Tectonic and sedimentary response to oblique and incipient continental - continental collision the easternmost Mediterranean (Cyprus)

Timothy C. Kinnaird
BSc (Hons) (St Andrews)

Thesis submitted for the degree of Doctor of Philosophy
University of Edinburgh

2008

Declaration

This thesis was composed by myself and is my own work, except where specifically stated.

Timothy Kinnaird
Edinburgh, 2007

Abstract

The main objective of this work was to understand fundamental processes related to incipient continental collision through studying the tectonostratigraphic evolution of Cyprus, in its Easternmost Mediterranean context. This was achieved by compiling structural, sedimentological and stratigraphic evidence from Late Cenozoic to Recent sequences, and by applying palaeomagnetic and luminescence methods of dating. In particular, the basin-fill of the Neogene basins provides a temporal and palaeogeographic control to interpret syn-depositional and post-depositional structural assemblages. Four neotectonic deformation phases are recognised. The Polis and Pissouri Basins originated as Tortonian depocentres in response to syn-depositional W-E/WSW-ENE D1 extension. The Maroni Basin originated as a Tortonian depocentre in response to syn-depositional NW-SE D1 extension. The difference in extension direction between west and south-central Cyprus is attributed to the curvature of the Cyprus Arc. The Middle - Late Pliocene D2 extensional/transtensional phase re-orientated the Neogene basins and resulted in syn-depositional NW-SE extension. A kinematic change occurred at ~3 Ma, attributed to the collision of the Eratosthenes Seamount with an active trench, the 'Cyprus Arc'. Early Pleistocene to Recent D3a transpression generated strike-slip faulting along E-W trends, conjugate left-lateral NNE-SSW-trending and right-lateral NNW-SSE-trending strike-slip faults and reactivated Tortonian D1 NW-SE and NE-SW structures. Middle Pleistocene to Recent D3b compression produced intense NE-SW contractional deformation orientated along NW-SE trends. Optically stimulated luminescence (OSL) dating was used as a tool to constrain the D3a/D3b events, by generating a chronology for their associated sediments. D3 transtensional lineaments originated in the early Pleistocene (174.1 ± 20.9 ka < D3a < 76.6 ± 16.43 ka), and are still active today (Cape Kiti: 38.1 ± 13.2 ka < D3a < 12.1 ± 0.1 ka). D3 compressional lineaments originated in the middle Pleistocene, and were still actively growing at 76.8 ± 31.6 ka. To constrain the timing of regional uplift in south and central Cyprus, a magnetostratigraphy was generated for the Plio-Pleistocene units of the Pissouri and Mesaoria Basins. The results indicate that rapid uplift began in the latest Pliocene (c. 2.14 – 1.95 Ma), coincident with the large-scale progradation of Gilbert-type fan deltas into the Pissouri Basin, and the incursion of large fluvial networks into the Mesaoria Basin.

In light of the new evidence, three alternative models for the Early Cenozoic to Recent tectonostratigraphic evolution of Cyprus are considered: model 1, subduction/incipient collision; model 2, advanced collision; and model 3, transpression**.** Some difficulties exist in detail, with all three models. However, at present the working hypothesis is as follows: areas to the east of Cyprus (Syria, S Turkey) were in a collisional setting from Mid-Miocene time onwards. Cyprus remained in an oceanic embayment (Levant Sea) further west and subduction continued during Miocene time. Compressional processes may have been active at depth during this time. Southward extension (trench roll-back) was taking place at a high structural level in S Cyprus, as with many other convergent margin settings (e.g. SW Peloponnese; Aleutians; Sunda arc). Subsequently, the collision of the Eratosthenes Seamount with the Cyprus Arc obstructed subduction and initiated rapid uplift of the Troodos Massif. The initial manifestation of this kinematic change was the generation of E-W-trending strike-slip faults and the development of conjugate left-lateral NNE-SSW-trending and right-lateral NNW-SSE-trending strike-slip faults. Transpression resulted in the reactivation of D1/D2 E-W, NE-SW and NW-SE structures. Subsequent deformation is documented in a compressional lineament in SW Cyprus. In addition, the over-riding plate in southwest Cyprus still appears to be undergoing gravity spreading outwards from the developing collision zone.

Acknowledgements

This thesis is dedicated to my family. I cannot thank you enough. Thanks Mum, thanks Dad, thanks Tamsin.

I owe many thanks to Alastair Robertson, my principal supervisor, for his advice, support and patience. I am greatly indebted to John Dixon, John Underhill and Costas Xenophontos, my second, third and fourth supervisors, for helpful discussion and advice at crucial moments. Ioannis Panayides, of the Cyprus Geological Survey Department (C.G.S.D), arranged logistical support, access to C.G.S.D. data and, gave help in the field. Thanks to all the people who have contributed to this work. David Sanderson and Chris Burbidge (Scottish Universities Environmental Research Centre) provided support, training and assistance with the luminescence technique. David Sanderson kindly arranged the financial grant for this work. Anthony Morris (University of Plymouth) kindly provided training, and has offered additional support with the palaeomagnetic technique. Thanks must be said to Wyn Williams (University of Edinburgh) for letting me use the palaeomagnetics Laboratory at the University of Edinburgh.

The research was funded by N.E.R.C. I also wish to thank the C.G.S.D. for their CASE contribution.

Thanks to all my friends over the last four years. I thank Peter Macintosh, Gillian McCay and Sarah Boulton for help in the field. In Cyprus, Efthimios Tsiolakis, Zeza Zomeni, Paul Croft, Brigetta Bailey, Duncan Howitt-Marshall all made my experience on the island an enjoyable one.

My final word is reserved for Kara. Thank you for always being there.

Chapter 1: Tectonic and sedimentary response to oblique and incipient continental – continental collision in the easternmost Mediterranean

1.1 Rationale

The Easternmost Mediterranean, defined as the region located east of Aegean (east of 28ºE longitude), is situated in a complex tectonic regime between the African, Arabian and Anatolian (Eurasian) plates (Figure 1-1). It is a collage of fragmented tectonic terranes, of which the island of Cyprus is an example. Since the early Mesozoic, rifting, subduction, obduction, continent-continent collision and transform faulting have occurred along the plate margins.

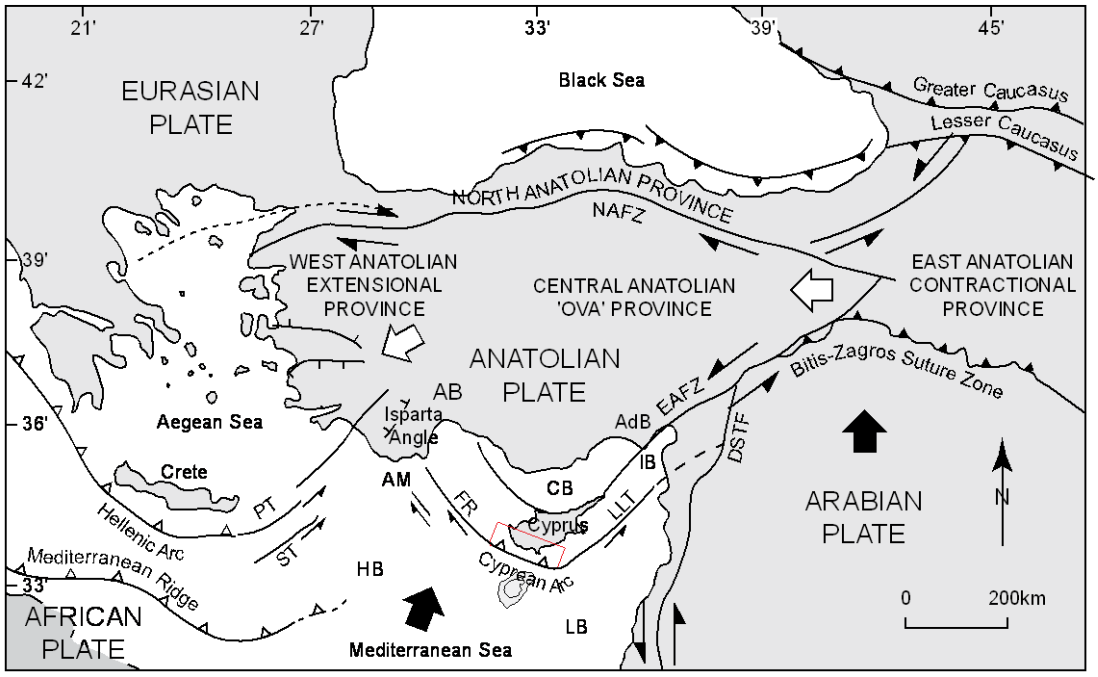

Figure 1-1: Tectonic framework of the eastern Mediterranean (after Zitter et al., 2003). Closed arrowheads indicate areas of crustal contraction. Open arrowheads indicate subduction zones. Large arrows indicate the relative plate motions of Africa and Arabia relative to a fixed Eurasia (McClusky et al., 2000). The Eratosthenes Seamount is shown to the south of Cyprus (in light grey). Abbreviations as follows: AdB = Adana Basin, AB = Antalya Basin, AM = Anaximader Mountains, CB = Cilica Basin, DSFZ = Dead Sea Transform Fault Zone, FR = Florence Rise, HB = Herodotus Basin, EAFZ = East Anatolian Fault Zone, IB = Iskenderun Bay, LB = Levant Basin, LLT = Latakia-Larnaka-Tartus ridges, NAFZ = North Anatolian Fault Zone, PT = Pliny Trench and ST = Strabo Trench

The present-day boundary between the African and Anatolian plates is represented by a deformation front, commonly termed the 'Cyprus Arc', located south of Cyprus, between the

island and the Eratosthenes Seamount (Ben-Avraham et al., 1995; Robertson et al., 1995a; Papazachos and Papaionnou, 1999; Vidal et al., 2000a,b; Woodside et al., 2002; Zitter et al., 2003). To the west of Cyprus, the Cyprus Arc extends along the Florence Rise (Woodside et al., 2002), and is probably connected to the Hellenic Arc in the Anaximander Mountains (Zitter et al., 2003) and/or Isparta Angle (Glover & Robertson, 1998; ten Veen et al., 2004). To the east of Cyprus, the plate boundary is suggested to extend from south Cyprus through the Iskenderun Bay towards the junction of the East Anatolian Fault (Ben-Avraham et al., 1995; Vidal et al., 2000a,b).

In the Middle Eastern region the suturing of the African and Eurasian plates was complete by 5 Ma, followed by the lateral expulsion of Anatolia westwards towards an Aegean subduction zone (Figure 1-1; Figure 1-2; Sengör et al., 1985; Robertson, 1990; 2000; Allen, 2004).

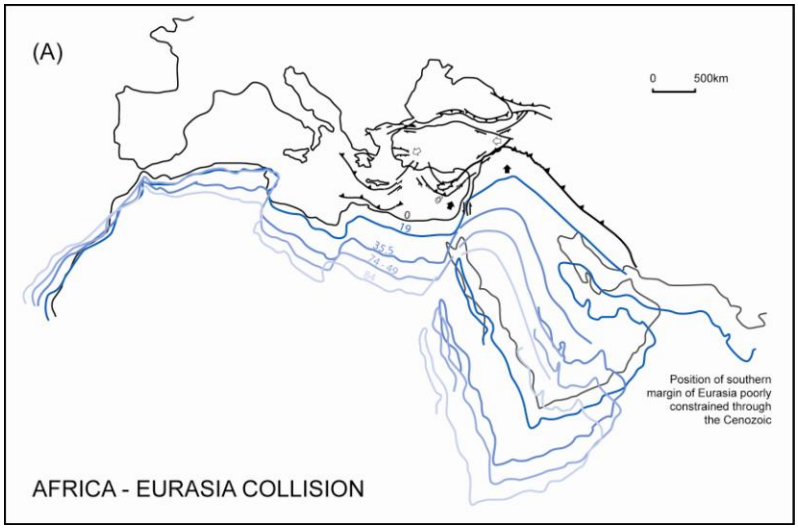

Figure 1-2: Convergent motion of Africa relative to Eurasia from Senonian (84Ma) to present time, from Allen, 2004.

In the Easternmost Mediterranean however, a relict of Mesozoic oceanic crust remained in a large embayment of the Mesozoic African continental margin allowing convergence to continue there along one, or both, of two important regional tectonic lineaments (Figure 1-1). The southernmost of these lineaments is the Cyprus Arc, while the second runs though the Kyrenia Range in the northern part of Cyprus (Figure 1-1; Robertson and Woodcock, 1986). There is currently considerable debate as to the relative roles of these two lineaments during Miocene to recent time and to their surface expression on land (Robertson, 1990; 2000; Soulas, 2003; Calon et al 2005a,b; Harrison et al., 2004a; Harrison and Tsiolakis, 2006).

This project aims to determine the kinematic evolution of the southern lineament, though analysing the tectonic and sedimentary expressions of this structure on land.

Due to the complexity of plate interactions in this region (Aksu et al., 2005), several different ideas exist as to the neotectonic setting of this deformation zone. One view is that a subduction zone exists between the south coast of Cyprus and the Eratosthenes Seamount, and that Africa and Anatolia are in incipient collision (Robertson, 1990; 2000). An alternative idea is that Africa and Anatolia are in a more advanced collisional setting (Sage and Letouzey, 1990; Soulas, 2003; Calon et al., 2005a,b). Yet, a third view is that strike-slip tectonics dominates the region and that no 'classical' subduction zone exists beneath Cyprus (Harrison et al., 2004a; Harrison and Tsiolakis, 2006). The tectonic setting of Cyprus, related to the collision of the African and Anatolian plates at the Cyprus Arc, has determined the deformation processes active on the island. As such, the geology of Cyprus offers an opportunity to study incipient continental collision and examine such problems as the role of palaeogeography, subduction versus overthrusting, and the importance of strike-slip deformation and terrane displacement.

This project forms one of several, process-orientated studies being supported by the Geological Survey Department of Cyprus. The framework for modern geological studies was provided by mapping by the Geological Survey Department of Cyprus, leading to the production of 1:250,000 maps and also memoirs covering much of Cyprus. Most relevant to this project are the maps of Bear and Morel (1960), Morel (1960), Pantazis (1967a,b), Malpas and Xentophontos (1992; 1999), Xenophontos et al. (1994) and Geological Survey Department of Cyprus (1995).

1.2 Areas investigated

The purpose of this section is to introduce the reader to the localities discussed within this thesis.

The island of Cyprus is formed from three amalgamated terranes, the central Troodos Massif, the southwesterly Mamonia Complex and the northerly Kyrenia Range (Figure 1-3). A varied carbonate and siliclastic sedimentary sequence fringes the Troodos Massif. A description of each of these terranes and, the circum-Troodos sedimentary cover is given in

chapter 2. The sedimentary succession contains a record of the Cenozoic tectonostratigraphic evolution of the island.

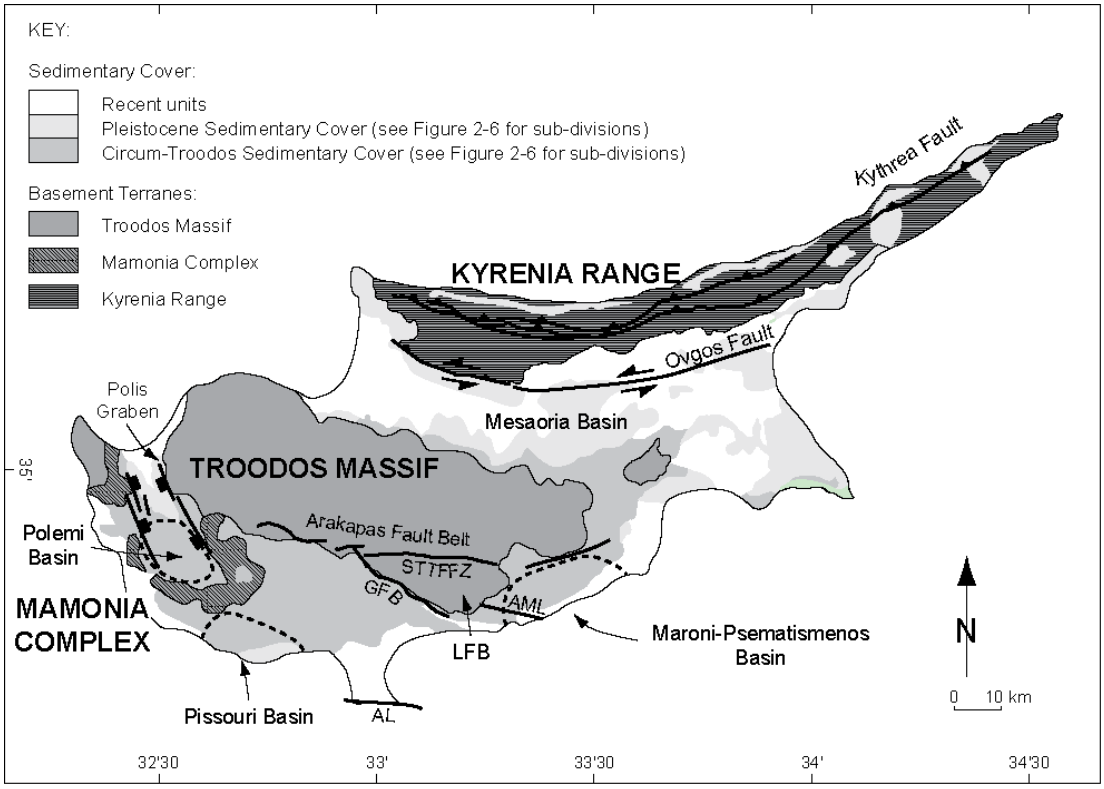

Figure 1-3: Simplified geological map of Cyprus

Three main basins are located to the south of the Troodos Massif: the Polemi Basin, the Pissouri Basin and the Maroni-Psematismenos Basin (Figure 1-3). A single basin is located to the north of the Troodos Massif, the Mesaoria Basin (Figure 1-3). Each basin is partly infilled by well-dated latest Cretaceous to Quaternary marine to non-marine sediments, including Late Miocene reef limestones (Follows et al., 1996), Messinian evaporites (Orszag-Sperber et al., 1989; Robertson et al., 1995b), Pliocene marginal to shallow-marine deposits (Payne and Robertson, 1995) and Quaternary non-marine to coastal deposits (Poole and Robertson, 1991; 1998; 2000). Stratigraphic, sedimentological and structural data were collected from within each of these basins (and from adjacent areas).

Figure 1-4: Map of Cyprus; illustrating the 'District' Divisions, and the location of cities and villages discussed in the text. Major Faults as mapped by the Cyprus Geological Survey are shown.

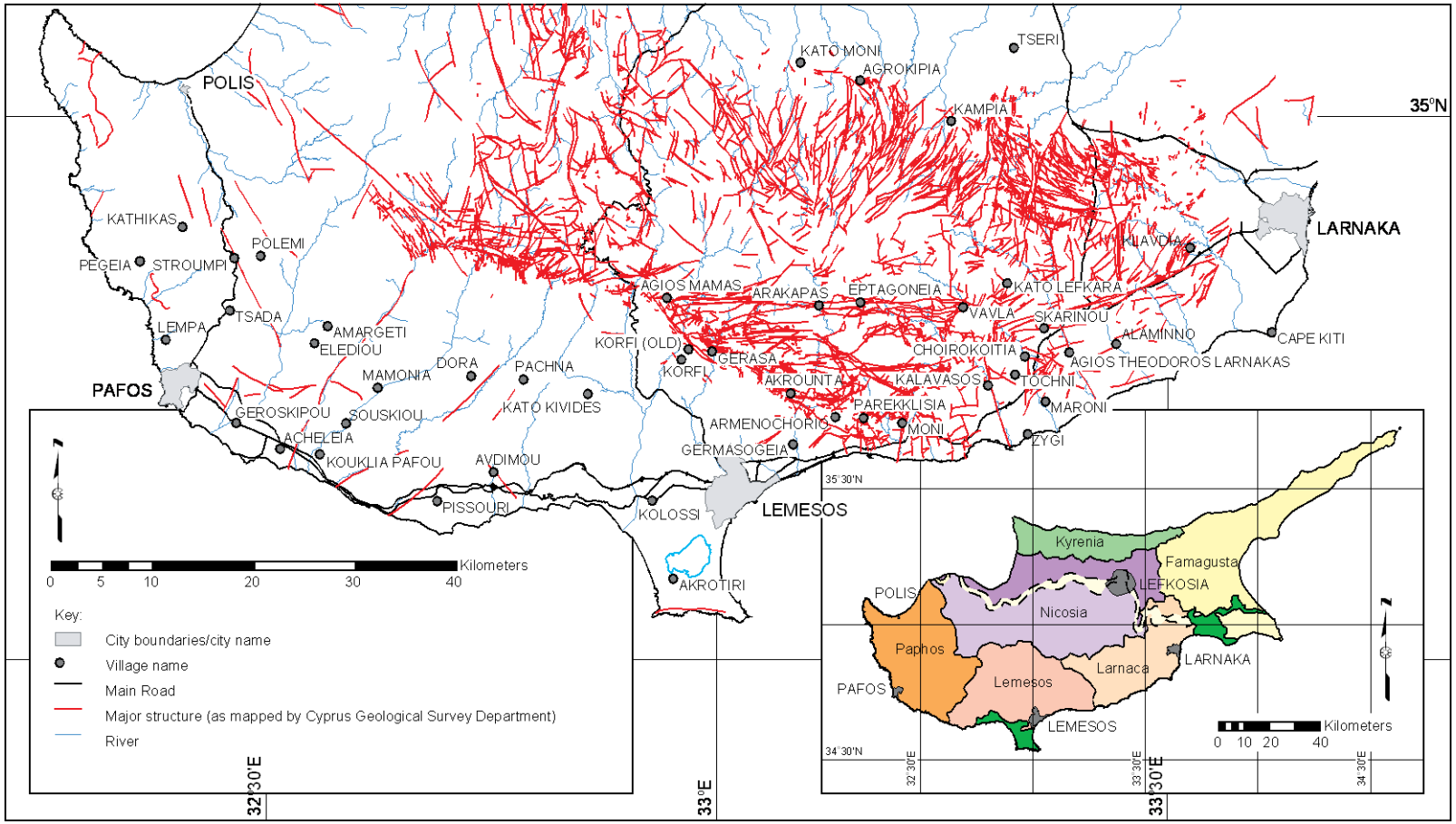

Figure 1-4: Map of Cyprus; illustrating the 'District' Divisions, and the location of cities and villages discussed in the text. Major Faults as mapped by the Cyprus Geological Survey are shown.

In the area studied there are four major cities – Paphos, Lemesos (Limassol), Larnaka (Larnaca) and Lefkosia (Nicosia; Figure 1-4). Numerous villages are distributed throughout the area under study (Figure 1-4). The author will frequently refer to the nearest town or village when discussing a rock unit, or structure.

1.3 Project Aims

The main aim of this thesis was to determine a model for the Late Cenozoic to Recent tectonostratigraphic evolution of Cyprus. This involved:

i. collecting detailed facies descriptions in each of the Neogene Basins (Figure 1-3), through sedimentary logging and geological mapping;
ii. collecting fault data from within each of the Neogene basins (Figure 1-3), through analysising data obtained from penetrative structures (faults, folds and their kinematic development in space and time) and syn-sedimentary structures (syn-sedimentary folds and growth faults).
iii. identifying active structures throughout Cyprus and determining their kinematic development through time; and
iv. establishing a geochronology for the Plio-Pleistocene successions of south and central Cyprus, using palaeomagnetic and luminescence methods of dating.

In the latter chapters of this thesis, three alternative models for the Late Cenozoic to Recent tectonostratigraphic evolution of Cyprus will be discussed. The three models will then be assessed in light of the new structural, sedimentary and chronological data presented in this thesis.

1.4 Methods Employed

Structural/geological mapping was undertaken at a variety of scales; reconnaissance fieldwork was undertaken on 1:50,000 scale maps and detailed work on 1:5,000 scale maps. Description of the stratigraphy, and its relation to the structural framework, was based on mapping and sedimentological logging, coupled with the collection of palaeocurrent and sedimentary structure data. Sedimentological logging was carried out at a variety of scales, depending on the detail required and the amount of continuous exposure. Standard

descriptive terms for lithology, texture and sedimentary structures are used. Lithological and palaeonotological samples were collected at selected intervals. A relative chronology was determined through palaeomagnetic sampling and optically stimulated luminescence profiling. The techniques employed in each method are discussed in more detail in their respective chapters.

1.5 Thesis organisation

The geodynamic and geological setting of the Eastern Mediterranean is introduced in chapter 2.

In chapter 3, a structural framework is established for south and central Cyprus. Structural data are presented for faults affecting each of the main lithostratigraphic units, so that the tectonic regime present during each of the main stratigraphic intervals can be assessed.

Chapters 4 and 5 establish a geochronological framework for the Plio-Pleistocene sedimentary successions of Cyprus. In chapter 4, magnetostratigraphies are generated for the Plio-Pleistocene units of the Pissouri and Mesaoria Basins. In addition, raised marine terrace deposits in southwest and south Cyprus are palaeomagnetically dated. Correlations are made between rock units found on the northern and southern flanks of the Troodos Massif. This allows the timing of uplift in Cyprus to be assessed. In chapter 5, optically stimulated luminescence dating of sediment is used as a tool to constrain the age of active faults in southwest and south Cyprus. In addition, the technique is used as a means to assess Late Pleistocene depositional processes and rates in areas of known tectonic disturbance.

An integrated sedimentological, structural and magnetostratigraphic study of the Pissouri Basin, south Cyprus, sheds light on the Late Pliocene to Holocene uplift history of the Troodos Massif, south Cyprus. Plio-Quaternary marine to non-marine sedimentary rocks in the Pissouri Basin provide an excellent record of subsidence and uplift. The results of this study are presented in chapter 6.

In chapter 7, a regional synthesis is established for the Late Cenozoic to Recent tectonostratigraphic evolution of Cyprus.

Chapter 2: Introduction to the geodynamic setting and evolution of the Eastern Mediterranean

2.1 Kinematic setting of the eastern Mediterranean Sea

2.1.1 Kinematic evolution of the Eastern Mediterranean from Jurassic to present

The development of the Tethyan region is intimately linked with the opening of the Atlantic Ocean to the west that began during the Triassic/Jurassic period. Numerous geological models for the evolution of the Tethyan system have been proposed (Robertson et al., 1996). These range from models involving a single Tethyan embayment separating Gondwana (Africa) from Eurasia (e.g. Dercourt et al., 1986; 1993), to those invoking an anastosmosing series of small ocean basins separating microcontinental terranes, which rifted off of the northern margin of Gondwana at various times during the Mesozoic (e.g. Şengör et al., 1984; Robertson and Dixon, 1984). In many models rifting of the Gondwanian margin was complete by the Middle to Late Triassic, forming the Neotethyan Ocean and several micro-continents. Remnants of these micro-continents can be seen as the Mamonia Complex in southwest Cyprus, the Moni Mélange in southern Cyprus and, as the Kyrenia Range in northern Cyprus (Robertson, 1990; Figure 1-3).

From Santonian time (85 Ma) to the late Cretaceous (65 Ma), the main relative motion of Africa with respect to Eurasia was in a north-south direction (Figure 1-2): this led to the progressive closure of Tethys through a variety of processes, including rifting, subduction, obduction, continent-continent collision and transform faulting. The northern part of Tethys amalgamated first, forming an 'isolated' northerly Neotethyan Ocean, and an 'open' southerly Neotethyan Ocean. In both the northerly and southerly Neotethyan ocean basins ophiolites were generated above northerly dipping subduction zones (Robertson, 2002; 2004). Within the southerly Neotethyan Ocean an intra-oceanic subduction zone apparently collided with the 'Arabian promontory' of the southerly continent during the Campanian to Maastrichtian, triggering the rotation of the Troodos micro-continent (Clube and Robertson, 1986; Clube et al., 1985). It was during this rotation that the Mamonia complex was juxtaposed with the Troodos ophiolite. Palaeomagnetic evidence (Morris et al., 2006) indicates an anticlockwise rotation of 90º for the Troodos Massif. As a result of collision, the Troodos Massif was tilted en mass to the south, producing a palaeoslope, which was

influential in the deposition of Lower Cenozoic carbonates and calciturbidites (Robertson, 1976).

By the Early Miocene (Aquitanian; 20 Ma) the whole Mediterranean region was in compression, with coincident back-arc extension; this resulted in the opening of the Aegean Sea (Figure 2-1; Le Pichon and Angelier, 1979; Jolivet et al., 2006). In Cyprus, the southern Neogene basins may have formed in response to regional back-arc extension (Payne and Robertson, 1995; 2000).

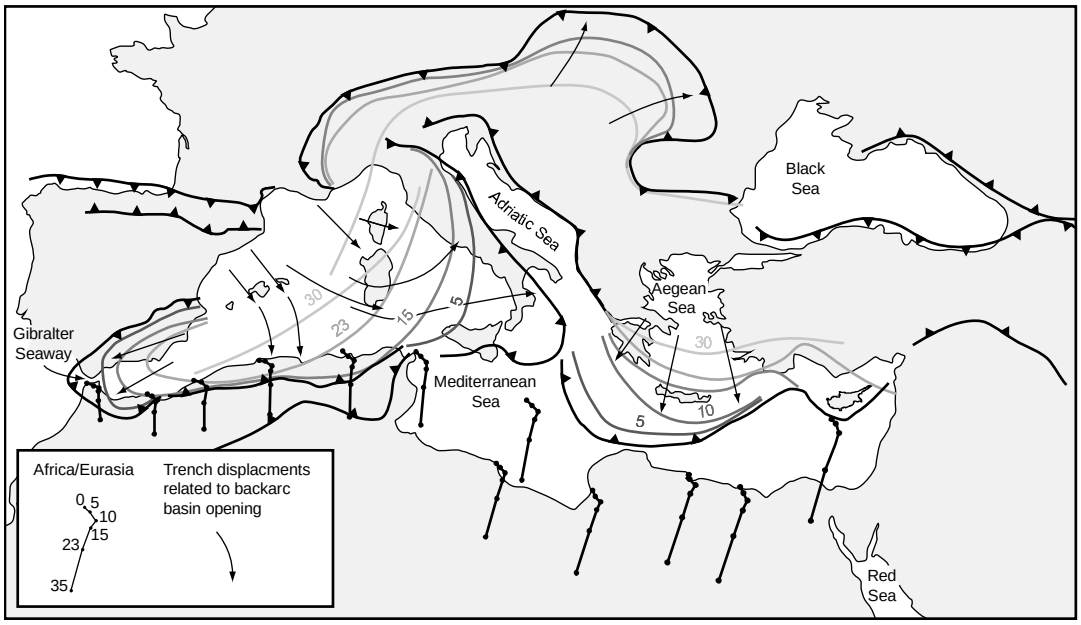

Figure 2-1: The position of the main convergent fronts and subduction zones from 30Ma to the Present in the Mediterranean Sea (Jolivet et al., 2006): Africa-Eurasia kinematics are modified from Dewey et al. (1989); the kinematics of the Anatolian block (5Ma to present) are modified from Le Pichon et al. (1995); the successive positions of the trenches were estimated from a variety of sources, including volcanic arc migration, the length of subducted slabs from tomography, the timing of backarc basin openings (Jolivet et al., 2006; and references therein); the backward motion of the subduction zones is constrained by the migration of volcanic arcs and high-pressure metamorphic rocks (Jolivet et al., 2006; and references therein)

During Middle to Late Miocene time (10 Ma), a drastic change occurred in Eastern Mediterranean tectonics, as the relative motion between Africa and Eurasia shifted from north-south to more northwest-southeast (Figure 2-1; Le Pichon and Anglier, 1979; Jolivet and Faccenna, 2000; Nocquet and Calais, 2004; Jolivet et al., 2006). The collision of the Arabian and Eurasian plates in eastern Turkey and in the Caucasus, linked to the opening of the Red Sea, led to the closure of the seaways between the Mediterranean and the Indian Ocean. This also triggered the westward extrusion of the Anatolian microplate, the reorganisation of the Cyprus-Hellenic subduction zone into two separate arcs and an increase

in extension tectonics in the Aegean and western Turkey. Closure of the Betic strait and Rifian Corridor (former Gibraltar seaway) between the Atlantic and Mediterranean isolated the Mediterranean waters, causing the 'Messinian' salinity crisis (Hsü et al., 1973). This, in combination with important environmental changes, lead to intense evaporation and deposition of thick halite and gypsum layers in deep basins (Flecker and Ellam, 1999; Flecker et al., 2002).

During Midde to Late Pliocene times (post-3.16 Ma), the convergence rate between Africa and Eurasia decreased by approximately 25% in the eastern Mediterranean, with the relative plate motion direction becoming more oblique (Figure 2-1; Calais et al., 2003). A change in the stress regime along the Africa-Eurasia plate boundary was reported by Armijo et al. (1992), who concluded that a phase of extension occurred in the Hellenic Arc in the early Pleistocene (~1 Ma).

2.1.2 Geodynamic setting of the Eastern Mediterranean region

Active deformation in the Eastern Mediterranean region is primarily controlled by the interaction of the African, Arabian and Eurasian lithospheric plates and the smaller Anatolian and Sinai microplates. The boundary between the African plate (inc. the Sinai plate) and the Anatolian microplate (as defined by the edge of the over-riding plate) is delineated by the Hellenic Arc and the Piny-Strabo Trenches in the west and the Florence Rise, Cyprus 'Arc' and the Latakia-Larnaka-Tartus Ridges in the east (Figure 1-1).

The partitioning of plate movements in the eastern Mediterranean has been recently clarified and quantified using GPS and SLR geodetic data (Reilinger et al., 1997; Kahle and Mueller, 1998; Kahle et al., 1998; McClusky et al., 2000; Anzidei et al., 2001; Nocquet and Calais, 2004; Mahmoud et al., 2005), finite element models (Lundgren et al., 1998) and sand-box experiments (Martinod et al., 2000). In a fixed Eurasia reference frame, the African Plate is presently moving in a northerly direction and the Arabian Plate in a north-northwesterly direction at velocities of ~ 6-10 and ~18-25 mm y^{-1}, respectively (McClusky et al., 2000). The differential motion between the African Plate and Arabian Plate is accommodated by the sinistral, transpressional Dead Sea Transform Fault. The collision between Africa and Arabia is accommodated by the Bitlis-Zagros fold-thrust belt. North-northwest 'pushing' of the Arabian microplate, in combination with the 'pulling' or basal drag associated with the subducting Africa slab beneath the Hellenic Arc, has resulted in the west-directed 'tectonic

escape' (and counter-clockwise rotation) of the Aegean-Anatolian Microplate (Reilinger et al., 1997; McClusky et al., 2000). The tectonic escape of the Aegean-Anatolian microplate is accommodated along two intra-continental transform faults: the dextral North Anatolian and sinistral East Anatolian faults (Şengör, 1979; Şengör et al., 1985). The Ecemiş Fault Zone (Central Anatolian Fault Zone) accommodates deformation internal to the Anatolian microplate (Jaffery and Robertson, 2001; Westaway et al., 2002; Jaffery and Robertson, 2004).

The western and central segments of the Hellenic and Cyprus 'Arcs' are nearly perpendicular to the present-day relative motion of the African and Anatolian plates, forming the 'subduction sutures' or regions of incipient collision (Figure 1-1). However, the Pliny-Strabo trenches and the Latakia-Larnaka-Tartus ridge are sub-parallel to the slip vector, with a predominantly sinistral transform motion (Figure 1-1). The leading edge of the African plate is apparently being subducted along the Hellenic Arc at a higher rate than the northward motion of the Africa plate itself, requiring that the Arc (and presumably the Aegean Sea) moves southwards relative to Eurasia proper (Royden et al., 1993; Kempler and Garfunkel, 1994; ten Veen and Kleinspehn, 2002; Rizzetto et al., 2004). Reilinger et al. (1997) predict 14 ± 5 mm yr^{-1} of north-south extension in the Aegean region. Subduction of the African plate is also thought to occur along the 'Cyprus Arc' and/or the Florence Rise, although it is less well defined in these regions than along the Hellenic Arc. Woodside et al. (2002) and Zitter (2003) suggest that the African and Anatolian plates have more or less sutured along the Florence Rise. This is associated with the development of positive flower structures existing in a ~15 km-wide arc-parallel dextral wrench zone. There is no evidence of typical 'slab-style' subduction along the arcuate Florence Rise today. However, the well-defined Wadati-Benioff zone delineated by Papazachos and Papaioannou (1999) suggests that the subduction of the African plate beneath the Aegean-Anatolian Microplate must have slowed-down or stopped only recently (Woodside et al., 2002; Zitter et al., 2003). The Cyprus Arc is probably connected to the Hellenic Arc via the Anaximander Mountains (Zitter et al., 2003) and/or Isparta Angle (ten Veen et al., 2004; Figure 1-1).

2.1.3 Geodynamic setting of Cyprus

The present day boundary between the African and Anatolian plates is represented by a deformation front, commonly termed the Cyprean Arc, located south of Cyprus, between the island and the Eratosthenes Seamount (Figure 2-2; Kemplar and Garfunkel, 1994; Ben-

Avraham et al., 1995; Robertson et al., 1995a; Papazachos and Papaionnou, 1999; Vidal et al., 2000a,b; Woodside et al., 2002 and Zitter et al., 2003). To the west of Cyprus, the Cyprean Arc extends along the Florence Rise (Woodside et al., 2002), through the Anaximander Mountains (Zitter et al., 2003) and is probably connected to the Hellenic Arc in the Isparta Angle, southwest Turkey (Figure 2-2; Glover and Robertson, 1998; Robertson et al., 2003; ten Veen, 2004; ten Veen et al., 2004). To the east of Cyprus, the plate boundary is suggested to extend from south Cyprus through the Iskenderun Bay towards the junction of the East Anatolian Fault (Figure 2-2; Ben-Avraham et al., 1995; Vidal et al., 2000a,b; Hardenberg and Robertson, 2007).

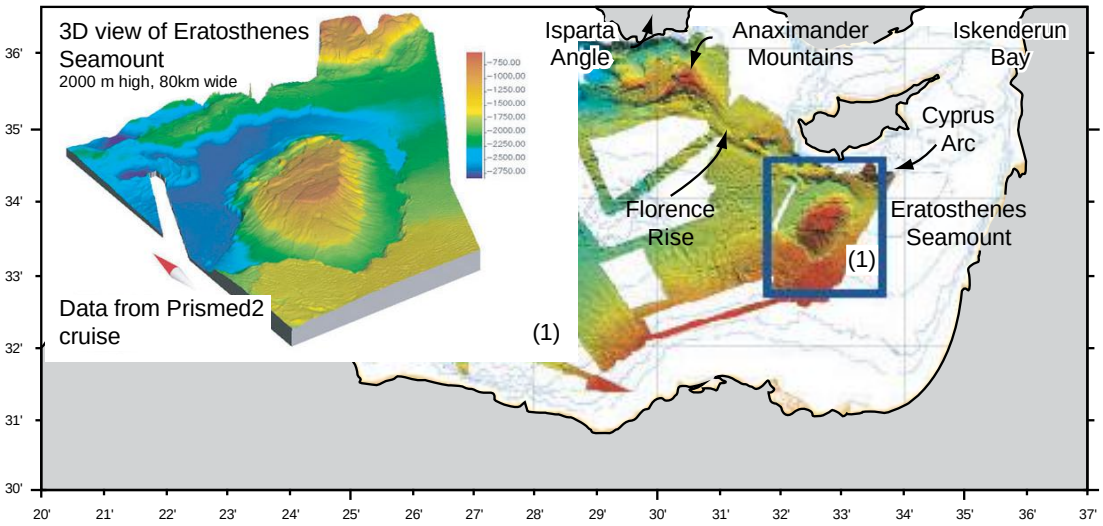

Figure 2-2: Bathymetry of the Eastern Mediterranean; note the bathymetry associated with the Eratosthenes Seamount, the Cyprean Arc, the Florence Rise and Anaximander mountains

Kahle et al. (1998) determined crustal strain rates for the region comprising the Hellenic Arc, the Aegean Sea, western Anatolia and the Cyprean Arc. The Cyprean Arc is associated with slight to moderate arc-normal compression (Figure 2-3a) within a weak transpressional setting (Figure 2-3b).

Mahmoud et al. (2005) developed an elastic block model (Figure 2-4), constrained by GPS results and consistent with regional tectonics, to estimate slip rates for the Sinai bounding faults, including the Gulf of Aqaba–southern Dead Sea fault system (left-lateral at ~4.4 ± 0.3 mm/yr), the Gulf of Suez (left-lateral at 1.9 ± 0.3 mm/yr, and extensional at 1.5 ± 0.4 mm/yr), and the Cyprus Arc (predominantly convergence at 8.9 ± 0.4 mm/yr along the western segment, and left-lateral ~6.0 ± 0.4 mm/yr along the eastern segment).

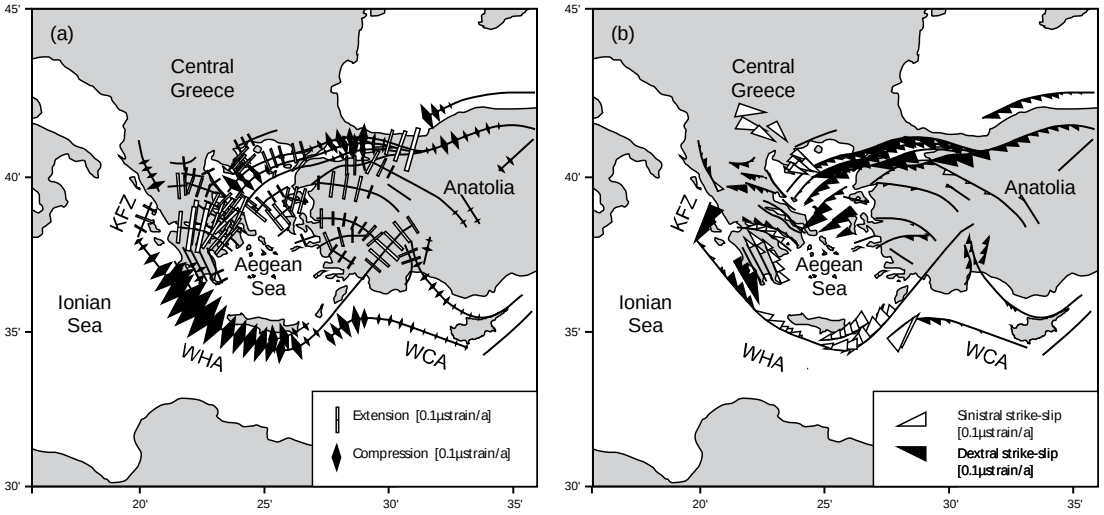

Figure 2-3: Scaled strain rates projected onto major faults: (a) normal strain; and (b) shear strain (Kahle et al., 1998). Abbreviations as follows: KFZ – Kephalonia Fault Zone; WCA – West Cyprus Arc; WHA – West Hellenic Arc

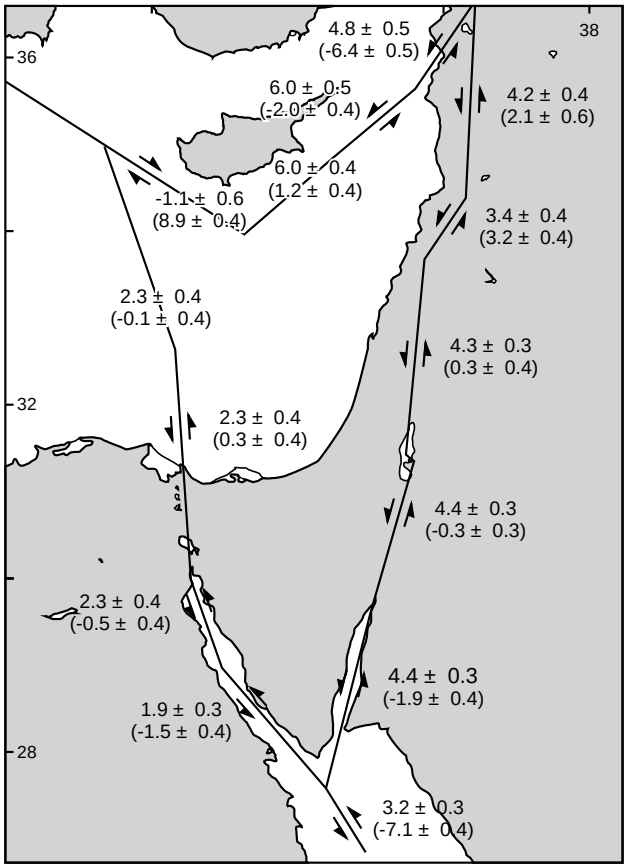

Figure 2-4: The elastic block model for the Sinai area created by Mahmoud et al. (2005). Numbers show fault strike-slip and fault normal slip rates, with 1σ uncertainties (fault normal component in brackets; negative for left lateral and extension). Faults are vertical, and assigned locking depths of 15km, except for the Gulf of Aqaba/Dead Sea fault system that has a locking depth of 13km, and the western Cyprus Arc that has a 30º dip to the NE. Slip rates are averages along each segment.

The model of Mahmoud et al. (2005) is derived from GPS-derived velocities obtained from a network of survey sites on the Sinai Peninsula and along the west side of the Gulf of Sinai; it does not take into account GPs-derived velocities obtained from a survey site on Cyprus. It represents the plate motion of the Sinai Peninsula relative to Nubia (Africa); the Sinai region is moving northward at the rate of 1.4 ± 0.8 mm yr^{-1} and westward at 0.4 ± 0.8 mm/yr west (Mahmoud et al., 2005).

Figure 2-5 illustrates the distribution of earthquake epicentres from deep and shallow earthquakes in the Mediterranean region.

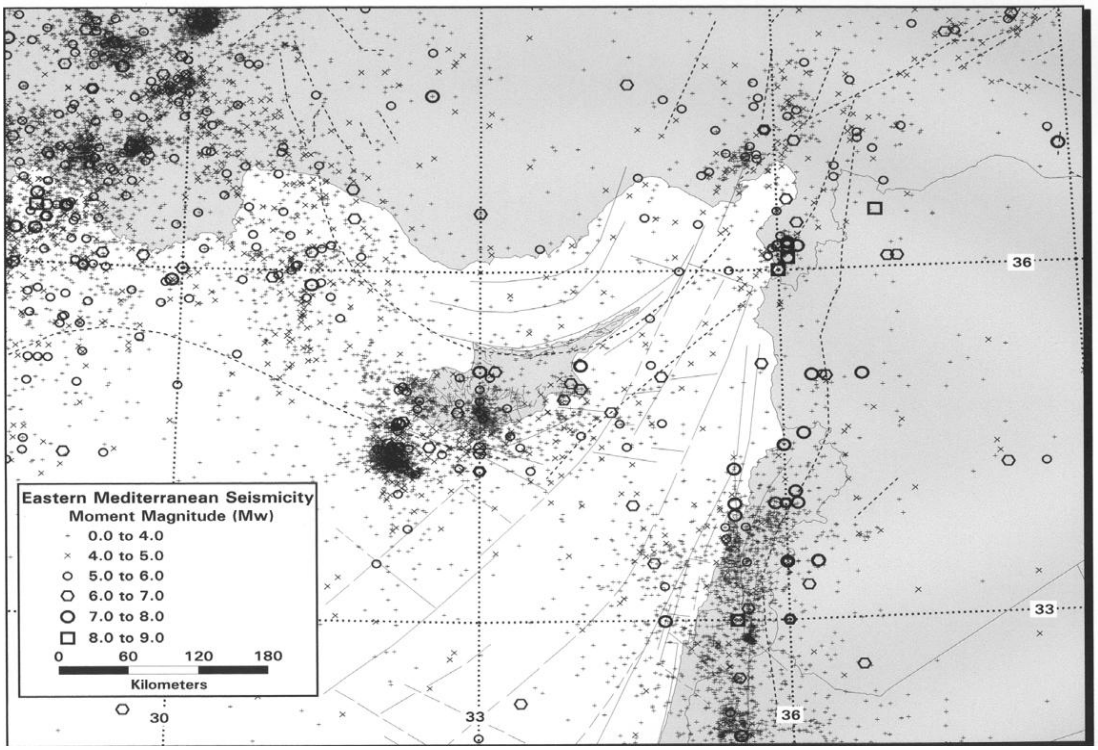

Figure 2-5: A map of all earthquakes in the historical record (from 2150BC through to 2000) in the Eastern Mediterranean region (Algermissen and Rogers, 2004). The solid lines offshore depict faults inferred from bathymetric data and geophysical surveys (adapted from Neev et al, 1985); the dashed lines are inferred faults (U.S. Geological Survey, 2000). The faults on Cyprus are mapped and inferred faults of unspecified age (Geological Map of Cyprus, 1995).

The most active areas are western Turkey, southeast Turkey (at the East Anatolian Fault), the Levantine coastal area, the Dead Sea rift in Syria, Israel, and Lebanon, and SW Cyprus. The Cyprus 'Arc' has experienced little seismicity over the last century (Ambrasey, 1962; Ambrasey and Adams, 1993). A prominent cluster of earthquakes is located to the southwest of Cyprus; this cluster demarcates the present plate boundary. The Eratosthenes Seamount is believed to be in the process of collision with the Cyprus active margin.

Focal mechanisms calculated for shallow (<30 km), major (M > 5) earthquakes in the Cyprean Arc are indicative of a mixture of faulting styles, but are dominantly strike-slip (Figure 2-6a; Arvidsson et al., 1998; Makris et al., 2000; Salamon et al., 2003; Pilidou et al., 2004).

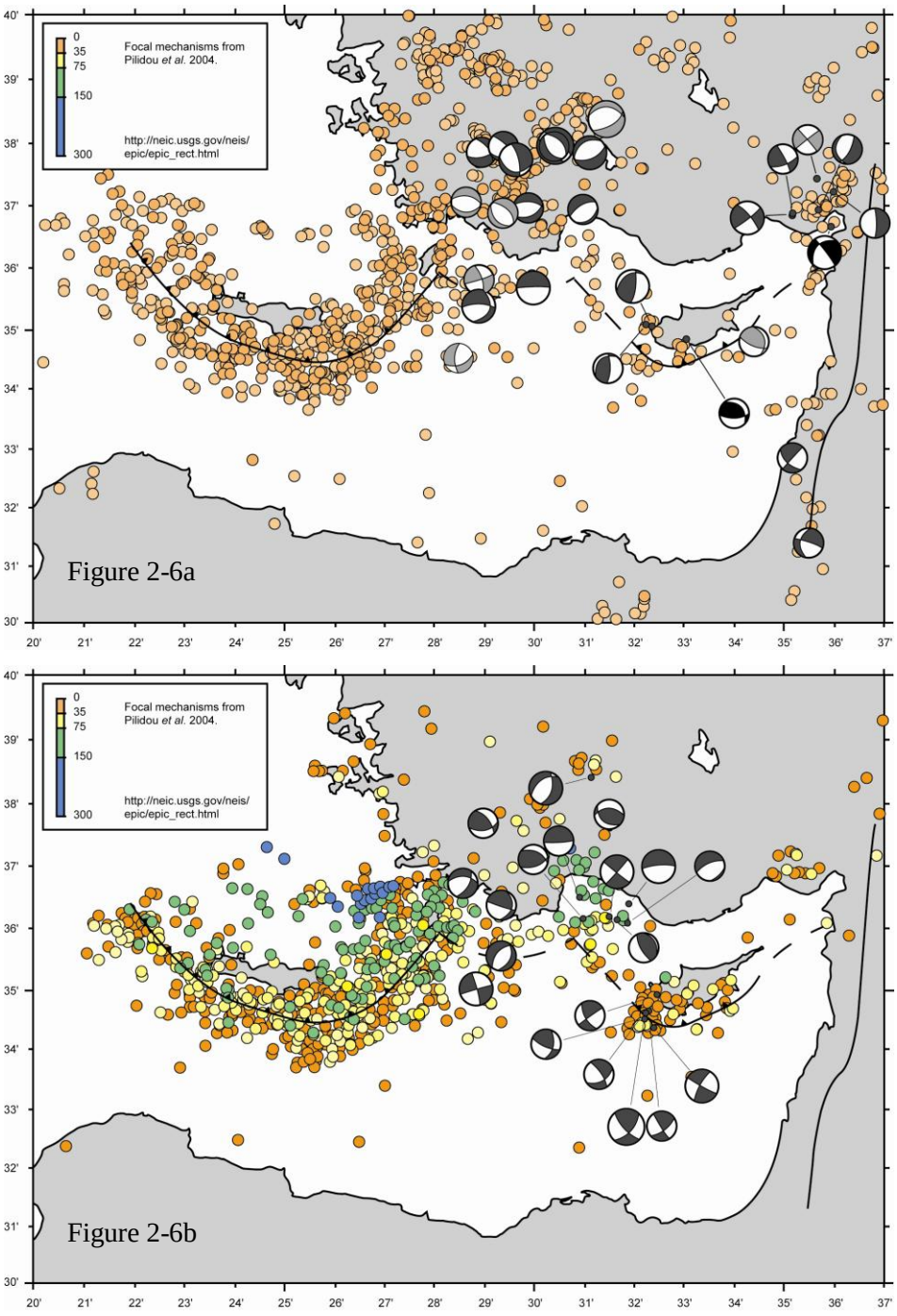

Figure 2-6: Focal mechanisms for (a) shallow and (b) deep earthquakes in the region of Cyprus (Pilidou et al., 2004).

Focal mechanisms derived for deep (>30km), major (M > 5) earthquakes, are again indicative of a mixture of faulting styles, but indicate that collision is occurring at depth (Figure 2-6b). The seismicity of the African-Anatolian plate boundary is reviewed in chapter 7. The observant reader will notice a discrepancy between the plate motion inferred in SW Cyprus by Mahmond et al. (2005) and the recorded seismicity; Mahmond et al.'s (2005) model is based on averaged GPS velocities in the Cyprus-Levant-Sinai region, whereas individual earthquakes record distinct events at the plate boundary.

2.2 The tectonostratigraphic framework of Cyprus

The island of Cyprus is formed from three amalgamated terranes; the upper Cretaceous Troodos Massif (Lapierre, 1972); the Triassic to lower Cretaceous Mamonia Complex (Robertson and Woodcock, 1979; Swarbrick, 1980); and the northerly Kyrenia Range (Robertson and Woodcock, 1986; Robertson, 1990) (Figure 2-7). A varied carbonate and siliclastic sedimentary sequence fringes the Troodos Massif.

2.2.1 The Troodos Massif

The Troodos ophiolite, exposed in central Cyprus (Figure 2-7), is thought to have formed at a spreading axis (Gass and Masson-Smith, 1963; Moores and Vine, 1971) in the Late Cretaceous (92 - 85 Ma; Gass et al., 1994; Mukasa and Ludden, 1987), above a northerly dipping subduction zone (Pearce et al., 1984; Clube and Robertson, 1986; Robertson, 1990). A generalised stratigraphy for the Troodos ophiolite is as follows, from the base upward: the lowest unit, comprised of upper mantle harzburgites, is overlain by layered cumulates, non-cumulate rocks (i.e. massive gabbro), sheeted dykes and finally pillow lavas (Figure 2-8). Three extrusive units are recognised: the Basal Group (lava screens within dykes); the Lower Pillow Lavas and the Upper Pillow Lavas.

The Troodos ophiolite is bounded to the south by an E-W-trending tectonic lineament, the South Troodos Transform Fault Zone (Figure 2-7).

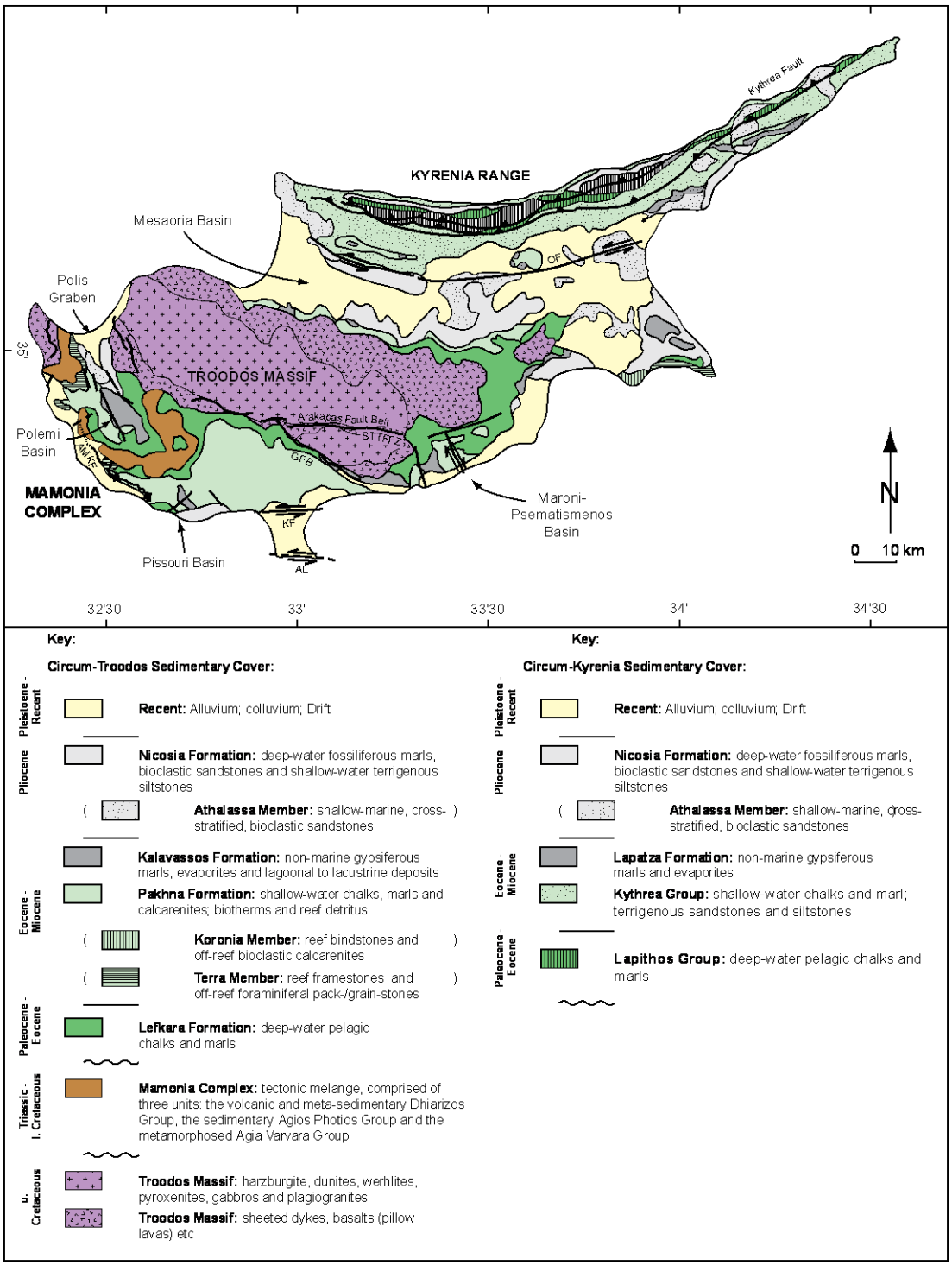

Figure 2-7: Simplified geological map of Cyprus illustrating the distribution of the basement terranes - the Troodos Massif in purple, the Mamonia Complex in brown, and the Kyrenia Range in green – and sedimentary cover. A distinction is made between circum-Troodos and circum-Kyrenia sediments. Abbreviations as follows: AL; Akrotiri lineament; AMKF – Agia Marinouda-Kouklia Fold; GFB – Gerasa Fault Belt; KF – Kolossi Fault; OF – Ovgos Fault; STTFZ – South Troodos Transform Fault Zone

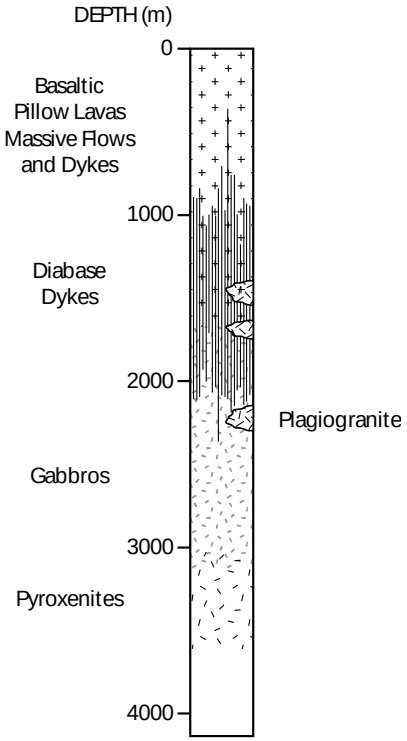

Figure 2-8: Stratigraphic column to show the main units of the Troodos ophiolite as inferred by the Cyprus Crustal Drilling Project (Moores and Vine, 1971)

2.2.2 The Mamonia Complex

The Mamonia Complex, exposed in west Cyprus (Figure 2-7), consists of broken formations and mélanges, comprised of sedimentary, volcanic and locally metamorphic rocks (Swarbrick, 1980). This tectonic mélange formed during Campanian/Maastrichtian collision of a 'Mamonia microcontinent' with the 'Troodos continent'; for Murton (1990) and Malpas et al., (1993), the Mamonia Complex was delaminated from its basement upon arrival at the N-dipping subduction zone and emplaced onto the forearc region of the Troodos microplate; for Clube & Robertson (1986), Swarbrick (1993) and McLeod & Murton (1995), the emplacement of the Mamonia Complex and Trooodos microplate took place along transcurrent faults which affected the Troodos southwestern margin, the Limassol Forest Block and Akamas Penisula (Figure 1-3). The Mamonia Complex and Troodos Massif are juxtaposed against each other along arcuate shear zones, in which slivers of transform lithosphere (including mantle harzburgite, gabbro, diabase and boninite) are entrained (Malpas et al., 1993; Bailey et al., 2000).

The Mamonia Complex is comprised of three units: the volcanic and meta-sedimentary Dhiarizos Group, the sedimentary Agios Photios Group and the metamorphosed Agia Varvara Group (Robertson and Woodcock, 1979; Swarbrick, 1980). The Dhiarizos Group is an assemblage of Triassic pillow lavas (Phasoula Formation; alkaline to tholeiitic basalts) and volcanic breccias (Loutra tis Aphroditis Formation) intercalated with pink calc-lutites and radiolarian mudstones, that occur in association with blocks of Triassic recrystallised algal/coral boundstones and shell-detrital limestones (Petra tou Romiou Formation). The Dhiarizos Group is believed to represent Late Triassic age oceanic floor and seamounts with carbonate atolls. New Nd and Pb isotopic data have shown that the whole Mamonia volcanic suite exhibits features of oceanic island basalts (OIB) (Lapierre et al., 2007). The Agios Photios Group consists of deepwater sediments, including Middle-Upper Triassic quartzose turbidites interbedded with pelagic mudstones and limestones (Vlambouros and Marona Formations), Jurassic radiolarian mudstones and redeposited carbonates/limestones (Episkopi Formation) and Lower Cretaceous quartzarenitic mud-flows (Akamas Member; Malpas et al., 1992).

The Agia Varvara Group, found in close proximity to the serpentinite shear zones, is comprised of amphibolite, metapelite, metachert and marble. It is thought to be the metamorphosed equivalent of the Dhiarizos Group. Bailey et al. (2000) identified three tectonic events of Upper Cretaceous age: (i) high temperature (c. 600ºC), transform-related, dextral strike-slip and localized metamorphism of the Mamonia Complex units (c. 90-83 Ma); (ii) retrograde hydration (<400ºC) during dextral transtension associated with the rotation of the Troodos micro-plate and the shallow-level emplacement of serpentinite (c. 83-73 Ma); and (iii) regional contractional reactivation at low temperatures, which ceased by the latest Maastrichtian (c. 65 Ma). Final welding between the Troodos and Mamonia terranes is represented by Maastrichtian debris flow deposits (Kathikas Formation), which contain clasts derived from both terranes (Swarbrick and Naylor, 1980).

2.2.3 The Kyrenia Range

The Kyrenia Range is a narrow arcuate deformed belt, several hundred kilometres long, mostly comprised of Mesozoic and Tertiary sedimentary rocks and subordinate volcanic and metamorphic rocks. Four rock groups, separated by major unconformities and each representing an important deformation event, are recognised (Robertson and Woodcock, 1986): (i) the Permian – Maastrichtian Trypa Group, comprised of Mesozoic shallow-water

carbonates, which where strongly deformed and metamorphosed in the early Late Cretaceous; (ii) the Maastrichtian – Early Eocene Lapithos Group, comprised of breccias and pelagic carbonates intercalated with mafic lavas, which were deformed and metamorphosed in the Late Eocene; (iii) the Early Oligocene to Messinian Kythrea Group, comprised of conglomerates, turbiditic sandstones and mudstones, bioclastic limestones and evaporites, which were deformed and uplifted in latest Miocene – Early Pliocene time; and, (iv) the Pliocene Mesaoria Group, which is comprised of conglomerates and marls.

2.2.4 Circum-Troodos sedimentary cover

A thick sequence (~200-1000m) of sedimentary rocks accumulated on the Troodos ophiolite, since the Late Cretaceous (92 - 85 Ma; Gass et al., 1994; Mukasa and Ludden, 1987). These sediments are termed the 'Circum-Troodos sedimentary sequence' (Figure 2-7; Figure 2-9). Recent research on this cover sequence has revealed information on the uplift history of the Troodos Massif (Robertson, 1977), the tectonic evolution of the eastern Mediterranean (Robertson, 1990; 2000) and Miocene-Recent climate and oceanographical changes (Davies, 2001; Read, 1993; Robertson et al., 1991)

Late Cretaceous deep-water metalliferous sediment and siliceous oozes of the Perapedhi Formation; and bentonitic clays and volcaniclastic sandstones of the Kannaviou Formation

Turonian (ca. 92-90 Ma; Blome and Irwin, 1985) deep water pelagic sedimentation, in the form of metalliferous sediment (umber) and siliceous oozes (radiolarites) of the Perapedhi Formation and Campanian – Maastrichtian bentonitic clays and volcaniclastic sandstones of the Kannaviou Formation, represent the first in situ sediments to be deposited on the newly created, topographically irregular ocean floor of the Troodos ophiolite (Robertson and Hudson, 1974; Robertson, 1976).

Paleocene – Oligocene deep-water pelagic carbonates of the Lefkara Formation

The Lefkara Formation can be divided into four lithological units, in ascending order these are: the Lower Marl Member, the Chalk and Chert Member, the Massive Chalk Member and the Upper Marl Member.

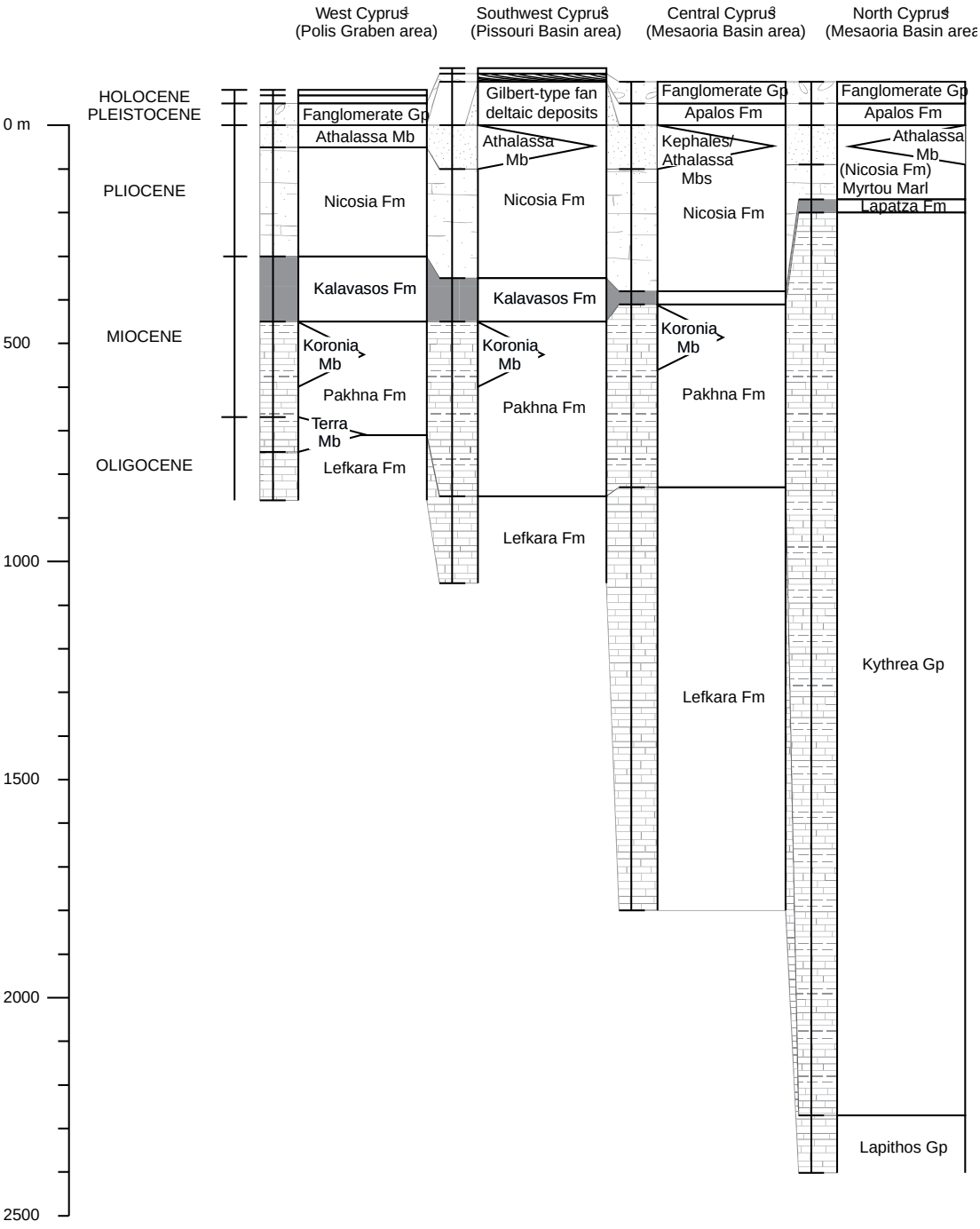

Figure 2-9: Stratigraphy of the circum-Troodos sedimentary cover. The age of the Kephales (Kakkaristra Formation) and Athalassa (Athalassa Formation) Members are consistent with geological data that existed before the completion of this project. Formation/Member thicknesses are as estimated by [1]Payne and Robertson (1995) and [2]myself (see chapter 6), and as known from boreholes, [3]Kato Lakatamia and 4Lefkoniko

The oldest of these, the Maastrichtian to Lower Eocene 'Lower Marl Member', consists of pinkish marls, white chalky marls and rare limestones and cherts (Kähler and Stow, 1998; Figure 2-10). The unit is thin and discontinuous. The maximum thickness of this unit is estimated between 25 and 100m. Burrows and bioturbational mottling are present

throughout. The overlying Lower to Middle Eocene 'Chalk and Chert Member' consists of regularly bedded chalks, marly chalks and thin marls, intercalated with silified micrites and cherts (Kähler and Stow, 1998; Figure 2-10). Normal grain-size grading, parallel lamination and cross-laminations are indicative of turbidite sequences, and reflect incomplete Bouma sequences (T_{de} and T_{cde}; Robertson, 1976). The upper part of this unit is marked by an increase in the proportion of these calciturbiditic horizons. The maximum thickness of this unit is 300m. The Upper Eocene to Lower Miocene 'Massive Chalk Member' is comprised of medium- to thickly-bedded massive chalks and rare, marly chalks (Figure 2-10). Chert is absent. It has a variable thickness between 70m and 250m. The Upper Eocene to Lower Miocene 'Upper Marl Member' is a succession of chert-free thin-bedded marls and chalky marls, which become increasingly calcarenitic up section (Figure 2-10). It has a variable thickness of between 0m and 200m.

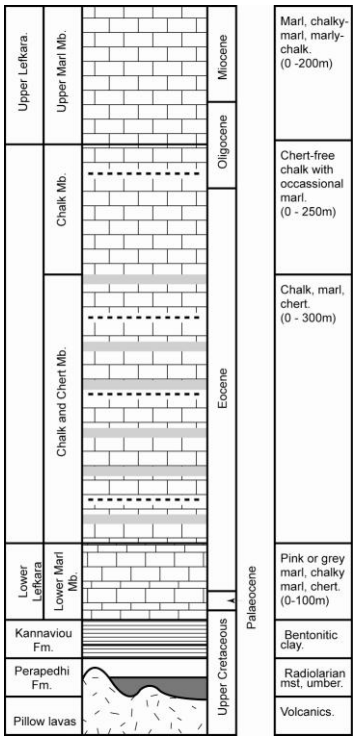

Figure 2-10: Standard stratigraphic column for the Lefkara Formation, showing age, units, principal lithologies and thickness variations (Kähler and Stow, 1998)

The Lefkara Formation is thought to represent sedimentation on the distal part of a carbonate slope-apron to basin plain setting, located in the western Tethyan Ocean (Kähler and Stow, 1998). A palaeographic reconstruction of the Lefkara Formation is shown in Figure 2-11. The earliest phase of Lefkara deposition, represented by the Lower Marl Member, was dominated by pelagic carbonate sedimentation (above the carbonate compensation depth), in

small ponded hollows on the surface of the Troodos Massif (Robertson and Hudson, 1974). The Kyrenia Range to the north was undergoing a period of subsidence, so that any material resedimented as turbidites and debrites from the Taurids was mostly trapped before reaching the Troodos terrane. The Chalk and Chert Member reflects a gradual increase in the influx of biogenic turbidites from the north i.e. uplift of the Kyrenia terrane at this time (Kähler and Stow, 1998) and/or local highs (Robertson, 1976). In southern Cyprus, facies variations, palaeocurrent measurements and the overall tectonic setting (intraformational slumps are common in the middle Lefkara units) indicate, that in general, the calciturbidites flowed from northeast to southwest down a regional palaeoslope. The Massive Chalk and Upper Marl Members reflect a return to slower rates of sedimentation (associated with significant depositional hiatuses in the rock record). Robertson (1976) identified in situ benthonic foraminifera in the upper levels indicating that by Oligoocene times, the seas around the Troodos margins were shallowing.

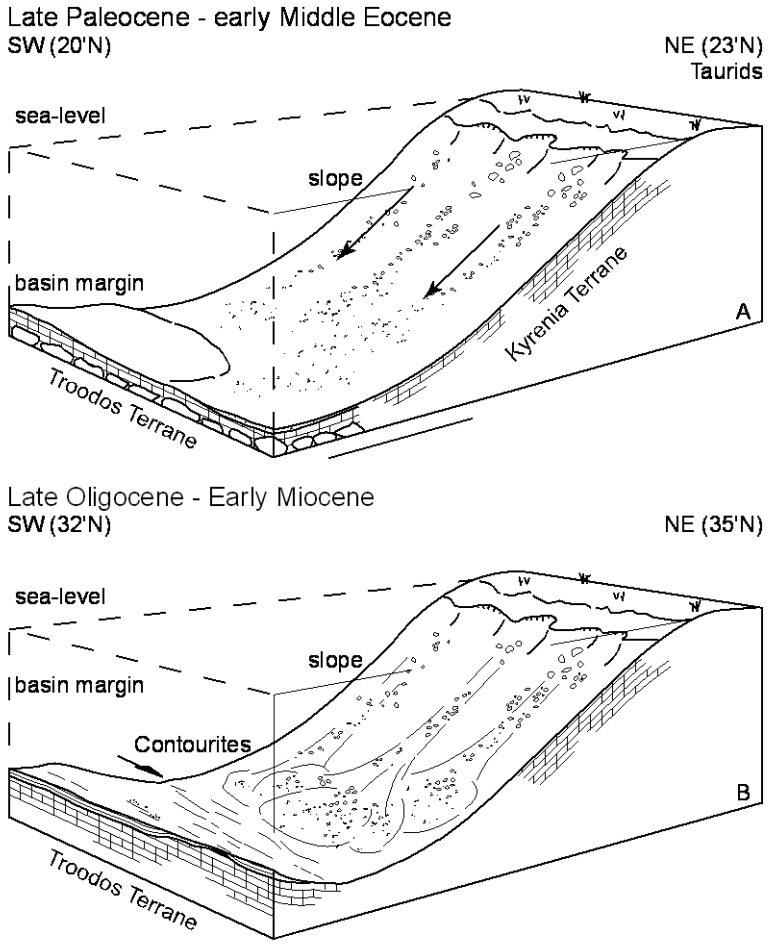

Figure 2-11: Palaeogeographical reconstruction of the local tectonic setting and depositional environments of the Lefkara Fomation. No precise scale is implied. The inferred palaeo-atitudes shown give an indication of the distance between the Taurid Range in the NE (Late Paleocene to early

Middle Eocene) and the uplifting Troodos terrane in the SE (Late Oligocene to Early Miocene) (Kähler and Stow, 1998)

Summary. The Maastrichtian to Late Oligocene/Early Miocene Lefkara Formation (Mantis, 1970), is a deep marine biogenic unit of c. 750 m thickness which represents approximately 50 Ma of dominantly foraminiferal and nannofossil chalks with subordinate radiolarian chert and secondary, bedded and nodular chert (BouDagher-Fadel and Lord, 2006).

Miocene carbonate and terrigenous (ophiolite-derived) sediments of the Pakhna formation

The Lefkara Formation is overlain by the Pakhna Formation. The age of the latest Lefkara and earliest Pakhna Formation sediments, and the nature of the boundary, varies depending on the tectonic setting of each individual basin and the deposition/preservation of sediments, i.e. Read (1993) dates the contact as latest Oligocene – earliest Miocene, and believes it to be conformable; elsewhere, most noteably in southern Cyprus, tectonically induced unconformities exist (Bagnall, 1960; Pantazis, 1967a,b; Eaton and Robertson, 1993). The Pakhna Formation reflects an abrupt change in sedimentation style from deep-water pelagic carbonates (Lefkara Formation) to shallower-water, pelagic and turbiditic carbonates and subordinate terrigenous (ophiolite-derived) sediments. Robertson (1998a) suggested that this change possibly corresponds to the onset of the present cycle of collision (see section 2.1.3): (i) deposition of the Lefkara Formation is believed to have abruptly terminated in response to Miocene uplift (Robertson, 1977), and; (ii) deposition of the Lefkara Formation occurred on a stable carbonate slope-apron or basin plain, whereas deposition of the Pakhna Formation occurred in localised tectonically controlled depressions (Eaton and Robertson, 1993).

A three-dimensional morphology and sedimentation history of the Pakhna Formation was identified by Eaton and Robertson (1993), based on (i) regional thickness variations, (ii) palaeocurrent data (Figure 2-12), (iii) slump orientations (Figure 2-12), and (iv) provenance studies. Four facies associations were recognised within the Pakhna Formation (Figure 2-12): the *basin-plain association*, the *basin-margin association*, the *gullied slope/channel-fill association* and the *peripheral sand association*.

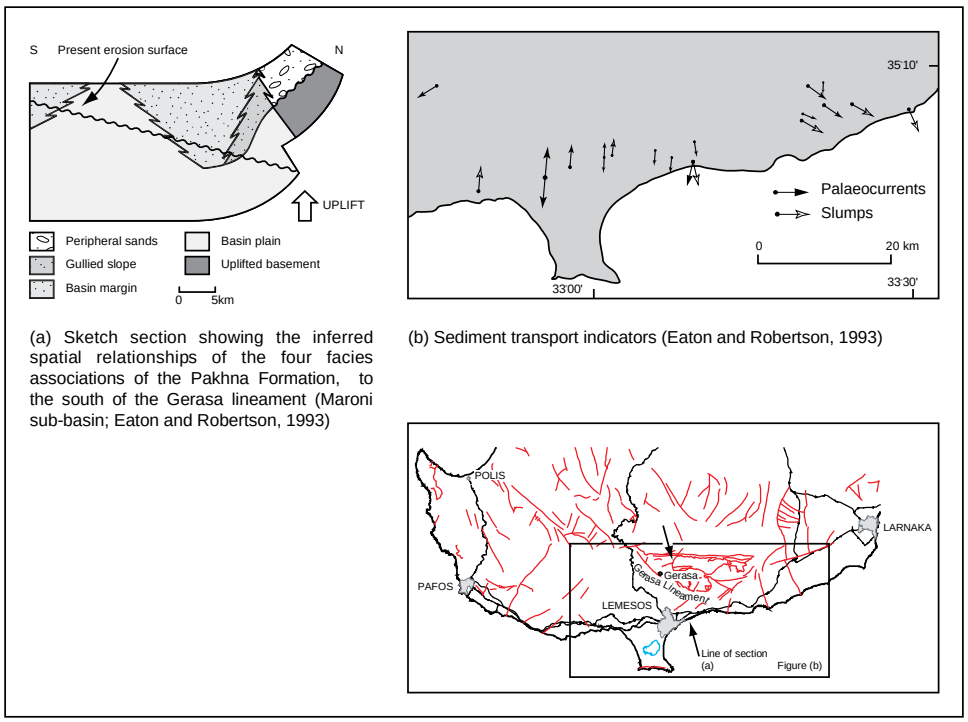

(a) Sketch section showing the inferred spatial relationships of the four facies associations of the Pakhna Formation, to the south of the Gerasa lineament (Maroni sub-basin; Eaton and Robertson, 1993)

(b) Sediment transport indicators (Eaton and Robertson, 1993)

Figure 2-12: (a) Sketch section showing the inferred spatial relationships of the four facies associations, to the south of the Gerasa lineament (Maroni-Psematismenos sub-basin; Eaton and Robertson, 1993). Note the shallowing-upward sequence and presence of margin facies, both to the north and south. Not to scale; (b) Sediment transport indicators (Eaton and Robertson, 1993)

A palaeographic reconstruction of each of the facies associations of the Pakhna Formation is shown in Figure 2-13. Deep-water, mainly hemipelagic sediments accumulated on the basin-plain. Deep water carbonate material was gravitationally reworked from marginal areas by turbidity currents and mass flow processes. Large volumes of mixed, ophiolite derived and bioclastic sediment were gravitionally transported into the basin within gullies and channels, as massive debris flows or turbities. Shallow-water bioclastic material, largely derived from patch reefs and benthic foraminiferal sands (Koronia Member, see below) in peripheral areas, situated along the southern flank of the ophiolitic terrane. Localised depocentres were created by tectonic movements at the beginning of the Miocene. The appearance of shallow-water-derived carbonate sediment a short distance above the base of the Pakhna Formation is attributed to tectonic uplift of marginal areas, both to the north and the south, giving rise, after transgression, to substantial areas of shallow-water carbonate production, including coral patch reefs (Koronia Member; see below).

In the absence of calcarenitic bands it is occasionally hard to distinguish between the upper Lefkara and lower Pakhna successions: typically, Pakhna Formation chalks contain more terrigenous material, are more intensely bioturbated, and contain more Troodos-derived

material than their Lefkara counterparts. In addition, Pakhna Formation chalk tends to be off-white in colouration, whereas Lefkara Formation chalk is white.

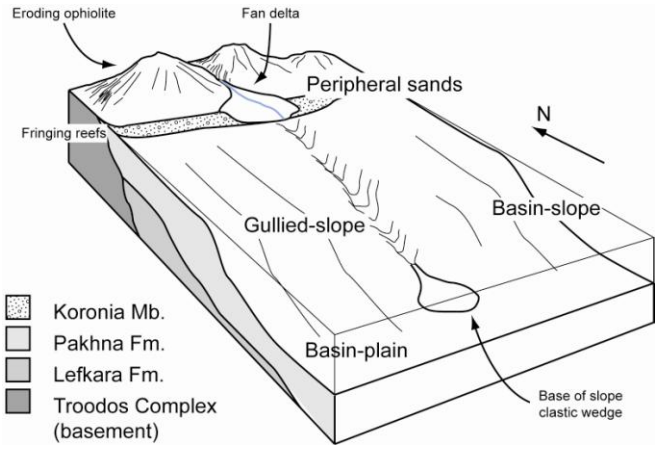

Figure 2-13: Simplified facies model for the Pakhna Formation. See text for detail (modified from Eaton and Robertson, 1993)

Summary. The Late Oligocene/Early Miocene to Tortonian Pakhna Formation is a hemipelagic unit of approximately 350-400 m thickness which represents approximately 16 Ma of mainly marl, chalk and calcarenite rich in planktonic foraminifera. It was deposited on a tectonically unstable shelf environment adjacent to the emerging Troodos island (BouDagher-Fadel and Lord, 2006).

Two phases of reef growth: the Aquitanian – Burdigalian Terra Member and the Tortonian Koronia Member

Two phases of reef growth are recognised within the Pakhna Formation: the Aquitanian-Burdigalian Terra Member and the Tortonian Koronia Member (Follows and Robertson, 1990; Follows, 1992). The Terra Member consists of diverse coral framestones, comprising faviids, domal poritids and secondary reef-dwelling corals. Its off-reef facies is comprised of benthonic foraminiferal packstones-grainstones (Follows et al., 1992). In contrast, the Koronia Member is a bindstone comprising monospecific, laminar poritid corals (Follows et al., 1992). Its off-reef facies comprises decimetre-thick beds of bioclastic reef detritus (Follows and Robertson, 1990; Follows, 1992).

There are differences between the first and second phases of reef development in primary reef construction, in regional distribution and in the level of background pelagic

sedimentation. The Terra Member reefs grew as upstanding patches under a relatively deep and calm sea, on isolated carbonate shelves (Follows, 1992). Local tectonic events and consequent sea-level fluctuations, possibly accentuated at times by global eustatic sea level movements, led to the Terra Member autochthonous shallow-water carbonate environment being repeatedly blanketed by pulses of reworked Oligocene chalk (Lefkara Formation; BouDagher-Fadel and Lord, 2006). In contrast, the Koronia Member grew in a shallower sea with varying turbulence, interspersed with oolite and bioclastic sands fringing a large, emergent land-mass. Regional tectonics had a limited influence on the evolution of the Terra Member reef phase; however, tectonics controlled reef location, clastic input and reef type during deposition of the later Koronia Member.

Messinian evaporites and lacustrine marls (Lago Mare sequence) of the Kalavasos Formation

Diatomaceous marls and microbial carbonates of the Pakhna Formation, (Krijgsman et al., 2002; Wade and Brown, 2005) are overlain by a variety of gypsum facies (Robertson et al., 1995b) and locally, in southern Cyprus, by lagoonal-lacustrine deposits and local palaeosols (Lago Mare sequence; Orszag-Sperber and Rouchy, 2000; Rouchy et al., 2001). This succession is termed the Kalavasos Formation. Three component lithostratigraphic units are recognised: the pre-evaporitic, the evaporitic and the post-evaporitic.

The pre-evaporitic unit is a transitional sequence between diatomateous chalks/marls and gypsum. This transitional interval, from cyclic carbonates to evaporites, is composed of indurated and finely laminated limestones which display features characteristic of microbial deposits, i.e. stromatolites. This interval can be correlated with similar units in other Mediterranean basins i.e. the Tripoli Formation on Sicily (Rouchy et al., 2001).

The evaporitic unit can be divided into several facies: (i) parallel-laminated gypsum (locally termed marmara); (ii) massive fine-grained gypsum (locally termed alabaster); (iii) banded-stacked selenite (defined by Follows, 1990); (iv) swallowtail selenite; and (v) botryoidal selenite (Robertson et al., 1995b). A simple facies model illustrating the inferred processes of primary gypsum deposition is shown in Figure 2-14.

The post-evaporitic unit, the Lago Mare succession, is a succession of marls, conglomerates, carbonates and palaeosols dated to the latest Messinian (Orszag-Sperber et al., 1989; Orszag-

Sperber and Rouchy, 2000; Rouchy et al., 2001). It is only locally preserved in southwest Cyprus at Pissouri village. The lower unit is comprised of marls, calcarenites and conglomerates. The upper unit is comprised of conglomerates, calcarenites and palaeosols. The palaeosols indicate that periods of subaerial exposure occurred in the Lago-Mare interval. The marls contain Ammonia beccarii and Cyprideis which are typical of brackish water environments (Rouchy et al., 2001).

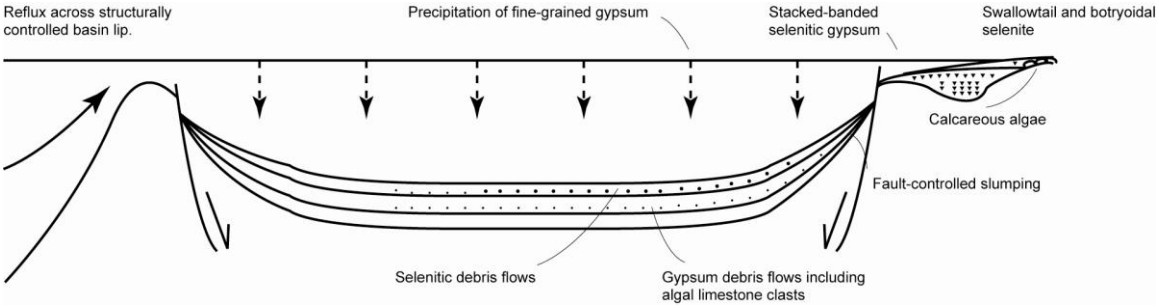

Figure 2-14: Simple facies model showing inferred processes of primary gypsum deposition in Cyprus, in which water depth plays an important role (Robertson et al., 1995b)

Summary. The restriction of the Mediterranean, during the Messinian salinity crisis, led to the deposition of gypsum and halite in small tectonically controlled sub-basins. Fine-grained gypsum (marmara and alabaster) precipitated in basinal areas, while *in situ* selenite (banded-stacked, swallowtail and botryoidal) formed in more marginal areas and within shallow lagoons. Reflooding of the 'evaporitic basins' led to a period dominated by brackish- and fresh-water environments, the 'Lago Mare'.

Pliocene marine marls of the Nicosia Formation (including bioclastic sandstones of the late Pliocene-early Pleistocene Athalassa Member (Athalassa Formation) and Pliocene deltaic and shoreline facies of the Kephales Member (Kakkaristra Formation))

The Kalavasos Formation is overlain by the Nicosia Formation. The Geological Survey Department of Cyprus recognise six members within the Nicosia Formation (Panayides et al., 2004): the Marine Marl Member, the Marine Littoral Member, the Lithic Sand Member, the Kephales Member, the Athalassa Member and the Aspropanboulos Member. The Marine Marl Member is the dominant unit, and is preserved throughout south and central Cyprus. The Marine Littoral and Lithic Sand Members occur at the top of the Pliocene succession.

The Aspropanboulos Member is only locally exposed. In the Mesaoria Basin, the Nicosia Formation has a maximum thickness of 900 m.

The Marine Marl Member (Nicosia Formation) consists of green-grey to dark-brown fossiliferous marl, silty marl, and small amounts of sandy marl. It displays an overall coarsening- and shallowing-upward trend from pure white micrites and marls to grey-brownish, fossiliferous marls and terrigenous (ophiolite-derived) siltstones. In more marginal areas, thin, discontinuous beds of coarser-grained sandstones and grits are noted. Macrofaunal and microfaunal assemblages suggest a shallowing-up from shelf (hundreds of metres) to shallow shelf (tens of metres) depth, from the base to the top of the Nicosia Formation. Macrofauna include bivalves and gastropods, and subordinate scaphopods, echinoderms, brachipods, annelids, arthropods and corals (McCallum and Robertson, 1995a). Microfauna include benthic foraminifera (e.g. Ammoniam, Cibicides, Elphidium and Patellina) and planktic foraminifera (e.g. Globigerina and Globorotalia) (McCallum and Robertson, 1995a). Plant debris is also locally abundant.

The Marine Littoral Member contains gravel, sand, and silt. It is typically cross-bedded and contains flat, rounded ‘beach’ pebbles and some oolitic sand.

The Lithic Sand Member is comprised of fine to coarse lithic sand and sandstone, derived dominantly from the Troodos ophiolite sequence. It includes subordinate horizons of marl and silty marl. It is gradational with the underlying Marine Marl Member.

The Kephales Member (Kakkaristra Formation) is comprised of deltaic, cross-stratified sandstones and conglomeratic lenses and shoreline, fine-grained, mud-free, well-sorted sandstones. Rare, localised subaerial facies of the Kephales Member are documented by McCallum and Robertson (1995a). The Kephales Member is a relatively thin unit (<15m) sandwiched between the shallow-marine facies of the upper part of the Nicosia Formation and the fluvial facies of the Apalos Formation (see below). A palaeographic reconstruction of each of the facies of the Kephales Member is shown in Figure 2-15

The Athalassa Member (Athalassa Formation) is comprised of Marine shallow-marine, cross-stratified, bioclastic rich, sandstones. McCallum and Robertson (1995b) identified three facies: (i) planar-stratified calcarenites, comprised of fine-grained, parallel-laminated calcarenites in thin, planar beds or lenses, (ii) cross-stratified calcarenites, comprised of fine

to locally medium-grained, tabular and trough cross-laminated calcarenites and medium- to coarse-grained, cross-bedded calcarenites, and (iii) fine-grained massive sandstones, comprised of very fine- to fine-grained, moderately sorted, slightly muddy, orange-yellow sandstones, which are poorly consolidated, generally structureless and thoroughly bioturbated.

The Aspropamboulos Member is comprised of fine-grained, crossbedded oolites. Its spatial distribution is restricted to a small area called 'Aspropamboulos', south of Laxia village.

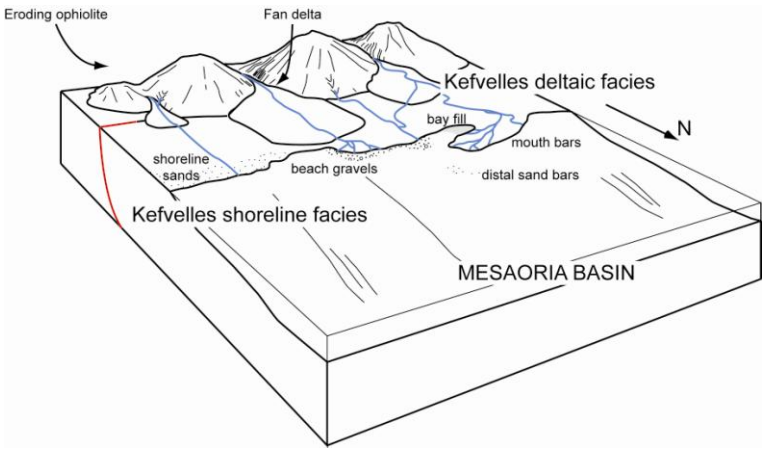

Figure 2-15: Palaeogeographical reconstruction of the local tectonic setting and depositional environments of the Kephales Member (Kakkaristra Formation). See text for detail (modified from McCallum and Robertson, 1995a)

McCallum and Robertson (1995a) interpreted Pliocene sedimentation in the Mesaoria basin to have been from a series of isolated fan-delta systems that built out from the uplifting Troodos Massif. The older fan-delta system, comprised of the Marine Marl, Marine Littoral and Lithic Sand Members (Nicosia Formation), was deposited when the Mesaoria Basin was actively subsiding (McCallum and Robertson, 1995a). It consisted of a number of small, isolated fan deltas which built across a narrow (< 5 km) largely submerged basin. In contrast, the younger fan-delta system of the Kephales Member (Kakkaristra Formation) was deposited when basin subsidence had virtually ceased and the Mesaoria seaway had filled to becomes a shallow, sandy platform. The renewed fan-delta sedimentation was initiated by uplift of the Troodos ophiolitic massif. In response to uplift, alluvial systems built northwards and coalesced at the coastline, giving rise to a large shelf fan delta that prograded into the basin. Athalassa Member (Athalassa Formation) carbonate sandbodies formed near the margin of the Kyrenia landmass and migrated southwards across a shallow marine platform (McCallum and Robertson, 1995b). Skeletal carbonate was formed in coastal areas

adjacent to the Mesaoria basins; this material was reworked offshore by storms. Minor tectonic activity and possibly eustatic transgression may have been responsible for triggering deposition of the Athalassa-type sediments.

Summary. The Nicosia Formation represents marine sedimentation, fluctuating between relatively deep water and shallower near-shore environments. The Kephales Member is a sequence of fan-delta deposits which include 'Gilbert-type' marine delta, bay and lagoonal facies, occurring on the southern side of he Mesaoria basin and consists of a series of siltstones, cross-bedded conglomerates and fine-grained sands with conglomeratic intercalations (Panayides et al., 2004). The Athalassa Member is made up of a series of fossiliferous medium to coarse-grained, cross-bedded calcarenites, interbedded with sandy fossiliferous marls (Panayides et al., 2004).

Please note that the Formation names and members used in this thesis are as defined by the Cyprus Geological Survey Department (Panayides et al., 2004) (Figure 2-9). The Cyprus Geological Survey Department recently revised the stratigraphic framework established in 1995 (1:250,000 geological map of Cyprus (Cyprus Geological Survey Department, 1995); compiled from stratigraphic data by Bellamy and Jukes-Brown (1905), Henson et al. (1949), Eaton (1987), Follows and Robertson (1990), McCallum and Robertson (1995a)). In the revised stratigraphy of Panayides et al. (2004): the Kakkaristra and Athalassa Formations are redefined as the Kephales and Athalassa Members of the Nicosia Formation. This follows re-mapping in the Greater Lefkosia (Nicosia) Area by Harrison et al. (2004b), which revealed that the 'Kakkaristra and Athalassa Formation' are overlain by the Nicosia Formation. The 'traditional' lithostratigraphic nomenclature as used by the Cyprus Geological Survey Department on their 1995 geological map of Cyprus, and as reviewed by McCallum and Robertson (1995a), is indicated in brackets after the new formational names.

Late Pliocene-early Pleistocene continental deposits of the Apalos Formation

The Nicosia Formation is overlain by the Apalos Formation. The Apalos Formation is comprised of stacked fluviatile deposits, consisting of rhymthically bedded units of gravels, flood deposits and palaeosols. Each stacked fluviate deposit has an internally distinctive, repeating sequence of channel gravels, red, oxidized, flood-plain sand and mud that are overprinted by soil horizons and caliche deposits. Each fan deposit has a different history.

The Apalos Formation has a variable thickness between 10 m and 60 m. It is only locally preserved in the Mesaoria Basin (Panayides et al., 2004).

Summary. The late Pliocene – early Pleistocene Apolos Formation is a succession of continental fluvial deposits and palaeosols. It is only preserved locally in the Mesaoria basin.

Late Pliocene-mid to late Pleistocene Fanglomerates and marine terrace deposits

The Pleistocene sedimentary succession includes both shallow marine and terrestrial deposits. A number of facies associations have been identified, including marine terraces (Poole et al., 1990; Poole and Robertson, 1991; 2000), fluvial terraces (McCallum, 1989; Poole, 1992; Poole and Robertson, 1998), soil horizons, havara and kafkalla (Schirmer, 1998; Stow et al., 1995). Havara is the local name given to tan to off-white, carbonaceous colluvial deposits of Quaternary age exposed throughout Cyprus. Kafkalla is the local name given to caliche, a layer of soil in which the particles are cemented together by lime.

Progressive uplift of the Troodos Massif and global eustatic sea-level change influenced Pleistocene sedimentation (Poole et al., 1990; Poole and Robertson, 1991; 2000). The locus of Pliocene-Recent uplift was concentrated on the Troodos Massif. Coarse clastic sediment was shed radially from the rising Troodos Massif (Figure 2-16). The main phase of Pleistocene uplift was marked by the deposition of the fluvial Fanglomerate Group (Poole and Robertson, 1991, 1998). The Fanglomerate Group consists mainly of conglomerates, with subordinate sand and silt. Its proximal facies are comprised of poorly sorted, weakly consolidated, immature, matrix-supported pebble-conglomerates. Its distal facies are represented by channelised units, overbank fines and palaeosols.

A series of raised marine terraces occur parallel to the present coastline. Poole and Robertson (1991) recognised and correlated five distinct marine terraces; the late Pliocene-early Quaternary - F0 terrace; the early-mid Quaternary – F1 and F2 terraces; and the late Quaternary F3 and F4 terraces. Fieldwork and aerial photography suggest that these terraces occur systemically along the south coast of Cyprus (Figure 2-16). Corals obtained from the latter terraces (F3 and F4) were dated with the uranium-series method (Poole et al., 1990); yielding ages of 185-192 ka and 116-130 ka respectively.

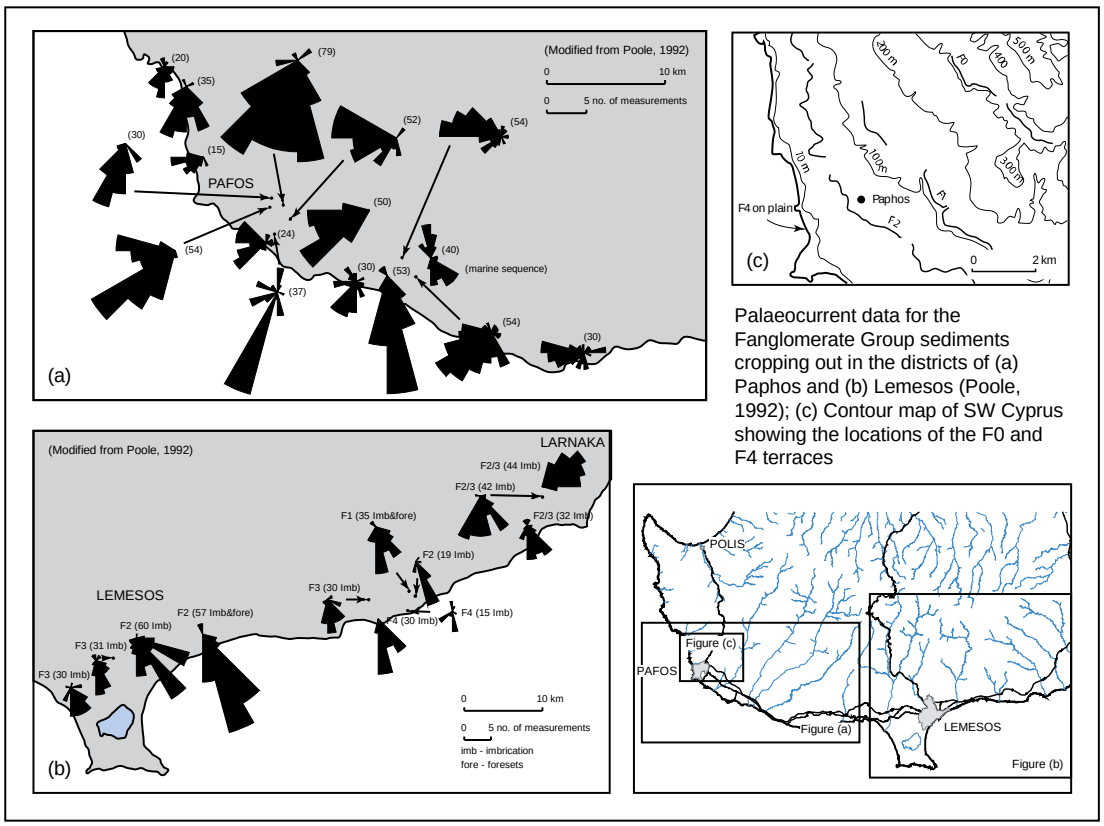

Palaeocurrent data for the Fanglomerate Group sediments cropping out in the districts of (a) Paphos and (b) Lemesos (Poole, 1992); (c) Contour map of SW Cyprus showing the locations of the F0 and F4 terraces

Figure 2-16: Palaeocurrent data for the Fanglomerate Group sediments cropping out in the districts of (a) Paphos and (b) Lemesos (Poole, 1992). Contour map of SW Cyprus showing the locations of the F0 to F4 terraces, and the occurrence of aeolinite (modified from Poole and Robertson, 1991)

Chapter 3: Structural development of the Maastrichtian to Recent Troodos cover sequence, Cyprus

3.1 Introduction

The main aim of this chapter is to systemically document structures that deform the Upper Cretaceous to Recent sedimentary cover, and in some places the ophiolite basement. The structures are interpreted in terms of local stresses, prior to considering them in a regional context. This chapter utilises a comprehensive set of fault data, combined with stratigraphic, geomorphologic and geochronological data obtained from each of the tectonically-controlled Neogene basins in southern, south-western and central Cyprus (Figure 3-1). In addition fault plane data were collected along the new highway between the towns of Lemesos and Paphos (Figure 3-2), where faulted Miocene-Recent sedimentary successions are superbly exposed.

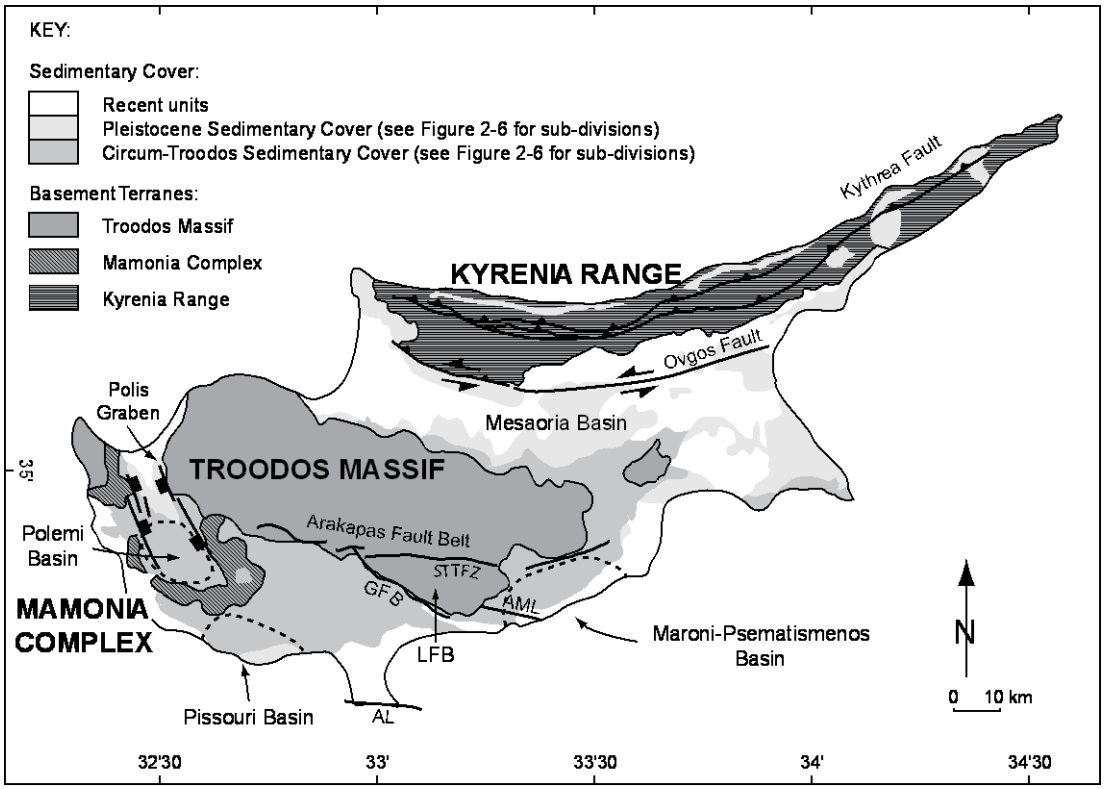

Figure 3-1: Simplified geological map of the island of Cyprus, indicating lower Cretaceous to lower Tertiary basement and the approximate location of the southern Neogene depositional basins.Abbreviations are as follow: AL = Akrotiri Lineament; AML = Agia Mavri Lineament; GFB = Gerasa Fault Belt (or alternatively, the Gerasa Lineament); STTFZ = South Troodos Transform Fault Zone

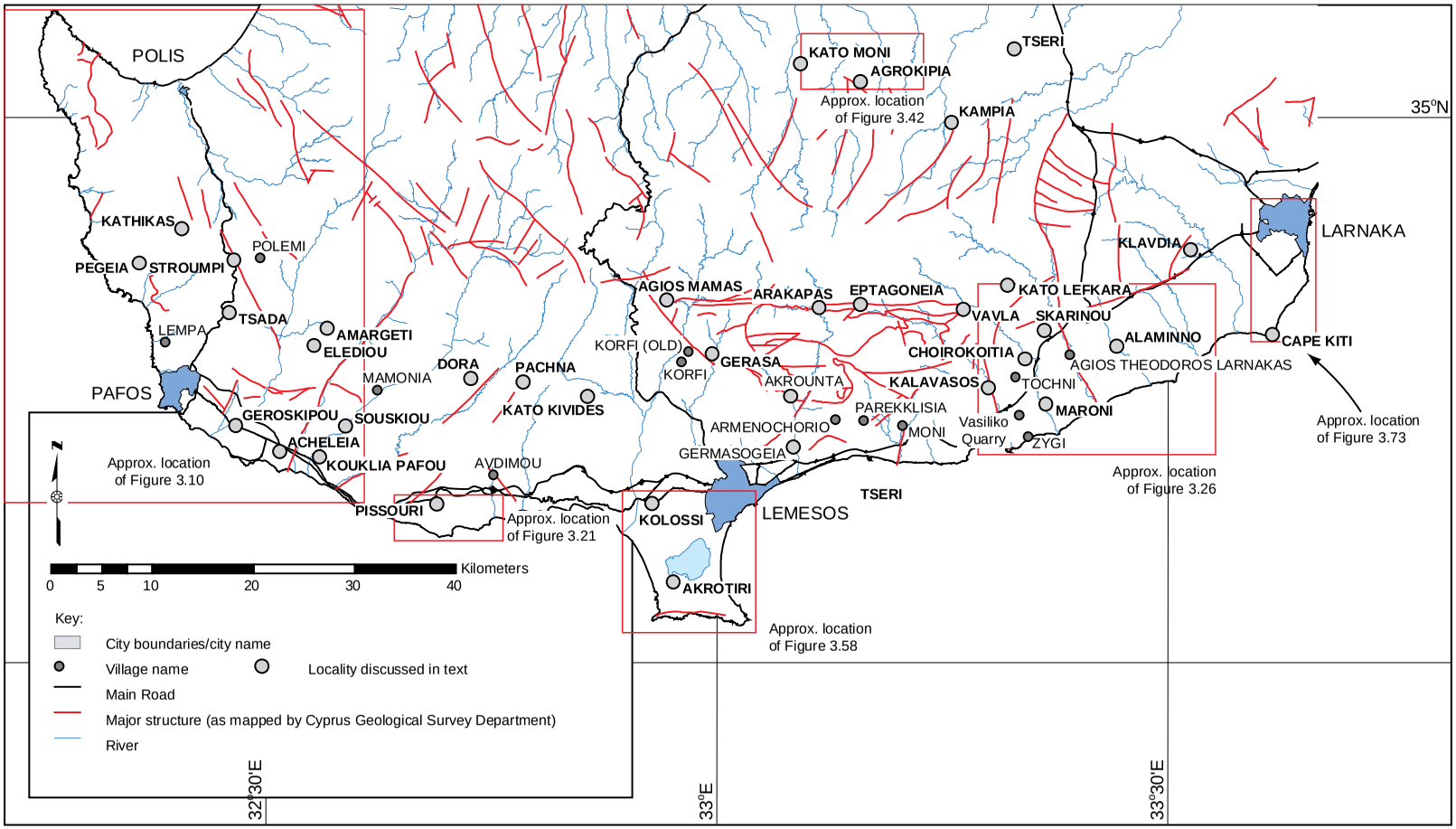

Figure 3-2: A map of south Cyprus, showing the location of the villages discussed in the text (created from GIS data supplied by the Cyprus Geological Survey Department). The approximate location of figures 3-10, 3-21, 3-26, 3-34, 3-42, 3-58 and 3-73 are shown

3.2 Methodology

It is recognised that identifying neotectonic fault patterns and dating their movements in south and central Cyprus is problematic: the best quantifiable fault data comes from Upper Cretaceous to Paleocene units; limited to relatively little quantifiable fault data comes from Miocene to Recent sediments (Figure 3-3). To overcome this problem the present study encompasses a range of disciplines, including geological mapping, structural analysis, detailed study of basin fills and geomorphology.

Commonly, faults may only be dated in terms of a maximum age provided by the age of the youngest affected stratigraphic unit. However, where fault-controlled sedimentological events have occurred the age of faulting may be better constrained. For example, faulting has controlled the distribution and orientation of channels throughout south Cyprus, including those within the Miocene Pakhna and Pliocene Nicosia Formations. A second example is that episodes of faulting in the Pliocene may be correlated with slumped units within the Nicosia Formation. Fault trends/kinematic indicators were measured at numerous sites throughout the Neogene basins. On fault planes in relatively hard sediments, such as the chalks of the Paleocene Lefkara Formation (see chapter 2), kinematic indicators are mainly offset marker horizons, sigmoidal gouge fabrics and drag folds (Figure 3-4). On fault planes in relatively soft sediments, such as the marls of the Pliocene Nicosia Formation (see chapter 2) kinematic indicators are mainly abrasive features (e.g. groove marks). Occasionally offset clasts were used in faulted conglomerates.

The sense of shear along faults was determined using offset stratigraphic markers, sigmoidal gouge fabrics and the orientation of drag folds (Figure 3-4). Many slickensided surfaces are accompanied by sharp, low steps that trend at right angles to the striations (Figure 3-4). The stepping direction of these rough surfaces can be used to determine the relative movement along the fault plane.

Figure 3-2: A map of south Cyprus, showing the location of the villages discussed in the text (created from GIS data supplied by the Cyprus Geological Survey Department). The approximate location of figures 3-10, 3-21, 3-26, 3-34, 3-42, 3-58 and 3-73 are shown

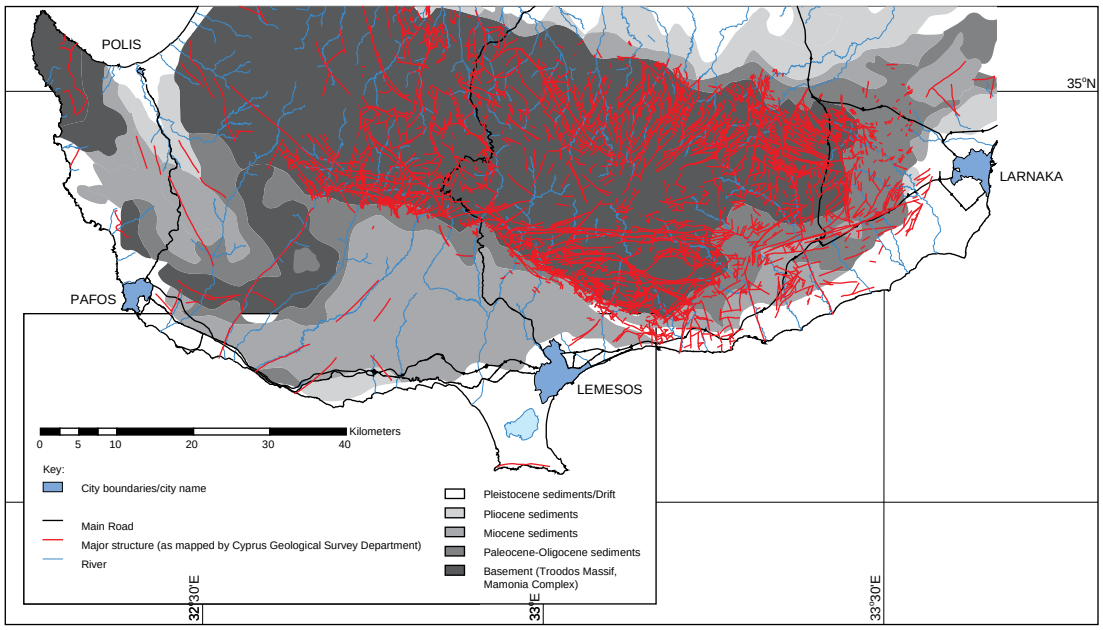

Figure 3-3: Outline map of south Cyprus. Main fault traces shown (data supplied by the Cyprus Geological Survey Department). Inset illustrates the distribution of Upper Cretaceous to Paleocene units (dark grey) and Miocene to Recent sediments (light grey).

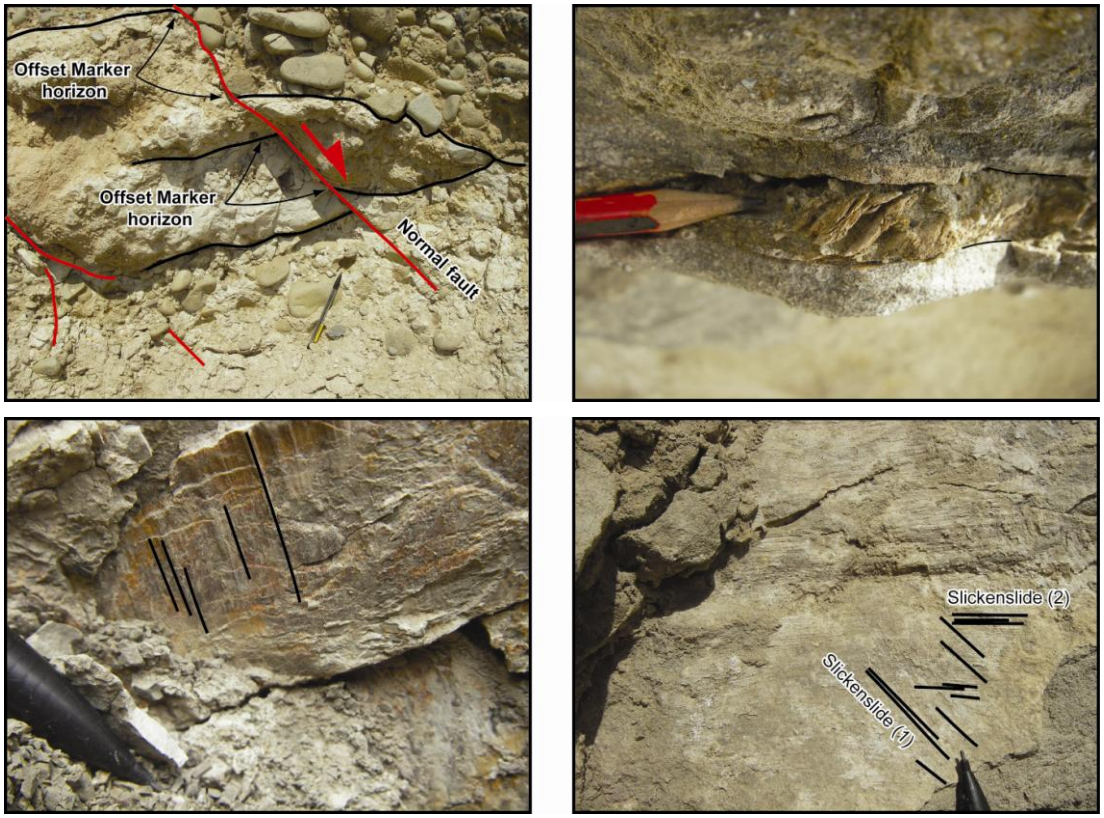

Figure 3-4: (top) Examples of kinematic indicators observed in the field: (left) prominent marker horizon offset by faults, the sense of offset indicators a normal offset; (b) sheared zone within sandstone, the fabric indicates a dextral offset; (bottom) Examples of slickenlines measured in the field: (left) fault plane with slickenlines orientated down dip, the 'stepped' profile of the fault plane allows one to assess the kinematics of the fault, in this instance normal; (right) fault plane with two

slickenlines, one indicating oblique movement (slickenline 1) and one indicating strike-slip movement (slickenline 2). In this example it is not possible to tell which slickenline overprints the other

Different generations of faults were discriminated based on several criteria: (i) cross-cutting relationships (chapter 3); (ii) the age of the oldest/youngest affected sediment (chapter 3); (iii) direct dating of individual faults using palaeomagnetic and luminescence methods (chapters 4 & 5) and; (iv) correlating sedimentological events in the hangingwall of the fault with movements along the fault (chapter 6). Many of the structures described in this chapter are believed to have reactivated. Reactivation is here defined as *the accommodation of geologically separable displacement events (intervals >1Ma) along pre-existing structures* (Holdsworth et al., 1997). Reactivated faults were identified based on: (i) discrepancies between kinematic indicators and modern/historic seismicity; (ii) offsets of geomorphological/anthropogenic features across ancient faults; (iii) changes in kinematic history indicated by overprinting structures; and (iv) repeated packages of fault talus, each deposit corresponding to movement on the fault. Where more than one episode of movement was recognised on a fault, several methods were employed to determine the relative age of the different events: (i) the slickensided surface was examined to determine if separate events were recorded by slickenlines (Figure 3-4); (ii) kinematic indicators (e.g. offset marker horizons, the orientation of drag folds and sigmoidal gouge fabrics) were compared with slickenline information to determine the last event to occur along the fault.

The fault data were mainly presented as great circle trends on lower hemisphere plots. The data are also presented as rose diagrams to highlight fault strike directions. Faults are assumed to be normal if the pitch of the slip indicator or rake (r) is $80° \leq r \leq 90°$ (pure dip-slip), as oblique-slip if $10° \leq r \leq 80°$, and as strike-slip if $r \leq 10°$. Faults are assumed to be reverse if the pitch of the slip indicator or rake (r) is $80° \leq r \leq 90°$ (pure reverse-slip), or oblique-slip if $10° \leq r \leq 80°$. Faults recording oblique-slip dominated by a dip-slip component are termed normal-sinistral or normal-dextral, whereas sinistral-normal or dextral-normal faults are dominated by a strike-slip component. In total 3,294 faults and 1,613 fractures were measured. Slip data were obtained from 1,413 faults.

The principal stresses responsible for the generation and subsequent deformation of each of the 'Neogene basins' were calculated using the dihedral protocol, initially described by Angelier and Mechler (1977). Fault kinematics were determined using the program Tectonicsfp v.1.6.2 of Franz Reiter and Peter Acs (a computer program for analysis of fault slip data). A sub-portion of data was analysed with the program GEOrient v.9 of Rob

Holcombe (a computer program for analysis of fault slip data); and the results of two programs cross-referenced. The two programs yielded similar results. Tectonicsfp was chosen as the program of choice, as its interface was found to be easier. The main assumptions in stress inversion procedures are that the fault population under study is the result of a single tectonic event governed by a single stress regime, that all faults move independently in response to the same mean stress tensor, and that faults slip in the direction of the slickenline on the fault plane (Gapais et al., 2000). However, in reality, measured fault populations are heterogeneous and result from the successive generation, reactivation, and rotation of faults throughout a deformation history. Pre-existing faults suffer the entire deformation history, whereas new faults may appear at any time during progressive deformation. Also, the spatial nonconformity of a stress field (e.g. transtensional /transpressional deformation) may contribute to the heterogeneity of measured fault populations (Gapais et al., 2000).

To counter these limitations, the fault data collected on Cyprus were segregated into subsets, and each was tested independently. The first subdivision was based on the age of the fault. Faults were segregated into different subsets based on cross-cutting relations, syn-depositional deformation and/or the age of the displaced rock unit. Meso-scale faults, which trend in a similar orientation to a basin-scale fault population were assigned to the age of that population. Temporal divisions include the Late Cretaceous (section 3.3.1), Early to Middle Miocene (section 3.3.2), Late Miocene to Middle Pliocene (section 3.3.3) and Late Pliocene to Recent (section 3.3.4). A second subdivision, based on the spatial variation in fault data, was created to test if the fault data had a dependence on area. The study area was divided geographically into several structural domains. Spatial divisions include the Polis Graben (section 3.3.3.1), the Pegeia region (section 3.3.3.1), the Pissouri Basin (section 3.3.3.3), the Maroni-Psematismenos Basin (section 3.3.3.4) and the Mesaoria Basin (section 3.3.3.6). The third division, based on fault-scale, was created to test if fault orientations/kinematics had dependence on scale. The data were divided into first- (basin-scale), second- and third-(minor) order faults. An arbitrary weighting ratio of 3:2:1 was applied to first-, second- and third-order faults, respectively. Weighting had minimal affect on the stress inversion results.

3.3 Structural framework of Cyprus

3.3.1 Late Cretaceous structures

3.3.1.1 The South Troodos Transform Fault

The Troodos ophiolitic massif is bounded to the south by the Arakapas fault belt (Figure 2-7; Figure 3-1). This major, east-west trending fault zone is comprised of an extensively sheared and brecciated basement of ophiolitic rocks, cut by elongate east-west trending slivers of sheared serpentinite. It represents the remnants of a Late Cretaceous oceanic transform fault (Moores and Vine, 1971). To the south of the fault belt lies the ophiolitic crust and mantle of the Limassol Forest Complex (Figure 3-1). The Limassol Forest Complex is comprised of strongly deformed, mantle rocks, generated within a transform fault zone (Simonian and Gass, 1978; Murton and Gass, 1986). It has been divided into two major parts: in the north and the far south, pillowed and massive lavas overlie an E-W trending sheeted dyke complex, which roots into massive gabbros; and in the centre, a layered sequence of mafic and ultramafic cumulates.

The term 'South Troodos Transform Fault Zone (STTFZ)' was proposed by Macleod (1988) to describe the Arakapas Fault Belt, and the part of the Limassol Forest Complex which formed within the transform zone. Palaeomagnetic evidence (Morris et al., 1990; Morris, 2003a) and structural data (MacLeod and Murton, 1993), suggest that deformation along the transform was right-lateral.

The STTFZ can be traced into southwest Cyprus as far as Kannaviou village (Figure 3-2; Robertson and Xenophontos, 1993). Beyond this, no link can be proved, as ophiolitic units in the Mamonia Complex are separated from the Troodos ophiolite by several arcuate structural lineaments. However, the studies of Swarbrick (1980) and Malpas et al. (1992) have shown that ophiolitic slivers in the Mamonia complex include lithologies that are similar to those within the STTFZ. It is, therefore, likely that these lineaments represent the former westward continuation of the STTFZ into SW Cyprus.

3.3.1.2 Mamonia Complex Fault Zone

In SW Cyprus, the Troodos Complex is juxtaposed against the older Mamonia Complex (see chapter 2) along a series of serpentinite-filled fault zones that define the Mamonia Complex

Suture Zone (MCSZ). Bailey et al. (2000; and references therein) identified two arcuate fault zones within the MCSZ. The southerly suture passes through the villages of Loutra tis Aphroditis, Mavrokolymbos, Marathounta, Agia Varvara and Phasoula (Figure 3-5). The northern suture delineates the south-western edge of the main Troodos Complex and can be traced through the villages of Kannaviou and Galataria (Figure 3-5).

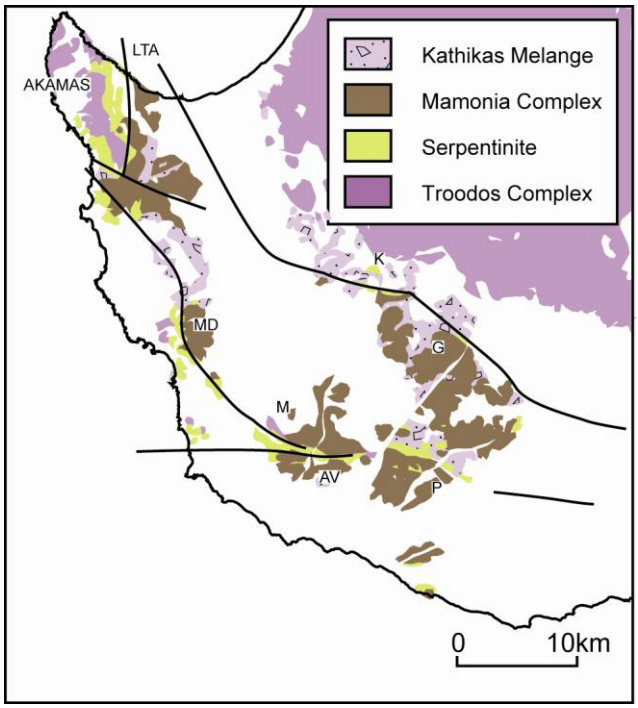

Figure 3-5: Geological map of SW Cyprus (modified from Bailey et al., 2000; geological data supplied by the Cyprus Geological Survey Department). The Mamonia Complex suture zone is defined by two main, serpentinite-filled fault zones, which are shown as black dashed lines. Localities referred to in the text are Galataria (G), Kannaviou (K), Loutra tis Aproditis (LTA), Mavrokolymbos Dam (MD), Marathounta (M), Agia Varvara (AV) and Phasoula (P).

The southern region of the MCSZ is characterised by E-W-striking, predominately sub-vertical, serpentinite-filled faults that separate a central silver of Troodos ophiolitic rocks from Mamonia Complex rocks to the north and south. The northern region of the MCSZ is characterised by N-S-striking, massive and variably serpentinized peridotite (predominantly harzburgite) bodies, which separate the Mamonia Complex in the east from Troodos ophiolitic rocks in the west.

3.3.2 Early – middle Miocene structures

Discrete WNW-ESE trending compressional lineaments are located in south and central Cyprus (Figure 3-1). These lineaments were initiated during the Early Miocene, as a response to a change in the regional stress regime, a result of a shift in the north-south convergence of the African and Anatolian plates. The lineaments ceased to be active by the Middle Miocene. The lineaments include: (i) the Gerasa lineament (or alternatively the Gerasa Fold and Thrust Belt of Morel, 1960); (ii) the Agia Mavri lineament (Eaton, 1987); (iii) the Akrotiri lineament (the Akrotiri high of Eaton, 1987) and (iv) the Petrounda lineament (McCallum, 1989).

3.3.2.1 The Gerasa Lineament

The Gerasa lineament, in south-central Cyprus, is a WNW-ESE-trending zone of thrusts and folds, which runs between Agios Mamas village in the west-northwest and Moni village in the east-southeast. The Germasogeia-Agios Mamas-Eptagoneia region, including the Gerasa Lineament and the South Troodos Transform Fault Zone, was mapped extensively by the Cyprus Geological Survey Department (Figure 3-6).

In the northwest, the Gerasa lineament is marked by southward thrusting and folding of the southern margin of the Limassol Forest ophiolite over the Lefkara Formation to the south. In the southeast, it is defined by large, tight upright folds, which could have formed above blind thrusts. The deformation is confined to a narrow lineament, c.30km long by 2km wide, adjacent to the southern margin of the Limassol Forest ophiolite. The lineament is thought to reflect the reactivation of an Upper Cretaceous zone of weakness. At Akrounta/Germasogeia Dam, ophiolite-gabbros overthrust ophiolitic pillow lavas/pillow breccias intercalated with inter-pillow sediments, pillow lavas overthrust bentonitic clays of the Upper Cretaceous Moni Melange, and bentonitic clays of the Moni Melange overthrust Paleocene to Oligocene chalks of the Lefkara Formation (Figure 3-7). Thrust planes dip north-northeast at 30º to 45º (Figure 3-8).

The lineament ceased to be active by the late Miocene (Tortonian), as evidenced by transgressive bioclastic limestones of the Koronia Member of the Pakhna Formation which unconformably overlie Troodos ophiolite pillow lavas, near Parekklisia village, the Moni Melange, near Armenochori village, and conformably overlie marls and calcarenite of the

Pakhna Formation, near Germasogeia Dam (Eaton and Robertson, 1993; Figure 3-7). The Koronia Member is not deformed by compressional faults.

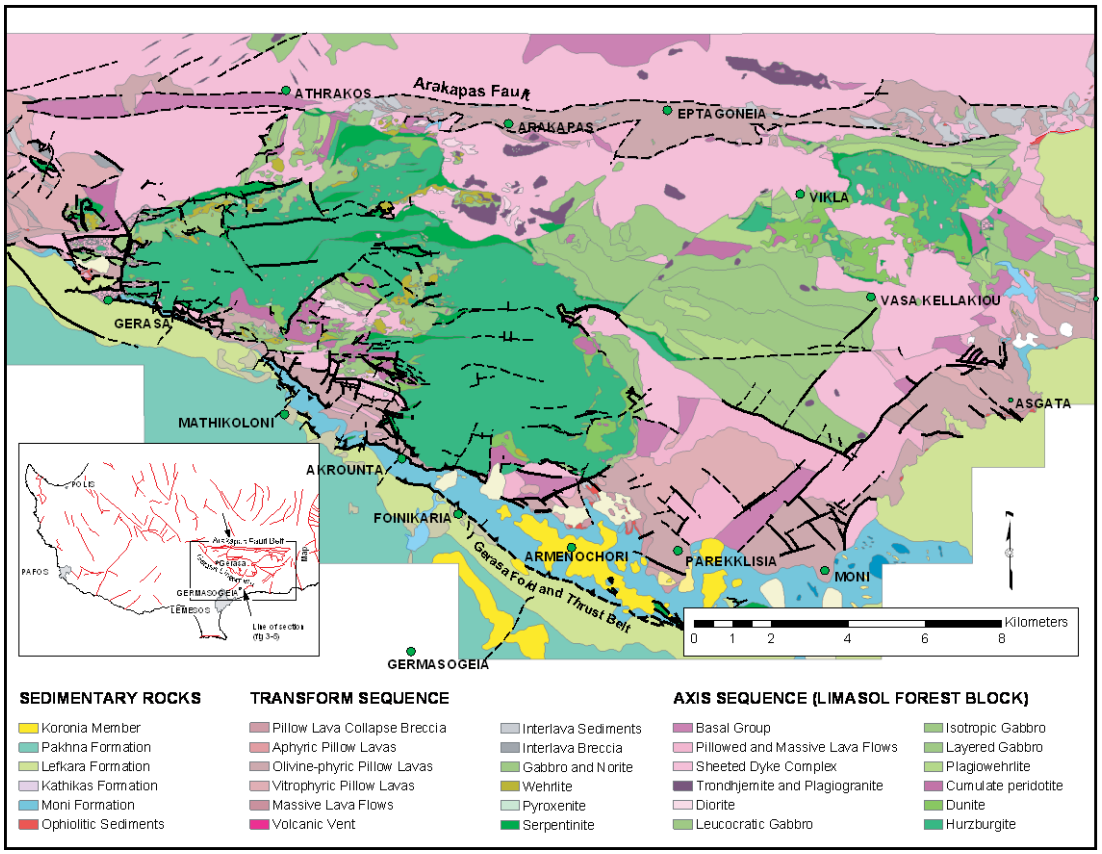

Figure 3-6: Geological map of the Germasogeia-Agios Mamas-Eptagoneia region. The map is compiled from GIS data supplied by the Cyprus Geological Survey Department. Line of cross-section shown

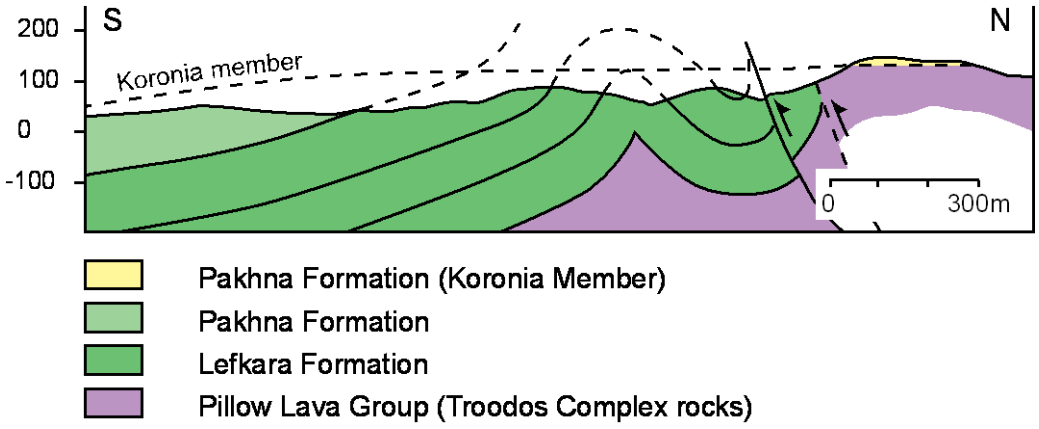

Figure 3-7: Simplified geological cross-section through the Gerasa lineament, which emphasises the structures discussed in the text (Eaton and Robertson, 1993). The location of the cross-section is shown in Figure 3-6

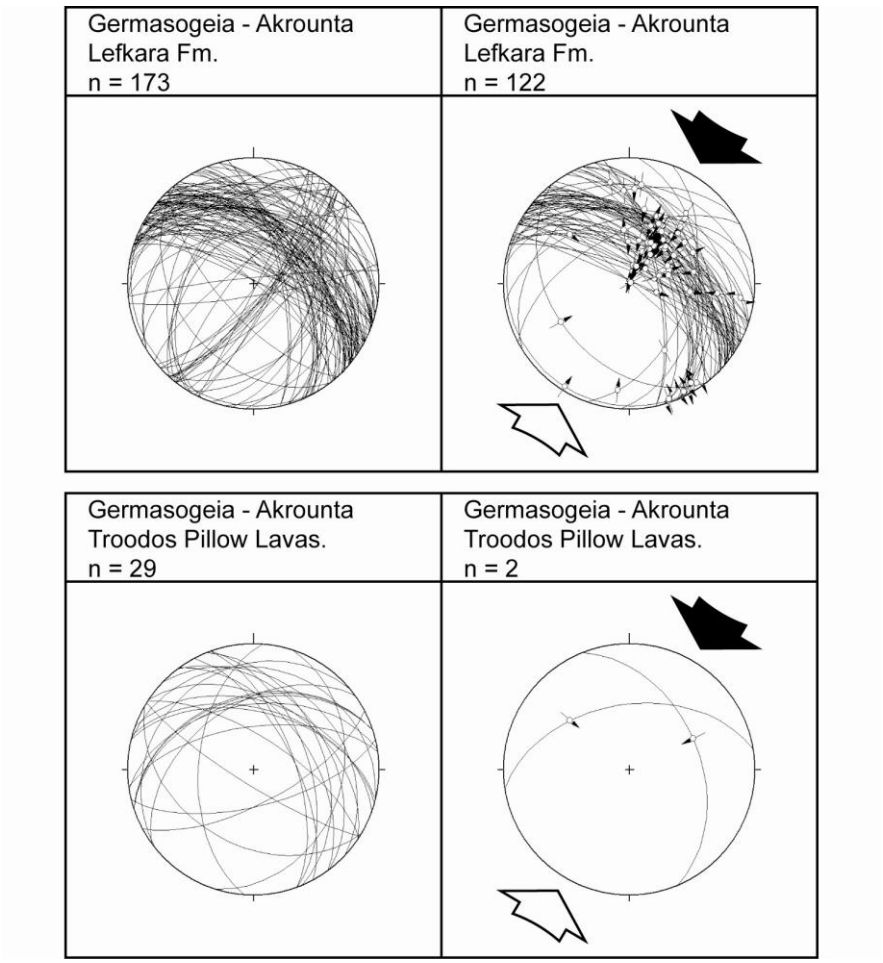

Figure 3-8: Top-to-the-SW thrusting in Troodos Pillow Lavas (Troodos ophiolite complex) and chalk of the Lefkara Formation; related to NW-SE compression along the Gerasa lineament. The lefthand column shows the orientation and dip of all measured faults; the righthand column shows the orientation and dip of measured faults with slickenlines. The great circles indicate the orientation and dip of the measured fault planes; the small arrows indicate the plunge and trend of the measured slickenlines; and the large arrows indicate the mean direction of thrusting

3.3.2.2 The Agia Mavri Lineament

The Agia Mavri Lineament, in south central Cyprus, is a WNW-ESE-trending belt of faulted and folded Paleocene – Miocene strata (Robertson et al., 1991). It runs between Agia Mavri village in the west-northwest and Mari village in the east-southeast (Figure 3-1). It is recognised mainly on the basis of numerous faults that cut the Lefkara and Pakhna Formations (Robertson et al., 1991). Near the faults that delineate the lineament, the middle Lefkara Formation contains conglomerates and clast-supported boulders. The conglomerates were presumably shed off an active submarine fault scrap. Near Mari village, the Pakhna Formation and overlying Messinian selenitic gypsum are disrupted, faulted, and folded into a

meso-scopic open syncline, striking WNW-ESE that plunges southeast-wards (Robertson et al., 1991). This suggests that the lineament was still active during the Messinian. There has been no movement along this lineament in the Plio-Quaternary (McCallum et al., 1993). Thus, the lineament was active during both the mid-Tertiary and Miocene.

3.3.2.3 The Akrotiri Lineament

A third lineament, the E-W-trending Akrotiri fault, is inferred to run through the southern tip of the Akrotiri Peninsula into offshore areas (Bear and Morel, 1960; Figure 3-1). Hydro-geological borehole studies indicate a juxtaposition of Triassic, Palaeozoic and Plio-Pleistocene units (Hadjistavrinou and Constantinou, 1977; Robertson et al. 1991). Coastal exposures, at the south coast of the Akrotiri Peninsula, include folded Triassic radiolarian cherts, overlain by Pliocene bioclastic carbonates and marls (Bear and Morel, 1960). Shallow seismic profiles reveal that the lineament can be traced offshore, as a broadly folded belt of Miocene strata. Post-Messinian, Plio-Pleistocene deposits are not affected, indicating that deformation had occurred previously (McCallum et al., 1993).

3.3.2.4 The Petrounda lineament

The Petrounda lineament, in south-eastern Cyprus, is a WNW-ESE-trending belt of folded and slumped Pakhna Formation strata that runs between Agios Theodoros Lemesou village in the west-northwest and Petrounda Point in the east-southeast (Robertson et al., 1991). Marked folding is visible in adjacent shallow seismic profiles (McCallum et al., 1993).

3.3.3 Early Miocene – Pliocene structures

Discrete NW-SE/NNW-SSE (southwest Cyprus), SW-NE (south-central Cyprus) and WNW-ESE (central Cyprus) trending extensional basins (Figure 3-1) formed during the Early to Middle Miocene.

3.3.3.1 The ‘Polis Graben’

The Polis Graben is a NW-SE/NNW-SSE-trending extensional depocentre located in west Cyprus (Figure 3-2). The graben is bounded to the east and west by major normal faults (Figure 3-9).

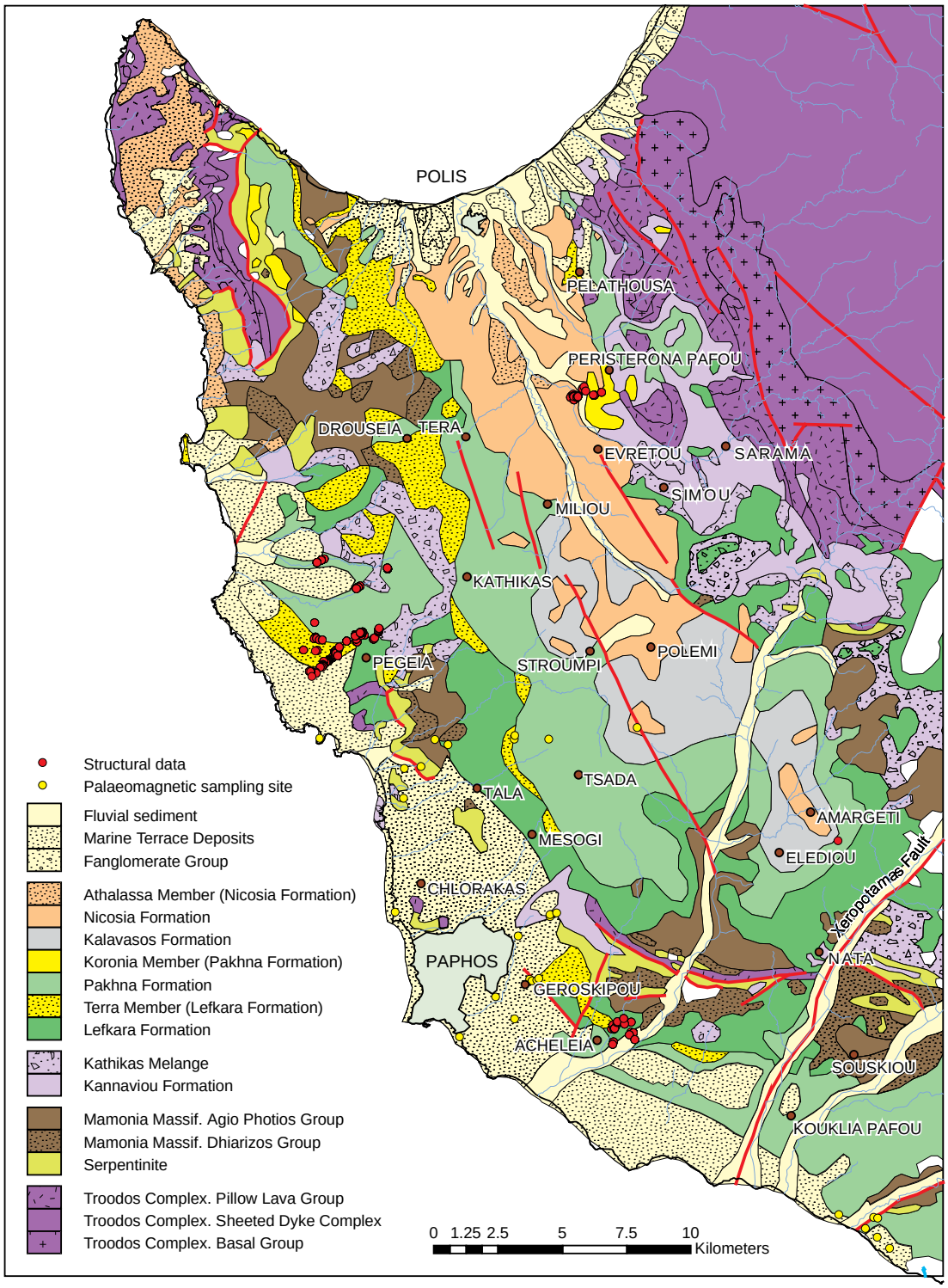

Figure 3-9: Geological map of the Polis Graben. The map was compiled from GIS data supplied by the Cyprus Geological Survey Department. The location of Figure 3-9 is shown in Figure 3-2

To the east the faults juxtapose basement rocks of the Troodos ophiolite against Lefkara/Pakhna Formation chalk, and to the west and south basement rocks of the Mamonia Complex against Lefkara/Pakhna Formation chalk (Figure 3-9). The basin is partly filled by

well-dated latest Cretaceous to Quaternary marine to non-marine sediments. 'Syn-rift' sediments include localised Late Miocene reef limestones (Follows et al., 1996), evaporites (Orszag-Sperber et al., 1989; Robertson et al., 1995b), Pliocene marginal to shallow-marine deposits (Payne and Robertson, 1995) and Quaternary non-marine to coastal deposits (Poole and Robertson, 1991; 1998; 2000). The 'Polemi Basin' (33°33'E, 35°00'N) is situated within the Polis Graben; it refers to the basin configuration immediately prior to, and during the Messinian (Wade and Brown, 2006; Figure 3-1).

Extensional faults are observed in the graben at a variety of scales; Payne (1995) defined four groups of faults/fractures within the Polis Graben, based on trend, displacement and magnitude: i.e. first-order (basin-bounding) faults, second-order faults, third-order (or minor) faults and extensional fractures.

First-order (basin-bounding) faults: First-order faults are those which bound the Polis Graben to the northeast and southwest, and cut Miocene and older strata. The northeast flank of the Polis Graben is characterised by a number of sub-parallel normal faults dipping at 50-60º towards the centre of the graben (Figure 3-9; Figure 3-10; Payne and Robertson, 1995). Payne and Robertson (1995) estimate vertical displacements of ~ 30-40 m. In contrast, the west flank is characterised by a single major normal fault dipping to the NE, with a vertical displacement of 50-100 m (Figure 3-9; Payne and Robertson, 1995). In addition, Payne (1995) identified several smaller NE- and SW- dipping (50-60º) normal faults in the axis of the Graben (Figure 3-9; Figure 3-10). Where exposed, basin-bounding faults can be traced vertically for up to c. 50 m. All faults show linear traces at outcrop, with no significant curvature. The cross-section in Figure 3-10 illustrates that these major faults bound kilometre-scale, back- and forward-rotated blocks. Bedding within the tilted first-order fault blocks is at an angle of 5º to 15º (Payne, 1995).

First order faults are only locally exposed but are otherwise inferred, based on: (i) an offset in stratigraphic units, (ii) a change in the regional dip/strike of beds, (iii) breaks in topography and (iv) vegetation contrasts. In general, two main trends in the strike of faults may be recognised: (i) a NNW-SSE (to NW-SE) trend, parallel or near parallel to the basin margin; and (ii) s NE-SW trend, orthogonal to the basin margin.

Second- and third-order (minor) faults: Second-order faults are those which bound small fault blocks on the margins of the graben, and within the graben axis. The west flank of the

Polis Graben is characterised by a number of sub-parallel normal faults, which bound small rotated blocks (Payne and Robertson, 1995). Fault dips are in the range of 50-70º. Bedding within the tilted blocks is at an angle of ~ 30º. Payne and Robertson (1995) estimate vertical displacements of ~ 10-50 m. Third-order faults dissect second-order fault blocks into smaller segments. Third-order faults typically occur at a spacing of a few metres, and have displacements of a few centimetres. Both sets of faults are orientated sub-parallel to the major bounding faults; no cross-cutting relationships are seen. Both sets of faults exhibit linear traces at outcrop (i.e. no evidence of significant curvature). In general, three main trends in the strike of faults are recognised: (i) a NNW-SSE trend, parallel or near parallel to the basin margin; (ii) a WNW-ESE trend, oblique to the basin margin; and (iii) a NE-SW trend, orthogonal to the basin margin.

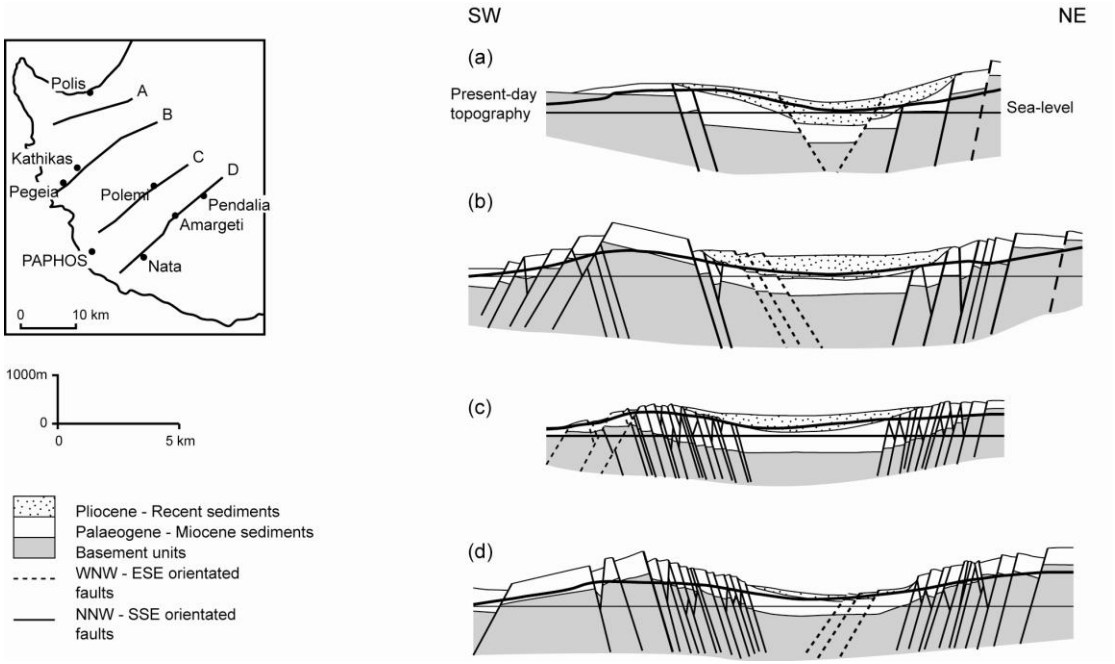

Figure 3-10: Structural cross-sections through the Polis Graben (Payne, 1995; Payne and Robertson, 1995; 2000). Thick lines denote first-order faults (dashed = inferred) and thin lines denote second-order faults. Section above present-day erosion level is the inferred original thickness of sediments (NB: basement level is arbitrary). Inset shows the location of the Polis Graben, the locations of the cross-sections and several villages discussed in the text below.

Extensional fractures: Extensional fractures are distributed throughout the Polis Graben. Two styles of joint patterns are observed: (i) single, parallel joints; and (ii) conjugate, intersecting joints. Jointing is particularly abundant in regions where there has been pervasive second- and third- order faulting. Lithological contrasts between hard and soft layers commonly affect the outcrop of joints. This probably reflects a combination of

different responses to stress in different lithologies, and poor preservation of fracture planes in the softer, more easily weathered beds.

In the following section, new structural data are presented for the Polis Graben. This data was collected to provide a framework on which to test existing models of basin development (Payne, 1995; Payne and Robertson, 1995, 2000) and facilitate comparisons between the Neogene basins. The new data are grouped by either age (of the affected rock) and/or location.

Paleocene chalks (Lefkara Formation): Paleocene chalks are cut by second- and third-order faults on both flanks, and in the axis of the Graben. Meso-structural data was collected from second- and third-order faults at two localities: (a) to the south of Kathikas village and (b) along a NW-SE transect between the villages of Mesogi, Tsada and Stroumpi (Figure 3-2; Figure 3-11a). Faults cutting Paleocene strata strike at a preferred orientation of N320-N000 (NNW-SSE to N-S), and dip to both the ENE and WSW. NNW-SSE-striking faults are observed to offset strata in a normal sense; where present, slickenlines indicate that this displacement is dip-slip to slightly oblique-slip.

Miocene chalks (Pakhna Formation): Miocene chalks are cut by second- and third-order faults on both flanks, and in the axis of the Graben. Meso-structural data was collected from third-order faults at two localities: (a) to the south of Kathikas village and (b) at Evretou Dam (Figure 3-2; Figure 3-11b; Figure 3-12). Three populations of faults where observed: (i) N340-N000- (NNW-SSE/N-S) striking, ENE- and WSW-dipping faults (Kathikas/Evretou Dam); (ii) N300-N270- (WNW-ESE/E-W) striking, SSW-dipping faults (Evretou Dam); and (iii) N040-N000- (NNE-SSW/N-S) striking, sub-vertical faults (Evretou Dam). The NNW-SSE- and WNW-ESE- striking fault sets offset strata in a normal sense (e.g. offset stratigraphic markers, drag folds); where present, slickenlines indicate that this displacement is dip-slip to slightly oblique-slip. The NNE-SSW-striking set of faults offset strata in a sinistral sense (e.g. offset stratigraphic markers, drag folds).

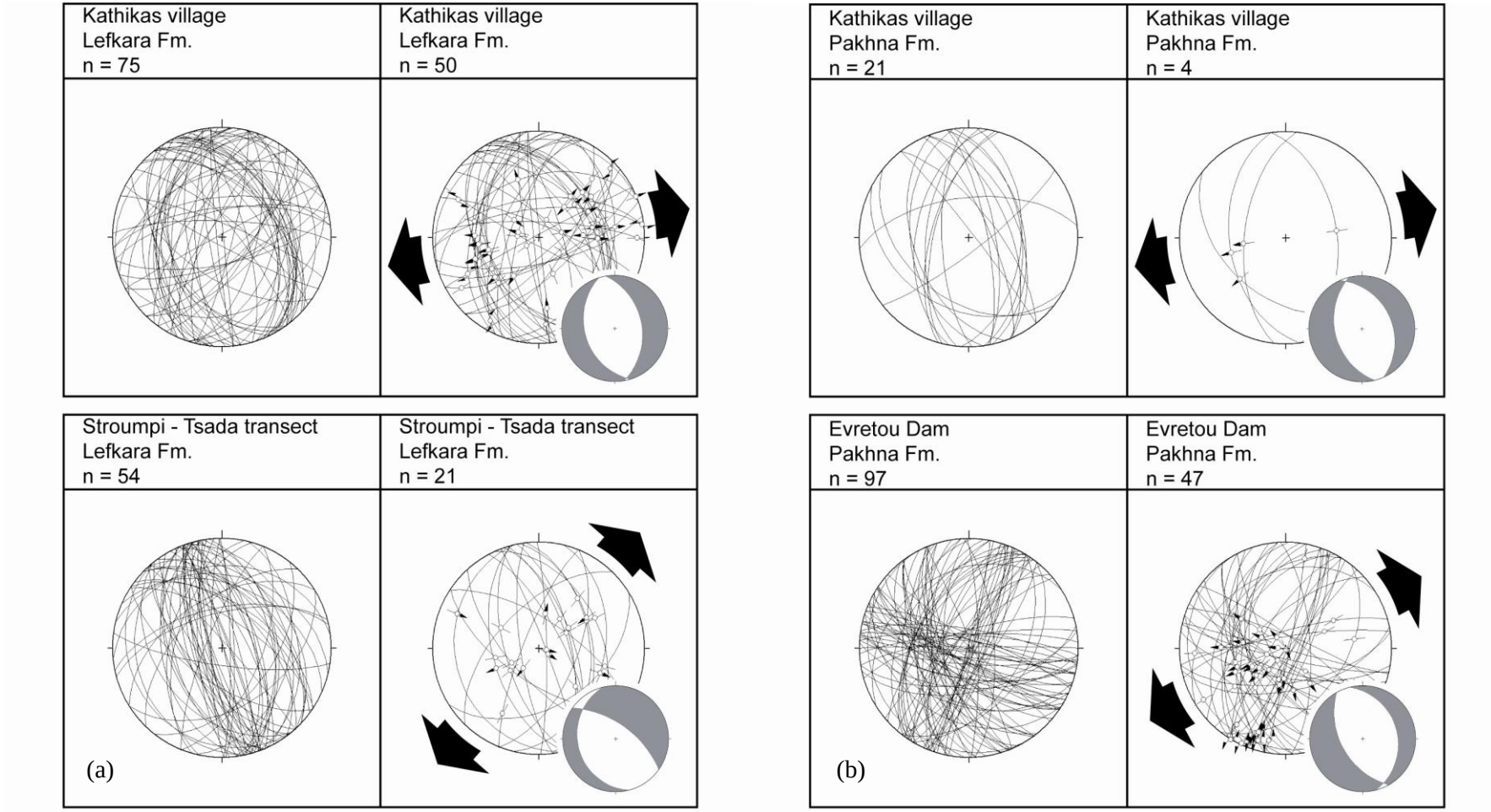

Figure 3-11: Faults affecting (a) Paleocene strata and (b) Miocene strata in the Polis Graben categorised by location. Lefthand column = all measured fault planes, righthand column = measured fault planes with slickenlines, great circle = orientation and dip of fault plane, small arrow = plunge and trend of slickenline and large arrow = mean direction of extension. The fault slip data collected at Evertou Dam is divided into normal and strike-slip sub- sets in Figure 3-12

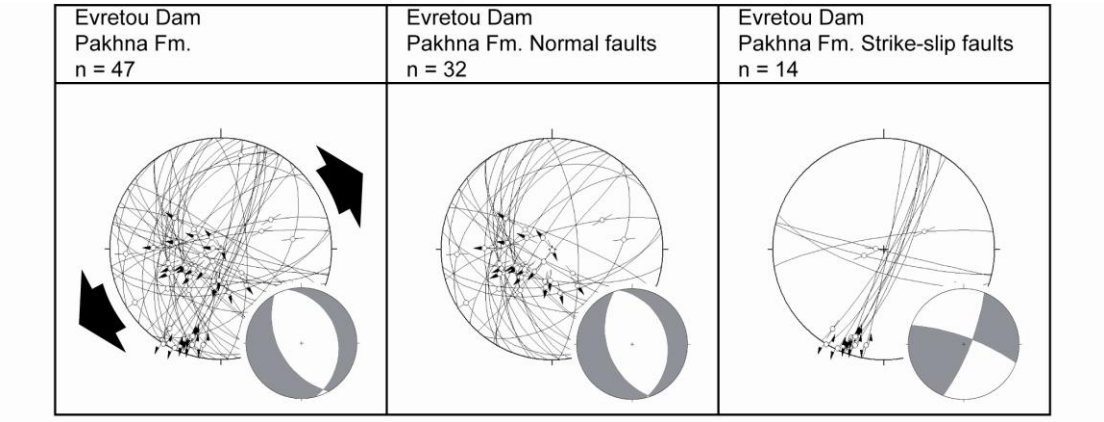

Figure 3-12: Fault data obtained from structures affecting Miocene-age strata in the Evretou Dam area (northern margin of the Polis Basin).

At Evretou Dam, the intersections of the NNW-SSE and NNE-SSW faults are marked by large amplitude (tens of metres) folds.

Late Miocene (Messinian) evaporites (Kalavasos Formation): Messinian evaporites are not commonly faulted within the Polis Graben. In this study, structural data were only collected from one locality, at Elediou village (Figure 3-2; Figure 3-13). Here, faults strike at a preferred orientation of N020-N040 (NNE-SSW to NE-SW) and dip to the WNW and ESE (Figure 3-13). No slip data were obtained.

Pliocene sediments (Nicosia Formation): Pliocene chalks are not commonly faulted within the Polis Graben. In this study, structural data were only collected from one locality, at Amargeti village (Figure 3-9; Figure 3-13). Faults strike at a preferred orientation of N280-N300 (WNW-ESE) and dip to the NNE and SSW. Faults dipping to SSW are more prevalent. No slip data were obtained. The independent study of Payne (1995) documents normal dip-slip faults affecting Pliocene strata at the villages of Miliou, Skoulli and Pelathousa (Figure 3-9; Figure 3-13). It is important to note that the NNW-SSE-striking fault set observed affecting Paleocene – Miocene strata does not affect Pliocene units.

Pleistocene to Recent fluvial gravels ('Fanglomerates'): Pleistocene to Recent fluvial to coastal deposits are not commonly faulted within the Polis Graben. In this study, structural data were only collected from one locality, at the Amargeti junction on the Nata-Pentalia road. Here, a sequence of Pleistocene marls, fluvial gravels, overbank fines and palaeosols are cut by a series of N280-N300- (WNW-ESE) trending, SSW-dipping normal faults

(Figure 3-13). No slickenlines or groove marks were noted. The sense of shear along the faults was determined using offset stratigraphic markers, imbricated clasts and the orientation of drag folds. The faults at Amargeti represent the 'youngest' phase of faulting in the Polis Graben; an optically stimulated luminescence dating study was initiated to constrain Pleistocene deformation in this area. The results of this study are presented in chapter 5.

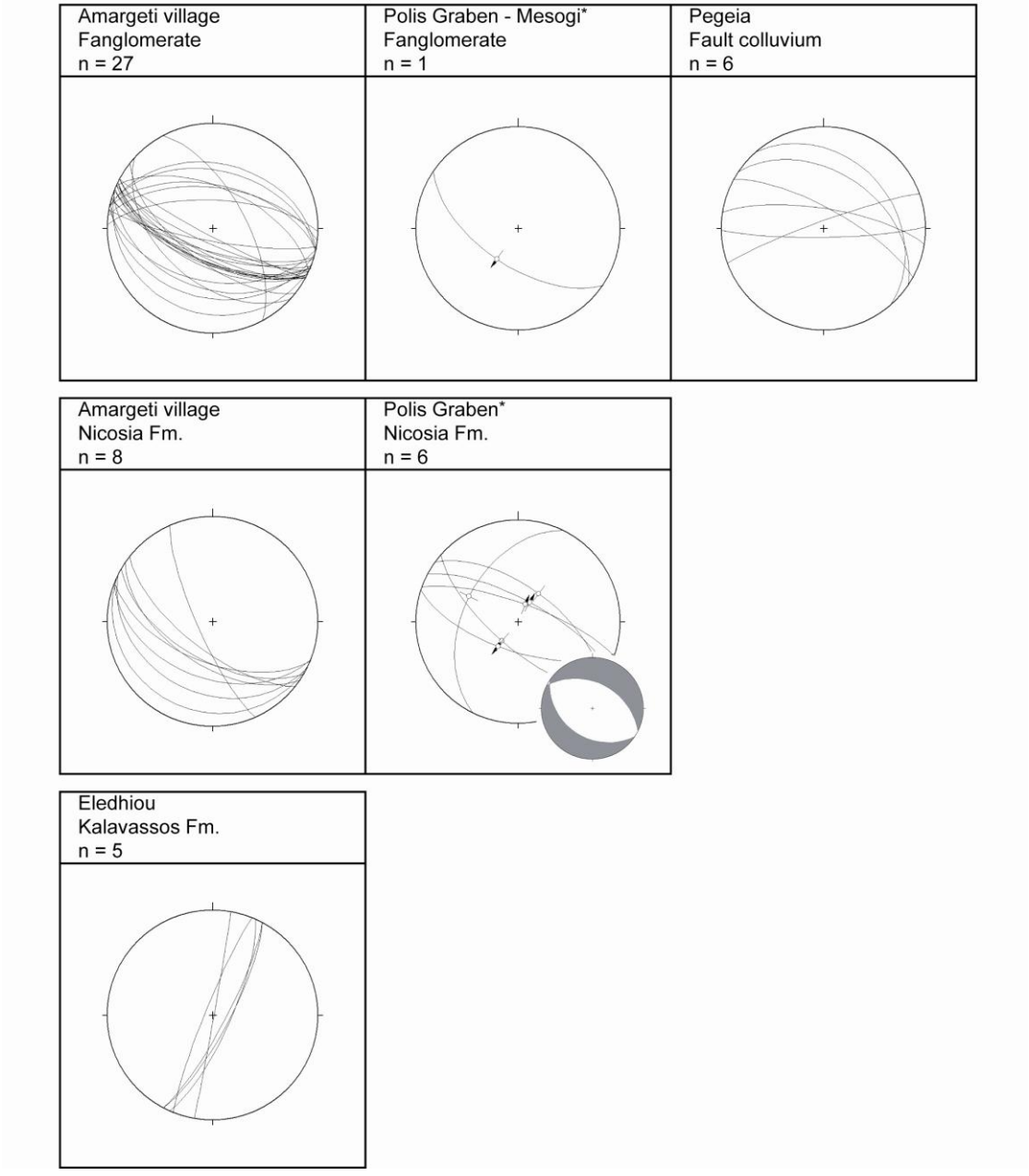

Figure 3-13: Fault data obtained from structures affecting Messinian-age strata at Eledio village, Pliocene-age strata at Amargeti village, and Pleistocene-age strata at Amargeti village and Pegeia village. The '' denotes data collected in the independent study of Payne (1995).*

The data presented above will now be examined to test the existing model of basin development (Payne, 1995; Payne and Robertson, 1995, 2000). The current hypothesis is that the onset of rifting in the Polis Graben began in the Tortonian. Pronounced faulting in the region occurred during the Messinian, followed by a period of tectonic quiescence in the Early to Middle Pliocene. Renewed faulting occurred in the latest Pliocene or early Pleistocene.

Figure 3-14 illustrates the distribution of faults affecting Paleocene and Miocene units in the Polis Graben. Three populations of faults were identified: (i) NNW-SSE-striking normal faults, parallel or near parallel to the basin margin; (ii) NNE-SSW/NE-SW-striking sinistral slip faults, oblique to the basin margin; and (iii) WNW-ESE-striking normal faults, orthogonal to the basin margin. The NNW-SSE-striking set of faults are believed to be the oldest, as these faults only affect Paleocene and Miocene chalks. No faults of this orientation are observed cutting Pliocene or younger strata. The WNW-ESE-striking set of faults are believed to be the youngest, as in addition to affecting Miocene strata, the faults also affect Plio-Pleistocene units (see above). Faults striking at a high angle to both these trends, i.e. at NNE-SSW/NE-SW, are observed at Evretou Dam. Here, NNE-SSW/NE-SW-striking faults displace faults of the main NNW-SSE trend. The faults are believed to form part of a larger transverse structure, which displaces basin-bounding faults on the eastern flank of the graben in the Sarama Valley area (Payne and Robertson, 1995). The fault data indicates two periods of deformation: an early extensional event forming NNW-SSE-striking faults in Miocene and older strata; and a later extensional event forming WNW-ESE-striking faults in Plio-Pleistocene strata.

Kinematic analysis of the fault-slip data yields information on the principal stress directions which controlled the formation of these faults. The NNW-SSE-striking set of structures was generated during east-northeast/west-southwest extension, with a maximum principal stress (σ_1) orientated vertical (059/86º) and intermediate (σ_2) and minimum (σ_3) principal stresses orientated horizontal (161/02º and 251/04º, respectively; Figure 3-15; Figure 3-16). To test whether the principal stresses derived from faults affecting Paleocene and Miocene strata were area specific, the data were analysed by locality, i.e. at Kathikas village, Evretou Dam and the Stroumpi-Tsada village transect (Figure 3-15). In each fault set, the strike of the faults is approximately perpendicular to the direction of the minimum principal stress resolved for that set (Figure 3-15). Fault data indicate that dip-slip displacements occur

parallel to the direction of the minimum principal stress. The development of NNW-SSE orientated structures in the Polis Basin is extensional, with only a minor element of transtension (Figure 3-15). The WNW-ESE-striking set of structures were generated during north-northeast/south-southwest extension, with a σ_1 orientated vertical (164/84º) and σ_2 and σ_3 orientated horizontal (300/03º and 030/03º, respectively; Figure 3-16).

Preliminary analysis of the new structural data obtained in the Polis Graben indicates that the chronology of deformation events established by Payne and Robertson (1995) is plausible. In later chapters of this thesis, further work will characterise the nature and timing of these deformation events; this will include luminescence dating of fault events (chapter 5) and a detailed study of the basin-fill of the Polis Graben (chapter 7).

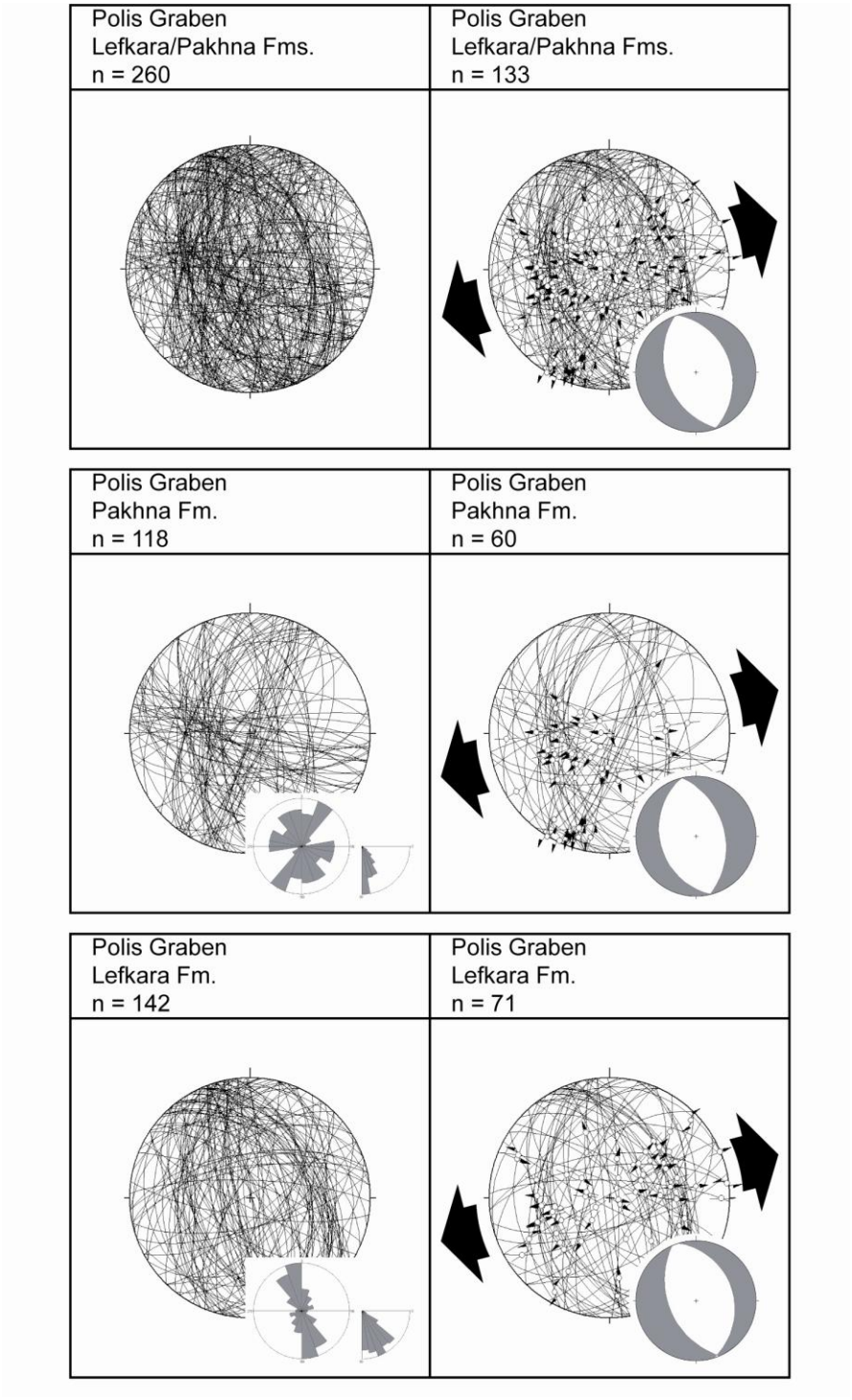

Figure 3-14: Fault data collected from structures affecting Paleocene and Miocene strata in the Polis Graben: (top) Strike directions of all faults measured in the Polis Graben; (centre) Strike directions of all faults in Miocene chalk (Pakhna Formation) in the Polis Graben; and (bottom) Strike directions of all faults in Paleocene chalk (Lefkara Formation).

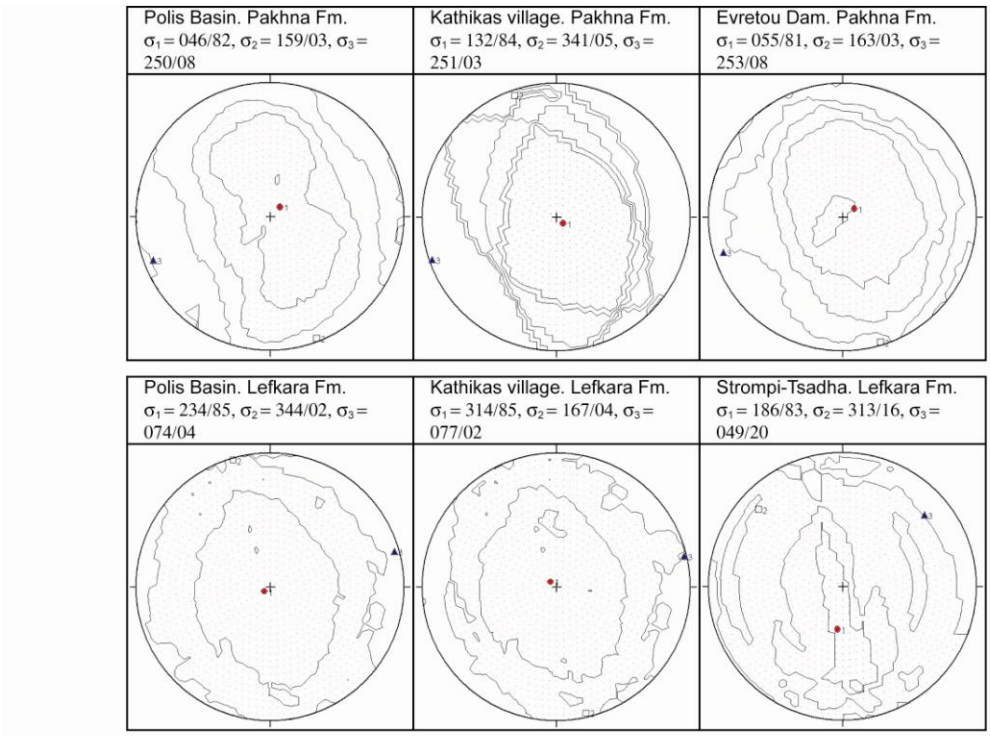

Figure 3-15: Principal stress directions in Paleocene and Miocene strata subdivided by location: (right) Principal stress directions derived for faults affecting Lefkara and Pakhna Formation chalk; (middle) Principal stress directions derived for faults affecting Lefkara and Pakhna Formation chalk at Kathikas village; and (left) Principal stress directions derived for faults affecting Lefkara and Pakhna Formation chalk between the villages of Strompi and Tsadha

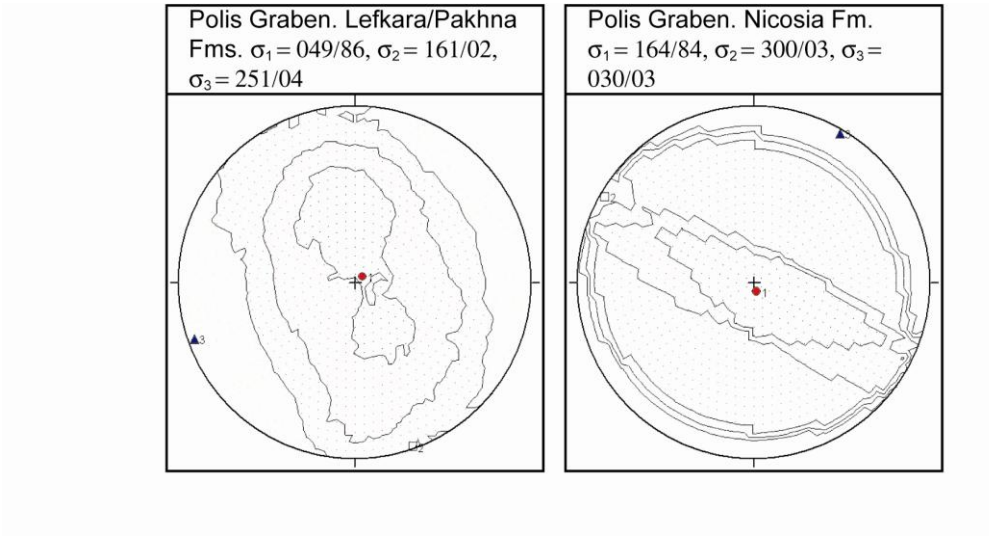

Figure 3-16: Deformation phases recognised in the Polis Graben: Tortonian, affects Paleocene and Miocene strata (Lefkara and Pakhna Formation chalk, respectively) and Pliocene, affects Pliocene and Pleistocene strata (Nicosia Formation marl)

3.3.3.2 The Pegeia Region

Payne and Robertson (1995; 2000) propose that the topography of the area to the south and west of the Polis Graben (Figure 3-9; hereafter referred to as the Pegeia region), is controlled by a system of mainly southerly dipping, WNW-ESE normal faults, which bound a series of down-faulted blocks of latest Cretaceous to Pliocene chalks, i.e. a half-graben (Figure 3-10; cross-section b). 'Syn-rift' sediments included localised Lower Miocene reef limestones (Follows et al., 1996), Pliocene marginal to shallow-marine deposits (Payne and Robertson, 1995b) and Quaternary non-marine to coastal deposits (Poole and Robertson, 1991; 1998; 2000).

In the following section, new structural data are presented for the Pegeia region. The data were collected to provide a framework on which to test the the existence of a half-graben in the region of Pegeia/Mesogi (Payne, 1995; Payne and Robertson, 1995, 2000) and determine if depositional/tectonic linkages exist between the Polis and Pegeia regions (Payne, 1995; Payne and Robertson, 1995, 2000). Fault orientations and kinematic data collected in the Pegeia area during this study differ from those measured by Payne and Robertson (1995; 2000). The present study has benefited from a number of new outcrops, created during construction of new tourist facilities. Payne and Robertson (1995) did not have access to these outcrops. The new data are grouped by either age (of the affected rock) and/or location.

Paleocene chalks (Lefkara Formation): Paleocene chalks are pervasively faulted throughout the Pegeia region. Meso-structural information was collected from second- and third-order faults cutting Paleocene chalks in the Pegeia/Mesogi region: at (a) Pegeia (Figure 3-17a) and (b) Mesogi (Figure 3-17b). Two populations of faults are observed at Pegeia: (i) N290-N320- (WNW-ESE/NW-SE) striking, NNE- and SSW-dipping faults; and (ii) N000- (N-S) striking, sub-vertical faults (Figure 3-17a). The WNW-ESE-striking set of faults offset strata in a normal sense. The senses of shear on the WNW-ESE-striking set of faults were determined from offset marker horizons, the orientation of drag folds and slickenlines (with steps as kinematic indicators). The slickensided surfaces are accompanied by sharp, low steps that trend at right angles to the striations; together these features imply normal dip-slip to slight oblique-slip displacements. The N-S-striking set of faults offset strata in a sinistral sense; slickenlines (with steps as kinematic indicators), when present, indicate sinistral to sinistral-normal displacements. Faults at Mesogi strike at a preferred orientation of N320-

N000 (NW-SE/N-S) and dip to SW and NE (Figure 3-17b). This set of faults offsets strata in a normal sense; where present, slickenlines indicate that this displacement is dip-slip.

Miocene chalks (Pakhna Formation): Paleocene chalks are pervasively faulted throughout the Pegeia region. Meso-structural information was collected from second- and third- order faults cutting Miocene chalks at two localities: at (a) Pegeia (Figure 3-17a) and (b) Mesogi (Figure 3-17b). Three populations of faults are observed at Pegeia: (i) N340-N000- (NNW-SSE/N-S) striking, ENE- and WSW-dipping, near vertical faults; (ii) N300-N340- (NW-SE) striking, NE-dipping faults; and (iii) N000-N020- (N-S/NNE-SSW) striking, sub-vertical faults. The NNW-SSE- and WNW-ESE-striking set of faults offset strata in a normal sense; where present, slickenlines indicate that this displacement is dip-slip. The NNE-SSW-striking set of faults are strike-slip in nature. The sense of shear on the NNE-SSW-striking faults was determined from offset marker horizons, fault geometries, slickenlines (with steps as kinematic indicators) and the orientation of drag folds. Two populations of faults are observed at Mesogi: (i) N300-N340- (NW-SE) striking, mainly SW-dipping faults; and N020-N060- (NE-SW) striking, mainly SE-dipping faults.

Pleistocene colluvium (recent fault detritus): Faults affecting Pleistocene colluvial deposits and palaeosols strike E-W, and dip preferentially to the S.

Fracture orientations: Four main orientations of fractures are seen in the Pegeia area (Figure 3-18). The most frequently observed trend is of NNW-SSE orientated fractures; i.e. at Pegeia in Miocene strata, and at Mesogi in Paleocene and Miocene strata. WNW-ESE fractures are observed cutting Paleocene chalks at Pegeia. Other fracture orientations in the Pegeia area include NE-SW and NNE-SSW. These are interpreted as cross-faults (conjugate sets) to the main, NNW-SSE and WNW-ESE orientated joint sets.

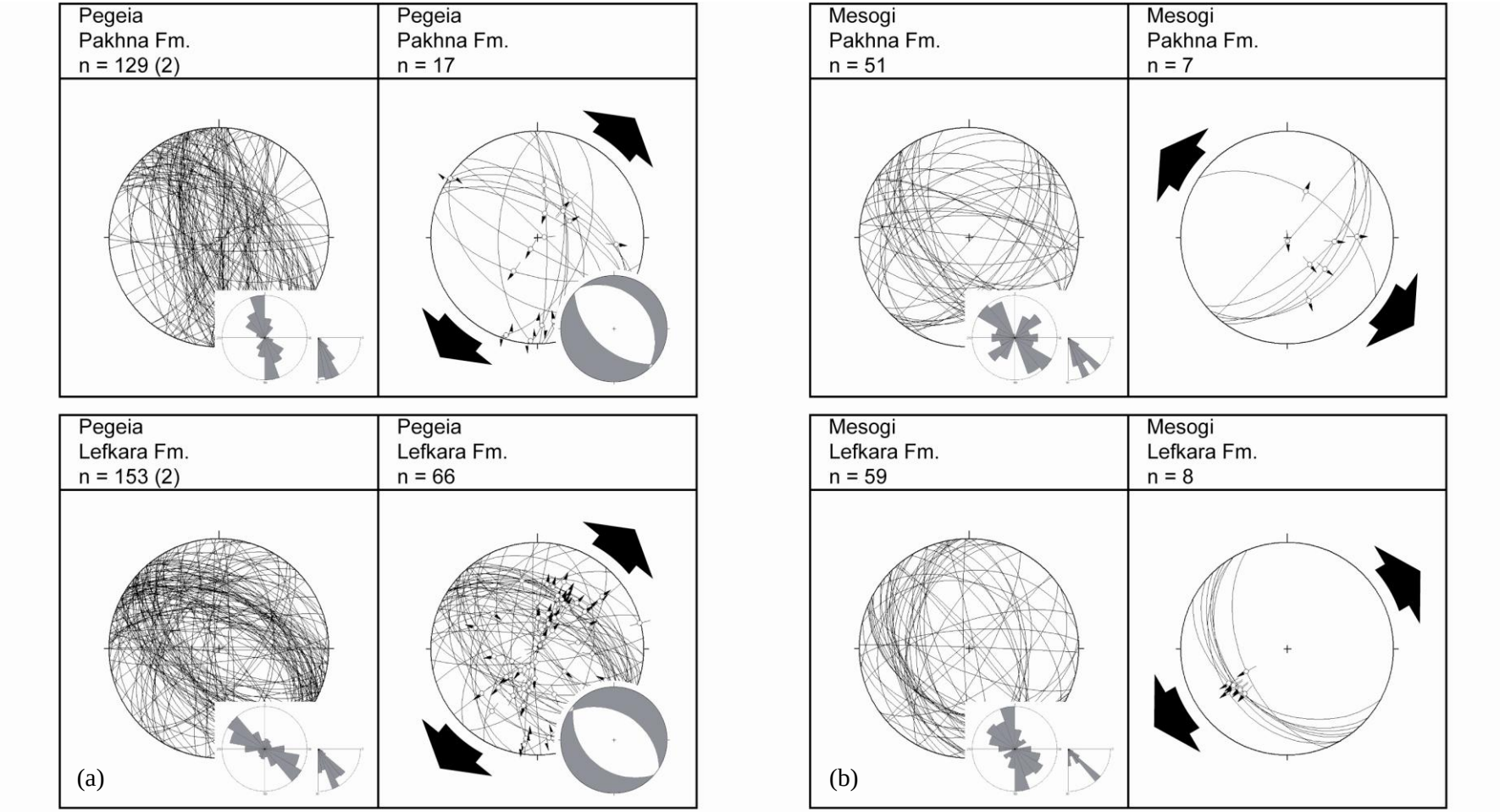

Figure 3-17: Strike directions for faults measured in Paleocene chalks (Lefkara Formation) and Miocene chalks (Pakhna Formation) at (a) Pegeia and (b) Mesogi. The numbers in brackets correspond to the number of measurements incorporated from Payne's (1995) study.

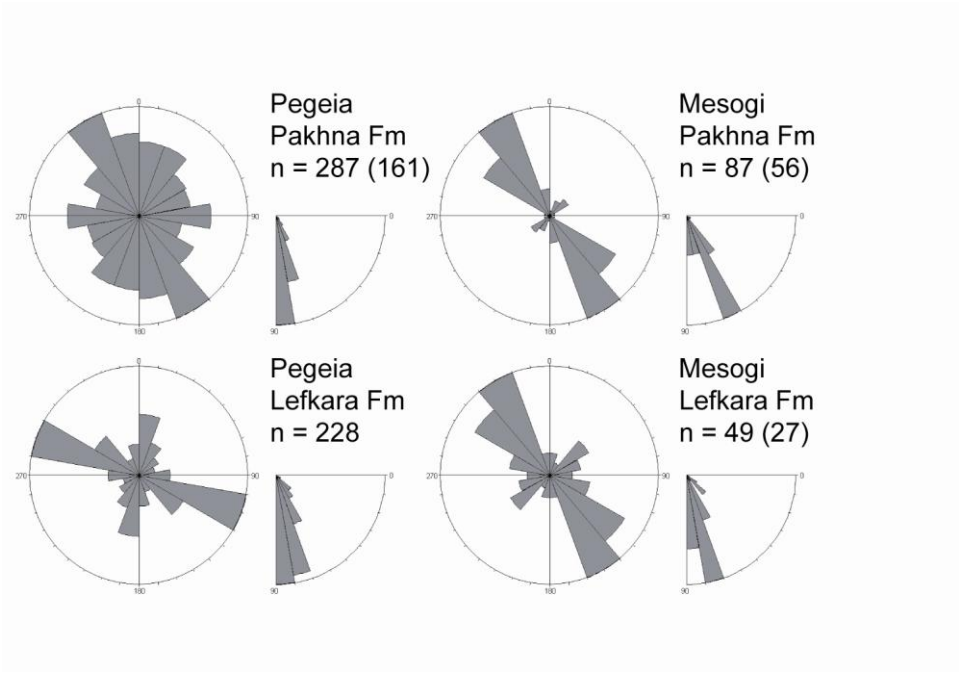

Figure 3-18: Strike directions for joints measured in Paleocene chalks (Lefkara Formation) and Miocene chalks (Pakhna Formation) at Mesogi. The numbers in brackets correspond to the number of measurements incorporated from Payne's (1995) study

The data presented above will now be examined to test the existing half-graben model for the Pegeia region (Payne, 1995; Payne and Robertson, 1995, 2000). The hypothesis of Payne and Robertson (1995) and Robertson (2000) is that latest Pliocene-early Pleistocene extension led to the formation of a half-graben in the Pegeia region. Payne and Robertson (1995) inferred a half-graben geometry based on a stepped topographic profile, west of Pegeia. They inferred three WNW-ESE-striking, SSW-dipping normal faults, which they believed down-faulted Pakhna Formation chalk and Quaternary marine terrace deposits (hence, the stepped topographic profile).

Reconnaissance mapping of the Pegeia region indicates that the stepped topographic profile, stated as evidence by Payne and Robertson (1995) for a system of WNW-ESE-striking, SSW-dipping normal faults, is actually a series of raised marine terraces. Raised marine terraces occur systematically throughout south Cyprus, various authors have attributed the terraces to eustatic sea-level changes and regional uplift of the Troodos Massif (see chapter 4; Poole and Roberton, 1991; 2000; Poole et al., 2001). Decimetre-scale normal faults do exist, although not on the same magnitude as proposed by Payne and Robertson (1995). Large normal faults, with vertical displacements of between 10 and 50m, are inferred based on (i) borehole data (Cyprus Geological Survey Department) that indicates that the base of

the Nicosia Formation occurs at different topographic heights (E. Tsiolakis, personal communication); (ii) offset stratigraphic markers, which indicate a repetition in a rare but prominent lignitic marker horizon in the Lefkara Formation; and (iii) a change in the regional dip/strike of beds (bedding within tilted blocks varies between 2 and 35º). No basin-scale faults, as observed in the Polis Graben, are observed at outcrop.

Figure 3-17 illustrates the distribution of faults affecting Paleocene and Miocene in the Pegeia region. Three populations of faults were identified: (i) NNW-SSE-striking normal faults; (ii) NNE-SSW/NE-SW-striking sinistral faults; and (iii) WNW-ESE-striking normal faults. NNW-SSE-striking, ENE- and WSW-dipping normal faults are observed cutting Pakhna Formation chalk in the east of the Pegeia region. WNW-ESE-striking, NNE- and SSW-dipping normal faults are observed cutting Lefkara and Pakhna Formation chalk throughout the Pegeia region. Fault plane solutions suggest that the WNW-ESE-striking set of faults were generated during NNE-SSW extension, with a σ_1 orientated vertical (130/87º) and σ_2 and σ_3 orientated horizontal (310/03º and 200/00º, respectively; Figure 3-19). Figure 3-19 indicates the principal stresses resolved for faults affecting Paleocene and Miocene strata in both Pegeia and Mesogi.

Preliminary analysis of the new structural data obtained in the Pegeia region indicates that a half-graben configuration for this area is questionable. In later chapters of this thesis, further work will characterise the nature and timing of faults in the Pegeia region; this will include luminescence dating of fault colluvium, to charactise the age of the youngest fault event (chapter 5) and a more detailed analysis of the Pegeia structures, considered in terms of a regional context (chapter 7). NNW-SSE-striking, ENE- and WSW-dipping normal faults are known to have been instrumental in forming the Polis Graben (see discussion above). WNW-ESE-striking normal faults were observed cutting Pliocene and younger chalk in the Polis Graben. Based on this data alone, it would appear that the orientation of faults in the Pegeia region is intrinsically linked to fault trends within the Polis region.

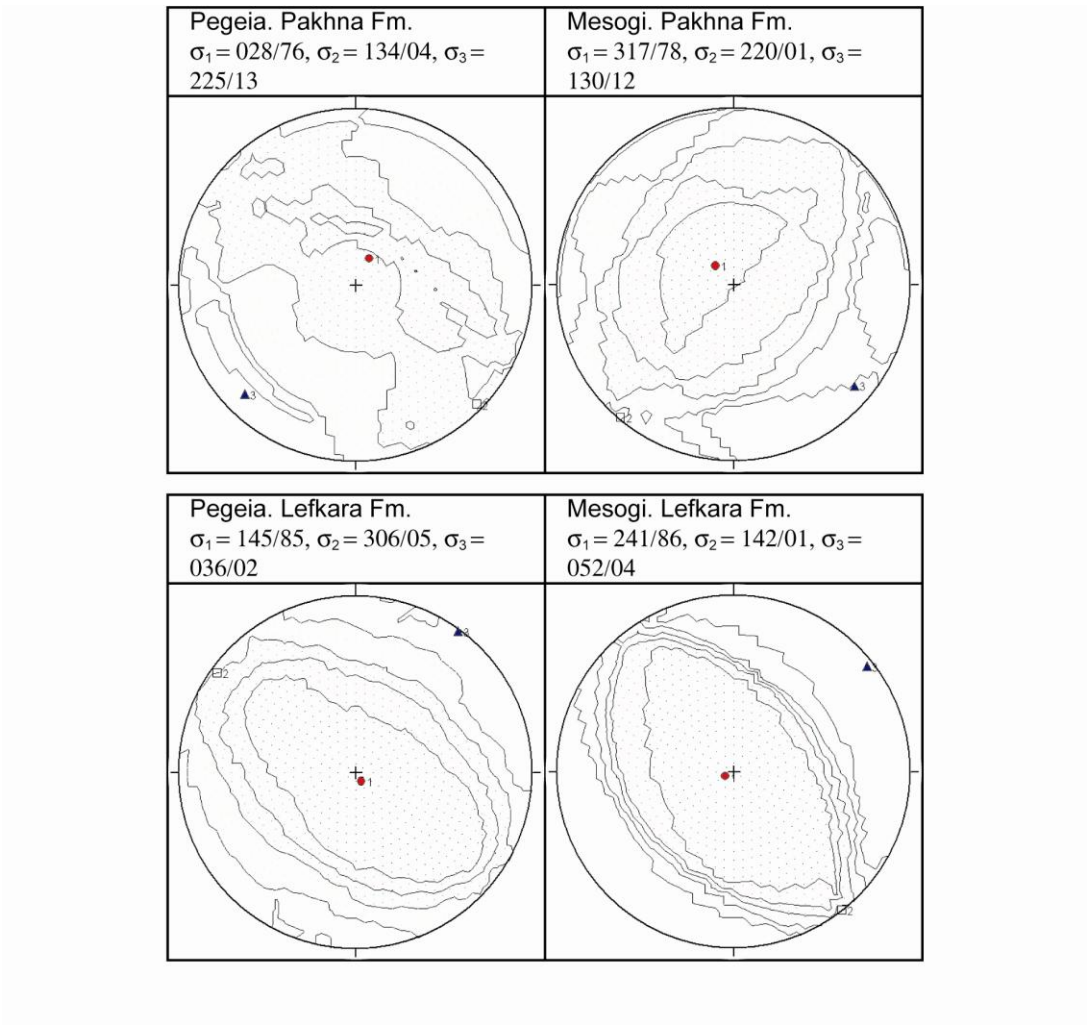

Figure 3-19: Principal stress directions resolved for faults affecting Paleocene and Miocene strata at Pegeia and Mesogi

3.3.3.3 The Pissouri Basin

The Pissouri Basin encompasses an area 23km east-west and 12km north-south, between Kouklia village to the west, Evidhimou Bay to the east and Pano Archimandrita village to the north (Figure 3-2). Detailed mapping was carried out of an area ~ 50km^2, in the vicinity of the villages of Pissouri and Pissouri Jetty (Figure 3-20). To date no detailed structural study has been undertaken in the Pissouri Basin. Payne and Robertson (1995) and Robertson et al. (1995b) inferred a model of basin evolution similar to that of the Polis Graben, based on the similar timing and orientation of faults in each basin.

Four groups of faults/fractures are defined within the Pissouri Basin, based on trend, displacement and magnitude: i.e. first-order (basin-bounding) faults, second-order faults, third-order (or minor) faults and extensional fractures.

First order (basin bounding) faults: Basin-bounding faults are inferred from borehole data; as (a) the spatial distribution and thickness of Messinian units and/or Pliocene marl varies throughout the basin; and (b) Miocene and Pliocene units are juxtaposed (without the intervening Messinian units; Figure 3-21). Inferred vertical displacements on first-order faults are believed to be at the scale of 100-200m. In the north of the basin, hydro-geological boreholes (data supplied by the Cyprus Geological Survey) encountered successions that pass down from Pliocene marls (Nicosia Formation), c. 25m - 40m thick, through gypsiferous deposits (Kalavasos Formation), c. 5m -100m thick, into carbonates (Pakhna Formation). In the east of the basin, the hydro-geological boreholes reveal a similar succession, with Pliocene marls, c. 20m thick, passing down through gypsiferous deposits, c. 50 metres thick, into Miocene carbonates. The gypsiferous units are inferred to pinch out laterally, and at the most eastern limit of the basin, Pliocene marls unconformably overlie Miocene carbonates. However, the hydro-geological boreholes in the axis of the basin reveal a different stratigraphic section: Pliocene marls reach a maximum thickness of c. 350m, and pass down into Miocene carbonates, with no intervening Messinian evaporites. There is one exception: c. 1km northwest of Pissouri Jetty, along the Pissouri Jetty/Pissouri village access road, borehole P2246 reveals a Mio-Pliocene succession. This succession is comprised of c. 70m of Pliocene marls, c. 100m of Messinian gypsiferous deposits, underlain by Miocene carbonates. 1km north-west of this borehole, borehole P2252, encounters a succession in which Pliocene marls rest unconformably on Miocene carbonates. It is believed that the orientation of the first-order faults must be sub-parallel to that of the second- and third-order faults.

Figure 3-20: Geological map of the Pissouri area, illustrating the distribution of lithostratigraphic units discussed in the text. Black lines denote roads. Thick black lines denote normal faults (downthrown side marked). Stars denote palaeomagnetic sampling sites (see section 6.3). Borehole data supplied by the Cyprus Geological Survey Department. Grid spacing is 1 kilometre.

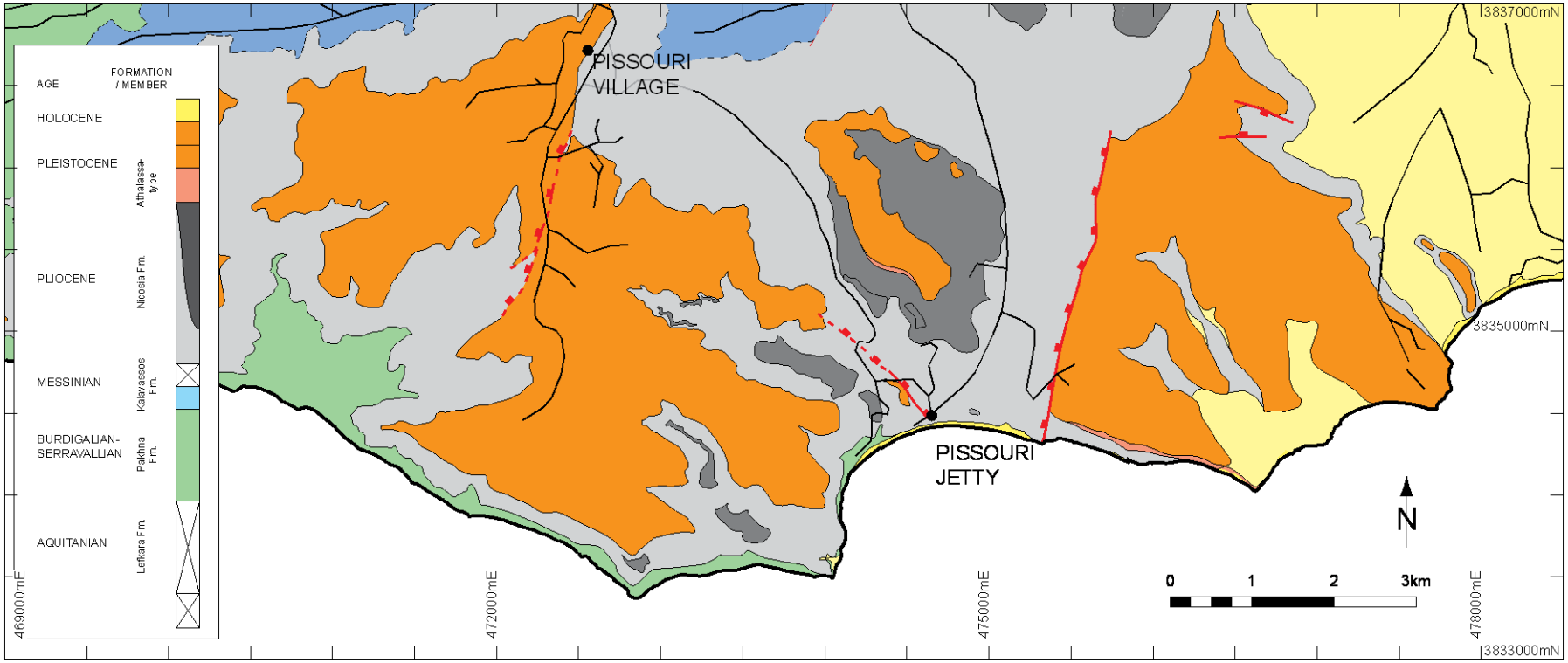

Figure 3-20: Geological map of the Pissouri area, illustrating the distribution of lithostratigraphic units discussed in the text. Black lines denote roads. Thick black lines denote normal faults (downthrown side marked). Stars denote palaeomagnetic sampling sites (see section 6.3). Borehole data supplied by the Cyprus Geological Survey Department. Grid spacing is 1 kilometre.

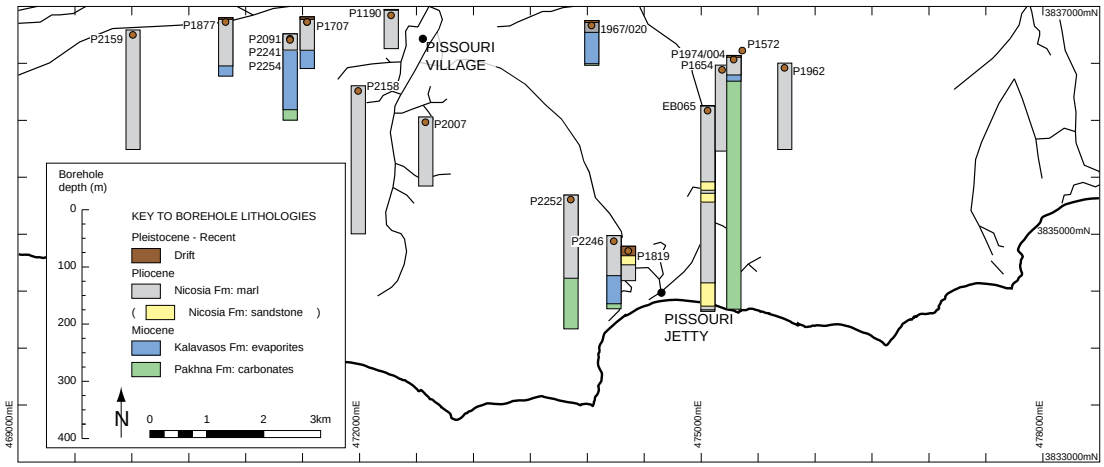

Figure 3-21: Outline map of the Pissouri area; indicating the location of hydro-geological boreholes in the region; and the spatial distribution of geological units at depth.

Second- and third-order (minor) faults: Second-order faults are those which bound small faults blocks on the margins, and in the axis of the Pissouri Basin. The centre of the basin is characterised by several NNE-SSW trending, westerly-dipping faults, associated with rotated fault blocks of Pliocene strata (see chapter 6). Fault scarps, perpendicular to the present coastline, east of Pissouri and Pissouri Jetty are recognised as active structures (see chapter 6). Fault dips are in the range of 50-70º. Bedding within the tilted blocks is at an angle of 5º to 30º. Abundant minor faults and fractures are seen in Lefkara and Pakhna Formation chalks at/or near the margins of the Pissouri Basin. Third order faults typically dissect second-order fault blocks into smaller segments. Displacements observed across minor faults are small, and vary from tens of centimetres to a few millimetres. In general, three main trends in the strike of faults may be recognised: (i) a NNE-SSW trend; (ii) a NW-SE trend; and (iii) a NNE-SSW/N-S trend.

Extensional fractures: Extensional joints are rarely preserved in Nicosia Formation sediments; however, where preserved they occur sub-parallel to the traces of second- and third-order faults.

In the following section new structural data are presented for the Pissouri Basin. This data was collected to provide a framework on which to test the existing model of basin development (Payne, 1995; Payne and Robertson, 1995, 2000) and facilitate comparisons between the Neogene basins. An integrated sedimentological, structural and magnetostratigraphic study of this basin is presented in chapter 6. The new data were grouped by either age (of the affected rock) and/or location.

Paleocene chalks (Lefkara Formation): Paleocene chalks only outcrop in the Pissouri region at a single locality, west of Pissouri village, on the Paphos-Lemesos old road. Here, faults strike at a preferred orientation of N290-N320 (NW-SE), and dip to the SW. No fault-slip data were obtained.

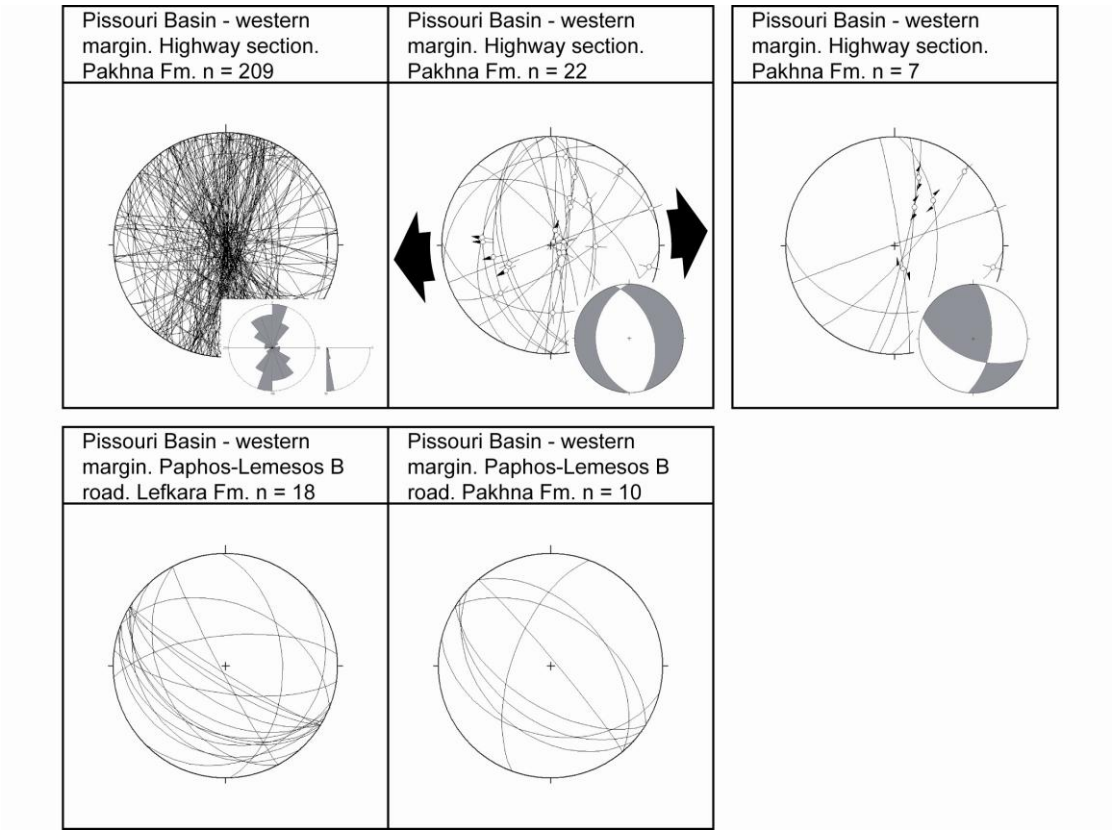

Figure 3-22: Strike directions of faults measured in Paleocene chalk and Miocene chalk, west of Pissouri village, by (top) the Paphos-Lemesos highway and (bottom) the Paphos-Lemesos road

Miocene chalks (Pakhna Formation): Miocene chalks are pervasively faulted throughout the Pissouri Basin. Meso-structural information was collected from third-order faults cutting Miocene strata at several localities: (a) to the west of Pissouri, at the contact between the Lefkara and Pakhna Formations (Figure 3-20; Figure 3-22); (b) to the west of Pissouri, along the Paphos-Lemesos highway (Petra Tou Romiou junction) (Figure 3-22); and (c) to the east of Pissouri, along the Paphos-Lemesos highway (Figure 3-23). Two populations of faults are observed cutting Miocene strata: at locality (a) faults strike at a preferred orientation of N290-N320 (NW-SE), and dip to the SW; at localities (b) and (c) faults strike at a preferred orientation of N350-N020 (N-S/NNE-SSW), and dip to the E and W.

All of the above faults were inferred to be normal in nature, based on offset stratigraphic markers and the orientation of drag folds. Slickensided surfaces were only observed at one locality, west of Pissouri at the Petra Tou Romiou junction of the Paphos-Lemesos highway. Two separate slickenlines (with steps as kinematic indicators) were observed on several of the slickensided surfaces: one slickenline implied a dip-slip movement (normal in nature) and the other a strike-slip movement (dextral in nature).

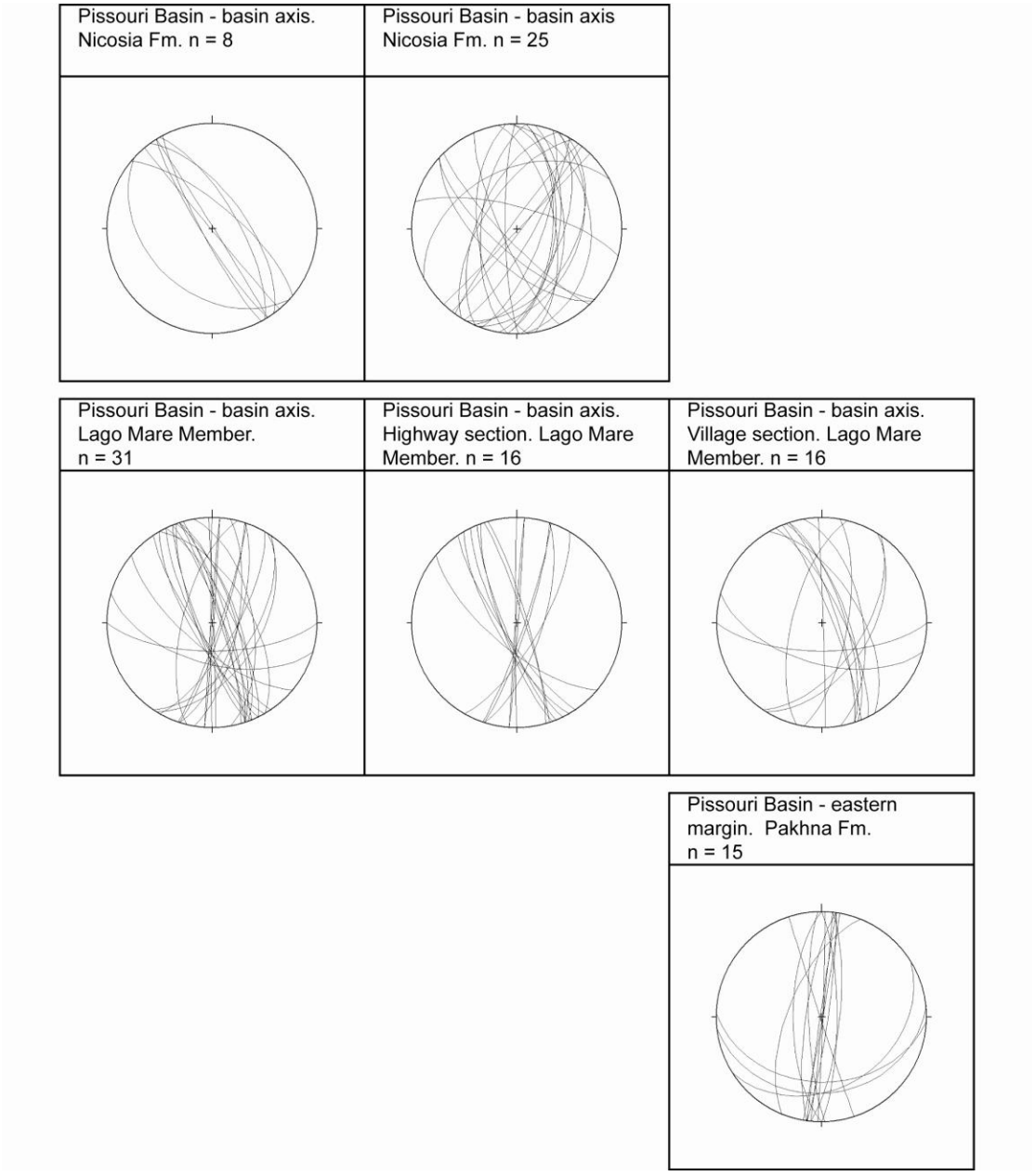

Figure 3-23: Strike directions of third-order faults measured at Pissouri: in the lower row structural data is presented for faults affecting Miocene strata (Pakhna Formation) at the eastern margin of the Basin; in the middle row structural data is presented for faults affecting Messinian deposits in the axis of the Basin; in the upper row structural data is presented for faults affecting Pliocene strata (Nicosia

Formation) in the axis of the Basin. Structural data presented for faults affecting Messinian strata were sub-divided by locality, i.e. Lago Mare village section and Lago Mare highway section

Messinian evaporites, marls and chalks (Kalavasos Formation): Messinian marls and chalks are pervasively faulted throughout the Pissouri Basin. Meso-structural information was collected from third-order faults affecting Messinian strata at two localities: at (a) (Lower) Pissouri village (the Pissouri village section of chapter 6) and (b) along the Paphos-Lemesos Highway (the Paphos-Lemesos highway section of chapter 6). Faults affecting Messinian strata strike N-S and dip to both the E and W (Figure 3-23).

Pliocene marls (Nicosia Formation): Pliocene marls are not commonly faulted within the Pissouri Basin. Meso-structural information was collected from third-order faults affecting Pliocene strata at two localities: at (a) Pissouri Jetty and (b) the Pakhna junction of the Paphos-Lemesos Highway. Faults affecting Pliocene strata strike at a preferred orientation of N320-020- (NNW-SSE/N-S) and dip to both the ENE and WSW. Some scatter is evident in the fault orientation data. No slip data were obtained.

Pleistocene gravels (Fanglomerate Group): Pleistocene gravels are not commonly faulted within the Pissouri Basin. In this study, structural data were only collected from one locality, at the Pissouri junction of the Paphos-Lemesos highway (Figure 3-24). Two populations of faults are observed in Pleistocene strata at the Pissouri junction of the Paphos-Lemesos highway: (i) a ~ N-S-striking, E- and W-dipping set; and (ii) a NE-SW-striking, NW-dipping set. No slip data were obtained.

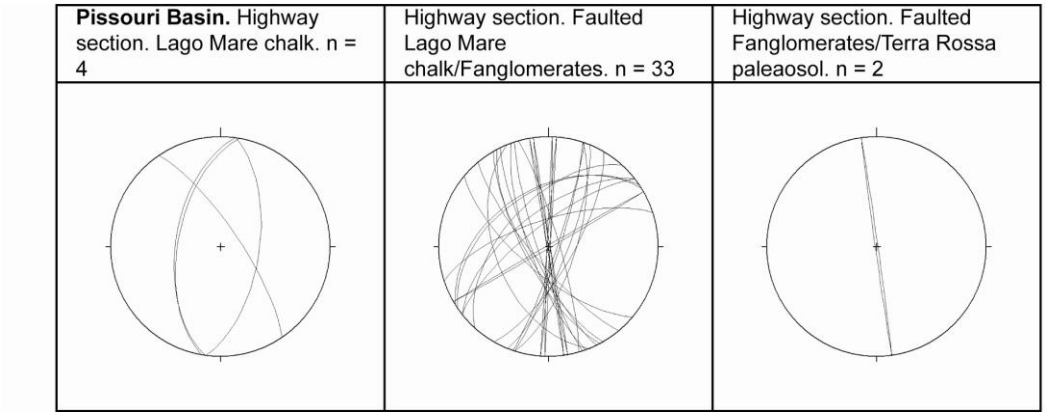

Figure 3-24: Structural data collected from faults affecting Messinian and Pleistocene strata in the Pissouri Basin

The data presented above will now be examined, to test the existing model of basin development. The current hypothesis is that the Pissouri Basin formed contemporaneously with the Polis Graben, under similar extensional stresses. Hence, the onset of 'rifting' in the Pissouri Basin is believed to have began in the late Miocene.

Figure 3-22 and Figure 3-23 illustrate the distribution of faults affecting Paleocene to Pleistocene strata in the Pissouri Basin. Three populations of faults were identified: (i) N-S-striking; (ii) NW-SE-striking; and (iii) E-W-striking predominantly normal faults. Kinematic analysis of the fault-slip data yields information on the principal stress directions which controlled the formation of these faults. The ~ N-S-striking set of structures was generated during east-northeast/west-southwest extension, with a σ_1 orientated vertical (216/80º) and σ_2 and σ_3 orientated horizontal (350/07º and 051/07º, respectively; Figure 3-25). The spatial distribution of Messinian evaporates was controlled by faulting (see above). Thus, the ~ N-S-striking sets of faults were believed to be active in the late Tortonian to early Messinian. Messinian evaporites are cut by ~ N-S faults. Messinian Lago Mare deposits and Pleistocene Fanglomerate gravels are cut by~ N-S, E-W and NE-SW faults. Dissolution of the underlying gypsiferous deposits created large (metre-wide) cavities, which were infilled by Lago Mare deposits. Collapse structures are associated with the margins of these cavities. It is believed that faults in the evaporitic succession (trending ~ N-S) acted as conduits for groundwater; hence dissolution cavities trend in a similar orientation to Messinian faults. Earlier structures (Tortonian/Messinian), therefore, largely control the spatial distribution of faults in Pleistocene and younger strata. No fault-slip data were obtained from the later faults.

The fault data indicate several periods of deformation: (i) an extensional event forming ~ N-S- and NW-SE-striking faults in Tortonian and older carbonates; (ii) an extensional event forming ~ N-S- and E-W-striking faults in Messinian evaporites/chalks; and an (iii) extensional event forming ~ N-S- and NE-SW-striking faults in Pleistocene strata. The normal faults observed cutting Messinian and older strata have been reactivated in a later phase of compression/transpression. This deformation is consistent with an approximate northeast σ_1 (059/01º) and an approximate northwest σ_3 (328/43º; Figure 3-25).

Preliminary analysis of the new structural data obtained in the Pissouri Basin indicates that the Polis Graben and Pissouri Basin may have formed contemporaneously. The principal stresses resolved for the late Tortonian to early Messinian structures in both the Pissouri and

Polis regions are comparable (σ_1; 216/80º : 234º/85º, σ_2; 350/07º : 344º/02º, and σ_3; 051/07º : 074º/04º; Pissouri : Polis, respectively), suggesting that they may have formed during the same episode of E-W extension. This hypothesis will be explored futher in chapter 7 of this thesis.

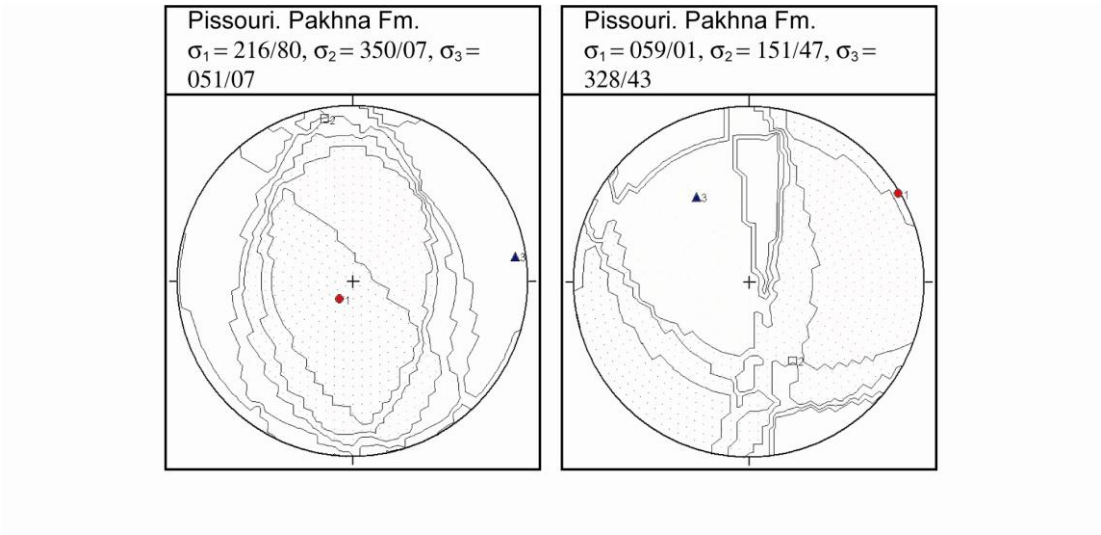

Figure 3-25: Principal stress directions resolved for faults affecting Miocene strata in the Pissouri Basin. Two deformation phases are recognised: Tortonian – Messinian extension which affects Pakhna and Kalavasos Formation strata; and Late Pliocene – Pleistocene transpression which reactivates earlier structures in Pakhna and Kalavasos Formation strata

3.3.3.4 The Maroni - Psematismenos Basin

The Maroni-Psematismenos Basin encompasses an area c. 14km east-west and c. 10km north-south (Figure 3-2). Reconnaissance mapping was carried out of an area c. 14km^2, in the vicinity of the villages of Choirokoitia, Tochni and Psematismenos (Figure 3-26). To date, no detailed structural study has been undertaken in the Maroni-Psematismenos Basin. In the northern part of the basin, the NNW-SSE trending Kalavasos-Vasilikós Valley, is bound to the east and west by first-order N020-N040- (NE-SW) trending, NW- and SE-dipping and N300-N320 (NW-SE) trending, NE- and SW-dipping normal faults. Both fault sets occur in association with rotated blocks of Lefkara and Pakhna Formation strata, and at one locality, Pleistocene colluvium (see chapter 5, section 5.6.1). Elsewhere in the basin, first-order, basin-bounding faults are inferred, based on several criteria: (i) an offset in stratigraphic units; (ii) a change in the regional strike of beds; and (iii) breaks in topography.

Figure 3-26 illustrates the distribution of first- and second-order faults in the Maroni-Psematismenos Basin. The map was compiled from GIS data supplied by the Cyprus Geological Survey Department. Bear (1960) and Pantazis (1967a,b) identified three populations of faults: (i) N330-N350 (NNW-SSE) striking faults; (ii) N070-N080 (ENE-WSW) striking faults; and (iii) N010-N040 (NNE-SSW to NE-SW) striking faults. Several NNW-SSE-striking, sub-vertical strike-slip faults have been identified in the axis of the Maroni Basin (Soulas, 2003). In addition to the NNW-SSE-striking fault set, the Maroni Basin is dissected by several ENE-WSW-striking, SSE-dipping normal faults. In the central axis of the basin, near Maroni village, Kalavasos Formation evaporites are cut by a conjugate set of fractures aligned N340-N020 (~ N-S) and N280-N300 (WNW-ESE).

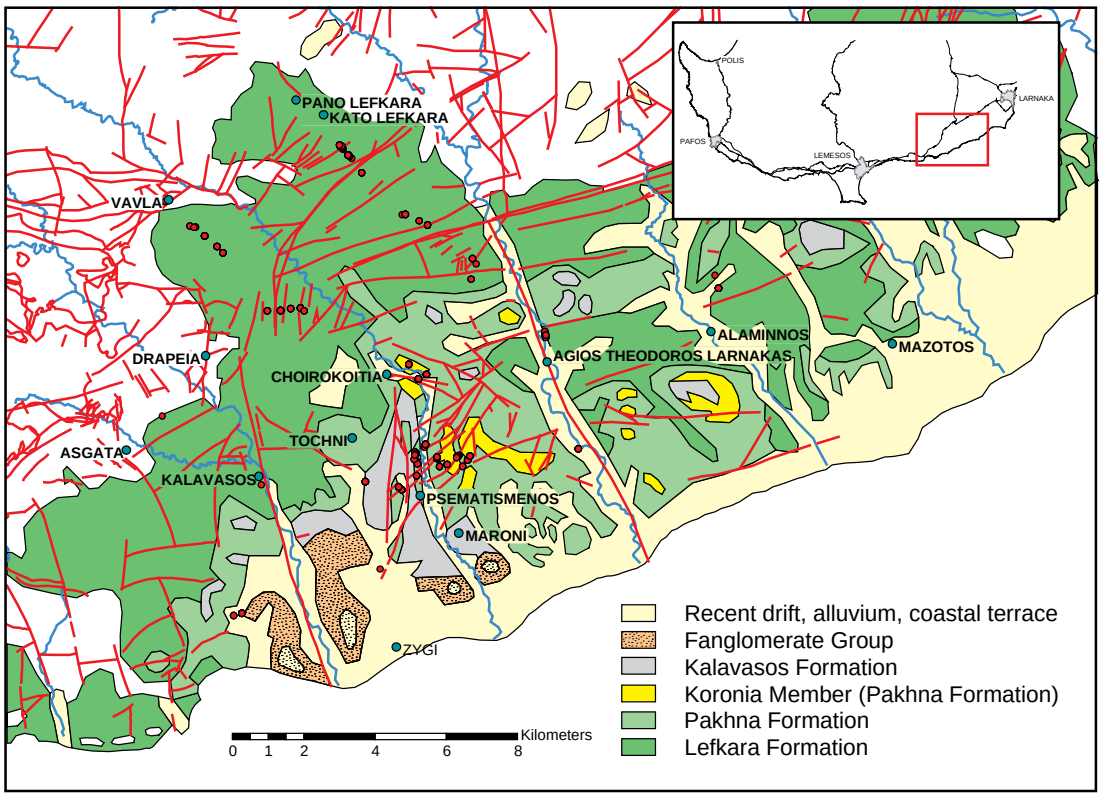

Figure 3-26: Geological map of the Maroni-Psematismenos Basin (data supplied by the Cyprus Geological Survey Department). Black dots denote village centres. Red dots denote localities at which structural data was collected.

In the following section new structural data are presented for the Maroni-Psematismenos Basin. An integrated sedimentological and structural account of the Kalavasos Vasilikós River valley is presented in chapter 5. The new data were grouped by either age (of the affected rock) and/or location.

Paleocene chalks (Lefkara Formation): Paleocene chalks are pervasively faulted throughout the Maroni-Psematismenos Basin. Faults affecting Paleocene strata are observed at, or near to, the villages of Kalavasos and Agios Theodoros Larnakas. Two populations of faults are observed at Kalavasos: (i) N010-N060- (NNE-SSW/NE-SW), WNW- and ESE-dipping faults; and (ii) N280-N330- (WNW-ESE/NW-SE), NNE- and SSW-dipping faults. Two populations of faults are observed at Agios Theodoros Larnakas: (i) N000-N020- (NNE-SSW) striking, WNW- and ESE-dipping faults and (ii) N280-N300- (WNW-ESE) striking, NNE-dipping faults (Figure 3-27a). The majority of the aforementioned faults are believed to be normal in nature, as they offset strata in a normal sense; where present, slickenlines (with steps as kinematic indicators) indicate that this displacement is down-dip to slightly oblique-slip in nature.

Miocene chalks (Pakhna Formation): Miocene chalks are pervasively faulted throughout the Maroni-Psematismenos Basin. Faults affecting Miocene strata are observed at, or near to, the villages of Psematismenos and Maroni. Faults strike at a preferred orientation of N020-N060 (NE-SW), and dip to the NW and SE. The majority of the faults are believed to normal in nature, as they offset strata in a normal sense; where present, slickenlines indicate that this displacement is dip-slip. There are subsets of reverse faults (13.2% of the total fault population), sinistral faults (12.2%) and dextral faults (2.4%). For each subset of faults, it is possible to identify slickensided surfaces associated with the faults. Frequently these surfaces are characterised by small steps orientated perpendicular to the main slickenline; from these observations it is possible to determine the kinematics of each fault.

Messinian gypsum breccias and gypsiferous marls (Kalavasos Formation): Meso-structural information was collected from third-order faults (Figure 3-28) and fractures (Figure 3-29) that cut Messinian-aged gypsiferous deposits at two localities: (a) to the north of Psematismenos village, and (b) in gypsum quarries, east of Maroni village. Faults strike at a preferred orientation of N060-N080 (ENE-WSW) and dip to both the NNW and SSE (Figure 3-28). The faults offset strata in a normal sense; where present, slickenlines indicate that this displacement is normal dip-slip to normal-sinistral.

Pliocene marls (Nicosia Formation): Faults affecting Pliocene strata were only observed at one locality in the Maroni-Psematismenos Basin, i.e. Vasiliko Quarry (Figure 3-2). Here, faults strike at a preferred orientation of N300-N320 (NW-SE) and dip to the NE (Figure 3-28). No slip data were obtained.

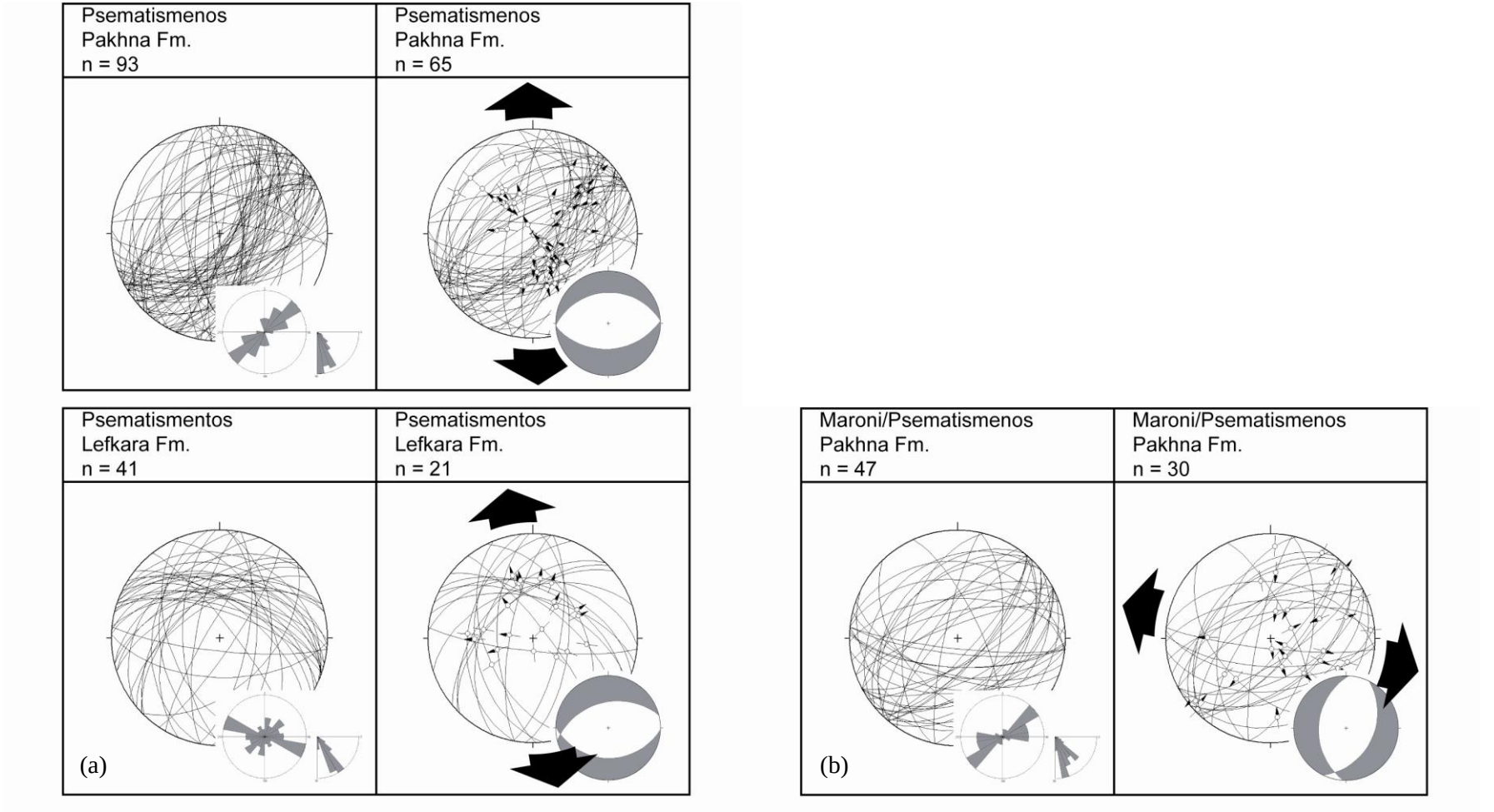

Figure 3-27: Fault data collected from structures affecting Paleocene chalk (Lefkara Formation) and Miocene chalk (Pakhna Formation) at (a) Psematismenos and (b) Maroni.

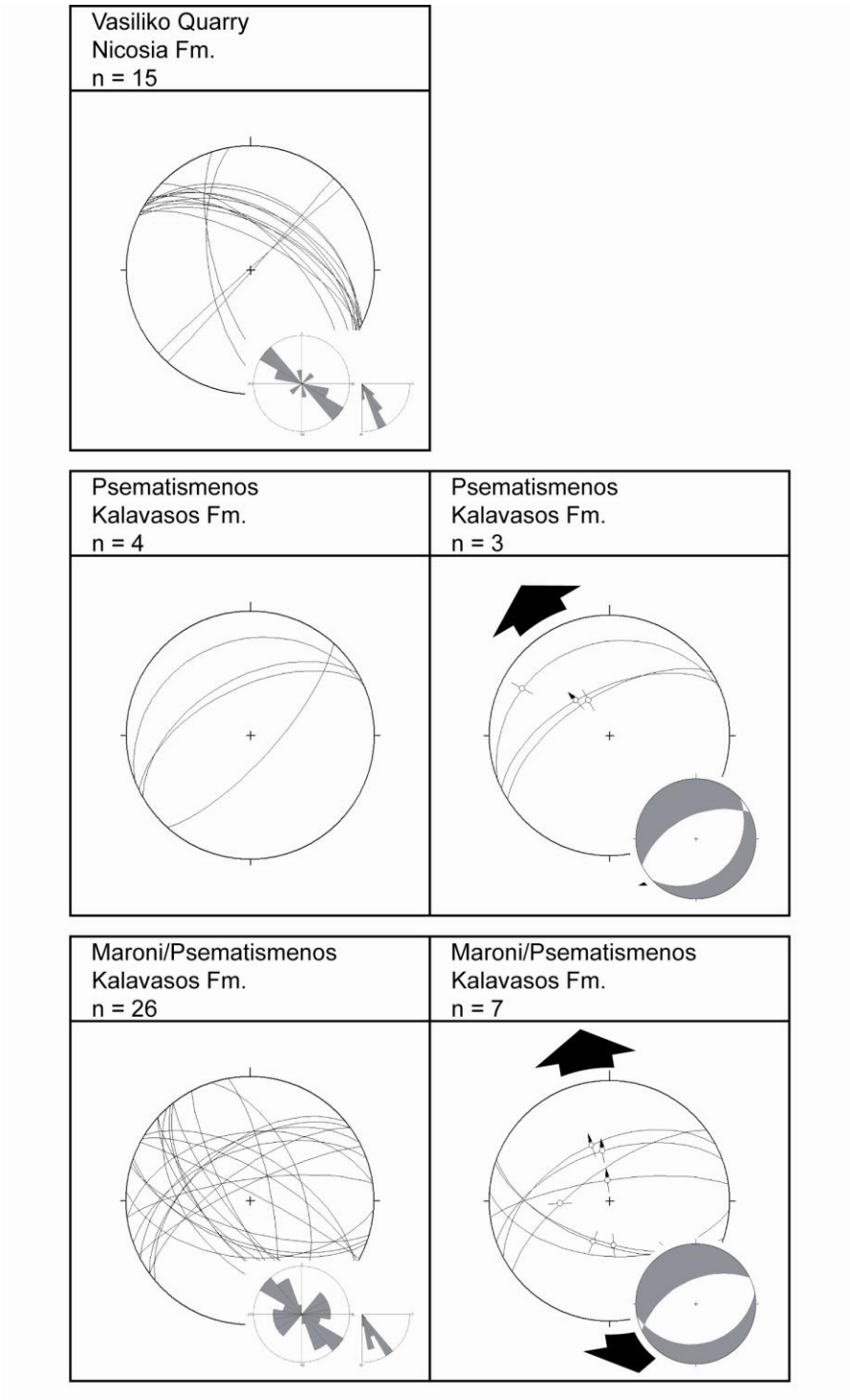

Figure 3-28: Fault data collected from structures affecting Messinian gypsiferous deposits (Kalavasos Formation) and Pliocene strata (Nicosia Formation) at Psematismenos and Maroni/Psematismenos.

Fracture orientations: Two main orientations of fractures are seen in the Maroni-Psematismenos Basin (Figure 3-29). The most frequently observed trend is of WNW-ESE/NW-SE fractures, as noted in Messinian evaporites at Maroni, in an abandoned gypsum

quarry and Pliocene marls at Vasiliko Quarry (Figure 3-29). The other fracture orientation in the Maroni-Psematismenos Basin has a ~ N-S trend.

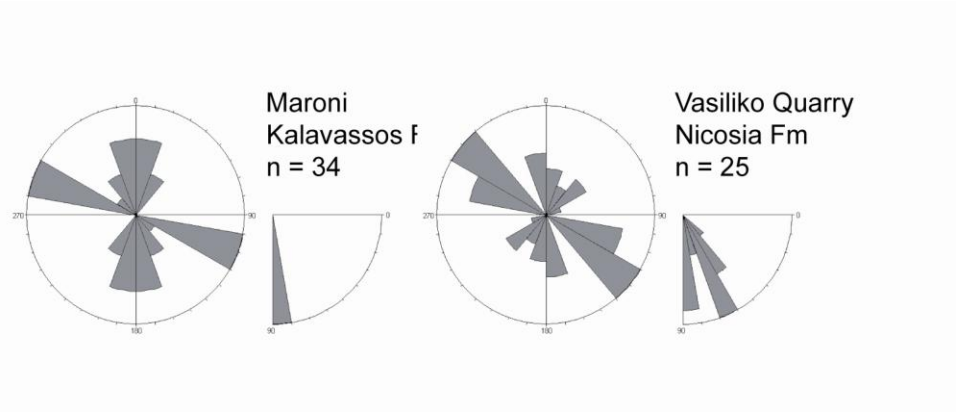

Figure 3-29: Strike directions for joints measured in Messinian evaporites (Kalavasos Formation) at Maroni and Pliocene marls (Nicosia Formation) at Vasiliko Quarry.

The new structural data presented above is now analysed to determine a structural framework on which models for the tectonic evolution of the basin can be built. Figure 3-30 illustrates the distribution of faults affecting Paleocene to Pleistocene strata in the Maroni-Psematismenos Basin. Three populations of faults are identified: (i) NE-SW- to ENE-WSW-striking normal faults; (ii) NE-SW-striking sinistral faults; and (iii) NNW-SSE- to NW-SE-striking extensional faults. Field observations described above indicate that the NE-SW-striking set of faults is the oldest, with faults affecting Paleocene and Miocene chalks. The ENE-WSW fault set is the youngest, with faults affecting Messinian gypsiferous deposits.

Kinematic analysis of the fault-slip data yields information on the principal stress directions which controlled the formation of these faults. The NE-SW-striking set of faults was generated during northwest to north-northwest/southeast to south-southeast extension, with a σ_1 orientated vertical (037/86º) and σ_2 and σ_3 orientated horizontal (246/03º and 156/02º, respectively; Figure 3-31; Figure 3-32). The ENE-WSW-striking set of faults were generated during north-northwest/south-southeast extension, with a σ_1 orientated vertical (140/77º) and σ_2 and σ_3 orientated horizontal (246/04º and 337/12º). To test whether the principal stresses derived from faults affecting Paleocene and Miocene strata were area specific the data were analysed by locality, i.e. those collected near Psematismenos and those collected near Maroni. The principal stresses resolved for faults affecting Miocene and Messinian strata at Psematismenos and Maroni are similar, i.e. in Miocene strata, σ_1; 332º/82º : 032º/79º (Psematismenos : Maroni), σ_2; 074º/01º : 224º/11º, and σ_3; 164º/06º : 134º/02º; and in

Messinian strata, σ_1; 181º/75º : 128º/76º, σ_2; 059º/08º : 248º/01º, and σ_3; 327º/13º : 340º/12º (Figure 3-32).

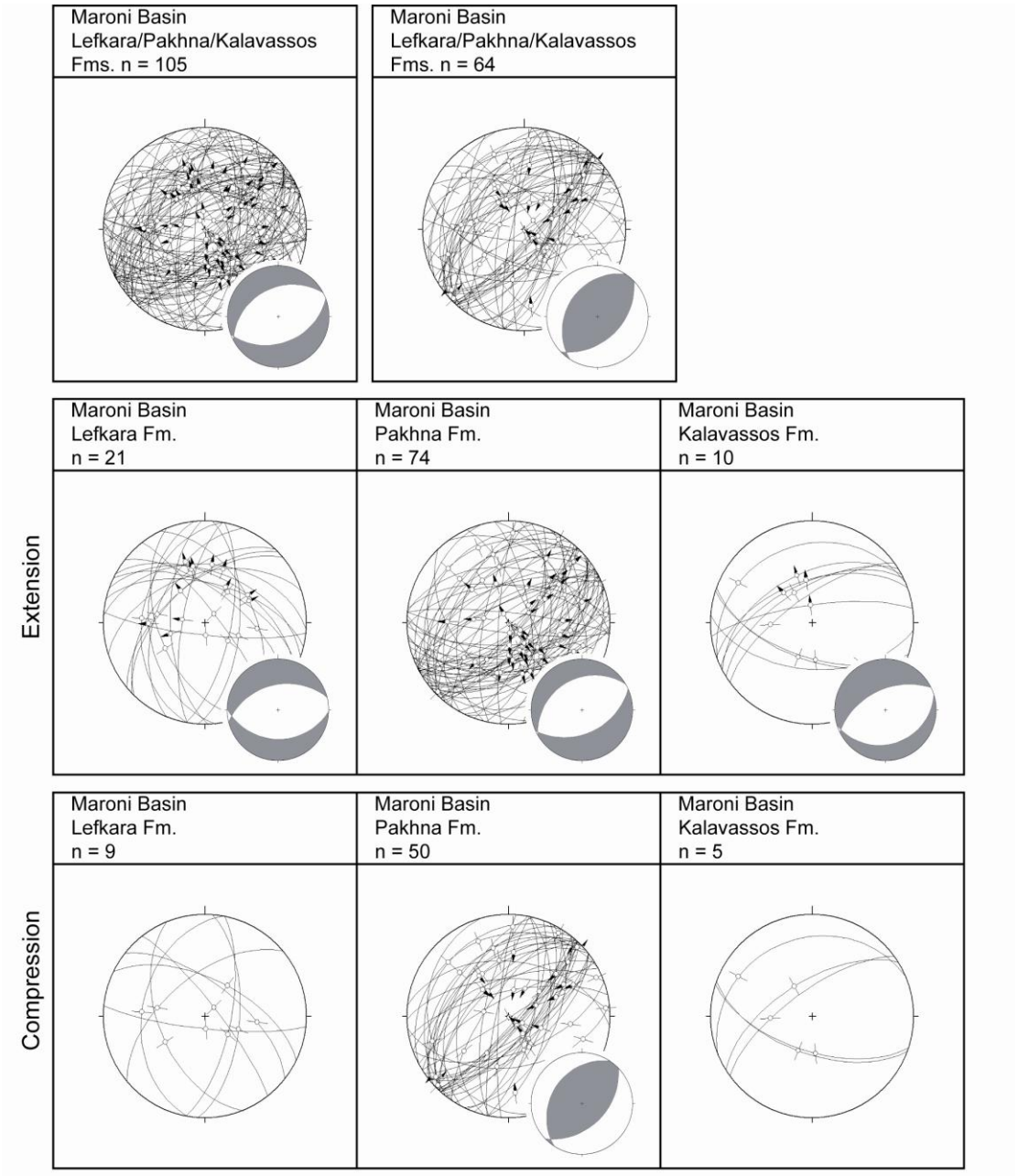

Figure 3-30: Fault data collected in the Maroni-Psematismenos Basin: Row 1: All fault data collected in the Maroni village region, sub-divided by kinematics; Row 2: Fault data collected from extensional faults in the Maroni village region, sub-divided by age of the affected rock; Row 3: Fault data collected from compressional faults in the Maroni village region, sub-divided by age of the affected rock

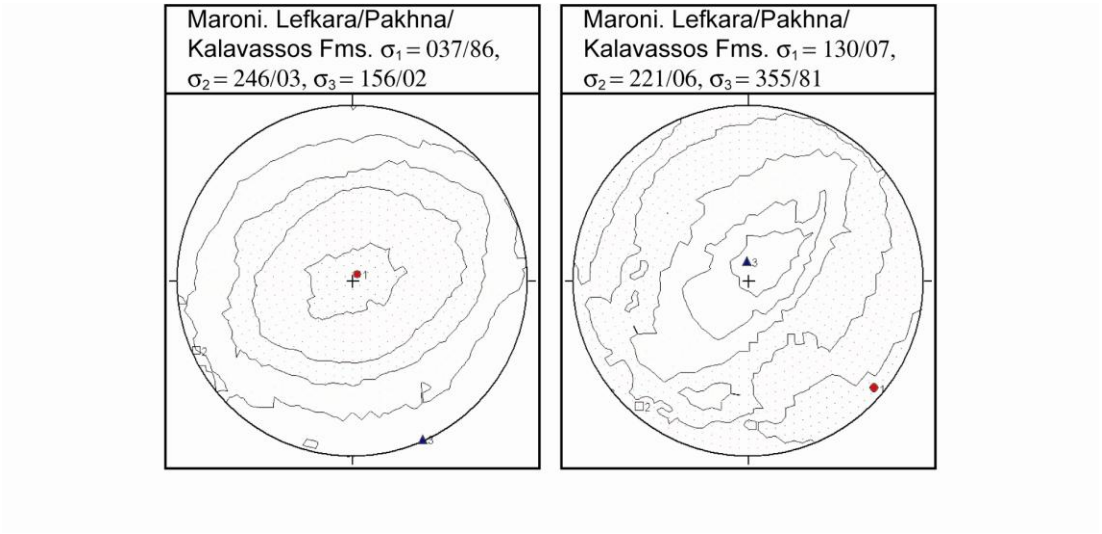

Figure 3-31: Principal stress directions determined for faults in the Maroni Basin, sub-divided by kinematics: lefthand column = principal stress directions determined for extensional structures, righthand column = principal stress directions determined for compressional structures

The normal faults observed cutting Messinian and older strata have been reactivated in a later phase of compression/transpression. The principal stresses resolved for the compressional event are consistent with σ_1 and σ_2 orientated horizontal (130/07º and 221/06º, respectively) and σ_3 orientated vertical (355/81º). To test whether the principal stresses derived for the reactivation of faults were area specific the data were analysed by locality, i.e. those collected near Psematismenos and those collected near Maroni. The principal stresses resolved for reactivated faults at Psematismenos and Maroni are similar, i.e. in Miocene strata, σ_1; 108/08º : 156/04º (Psematismenos : Maroni), σ_2; 199/08º : 248/15º, and σ_3; 336/79º : 059/74º (Figure 3-33).

To conclude, three deformation events are recognised in the Maroni-Psematismenos Basin: (i) an early phase of NW-SE Late Miocene (Tortonian?) extension, which generated NE-SW faults; (ii) a later phase of NNW-SSE Messinian extension, which generated ENE-WSW faults; and (iii) a late (post-Messinian) phase of NW-SE compression, which led to the reactivation of earlier structures.

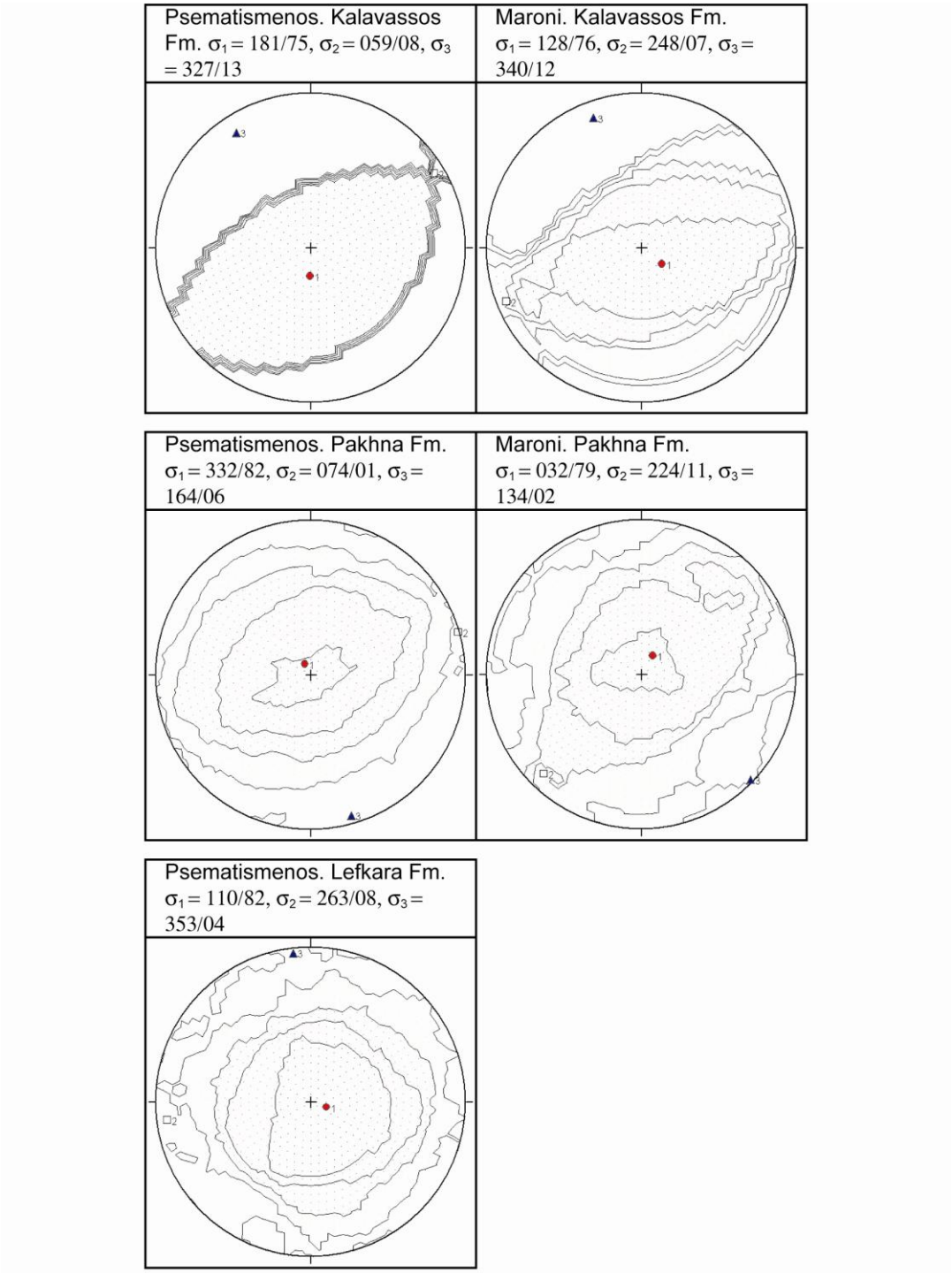

Figure 3-32: Principal stress directions resolved for extensional faults affecting Paleocene strata (Lefkara Formation), Miocene strata (Pakhna Formation) and Messinian deposits (Kalavasos Formation) at (a) Psematismenos; and (b) Maroni/Psematismenos

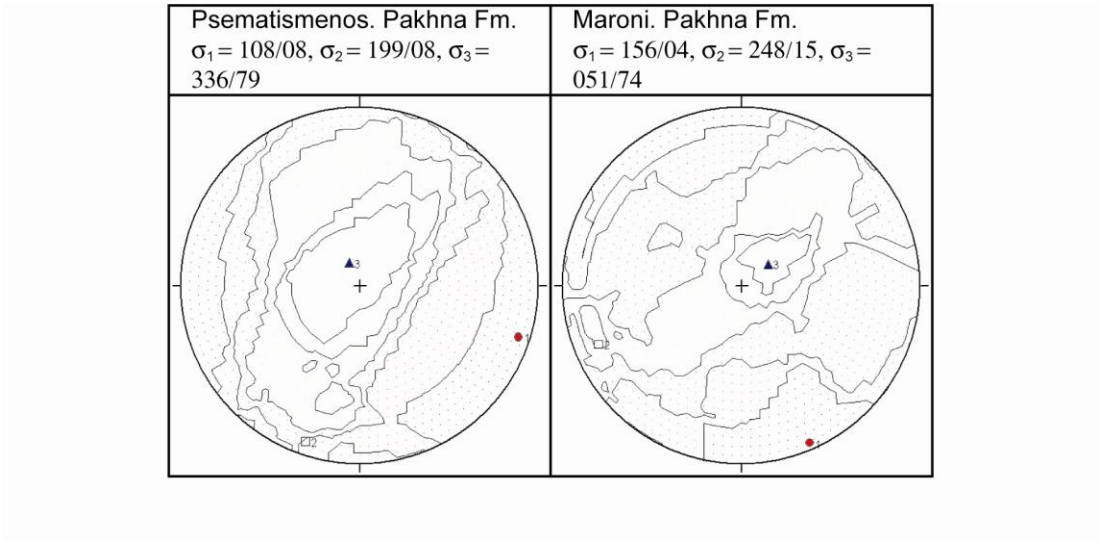

Figure 3-33: Principal stress directions determined for faults in the Maroni Basin , sub-divided by kinematics: lefthand column = principal stress directions determined for extensional structures, righthand column = principal stress directions determined for compressional structures

3.3.3.5 Depositional/tectonic linkages between basins (south coast)

To establish whether syn-depositional linkages could exist between the Neogene extensional basins of south and south-west Cyprus, structural data were collected along several c. north-south transects, between the villages of Kouklia and Dora, Avidimou and Pano Kivides, Choirokoitia and Vavla, Skarinou and Kato Lefkara, and along the Kouris River (Figure 3-34).

Kouklia-Dora transect: Meso-structural data were collected from third-order faults affecting Miocene strata along a north-south transect between Kouklia village and Dora village (Figure 3-34). Faults strike with a preferred orientation of N340-N020 (~ N-S), and dip to the W and E (Figure 3-35). The N-S faults are believed to be normal, due to offset stratigraphic markers and the orientation of drag folds. The N-S faults are believed to have been reactivated during a later phase of compression/transpression. Slickensided surfaces associated with the third-order faults have two slickenlines; one slickenline (with steps as kinematic indicators) indicates a normal dip-slip displacement, the other a strike-slip displacement. This latter movement may have been dextral in nature (determined through examining steps on the slickensided surface).

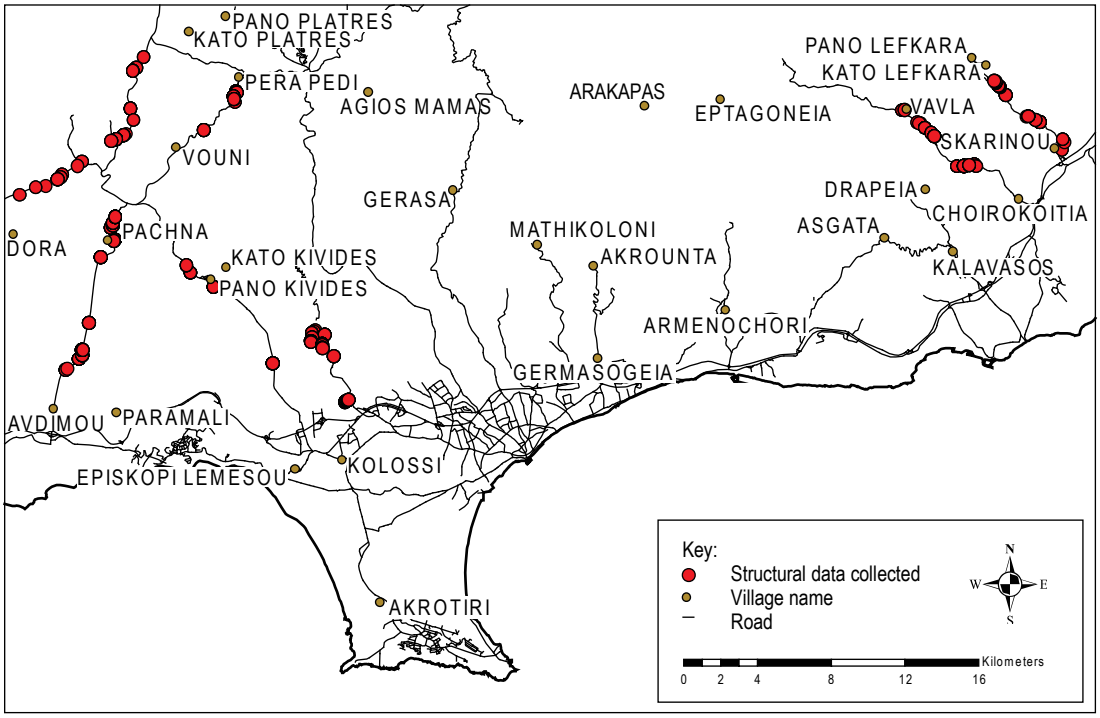

Figure 3-34: Simplified road map of South-central Cyprus. The circles denote sites at which structural data was collected during c. north – south trending transects i.e. from left to right, Kouklia - Dora, Avdimou - Pera Pedi (Kivides), Kouris river, Choirokoitia - Vavla and Skarinou - Kato Lefkara.

Kivides Road transect: Meso-structural data were collected from extensional fractures affecting Paleocene and Miocene strata between the villages of Avdimou, Pera Pedi and Pano Kivides (Figure 3-34; Figure 3-36). Fractures cutting Paleocene chalks strike at a preferred orientation of WNW-ESE to W-E. In contrast, fractures cutting Miocene strata strike at preferred orientations of WSW-ENE and NW-SE.

Kouris River transect: Meso-structural data were collected from extensional fractures affecting Miocene strata in the vicinity of the Kouris River, near Kouris Dam (Figure 3-36). Two main orientations of fractures are evident. The most frequent trend is of WSW-ENE to SW-NE orientated fractures. A second trend is NNW-SSE. This sub-set of faults is interpreted as cross-faults (conjugate sets) to the main, WSW-ENE- to SW-NE-orientated joint sets.

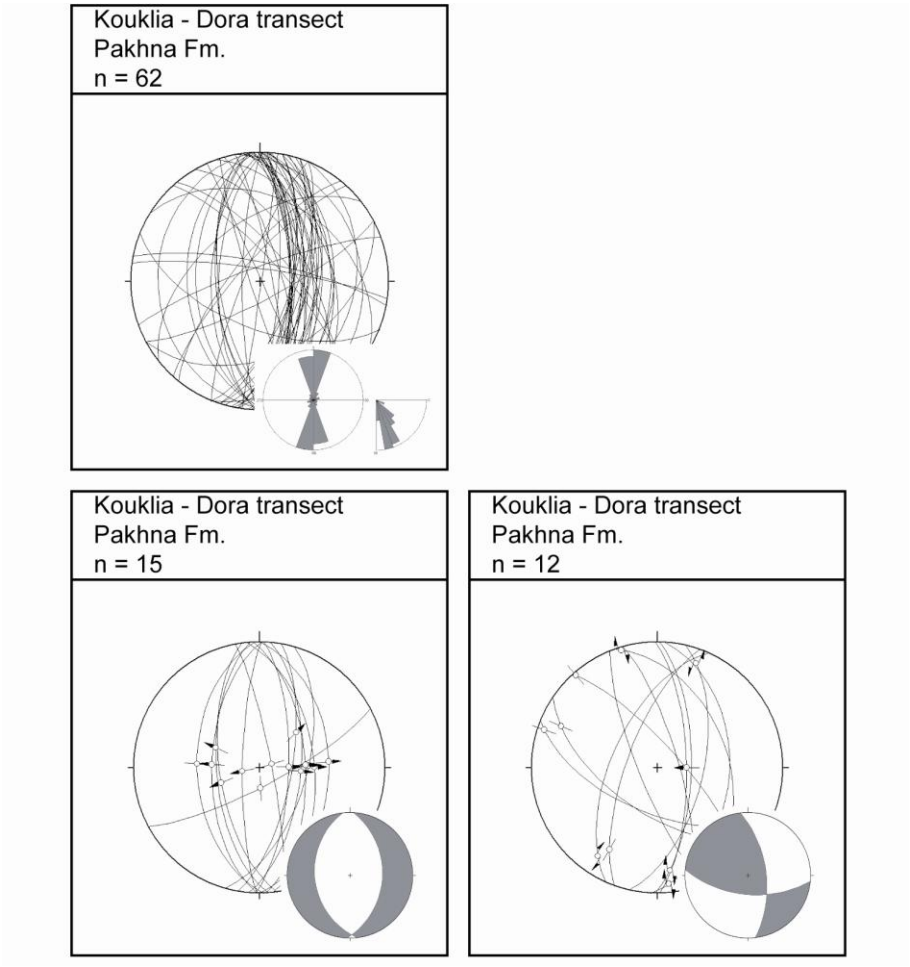

Figure 3-35: Fault data collected from structures affecting Miocene chalks (Pakhna Formation) along a north-south transect between Kouklia and Dora villages.

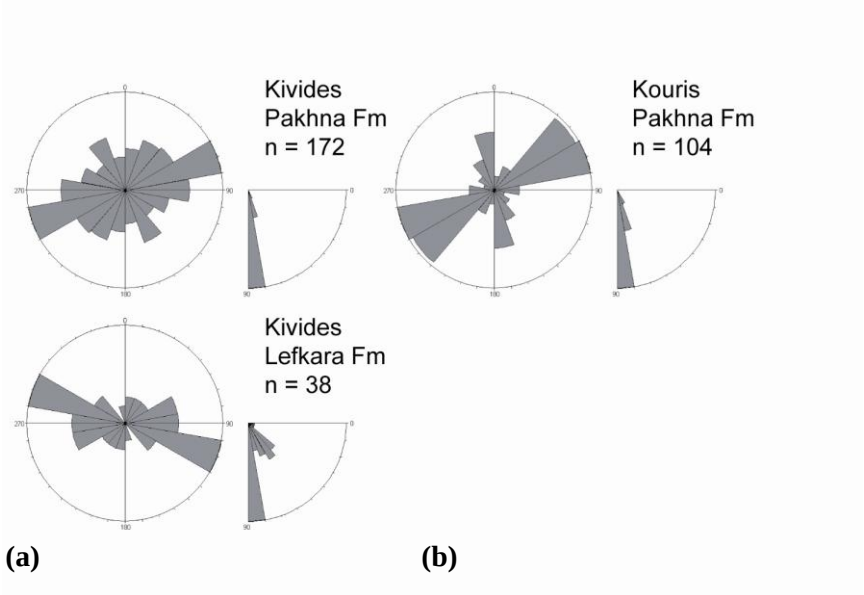

Figure 3-36: Strike directions of joints measured in Miocene chalk at (a) Kivides and (b) in the vicinity of Kouris River, near to Kouris River Dam

Choirokoitia transect: Meso-structural data were collected from faults affecting Paleocene strata along a NW-SE transect between the villages of Choirokoitia and Vavla (Figure 3-34; Figure 3-37) and, from faults affecting Miocene strata at, or near, the Choirokoitia Neolithic settlement. A single population of faults is observed in Paleocene strata at Choirokoitia; faults strike at a preferred orientation of N030-N060 (NE-SW) and dip to both the NW and SE. Three population of faults are observed cutting Miocene strata at Choirokoitia: a (i) N340-N000 (NNW-SSE) striking, ENE- and WSW-dipping set; (ii) N080-N290- (E-W) striking, S-dipping set; and (iii) N000-N020- (NNE-SSW) striking, WNW- and ESE-dipping set. The NNW-SSE- and E-W-striking sets of faults offset strata in a normal sense, and are thus believed to be extensional; where present, slickenlines indicate that this displacement is dip-slip to slight oblique slip. The NNE-SSW-striking set of faults are dextral in nature; slickenlines on the slickensided surfaces indicate that this offset is strike-slip to oblique-slip (dextral to dextral-normal).

Lefkara transect: Meso-structural data were collected from faults affecting Paleocene strata along a NW-SE transect between the villages of Skarinou and Kato Lefkara (Figure 3-38). Faults along this transect strike at a preferred orientation of N040-N070 (NE-SW) and dip to both the NW and SE. Offset marker horizons, the orientation of drag folds and steps on slickensided surfaces all indicate that these faults are normal in nature.

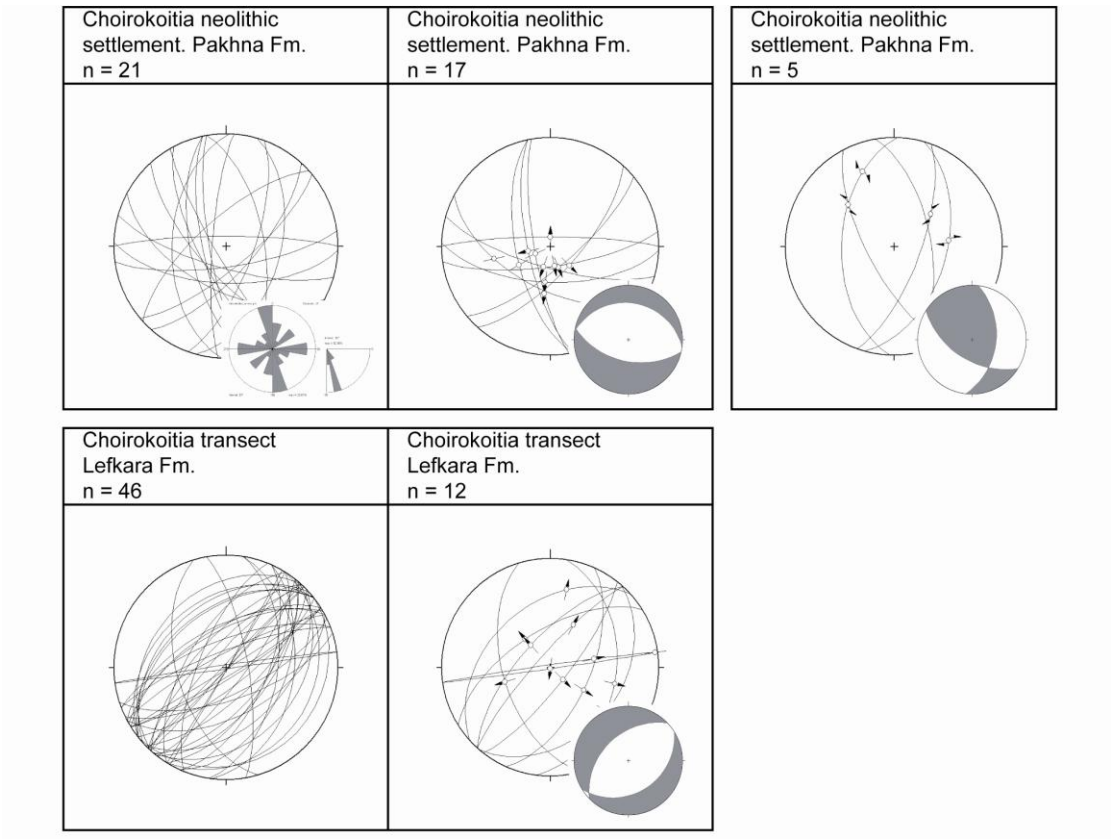

Figure 3-37: Fault data collected from faults affecting Paleocene and Miocene strata in the region around Choirokoitia village.

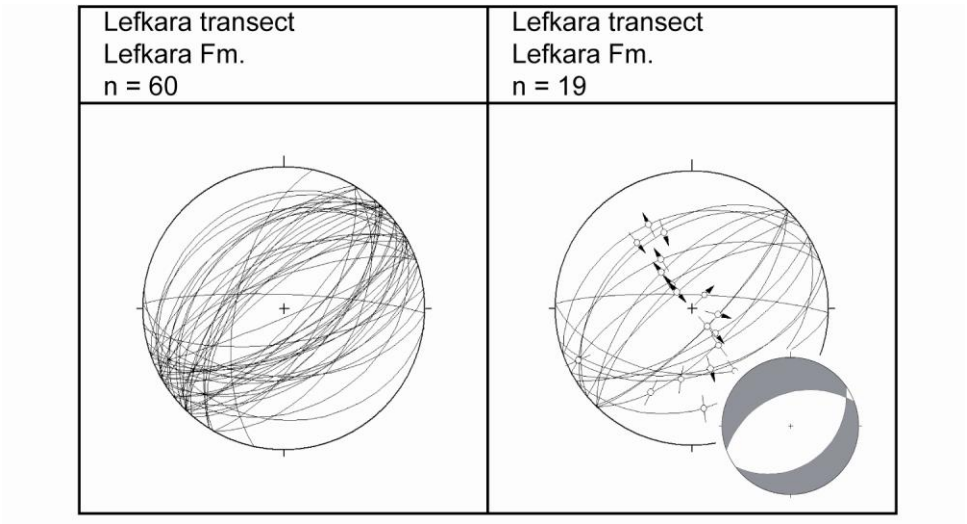

Figure 3-38: Fault data collected from structures affecting Paleocene strata between the villages of Skarinou and Kato Lefkara

The new structural data presented above are now examined to determine if tectonic/depositional linkages occur between the Neogene basins. The deformation phases recognised in each of the studied Neogene basins (Polis, Pissouri and Maroni-Psematismenos) are also observed in adjacent areas, at Kouklia-Dora, between the Polis Graben and Pissouri Basin, and at Choirokoitia-Vavla and Skarinou-Kato Lefkara, NNW of the Maroni-Psematismenos Basin. Late Miocene E-W extension generated ~ N-S-striking faults in Miocene strata at Kouklia, in response to east/west extension, consistent with a σ_1 orientated vertical (335/85º) and σ_2 and σ_3 orientated horizontal (178/05º and 088/02º, respectively; Figure 3-39). The principal stresses resolved for faults at Kouklia, are similar to those determined at Polis and Pissouri.

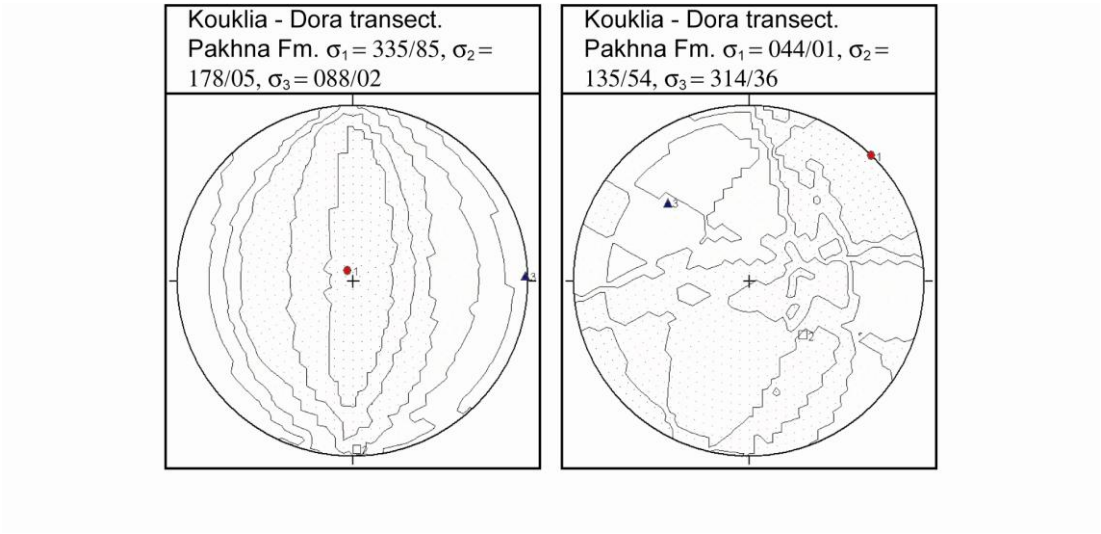

Figure 3-39: Principal stress directions resolved for faults affecting Miocene strata between the villages of Kouklia and Dora, sub-divided by kinematics: lefthand column = principal stress directions determined for extensional structures, righthand column = principal stress directions determined for compressional structures

Late Miocene NW-SE extension generated NE-SW-striking faults in Paleocene strata at Choirokoitia and Kato Lefkara; localised Late Miocene extension generated ~ N-S- and E-W-striking faults in Miocene strata at Choirokoitia. The NE-SW-striking set of structures at Kato Lefkara were generated during northwest/southeast extension, with a σ_1 orientated vertical (123/85º) and σ_2 and σ_3 orientated horizontal (236/02º and 326/05º, respectively). The principal stresses resolved for faults affecting Paleocene strata at Choirokoitia and Kato Lefkara are similar, i.e. σ_1; 093/82º : 209/81º (Choirokoitia : Kato Lefkara), σ_2; 231/06º : 063/63º, and σ_3; 322/05º : 332/05º (Figure 3-40). The N-S- and E-W-striking sets of faults at Choirokoitia Neolithic settlement were generated during north-northeast/south-southwest

extension, with a σ_1 orientated vertical (020/77º) and σ_2 and σ_3 orientated horizontal (281/02º and 191/12º, respectively). The principal stresses resolved for faults at Choirokoitia and Kato Lefkara, are similar to those determined at Maroni and Psematismenos.

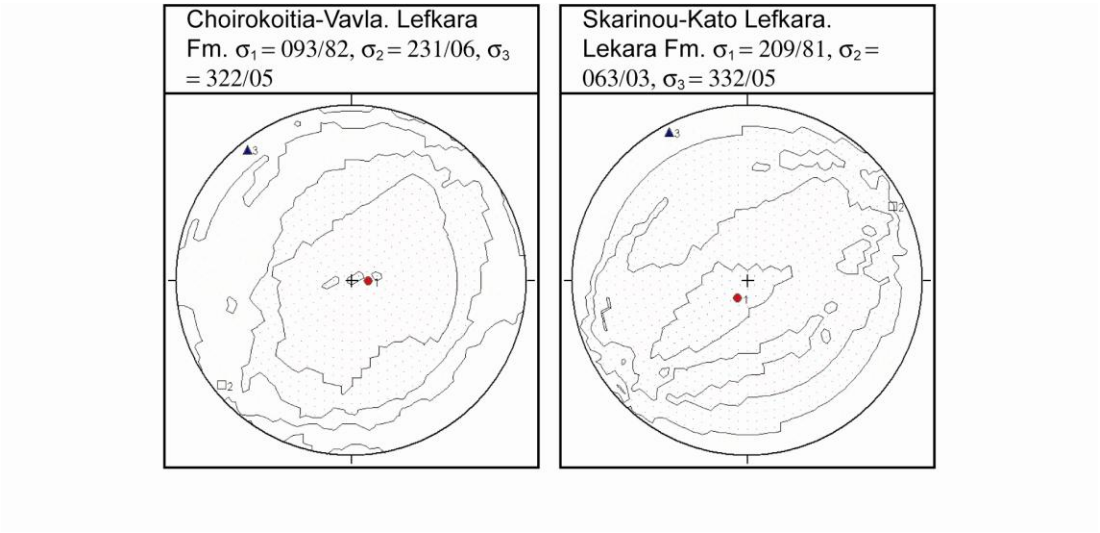

Figure 3-40: Principal stress directions resolved for faults affecting Paleocene strata at Choirokoitia and Kato Lefkara

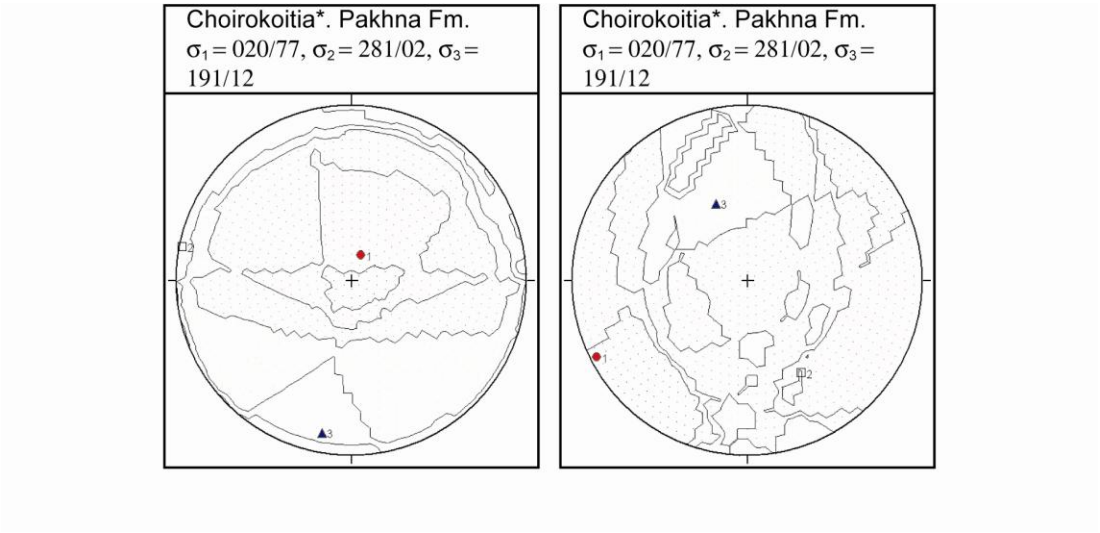

*Figure 3-41: Principal stress directions resolved for Miocene strata at Choirokoitia *Neolithic settlement, sub-divided by kinematics: lefthand column = principal stress directions determined for extensional structures, righthand column = principal stress directions determined for compressional structures*

Many of the normal faults discussed above have been reactivated in a later phase of compression/transpression. The principal stresses resolved for the compressional event at Choirokoitia Neolithic Settlement are consistent with σ_1 and σ_2 orientated horizontal (243/4º

and 150/39º, respectively) and σ_3 orientated vertical (338/51º). Further work is carried out to characterise the nature of this event in later chapters of this thesis.

In summary, Late Miocene extension was a pervasive event and was not restricted to the Neogene basins. Tectonic linkages occur between the southern Neogene basins.

3.3.3.6 The Mesaoria Basin

The Mesaoria Basin is a W-E-trending sedimentary basin located in central Cyprus, between the ophiolitic Troodos Massif to the south and the Kyrenia Range to the north (Figure 3-1). The basin is partly filled by well-dated latest Cretaceous to Quaternary marine to non-marine sediments. 'Syn-rift' sediments include localised Late Miocene reef limestones (Follows et al., 1996), evaporites (Robertson et al., 1995b), Pliocene marginal to shallow-marine deposits (McCallum, 1989; McCallum and Robertson, 1995a,b) and Pleistocene continental deposits (Weber et al., 2006). Follows (1992) and Follows et al. (1996) defined four groups of faults/fractures within the Mesaoria Basin, based on trend, displacement and magnitude: i.e. first-order (basin-bounding) faults, second-order faults, third-order (or minor) faults and extensional fractures. The summary below is based on the work of Follows (1992) and Follows et al. (1996). Figure 3-42 is a simplified geological map of the southern margin of this basin.

First-order faults: Zomenis (1972) and Follows and Robertson (1990) identified basin-bounding, first-order faults along the southern margin of the Mesaoria Basin. The north flank of the Troodos Massif is characterised by a number of sub-parallel normal faults dipping at 50-60º towards the centre of the basin (Follows and Robertson, 1990). Follows and Robertson (1990) estimate vertical displacements of ~ 30-40 m. These faults bound fault blocks, which are strongly forward tilted (i.e. northwards) or more gently back-rotated (i.e. southwards) (Follows and Robertson, 1990; Robertson et al., 1995b). Two main populations of faults were identified: (i) E-W-striking, N-dipping normal faults; and (ii) N-S- to NNE-SSW-striking sinistral faults.

Second- and third- order faults: The north flank of the Troodos Massif is cut by numerous second- and third-order faults, which dissect the first-order fault blocks into smaller segments. Both sets of faults are orientated sub-parallel to the main first-order faults. Follows and Robertson (1990) estimate vertical displacements of 10-30m on second-order

faults, and 1- 5m on third-order faults. Two main populations of faults were identified: (i) E-W-striking, N-dipping normal faults; and (ii) N-S- to NNE-SSW-striking sinistral faults.

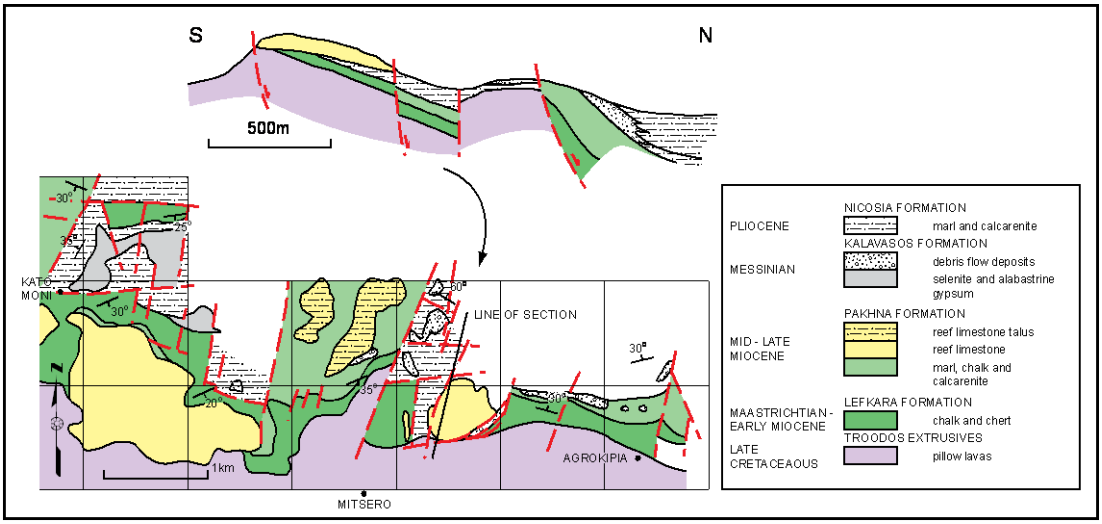

Figure 3-42: Simplified geological map of the Tertiary carbonate facies exposed along the northern flank of the Troodos Massif (modified from Follows, 1992). The location of this figure is shown on Figure 3-2

At present, there is a debate in the literature as to whether the Mesaoria Basin evolved as: a half-graben, in response to backarc extension in the Late Oligocene/Early Miocene; a piggy-back basin, between the active fronts of the Troodos-Larnaka culmination and the Kyrenia fold/thrust belt; or as a pull-apart basin within a left-lateral strike-slip system. Each of these models is discussed in chapter 7. A tectonic model for the evolution of the Mesaoria Basin is not within the remit of this project. New structural data were collected along the southern margin of the Mesaoria Basin. The central and northern parts of the basin were not studied. The data was collected to facilitate comparisions between the Neogene basins to the north and south of the Troodos Massif. This database provides a means to critically appraise existing models of basin evolution for the Mesaoria Basin (Follows and Robertson, 1990; Follows, 1992; McCallum and Robertson, 1995a,b; Robertson et al., 1995b; Follows et al., 1996; Harrison et al., 2004; Calon et al., 2005a,b). Structural data were grouped by either age (of the affected rock) and/or location.

Upper Cretaceous Pillow Lavas: Meso-structural data were collected from minor faults affecting Upper Cretaceous Pillow Lavas of the Troodos Ophiolite Complex at two localities: (a) Polikiton village (Figure 3-43) and (b) Agrokipia village (Figure 3-44). At both localities, faults strike at a preferred orientation of N020-N040 (NE-SW), and dip steeply to

the NW and SE. The slickensided surfaces of the fault planes have well-developed slickenlines, steps associated with the formation of the striations indicate that the faults are sinistral to sinistral-normal.

Paleocene chalks (Lefkara Formation): Meso-structural data were collected from third-order faults affecting Paleocene rocks at two localities: (a) Polikiton (Figure 3-43) and (b) Agrokipia (Figure 3-44). Three populations of faults are observed in Paleocene strata at Polikiton: (i) a N290-N320- (WNW-ESE/NW-SE) striking, NNE- and SSW-dipping set; (ii) a N000-N040- (N-S/NNE-SSW) striking, E- and W-dipping set; and (iii) a N010-N020- (NNE-SSW) striking set of sub-vertical faults. The main fault orientation is WNW-ESE. Faults of a WNW-ESE- and N-S- orientation offset strata in a normal sense; slickenlines, where present indicate dip-slip to oblique-slip displacements. NNE-SSW-striking faults are strike-slip in nature. NNE-SSW-strikings faults cut and offset both the WNW-ESE- and N-S-striking faults in a sinistral sense. The slickensided surfaces of the NNE-SSW-trending fault planes have well-developed slickenlines, steps associated with the formation of the striations indicate that the faults are sinistral to sinistral-normal. A single fault population is observed in Paleocene strata at Agrokipia; faults strike at a preferred orientation of N000-N050 (N-S/NE-SW) and dip to the W.

Miocene chalk (Pakhna Formation): Meso-structural data were collected from faults affecting Miocene strata at several localities, at/or near the villages of: (a) Polikiton (Figure 3-43), (b) Agrokipia (Figure 3-44), (c) Kampia (Figure 3-45a) and (d) Kato Moni (Figure 3-45b). No preferred orientation of faulting was noted in Miocene strata at/or near Polikiton. A single fault population is observed in Miocene strata at Agrokipia; faults strike at a preferred orientation of N280-N300 (WNW-ESE) and dip to the NNE and SSW. WNW-ESE-striking faults at Agrokipia offset Miocene strata in a normal sense (e.g. offset stratigraphic markers); where present, slickenlines indicate that this displacement is dip-slip.

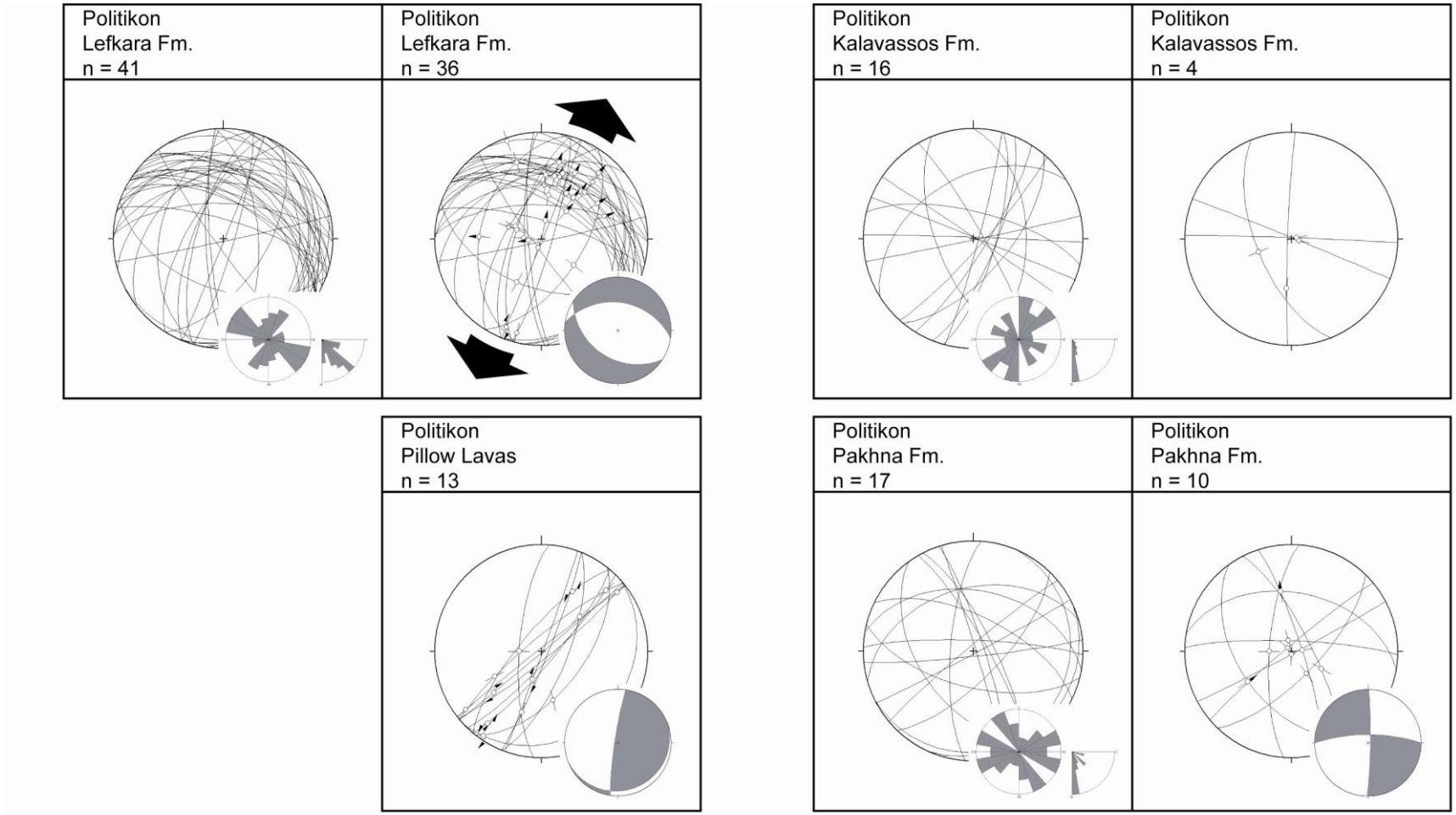

Figure 3-43: Fault data collected from structures affecting Late Cretaceous Troodos Pillow Lavas, Paleocene chalk (Lefkara Formation), Miocene chalk (Pakhna Formation) and Messinian evaporites (Kalavasos Formation) at/or near Polikiton village

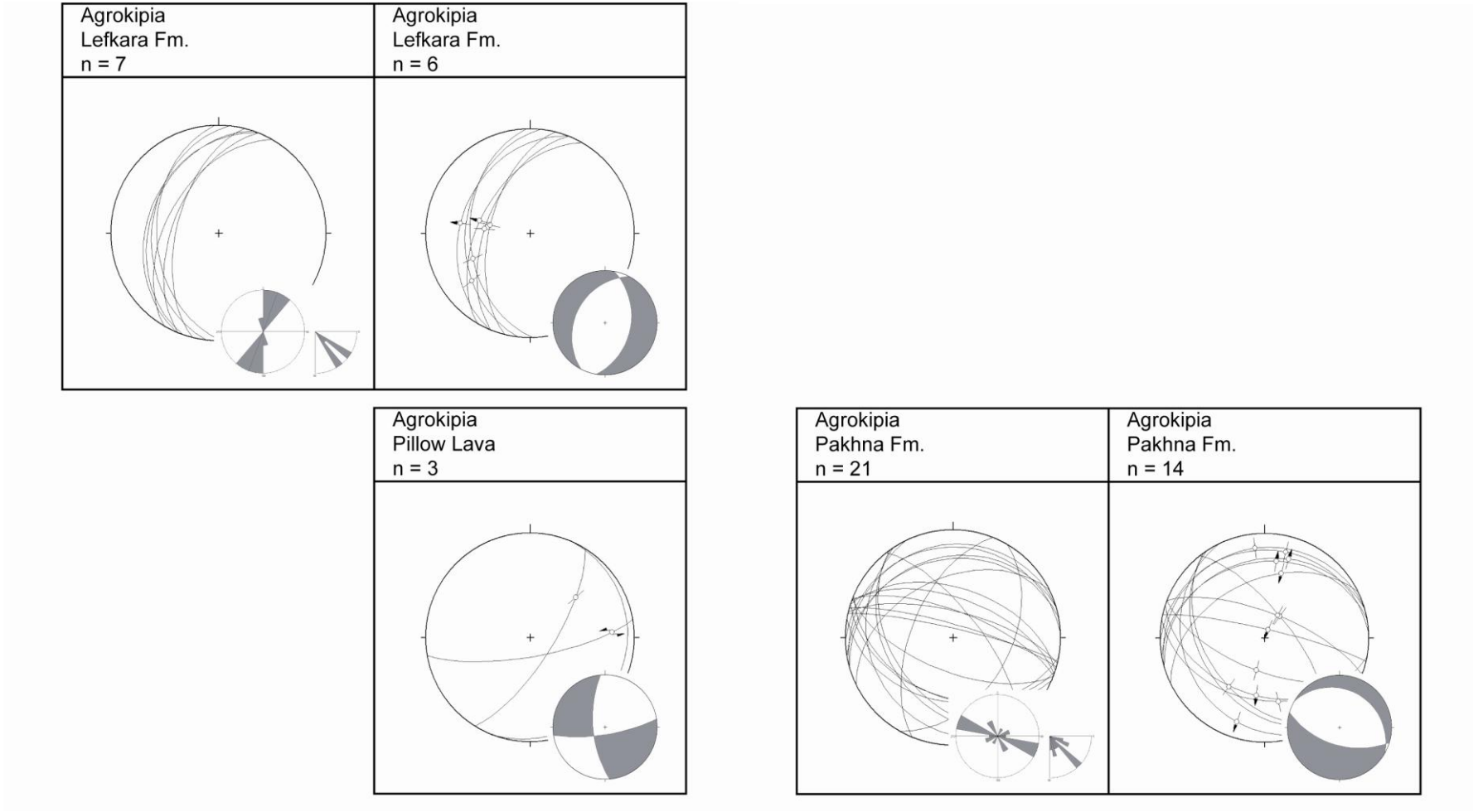

Figure 3-44: Fault data collected from structures affecting Late Cretaceous Troodos Pillow lavas, Paleocene chalk (Lefkara Formation) and Miocene chalk (Pakhna Formation), at/or near, Agrokipia village

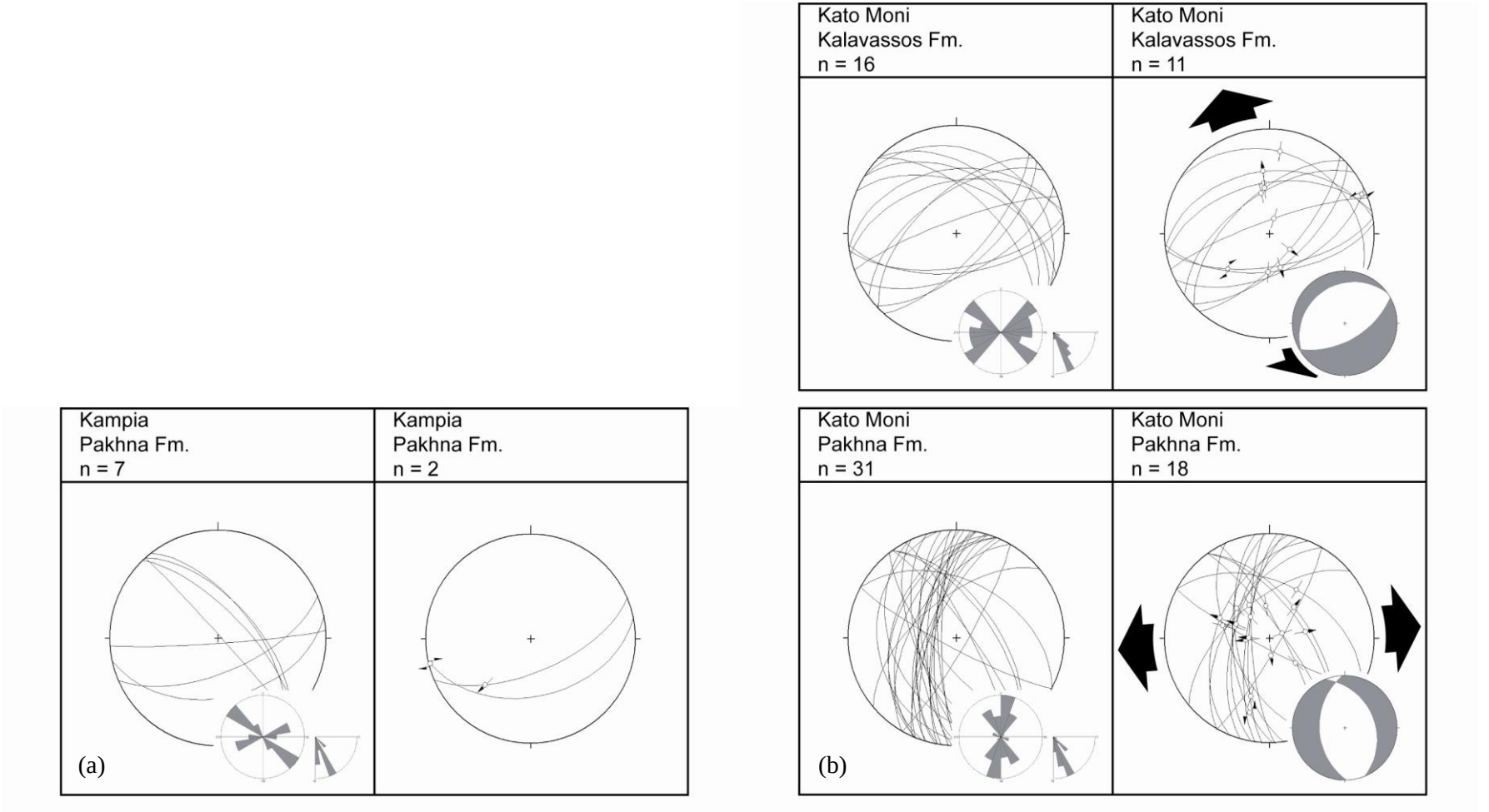

Figure 3-45: Fault data collected from structures affecting Miocene strata at/or near (a) Kampia village and (b) Kato Moni

Faults at Kampia strike in a similar direction to those at Agrokipia (Figure 3-44; Figure 3-45). In contrast, faults affecting Miocene strata at Kato Moni strike at a preferred orientation of N000-N020 (NNE-SSW) and dip to the WNW. NNE-SSW-striking faults at Kato Moni offset Miocene strata in a normal sense (e.g. offset stratigraphic markers); where present, slickenlines indicate dip-slip displacements.

Messinian evaporites (Kalavasos Formation): Meso-structural data were collected from faults affecting Messinian strata at two localities: (a) Polikiton (Figure 3-43) and (b) Kato Moni (Figure 3-45b). No preferred orientation of faulting was noted in Messinian strata at/or near Polikiton. No fault-slip data were obtained at Polikiton. At Kato Moni faults strike at a preferred orientation of N040-N070 (WSW-ENE) and dip to the NNW and SSE. This population of faults offsets Messinian strata in a normal sense (e.g. offset stratigraphic markers); when present, slickenlines indicate that this displacement is dip-slip.

Follows and Robertson (1990) argue that the first evidence of tectonic instability in the Mesaoria Basin occurred during the Tortonian, as recorded in the deposition and deformation of the Pakhna Formation. Tectonic disturbance resulted in Pakhna Formation strata being tilted a few degrees to the north. They argue that syn-depositional E-W-striking, normal faults controlled the location and development of Tortonian Koronia Member reefs. E-W striking depocentres were compartmentalised by NE-SW-trending transverse faults (Follows and Robertson, 1990). Follows and Robertson (1990) believe that the E-W-trending faults were still active in the Messinian and Early Pliocene.

Figure 3-46 illustrates the distribution/orientations of faults affecting Paleocene to Pleistocene strata along the southern margin of the Mesaoria Basin. Three populations of faults are identified: (i) N-S/NNE-SSW-striking normal faults; (ii) WSW-ENE-striking normal faults; and (iii) compartmentalising NNE-SSW/NE-SW-striking strike-slip faults.

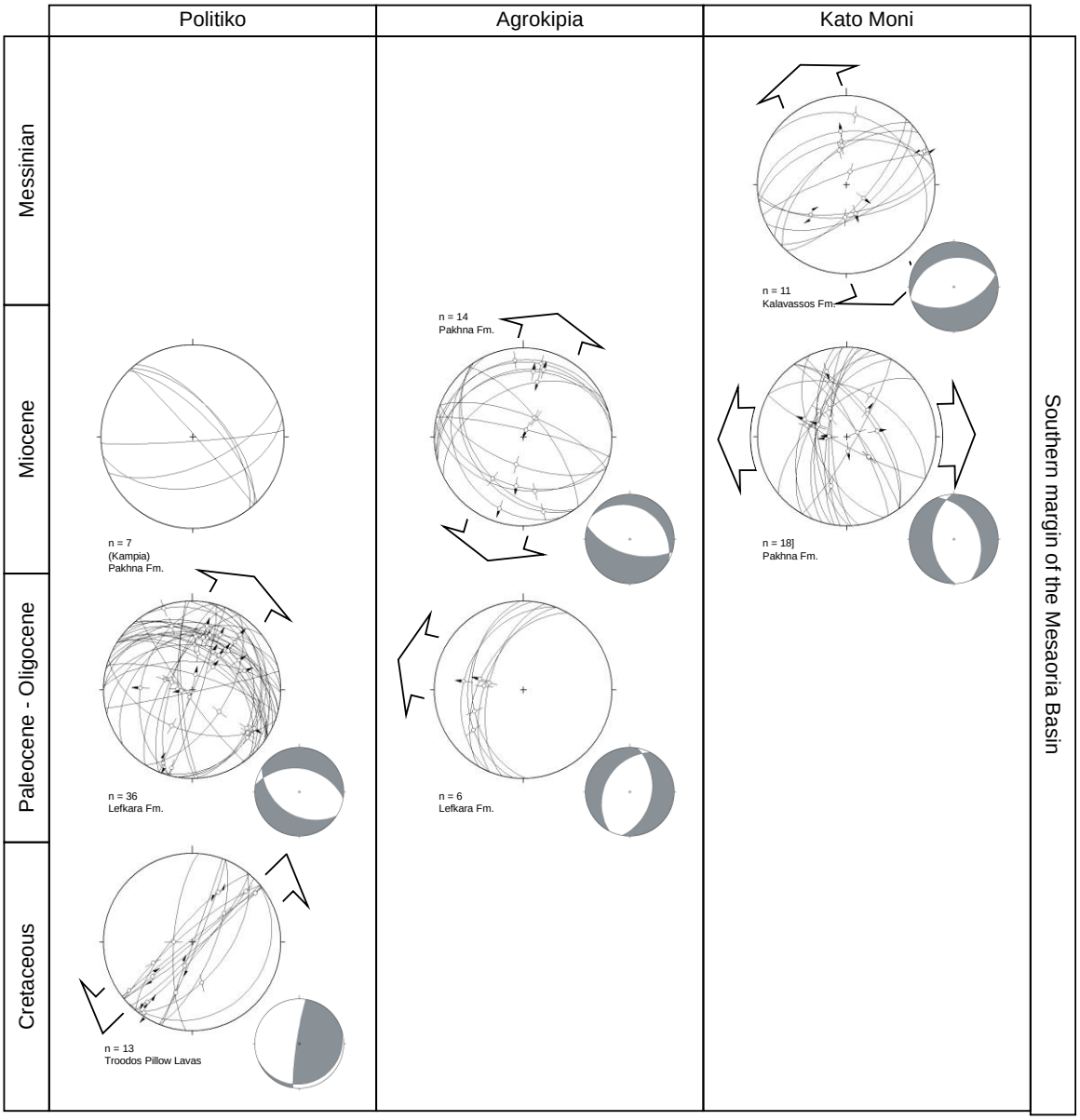

Figure 3-46: New structural data collected from faults affecting each of the main stratigraphic intervals: the Cretaceous, the Paleocene-Oligocene, the Early to Late Miocene and the Late Miocene (Messinian). The data are separated by temporal and spatial divisions (see description in text)

Field observations described above indicate that the N-S/NNE-SSW-striking set of faults are the oldest, with faults affecting Paleocene and Miocene chalks. The ENE-WSW-striking set of faults are believed to be younger, with faults affecting Messinian gypsiferous deposits. Faults of a N-S orientation affect Paleocene strata at Agrokipia and Miocene strata at Kato Moni (Figure 3-46). Faults of an ~ E-W orientation affect Paleocene strata at Polikiton, Miocene strata at Agrokipia and Messinian strata at Kato Moni (Figure 3-46). The N-S-striking set of faults were generated during northwest to east/west extension, with a σ_1 orientated vertical (053/84º) and σ_2 and σ_3 orientated horizontal (286/04º and 196/05º, respectively; Figure 3-47). The ENE-WSW-striking set of faults were generated during north-

northwest/south-southeast extension, with a σ_1 orientated vertical (163/82º) and σ_2 and σ_3 orientated horizontal (359/08º and 264/02º; Figure 3-47).

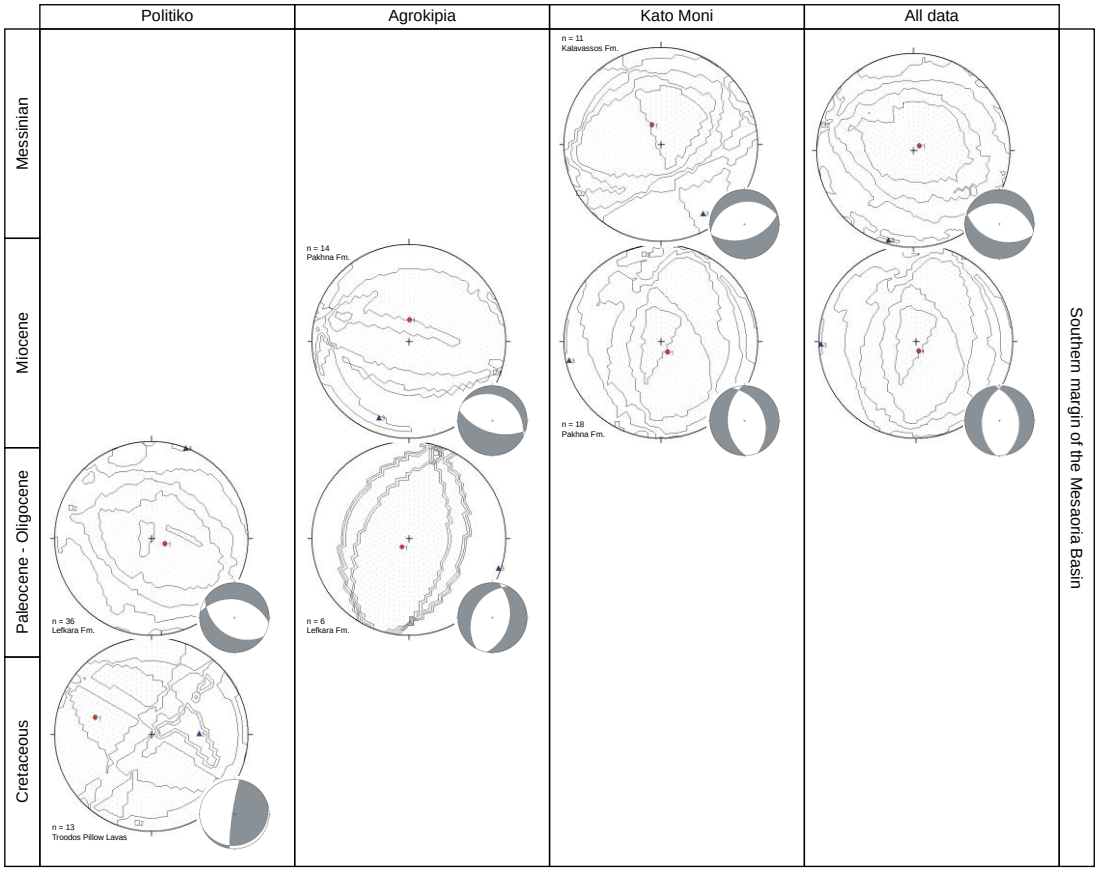

Figure 3-47: Principal stress directions resolved for faults affecting Late Cretaceous Pillow Lavas at Polikiton, Lefkara Formation chalk at Polikiton and Agrokipia, Pakhna Formation chalk at Agrokipia and Kato Moni and Kalavasos Formation evaporites at Kato Moni

The new data indicates that E-W extensional stress propagated along the southern margin of the Mesaoria Basin from the east to the west in the Middle to Late Miocene; and that N-S extensional stress propagated along the southern margin of the Mesaoria Basin from the east to the west in the Late Miocene (to Early Pliocene?). NE-SW- to NNE-SSW-striking transverse faults offset Paleocene to Messinian strata, N-S- and E-W-striking normal faults in a sinistral sense. Similar NNE-SSW/NE-SW-striking sinistral faults were mapped by R. Harrison and the Cyprus Geological Survey in the Lefkosia (Nicosia) Area (Figure 3-48; Harrison et al., 2004b) and by G. McCay in the Kyrenia Range (G. McCay, personal communication). This would suggest that the NNE-SSW/NE-SW striking faults extend across the Mesaoria Basin.

In summary, three different deformation events are recognised along the southern margin of the Mesaoria basin: (i) an early phase of E-W Middle to Late Miocene extension, which generated N-S faults; (ii) a later phase of NNE-SSW Late Miocene extension, which generated WNW-ESE faults; and (iii) a third event, which formed NE-SW- to NNE-SSW-striking sinistral faults. The latter event is believed to be longlived: NNE-SSW-striking faults were active during the initiation of E-W- and N-S-striking extensional faults (Follows and Robertson, 1990) and continue to be active at present (Harrison et al., 2004b).

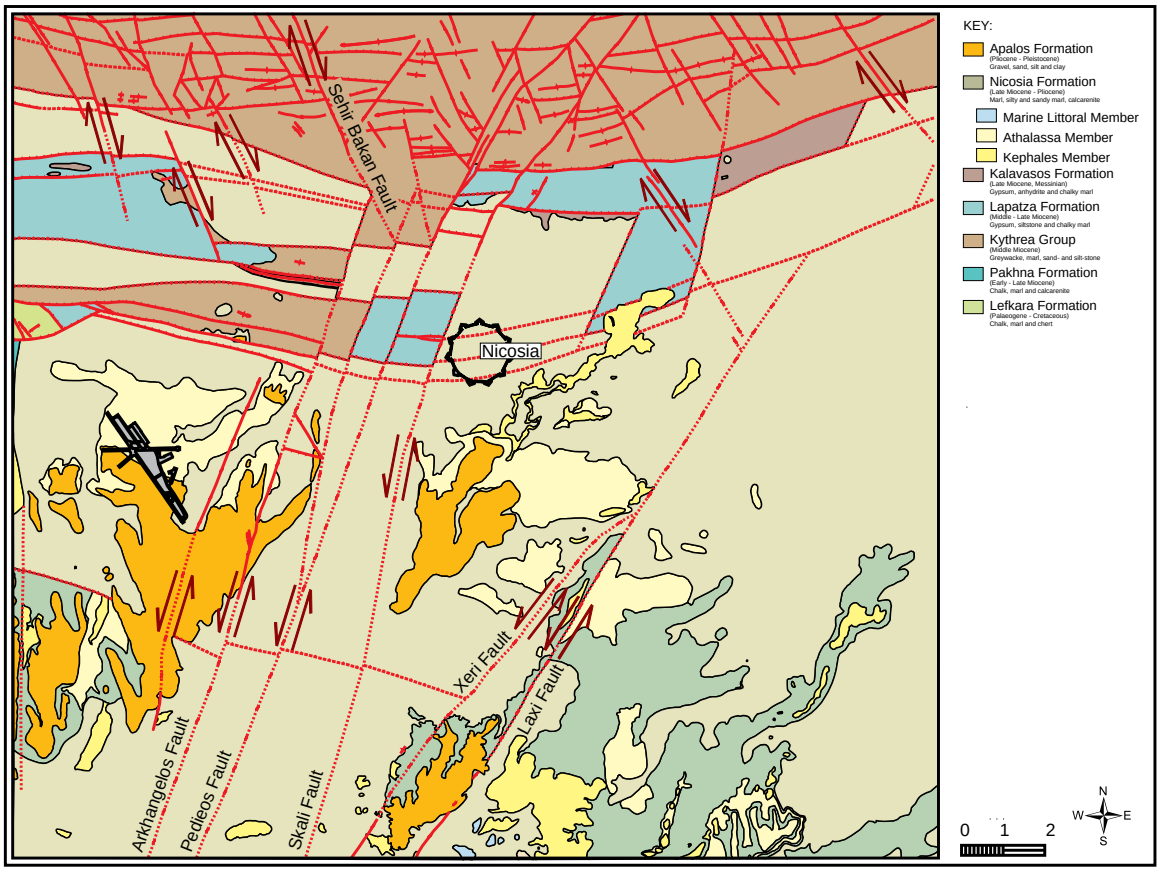

Figure 3-48: Geological map of the Greater Lefkosia (Nicosia) area (Harrison et al., 2004b). The map illustrates the trend of faults in the Lefkosia region – note, the continuation of NNE-trending strike-slip faults across the Mesaoria Basin. Structures discussed in chapter 7 are named

3.3.4 Late Pliocene to Recent structural framework

3.3.4.1 The Agia Marinouda - Kouklia Fold

The Agia Marinouda – Kouklia fold is an arcuate, NW-SE-trending antiform of deformed Paleocene to Miocene strata and Pleistocene marine sediments. The Agia Marinouda – Kouklia fold outcrops parallel to the coast, between Geroskipou town and Kouklia village. A

transverse strike-slip zone, the Ktima fault system of Soulas (1999), separates the Agia Marinouda – Kouklia fold belt into two segments: (i) between Kouklia village and the Khapotami River mouth – a distance of c. 3km (The Kouklia Fold); and (ii) between Agia Marinouda and the Paphianna hotel, to the NE of Geroskipou – a distance of ~ 3km (The Agia Marinouda Fold) (Figure 3-49).

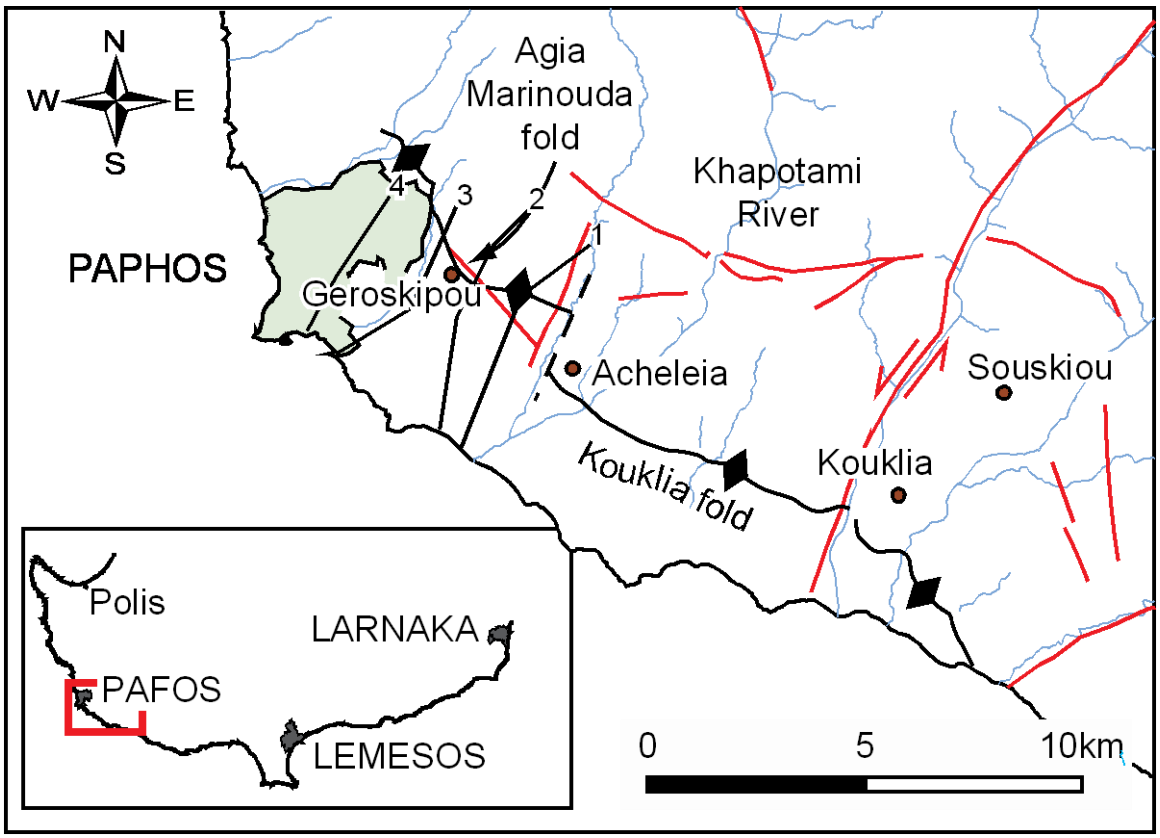

Figure 3-49: Simplified structural map of southwest Cyprus indicating the approximate location of the Agia Marinouda Fold. The location of the cross-sections shown in Figure 7-22 and Figure 7-23 are shown

The geometry of the Kouklia Fold varies along strike: to the northwest the fold is approximately cylindrical, with a sub-vertical axial plane trending 150°E; to the southeast the fold is sigmoidal, with a west-vergent axial plane undulating between 010° and 145° (Soulas, 1999). The geometry of the Agia Marinouda fold is constant along strike. At Agia Marinouda, in the town of Geroskipou, the anticline axis is seen to strike at ~ 105° between the Krochatis River (which follows a small transverse fault – striking 028°) and the Paphianna hotel. The axial plane of this segment of the fold is sub-vertical (Soulas, 1999).

Several key areas warrant fuller description:

Kouklia. The Kouklia fold locally deforms a Pleistocene marine terrace at the Happy Valley junction of the Paphos-Lemesos highway. Middle to upper Pleistocene marine terrace deposits are tilted to sub-vertical on the western flank of the fold and to 45° on its eastern flank.

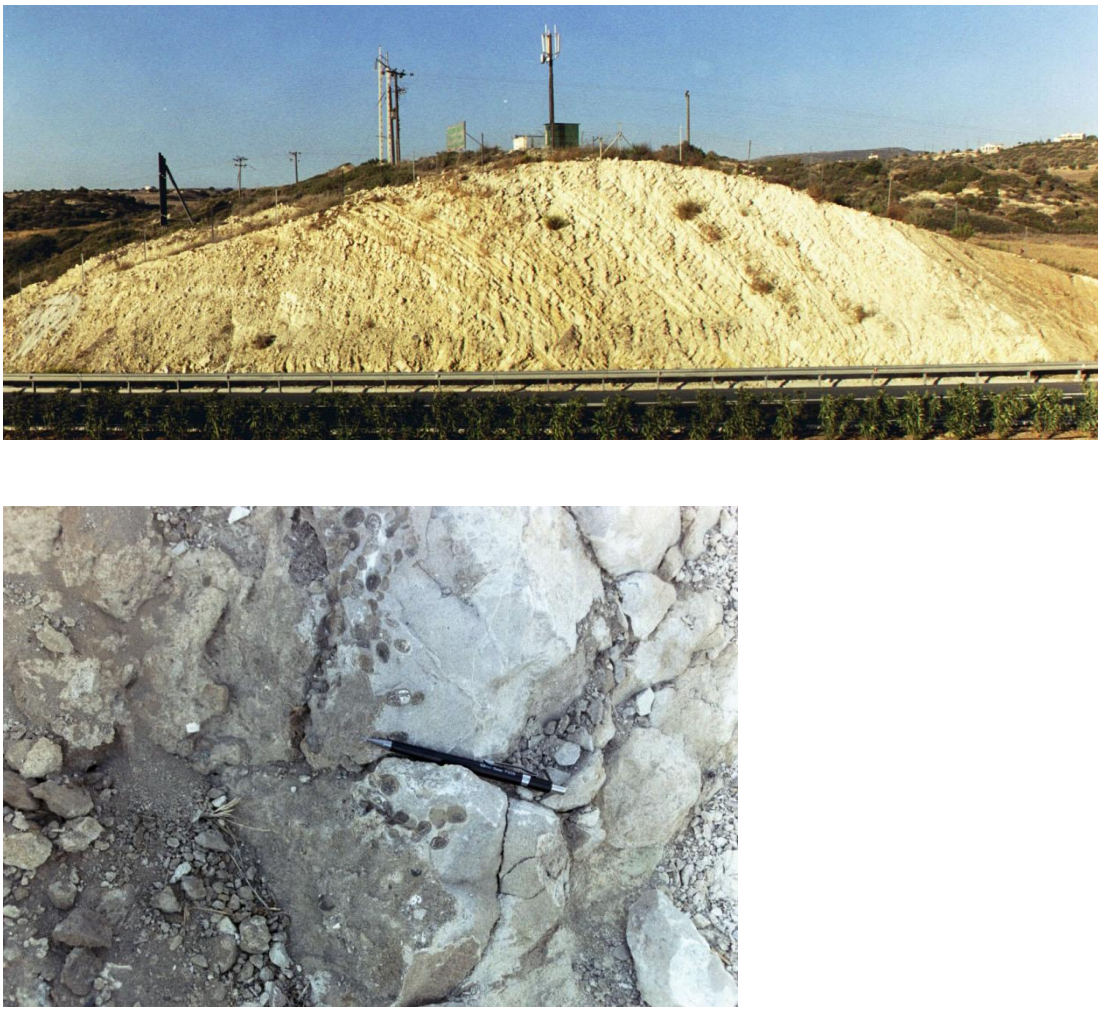

Figure 3-50: The Kouklia fold: (top) Pakhna strata deformed as an anticline (the hinge of the fold is exposed in the bottom left of the photograph); (bottom) Tilted marine terrace. Burrowing bivalves indicate that the surface was previously exposed at sea level.

Geroskipou. To the north of Geroskipou, where the axial trace of the fault passes the Miji stream (which follows a small transverse structure – striking ~ N030°), the fold locally deforms a 15 metre-thick succession of middle Pleistocene to Holocene sediments (Figure 3-51). Rhythmically bedded colluvial deposits and palaeosols are preserved on the northern flank of the Agia Marinouda fold, in the village of Geroskipou. This strata is believed to have been deposited during active growth of the fold, as: (i) late middle Pleistocene sediments rest unconformably, but with only slight angular discordance (c. 5-10°) on Paleocene – Oligocene deepwater Lefkara Formation chalks (Figure 3-51); (ii) middle Pleistocene strata at the base

of the succession has a dip of >50º; whereas (iii) late Pleistocene strata at the top of the succession dip at a few degrees (~ 1-5º) to near horizontal.

Figure 3-51: Syn-tectonic tilting of a late Pleistocene to Holocene sequence of palaeosols and colluvium indicates growth of the Agia Marinouda fold during the late Pleistocene. Photographs taken looking west

Agia Marinouda. To the north of the church in Agia Marinouda, and behind the Agia Marinouda fold, a sequence of WNW-ESE-trending, NNE-dipping faults cut Paleocene strata (Figure 3-52). Fault plane solutions suggest that the tectonic regime responsible for the generation of these faults was characterised by broadly NNE-SSW compression.

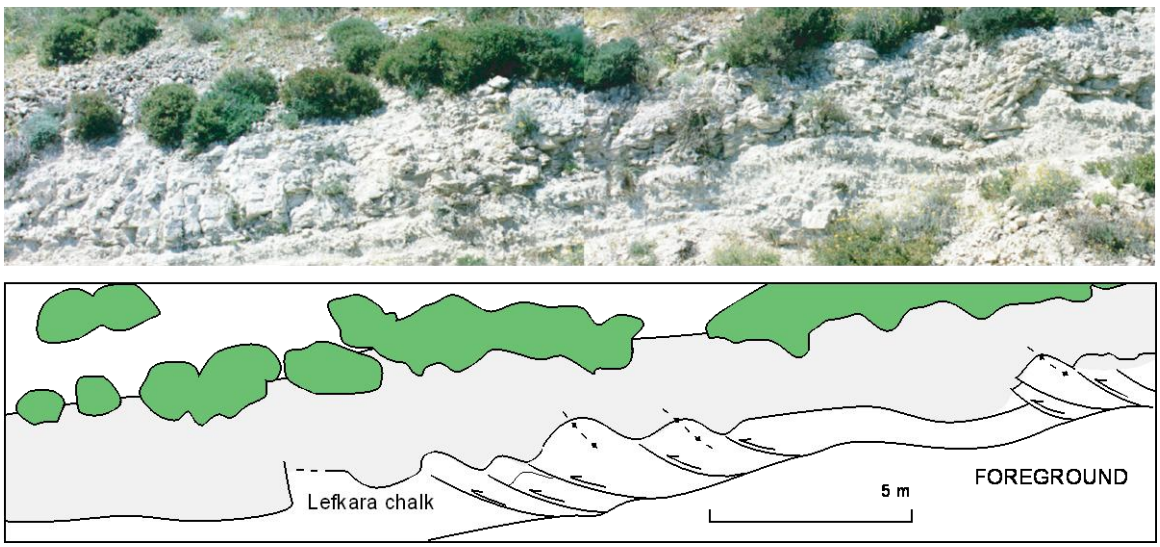

Figure 3-52: Top to the SW thrusts in Paleocene chalk, north of Agia Marinouda church. Photograph taken looking west

Acheleia. At Acheleia Dam, to the north of the Agia Marinouda Fold, a sequence of NNE-SSW-trending, predominately ESE-dipping faults cut Miocene strata (Figure 3-54; Figure 3-53).

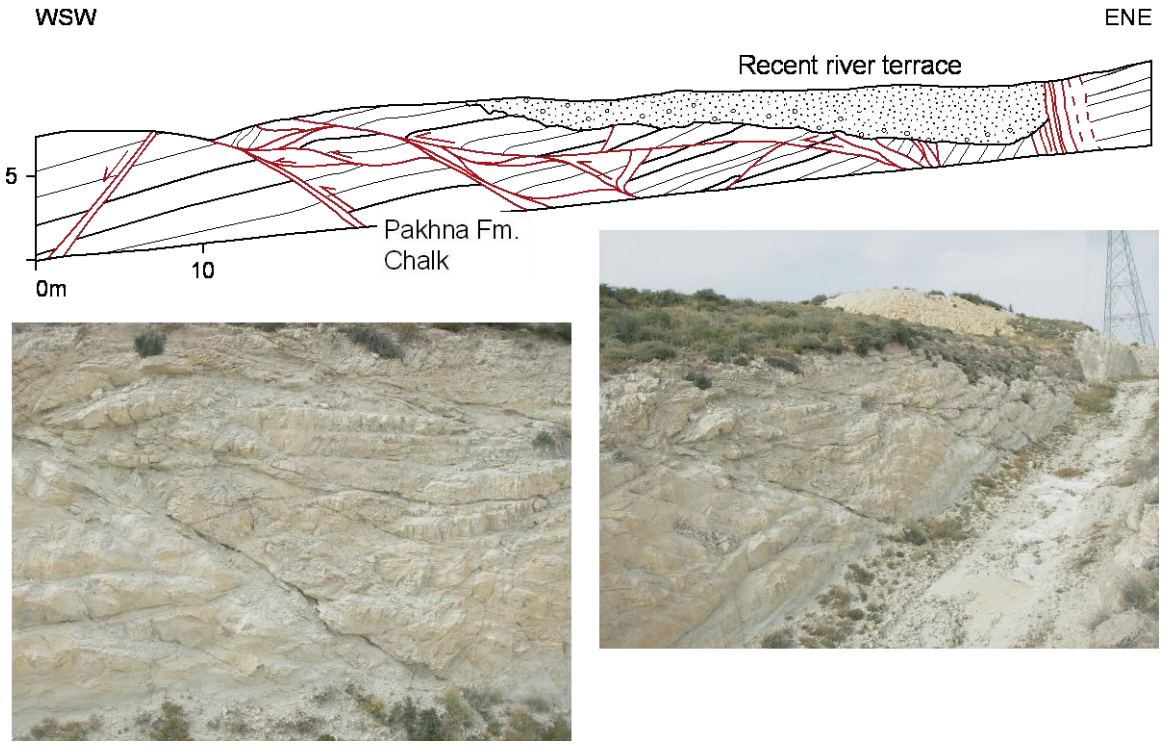

Figure 3-53: Top to the SW thrusts in Miocene chalk, near Acheleia Dam (modified from Soulas et al., 2005). Photographs illustrate extensional collapse in the footwall and thrust geometries in the hangingwall. Photographs taken looking west

The faults strike at a preferred orientation of N020-N040 (NNE-SSW to NE-SW) and dip predominantly to the ESE. Elsewhere in the area, NNE-SSW-striking faults dip to the ESE and WSW (Figure 3-54). The faults shown in Figure 3-53 are clearly reverse; slickenlines (with steps as kinematic evidence) on the fault planes indicate that this displacement is reverse dip-slip. In the wider area, both normal and reverse NNE-SSW- and NE-SW-striking faults are observed (Figure 3-53).

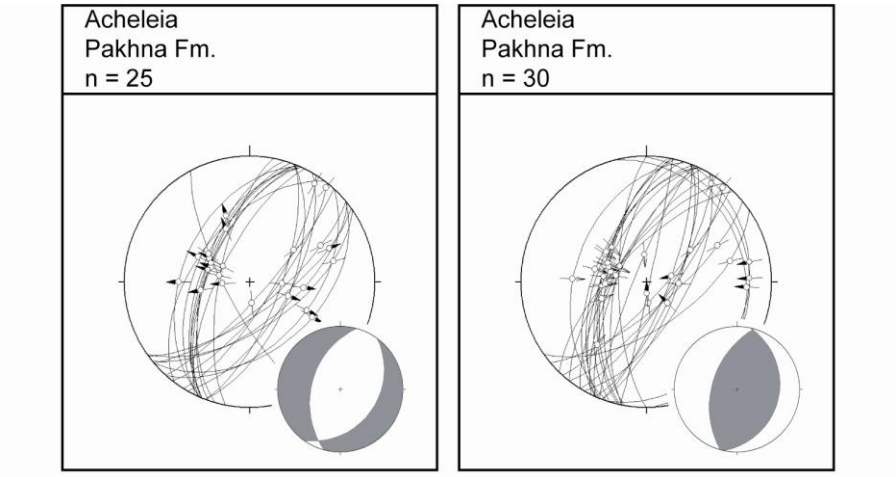

Figure 3-54: Fault data collected from structures affecting Miocene strata at Acheleia Dam.

Acheleia Industrial Park (Eurogum Quarry). Further south, in the Acheleia Industrial Park (Eurogum Quarry), a prominent NNE-SSW-striking, ESE-dipping fault juxtaposes Lefkara Formation chalk and chert (in the footwall) against Pakhna Formation chalk (in the hangingwall) (Figure 3-55). This structural/stratigraphic configuration is only possible if the fault was originally normal (or transtensional), i.e. the fault was generated during a phase of WNW-ESE extension. However, slickenlines on the slickensided surface of the NNE-SSW-orientated fault reveal a different kinematic history; steps associated with the development of the slickenlines indicate that the latest displacement was reverse dip-slip (top-to-the-west thrusting), i.e. the fault must have subsequently been reactivated during a phase of broadly WNW-ESE compression. Elsewhere in the quarry, comparable NNE-SSW-trending, WNW- and ESE-dipping faults cut Paleocene (Lefkara Fm) and Miocene (Pakhna Fm) strata. The slickensided surfaces of these faults shed further light on the neotectonic history of this site. Several of the surfaces have two discrete slickenlines (orientated orothogonal to one another), steps associated with the development of these slickenlines indicate two displacements: one implies normal dip-slip and one implies reverse oblique-slip (Figure 3-56).

The NNE-SSW-striking set of faults were generated during west-northwest/east-southeast extension, with a σ_1 orientated vertical (054/78º) and σ_2 and σ_3 orientated horizontal (203/10º and 294/16º, respectively; Figure 3-57); and reactivated during west-northwest/east-southeast compression, with a σ_3 orientated vertical (070/71º) and σ_1 and σ_2 orientated horizontal (261/19º and 170/03º, respectively).

Figure 3-55: Abandoned quarry at the Eurogum factory, Acheleia Industrial site. The fault plane in the centre of the photograph trends NNE-SSW; and juxtaposes Pakhna Formation chalk (in the hangingwall) against Lefkara Formation chalk and chert (in the footwall)

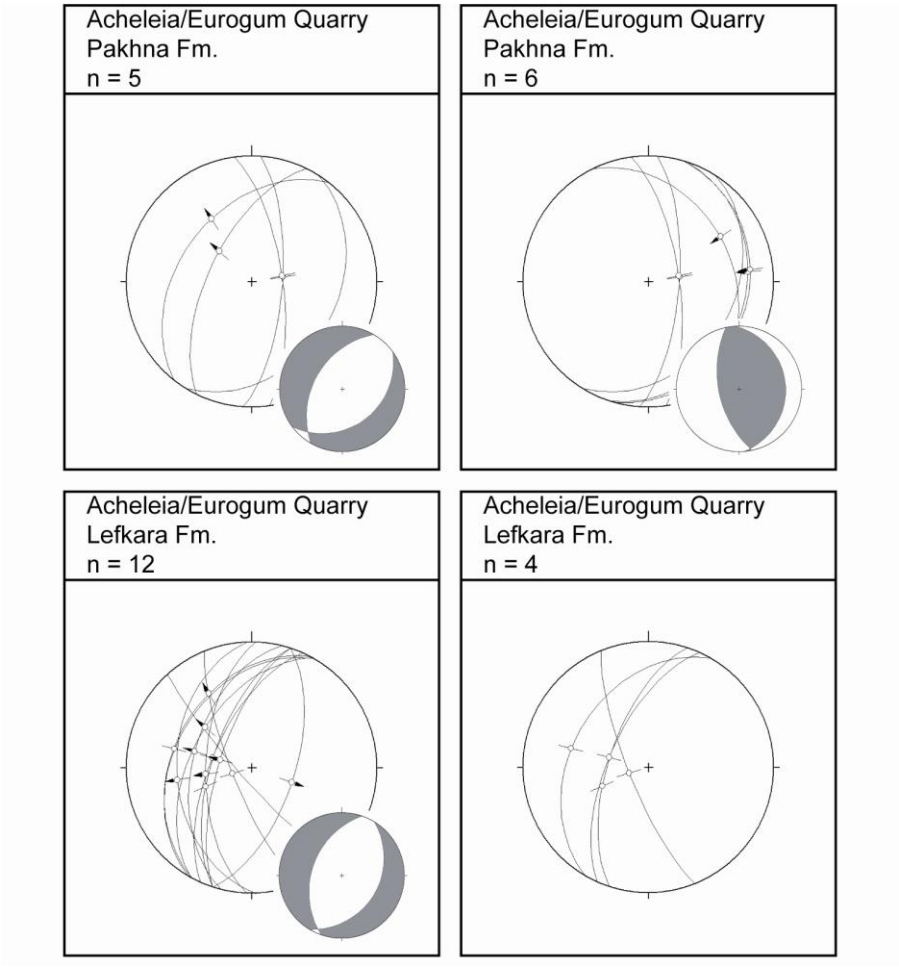

Figure 3-56: Fault data collected from structures affecting Paleocene and Miocene strata at the Eurogum Quarry, Acheleia

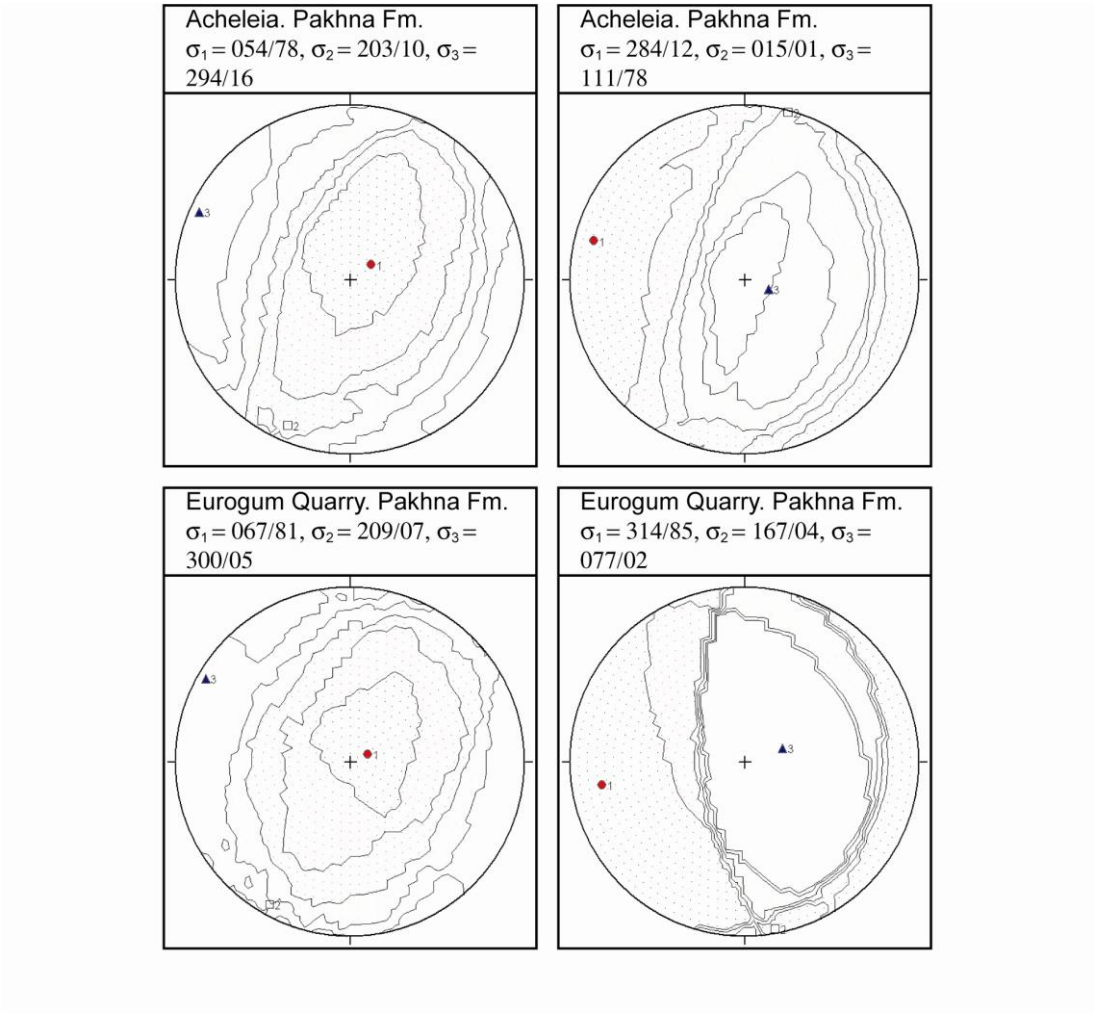

Figure 3-57: Principal stresses resolved for structures affecting Miocene strata in the Acheleia village region, sub-divided by kinematics: lefthand column = principal stress directions determined for extensional structures, righthand column = principal stress directions determined for compressional structures

3.3.4.2 Kolossi

The Kolossi Lineament (or alternatively, the Trakhoni fault system of Soulas (1999)) is a belt of deformed Pakhna Formation chalks, Nicosia Formation marls and Pleistocene gravels, overlain unconformably by Holocene? soils and gravels. It is located to the south/southwest of Lemesos, and extends from Episkopi Bay (south of Kourion), through the villages of Vounaro and Trakhoni to Akrotiri Bay (Figure 3-58). The lineament is thought to be a continuation of structures seen offshore in seismic surveys (McCallum et al., 1993; Ben-Avraham et al., 1995; Vidal et al., 2000a,b).

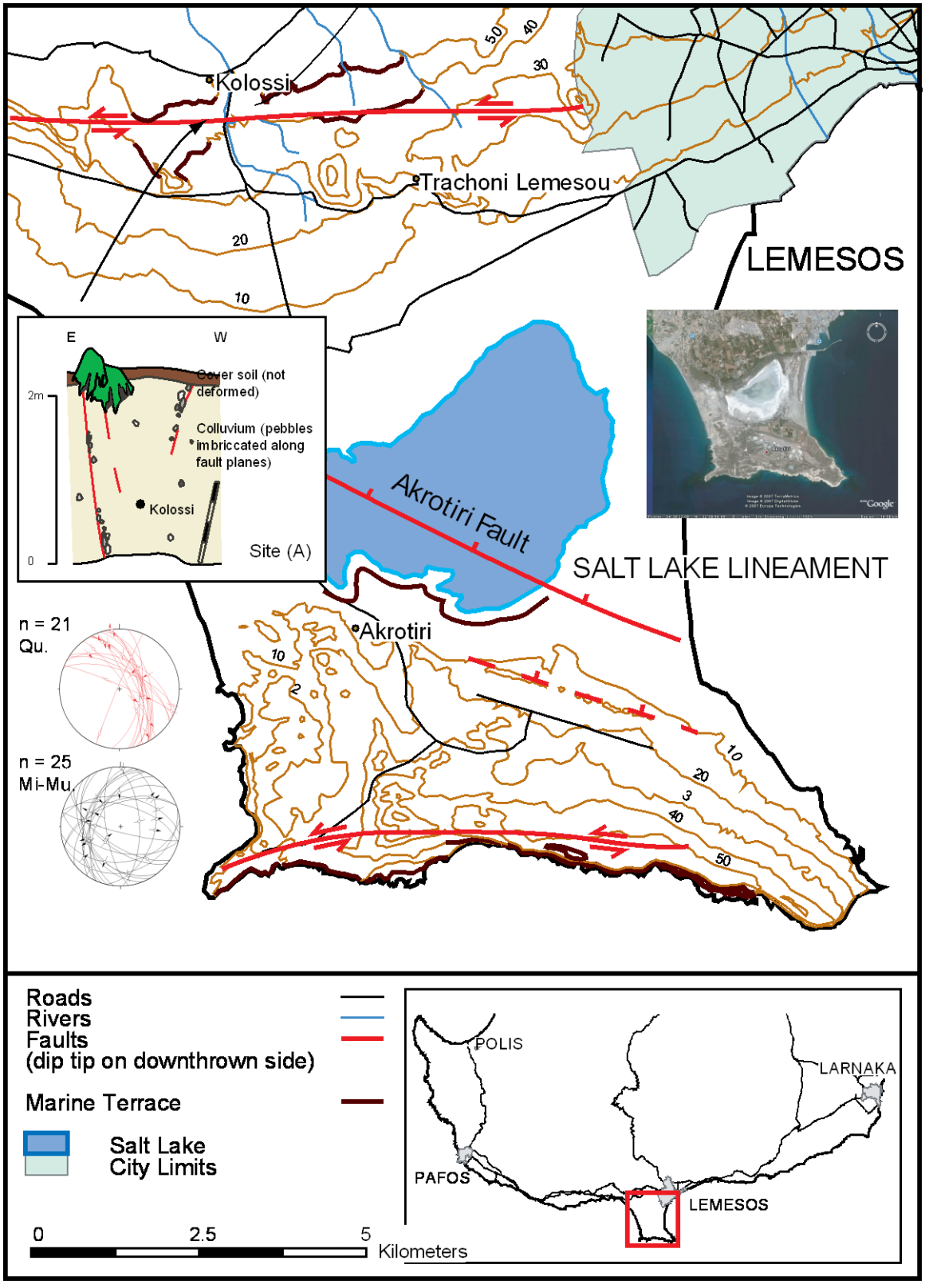

Figure 3-58: Map of the Kolossi area. The approximate location of the Kolossi and Akrotiri Faults are shown. The insets include (in a clockwise direction): (a) sketch of the section sampled/profiled for OSL dating at the Kolossi football stadium, (b) satellite image of the Kolossi/Lemesos region, clearly illustrating the Akrotiri Fault and (c) fault plane data, including slickenline lineations, for the Kolossi Fault. The NNE-SSW- and NNW-SSE-striking faults are interpreted as conjugate faults to the main E-W trend (see chapter 5, section 5.5.2). Abbreviations are as follows: Mi-Mu = Pakhna Formation, Qu = Quaternary

The lineament is mainly identified by remote sensing methods (i.e. satellite imagery and aerial photography), as it is largely obscured by intensive agricultural activity and the suburban development of Lemesos. Analysis of historical maps (Ortelius, 1573; Janssonius, 1652; Coronelli, 1692; in Soulas, 1999) suggests that the Kouris River has altered its course, historically, along the trend of the Kolossi Lineament. Borehole studies (Greitzer and Constantinou, 1968; Soulas, 1999) indicate a juxtaposition of Miocene and Pliocene units. The fault is believed to be a complex left-lateral strike-slip system, with sub-vertical to slightly inclined fault planes (Soulas, 1999).

3.3.4.3 Arakapas/Gerasa

Figure 3-59 illustrates the distribution of faults in the Germasogeia-Agios Mamas-Eptagoneia region. The faults can be spilt into two populations: a northerly set, between Agios Mamas and Eptagoneia, of the Arakapas Fault Belt (see section 3.3.1.1) and a southerly set, between Gerasa and Parekklisia, of the Gerasa Fault Belt (see section 3.3.2.1). It has recently been suggested that the Arakapas Fault Belt, i.e. the northerly fault set, was reactivated in the Quaternary in a left-lateral sense, and that the Gerasa lineament was reactivated in a right-lateral sense (Soulas, 2003).

Six groups of faults and fractures have been identified in the Germasogeia-Agios Mamas-Eptagoneia region, based on topographic breaks and depressions, stream/ridge offsets and fault scarps (Soulas, 2003):

i. The Arakapas Fault Zone, between Agios Mamas and Eptagoneia, is comprised of E-W-trending, sub-vertical faults, with sub-horizontal displacements (Figure 3-59);
ii. The Agios Konstantinos fault zone trends WSW-ENE for up to 10 to 11 km (Figure 3-59). It diverges from the Arakapas Fault Zone at Arthrakos, 3 km west of Kato Khorio village. It is divided into two segments: between Zoopigi and Agios Pavlos village, the fault is sub-vertical with a left-lateral sense of displacement; and east of Agios Konstantinos, where the fault separates into a further three splays, each sub-vertical with sub-horizontal movements;
iii. The Limassol Forest frontal thrust, which trends NW-SE between Agios Mamas and Parekklisia, a distance of 4.5 - 5 km (Figure 3-59);
iv. The Gerasa fault system trends sub-parallel to the Limassol Forest frontal thrust, between Agios Mamas and Parekklisia (Figure 3-59). It is believed to be a sub-vertical, en echelon, right-lateral strike-slip system (Soulas, 2003).

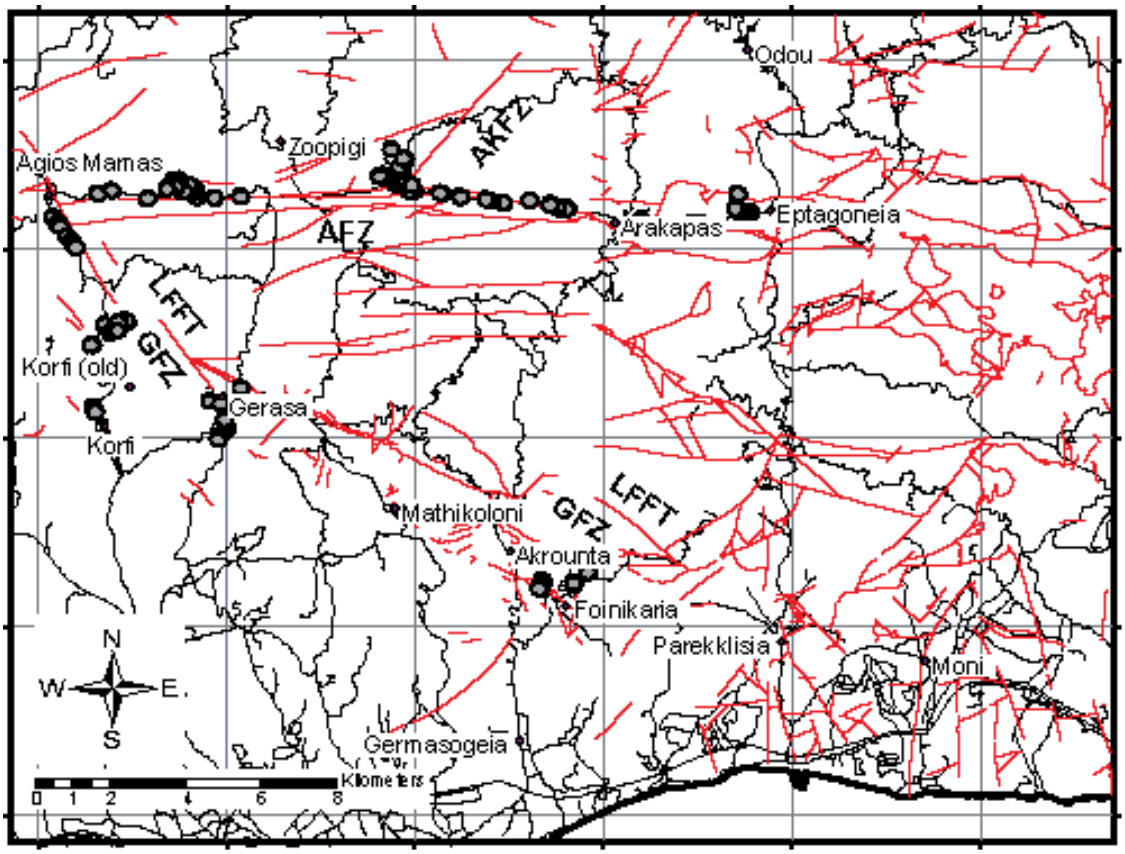

Figure 3-59: Distribution of faults in the Germasogeia-Agios Mamas-Eptagoneia area. Red lines denote faults and faint black lines denote roads. The grey circles denote sites from which fault orientation/slip data were collected. Abbreviations as follows: AFZ = Arakapas Fault Zone, AFFZ = Agios Konstantinos Fault Zone, GFZ = Gerasa Fault Zone and LFFT = Limassol Forest Frontal Thrust. The locations of villages discussed in the text are shown. This map was created from a GIS database supplied by the Cyprus Geological Survey Department.

v. The Moniatis fault system, between Agios Mamas and Pano Platres, comprised of two sets of sub-parallel, WNW-ESE-trending, sub-vertical faults, with right-lateral displacements; and

vi. The Pelendria fault system, to the east of Pelendria village, comprised of WNW-ESE, sub-vertical faults, with left-lateral displacements.

To determine if the Arakapas and Gerasa Fault Belts have been reactivated in the Quaternary, new structural data was collected from faults affecting Cretaceous to Paleocene strata in each fault zone. Localities at which structural data were collected are shown in Figure 3-59. Structural data are grouped by locality and the age of the affected rock.

Eptagoneia: Meso-structural data were collected from faults affecting Upper Cretaceous Sheeted Dykes and Pillow Lavas of the Troodos ophiolitic complex at/or near the village of Eptagoneia. Faults in the Sheeted Dyke Complex (SDC) strike at a preferred orientation of

NW-SE and dip to the SW (Figure 3-60a). Two populations of faults are observed cutting the pillow lavas: (i) NNW-SSE-striking, ENE- and WSW-dipping right-lateral faults; and (ii) ENE-WSW-striking, NNW- and SSE-dipping left-lateral faults (Figure 3-60). The sense of shear on all faults was determined from the slickensided surface of each fault, slickenlines on this surface frequently develop with small steps which indicate the direction of movement. Additionally, in faults affecting sheeted dykes, offset dykes and drag folds were used as evidence of kinematic behaviour; and in faults affecting pillow lavas, drag folds. A number of different displacements were noted within the Sheeted Dykes: several faults are dextral/dextral-normal (40.0% of total number of faults measured); several faults are normal dip-slip (33.3%); several faults are sinistral (20.0%); and the remainder are reverse dip-slip (6.7%).

Arakapas: Meso-structural data were collected from Upper Cretaceous Sheeted Dykes and Pillow Lavas at/or near the village of Arakapas. Faults in the Sheeted Dykes strike at a preferred orientation of WNW-ESE and dip to the SSW (Figure 3-60b). A similar trend is observed in faults affecting Pillow Lavas at Arakapas (Figure 3-60b). Faults affecting the Sheeted Dykes and Pillow Lavas share similar displacement characteristics: in trend, kinematics and sense. A number of different displacements are noted (kinematic indicators are as listed above): most faults are sinistral (58.5%), but dextral (14.6%), normal (22.0%) and reverse (4.9%) faults do occur in smaller abundance.

Konstantinos: Meso-structural data were collected from faults that affect the Sheeted Dykes in the vicinity of the village of Konstantinos. In general, faults strike with a preferred orientation of W-E and dip to the S. A minor sub-set of faults strike at a preferred orientation of NNW-SSE and dip to both the W and E (Figure 3-61). The majority of displacements are sinistral (80.0%; kinematic indicators are as listed above). Less common are dextral (16.7%) and normal (3.3%) faults.

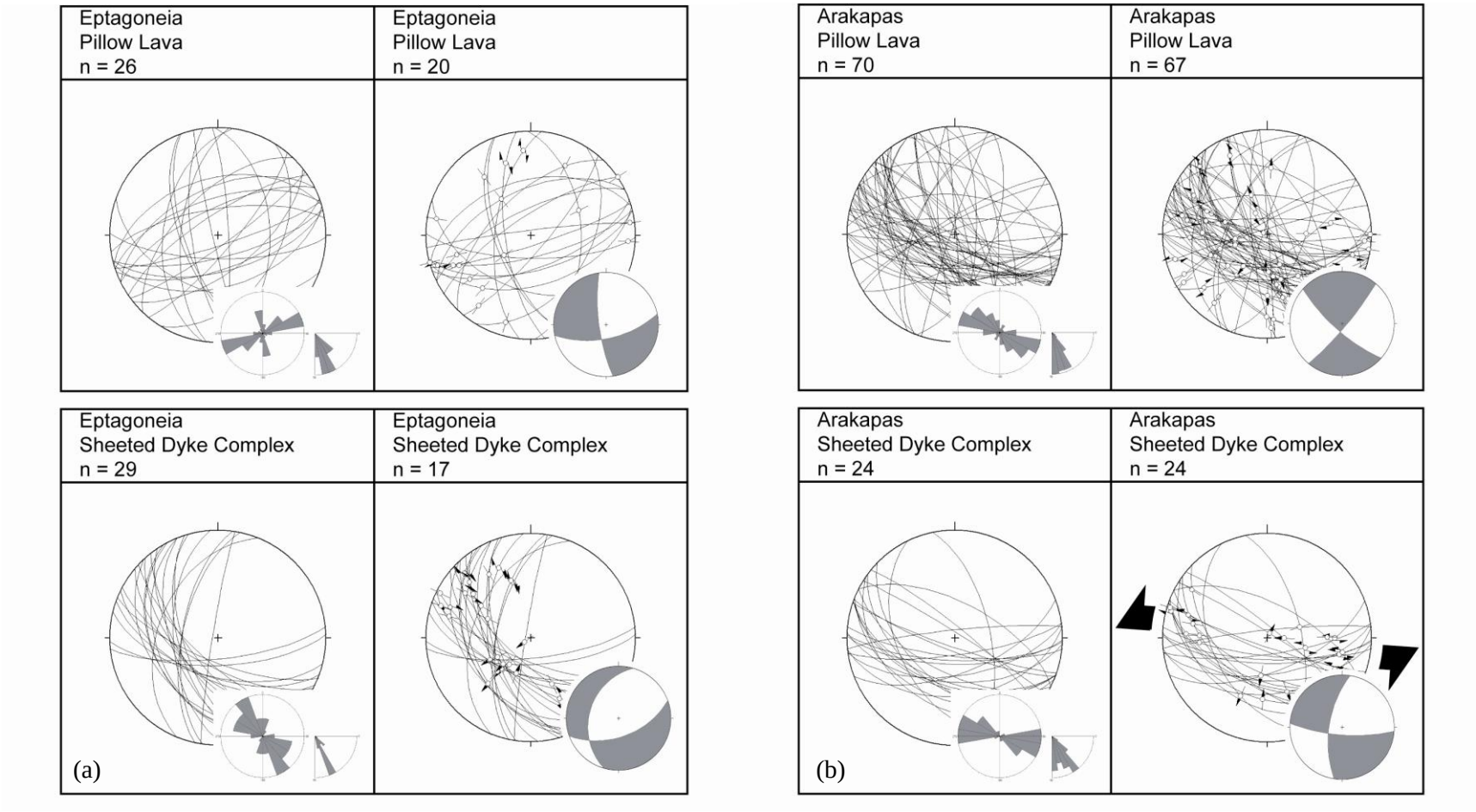

Figure 3-60: Fault data collected from structures affecting Upper Cretaceous Sheeted dykes and Pillow Lavas at/or near (a) Eptagoneia and (b) Arakapas

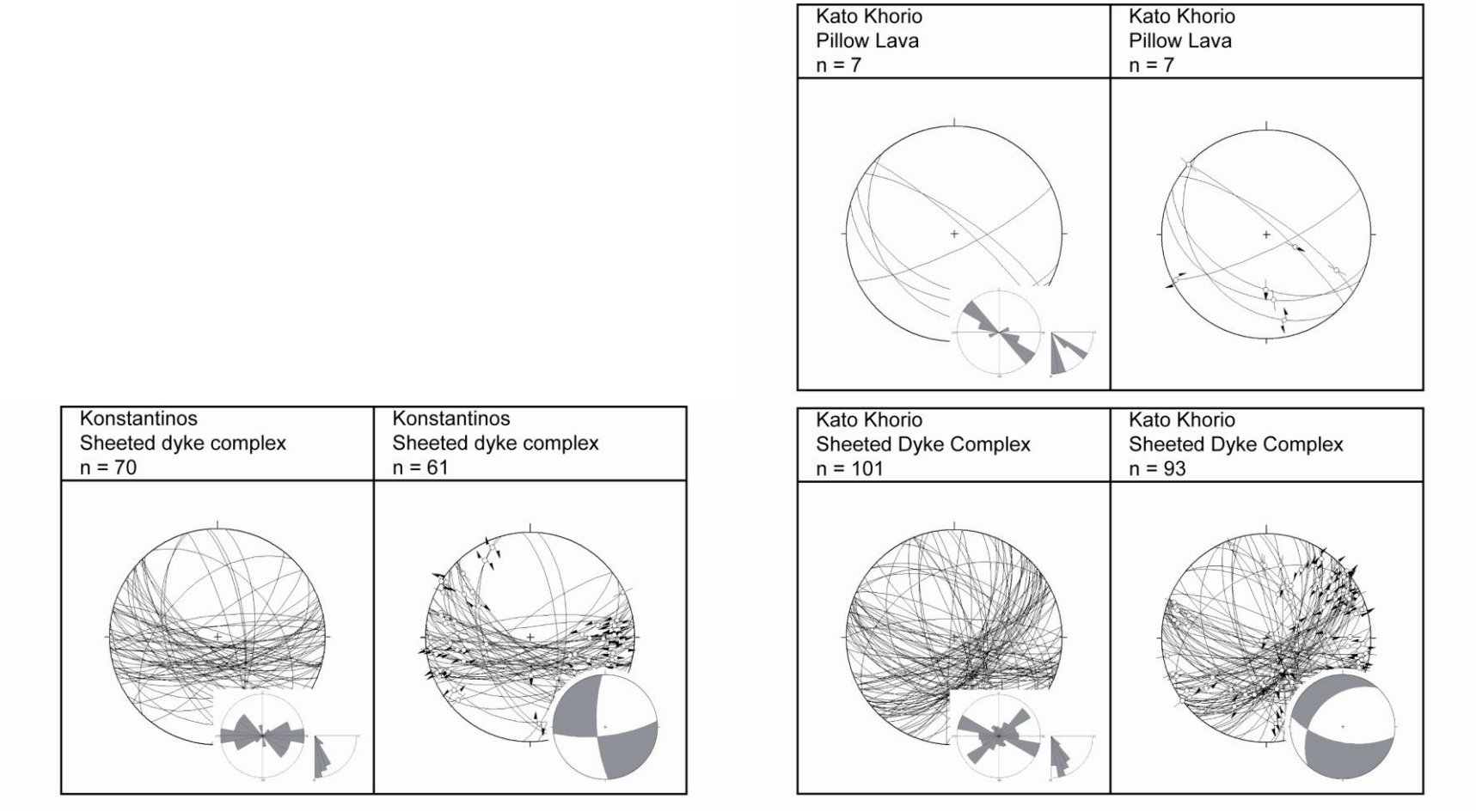

Figure 3-61: Fault data collected from structures affecting (a) Upper Cretaceous Sheeted Dykes at/or near to Konstantinos and (b) Upper Cretaceous Sheeted Dykes Pillow Lavas at/or near Kato Khorio.

Kato Khorio: Meso-structural data were collected from faults affecting Upper Cretaceous Sheeted Dykes and Pillow Lavas at/or near the village of Kato Khorio. Faults affecting the Sheeted Dykes strike at three preferred orientations, either: (i) WNW-ESE, (ii) NE-SW or (iii) NNW-SSE, and dip to the SSE, SE and WSW/ENE respectively (Figure 3-61b). Kinematic indicators, as listed above, indicate that the majority of the faults are sinistral (63.3%). Normal (17.1%), dextral (17.1%) and reverse (2.4%) faults are less common. A limited amount of fault data were collected from faults cutting Pillow Lavas: these faults are observed to strike at a preferred orientation of NW-SE, and dip shallowly to the south, but steeply to the north.

Agios Mamas: Meso-structural data were collected from faults affecting the Sheeted Dyke Complex near the village of Agios Mamas. Faults strike at a preferred orientation of NW-SE and dip predominantly to the SW. Other fault orientations are N-S and WSW-ENE (Figure 3-62). The kinematic indicators listed above indicate that the majority of the faults are sinistral (57.1%). Dextral (39.3%) and normal (3.6%) faults are less common. No dependence was noted between the strike of the fault and its displacement.

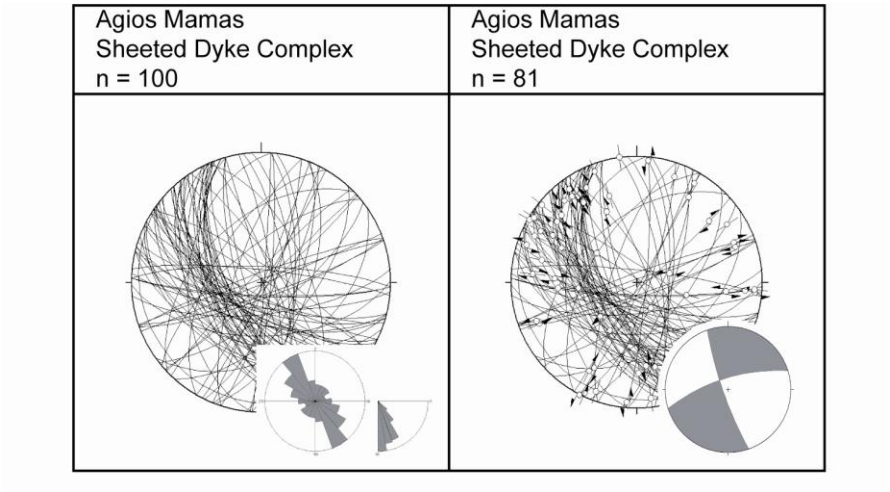

Figure 3-62: Fault data collected from structures affecting Upper Cretaceous Sheeted Dykes at/or near Agios Mamas

Gerasa: Meso-structural data were collected from faults affecting Upper Cretaceous Pillow Lavas and Paleocene chalks (Lefkara Formation) at Gerasa (Figure 3-63). A limited amount of fault data was collected from faults cutting Pillow Lavas. Where observed, faults strike at a preferred orientation of NW-SE, and dip shallowly to the southwest, but steeply to the northeast. A single slickensided surface sheds light on the kinematics of this population:

slickenlines (with steps as kinematic evidence) indicate that the faults are reverse dip-slip. Faults affecting Paleocene strata strike at two preferred orientations, either NE-SW or NW-SE. The NE-SW striking set of faults dips to the SE, whilst faults of the NW-SE set dip both to the SW and NE. Of the two main populations, the NW-SE-striking set of faults is characterised by reverse displacements (30.8%), indicating top-to-the-NE thrusting and, the NE-SW-striking set of faults by dextral (38.5%) and sinistral (30.8%) offsets (kinematic indicators are as listed above).

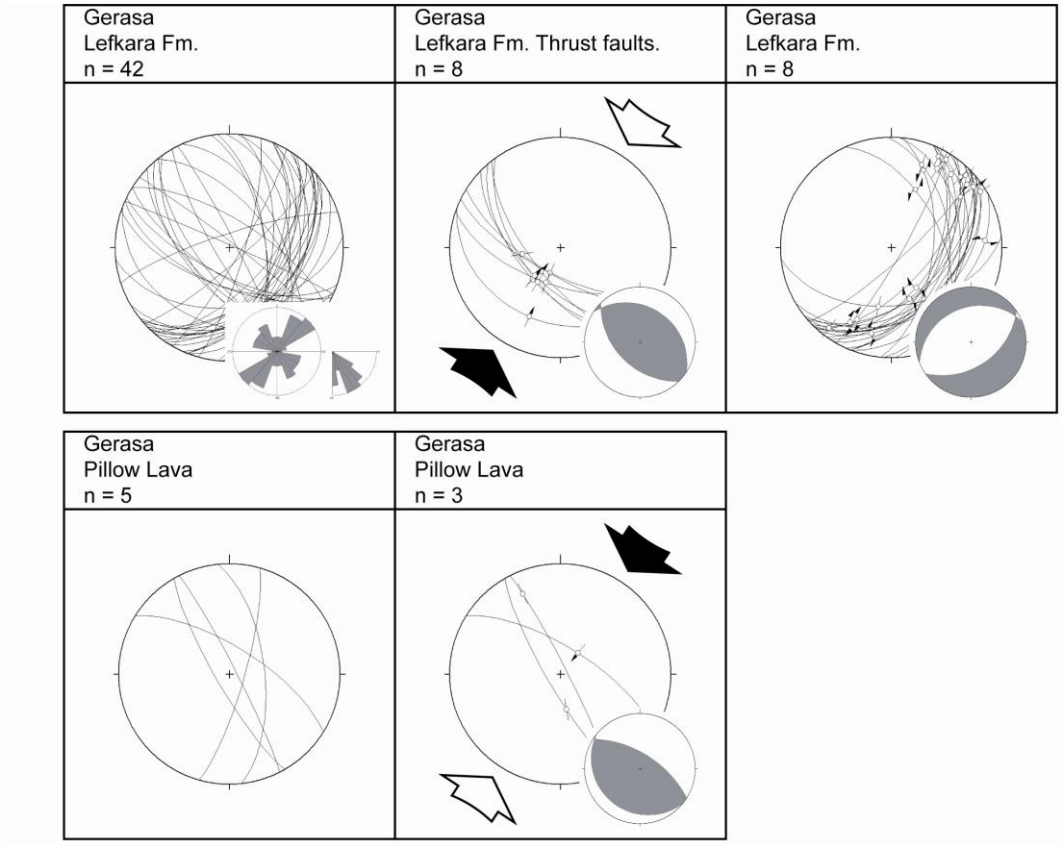

Figure 3-63: Fault data collected from structures affecting Upper Cretaceous Pillow Lavas and Paleocene chalk (Lefkara Formation, at/or near Gerasa

Mathikoloni: Meso-structural data were collected from faults affecting Paleocene strata at Mathikoloni (Figure 3-64). No preferred orientation was noted. In Figure 3-64 the faults are categorised by type: extensional faults (63.3%), with normal dip-slip displacements, trend c. WNW-ESE, and imply c. N-S extension; whereas strike-slip faults trend c. NE-SW, and imply sinistral displacement (30.0%).

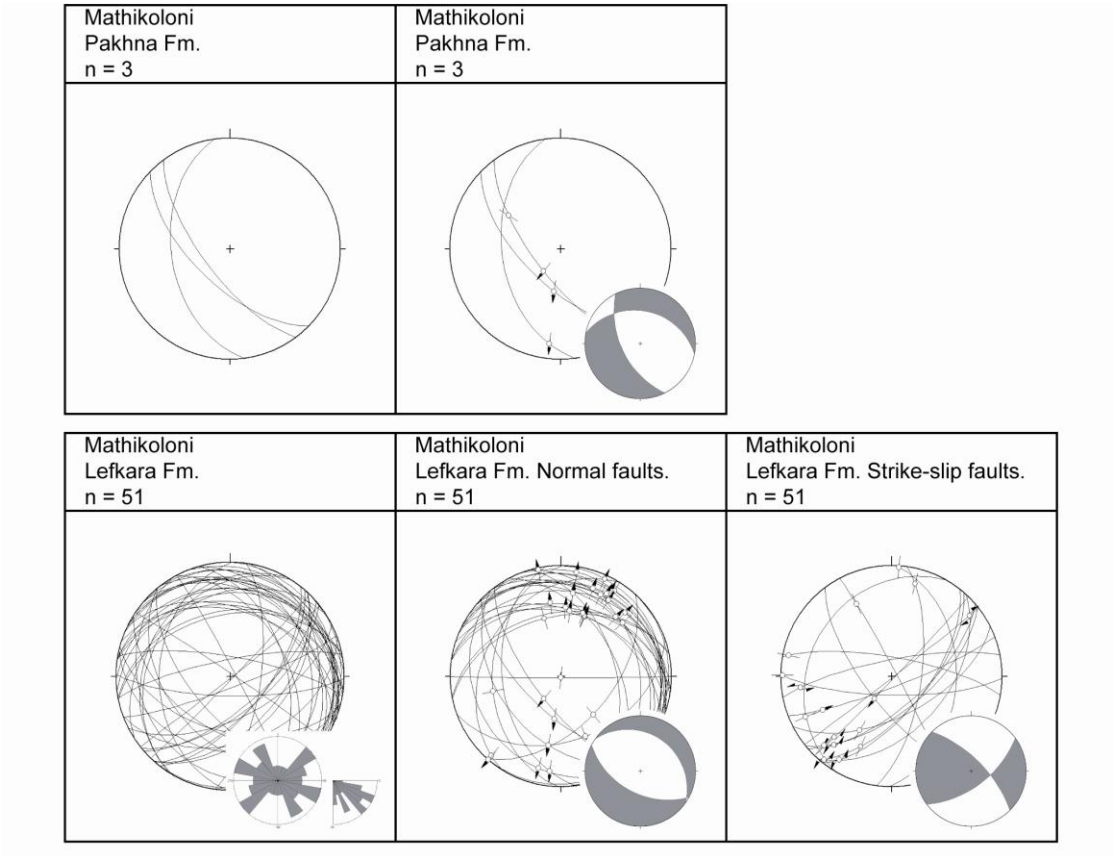

Figure 3-64: Fault data collected from structures affecting Paleocene chalks (Lefkara Formation) in the vicinity of Mathikoloni village. Slip data are categorised by type

Germasogeia: Meso-structural data was collected from faults affecting Upper Cretaceous Pillow Lavas and Paleocene chalks at Akrounta village and Germasogeia Dam (Figure 3-65). Faults cutting Pillow Lavas strike at two preferred directions either ENE-WSW or NNW-SSE and dip to the NNW and ENE respectively. Faults affecting Lefkara chalk strike at two preferred orientations either NW-SE or NE-SW. The main population of faults is the set that strikes NW-SE and dips preferentially to the NE. The NW-SE-trending faults can be split into three further groups, based on the kinematic data obtained from slickensided surfaces: the predominant set of faults are reverse dip-slip to oblique-slip, a second set of faults are sinistral strike-slip, and a third set of faults are normal dip-slip.The reverse faults were generated during a top-to-the-SW thrust event, whereas the normal faults formed in response to NE-directed extension.

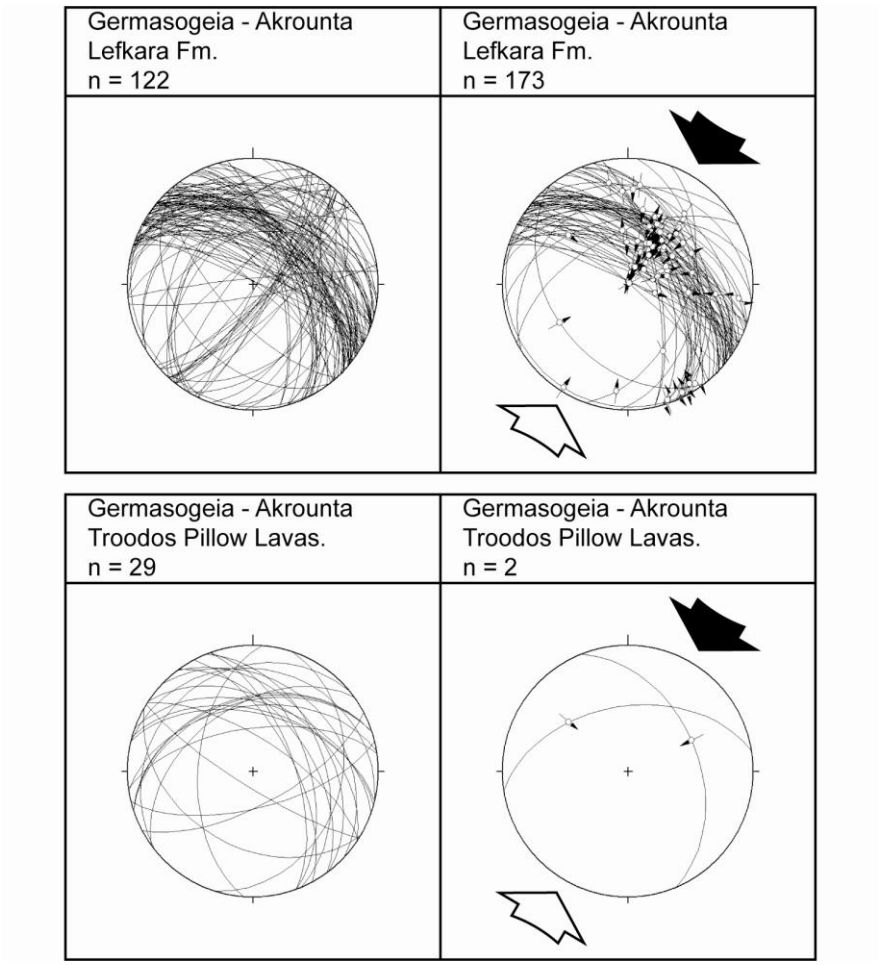

Figure 3-65: Fault data collected from structures affecting Upper Cretaceous Pillow Lavas and Paleocene chalks (Lefkara Formation) near Germasogeia Dam.

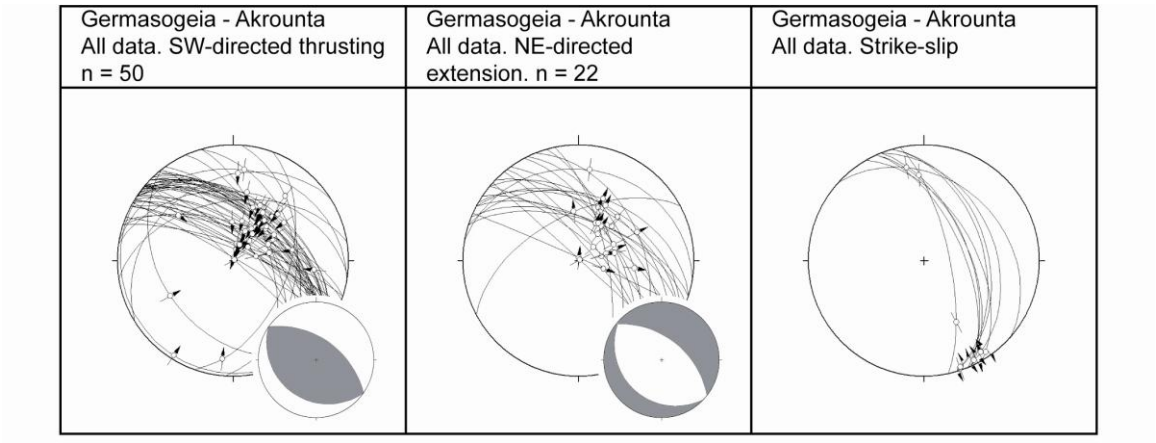

Figure 3-66: Different deformation phases noted at Germasogeia Dam-Akrounta: SW-directing thrusting, NE-directed extension and transtension

The data presented above are now examined to determine whether the Arakapas and Gerasa Fault Belts have been re-activated in the Quaternary. Soulas (2003) proposes that the Arakapas Fault Belt was reactivated in a sinistral sense, whilst the Gerasa Fault Belt was reactivated in a dextral sense. Figure 3-67 summarises the structural data collected in the Arakapas region, Figure 3-68 summarises the structural data collected in the Gerasa region.

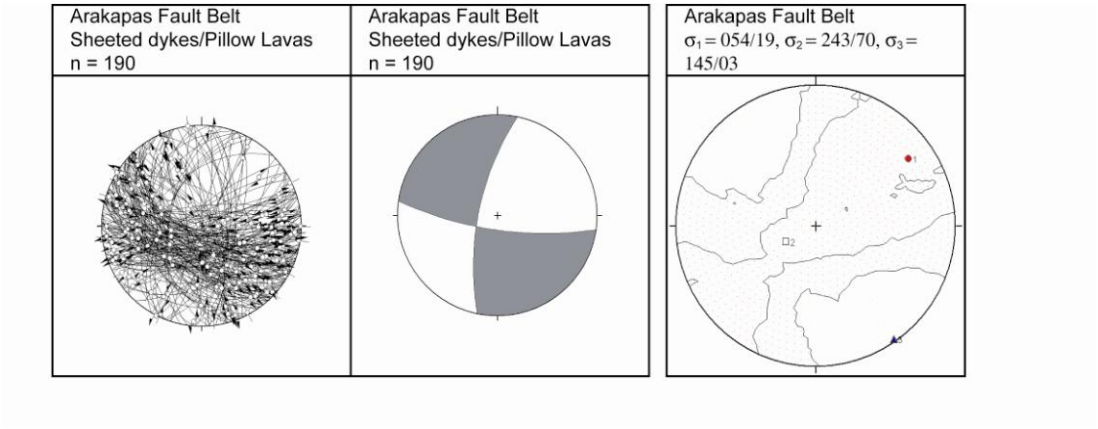

Figure 3-67: Fault-slip data obtained for faults affecting Late Cretaceous sheeted dykes and pillow lavas, between the villages of Eptagoneia and Agios Mamas

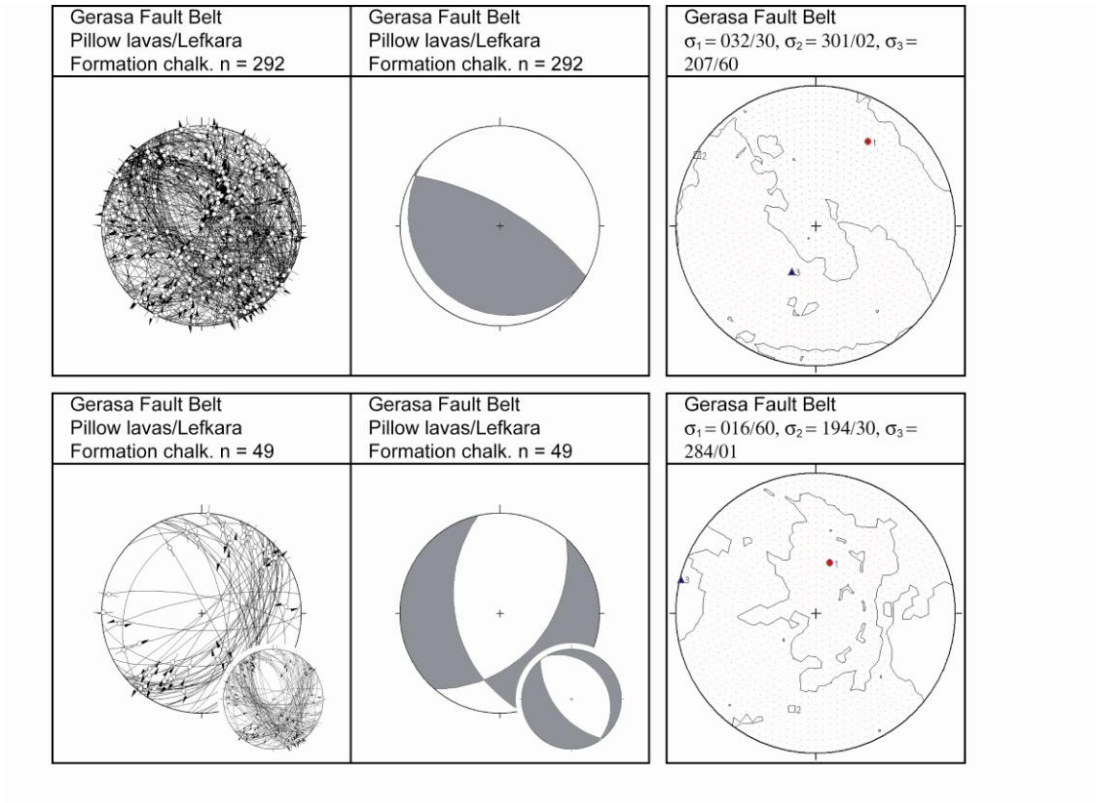

Figure 3-68: Fault-slip data obtained for faults affecting Late Cretaceous sheeted dykes and pillow lavas, between the villages of Eptagoneia and Agios Mamas

Three groups of faults/fractures were recognised in the Arakapas Fault Belt based on trend, dip and offset: (i) a NW-SE to WNW-ESE trend; (ii) a SW-NE trend; and (iii) a N-S trend. Meso-structural information was collected for 381 faults affecting Late Cretaceous Sheeted Dykes and Pillow Lavas, between the villages of Eptagoneia and Agios Mamas; of these faults 59.0% had sinistral displacements, 20.1% had dextral displacements, 17.9% had normal offsets and 3.0% had reverse offsets. Palaeomagnetic evidence (Morris et al., 1990; Morris, 2003a) and structural data (MacLeod and Murton, 1993), suggest that Late Cretaceous deformation along the South Troodos Transform Fault Zone (a segment of the Arakapas Fault zone, see chapter 3) was right-lateral. Fault plane solutions suggest that the Upper Cretaceous structures have subsequently been reactivated, as they indicate that the Arakapas Fault belt is subject to E-W, left-lateral transpression (Figure 3-67). It is not possible to constrain the age at which reactivation occurred, as outcrops younger than the late Cretaceous are not affected by faulting. Soulas (2001, 2003) states various geomorphological features, including offset streams and ridges, topographic breaks, depressions and highs, as evidence that the Arakapas Fault Belt was reactivated in a sinistral sense during the Quaternary.

Two groups of faults/fractures were recognised in the Gerasa Fault Belt, based on trend, dip and offset: (i) a NW-SE to WNW-ESE trend; and (ii) a SW-NE trend. Meso-structural information was collected for 292 faults affecting Late Cretaceous Sheeted Dykes and Pillow Lavas and Paleocene chalk, between the villages of Agios Mamas and Akrounta/Germasogeia Dam; of these faults 30.6% had sinistral displacements, 20.4% had dextral displacements, 25.2% had normal offsets and 23.8% had reverse offsets. The fault data are segregated into two data sets: set (i) encompasses all structures collected in the region, the fault-plane solution for this data set implies top-to-the-SW thrusting; set (ii) has been filtered to remove structures that relate to the Early Miocene event, the remaining structures are characterised by NE-SW-striking sinistral and NNW-SSE-striking dextral strike-slip faults. During the Early to Middle Miocene, the ophiolitic terrain of the Limassol Forest Block was deformed and thrust southward over the Early Cenozoic sedimentary cover. The fault-plane solution for this data set implies a small amount of right-lateral slip on a NNW-SSE plane. It is not possible to constrain the age at which reactivation occurred, as outcrops younger than the Miocene are not affected by faulting. Soulas (2001, 2003) states various geomorphological features, including offset streams and ridges, topographic breaks, depressions and highs, as evidence that the Gerasa Fault Belt was reactivated in a dextral sense during the Quaternary.

New structural data indicates that both Late Cretaceous structures in the Arakapas Fault Belt and Early Miocene structures in the Gerasa Fault Belt have subsequently been reactivated. The Arakapas fault belt is characterised by left-lateral deformation and the Gerasa fault belt by extension, with a minor right-lateral component on a NNW-SSE plane. The geomorphological features listed by Soulas (2001, 2003) as evidence for Quaternary movements, i.e. offset streams and ridges, topographic breaks, depressions and highs were studied. The data were inconclusive: (i) offset streams and ridges commonly occur along lithological boundaries, and could be alternatively explained by differential weathering; and (ii) offset streams and ridges not associated with lithological changes indicate both dextral and sinistral displacements. Further data are required to test this hypothesis. Earthquake data imply that both regions are seismically active (Algermissen and Rogers, 2004, see section 7.3).

3.3.4.4 Larnaka to Cape Dolos

A series of ENE-WSE-, to NE-SW-trending faults have been mapped in the Larnaka District by Soulas et al. (2005). These faults are confined between NW-SE-trending tranverse structures. All structures are believed to have been active in the Pleistocene to Recent.

East-northeast/west-southwest to north-northeast/south-southwest-trending faults

ENE-WSW/NNE-SSW-trending faults, as observed at the villages of Kato Khorio, Alaminno and Klavdia, juxtapose Lefkara and Pakhna Formation chalks (Figure 3-69). As the juxtaposition of the units occurs along SSE- to ESE-dipping fault plane, and as the faults dip in the direction of the Pakhna Formation it is believed that the faults were originally normal in nature. This sense of displacement is in conflict with that indicated by slickenlines (and associated steps) on the fault plane. The slickenlines indicate that this last movement was dip-slip to slight oblique-slip. The stepped grooves on the slickensided surface indicate that this displacement was reverse.

The Maroni-Psematismenos Basin is located immediately SW of the area under study; extensional ENE-WSW-trending structures formed in this basin in the Late Miocene. The formation of ENE-WSW/NNE-SSW-trending faults in the Larnaka District are tentatively correlated with the formation of ENE-WSW-trending structures in the Maroni Basin. The

reactivation of faults in the Larnaka District must have occurred after this event, i.e. post-Miocene.

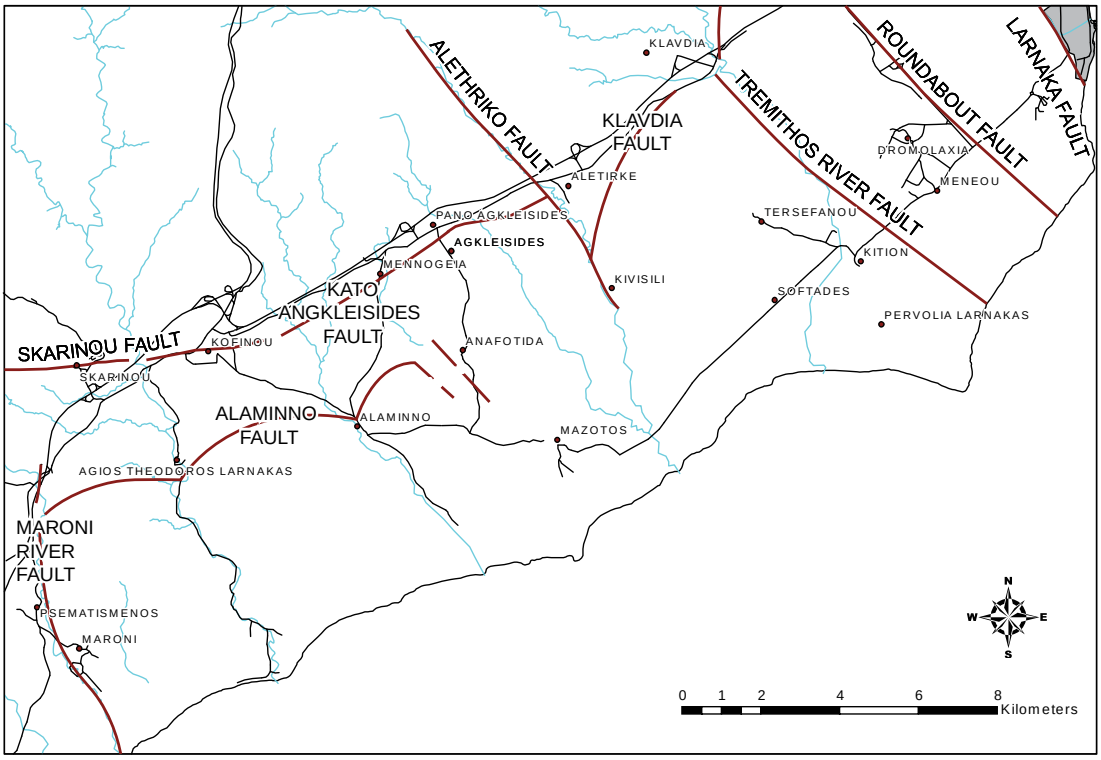

Figure 3-69: East-northeast/west-southwest to north-northeast/south-southwest trending faults in the Larnaka district, south-central Cyprus

The Kato Khorio Fault is approximately 3.5 km long, trends N-S to NE-SW and dips between 40º and 50º to the SE (Figure 3-69). Meso-structural information were collected in Paleocene strata along the strike of this fault (Figure 3-70). Faults measured in Miocene-aged rocks between Alaminno and Kato Agkleisides villages have a preferred NE-SW orientation and dip at approximately 30º to the SE (Figure 3-70). The Klavdia Fault is c. 5 km long, trends NE-SW to ENE-WSW (i.e. at c. 065º) and, dips between 30º - 80º to the SE (Figure 3-69). Meso-structural information was collected in Miocene strata along the strike of this fault (Figure 3-70). Analysis of slip-data obtained from each lineament indicates top-to-the-NW to top-to-the-N thrust faulting. At Klavdia, a sub-set of faults are believed to be extensional; Paleocene strata is offset in a normal sense. Quaternary displacements along these lineaments have been inferred for several reasons: firstly, at Kato Khorio, Lefkara Formation chalks are overthrust above recent colluvial deposits; and secondly, near Klavdia, several small streams are perched above a topographic high, implying that the ridge was uplifted in Recent times (Soulas et al., 2005).

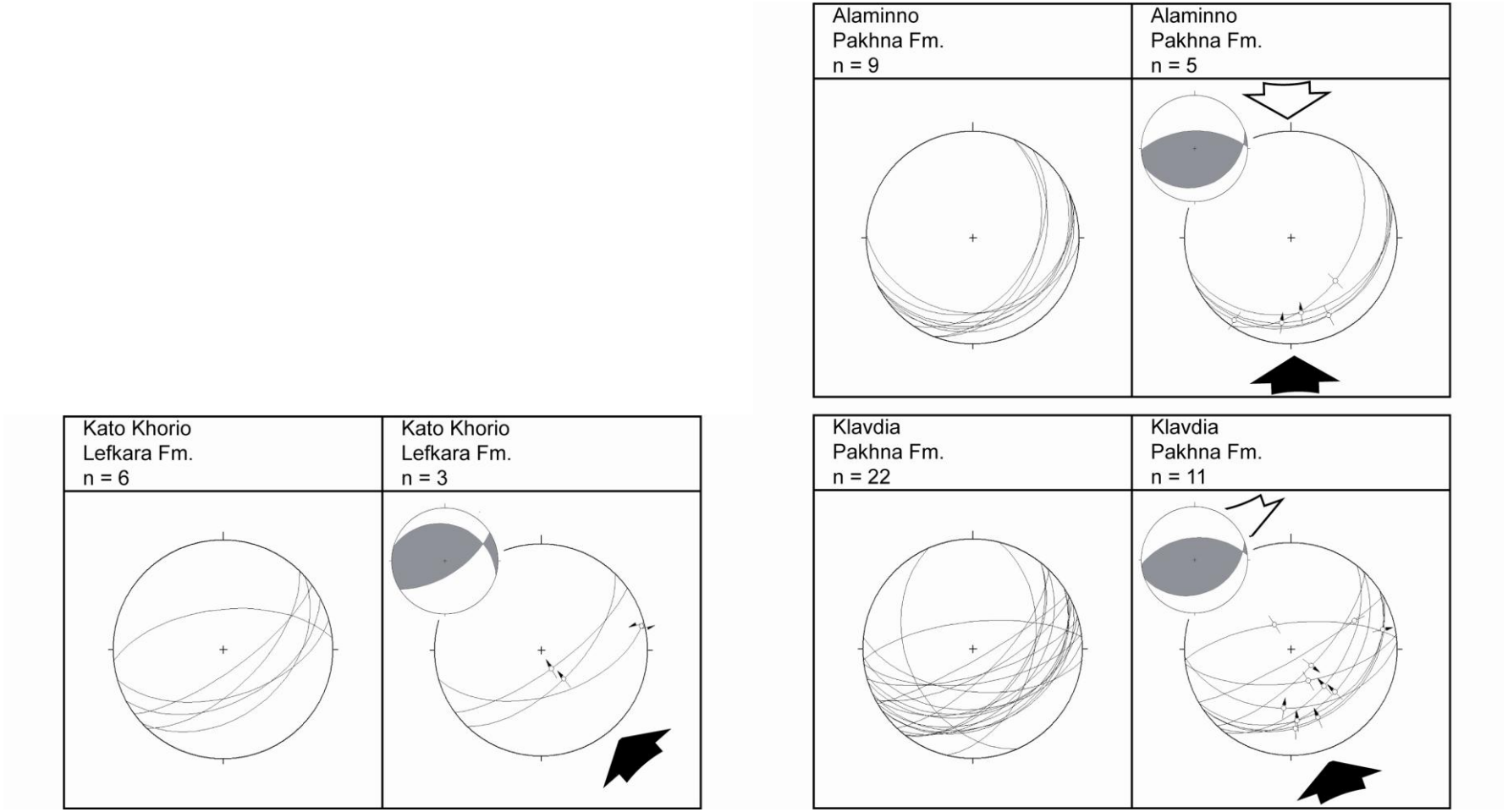

Figure 3-70: Fault data collected from structures affecting (a) Paleocene strata at or near the village of Kato Khorio, Larnaka District; and, (b) Miocene strata at or near the villages of Alaminno and Klavdia

Northwest-southeast transverse structures

NW-SE transverse structures bound the Kato Khorio, Klavdia and Alaminno lineaments (Figure 3-69). Soulas et al. (2005) identified several structures, i.e. (i) the Roundabout – Airport Fault, a NW-SE trending, right-lateral lineament, in which the NE side is downthrown; (ii) the Tremithos River Fault, sub-parallel to the Airport Fault and also right-lateral; (iii) the Alethriko Fault, a relict, pre-Pliocene structure; and the Cape Kiti Fault, a NNE-SSW trending, left-lateral lineation.

The fault-slip data discussed above are summarised in Figure 3-71. The regional stresses determined for faults affecting Paleocene and Miocene strata in the Larnaka District are shown in Figure 3-72. As the ENE-WSW/NNE-SSW-trending structures are known to have originated as normal structures, and assuming that displacements were normal dip-slip, it was possible to calculate the principal stresses responsible for the generation of the faults i.e. σ_1; 250º/83º, σ_2; 057º/07º, and σ_3; 147º/02º. The values obtained are comparable to those resolved for faults affecting Paleocene, Miocene and Messinian strata in the Maroni Basin (Figure 3-31), suggesting that this was a valid assumption. The principal stresses resolved for the compressional phase of deformation are σ_1; 353º/07º, σ_2; 085º/13º, and σ_3; 237º/75º.

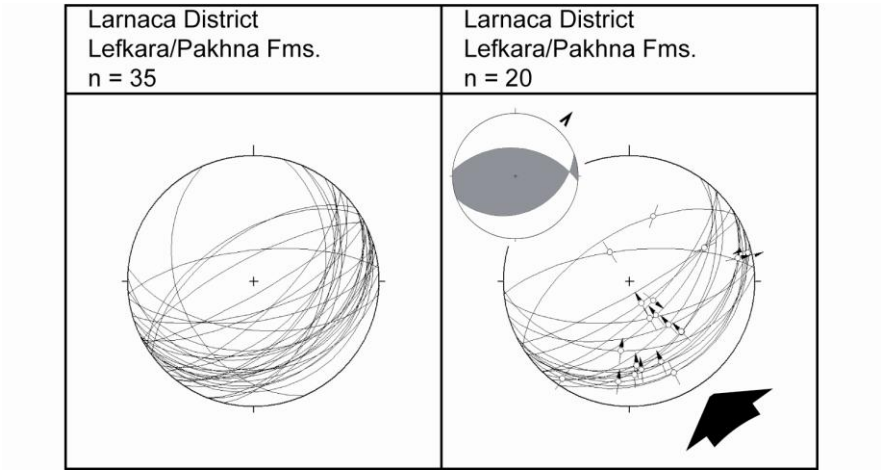

Figure 3-71: Fault data collected throughout the Larnaka District, from structures affecting Paleocene and Miocene strata.

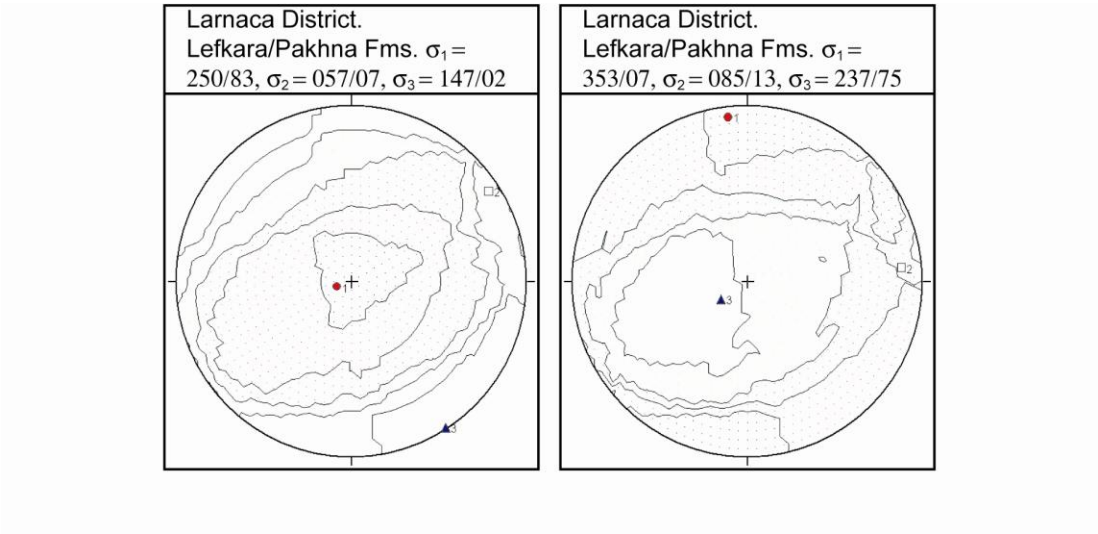

Figure 3-72: Principal stress directions resolved for faults affecting Paleocene and Miocene strata in the Larnaka district

3.3.4.5 Cape Kiti

The Larnaka Fault Zone (LFZ), is comprised of braided NNE-SSW trending left-lateral, steeply dipping fault strands, which have been active in the Late Pleistocene and Holocene (R. Harrison and E. Tsiolakis, personal communication). It is located in south-central Cyprus, in the district of Larnaka (Figure 3-73), and extends from Cape Kiti, through the Kiti Medieval Tower, towards the village of Pergamos; a distance of > 30km. Bathymetric data suggests that the Cape Kiti lineament extends many more km to the SSW, where it intersects with the Cyprus Arc (R. Harrison and E. Tsiolakis, personal communication). The southernmost strand of the Larnaka Fault Zone is the Cape Kiti Fault. It is a tectonically active zone, consisting of several braided, steeply dipping fault strands, with a relief formed by a series of uplifted marine terraces. The Cape Kiti Fault may be traced inland towards the city of Larnaka (Figure 3-73), through a series of uplifted marine terraces (sand dunes) and local depressions (salt-lakes). In Larnaka itself, beside the causeway crossing Larnaka salt-lake, a linear ridge comprised of Nicosia marls and gravels is cut by parallel faults, which trend in a similar direction as the faults at Cape Kiti (Figure 3-73).

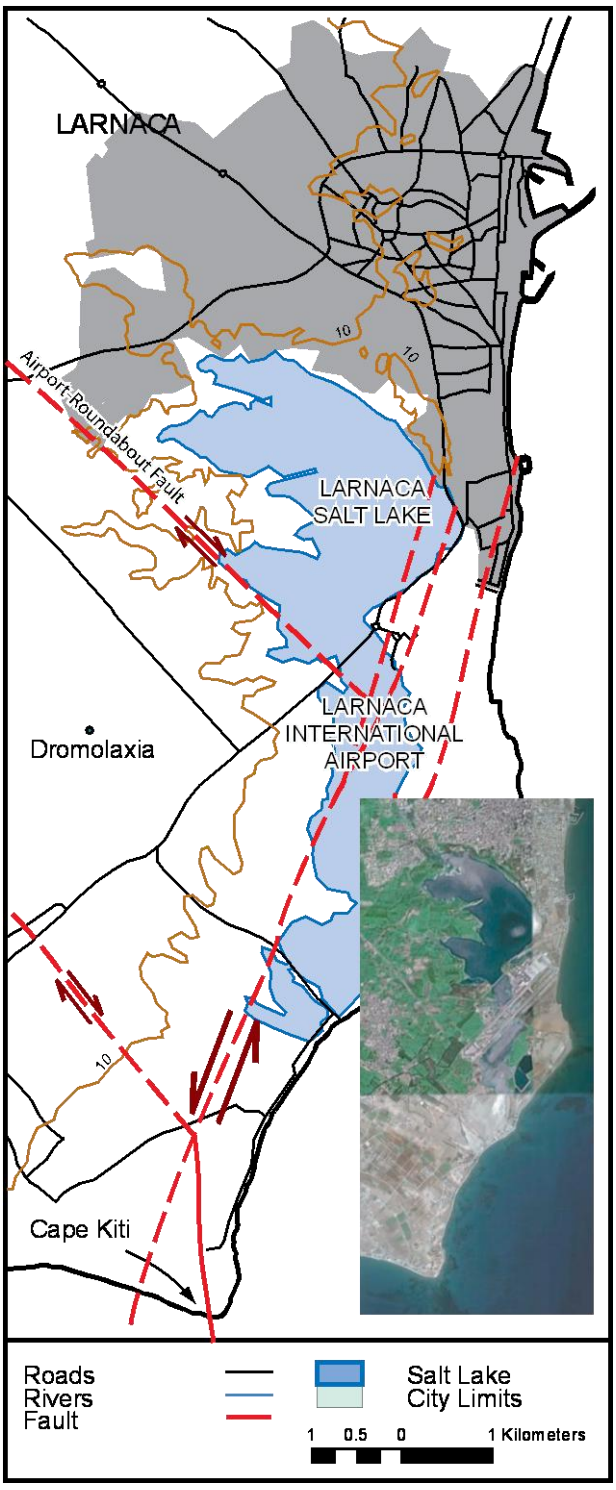

Figure 3-73: Map of the Cape Kiti Fault, the southernmost strand of the Larnaka Fault Zone. Fault traces are as mapped by Harrison and Tsiolakis (2006). The location of this figure is shown in Figure 3-2

The southern tip of the Cape Kiti Fault is exposed at Cape Kiti (Figure 3-73). Richard Harrison, of the U.S. Geological Survey (U.S.G.S), and Efthimios Tsiolakis, of the Cyprus

Geological Survey have extensively examined the fault at this locality: Late Pleistocene terrestrial deposits are juxtaposed against Holocene beach deposits (Figure 3-74). To the west of the lineament (c. 100m), a borehole informs us that the top of the Pliocene Nicosia Formation occurs at a depth of 16m beneath the surface, and that the top of the Miocene Pakhna formation occurs at a depth of 34m. This implies that there has been a minimum of 34m of stratigraphic throw across the structure in the Quaternary; the amount of horizontal movement is undeterminable, but is considered to be significantly greater than the vertical offset. Miocene Pakhna Formation chalks, located in the footwall of the fault, have been rotated to dip at 10° - 25° to the west. The chalks are cut by numerous extensional faults down-stepping to the east, which represent extension away from the uplifted zone (Figure 3-75).

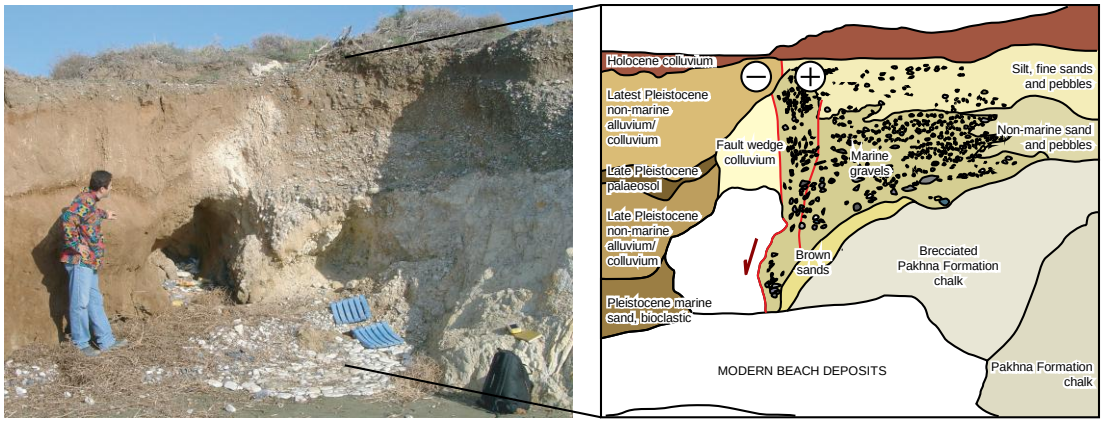

Figure 3-74: The Cape Kiti Fault: Pleistocene terrestrial deposits juxtaposed against Holocene beach deposits (R. Harrison). Photograph taken looking north

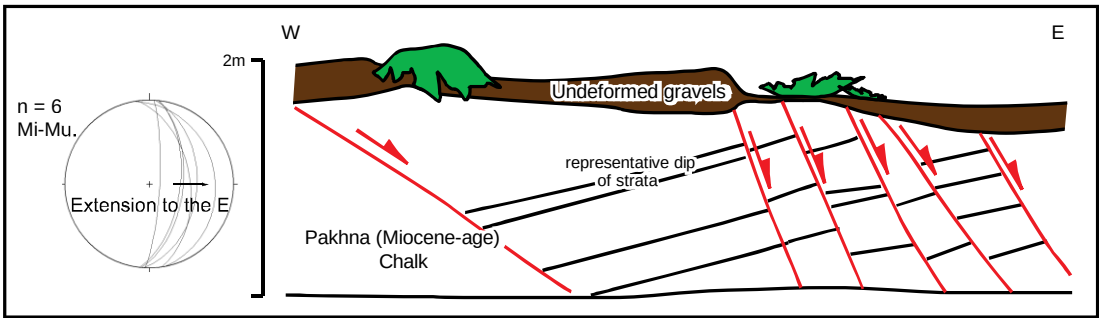

Figure 3-75: The Cape Kiti Fault: Extension in Pakhna Formation chalks exposed at Cape Kiti.

3.4 Discussion

A large amount of new structural data was collected throughout the south of Cyprus: in particular, this includes fault data: from each of the main Neogene basins and adjacent areas (Figure 3-1); from E-W-, NNE-SSW- and NNW-SSE-trending strike-slip faults in the Lemesos and Larnaka districts (Figure 3-2) and; from folded strata in Paphos district (Figure 3-2). An attempt is now made to correlate tectonic events throughout Cyprus.

The data collected in each of the Neogene basins and in adjacent areas alludes to a period of extension that was prelevant throughout the south of Cyprus (Figure 3-76). This event is broadly constrained to the late Miocene. In the Polis Graben this event formed NNW-SSW-striking normal faults; in the Pissouri Basin it formed ~N-S-striking normal faults; in the Maroni-Psematismenos Basin it formed NE-SW-striking faults; and in the Mesaoria Basin it formed ~N-S- and ~E-W-striking normal faults along its southern margin. NNW-SSE-striking faults observed in the Polis Graben are believed to have formed in the Late Miocene, as the faults only affect Paleocene and Miocene chalks. No faults of this orientation are observed cutting Pliocene or younger strata. In the Pissouri Basin, N-S-trending faults are believed to have controlled the distribution of faults in Messinian evaporites. In latter chapters of this thesis chronological evidence and sedimentological data is presented to further characterise the timing of this event.

Payne and Robertson (1995) attributed the formation of WNW-ESE-striking faults in the Polis Graben and Pegeia region to a discrete NNE-SSW extensional event. As the faults are observed cutting Pliocene and early Pleistocene strata they believed this event to occur in the Late Pliocene. WNW-ESE-striking faults affecting Messinian and Pliocene strata are observed in the Mesaoria Basin. It is possible that these faults may have formed during the same event. However, further work is required to validate or refute this statement.

The data also alludes to a period of compression/transpression that occurred post-Miocene. This event is recognised throughout the south of Cyprus (Figure 3-77): in W Cyprus, N-S- and NNE-SSW-striking structures have been reactivated in E-W/WNW-ESE compression; in SW Cyprus, N-S-striking structures have been reactivated in transpression; in south central Cyprus, NE-SW-striking structures have been reactivated in NW-SW compression.

In W Cyprus, the Agia Marinouda Fold deforms Pleistocene strata; in central Cyprus, the Kolossi Fault cuts Pleistocene strata; in south central Cyprus, sinistral NNE-SSW-striking and dextral NNW-SSE-striking faults in the Larnaka region are believed to have been active in the Pleistocene/Recent (Soulas et al., 2005). This indicates a pervasive compressional/transpressional event throughout the south of Cyprus. As the numerous structures listed above allude to this event occurring during the Pleistocene/Recent, it is believed that reactivation of the structures in Neogene Basins and adjacent areas occurred during this interval.

Figure 3-76: Extension in the Late Miocene: structural data collected in each of the Neogene basins and in adjacent areas, alludes to a period of extension throughout the south of Cyprus. This event is broadly constrained to the late Miocene (see discussion in text)

Figure 3-77: Post-Miocene compression: structural data collected in each of the Neogene basins and in adjacent areas alludes to a period of compression throughout the south of Cyprus. This event is broadly constrained to the Pleistocene/Recent (see discussion in text)

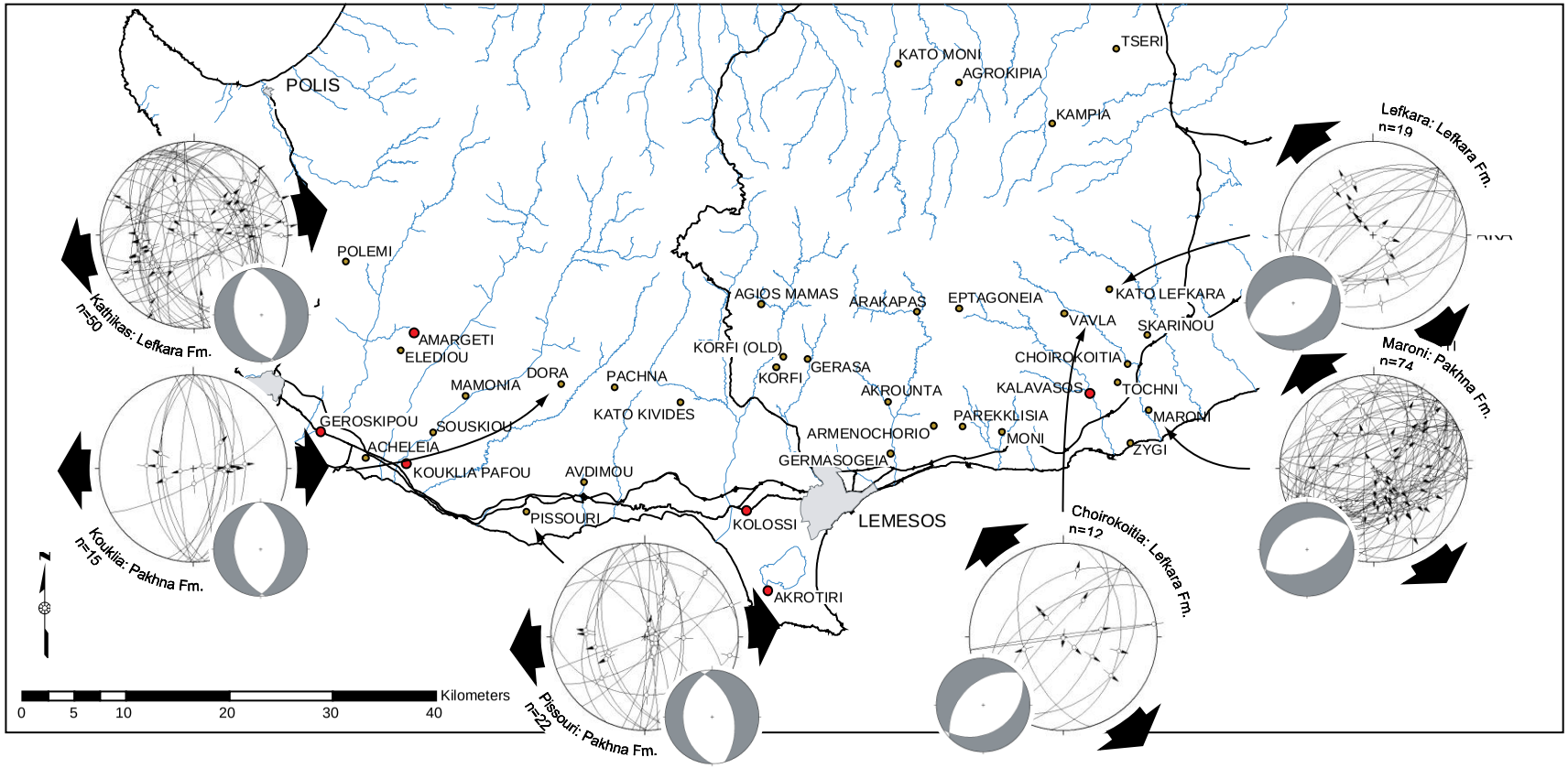

Figure 3-76: Extension in the Late Miocene: structural data collected in each of the Neogene basins and in adjacent areas, alludes to a period of extension throughout the south of Cyprus. This event is broadly constrained to the late Miocene (see discussion in text)

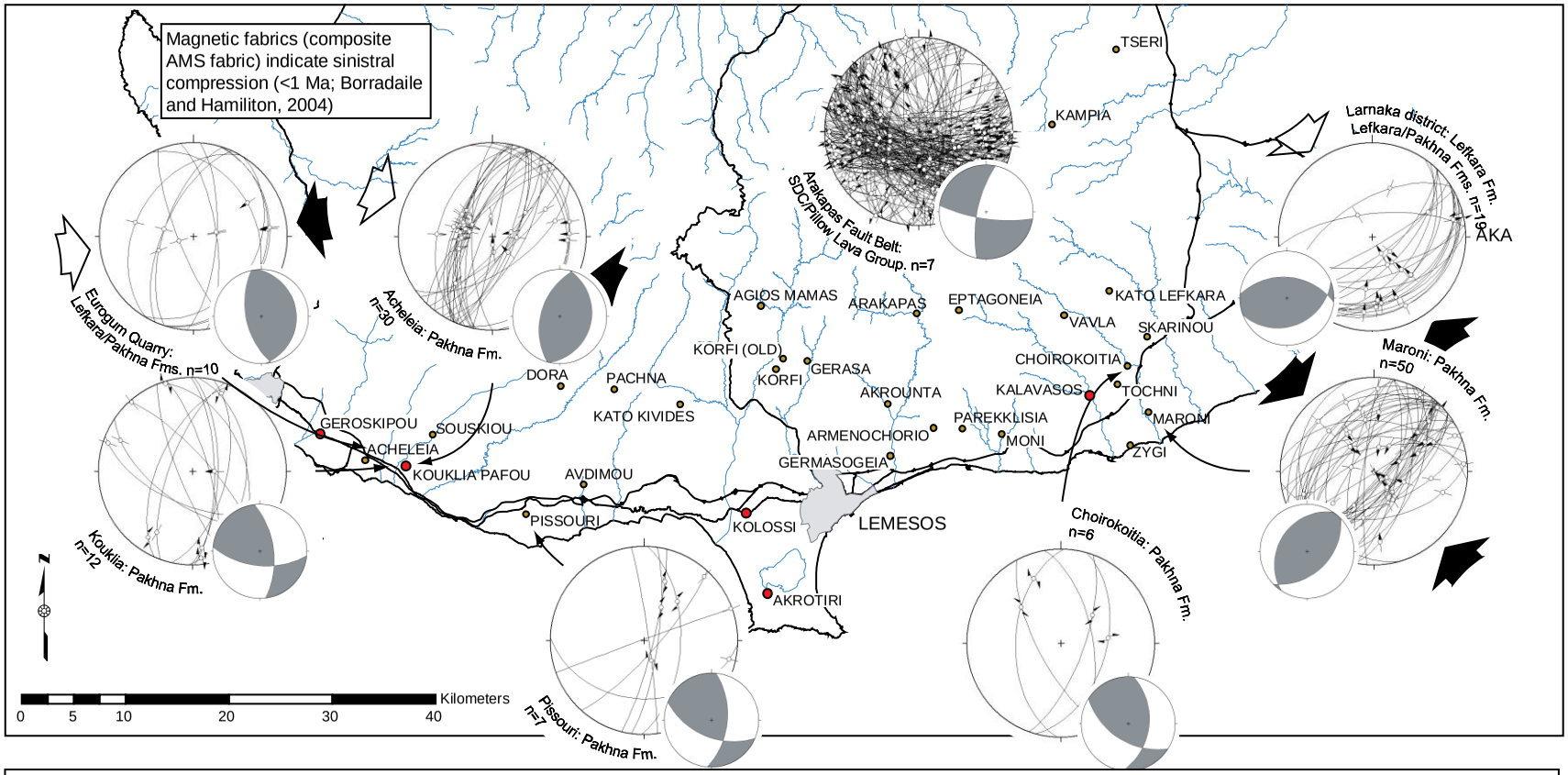

Figure 3-77: Post-Miocene compression: structural data collected in each of the Neogene basins and in adjacent areas alludes to a period of compression throughout the south of Cyprus. This event is broadly constrained to the Pleistocene/Recent (see discussion in text)

3.5 Conclusions

In this chapter a large amount of new structural data were presented for south and central Cyprus, for faults and folds affecting each stratigraphic interval of the circum-Troodos sedimentary cover.

On the basis of this work a tentative chronology of tectonic events in Cyprus is established: *D1: Late Miocene extension:* E-W extension in west and southwest Cyprus led to the formation of faults of a N-S orientation, whereas in south central Cyprus, NW-SE extension led to the formation of NE-SW faults; *D2?: Late Pliocene extension:* Localised NNE-SSW extension led to the formation of WNW-ESE faults in the Polis Graben and Pegeia region; and *D3: Pleistocene/Recent compression/transpression:* A pervasive compressional/transpressional event occurred throughout the south of Cyprus, this led to the reactivation of pre-existing structures (D1), the formation of E-W- and NNE-SSW-trending sinistral faults and NNW-SSE-trending dextral faults. The Agia Marinouda Fold also formed at this time.

The nature and timing of the separate tectonic events will be constrained further in later chapters. This will involve relative and absolute methods of dating of the faults (palaeomagnetic profiling and luminescence dating methods; chapters 4 and 5), correlating discrete sedimentological events to periods of fault displacement (chapters 6 and 7) and examining modern/historical seismic records (chapter 7).

Chapter 4: Magnetostratigraphy for the Plio-Pleistocene circum-Troodos sedimentary cover

4.1 Introduction

Neotectonic and geomorphological studies in Cyprus indicate that convergence between Africa and Anatolia is presently occurring, with active structures distributed over much of the island (see chapter 3 and the work of Soulas, 1999; 2001; 2003; Harrison et al., 2004a,b). Some parts of Cyprus are undergoing uplift, as evidenced by raised marine terraces (this chapter and the work of Poole and Robertson, 1991, 2000), incised/abandoned fluvial channels (Poole, 1992; Poole and Robertson, 1998; Vita-Finzi, 1993) and localised gravitational faulting (Soulas, 2003). At present, only a relative chronology exists for much of the Plio-Quaternary sedimentary succession of southern Cyprus. An integrated study combining magnetostratigraphy, luminescence profiling, sedimentology and geomorphology was devised to obtain a more robust chronological framework.

The aim of this chapter is to establish a magnetostratigraphy for the Plio-Pleistocene circum-Troodos sedimentary cover. It is important to establish a detailed stratigraphy for the Plio-Pleistocene, as it is within this time interval that the Eratosthenes Seamount collided with the Cyprus trench (Robertson et al., 1995a; Payne and Robertson, 1995, 2000; Robertson, 1998b) or Cyprus transform plate boundary (Harrison et al., 2004a, Harrison and Tsiolakis, 2006). The collision of the Seamount with the 'Cyprus active margin' led to accelerated uplift, emergence, and then erosion of the island, centred on the Troodos Massif. Thus, if one can obtain a detailed geochronological framework for the Plio-Pleistocene successions of south and central Cyprus, one can assess rates of Plio-Pleistocene uplift. The data will be extrapolated to improve our understanding of the timing (this chapter) and consequences (see discussion in Chapter 7) of the collision of the Eratosthenes Seamount with the active margin.

Palaeomagnetic age profiling has become a widely used chronological tool of choice to characterise stratigraphy and independently test correlations and depositional frameworks (e.g. Richter et al., 1998; Homke et al., 2004; Vasiliev et al., 2005)

4.2 Lithostratigraphic units

The lithostratigraphic units discussed in this chapter are described in Chapters 2 and 6.

4.3 Previous work

The first palaeomagnetic studies of the Troodos extrusive sequences and overlying sedimentary cover were initiated to constrain the timing and duration of its rotation. Clube (1985) and Morris (1990) compiled authorative syntheses on all previous work prior to the late 1980s. The reader is referred to these syntheses to see a description of this body of work.

The characteristic remanent magnetisation retained by the umbers and lowermost radiolarites of the Perapedhi Formation (ca. 90.4 - 74.0 Ma; Blome and Irvine, 1985) was found by Morris (1990) to be indistinguishable from that of the underlying extrusives (Figure 4-1; Table 4-2). Hence, rotation of the ophiolite complex must have been initiated after the deposition of these sediments.

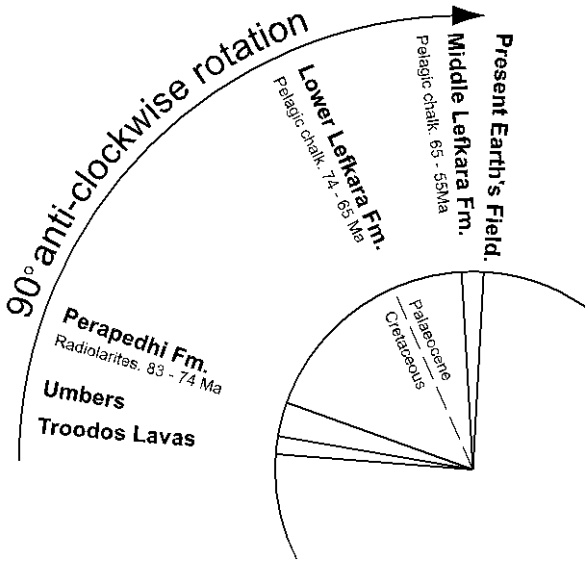

Figure 4-1: The rotations of the cover rocks and the underlying tectonic units as revealed by palaeomagnetic studies. (Clube and Robertson, 1986; modified from Lagroix and Borradaile, 2000)

Declination data from the overlying Lefkara Formation pelagic chalks indicated at least 60º rotation between the Upper Campanian (c. 74 Ma) and the end of the Late Paleocene (c. 55 Ma) (Figure 4-1; Table 4-2; Clube, 1985). Rotation was essentially complete by the end of the Lower Eocene (c. 50 Ma) (Figure 4-1; Table 4-2; Clube, 1985). Younger, Miocene

sediments were found to consistently retain a stable remanent magnetisation orientated close to north, or the south, suggesting that only minor rotation of the underlying ophiolitic basement took place after the end of the Lower Eocene (Figure 4-1; Table 4-2; Clube, 1985).

Site	**Age**	**N**	**Geographic**				**Stratigraphic**			
			Dec	**Inc**	**α_{95}**	**K**	**Dec**	**Inc**	**α_{95}**	**K**
Eastern Limassol Forest Complex										
AS	UPL Pillows/seds	14	266	2	6.2	42	282	46	6.2	42
AC	Perapedhi Umbers	5	293	41	3.1	597	282	39	3.1	597
DH	Perapedhi Umbers	9	269	21	8.2	40	277	26	5.8	81
AU	Perapedhi Umbers	4	285	26	11.8	61	274	23	11.8	61
	Perapedhi Radio.	8	304	23	7.0	63	306	20	7.0	63
Eastern flank of Troodos Massif										
MP	UPL Pillows	9	294	4	6.3	68	305	33	6.3	68
	Perapedhi Umbers	10	284	-3	7.1	47	286	17	7.1	47
Arakapas Fault Belt										
MD	UPL Sediments	17	313	45	3.4	112	311	29	2.6	193
LY	LPL Sediments	7	270	15	9.0	46	267	51	8.7	49
VL	LPL Haem. Shales	17	266	-3	6.1	35	270	23	5.9	38
VR	Perapedi Umbers	5	268	11	8.0	92	266	30	8.0	92
	Perapedi Radio.	17	307	-5	3.7	95	304	28	3.2	127
PU1	Perapedi Umbers	9	358	33	5.1	101	358	34	5.1	101
PU2	Perapedi Umbers	7	284	21	10.9	31	274	29	9.8	39
Troodos Reference Direction										
TMV							276	32		

Table 4-1: Summary of the Palaeomagnetic results obtained by Morris (1990): N = number of localities; number of samples; Dec = declination; Inc = Inclination; α_{95} = radius of the 95% cone of confidence; K = Fisher precision parameter; Geographic = as measured; Stratigraphic = corrected for tectonic tilt

Lithology/Locality	**Age**	**N**	**n**	**Dec**	**Inc**	**α_{95}**
Pelagic chalks	Lower Eocene	5	136	357	38	10.1
Pelagic chalks	Maastrichtian-Paleocene (Reverse)	6	101	152	-14	15.3
Pelagic chalks	Maastrichtian-Paleocene (Normal)	5	116	336	32	13.2
Radiolarites (North Troodos)	Campanian	1	25	289	13	23.9
Umbers (north Troodos and Southern Limassol Forest areas)	Turonian	5	56	279	6	28.6
Akamas	Turonian	3	217	276	41	14.1
Troodos Pillow Lavas (north Troodos, Akamas and Southern Limassol Forest areas)	Turonian	11	663	274	36	12.3

Table 4-2: Summary of the Palaeomagnetic results obtained by Clube (1985): N = number of localities; n = number of samples; Dec = declination; Inc = Inclination; α_{95} = radius of the 95% cone of confidence.

Subsequent palaeomagnetic studies in Cyprus fall into one of two caterogies, those which seek to establish a chronology for the circum-Troodos sedimentary cover, and those which

seek to define magnetic fabrics within the circum-Troodos sedimentary cover. Krijgsman et al. (2002) generated a magnetostratigraphy for the Tortonian/Messinian boundary, to study the onset of the Messinian Salinity Crisis (Krijgsman et al., 2002). This work is reviewed in chapter 6. Weber et al. (2006) generated a magnetostratigraphy for the middle to late Pleistocene Apalos Formation and the overlying Fanglomerate Group. No palaeomagnetic age data exists for the period between the Early Pliocene and Middle Pleistocene.

Magnetic fabric studies, using the Anisotropy of Magnetic Susceptibility (AMS) and Anisotropy of Anhysteretic Remanence (AARM), have revealed information on neotectonic stresses in the circum-Troodos sedimentary cover of Cyprus (Lagroix and Borradaile, 2000; Borradaile and Hamilton, 2004). The AMS foliation observed in Lefkara, Pakhna and Nicosia Formation chalk and marl reveals a south-directed movement (S-vergent) away from the Troodos ophiolite (Lagroix and Borradaile, 2000). A complimentary investigation of magnetic fabrics in the sedimentary cover was carried out by Borradaile and Hamilton (2004). Borradaile and Hamilton (2004) identified, within the Polis Graben, an AMS petrofabric which indicated NE-SW extension. The AARM subfabric correlates with this rifting event with a NNE lineation. This work is reviewed in chapter 7.

The present magnetic inclination and declination of Cyprus (35° 00 N, 33º 00 E) are 49.9˚ and -13.1˚ respectively (Geomagix for Win95, version 1.0, John Quinn).

4.4 Methodology (Sample collection, preparation and analysis)

At each locality, a bed was identified for sampling and cleaned. Sub-samples were collected at different vertical heights and horizontal distances to test whether there was a vertical or horizontal variation in magnetic remanence. Three to nine cores were collected from each site. In lithified units, a pedestal drill was used to extract 1-inch diameter cores from the rock face. In unconsolidated sediments, plastic tubes, measuring an inch in diameter and several inches in length, were inserted into the sample horizon. The orientation of the collected core, with respect to the units bedding, was measured by sun and magnetic measurements prior to extraction. In the laboratory, visibly altered sections of the cores were removed.

Palaeomagnetic samples were analysed at the Institute of Earth Sciences, University of Edinburgh, using a nitrogen SQUID magnetometer. The Natural Remanence (NRM) of each

rock sample was subject to progressive Alternating Field (AF) demagnetisation, with steps of 2 Oe between 0 and 30 Oe and 5 Oe between 30 and 80 Oe. A sub-group of cores were subjected to thermal demagnetisation, with steps of 50°C between 100°C and 500°C and 20°C between 500°C and 600°C. The results were evaluated using Zeijderveld plots (orthogonal projections) of the remanence vectors. Components of magnetisation were recognised by eye, and their direction determined through principal component analysis, using the 'PMGSC: Palaeomagnetism Data Analysis' program (version 4.2) of Enkin et al. 2000.

Rock magnetic tests were preformed at the Univeristy of Plymouth by Dr Anthony Morris. The rate of acquisition of isothermal remanence (IRM) was studied for selected samples (in fields up to 0.8 T). Rock samples were exposed to successively higher direct magnetic fields at incremental steps, produced by a pulse magnetiser and the IRM measured, using a spinner magnetometer. This technique provides a rapid and effective method for distinguishing the presence of Ti-poor titanomagnetites and Ti-poor ilmenohaematites (Tarling, 1983): (i) single and multi-domain titanomagnetite (and maghemite) grains reach saturation in fields of 0.05 - 0.2 T, (ii) single domain needle-shaped magnetite grains may have peak coercivities of up to 0.3 T, and (iii) haematite and goethite grains reach saturation in fields of over 1 - 3 T. Therefore, if direct magnetic fields are applied in incremental steps the magnetization becomes saturated and essentially constant before 1 T for low coercivity magnetite and maghemite, but continues to increase at higher fields for haematite and goethite. The advantage of this technique for identifying the potential carriers of natural remanence is that it does not involve chemical changes to the rock, since no heating is required.

Dunlop (1972) described a method of deriving the remanent coercivity spectra of a sample from the IRM vs. applied field characteristic. Dunlop (op. cit.) demonstrated that the coercivity spectrum may be approximated by the incremental isothermal remanent moment, Dmr, in equal applied field intervals, DH, as determined from the IRM acquisition curve. This incremental spectrum is easier to calculate than the continuous spectrum determined from the point-by-point slope of the IRM curve, which is not justified by the limited number of measurements made.

In addition to the IRM acquisition experiments, a selection of samples were subjected to backfield IRM experiments; the 0.8 T IRM was gradually reduced to zero intensity by applying stepwise increasing direct magnetic fields in the opposite direction. The applied

field that results in a zero net magnetization during this procedure provides a magnetic hysteresis parameter known as the coercivity of remanence. This is a good indicator of magnetite grain size, which may be substantially different from the sedimentary grain size of the rocks

4.5 Palaeomagnetic age profiling: results

Zeijderveld plots of representative normally magnetised specimens are shown in Figure 4-2 (a-c) and of reversely magnetised specimens in Figure 4-3 (a-c).

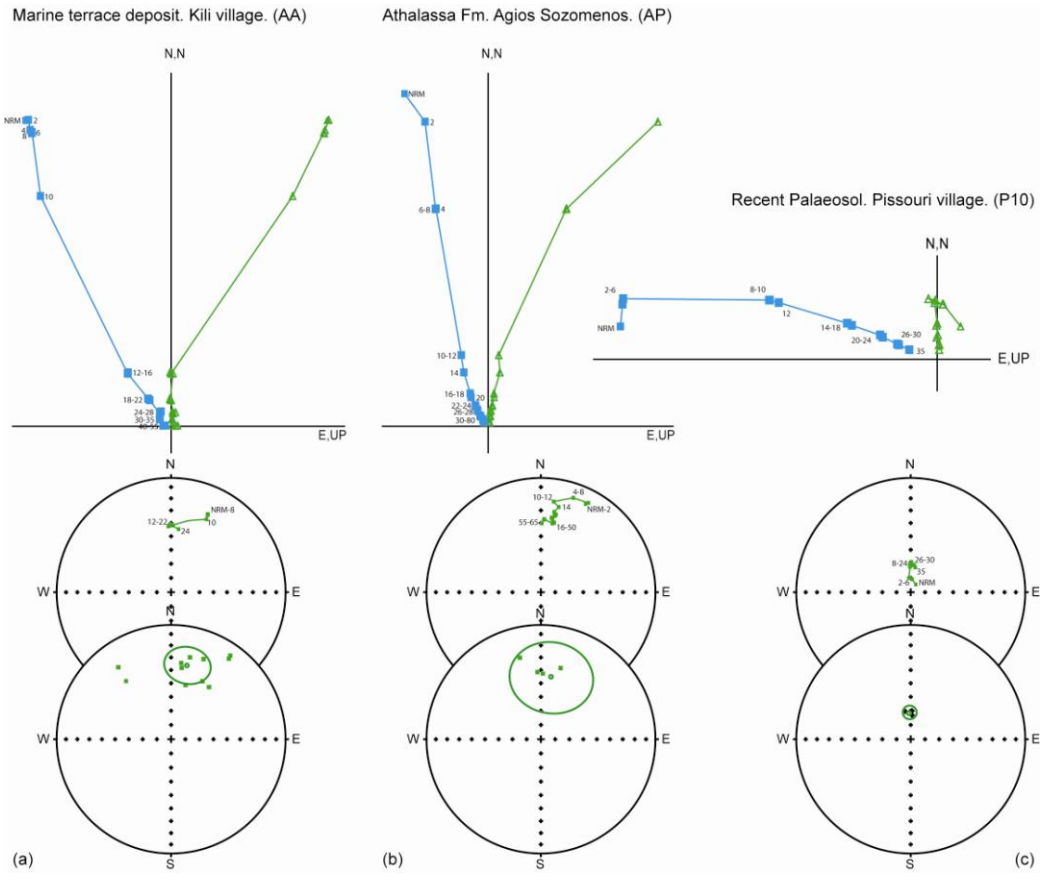

Figure 4-2: AF demagnetisation of representative samples: (a) Kili village, Paphos district: marine terrace deposit; (b) Agios Sozomenos, Lefkosia (Nicosia) district: Athalassa Formation; (c) Pissouri village, Pissouri district: Recent palaeosol.

The reliability of the demagnetisation data was determined by the inspection of the Zeijdervled plots and by intensity-decay curves. Each sample was ranked on an arbitary scale of 'A', 'B' or 'C' (Richter et al., 1998). A sample was given an 'A' ranking if there was an obvious, uniformly stable direction that was clearly identifiable over multiple

demagnetisation steps. 'B' rankings were given to samples that were less stably magnetized than category 'A', but still gave a relatively clear indication of primary polarity. Directional scatter during demagnetization was usually relatively high in such samples. Finally, if a sample displayed no obvious characteristic remanence component, it was given a 'C' ranking. This category usually included samples that were either weakly magnetized or behaved erratically. No interpretation was attempted for such samples.

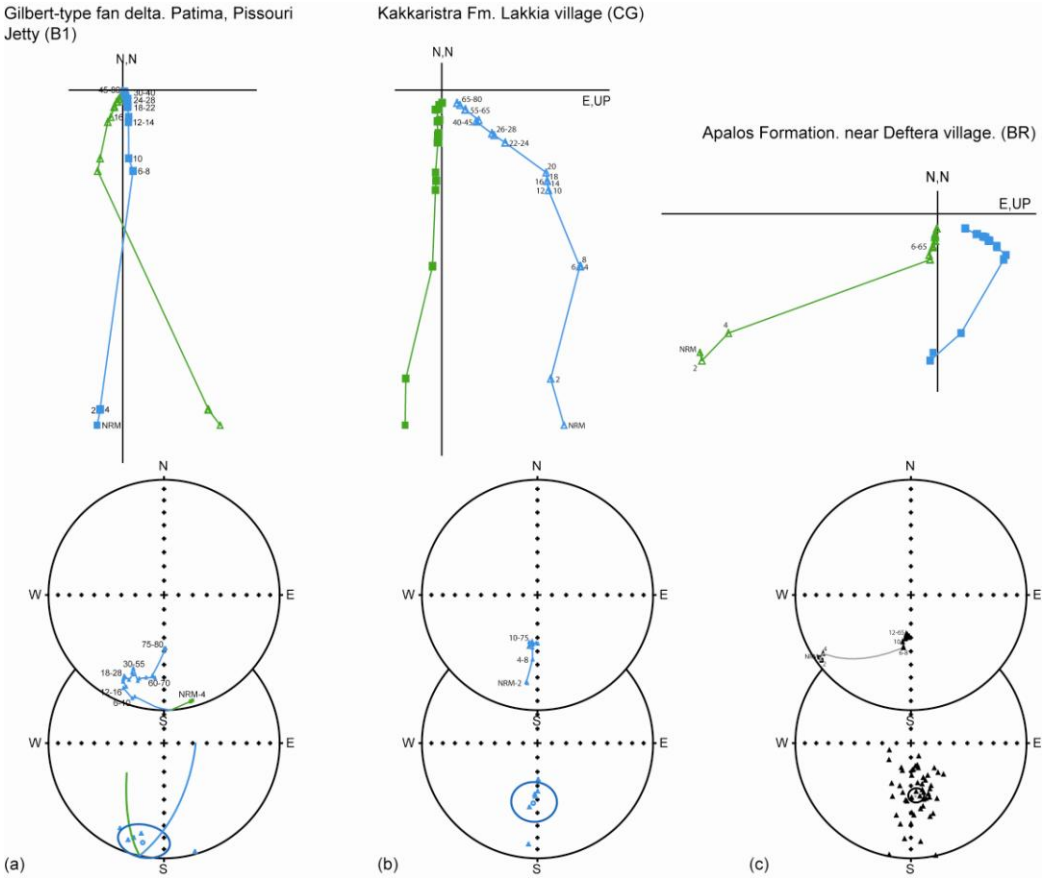

Figure 4-3: AF demagnetisation of representative samples: (a) Pissouri village, Pissouri district: Gilbert-type fan delta deposit; (b) Lakkia village, Lefkosia (Nicosia) district: Kephales Member; and (c) Deftera village, Lefkosia (Nicosia) District: palaeosol

The Characteristic Remanant Magnetisation (ChRM) obtained for each of the measured samples is shown in Figure 4-4. The mean declination and inclination calculated for each site is presented in Table 4-2.

Formation/Member/Location/ (Lithology)	Age	N	n	Dec	Inc	α_{95}	K
Pleistocene – Recent Marine Terraces: Paphos, Kouklia and Lemesos							
Paphos, Kouklia and Lemesos (aeolintes, calcarenties, bioclastic limestones and palaeosols)	Early Pleistocene to Recent	20	48	4.6	69.2	4.6	8.6
Plio-Pleistocene boundary: Mesaoria Basin							
Apalos Formation. Abandoned quarry, near Deftera/Tseri-Lefkosia (Nicosia) road section. (palaeosols)	Early Pleistocene- late early Pleistocene	2	54	173.2	-53.0	5.0	15.8
Athalassa Member (Athalassa Formation). Abandoned quarry, near Deftera. (calcarenite) – BZ	Late Pliocene – late middle Pleistocene	1	5	187.9	-37.6	10.2	57.3
Athalassa Member (Athalassa Formation). Makareion Football stadium. (calcarenite) – BG	Late Pliocene – late middle Pleistocene	1	5	341.1	42.5	29.9	7.5
Athalassa Member (Athalassa Formation). NW of Lefkosia (Nicosia) airport. (calcarenite) – CH	Late Pliocene – late middle Pleistocene	1	2	353.9	74.4	52.7	24.6
Athalassa Member (Athalassa Formation). E of Lefkosia (Nicosia) airport. (calcarenite) – BF	Late Pliocene – late middle Pleistocene	1	1	195.5	-54.7	3.2	99.6
Athalassa Member (Athalassa Formation). Agios Sozomenos. (calcarenite) – AP	Late Pliocene – late middle Pleistocene	1	11	12.7	34.6	14.6	10.7
Athalassa Member (Athalassa Formation). Abandoned quarry, Mammari. (calcarenite) - BE	Late Pliocene – late middle Pleistocene	1	2	162.0	-60.3	13.9	323.8
Athalassa Member (Athalassa Formation). Abandoned quarry, CTKA headquarters (calcarenite) - CD	Late Pliocene – late middle Pleistocene	1	3	197.3	-46.2	46.1	8.2
Athalassa Member (Athalassa Formation). Essovouyes. (calcarenite) – AO	Late Pliocene – late middle Pleistocene	1	1	172.1	-46.0	23.2	4.8
Kephales Member (Kakkaristra Formation). Kephales (calcarenite/sandstone)	Early Pleistocene	1	6	186.1	-51.3	14.2	23.2
Plio-Pleistocene boundary: Pissouri Basin							
Pissouri village. (palaeosol)	Late Pleistocene	1	3	357.7	71.1	4.6	650.2
Pissouri village. (palaeosol)	Early Pleistocene	1	2	166.3	-54.7	16.3	235.7
Gilbert-type Fan Delta. Patima, Pissouri Jetty (calcarenite)	Early Pleistocene	2	9	186.5	-13.5	13.2	16.2
Nicosia Formation. Mandra tou Yerolemou, Pissouri (sandstone/marl)	Late Pliocene	6	15	15.1	58.1	5.6	48.3

Table 4-3: Summary of Palaeomagnetic results obtained during this study: N = number of localities; n = number of samples; Dec = declination; Inc= inclination; α_{95} = radius of the 95% zone of confidence; and K = Fischer precision parameter

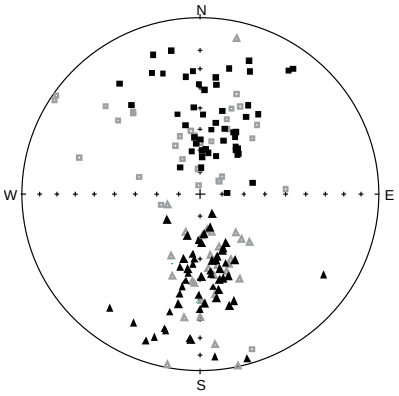

Figure 4-4: Equal-area projection showing the distribution of all ChRM directions (n = 173). Triangles (squares) represent projections on the lower (upper) hemisphere. 'A' ranked samples are indicated by a closed square or triangle, and 'B' ranked samples are indicated by an open square or triangle.

4.5.1 Rock magnetic tests

Typical results of the IRM analyses are shown in Figure 4-5a and Figure 4-5b. The solid curves of Figure 4-5a represent the stepwise increase in isothermal remanent magnetization produced by successively increasing applied fields, while the histograms of Figure 4-5b show the rate of change of IRM, i.e. the incremental coercivity spectrum (Dunlop, 1972). The rapid initial rise and subsequent flattening off of curves above 0.2 T indicates that magnetite is the main magnetic mineral present in all the sampled lithologies.

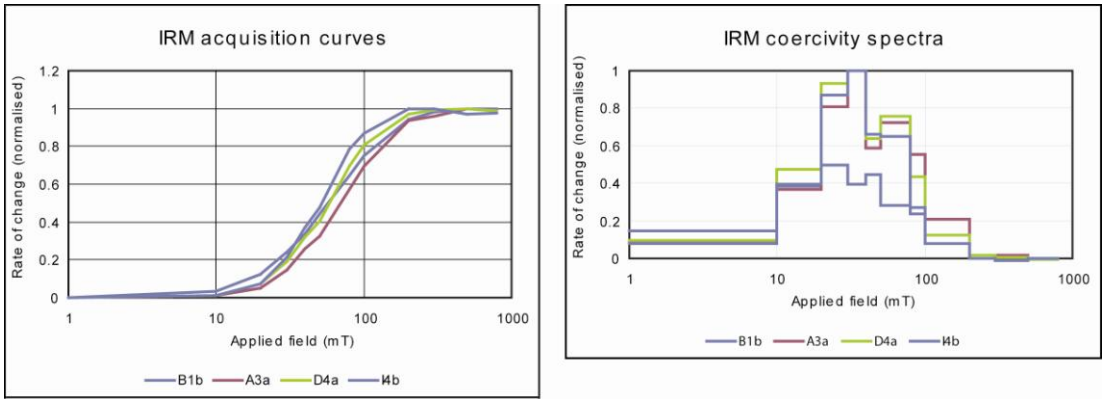

Figure 4-5: IRM (a) acquisition curves and (B) coercivity spectra for a number of selected samples, including calcarenites (B1b/A3a) collected at Pissouri (Gilbert-type fan delta deposits) and marine terrace deposits (D4a/I4b) collected at Paphos

Coercivity of remanence values were found to be in the range 35-47 mT, indicating magnetite grain sizes in the pseudo-single-domain field (0.1-1.0 μm) (Morris, 2003b). It seems likely that the magnetization in these samples is carried by a combination of fine,

detrital grains of magnetite and magnetite occurring as inclusions within silicate grains derived from erosion of source rocks in the Troodos ophiolite and Mamonia Complex.

4.5.2 Pleistocene-Holocene boundary: Paphos, Kouklia and Lemesos, SW Cyprus

Palaeomagnetic samples were collected from a series of raised marine terraces, in the districts of Paphos (Figure 4-6 and Figure 4-7) and Lemesos (Figure 4-8). Marine terrace sediments are best developed in areas of minimal clastic run-off from the uplifting Troodos Massif, especially in the southwest and south of the island (e.g. in the area in and around Paphos).

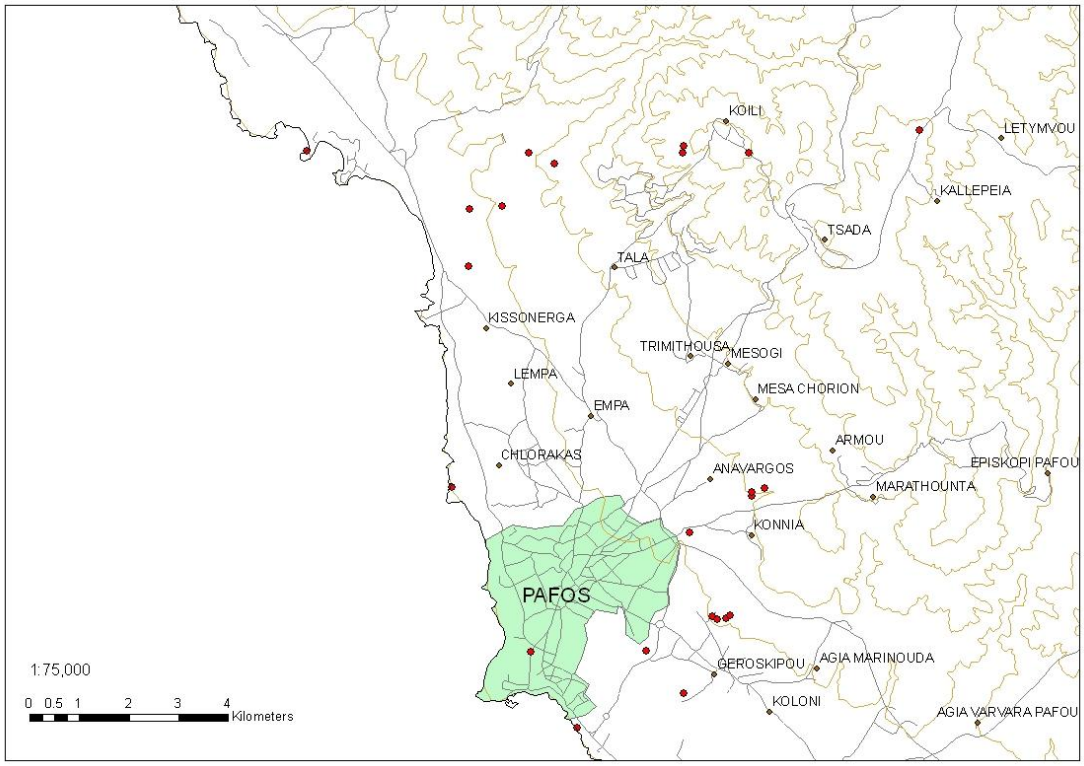

Figure 4-6: Locations of palaeo-magnetic sampling sites in Paphos District. Compiled from GIS data supplied by the Cyprus Geological Survey Department.

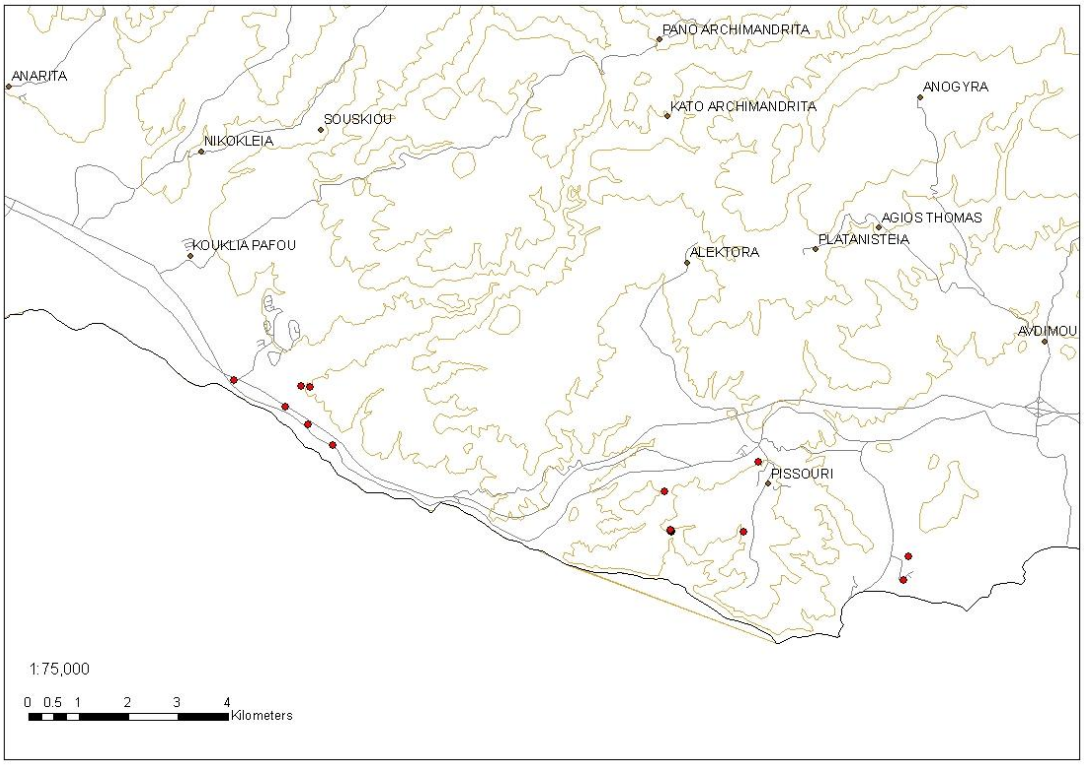

Figure 4-7: Location of palaeomagnetic sample sites at Kouklia and Pissouri. Compiled from GIS data supplied by the Cyprus Geological Survey Department.

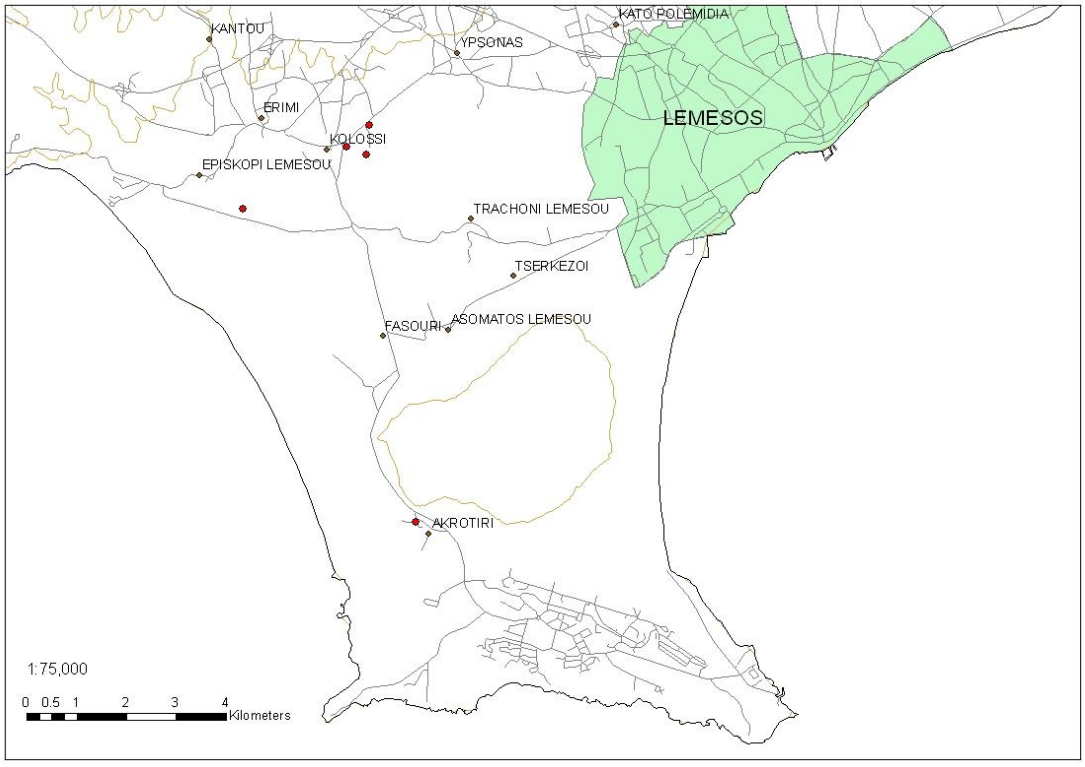

Figure 4-8: Locations of palaeo-magnetic sampling sites in Lemesos district. Compiled from GIS data supplied by the Cyprus Geological Survey Department.

In almost all samples collected, detailed AF demagnetization revealed rather simple properties of characteristic remanent magnetization. Eighteen 'A'-ranked and thirteen 'B'-ranked hard rock samples and six 'A'-ranked and three 'B'-ranked soft rock samples were obtained from raised beach deposits in the vicinity of Paphos. In addition, a further five 'A'-ranked samples and three 'B'-ranked rock samples were obtained from marine terraces in the vicinity of Kouklia, Lemesos and Larnaka.

The characteristic remanent magnetization obtained for the Paphos and Larnaka district terrace samples is directed to the north and downward (Dec: 4.6º, Inc: 69.2º, α95: 8.6, k: 6.6, n: 48) (Figure 4-9).

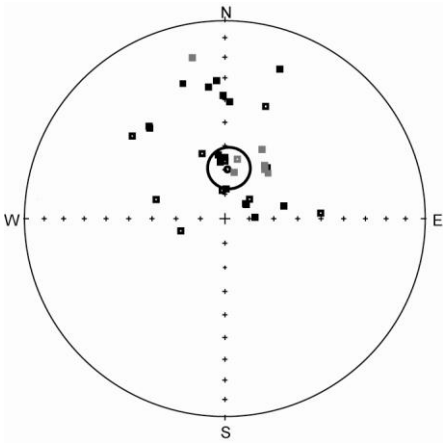

Figure 4-9: Equal-area stereographic projections of characteristic directions (normal and reversed polarities) from samples of bioclastic sandstones and limestones, aeolinites and palaeosols (raised terrace deposits) collected at Paphos (Black squares) (see Figure 4-6 for sample locations) and Kouklia/Lemesos (Grey squares) (see Figure 4-7 for sample locations). 'A'-ranked samples are indicated by closed squares or triangles; 'B'-ranked samples are indicated by an open squares or triangles. The large black circle indicates the mean direction; the 95% confidence limit ellipsoid is shown

Discussion: Poole and Robertson (1991) recognised and correlated five distinct marine terraces, the late Pliocene-early Quaternary – F0 terrace; the early-middle Quaternary – F1 and F2 terraces; and the late Quaternary, F3 and F4 terraces. Corals obtained from the lower, younger terraces (F3 and F4) have been dated by the uranium-series method (Poole et al., 1990); yielding ages of 185-192 ka and 116-130 ka respectively. Poole and Robertson's (1991) stratigraphic framework suggest that the marine terraces are Plio-Pleistocene in age. Given the absence of any reversely magnetised samples, it seems likely that the raised beach deposits were deposited during the Brunhes chron (i.e. < 0.78 Ma). Young, alternative ages of 1.07-0.99 Ma, 1.24-1.22 Ma or 1.95-1.77 Ma are all possible, given the positive polarity

of the samples – however, these ages are deemed unlikely given the stratigraphic constraints mentioned above. Regardless, the data indicates that the marine terraces preserved at Paphos and Lemesos are possibly 'young' (<0.78 Ma), and that rates of uplift in southwest Cyprus are moderately high: possibly 60+ m of uplift in under 780 ka (c 0.08mm/yr).

4.5.3 The Plio-Pleistocene boundary: Mesaoria Basin, central Cyprus

To determine a magnetostratigraphy for the Plio-Pleistocene infill of the Mesaoria Basin, samples were collected from the Kephales Member of the Nicosia Formation (Kakkaristra Formation), the Athalassa Member of the Nicosia Formation (Athalassa Formation) and the Apalos Formation. The Kephales Member (Kakkaristra Formation) was sampled at Lakkia village (WGS 84 533583E/3883438N). The Athalassa Member (Athalassa Formation) was sampled at a number of localities, at a range of stratigraphic heights and topographic elevations. The Apalos Formation was sampled at two localities: (i) along the newly constructed Tseri – Lefkosia (Nicosia) road (WGS84 36N 531504E/3881390N to 531631E/3881436N), and (ii) at an abandoned quarry, near the village of Deftera (WGS84 36N 522715E/3882986N to 522318E/3883305N).

In almost all the samples, detailed Alternating Field demagnetization (AF) revealed rather simple properties of characteristic remanent magnetization. Six 'A'-ranked hard rock samples were collected from a calcarenitic lens within the Kephales Member (Kakkaristra Formation). Twenty 'A'-ranked and fifteen 'B'-ranked hard lithified rock samples were obtained from bioclastic calcarenites of the Athalassa Member (Athalassa Formation). Fifty-four soft rock samples were obtained from palaeosols and sands of the Apalos Formation: section (i) yielded five 'A'-ranked and sixteen 'B'-ranked samples and section (ii) yielded twenty 'A'-ranked and thirteen 'B'- ranked samples. The declination and inclination calculated for each sample, together with the mean declination and inclination calculated for each site are shown in Table 4-4.

Site	Location	Lithology	n	Dec	Inc	α_{95}	K
BZ	Abandoned quarry, near Deftera village	Calcarenite	5	187.9	-37.6	10.2	57.3
				194.9	-22.3	9.4	31.0
				180.2	-35.1	4.3	113.7
				180.9	-42.4	5.6	85.5
				191.7	-41.8	8.3	20.7
				191.0	-45.5	5.3	75.2
BG	Makareion Football Stadium, Lefkosia	Calcarenite	5	341.1	42.5	7.5	29.9
				338.2	27.4	6.9	34.1
				341.2	18.3	4.2	174.8
				351.5	60.5	16.1	23.5
				43.7	65.1	7.0	30.8
				312.8	28.0	6.2	69.9
CH	NW of Lefkosia (Nicosia) Airport, Lefkosia	Calcarenite	2	353.9	74.4	52.7	24.6
				348.6	85.9	11.6	34.3
				354.7	62.8	6.0	235.4
BF	E of Lefkosia (Nicosia) Airport	Calcarenite	1	195.5	-54.7	3.2	99.6
AP	Agios Sozomenos village	Calcarenite	11	12.7	34.6	14.6	10.7
				322.2	36.6	2.7	364.3
				323.7	23.9	5.8	92.1
				36.1	43.6	5.9	40.0
				22.1	26.3	7.4	22.8
				7.6	34.0	7.0	30.8
				28.4	42.5	3.8	95.2
				13.0	28.2	4.0	92.3
				15.0	49.9	5.4	55.1
				8.5	37.7	7.9	24.4
				36.6	13.1	2.2	482.7
				35.7	15.4	837.2	1.5
AQ	Arounas Hill	Calcarenite	5 (2)	295.8	2.7	9.1	71.3
				305.3	5.1	1.6	617.4
				303.3	5.6	1.9	405.6
				282.5	-2.4	7.5	27.0
				293.9	1.8	3.4	163.8
				294.2	3.2	2.3	277.1
CD	CKTA headquarters	Calcarenite	3	197.3	-46.2	46.1	8.2
				218.4	-18.7	15.9	24.1
				172.5	-52.0	30.1	3.0
				187.1	-61.9	3.1	179.7
BE	Mammari village	Calcarenite	2	162.0	-60.3	13.9	323.8
				156.9	-62.4	3.3	146.0
				166.4	-58.1	4.6	57.4
AO	Essovouyes	Calcarenite	2 (1)	172.1	-46.0	23.2	4.8
				172.1	-46.0	23.2	4.8
				123.3	-17.7	3.6	161.7

Table 4-4: Palaeomagnetic data collected for the Athalassa Formation: site = site code/laboratory sample number; n = number of samples; Dec = declination; Inc = inclination; α95 = radius of the 95% zone of confidence; and K = Fischer precision parameter

4.5.3.1 Kephales Member of the Nicosia Formation (Kakkaristra Formation)

The characteristic remanent magnetization obtained for the calcarenites of the Kephales Member (Kakkaristra Formation) is directed to the south and upwards (Dec: 186.1º, Inc: -51.3º, α95: 14.2, k: 23.2, n: 6; Figure 4-10a).

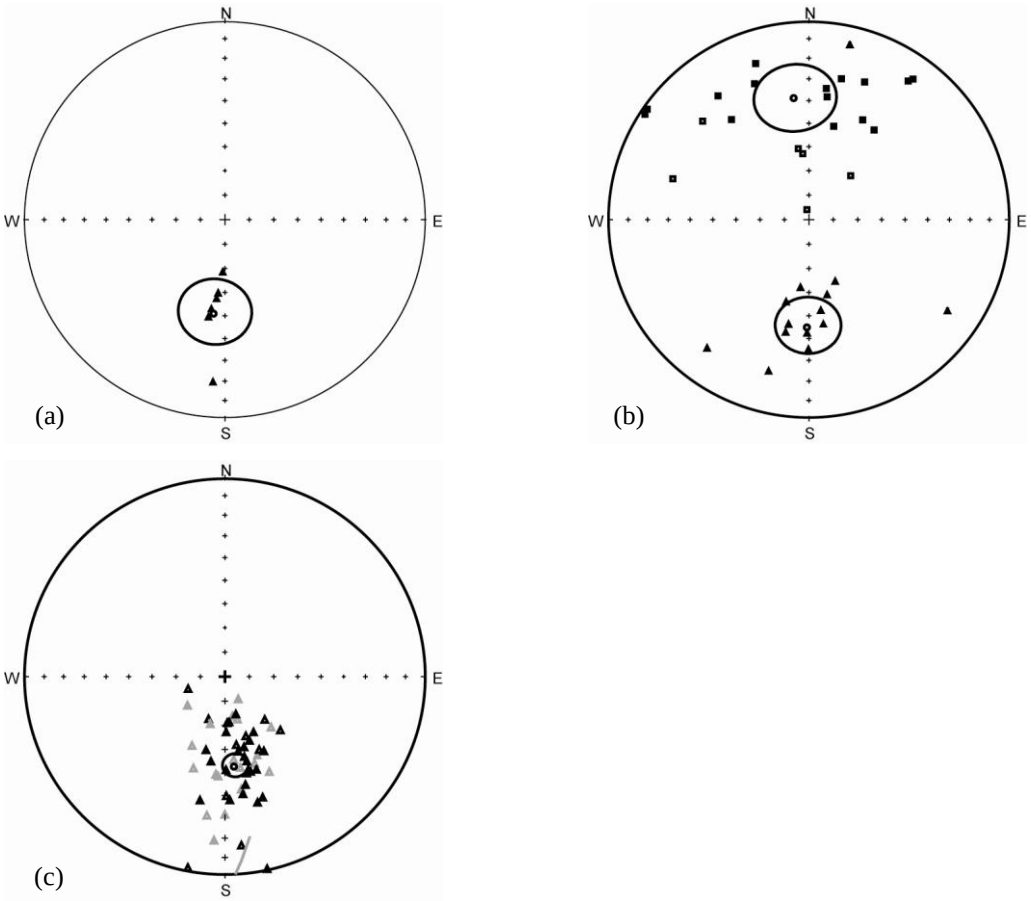

Figure 4-10: (a) Equal-area stereographic projections of characteristic directions (normal and reversed polarities) obtained from calcarenites of the Kephales Member (Kakkaristra Formation) (Lakkia village, near Tseri); (b) Equal-area stereographic projections of characteristic directions (normal and reversed polarities) of samples collected from the Athalassa Formation; (c) Equal-area stereographic projections of characteristic directions (normal and reversed polarities) obtained from samples collected from the Apalos Formation along (i) the newly constructed Tseri-Lefkosia (Nicosia) road (light grey), and (ii) in a quarried section near Anagyia (black).
'A'-ranked samples are indicated by a closed square or triangle, and 'B'-ranked samples by an open square or triangle. The large black circle indicates the mean direction; the 95% confidence limit ellipsoid is shown

4.5.3.2 Athalassa Member of the Nicosia Formation

A characteristic remanent magnetization is identified in bioclastic calcarenites and sandstones of the Athalassa Member (Athalassa Formation), directed either to the north and downwards (Table 4-4) or to the south and upwards (Table 4-4; Figure 4-10b).

4.5.3.3 Apalos Formation

A characteristic remanent magnetization is identified in continental deposits of the Apalos Formation, directed to the south and upwards (Dec: 173.2º, Inc: -53.0º, α95: 5.0, k: 15.8, n: 54) (Figure 4-10c). The characteristic remanent magnetization obtained at the Tseri-Lefkosia road section (Dec: 177.0º, Inc: -53.1º, α95: 8.7, k: 15.2, n: 20; Figure 4-11) and at Deftera village quarry (Dec: 172.5º, Inc: -52.5º, α95: 3.2, k: 6.8, n: 32; Figure 4-12).

Figure 4-11: (a) Sketch of sampled section in Apalos Formation gravel, flood deposits and palaeosols, along the Tseri – Lefkosia (Nicosia) road; (b) Magnetostratigraphy established for Apalos Formation gravel, flood deposits and palaeosols, along the Tseri – Lefkosia (Nicosia) road.

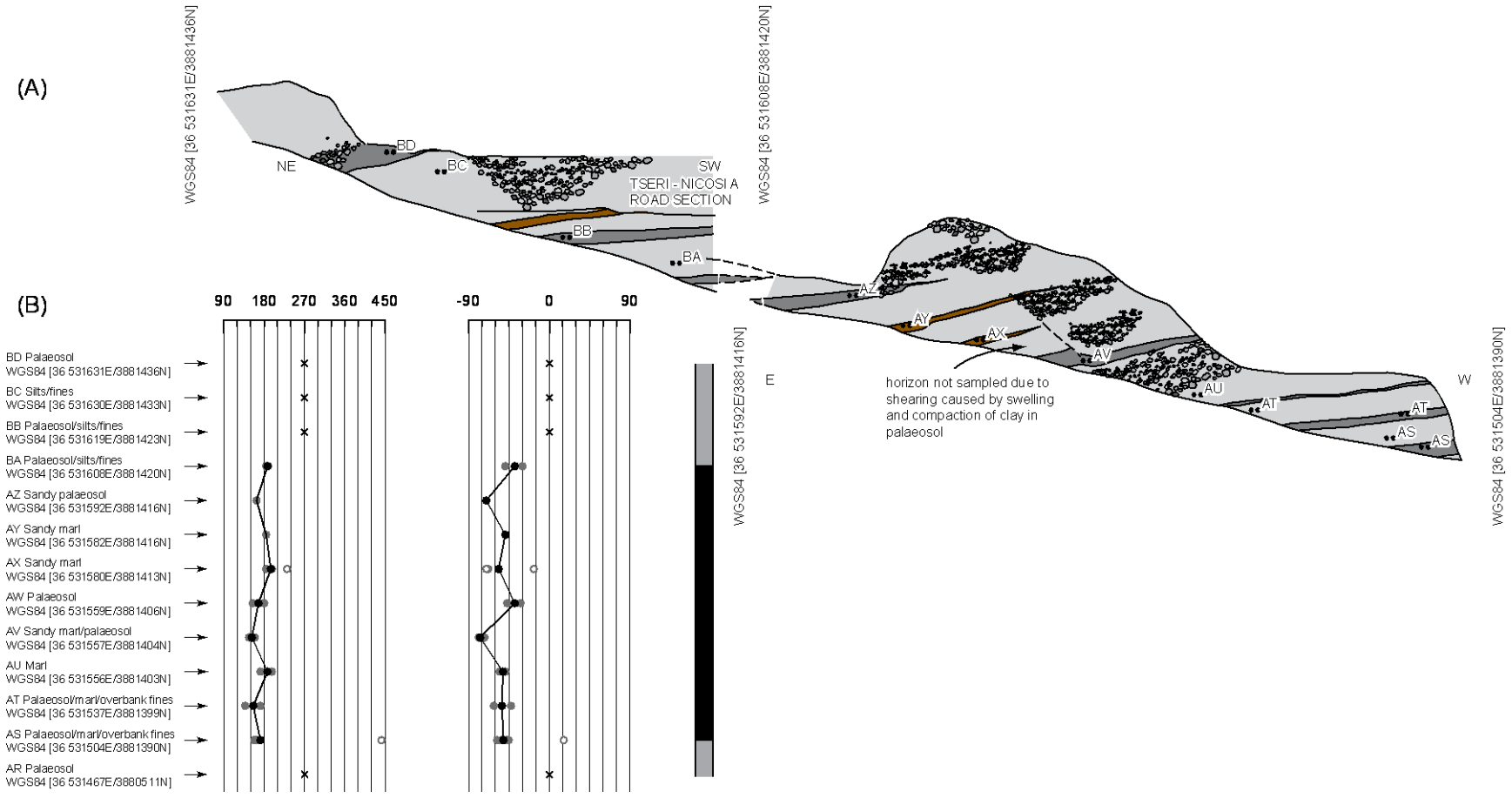

Figure 4-11: (a) Sketch of sampled section in Apalos Formation gravel, flood deposits and palaeosols, along the Tseri – Lefkosia (Nicosia) road; (b) Magnetostratigraphy established for Apalos Formation gravel, flood deposits and palaeosols, along the Tseri – Lefkosia (Nicosia) road.

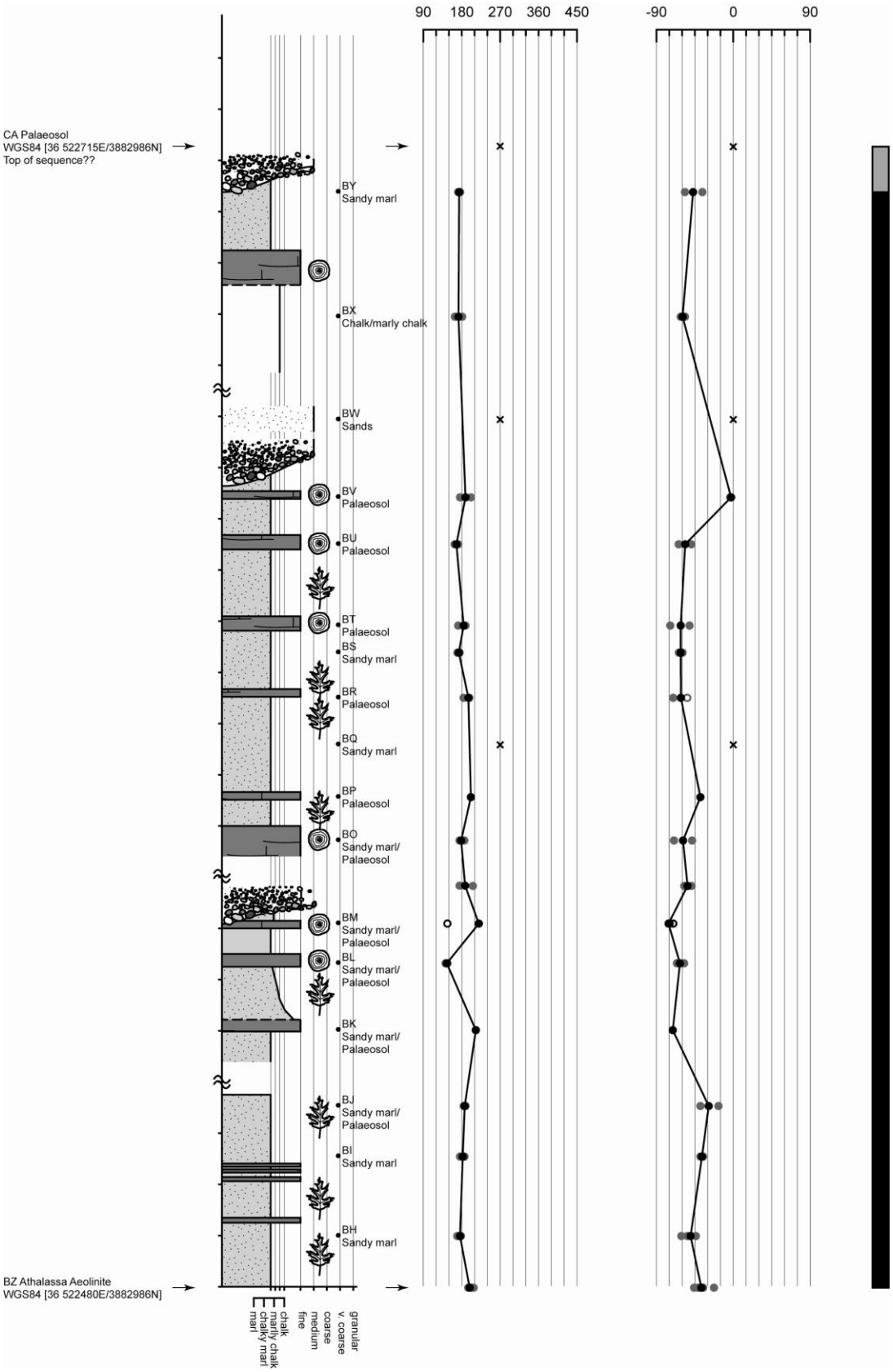

Figure 4-12: Composite stratigraphic section through the Apalos Formation from its base overlying the Kakkaristra Formation, to its top, at an abandoned quarry, near Deftera village.

Discussion: In McCallum and Robertson's (1995a) stratigraphic framework, the Kakkaristra Formation overlies the Nicosia Formation with an angular unconformity. In the revised stratigraphic framework of the Cyprus Geological Survey Department (Panayides et al., 2004), the Kakkaristra Formation is identified as a component member of the Nicosia Formation, i.e. the Kephales Member, due to it lateral equivalence with, and encasement within the Nicosia Formation. To the south of Lefkosia (Nicosia), the Kephales Member occurs as a coarse-grained deltaic sequence, containing sets of foreset strata in excess of 8 m thick; whilst in Lefkosia (Nicosia), the unit occurs as a channelised, ortho- and para-conglomeratic submarine shelf debris-flow deposit (Panayides et al., 2004; Harrison et al, 2004b). The biostratigraphy of the Nicosia Formation is currently being revised. Efthimios Tsiolakis of the Cyprus Geology Survey identified the planktonic foraminifera, *Gt. inflata* within the upper part of the Nicosia Formation (Figure 4-13). *Gt. Inflata* has a first occurrence at 2.13 Ma (Sprovieri et al., 1998) – 2.09 Ma (Lourens et al., 1996) (Figure 4-13). In the revised stratigraphic framework of the Cyprus Geological Survey (Panayides et al., 2004) the Kephales Member is a facies variation of the upper part of the Nicosia Formation. Given this stratigraphic framework, it seems likely that the Kephales Member (Kakkaristra Formation) was deposited during the Matuyama Chron, prior to the onset of the Olduvai Subchron (i.e. between 2.58 – 1.95 Ma).

Athalassa-type bioclastic calcarenites overlie marls of the upper Nicosia Formation (E. Tsiolakis, personal communication) at Essovouyes, near Louroukina village (WGS84 36N 546492E/3874301N). A characteristic remanent magnetization was obtained directed to the south and upward (Dec: 172.1º, Inc: -46.0º, α95: 23.2, k: n/a, n: 1). The preliminary biostratigraphy established for the upper part of the Nicosia Formation indicates that deposition occurred at approximately ~ 2.13 Ma. The characteristic remanent magnetization obtained for the Athalassa-type bioclastic calcarenite at this locality indicates that the deposition of this unit occurred during the Matuyama Chron, immediately prior to the onset of, or immediately after the Olduvai subchron, i.e. at < 1.95 Ma and > 1.77 Ma respectively (Figure 4-14). However, given the age of the Nicosia Formation at this locality, the former is deemed more likely, i.e. deposition occurred between 2.14 – 1.95 Ma (Figure 4-14). Athalassa-type bioclastic calcarenites were also sampled at Mammari village, in an abandoned quarry (WGS84 36N 518245E/3892424N), and at the CKTA (Cyprus Telecommunications) head office, in a second abandoned quarry (WGS84 36N 533670E/3889432N).

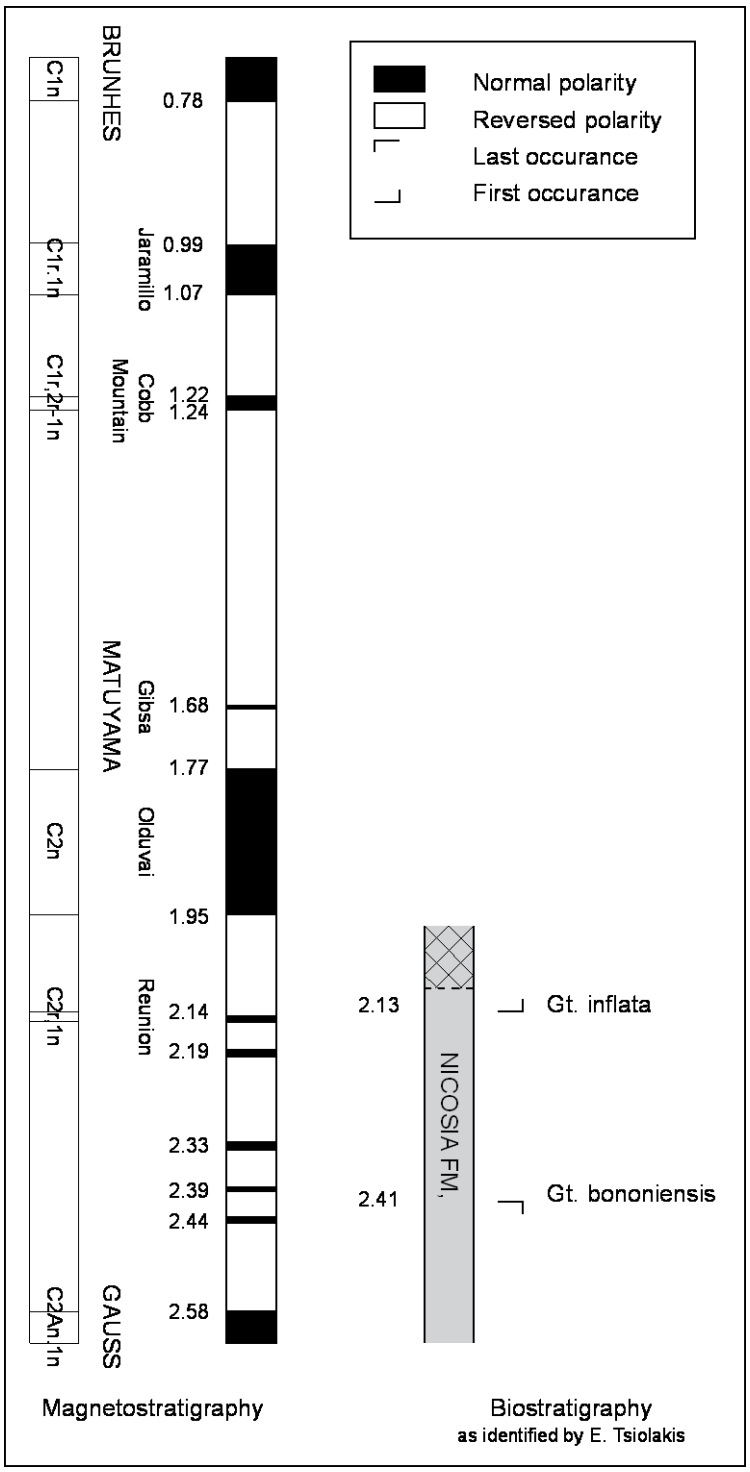

Figure 4-13: The Palaeomagnetic record (2.58 - 1.24 Ma) and preliminary biostratigraphy of the Nicosia Formation (personal communication, E. Tsiolakis)

The characteristic remanent magnetization obtained for both localities was directed to the south and upward (Marammi: Dec: 162.0º, Inc: -60.3º, α95: 13.9, k: 323.8; n: 2 and CKTA: Dec: 197.3º, Inc: -46.2º, α95: 46.1, k: 8.2; n: 3). The unit at Mammari overlies marls of the upper Nicosia Formation (E. Tsiolakis, personal communication). Following the reasoning of

above it is believed that deposition of this unit occurred between 2.14 – 1.95 Ma (Figure 4-14). In contrast, the exact position of the Athalassa-type calcarenite at CKTA, within the Plio-Pleistocene stratigraphic framework is not known: all that can be stated is that deposition occurred either prior to 1.95 Ma or after 1.77 Ma.

Athalassa-type bioclastic calcarenites at Agios Sozomenos (WGS84 36N 538758E/3879504N), and Aronas Hill (WGS84 36N 537350E/3887655N) yield a characteristic remanent magnetization directed to the north (northwest) and downwards (Dec: 12.7º, Inc: 34.6º, α95: 14.6, k: 10.7, n: 13 and Dec: 295.8º, Inc: 2.7º, α95: 9.1, k: 71.3, n: 5 (2), respectively). The calcarenitic bodies at Agios Sozomenos and Aronas Hill occur at a lower topographic elevation than the unit observed at Essovouyes (or its lateral equivalents). They are believed to onlap, or downcut into, Essovouyes-type units. The positive polarity obtained for the Agios Sozomenos-type units, indicate that deposition could have occurred during either the Olduvai or Gibsa Subchrons of the Matuyama Chron, i.e. between 1.95 and 1.77 Ma, or at 1.66 Ma, respectively (Figure 4-14). Sufficient data are not available to distinguish in which of these periods this unit of the Athalassa Member was deposited.

Athalassa Formation bioclastic sandstones directly underlie continental deposits of the Apalos Formation at Deftera village (WGS84 36N 522480E/3883438N) and Makareion Football Stadium, Lefkosia (WGS84 36N 528278E/3889552N). The site at Deftera yielded a characteristic remanent magnetization directed to the south and upwards (Dec: 187.9º, Inc: -37.9º, α95: 10.2, k: 57.3, n: 5). The site at the Makareion football stadium yielded a characteristic remanent magnetization directed to the north and downwards (Dec: 341.1º, Inc: 42.5º, α95: 7.5, k: 29.9, n: 5). The Apalos Formation is believed to be Pleistocene in age (see below). In this stratigraphic framework, the Athalassa Formation at Deftera was deposited in the earliest Pleistocene, between 1.77 and 1.07 Ma, and at the football stadium at Makareion during either the Gibsea or Cobb Mountain event, i.e. at 1.66 Ma or 1.24 – 1.22 Ma, respectively (Figure 4-14).

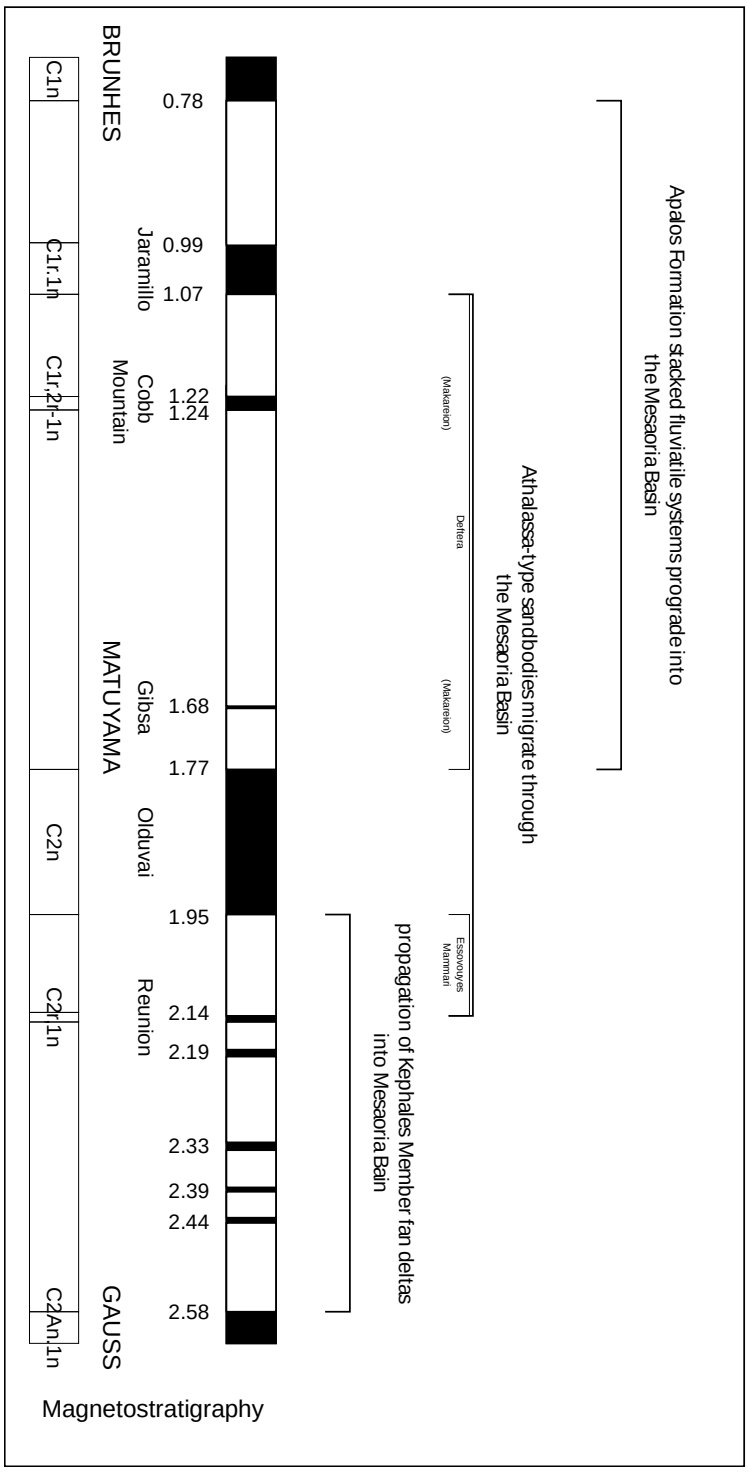

Figure 4-14: Possible correlations of the magnetostratigraphic profile obtained in the Mesaoria Basin to the palaeomagnetic record

The Nicosia Formation is overlain by muddy, calcareous, caliche-like sediments, which have been interpreted by McCallum and Robertson (1995a) to mark the rapid emergence of the Mesaoria Basin in the Late Pliocene-early Pleistocene (McCallum and Robertson, 1995a) (now known to be earliest Pleistocene: this study), heralding deposition of the non-marine

Apalos Formation. Weber et al. (2006) established a preliminary magnetostratigraphy for the Apalos Formation, from bottom to top, with a reversed-normal-reversed main polarity pattern, believed to indicate deposition during mainly the Matuyama chron, with the normal polarity zone representing the Jaramillo subchron (1.07 – 0.99 Ma). The results of the present study validate this claim: it is likely that the stacked system of superimposed fluviatile sediments, comprising the Apalos Formation were deposited during the Matuyama Chron, following the Olduvai subchron (1.77 – 0.78 Ma; Figure 4-14).

4.5.4 Plio-Pleistocene boundary: Pissouri, southwest Cyprus

Palaeomagnetic samples were collected from several sites in the Pissouri village area: at (i) Mandra tou Yerolemou, Pissouri (WGS84 36N 470644E/3835477N), where marls and sandstones of the upper part of the Nicosia Formation are exposed; at (ii) Patima, Pissouri Jetty (WGS84 36N 475331E/3834457N and 475438E/3834930N), where calcarenites of Stow et al.'s (1995) Gilbert-type fan deltas are exposed; and at (ii) Pissouri village (WGS84 36N 470524E/3836243N and 472421E/3836840N), where interbedded aeolinites and palaeosols are exposed (Figure 4-15).

In almost all samples, stepwise AF demagnetization revealed rather simple properties of natural remanent magnetization. Nine 'A'-ranked samples and six 'B'-ranked samples were obtained from homogenous marls and sandstones of the upper part of the Nicosia Formation. Six 'A'-ranked samples and three 'B'-ranked samples were obtained from calcarenites of Stow et al.'s (1995) Gilbert-type fan deltas. Six 'A' ranked-samples were obtained from the palaeosols and aeolinites overlying the Gilbert-type fan deltas.

A maximum peak field of around 16 mT was sufficient to remove a secondary overprint of viscous origin. Above this field a characteristic remanent magnetization was identified, which was directed to the north and downwards for marls and sandstones of the upper part of the Nicosia Formation (Dec: 15.1º, Inc: 58.1º, α95: 5.6, k: 48.3, n: 15) and the most recent palaeosol horizon (Dec: 357.7º, Inc: 71.7º, α95: 4.6, k: 650.2, n: 3), and directed to the south and upwards for calcarenites of Stow et al.'s Gilbert-type fan deltas (Dec: 186.5º, Inc: -13.5º, α95: 13.2, k: 16.2, n: 9) and the oldest palaeosol horizon (Dec: 166.3º, Inc: -54.7º, α95: 16.3, k: 235.7, n: 2) (Figure 4-16).

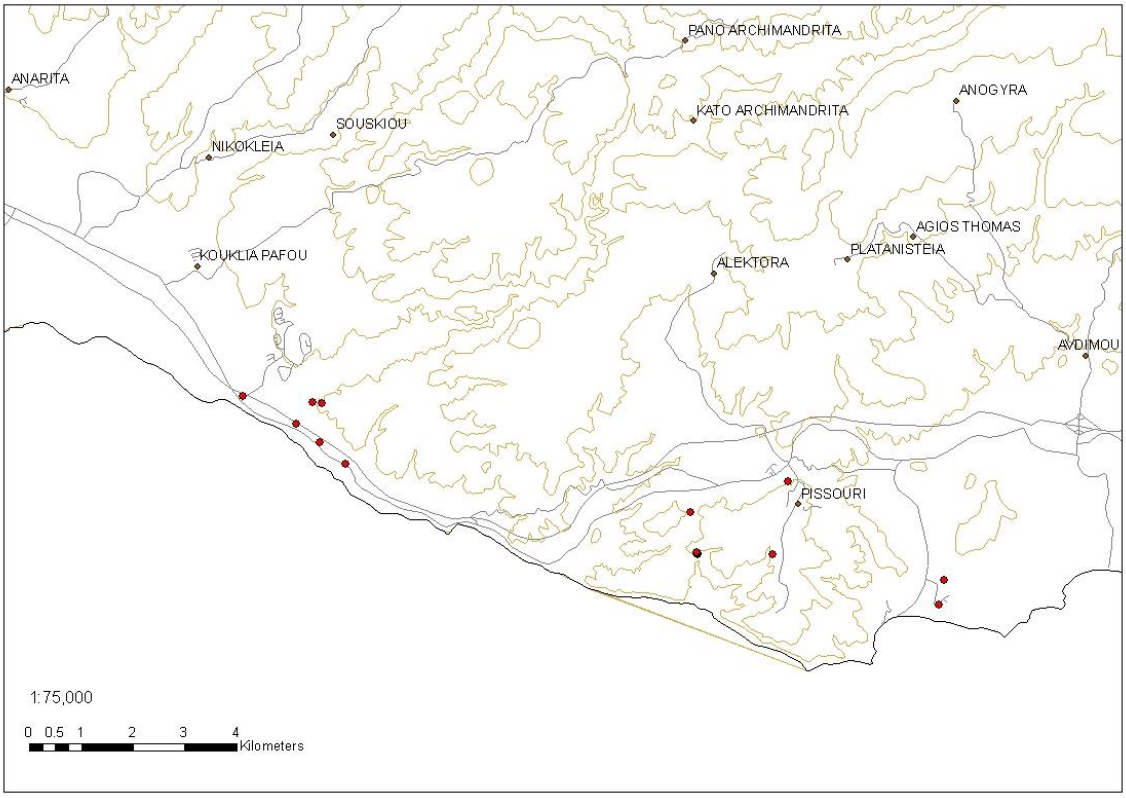

Figure 4-15: Location of palaeomagnetic sample sites at Kouklia and Pissouri. Compiled from GIS data supplied by the Cyprus Geological Survey Department.

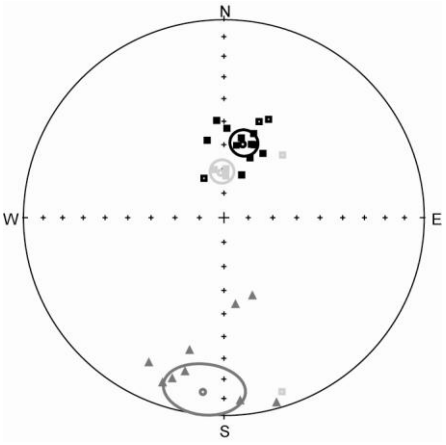

Figure 4-16: Equal-area stereographic projections of characteristic directions (normal and reversed polarities) obtained from samples of marl and sandy marl of the uppermost part of the Nicosia Formation (black), calcarenites of Stow et al.'s (1995) Gilbert-type fan deltas (medium grey) and also from recent palaeosols (light grey). 'A'-ranked samples are indicated by a closed square or triangle, whereas 'B' ranked samples are indicated by an open square or triangle. Mean directions with 95% confidence are illustrated. The large circles indicate the mean directions; the 95% confidence limit ellipsoids are shown

Discussion: The composite stratigraphic section shown in Figure 4-17 was compiled from data collected at Mandra tou Yerolemou (Pissouri), Pissouri village and Patima (Pissouri Jetty); it incorporates sedimentological data (e.g. logs) from the upper part of the Nicosia Formation, calcarenites of Stow et al.'s (1995) Gilbert-type fan delta deposits and the upper sequence of interbedded aeolintes and palaeosols (see chapter 6).

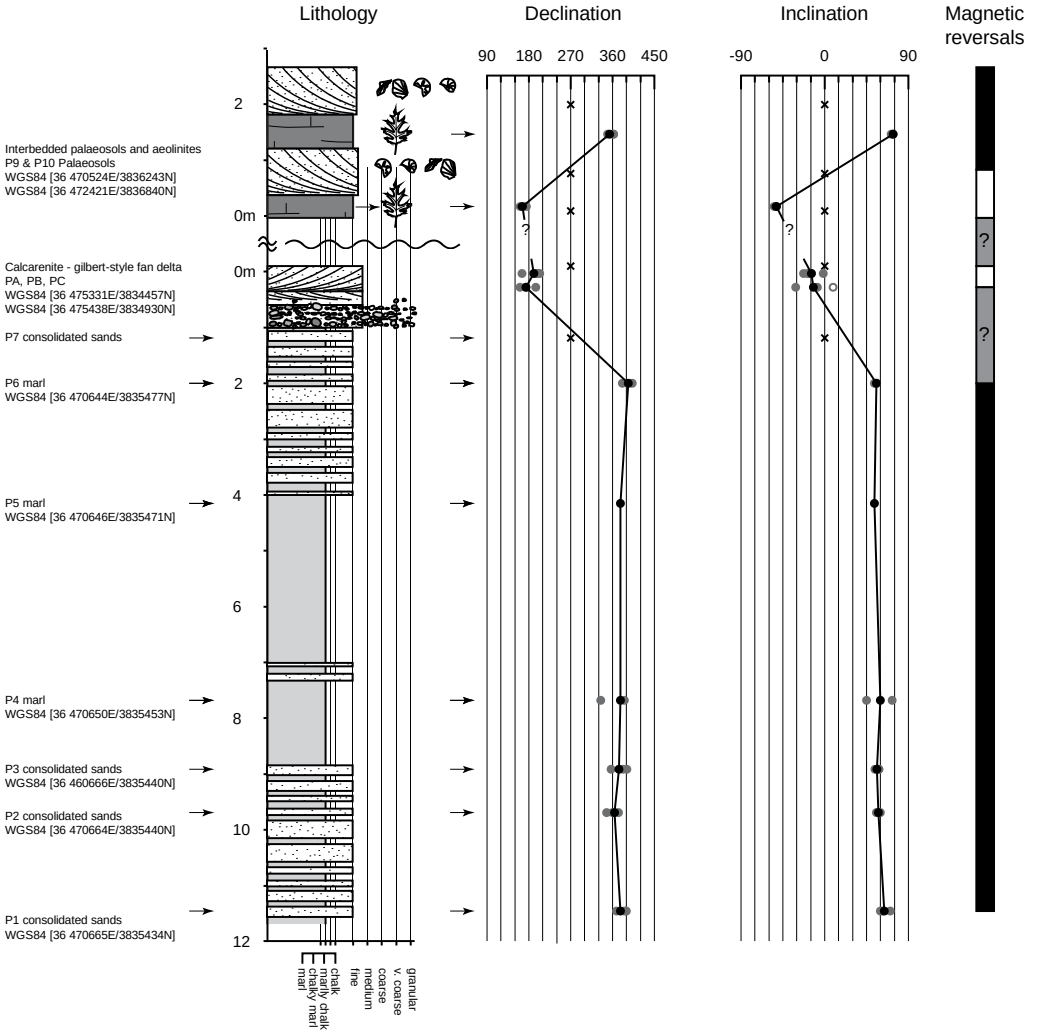

Figure 4-17: Composite stratigraphic section through the upper units of the Nicosia Formation, Stows et al.'s (1995) Gilbert-style fan deltas and overlying palaeosols and aeolinites. Sample horizons marked (Samples that didn't yield a palaeomagnetic signal are marked by a cross). The figure incorporates the results of the palaeomagnetic study (the presentation of the palaeomagnetic data is as in Figure 6-10).

The characteristic remanant magnetisation is carried by magnetite originating from the nearby Troodos Ophiolite Complex. A preliminary magnetostratigraphy, with a normal-reversed-normal main polarity pattern, is observed at Pissouri (Figure 4-17). Magnetostratigraphic data for the lower part of the Nicosia Formation was obtained by Clube (1985) (Dec: 002.3º, Inc: 56.3º, α95: 10.2, k: 5.6, n: 34; Figure 4-18).

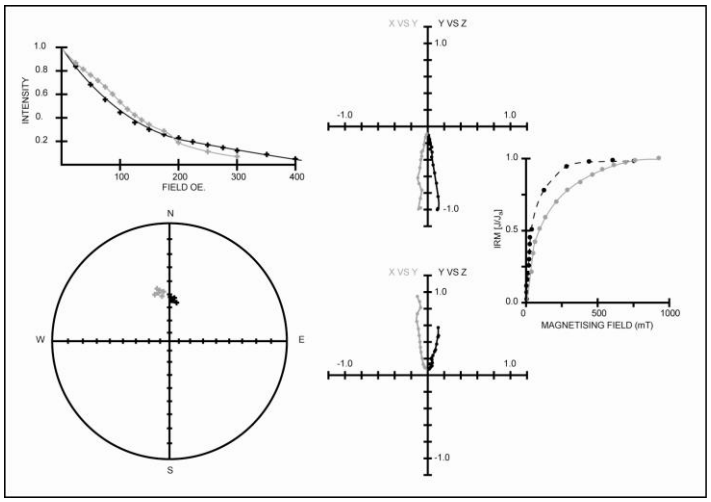

Figure 4-18: AF demagnetisation plots and IRM acquisition curves of Clube (1985) for (A) ophiolite-derived sediment, collected at Tochni (black circles) and (B) Pliocene marl, collected from the Polis Graben (grey circles).

This data, and the palaeotological data of others (Orszag-Sperber et al., 1989; Rouchy et al., 2001), indicate that the lower- and middle-parts of the Nicosia Formation are Pliocene in age. Given the age estimate of the succession as late Pliocene to early Pleistocene, the following magnetostratigraphy can be proposed:

i. Nicosia Formation marls were deposited either during the Reunion (**2.15 – 2.14 Ma**) or Olduvai subchron (1.95 - 1.77 Ma) of the Matuyama chron (Dec: 15.1º, Inc: 58.1º, α95: 5.6, k: 48.3, n: 15) (Figure 4-19);
ii. Calcarenites of Stow et al.'s Gilbert-type fan deltas were deposited during the Matuyama chron, either prior to or after the Olduvai subchron, i.e. between **2.14 and 1.95 Ma** or between 1.77 and 1.66 Ma respectively (Dec: 186.5º, Inc: -13.5º, α95: 13.2, k: 16.2, n: 9) (Figure 4-19);
iii. The first of the palaeosol horizons were deposited during the Matuyama chron, either prior to or after the Olduvia subcron, i.e. between 2.14 and 1.95 Ma or between 1.77 and 1.66 Ma respectively (Dec: 166.3º, Inc: -54.7º, α95: 16.3, k: 235.7, n: 2) (Figure 4-19); and
iv. The upper palaeosol horizon were deposited during the Brunhes chron (< **0.78 Ma**) (Dec: 357.7º, Inc: 71.1º, α95: 4.8, k: 650.2, n: 3) (Figure 4-19).

Higher resolution palaeomagnetic profiling needs to be undertaken to accurately constrain the age of each of these lithostratigraphic units; however, based on published palaeontological evidence (Orszag-Sperber et al., 1989; Rouchy et al., 2001) and previous

palaeomagnetic studies (Clube, 1985) the author cautiously proposes that the ages given in bold are the more realistic.

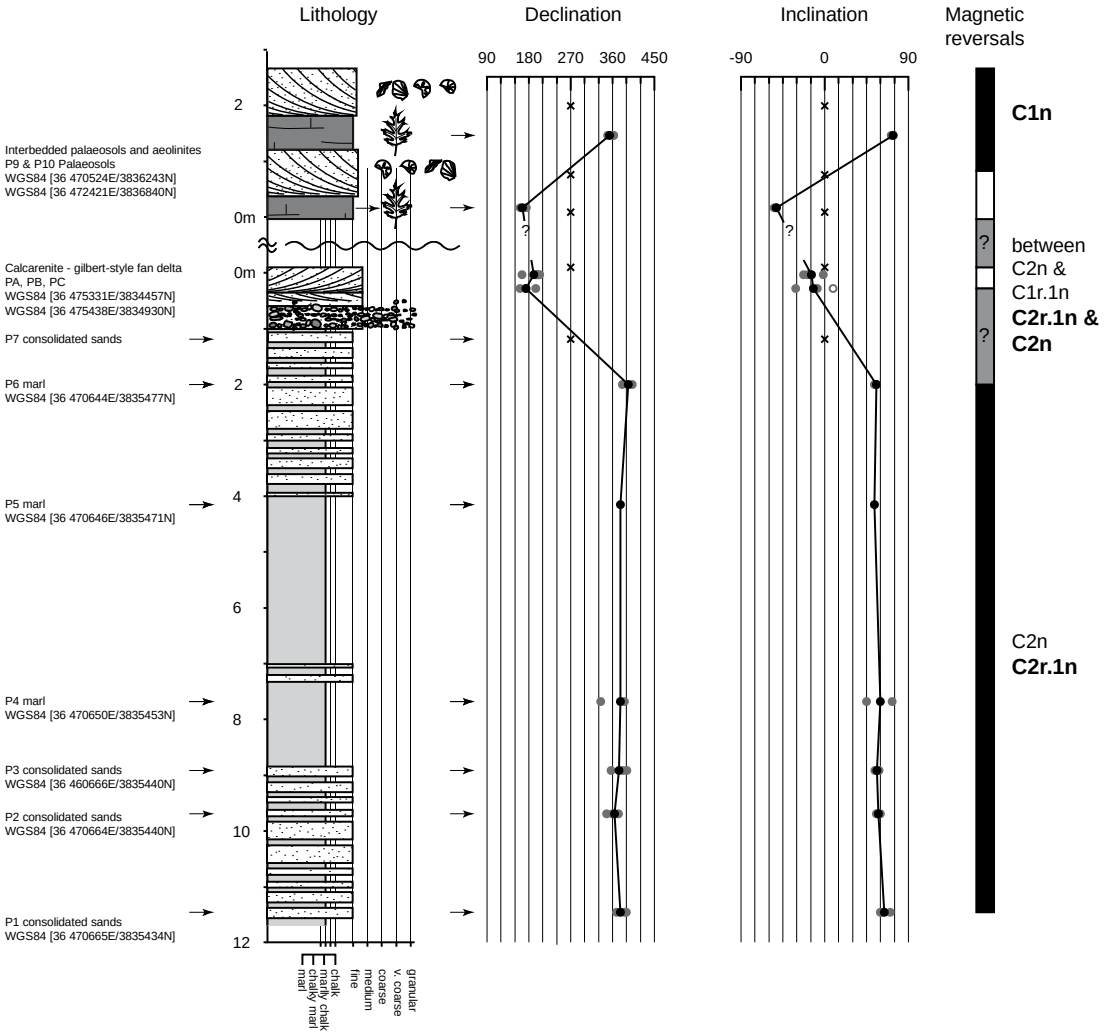

Figure 4-19: Possible correlations of the magnetostratigraphic profile obtained at Pissouri to the palaeomagnetic record (Cande & Kent, 1995); the favoured correlation is indicated in bold

4.6 Magnetostratigraphy

A composite magnetostratigraphic framework for the Plio-Pleistocene units of southern and central Cyprus is shown in Figure 4-20 (age constraints shown in bold are the preferred interpretation):

i. The marine terraces observed at Paphos at elevations above sea level of c. 0m, 1m, 50m, 100m, 125m, 200m, 270m and 500m were all cut, and subsequently infilled post 0.78 Ma;

ii. Marine terraces observed at Kouklia at elevations of c. 25m, 40m, 50m, 100m and 120 m were all cut, and subsequently infilled post 0.78 Ma;

iii. Marine terraces observed in the Lemesos District at elevations of c. 10m (Akotiri), 30m (Akotiri Police Station), 50m, 60m and 65 m were all cut, and subsequently infilled post 0.78 Ma;

iv. In the Mesaoria Basin, marls and sandy marls of the upper part of the Nicosia Formation (E. Tsiolakis, personal communication) are transgressed by (a) marine conglomerates and calcarenites of the Kephales Member at Lakkia village and (b) channelised bioclastic sandstones of the Athalassa Member at Essovouyes, near Louroukina village;

v. Kephales Member fan-deltas prograded into the Mesaoria Basin from the southern margin of the basin during the latest Pliocene (2.58 – 1.95 Ma);

vi. Athalassa-type bioclastic sandstones prograded into the Mesaoria Basin during the latest Pliocene – earliest Pleistocene (2.14 – 1.22 Ma);

vii. Stacked fluviatile systems prograded into the Mesaoria Basin from the southern margin of the Basin during the earliest Pleistocene (1.77 – 0.78 Ma) (Apalos Formation);

viii. Marls and sandy marls assigned to the upper part of the Nicosia Formation (E. Tsiolakis, personal communication), located at Mandra tou Yerolemou in the Pissouri Basin, were either deposited during the Reunion (**2.15 – 2.14 Ma**) or Olduvai (1.95 – 1.77 Ma) subchron of the Matuyama Chron;

ix. Gilbert-type fan-deltas prograded into the Pissouri Basin from the northern margin of the basin during the latest Pliocene - earliest Pleistocene (**2.14 – 1.95 Ma** or 1.77 – 0.78 Ma);

x. Higher in the Plio-Pleistocene sequence, aeolinites are interbedded with Terra Rosa-type palaeosols. The lowermost palaeosol sampled was deposited in the Matuyama Chron, following the Olduvai subchron (1.77 – 0.78 Ma). The uppermost palaeosol sampled was deposited in the Brunhes Chron (0.78 Ma - present).

Figure 4-20: Magnetostratigraphy of the Plio-Pleistocene circum-Troodos sedimentary cover. Unit thicknesses not to scale.

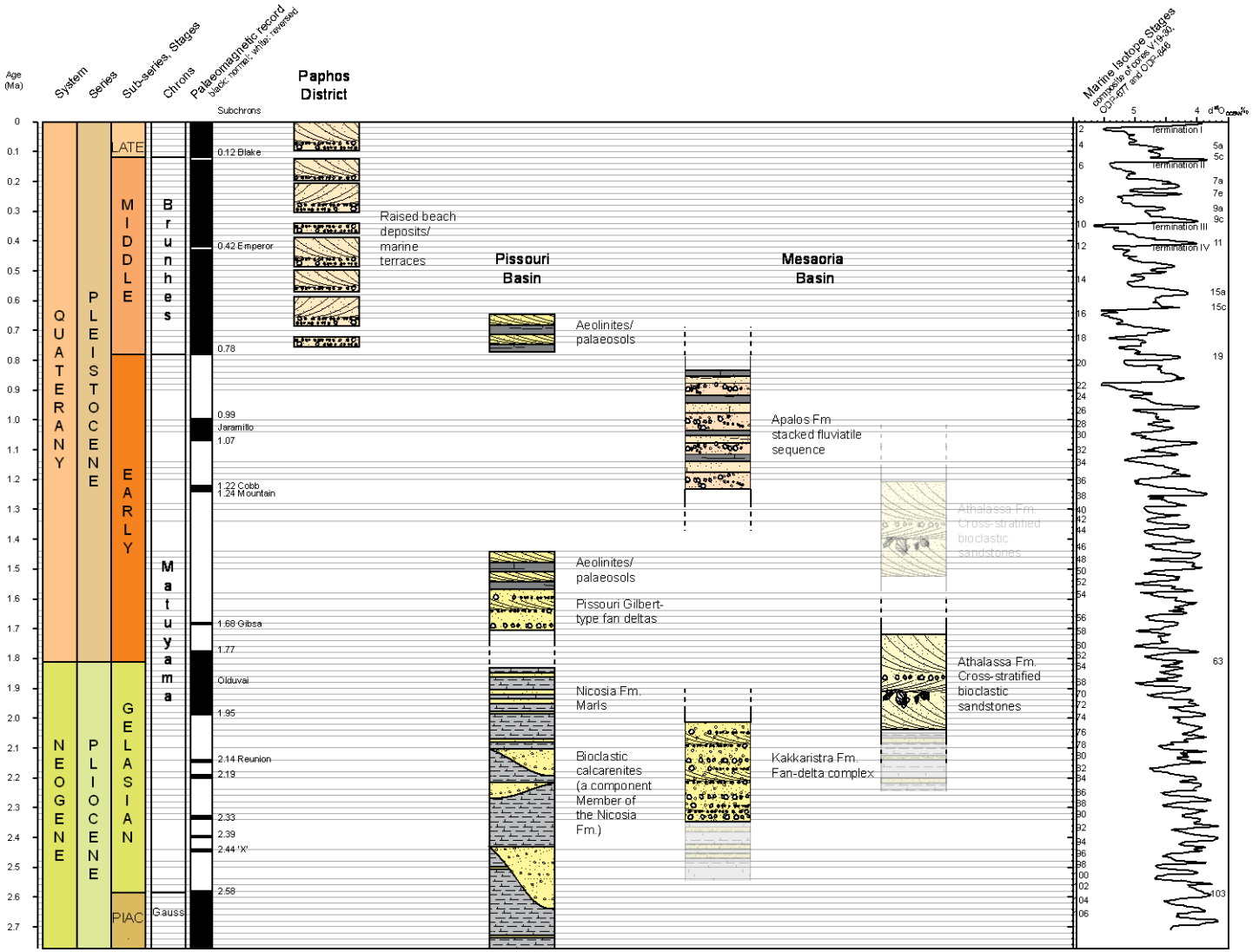

Figure 4-20: Magnetostratigraphy of the Plio-Pleistocene circum-Troodos sedimentary cover. Unit thicknesses not to scale.

4.7 Tectonic versus eustatic sea-level change at the Cyprus active margin

Any interpretation involving tectonic uplift of Cyprus must first take into account Quaternary sea-level change. Robertson et al. (1991), Poole and Robertson (1991) and McCallum and Robertson (1995a) evaluated the influences of tectonic and eustatic sea-level change on sedimentation at the Cyprus active margin. They concluded that tectonics exerted the dominant influence on sedimentation, modified by the effects of global sea-level changes:

4.7.1 Middle to Late Pliocene

McCallum and Robertson (1995a) envisaged the following main controls on sedimentation in the Mesaoria Basin, during the Middle to Late Pliocene as:

i. Sea-level rise, following the Mediterranean Salinity Crisis, led to the deposition of deep-water marls (i.e. the lower marls of the Nicosia Formation). Channel cutting, during this period of well-documented sea-level rise (Hsü et al., 1973; Jolivet et al., 2006), cannot simply reflect a lowstand, but must instead be related to tectonics and basin morphological factors (McCallum and Robertson, 1995a).
ii. The cutting and filling of channels in the middle to upper parts of the Nicosia Formation could be related to lowstand events, superimposed on the longer term subsidence and progressive infill of the Mesaoria Basin (McCallum and Robertson, 1995a).

4.7.2 Late Pliocene

McCallum and Robertson (1995a) evaluated the dominant controls on deposition of the Kephales Member (Kakkaristra Formation) in the Mesaoria Basin during the late Pliocene as:

i. Uplift of the Troodos Massif during the late Pliocene (Robertson, 1977; McCallum and Robertson, 1990), led to an influx of coarse clastics into the Mesaoria Basin and onset of deposition of the Kephales fan-delta (2.58 – 1.95 Ma).

ii. Local incision of the Kephales fan-delta (Kakkaristra Formation) into marine facies of the Nicosia Formation was due to climatic and/or eustatic effects.
iii. Climatic and eustatic effects could have influenced phases of fan-delta construction in the Kephales Member (Kakkaristra Formation), including the development of Gilbert-type-profile mouth bars (McCallum and Robertson, 1995a).

McCallum and Robertson (1995b) established the dominant controls on deposition of the Athalassa Formation, in the Mesaoria Basin, during the Late Pliocene to be:

i. Uplift of the Kyrenia Range, at the beginning of Athalassa Member times (2.14 – 1.22 Ma) (McCallum and Robertson, 1990) increased the area of coastal carbonate sands, providing a source of sand for the Mesaoria Basin.
ii. During eustatically initiated transgression, this sediment was reworked southwards from the Kyrenia landmass.
iii. In addition, McCallum and Robertson (1995b) postulate that accompanying climate change and increased wind activity may have enhanced the ability to transport sand offshore to the south.

Stow et al. (1995) established the dominant controls on deposition of the Gilbert-type fan deltas, in the Pissouri Basin, during the Late Pliocene as:

i. Uplift of the Troodos Massif, in the Late Pliocene (Robertson, 1977; McCallum and Robertson, 1990), led to a significant infux of coarse clastics and deposition of the Gilbert-type fan deltas.
ii. High-frequency sea level fluctuations do not appear to have influenced sedimentation (Stow et al., 1995).

4.7.3 Late Pliocene – early Pleistocene

Influxes of coarse clastic material into the Mesaoria Basin and the Pissouri Basin have been attributed to pluvial periods, when erosion of the uplifting Troodos Massif was most dominant. In contrast, thick palaeosol deposits are thought to represent interpluvial periods (Weber et al., 2006). Stacked fluviate deposits, consisting of rhymthically bedded units of gravels, flood deposits and palaeosols (Apalos Formation), therefore, record climatic

fluctuations in the Mesaoria Basin. Similarly, stacked conglomerates and palaeosols in the Pissouri Basin record climatic fluctuations.

4.7.4 Early Pleistocene – Late Pleistocene

Shallow-marine (littoral) carbonates in coastal Cyprus developed in response to the interplay between regional tectonic uplift, focussed on the Troodos Massif and eustatic sea-level change/climate change (Poole and Robertson, 1991; 2000). Each of the four main terraces (F1 – F4: see section 4.5.2) identified by Poole and Robertson (1991), show a similar history of deposition:

i. Marine transgression, with development of a localised conglomerate lag;
ii. Maximum marine transgression (maximum flooding surface), associated with the growth of Scleractenian corals and calcareous algae;
iii. Gradual marine regression, recorded in carbonate grainstones and local packstones; and
iv. Maximum marine regression, recorded in cross-bedded, carbonate sands (aeolinites).

4.8 Implications for the Plio-Recent tectono-stratigraphic evolution of Cyprus

Sedimentological and magnetostratigraphic evidence from the circum-Troodos sedimentary cover provides insights into the Plio-Pleistocene tectonostratigraphic evolution of south Cyprus.

Sedimentary evidence has established that the Limassol Forest ophiolite of southern Cyprus was wholly emergent and eroding in Early Miocene time (see discussion in chapter 3, section 3.4.5), while the main Troodos ophiolite remained mainly submerged, with little erosion until early-late Pliocene time (Robertson, 1977; McCallum, 1989). Pronounced uplift of the Troodos ophiolite began in the Late Pliocene (>2.14 Ma).

4.8.1 Paphos District

Rapid tectonic uplift, coupled with the effects of eustatic sea-level change, resulted in the development of shallow-marine and aeolian sequences in coastal areas of southwest and

south Cyprus. Palaeomagnetic age profiling of littoral marine terraces developed at c. 0m, 1m, 50m, 100m, 125m, 200m, 270m and 500m in the Paphos District indicate that all these terraces were, cut and subsequently covered by littoral sediments post 0.78 Ma

4.8.2 The Mesaoria Basin

Tectonic activity has played a major role in controlling the architecture of the Plio-Pleistocene Mesaoria Basin. McCallum and Robertson (1995a) suggest that the Nicosia Formation fan-delta system evolved as a response to uplift, emergence and erosion of the Troodos Massif, during the Early Pliocene. Extensional faulting along the southern margin of the Mesaoria Basin was active at this time (see chapter 3). McCallum and Robertson (1995a) argue that the fault block morphology in this part of the basin contributed to sediment transportation paths and depositional sites. In addition, steepened slopes associated with the faulted margin at its hinterland helped control the formation of channels and subaqueous fan-delta fronts, which were filled mainly with mass-flow deposits.

McCallum and Robertson (1995a) argue that the onset of deposition of the Kephales fan-delta system marked a second pulse of uplift of the Troodos Massif (2.56 – 1.95 Ma; this study). A significant hiatus in deposition occurred prior to the progradation of the Kephales fan-delta into the basin. McCallum and Robertson (1995a) map a local, angular unconformity at the base of the 'Kakkaristra Formation' near the village of Potami. This implies a second pulse' of uplift, with local deformation and tilting of earlier strata. Major restructuring did not occur, however, and the relatively gentle morphology of the basin at this time was not significantly affected. As the basin was already, largely infilled, the Kephales fan-delta prograded onto a shallow water sedimentary platform. Contemporaneously, shallow-marine, carbonate sandbodies, migrated southwards across the shallow water platform from an origin at the southern margin of the Kyrenia landmass (Althalassa Formation bioclastic calcarenites, 2.14 – 1.22 Ma). Rapid emergence of the Mesaoria Basin in the earliest Pleistocene (1.77 – 0.78 Ma), led to a stack of fluviatile systems (rhythmically bedded gravels, sandy/silty overbank fines and palaeosols), which prograded out from the Troodos Massif. McCallum and Robertson (1990) identified a transitional facies between the Nicosia and Apalos Formations that was comprised of muddy, calcareous, caliche-like sediments.

4.8.3 The Pissouri Basin

In the Pissouri region, pronounced uplift of the Troodos ophiolite is coincident with the large-scale progradation of Gilbert-type fan-deltas into the Pissouri Basin (< 1.77 Ma) (see discussion in chapter 6). Rapid emergence of the Pissouri Basin in the earliest Pleistocene (2.14 – 1.95 or 1.77 – 1.66 Ma), and compartmentalisation by large north-south trending faults (see chapter 3, section 3.4.3), resulted in the Pissouri region behaving as an independent fault block. The Gilbert-type fan-delta succession was followed by rhythmically bedded basal clastic lags, aeolinites and palaeosols (1.77 – present).

4.9 Conclusions

A magnetostratigraphy has been established for the Plio-Pleistocene circum-Troodos sedimentary cover, in which (when more than one interpretation is given, the age constraint given in bold is the preferred age):

i. The uppermost Nicosia Formation in the Pissouri Basin was deposited during either the Reunion or Olduvai subchron of the Matuyama Chron, either at **2.14 – 1.95 Ma** or 1.95 – 1.77 Ma;

ii. Pronounced uplift of the Troodos Massif began in the Late Pliocene (< 2.14 Ma). This is coincident with the Kephales fan delta prograding into the Mesaoria Basin (2.14 – 1.95 Ma), Athalassa-type sandbodies migrating through the Mesaoria Basin (2.14 – 1.24 Ma) and large Gilbert-type fans prograding into the Pissouri Basin (either between **2.14 – 1.95 Ma** or between 1.77 – 1.66 Ma).

iii. Uplift of the Troodos Massif continued into the early Pleistocene, as recorded by rhythmically bedded fluvial gravels, sandy/silty overbank fines and palaeosols of the Apalos Formation (> 0.78Ma), which aggraded into the Mesaoria Basin as a stacked fluviatile system; and rhythmically bedded basal clastic lags, aeolinites and palaeosols (1.77 – present), which followed deposition of the Gilbert-type fan deltas in the Pissouri Basin.

iv. The marine terraces of the Paphos, Kouklia and Lemesos areas were all cut, and subsequently covered by littoral sediments post 0.78 Ma, suggesting that Cyprus was still undergoing high rates of uplift in the Middle to Late Pleistocene. The

marine terraces are broadly correlative with the uppermost palaeosols and aeolinites at Pissouri.

Chapter 5: Late Pleistocene and Holocene tectonics and depositional processes

5.1 Introduction

The aim of this chapter is to summarise the data obtained from the Optically Stimulated Luminescence (OSL) section of the integrated Plio-Pleistocene chronological study (see discussion in chapter 3, section 3.1). The aims of the luminescence study are twofold: (i) to constrain the timing of Pleistocene deformation (e.g. episodes of failure along the Kolossi and Cape Kiti Fault lineaments and the growth of the Agia Marinouda Fold), and (ii) to assess Late Pleistocene depositional processes and rates in areas of known tectonic disturbance. An integrated sedimentological, structural and luminescence study was untaken in the Kalavasos village (Figure 5-1) region to allow a better understanding of the controls on landscape evolution, in an area of known tectonic instability.

As the luminescence dating method had not been applied to sediments in Cyprus prior to this study, it was deemed prudent to test the technique independently. The OSL method was used to date the pit-fill from two hollows of archaeological interest at Kissonerga-Mylouthkia, Paphos, southwest Cyprus. Optically stimulated luminescence ages of quartz extracts in Neolithic pits at Kissonerga-Mylouthkia, correlate with published AMS results (calibrated radiocarbon dates range between 8740 and 6690 BP; OSL dates between 9600 and 7700 BP; Kinnaird et al., 2008).

Optical dating was carried out at the Scottish Universities Environmental Research Centre (SUERC), in the luminescence laboratory under the supervision of David Sanderson, Chris Burbidge and Rob Bingham. The technical sections of this report were written in collaboration with David Sanderson as an interim report. This was entitled ‘Optically stimulated luminescence dating of sediments from south-western and southern Cyprus; assessing Pleistocene – Holocene depositional rates and tectonic processes’. All interpretations and conclusions are my own.

Figure 5-1: A map of south Cyprus, showing the location of the sequences discussed in the text (created from GIS data supplied by the Cyprus Geological Survey Department). The location of figures 3.58, 3.7, 5.2 and 5.12 are shown

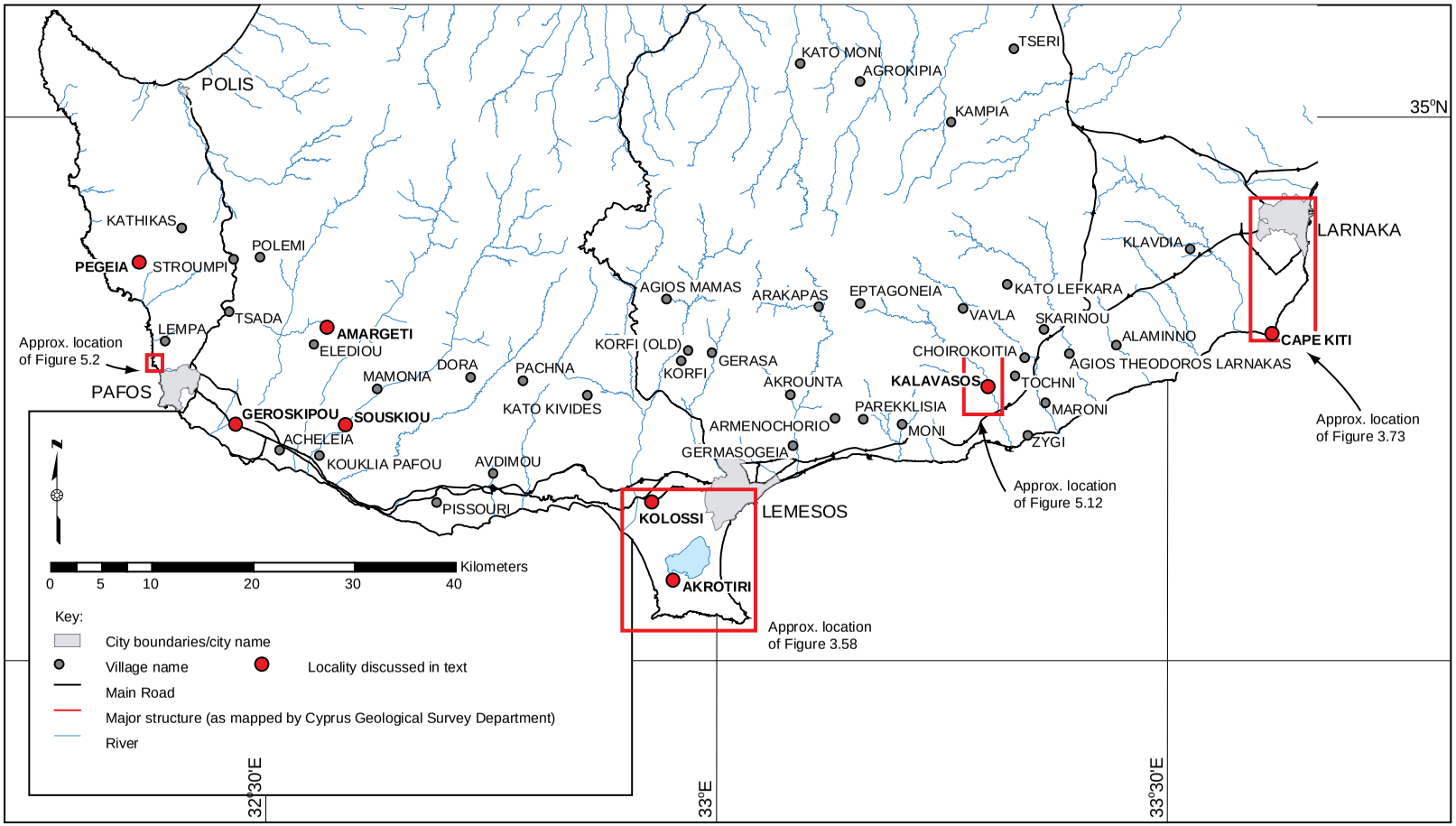

Figure 5-1: A map of south Cyprus, showing the location of the sequences discussed in the text (created from GIS data supplied by the Cyprus Geological Survey Department)

5.2 The Luminescence technique

A brief introduction to the luminescence technique is given below. For a more comprehensive review on the technique, see Prescott and Robertson (1997), Stokes et al. (1999), Aitken (1999) and Duller (2004). Optical stimulated luminescence (OSL) dating provides a means to determine the burial age of sediments that have been exposed to sunlight (bleached) prior to deposition and burial. The calculated age is the time elapsed since the last bleaching advent.

The Theory: All sediments and soils contain trace amounts of radioactive isotopes including uranium, thorium, rubidium and potassium (U, Th, Rb and K). These isotopes slowly decay over time and the ionizing radiation they produce is absorbed by other constituents of the soils/sediments, including quartz and most feldspars. Both quartz and feldspar contain small imperfections or defects within their crystalline lattice, which can store energy in the form of electrons. Electrons may be evicted from their stable ground state by the addition of energy to the system, e.g. from exposure to ionizing radiation emitted during radioactive decay. The flux of ionizing radiation, both from cosmic radiation and from natural radioactivity, excites electrons from atoms in the crystal lattice into the conduction band where they can move freely. Most excited electrons will soon recombine with lattice ions, but some will be trapped, storing part of the energy of the radiation in the form of trapped electric charge. With time, the ionizing radiation field around the material causes the trapped electrons to accumulate.

If one stimulates the crystalline material, through either thermal (TL) or optical (OSL) irradiation, then the trapped electrons are given sufficient energy to escape from the lattice defect. Following their escape they recombine with a lattice ion and in doing so energy is emitted in the form of photons, which are detectable in the laboratory. The amount of photon energy produced is proportional to the number of trapped electrons that escape during ionisation, which is in turn proportional to the radiation dose accumulated. Photon emission or luminescence emission following thermal stimulation is termed thermo-luminescence (TL) and emission following optical stimulation is termed optically stimulated luminescence (OSL).

In the laboratory, the accumulated or ‘natural’ radiation dose can be measured, but this by itself is insufficient to determine the time since the zeroing event. The ‘natural’ signal that

results from the natural radiation during burial (i.e. radioactive decay of K, U, Th and Rb within the sample and its surroundings and the radiation dose from cosmic rays) is compared with signals from the sample that result from known doses of radiation, administered by a calibrated radiation source.

The 'equivalent dose' is the laboratory dose of nuclear radiation needed to induce luminescence equal to the natural signal. The dose rate is determined by measuring the alpha radioactivity (the U and Th content) and the potassium content (K-40 is a beta and gamma emitter) of the sample material. In addition, the contribution from cosmic radiation is assessed, either through measuring the gamma radiation in the field, or calculating it from the alpha radioactivity and potassium content of the sample environment. A luminescence age is calculated by dividing the one quantity by the other i.e.

$$\text{burial age (ka)} = \frac{\text{equivalent dose (Gy}}{\text{dose rate (Gy/ka)}}$$

A sample in which the mineral grains have all been exposed to at least a few seconds of daylight can be said to be of zero age, i.e. when excited it will not emit photons. The older the sample is, the more photons it emits.

Analytical procedure: OSL and TL measurements are made on small (typically 4-6mg) aliquots of refined quartz or feldspar (of a limited grain size) from the sample to be dated. As each aliquot is apt to contain a mix of grains, some of which are well bleached, and others that are poorly bleached/or not bleached at all, it is necessary to measure several aliquots to estimate a pooled equivalent dose and assess levels of scatter.

There are three widely used strategies for obtaining a palaeodose: (i) the additive dose method, (ii) the regeneration method and (iii) the Australian slide mechanism (Stokes, 1999). In (i) a measurement of the natural luminescence intensity is made from one aliquot, and of aliquots which have been subjected to additional amounts of ionizing radiation. The resulting luminescence versus the added radiation dose growth curve may then be used to define the trend of signal growth with dose. With this information, the palaeodose may be estimated by extrapolating the trend line back to its x-axis intercept. In (ii), a measurement is made of the natural luminescence intensity and of luminescence intensities at a range of OSL signals. In the single-aliquot regenerative dose protocol (SAR) (Murray and Wintle, 2000; Sanderson et

al., 2001) each natural or regenerated OSL signal is corrected for changes in sensitivity using the luminescence response to a subsequent test dose. The palaeodose is estimated by projecting the natural aliquot intensity level onto the regenerated growth curve. In (iii), both additive dose and regeneration techniques are applied to separate sets of aliquots and the palaeodose is calculated as the amount of shifting along the x-axis to produce a single well-defined growth curve. In each of these methods, the typical approach is to use a large (up to 80) number of aliquots for the determination of the palaeodose. In the present study method (ii) was employed. The single-aliquot-regenerative-dose protocol proposed by Murray and Wintle (2000) was used to generate equivalent doses. This is the protocol adopted by SUERC in all dating applications.

5.3 Methodology

5.3.1 Sample collection and preparation

Samples were collected from cleaned vertical faces by inserting opaque plastic and/or stainless steel tubes into the soil profiles. The samples were collected in natural daylight, but were wrapped immediately in opaque black plastic bags. Each bag was sealed individually to retain soil moisture. Two types of samples were collected: (i) small (several cm^3 of material) sediment samples to be used in luminescence profiling; and (ii) large (tens to hundreds of cm^3 of material) sediment samples to be used in full luminescence dating.

All sample handling and preparation was conducted under safelight conditions in the SUERC luminescence dating laboratories. Laboratory sample labels and contextual notes are given in Table 5-1. Approximately 100-200 g of material was collected from the central, light protected core of the tubes, and wet sieved to obtain 2 fractions: 90-150 microns for initial tests - ‘polymineral’, and 150-250 microns for dating measurements - ‘quartz’. Both fractions were treated with 1M HCl for 30 minutes to dissolve carbonates. The coarser fraction was then treated with 15% HF (followed by washing in HCl) and density separated at 2.52, 2.58, 2.62, and 2.74 gcm^{-3}. Quartz was isolated from the 2.62-2.74 gcm^{-3} fraction by etching in 40% HF for 40 minutes (and washed in HCl). The 90-150 micron polymineral and 150-250 micron quartz grains were presented for measurement as mono-layers on 10 mm diameter, 0.25 mm thick stainless steel disks, fixed with silicone oil.

5.3.2 Water content measurements

For each sample, the actual weight (that which the sample was received at (*w*), the saturated weight (*Sw*) and the dried weight (*dw*) were obtained using a balance.

The fractional water content (by weight), *fw*, was calculated as:

$$fw = \left[\frac{w - dw}{w}\right] \times 100$$

and the saturated water content (by weight), *sw*, was calculated as:

$$sw = \left[\frac{sw - dw}{w}\right] \times 100$$

Site context. Label allocated in the field	Label assigned in the laboratory (SUTL no.)	Description of sample	Sample weights (g)
Kalavasos-Matrou01: Interbedded havara/palaeosols sequence	SUTL 2014	Palaeosol; light brown to brown-grey; humic to strongly humic; pebbles; scarce cobbles; very rare boulders; predominantly of chalk; rare ophiolite-derived material.	129.2[1], 149.2[2], 109.1[3]
Kalavasos-Vasilikós01: Interbedded havara/palaeosol sequence	SUTL 2017	Palaeosol; brown to dark brown; humic to strongly humic; rare pebbles; predominantly of chalk; rare ophiolite-derived material.	30.3[1], 42.5[2], 21.8[3]
Kalavasos02 Interbedded havara/palaeosol sequence. Near horse farm	SUTL 2047	Palaeosol; brown to dark brown; humic to strongly humic; rare pebbles; predominantly of chalk; rare ophiolite-derived material.	187.7[1], 250.0[2], 169.5[3]
Kalavasos03 Interbedded havara/palaeosol sequence. Near horse farm	SUTL 2048	Palaeosol; brown to dark brown; humic to strongly humic; rare pebbles; predominantly of chalk; rare ophiolite-derived material.	113.5[1], 144.2[2], 98.8[3]
Amargeti01: Collected from the hanging-wall, of youngest fault observed at Amargeti	SUTL 2019	Palaeosol; chalky; tan to light grey; contains some charcoal.	24.4[1], 37.1[2], 20.7[3]
Amargeti02: Collected from the foot-wall, of youngest fault observed at Amargeti	SUTL 2020	Palaeosol; brown to brown red; humic to strongly humic; clayey; contains some charcoal.	21.8[1], 30.3[2], 16.7[3]
Amargeti03: Collected from the hanging-wall, of youngest fault observed at Amargeti	SUTL 2021	Palaeosol; chalky; tan to light grey; contains some charcoal.	26.6[1], 40.0[2], 17.4[3]
Geroskipou01: Interbedded havara/palaeosols sequence. Sample taken 2m beneath top of section.	SUTL 2023	Palaeosol; brown to brown red; clayey; contains some charcoal.	113.4[1], 149.4[2], 87.3[3]
Geroskipou02: Interbedded havara/palaeosols sequence. Sample taken 1.5m from base of section.	SUTL 2043	Palaeosol; light brown to grey-brown; pebble-sized clasts of chalk and chert; chalky matrix.	196.7[1], 274.8[2], 170.0[3]
Geroskipou03 Interbedded havara/palaeosols sequence. Sample taken 5.5m from base of section.	SUTL 2044	Palaeosol; light brown to grey-brown; pebble-sized clasts of chalk and chert; chalky matrix.	183.7[1], 201.8[2], 168.9[3]
Kolossi01	SUTL 2045	Colluvium; chalky matrix; angular clasts of chalk and ophiolite-derived material; no internal stratification;	158.8[1], 190.3[2], 139.0[3]

		clasts imbricated along fault planes.	
Kolossi02	SUTL 2046	Sands; fine- to medium- grained; sub-rounded; ophiolite-derived material.	177.7[1], 205.2[2], 167.9[3]
Akoteri. Aeolinite deposit	SUTL 2025	Sands; fine- to medium- grained; rounded; ophiolite-derived material.	212.7[1], 300.2[2], 205.9[3]
Cape Kiti. Aeolinite deposit. Uplifted zone	SUTL 2026	Sands; fine- to medium- grained; rounded ophiolite-derived material.	83.0[1], 115.1[2], 80.2[3]
Kissonerga-Mylouthkia01. Archaeological context 'Feature 2208'. Sample taken from beneath organic layer.	SUTL 1581	Colluvium; clay-silt matrix; rounded – angular clasts of chalk; shell fragments.	205.4[1], 231.4[2], 185.4[3]
Kissonerga-Mylouthkia02 Archaeological context 'Feature 2207'	SUTL 1582	Colluvium; clay-silt matrix; rounded – angular clasts of chalk; shell fragments.	217.3[1], 302.1[2]

Table 5-1:Sampling data from all samples collected in the field
[1]Weight as received; [2]Weight when saturated; and [3]Weight when dry.

5.3.3 Dose rate measurements

Dose rate measurements from the dating samples were undertaken by High Resolution Gamma Spectrometry (HRGS), and Thick Source Beta Counting (TSBC). In addition in situ gamma spectrometry was undertaken using a portable spectrometer (Rainbow 1-7010) with a 1"x1" NaI detector probe.

A 50g portion of dried sediment from each sample was removed to determine beta dose rates using the SUERC HRGS system, a 50% relative efficiency 'n' type hyperpure Ge detector (EG&G Ortec Gamma-X) operated in a low background lead shield with copper lining. To allow radon equilibrium, the samples were sealed in Sterilin Petri dishes for a minimum of 2-3 weeks prior to measurement. Gamma ray spectra were recorded over the 30 keV to 3 MeV range for each sample, interleaved with known background and Shap Granite Standard measurements. Counting times of 80 ks per sample were used. The spectra were analysed, using the software programme, Maestro. Count rates (with their statistical counting uncertainties) were determined for ^{40}K, and for selected nuclides in the U decay series (^{234}Th, ^{236}Ra & ^{235}U, ^{214}Pb, ^{214}Bi and ^{210}Pb) and the Th decay series (^{238}Ac, ^{212}Pb and ^{208}Tl). Net rates and activity concentrations for each of these nuclides were determined relative to the standard by weighted comparisons. The internal consistency of nuclide-specific estimates for U and Th decay series nuclides were accessed relative to measurement precision. Weighted

combinations were used to estimate mean activity concentrations (in Bq kg^{-1}) and elemental concentrations (% K and ppm U, Th) for the parent activity. The data were then used to determine dry infinite matrix dose rates for alpha, beta and gamma radiation.

A 20 gram portion of dried sediment from each sample was removed to determine beta dose rates using the SUERC TSBC system (Sanderson, 1988). Sample count rates were determined with six replicate 600 second counts for each sample. Dry infinite-matrix dose rates were calculated by scaling the net count rate of the sample to a reference material, the SUERC Shap granite, which has a working beta dose rate of 6.245 ± 0.062 mGy a^{-1}. The estimated errors combine counting statistics, observed variance and the uncertainity on the reference value.

The results of the HRGS and TSBC analyses were used to estimate internal alpha activity, model cosmic ray dose rates, and determine the overall effective dose rates for age estimation.

5.3.4 Stored dose measurements

OSL measurements were carried out using a RISO TL/OSL automated machine. Luminescence from the quartz fraction was stimulated using blue diodes (470 Δ 20nm) with detection in the ultraviolet defined by two Hoya U340 filters (Botter-Jensen et al., 2000; Spencer and Sanderson, 2002). A single aliquot regenerative-dose (SAR) protocol (Murray and Wintle, 2000; Sanderson et al., 2001) was used to determine the equivalent dose on each disc measured. In the SAR method, each natural or regenerated OSL signal is corrected for changes in sensitivity using the luminescence response to a subsequent test dose. Regenerative dose response curves were constructed using doses of 8, 16, 24, 32 and 40 Gy (and in several samples 80 and 120 Gy), with a test dose of 4 Gy. A second dose of 8 Gy was applied at the end of the run as a further sensitivity check. To ensure the prepared quartz contained no significant feldspar grains or micro-inclusions, a feldspar contamination test was carried out at the end of each run (the IRSL was read out after the sample was subjected to 8Gy). To assess the dependence of equivalent dose on preheat temperature, four different preheat temperatures were investigated (220, 240, 260 and 280 °C).

Discs were rejected from further analysis based on the 8Gy recycling ratio test and feldspar contamination. The weighted mean equivalent dose was then calculated for each sample from the remaining individual single aliquot equivalent dose values.

Stored dose measurements were preformed on both luminescence profiling and full-dating samples. There was no difference in the luminescence dating protocol employed; however, fewer aliquots were prepared for the profiling samples (1-2) than for the full-dating samples (<20 aliquots). When determining a luminescence age one averages the equivalent dose obtained from each aliquot, thus when a greater number of aliquots are measured the age is more accurate. Luminescence profiling is still a valid tool as it allows one to perform cheap and rapid measurements. Full-dating samples yield the preferred age. Profiling samples provide a means to bracket/constrain this age.

5.4 The Neolithic settlement at Mylouthkia-Kissonerga (an independent age control).

Mylouthkia is a severely eroded coastal settlement located at the northern end of the Ktima Lowlands in the Paphos District, western Cyprus (Figure 5-2a). It is comprised of two distinct sites separated by a millennium, but physically by only a few hundred yards; assigned to the Cypro-Pre-Pottery Neolithic B (Cypro-PPNB) and Early Chalcolithic (Figure 5-2b) periods. A detailed account of the excavations at Mylouthkia is provided by Peltenburg (2003). As of 2000, the Lemba Archaeological Project (University of Edinburgh) had identified five wells, a semi-subterranean structure and three pits belonging to the Aceramic Neolithic. Rescue excavations in March, 2000, necessitated by construction of a new tourist village on the Neolithic site, revealed a number of important features thought to date from the Aceramic Neolithic.

Sample 'SUTL1581' was taken from the fill of one of these features, a large hollow, (designated 'Feature 2208') which measures c. 11 metres from north to south, and is generally < 1 metre deep. In the centre of this hollow, a basal depression exists which is c. 0.60 metres deeper than the adjacent base level. It is filled with a sequence of pale to dark grey ashy layers, silts and gravels. The OSL sample was taken from the lower portion of this fill. The absence of pottery and the presence of a single worked flint suggests that this feature probably dates from the early (Cypro-PPNB) phase at Mylouthkia. Sample

'SUTL1582' was taken from the fill of a second feature of unknown extent (designated 'Feature 2207'). Cursory cleaning and examination of the exposed section yielded two stone vessel fragments and two pieces of worked flint, which combined with the absence of pottery, suggest that the feature should also belong to the earlier (Cypro-PPNB) phase of use of the site. Future excavation may yield material that can be dated by the radiocarbon method, which would provide a powerful cross-check on the results obtained using the OSL method.

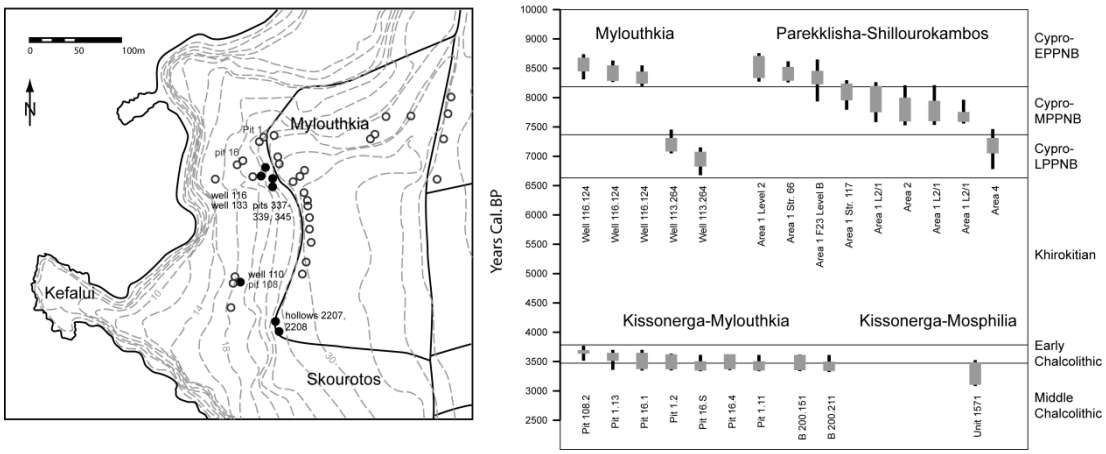

Figure 5-2: (a) Site plan with location of surveyed and excavated features; closed circles denote Cypro-PPNB structures; open circles denote Chalcolithic structures. Features described in the text are labelled; (b) Radiocarbon dates (single standard deviation) from sites of the Cypro-PPNB period, i.e. Mylouthkia and Parekklisha-Shillouokambos (modified from Peltenburg et al., 2003; Guilaine et al., 2000). The reader is referred to Figure 5-1 to see the location of Figure 5-2

5.5 Middle Pleistocene to Holocene tectonics

The main objective of the luminescence study was to constrain the timing of Pleistocene deformation, described and discussed in the chapter 3. Two luminescence methods have previously been employed in the dating of neotectonic faults. The first, 'earth systems approach', is based on luminescence dating of buried soils, colluvium and/or fluvial sediments, which are offset by, or overlay faults. The basic premise is that prior to burial, sediments at the surface of the soil/colluvium/fluvial deposit are exposed to sunlight (bleached), thereby resetting their luminescence clock. The second, 'the experimental approach', is based on luminescence dating of fault gouges. This technique is based on the premise that during faulting, the geological luminescence of minerals constituting the fault gouge would be reset due to frictional heating and/or cataclastic deformation. The 'earth systems approach' was used in this study.

5.5.1 The Agia Marinouda and Kouklia Folds

Pleistocene/Recent compression produced N-S contraction along E-W trends (see chapter 3). The Agia Marinouda – Kouklia fold formed in response to this phase of compression. A description of the Agia Marinouda – Kouklia fold belt is given in chapter 3. The fold zone experienced several episodes of active growth, which extend back at least to the middle Pleistocene. Marine terrace deposits at Kouklia are deformed; similar terrace deposits exposed laterally and dated by the palaeomagnetic technique yield ages between 0.78 (middle Pleistocene) and 0 Ma (see chapter 4). Rhythmically bedded colluvial deposits and palaeosols are preserved on the northern flank of the Agia Marinouda fold, at Agia Marinouda in the village of Geroskipou (Figure 5-3; Figure 5-4). Three full-dating samples and five profiling samples were collected from this sequence of growth strata (Table 5-1), to characterise the temporal and spatial development of the Agia Marinouda fold.

Figure 5-3: Growth strata preserved on the northern limb of the Agia Marinouda fold: Rhythmically bedded colluvial deposits and palaeosols

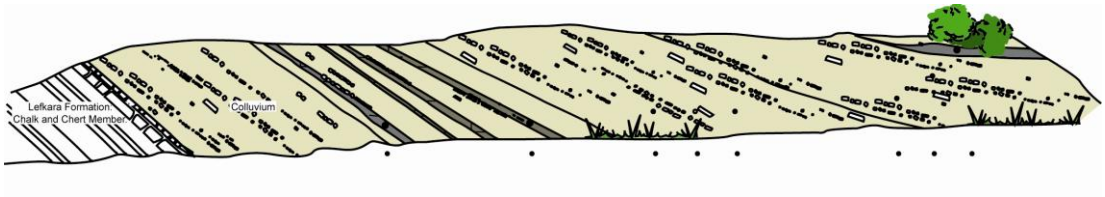

Figure 5-4: Sketch of the deformed, syn-tectonic strata seen at Geroskipou, on the northern flank of the Agia Marinouda fold. Black dots indicate horizons sampled

5.5.2 The Kolossi fault

Pleistocene/Recent transpression reactivated Late Miocene NW-SE and NE-SW structures, generated strike-slip faulting along E-W trends, and conjugate sinistral NE-SW-trending and dextral NW-SE-trending strike-slip faults (see Chapter 3; Harrison et al., 2002; 2004; Soulas, 1999; this study: chapter 3). The Kolossi Fault lineament formed in response to this phase of transpression. A description of the Kolossi Fault lineament is given in chapter 3.

The Kolossi Fault lineament is exposed at two localities (Figure 3-58): at (i) the Kolossi Football stadium, where Pliocene Nicosia Formation marls and middle Pleistocene(?) gravels are juxtaposed (Figure 5-5); and at (ii) an abandoned quarry (now used as a goat pen), c.750m south, where Miocene Pakhna Formation chalks and middle Pleistocene gravels are juxtaposed (Figure 5-6). At site (i) middle Pleistocene fluvial gravels (overspill from the Kouris River?) are cut by NW-SE-trending dextral and dextral-normal faults (Figure 5-5; Figure 5-7). Pebbles are imbricated along the fault planes. At site (ii) sheared Pakhna Formation chalks and middle Pleistocene gravels (equivalent to site i) are cut by normal/normal-sinistral NE-SW-trending faults. The dextral NW-SE-trending and the normal-sinistral NE-SW-trending strike-slip faults are interpreted as conjugate faults to the main E-W trend of the Kolossi Fault lineament. At site (ii) the sheared chalk/gravel unit is overlain by a horizon of well-sorted aeolinite sands (Figure 5-6). This unit is not affected by the underlying faults. Full-dating samples were collected from the deformed unit (site i) and the overlying sands (site ii), to constrain episodes of failure on the Kolossi Fault lineament. In addition, a full-dating sample was collected from an aeolinitic body outcropped at the village of Akotiri.

Figure 5-5: Deformed Pliocene marls and Pleistocene gravels at the Kolossi football stadium, Kolossi, Kolossi Faultft) Exploration trench, Kolossi football stadium; (right) Imbriccated clasts along Pleistocene fault plane, Kolossi football stadium

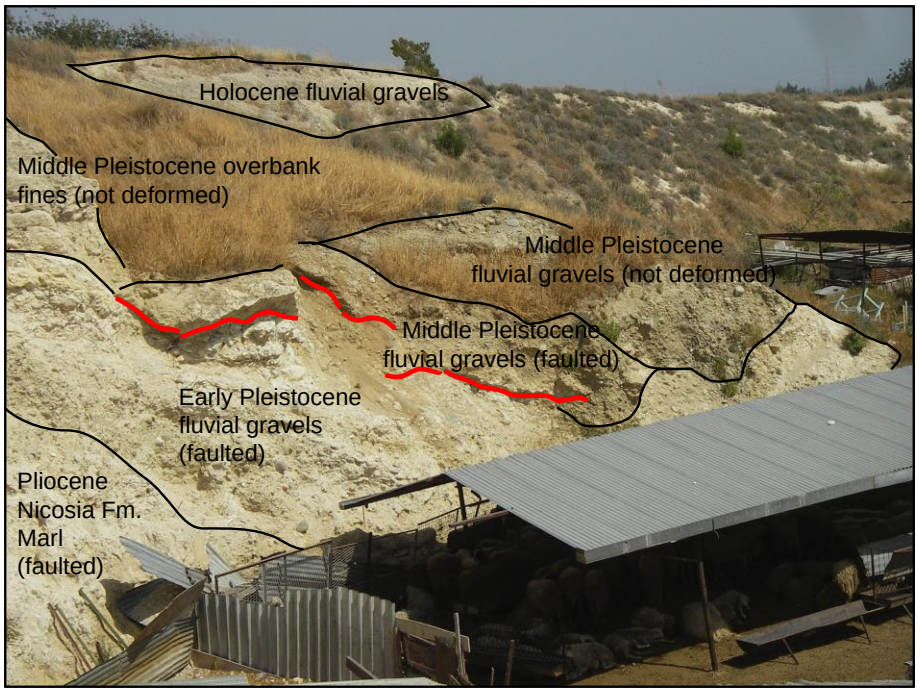

Figure 5-6: Deformed Pliocene marls and middle Pleistocene gravels overlain by undeformed late Pleistocene sand, abandoned quarry, Kolossi, Kolossi Lineament: (clockwise from top) deformed Pliocene marls and Pleistocene gravels; unconformably overlain by undeformed late Pleistocene gravels and sands; detail in deformed Pleistocene gravels

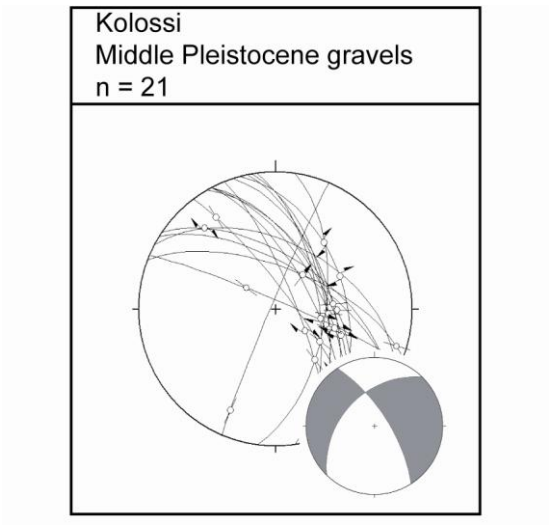

Figure 5-7: Structural data collected from faults affecting middle Pleistocene gravels at the Kolossi football stadium, Kolossi, Kolossi Fault lineament

5.5.3 The Cape Kiti Fault

A description of the Cape Kiti fault is given in chapter 3. The southern tip of the Cape Kiti Fault is exposed at Cape Kiti (Figure 3-51). Late Pleistocene terrestrial deposits are juxtaposed against Holocene beach deposits. Richard Harrison and Efthimios Tsiolakis believe that failure occurred along the fault in the late Pleistocene, based on optical stimulated luminescence (OSL) dates obtained on either side of the fault: a brown sand horizon in the footwall of the fault yielded an OSL age of 12,100 ± 1,090 BP; fault-derived colluvium in the shear zone of the fault yielded an OSL age of 12,500 ± 1,250 BP; and a brown palaeosol horizon in the hangingwall of the fault yielded an OSL age of 16,030 ± 2,460 BP (Figure 5-8; R. Harrison, personal communication). On the basis of this study, R. Harrison and E. Tsiolakis propose three episodes of faulting: the youngest event at 12,100 ± 1,090 (Holocene) BP; an intermediate event at 12,500 ± 1,250 BP; and the oldest event at 16,030 ± 2,460 BP (Pleistocene) (R. Harrison, personal communication).

Figure 3-73 illustrates the distribution of faults in the Larnaka Fault Zone. The Cape Kiti Fault may be traced inland towards the city of Larnaka through a series of uplifted marine terraces (sand dunes) and local depressions (salt lakes; Figure 5-9). A sample was collected from the base of an uplifted marine terrace to constrain the rate of uplift in the middle Pleistocene along the Cape Kiti Fault.

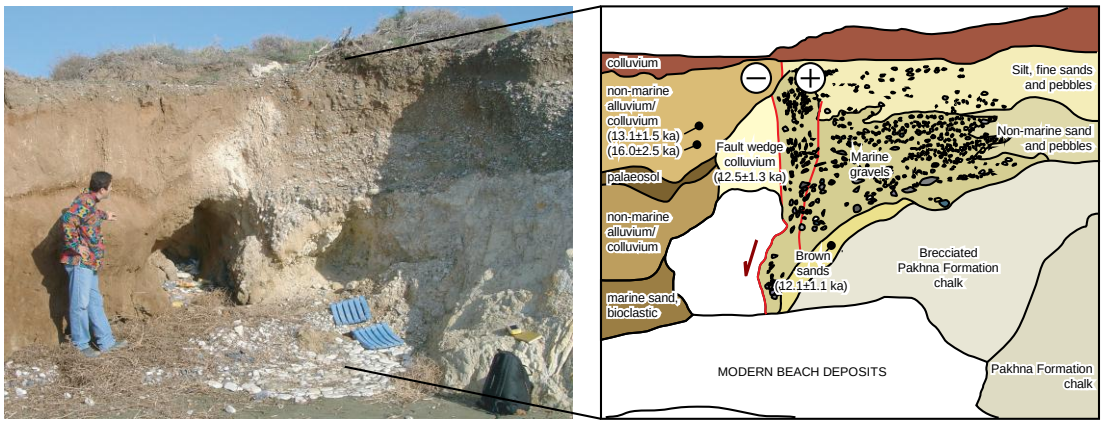

Figure 5-8: The Cape Kiti Fault: Pleistocene terrestrial deposits juxtaposed against Holocene beach deposits (R. Harrison). Photograph taken looking north. The results of the OSL study of Harrison and Tsiolakis are shown. Data kindly supplied by R. Harrison

Figure 5-9: The Cape Kiti Fault is traced north, from its exposure on the coast, through a series of uplifted marine terraces and local depressions to the city of Larnaka

5.5.4 Extensional faulting at Amargeti

At Amargeti village (Figure 5-1), a Plio-Pleistocene sequence of marls, fluvial gravels, overbank fines and palaeosols is cut by a series of WNW-ESE, SSW-dipping normal faults (Figure 5-10; Figure 5-11). The village of Amargeti is located in the centre of the Polis

Graben. Previous workers (Payne and Robertson, 1995; 2000) have inferred from this evidence that the Polis Graben was active in the Pleistocene. OSL samples were collected to constrain the age of faulting in this area.

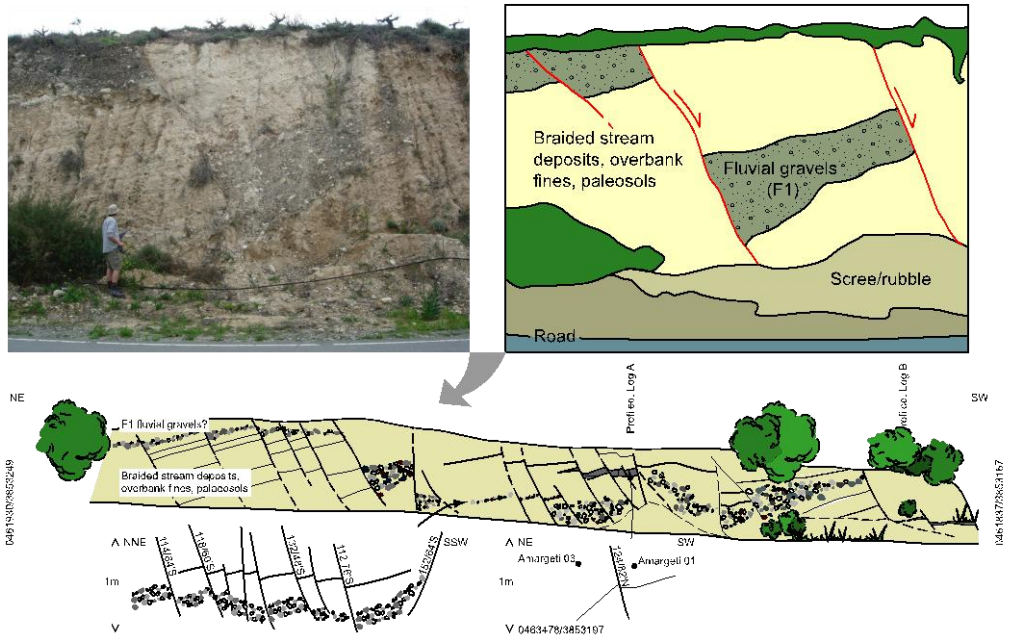

Figure 5-10: Extensional faulting at Amargeti. The section shown in photograph is approximately six metres in height

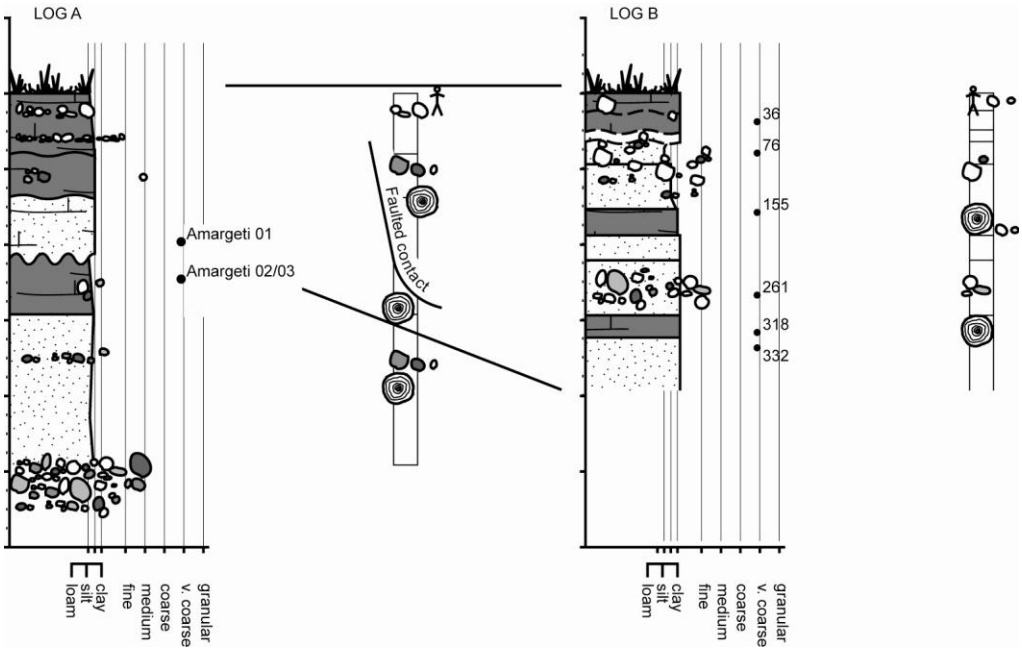

Figure 5-11: Extensional faulting at Amargeti: profiled section. The number beside the sampled horizon corresponds to its depth from the present land surface (in cm)

5.6 Late Pleistocene to Holocene depositional processes

A second objective of the luminescence study was to assess late Pleistocene depositional processes and rates, both in stable regions and in regions that are known to be tectonically unstable. In order to achieve this objective, colluvial/palaeosol sequences were studied at and in close proximity to the villages of Kalavasos, Souskiou and Pegeia (Figure 5-1). Colluvial/palaeosol profiles store morphological data related to the eroded slope and, retain a record of climatic, anthropogenic and tectonic (e.g. seismic-induced slope failures) processes. If climatic and anthropogenic signals can be accounted for, the signal that remains includes information on the processes active on the eroded slope, including slope instabilities i.e. a tectonic overprint.

The Cypriots have a local name for deposits of colluvium, 'havara'. Typically, it occurs as a surficial, white to buff, fine, chalky porous powder, mixed with angular to sub-rounded heterolithic (although predominantly limestone) clasts. It occurs in several facies associations: (i) as slope debris, a chaotic assemblage of angular limestone clasts and sand-silt, at the toes of slopes in limestone upland areas; (ii) as debris cones, alternating clast-rich/clast-free horizons of colluvium, at the toes of slope concavities, in dales and small valleys; and (iii) as a surficial veneer, i.e. a silty, sandy fine-grained colluvium (Schrimer, 1998).

5.6.1 Vasilikós Valley (Kalavasos)

The NNW-SSE trending Vasilikós Valley, in which the village of Kalavasos is located (Figure 5-12), is bounded to the east and west by NE-SW trending, NW- and SE-dipping and WNW-ESE-trending, NNE- and SSW-dipping normal faults (Figure 5-13; Figure 5-14). The Vasilikós is the westernmost of a series of rivers which, in a broadly radial pattern, drain the south-eastern slopes of the Troodos Massif. In 1985 the Kalavasos Dam was constructed on the Vasilikós River. In its upper reaches the catchment is underlain by igneous rocks of the Troodos Ophiolite complex. In its lower reaches the catchment is underlain by sedimentary rocks of Upper Cretaceous to Pliocene age (Figure 5-12).

Tan to off-white colluvial deposits (i.e. Havara) comprised of alternating sequences of clast-supported and matrix-supported breccia-conglomerates, in clast-rich and clast-free horizons, in a silty, powdery matrix, occur at the toes of slopes in the Vasilikós Valley. Palaeosol

horizons occur in association with the colluvial deposits. Frequently these deposits are banked up against the valley bounding NE-SW- and WNW-ESE-trending faults. At a number of localities, interbedded sequences of havara and palaeosols are tilted (with stratigraphic dips of between 2º and 20º), presumably due to movement on the active faults. Faults affecting havara/palaeosol strata are inferred based in the presence of: (i) an offset in stratigraphic units, (ii) a change in the regional dip/strike of beds, (iii) breaks in topography and (iv) vegetation contrasts.

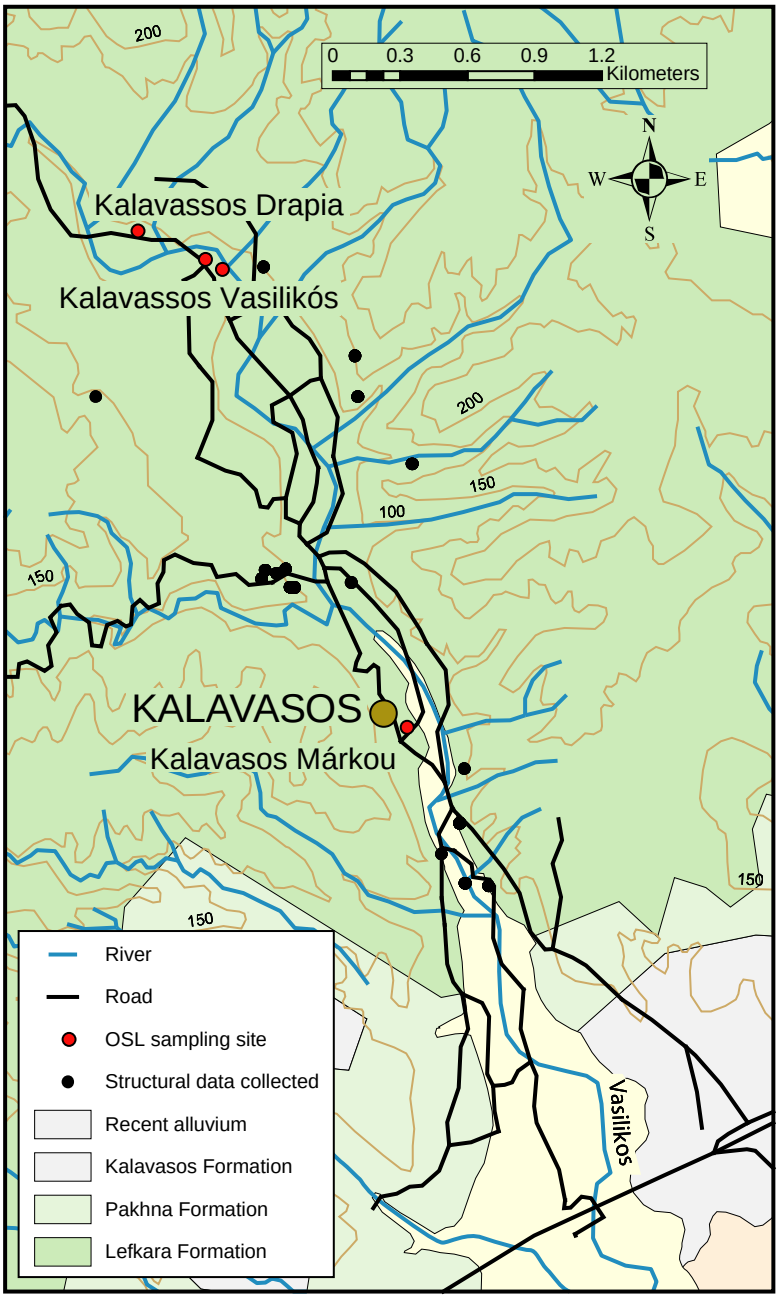

Figure 5-12: Topographic map of the Vasilikós Valley (created from GIS data supplied by the Cyprus Geological Survey Department)

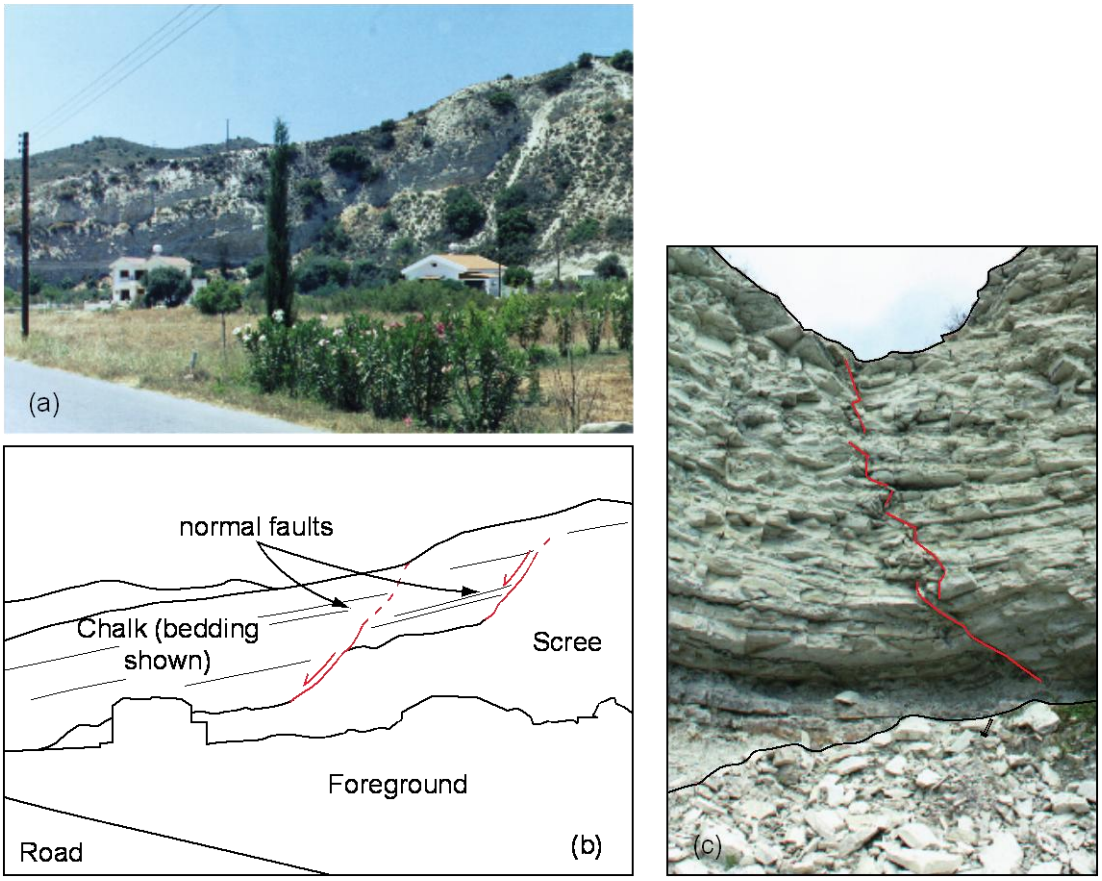

Figure 5-13: Faults bounding the Vasilikós Valley: (a and b) valley-bounding 1st order faults; (c) minor 3rd order faults

The NE-SW and NE-SW faults are believed to be normal in nature; the shear of displacement was determined from offset stratigraphic markers and the orientation of slickenlines (with steps as kinematic evidence) on the fault surfaces. Fault-slip data collected throughout the Vasilikós Valley, from both the NE-SW- and WNW-ESE-trending faults, indicate that the majority of displacement are normal dip-slip (Figure 5-15). It is possible to generate normal dip-slip NE-SW- and WNW-ESE-trending structures in an ENE-WSW extensional regime (Figure 5-15). The principal stresses resolved for faults affecting Paleocene strata in the Vasilikós Valley are σ_1; 029º/80º, σ_2; 149º/05º and σ_3; 238º/09º (Figure 5-16).

In chapter 3, it was established that Late Miocene (Tortonian?) E-W/ENE-WSW and NW-SE D1 extension generated N-S- and NNW-SSE-trending faults in the Polis Graben and Pissouri Basin and NE-SW-trending faults in the Maroni-Psematismenos Basin. The principal stresses resolved for faults affecting Paleocene strata in the Vasilikós Valley

correlate with those derived for faults affecting Miocene strata in the Polis Graben. Thus, faults affecting Paleocene strata in the Vasilikós Valley were presumably generated during D1 extension. Rotated fault-blocks of Pleistocene havara/palaeosol strata indicate that the Vasilikós Valley is still actively extending.

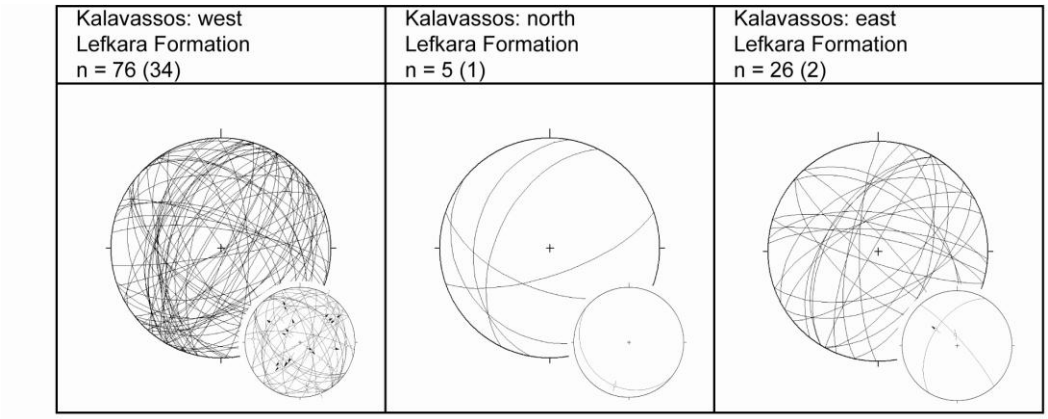

Figure 5-14: Fault data collected from structures affecting Paleocene chalk in the Vasilikós Valley separated by area: west, east and north

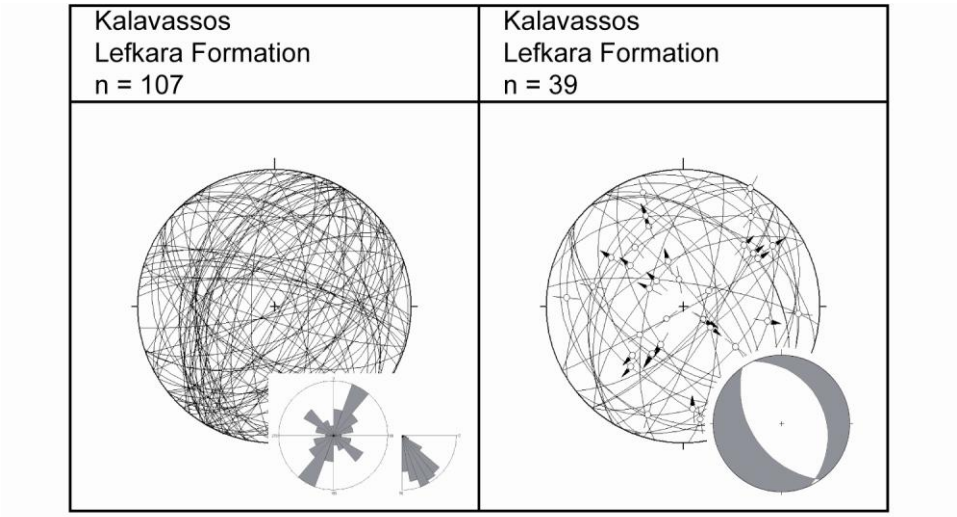

Figure 5-15: Fault data collected from structures affecting Paleocene chalk in the Vasilikós Valley

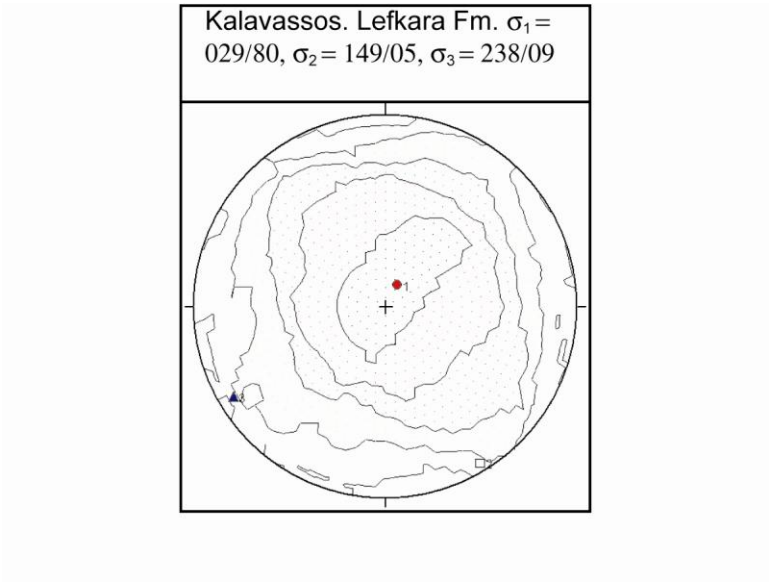

Figure 5-16: Principal stresses resolved for faults affecting Paleocene strata in the Vasilikós Valley

To obtain data on landscape evolution in the Vasilikós Valley several sections of havara/palaeosol were dated using the technique of optical stimulated luminescence. Three successions of interbedded havara and palaeosol were examined. The first site, at Kalavasos Márkou, is located in an upland area, 30m above the valley floor. No faults are observed in the immediate vicinity. The site at Kalavasos Márkou was selected to assess whether it is possible to isolate a climatic signal in a sequence of havara/palaeosol. The second site, at Kalavasos Vasilikós, is located in the centre of the valley, c. 15m above the Vasilikós river bed. The third site, at Kalavasos Vasilikós – Drapia horse farm, is located in the centre of the valley, on the valley floor. The succession at Kalavasos Vasilikós-Drapia was deposited pre- to syn-faulting; whereas the sucession at Kalavasos Vasilikós was deposited post-faulting. The site at Kalavasos Vasilikós overlies the site at Kalavasos Vasilikós-Drapia. The latter two sites were selected to assess whether it is possible to isolate a tectonic signal in a sequence of havara/palaeosol and to constrain the age of faulting in the Vasilikós Valley. The three sections studied are discussed in detail below.

5.6.1.1 Kalavasos Márkou

A section through an interbedded havara/palaeosol sequence was logged in Kalavasos, behind the house of Charálampos Varélla, 150m south of the village church. The Greek name for this locality is ‘Spílios tou Papá Márkou (Σπήλιος του Παπά Μάρκου)’, which translates as the ‘Caves of Father Márkou’. This site is referred to here as Kalavasos Márkou.

The site is a slope-cut, located 30m above the valley bottom at the first flattening of the slope toe (Figure 5-17).

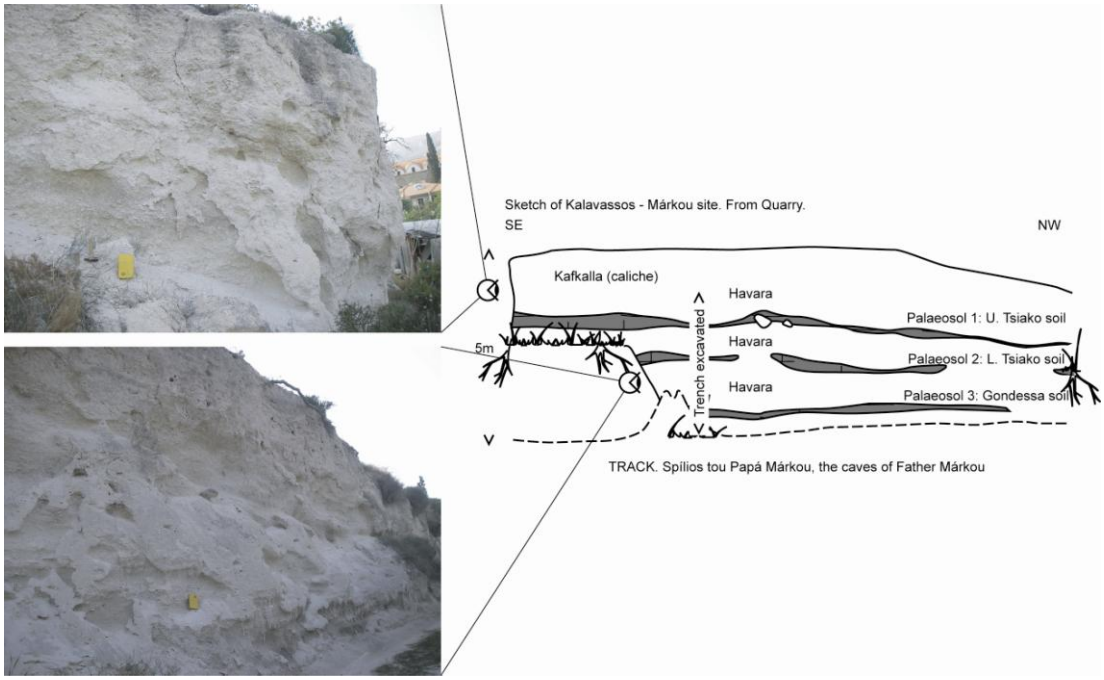

Figure 5-17: Sketch of the havara/palaeosol sequence at Kalavasos Márkou. The trenches excavated for OSL profling/sampling are shown.

The stratigraphy includes the following layers from top to bottom (Figure 5-17; Figure 5-18a):

i. ~ 1.5 metre-thick, grey, anthropogenic colluvium; silty, powdery, sub-angular to rounded, clasts and pebbles of chalk (and subordinate Troodos-derived material); with autochthonous surface soil; crudely stratified; perforated by burrows.

ii. ~ 0.5 metre-thick, tan to off-white, colluvial deposit (i.e. havara), a silty, powdery, alternating sequence of clast-rich/clast-free horizons; sub-angular pebbles; rare boulders of chalk. Schrimer (1998) obtained a radiocarbon age of 27.4 ± 1.6 ka from a piece of charcoal at the base of this unit.

iii. ~ 1.5 metre-thick grey-brown palaeosol; humic; isolated clasts/pebbles of chalk (and subordinate Troodos-derived material).

iv. ~ 0.5m metre-thick, tan to off-white, colluvial deposit (i.e. havara); silty; powdery; alternating sequence of clast-rich/clast-free horizons; sub-angular

pebbles; rare boulders of chalk. Imbrication indicates a east-ward component to flow (i.e. towards the axis of the valley).

v. ~ 1.5m metre-thick grey-brown palaeosol; humic; isolated clasts/pebbles of chalk (and subordinate Troodos-derived material).

vi. ~ 0.5m metre-thick, tan to off-white, colluvial deposit (i.e. havara), a silty, powdery; alternating sequence of clast-rich/clast-free horizons; sub-angular pebbles; rare boulders of chalk

vii. ~ 1.5m light-brown, to brown-grey, palaeosol; humic to strongly humic; isolated clasts/pebbles of chalk (and subordinate Troodos-derived material); scarce Troodos-derived gravels; nested charcoal. Schrimer (1998) obtained a radiocarbon age of 32.0 ± 0.9 ka from a piece of charcoal from within a 10cm large slab of black-brown humic soil with a reddish aureole (presently buried). Base of unit not seen.

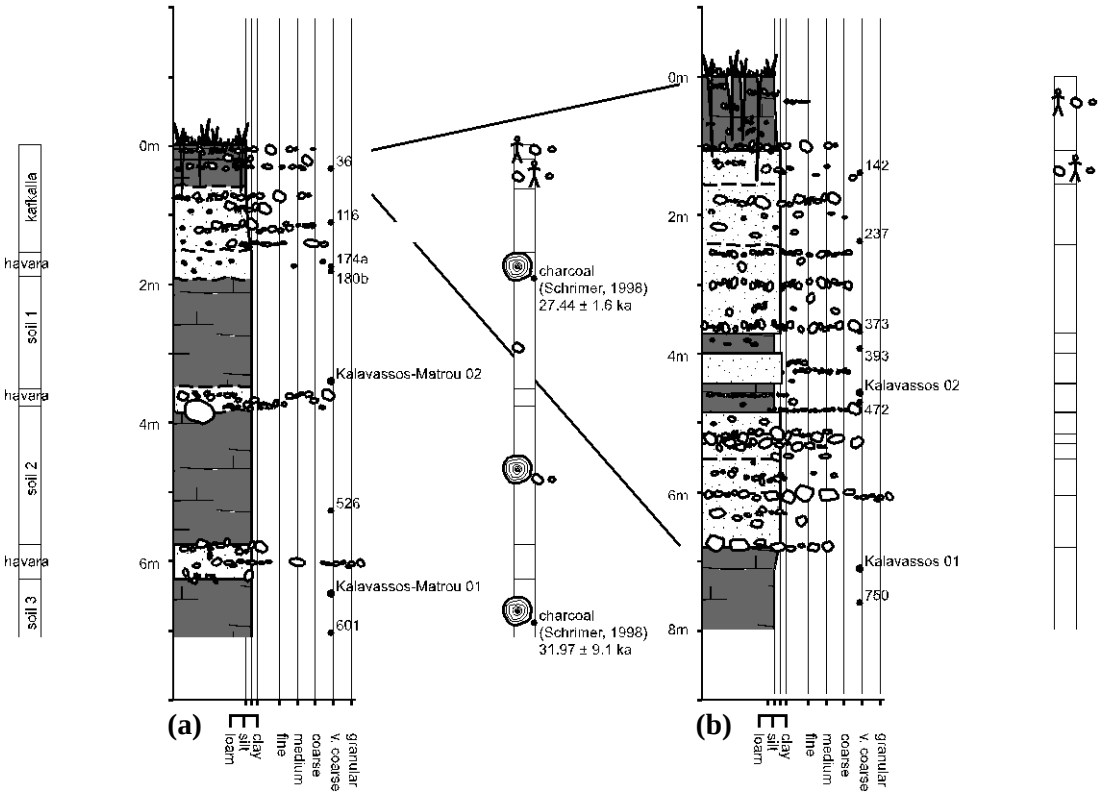

Figure 5-18: Sedimentary logs through the havara/palaeosol sequences: (a) at Kalavasos Márkou and (b) at Kalavasos Vasilikós. Horizons sampled for OSL profiling and for full OSL dating are indicated. The number beside the sampled horizon corresponds to its depth from the present land surface (in cm). The key to the sedimentary logs is given in Appendix A

5.6.1.2 Kalavasos Vasilikós

A second section of interbedded havara horizons and palaeosols was logged at Kalavasos Vasilikós, which is located ~ 1km north-northwest of the village of Kalavasos on the Kalavasos - Asgata road.

The stratigraphy includes the following layers from top to bottom (Figure 5-18b):

i. ~ 1.0 metre-thick, grey, anthropogenic colluvium; silty, powdery; sub-angular to rounded clasts and pebbles of chalk (and subordinate Troodos-derived material); with autochthonous surface soil; strongly humic; crudely stratified; perforated by burrows.
ii. ~ 3 metre-thick, tan colluvial deposit (i.e. havara); silty; powdery; an alternating sequence of clast-rich/clast-free horizons; poorly sorted; sub-angular pebbles and rare boulders of chalk; clasts of chert from the Lefkara Formation (and subordinate Troodos-derived material).
iii. ~ 1 metre-thick brown, palaeosol; silty; locally humic; contains scare charcoal; poorly sorted, isolated clasts/pebbles of chalk (and subordinate Troodos-derived material); crudely stratified.
iv. ~ 2 metre-thick, brown to grey-brown, colluvial deposit (i.e. havara); an alternating sequence of clast-rich/clast-free horizons; poorly sorted; sub-angular pebbles and rare boulders of chalk; clasts of chert from the Lefkara Formation (and subordinate Troodos-derived material); some crude imbrication. Larger clasts are comprised of predominantly chalk of the Lefkara Formation, and are angular to sub-rounded in shape.
v. ~ 1 metre-thick, brown to dark brown palaeosol; humic to strongly humic; isolated clasts/pebbles of chalk and rare Troodos-derived material.
vi. ~ 2 metre-thick, colluvial deposit (i.e. havara). Base of Quaternary sequence rests on brecciated Lefkara Formation chalk.

5.6.1.3 Kalavasos Vasilikós – Drapia horse farm

A large, fault-bounded block of interbedded havara and palaeosols is exposed at Drapia horse farm, Kalavasos (Figure 5-19). Full dating and profiling samples were collected through the succession, from its base to its middle.

Figure 5-19: Panorama of back-rotated colluvium and palaeosols. The photographs were taken looking due south from the Drapia horse farm. Faults bound the Vasilikós valley margins

5.6.2 Souskiou

Katleen Decker, of the University of Tübingen, logged a section of interbedded havara horizons and palaeosols at Souskiou, a prehistoric settlement near the village of Kouklia (Figure 5-1; Figure 5-20). She established a chronology based on the presence of archaeological artefacts in the soil/colluvium horizons. Several OSL full-dating samples were collected from the sequence to constrain depositional rates and its age.

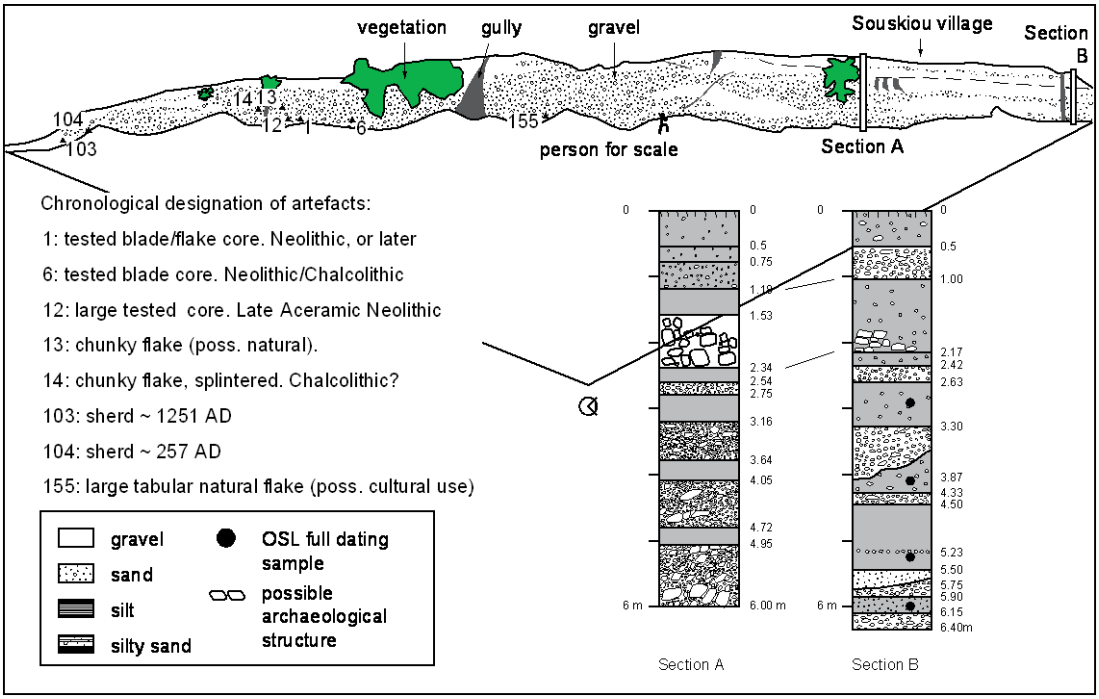

Figure 5-20: Sedimentary logs through the havara/palaeosol sequences at Souskiou (Kouklia). Horizons sampled for full OSL dating are indicated. The number beside the sampled horizon corresponds to its depth from the present land surface (in metres). Figure drafted by Katleen Decker

5.6.3 Pegeia

A fifth section of interbedded havara (m-scale) and palaeosols (dcm-scale) was logged at Pegeia, a village to the northwest of Paphos (Figure 5-1). The base of the sequence is not exposed at this locality; however, along strike the colluvium rests unconformably on brecciated Lefkara Formation chalk. It is not known whether this chalk is in situ or downfaulted/land slipped. Several OSL profiling samples were collected from this sequence to constrain depositional rates and its age.

The stratigraphy includes the following layers from top to bottom (Figure 5-21):

i. ~ 0.25 metre-thick brown, to red, autochthonous soil; strongly humic; reworked, rounded, to subrounded, pebbles of chalk (and subordinate Troodos-derived material).

ii. ~ 3 metre-thick tan to red-brown colluvial deposit; humic; chalky; reworked, rounded to subrounded pebbles of chalk, calcarenites (Terra Member limestone),

chert and subordinate Troodos-derived material; crudely stratified; some clast imbrication.

iii. ~ 0.5 metre-thick brown palaeosol; strongly humic; rounded pebbles of chalk and Troodos-derived material. Base of section not exposed, although the colluvium rests on brecciated Lefkara Formation chalk along strike.

The havara/palaeosol succession profiled above is interpreted as a body of fault colluvium, related to the recent phase of gravitational faulting.

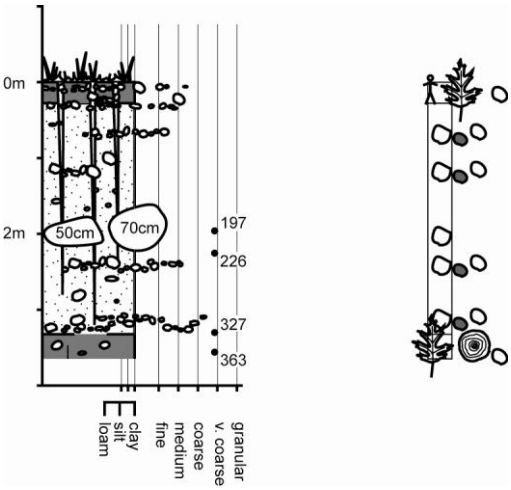

Figure 5-21: Sedimentary log through the colluvium/palaeosol sequence at Pegeia. Horizons sampled for OSL profiling are indicated. The number beside the sampled horizon corresponds to its depth from the present land surface. The key to the sedimentary logs is given in Appendix A

5.7 Results

5.7.1 Exploratory measurements

Exploratory measurements were performed on discs of plagioclase/K feldspar/quartz (polymineral) and etched quartz extracts. The measurements were designed to make preliminary equivalent dose estimates for the polymineral and quartz separates; to assess luminescence sensitivity, evaluate dating suitability, and to decide on the most appropriate dating procedure. Both separates were subjected to infra-red stimulated luminescence (IRSL) and thermoluminescence (TL). The polymineral separates had poor IRSL and TL responses, indicating that the feldspar in the samples wasn't suitable for dating in the luminescence procedure. The quartz separates had no response under either stimulation, implying little/or no feldspar contamination. This indicates that the quartz separates are 'clean', i.e. that they

contain no contaminates that will alter the luminescence sensitivity. The quartz separate is deemed the most appropriate for dating in the luminescence procedure.

5.7.2 Dose rate measurements and calculations

Dose rates were estimated from laboratory measurements by TSBC and HRGS. All laboratory measurements were conducted on dried samples.

Table 5-2 presents the results from each sample obtained from HRGS, both as activity concentrations (Bq kg^{-1}) and as equivalent concentrations, assuming in the case of the U and Th series full series equilibrium. The data were calibrated with respect to the Shap Granite standard. Mean parent concentrations from all four samples were 0.86 ± 0.07% K, 2.38 ± 0.31 ppm U and 0.57 ± 0.07 ppm Th.

Table 5-3 correlates dose rates from TSBC and HRGS. HGRS measurements were conducted with sealed samples which had been stored for radon accumulation. TSBC measurements were conducted in open geometry after drying the sample, and therefore aren't expected to retain full equilibrium radon levels. This is reflected in the results obtained.

Table 5-4 presents measured and assumed water content for all samples. Water content corrections need to be applied to the average beta dose rate from HRGS and TSBC (Zimmerman, 1971), and to the dry gamma dose rates determined by HRGS. The mean value for the effective beta dose rate is 0.99 ± 0.04; as determined by the water content and grain size attenuation corrections. Calculated wet gamma dose rate values by HRGS are also tabulated.

Sample (SUTL)	Activity Concentrations/ Bq Kg^{-1}			Equivalent Concentrations[1,2]		
	K	U	Th	K (%)	U (ppm)	Th (ppm)
2014	82.255 ± 11.74	1.151 ± 0.801	5.433 ± 1.418	0.266 ± 0.038	0.093 ± 0.065	1.339 ± 0.350
2017	409.17 ± 19.10	16.645 ± 2.231	23.663 ± 2.496	1.323 ± 0.062	1.348 ± 0.181	5.832 ± 0.615
2019	190.42 ± 15.62	7.179 ± 1.811	5.217 ± 2.173	0.616 ± 0.050	0.581 ± 0.147	1.286 ± 0.536
2020	513.07 ± 18.83	5.569 ± 1.696	14.197 ± 2.203	1.659 ± 0.061	0.451 ± 0.137	3.499 ± 0.543
2021	130.48 ± 14.79	4.770 ± 1.701	7.122 ± 2.098	0.422 ± 0.048	0.386 ± 0.138	1.755 ± 0.517
2023	415.20 ± 15.64	5.232 ± 0.995	28.128 ± 1.722	1.343 ± 0.051	0.424 ± 0.081	6.933 ± 0.424
2025	100.63 ± 8.48	-1.222 ± 0.449	-4.279 ± 0.652	0.325 ± 0.027	-0.10 ± 0.036	-1.05 ± 0.161
2026	120.37 ± 9.03	4.015 ± 0.438	1.638 ± 0.751	0.389 ± 0.029	0.325 ± 0.035	0.404 ± 0.185
2043	322.67 ± 14.84	9.025 ± 1.091	12.300 ± 1.572	1.043 ± 0.048	0.731 ± 0.088	3.032 ± 0.388
2044	491.83 ± 16.94	18.886 ± 1.314	26.615 ± 1.779	1.590 ± 0.055	1.529 ± 0.106	6.560 ± 0.439
2045	36.602 ± 8.16	8.397 ± 0.542	2.953 ± 0.769	0.118 ± 0.026	0.680 ± 0.044	0.728 ± 0.190
2046	122.43 ± 8.94	1.445 ± 0.459	2.692 ± 0.762	0.396 ± 0.029	0.117 ± 0.037	0.663 ± 0.188
2047	64.71 ± 12.53	6.044 ± 0.939	4.233 ± 1.461	0.209 ± 0.041	0.489 ± 0.076	1.043 ± 0.360
1328	158.81 ± 15.14	35.432 ± 2.862	7.173 ± 2.186	0.514 ± 0.049	2.869 ± 0.232	1.768 ± 0.539
1330	204.60 ± 15.65	37.676 ± 3.175	13.529 ± 2.164	0.662 ± 0.051	3.051 ± 0.257	3.335 ± 0.533
1581	316.38 ± 21.38	37.812 ± 4.200	1.332 ± 0.241	1.023 ± 0.069	3.062 ± 0.340	0.328 ± 0.059
1582	268.78 ± 20.80	37.282 ± 4.089	2.961 ± 0.270	0.869 ± 0.067	3.028 ± 0.331	0.730 ± 0.067

Table 5-2: Activity and Equivalent concentrations of K, U and Th for samples SUTL 1581-1584 as determined by HRGS

[1] Conversion factors (based on OECD, 1994): 40K: 309.26 Bq kg-1 %K-1; 238U: 12.34787 Bq kg-1 ppmU-1; 232Th: 4.057174 Bq kg-1 ppmTh-1

[2] Working values for Shap granite: K(%) – 4.43 ± 0.03; U(ppm) – 12.00 ± 0.06; Th(ppm) – 28.5 ± 0.36; K - 1370 ± 10; U – 148.2 ± 7.4; Th – 115.6 ± 1.1

Sample (SUTL)	Dry Infinite Matrix dose rates[1] by HRGS / mGya-1									TSBC / mGya-1		
	Dα (dry)			Dβ (dry)			Dγ (dry)			Dβ (dry)		
2014	1.249	±	0.315	0.273	±	0.034	0.144	±	0.021	0.450	±	0.039
2017	8.056	±	0.677	1.462	±	0.060	0.774	±	0.041	1.649	±	0.053
2019	2.566	±	0.568	0.633	±	0.050	0.281	±	0.034	0.706	±	0.042
2020	3.839	±	0.554	1.543	±	0.057	0.632	±	0.035	1.629	±	0.057
2021	2.371	±	0.541	0.457	±	0.047	0.236	±	0.033	0.617	±	0.041
2023	6.301	±	0.385	1.375	±	0.045	0.729	±	0.027	1.551	±	0.052
2025	-1.054	±	0.156	0.225	±	0.024	0.013	±	0.011	0.299	±	0.038
2026	1.202	±	0.169	0.382	±	0.025	0.152	±	0.013	0.481	±	0.040
2043	4.272	±	0.377	1.059	±	0.043	0.491	±	0.025	1.106	±	0.047
2044	9.098	±	0.439	1.731	±	0.050	0.896	±	0.029	2.548	±	0.069
2045	2.428	±	0.186	0.218	±	0.023	0.144	±	0.013	0.259	±	0.037
2046	0.816	±	0.173	0.365	±	0.025	0.143	±	0.013	0.412	±	0.039
2047	2.131	±	0.340	0.275	±	0.037	0.160	±	0.023	0.622	±	0.041
1328	9.248	±	0.836	0.896	±	0.055	0.544	±	0.040	0.887	±	0.044
1330	10.943	±	0.816	1.090	±	0.058	0.681	±	0.042	0.801	±	0.043
1581	8.752	±	0.946	1.306	±	0.076	0.615	±	0.042	1.716	±	0.068
1582	8.952	±	0.922	1.185	±	0.074	0.595	±	0.042	1.707	±	0.065

Table 5-3: Dose rates determined by TSBC and HRGS

[1] *Based on Dose Rate conservation factors from Aitken, 1983.*

Sample (SUTL)	Water Content			Effective β dose rate[1] / mGya^{-1}	D_γ (wet) by HRGS[3] / mGya^{-1}	Effective γ dose rate[3] / mGya^{-1}	Total dose rate[2] / mGya^{-1}
	FW / %	SW / %	Assumed / %				
2014	18.42	36.76	15 ± 5	0.276 ± 0.025	0.123 ± 0.019	0.123 ± 0.019	0.584 ± 0.037
2017	38.99	94.95	15 ± 5	1.250 ± 0.077	0.696 ± 0.050	0.696 ± 0.050	2.131 ± 0.083
2019	17.87	79.23	15 ± 5	0.514 ± 0.037	0.241 ± 0.032	0.241 ± 0.032	0.940 ± 0.053
2020	30.54	81.43	15 ± 5	1.294 ± 0.079	0.568 ± 0.043	0.568 ± 0.043	2.047 ± 0.084
2021	52.87	129.9	15 ± 5	0.432 ± 0.035	0.213 ± 0.032	0.213 ± 0.032	0.830 ± 0.043
2023	29.9	71.13	15 ± 5	1.179 ± 0.071	0.656 ± 0.041	0.656 ± 0.041	2.020 ± 0.077
2025	3.3	45.8	15 ± 5	0.210 ± 0.021	0.011 ± 0.005	0.011 ± 0.005	0.406 ± 0.031
2026	3.49	43.52	15 ± 5	0.333 ± 0.025	0.130 ± 0.012	0.130 ± 0.012	0.648 ± 0.035
2043	15.71	61.65	15 ± 5	0.831 ± 0.050	0.421 ± 0.029	0.421 ± 0.029	1.437 ± 0.056
2044	8.76	19.48	15 ± 5	1.631 ± 0.092	0.768 ± 0.044	0.768 ± 0.044	2.584 ± 0.104
2045	5.84	22.22	15 ± 5	0.177 ± 0.019	0.124 ± 0.012	0.124 ± 0.012	0.486 ± 0.030
2046	14.24	36.91	15 ± 5	0.301 ± 0.024	0.123 ± 0.006	0.123 ± 0.006	0.608 ± 0.034
2047	10.74	47.49	15 ± 5	0.338 ± 0.027	0.137 ± 0.021	0.137 ± 0.021	0.660 ± 0.040
1328	-	-	15 ± 5	0.703 ± 0.048	0.490 ± 0.044	0.667 ± 0.051	1.466 ± 0.062
1330	-	-	15 ± 5	0.706 ± 0.046	0.584 ± 0.046	0.681 ± 0.050	1.524 ± 0.061
1581	10.79	24.81	15 ± 5	1.149 ± 0.072	0.527 ± 0.044	0.527 ± 0.044	1.861 ± 0.087
1582	-	-	15 ± 5	1.095 ± 0.069	0.510 ± 0.043	0.510 ± 0.043	1.790 ± 0.083

Table 5-4: Annual dose rates

[1] Effective beta dose rates combine water content corrections with inverse grain size attenuation factors obtained by weighting the 200 micron mean grain size attenuation factors of Mejdahl (1979) for K, U and Th sources by the relative contributions to beta dose rate from each source determined by HRGS.

[2] These rates are based on a γ water correction on the D_γ (dry) by HRGS.

[3] Obtained from the combination of effective beta and gamma dose rates and an additional 0.185 mGya^{-1} allowance for the dose rate due to cosmic radiation (Prescott and Hutton, 1994).

5.7.3 Single aliquot OSL results

Data derived from the SAR dose determinations were analysed at two scales; individual dose response curves were analysed using the Risø 'Analyst' program and composite data sets were explored using Excel spreadsheets and Jandel Sigmaplot software. The OSL decay shape and signal consistency for each individual measurement (i.e. aliquot) was compared to that recorded for all other measurements in a sample set (i.e. 4 to 20 aliquots). Background checks were consistent through all measurements. A final check for IRSL displayed a zero response in all samples. OSL signals were evaluated for equivalent dose estimates. Poorly bleached aliquots were rejected from further analysis based on the recycling ratio and feldspar contamination. A small number of outlying data points were also excluded from the final analysis. In general, there was no evidence of significant differences in normalised OSL ratios (both in natural and regenerated dose points) between subsets of discs pre-heated at temperatures from 220°C to 280°C.

Accordingly, composite dose response curves from selected discs for each sample were constructed and used to estimate equivalent dose values for each individual disc and their combined sets. The growth curve data were fitted with a single saturating exponential function and the equivalent dose was estimated by interpolation with the net-natural sensitivity-corrected luminescence level. The distribution in equivalent dose values was examined using weighted mean histogram plots (after Duller et al., 2000; Spencer and Sanderson, 2002). To check for the presence of non-uniformity (sample heterogeneity) in sample radiation dose histories, aliquot intensity and equivalent doses were compared.

A recognised problem in the accurate dating of sediments using a multi-grained approach is an overestimation in equivalent dose due to stimulation of a mixed dose population consisting of bleached, partially bleached or unbleached grains (Olley et al., 1999), i.e. fluvial gravels are apt to contain a mix of grains, some of which were well bleached at deposition and others that, under a cover of water, were bleached insignificantly to zero the optical dating signal (i.e. a response to the filtering and attenuation of the solar spectrum in water). The best estimate of the true burial dose is often considered to be the lowest measured, or population of dose(s) (Olley et al., 1998; 1999; Lepper et al., 2000; Fuchs and Lang, 2001). In single-aliquot dating techniques several methods have been used to exclude insufficiently bleached signal components from the equivalent dose estimation, including the use of radial plots (Galbraith, 1990), weighted histograms (Spencer and Sanderson, 2002),

de-convolution methods (Lepper et al., 2000), f-statistics (Spencer et al., 2003) and dose-recovery comparisons (Zhang et al., 2003). However, all of the foregoing are based on rather large sets of aliquots (or grains) (i.e. 50 plus aliquots (or grains)) and cannot be used if only a small number are available, as for samples collected at Agia Marinouda, Kolossi, Cape Kiti and Amargeti. Due to the limited amount of quartz in the sediment only 5-20 aliquots could be measured for each sample. As expected all of the OSL samples gave scattered equivalent dose distributions (see text below). However, valid and informative ages can be obtained, if one has a detailed knowledge of the site/sample context and location; including stratigraphical/sedimentological data, knowledge of the sediment transport process and the provenance of the sand/soil/sediment.

5.7.4 The Neolithic settlement at Kissonerga-Mylouthkia (an independent age control).

Table 5-5 summarises the SAR characteristics and results, together with age determinations based on unweighted and weighted combinations of data from the individual discs, for the two samples collected at Kissonerga-Mylouthkia.

Sample (SUTL)	**1581**	**1582**
Location:	**Kissonerga-Mylouthkia**	**Kissonerga-Mylouthkia**
Recycling ratio	1.00 ± 0.01	0.99 ± 0.01
D_e at 220°C / Gy	16.43 ± 2.24	12.94 ± 1.57
D_e at 240°C / Gy	16.94 ± 0.52	15.38 ± 1.64
D_e at 260°C / Gy	17.01 ± 1.56	16.32 ± 3.47
D_e at 280°C / Gy	17.51 ± 1.81	15.24 ± 0.20
Combined D_e / Gy	16.97 ± 0.83	14.97 ± 1.04
Total dose rate / $mGya^{-1}$	1.860 ± 0.090	1.790 ± 0.080
Age / ka	**9.12 ± 0.49**	**8.37 ± 0.61**
Age / years BP	**9118 ± 493**	**8368 ± 613**
Weighted D_e / Gy	17.13 ± 1.21	14.44 ± 1.64
Age / ka	9.20 ± 0.78	8.07 ± 0.99
Age / years BP	9206 ± 779	8068 ± 992

Table 5-5: Summary of SAR results from samples collected at Kissonerga-Mylouthkia

The two hollow- or pit-like features 2207 and 2208 at Mylouthkia (see section 5.4) yielded OSL ages of 8.37 ± 0.61 ka and 9.12 ± 0.49 ka, respectively. AMS results from charred

seeds and cereal grains date wells at the same site to the late 10th and 9th millennium; i.e. period 1A well 166 (Section 5.4, Figure 5-2a) has a coherent set of three later 10th millennium BP AMS dates from barley and other short-lived cereal grains (Section 5.4, Figure 5-2b); period 1B well 133 (Section 5.4, Figure 5-2a; Peltenburg et al., 2003) has two later 9th millennium AMS dates from charred seeds (Section 5.4, Figure 5-2b; Peltenburg et al., 2003). Hollow/pit 2208 may, thus be designated as a Period 1A PPNB-Cypro feature and hollow/pit 2207 a Period 1B PPNB-Cypro feature.

Summary: Optically stimulated luminescence ages of quartz extracts in Neolithic pits at Kissonerga-Mylouthkia, correlate with published AMS results (Kinnaird et al., in press; Table 5-6).

Locality:	Sample no.	Material	Years BP	Calibrated BC*
Well 116.124	Ox A-7460	Barley	9316 ± 60†	8740 – 8320
Well 116.123	AA-33128	Grain	9235 ± 70†	8630 – 8280
Well 116.124	AA-331129	Grain	9110 ± 70†	8540 – 8490 8490 – 8200
Well 133.264	Ox A-7461	Pistacea sp.	8185 ± 55†	7450 – 7430 7350 – 7060
Well 133.264	AA-33130	Lolium sp.	8025 ± 65†	7140 – 6690
Pit 1/ '2208'	SUTL 1581	-	9118 ± 493	9610 – 8625
Pit 2/ '2207'	SUTL 1582	-	8367 ± 612	8975 – 7755

Table 5-6: A comparison of AMS and SAR OSL results from Kissonerga-Mylouthkia

† denotes AMS result

** the radiocarbon dates were calibrated using the program Oxcal v.3.9 of Christopher Ramsey (a computer program to calibrate radiocarbon dates and facilitate analysis of archaeological stratigraphy)*

5.7.5 Middle Pleistocene – Recent tectonics

The SAR protocol described in section 5.3 was used to obtain equivalent dose estimates from samples collected at, or near the villages of Agia Marinouda, Kolossi, Cape Kiti and Amargeti.

5.7.5.1 The Agia Marinouda and Kouklia Fold

Table 5-7 summarises the SAR characteristics and results, together with age determinations based on unweighted and weighted combinations of data from the individual discs, obtained for three samples collected at the village of Gerospikou.

Sample (SUTL)	**2023**	**2043**	**2044**
Location:	**Geroskipou-1**	**Geroskipou-2**	**Geroskipou-3**
Recycling ratio			
D_e at 220°C / Gy	59.18 ± 2.28	-	41.22 ± 19.78
D_e at 240°C / Gy		98.69 ± 40.32	87.78 ± 20.35
D_e at 260°C / Gy	-	-	82.62 ± 18.93
D_e at 280°C / Gy	-	-	90.86 ± 13.93
Combined D_e / Gy	-	-	75.62 ± 9.20
Total dose rate / $mGya^{-1}$	2.020 ± 0.077	1.437 ± 0.056	2.584 ± 0.104
Age / ka	**29.27 ± 5.41**	**68.68 ± 28.19**	29.26 ± 5.60
Age / years BP	29273 ± 5407	68683 ± 28187	29262 ± 5598
Weighted D_e / Gy	-	-	85.35 ± 17.08
Age / ka	-	-	**33.03 ± 6.74**
Age / years BP	-	-	33028 ± 6741

Table 5-7: Summary of SAR results from the site at Geroskipou

In total, three full-dating and five profiling samples, were collected at Geroskipou, and dated by the SAR OSL protocol. A limited amount of quartz was extracted from the Geroskipou samples: sample SUTL 2044 yielded enough quartz to make 16 aliquots, samples 2023 and 2043 only yielded enough quartz to make 2 aliquots each. The luminescence properties of sample 2044 were studied, and the results extrapolated to obtain data for 2023 and 2043. Equivalent doses were obtained from 16 aliquots produced from quartz extracted from a palaeosol horizon at Geroskipou. An age estimate for SUTL 2044 was obtained by using the mean equivalent dose (i.e. the robust mean was calculated by the use of an in-house Excel program, which removed any data outwith 2 standard deviations in a continuous loop, so that data excluded from the last calculation were not included in the next. This method only removes the most extreme outliers. Of the 16 aliqouts measured, 13 were within 2σ (95% confidence level) of the robust mean (Figure 5-22a).

The equivalent dose distribution obtained for sample 2044, collected at Geroskipou, is a multi-peaked spectra spanning 112.6 ± 3.6 to 62.6 ± 2.7 Gy, but dominated by clusters at 106.7 ± 0.4, 77.9 ± 1.6 and 64.2 ± 1.6 Gy (Figure 5-22b). There was a significant difference in normalised OSL ratios (both in natural and regenerated dose points) between the subsets of discs pre-heated at temperatures of 220°C and between 240°C and 280°C. The luminescence signal at 220°C was unstable (Figure 5-23). The equivalent doses obtained at a preheat of 220°C were disregarded from further analysis. The equivalent dose distribution histogram for sample SUTL 2044 is shown in Figure 5-22b.

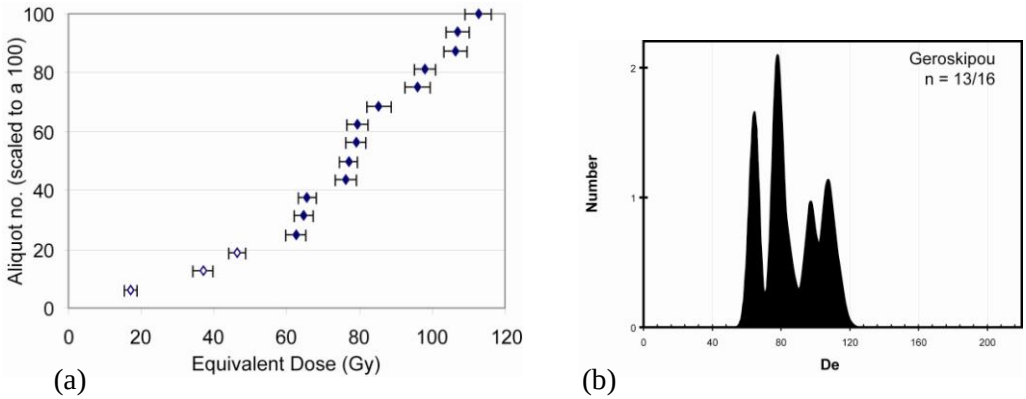

Figure 5-22: (a) Equivalent dose distributions of quartz extracted from a sample at Geroskipou. Closed diamonds denote data that are within 2σ of the mean. Open diamonds denote data that are outwith 2σ of the mean and (b) Weighted histograms of SAR equivalent doses

The results of the OSL dating/profiling study are shown in Figure 5-24. The two lower full-dating samples and all of the profiling samples yield stratigraphically consistent dates (Figure 5-24). The third full-dating sample, SUTL 2023 yielded at erroneous result: its age was calculated from an equivalent dose obtained at a preheat of 220°C. The luminescence signal obtained at 220°C was shown above to be unstable.

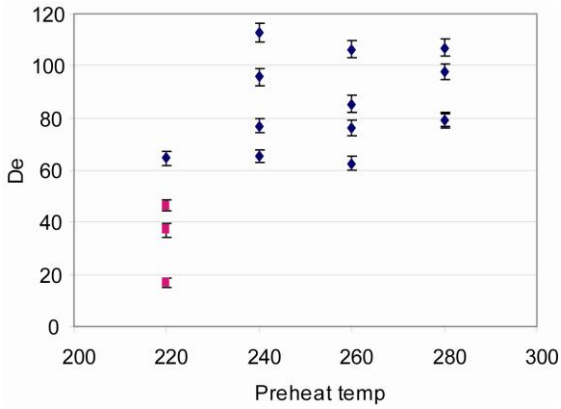

Figure 5-23: Preheat plateaus for quartz extracted from sample SUTL 2044 (Geroskipou). Due to scatter, no dependence of equivalent dose and preheat can be observed. Diamonds denote data that are within 2σ of the mean. Squares denote data that are outwith 2σ of the mean.

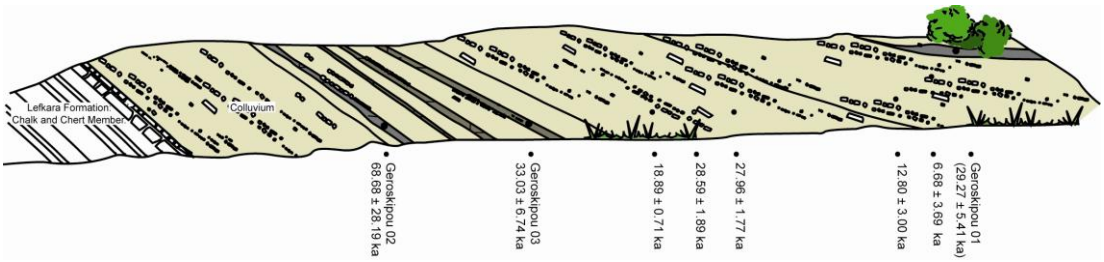

Figure 5-24: Sketch section of the growth strata observed at Agia Marinouda, Geroskipou. The results of the OSL study are shown

5.7.5.2 The Kolossi lineament

Table 5-8 summarises the SAR characteristics and results, together with age determinations based on unweighted and weighted combinations of data from the individual discs, obtained for samples collected at Kolossi and Akrotiri.

Sample (SUTL)	**2025**	**2045**	**2046**
Location:	**Akrotiri**	**Kolossi Football stadium**	**Kolossi Goat farm**
Recycling ratio			
D_e at 220°C / Gy	20.01 ± 1.46	92.39 ± 68.03	39.99 ± 5.05
D_e at 240°C / Gy	24.50 ± 1.71	81.05 ± 27.85	43.15 ± 24.40
D_e at 260°C / Gy	22.86 ± 3.56	92.66 ± 29.52	73.72 ± 4.43
D_e at 280°C / Gy	-	144.61 ± 55.27	54.21 ± 6.18
Combined D_e / Gy	22.46 ± 1.40	102.68 ± 24.15	52.77 ± 6.51

Total dose rate / mGya^{-1}	0.406 ± 0.031	0.486 ± 0.030	0.608 ± 0.034
Age / ka	55.26 ± 4.22	211.37 ± 76.07	86.76 ± 20.66
Age / years BP	55261 ± 4216	211365 ± 76066	86756 ± 20659
Weighted D_e / Gy	22.95 ± 2.83	84.58 ± 8.70	46.58 ± 9.66
Age / ka	**56.46 ± 8.17**	**174.12 ± 20.90**	**76.58 ± 16.43**
Age / years BP	56464 ± 8173	174118 ± 20903	76576 ± 16433

Table 5-8: Summary of SAR results from sites at Kolossi/Akrotiri

In total three full dating samples, were collected at Kolossi and Akrotiri, and dated by the OSL SAR protocol. Sufficient quartz was extracted from samples SUTL 2045 and 2046 to produce 16 and 20 aliquots, respectively. For all three samples, there was no evidence of significant differences in normalised OSL ratios (both in natural and regenerated dose points) between the subsets of discs pre-heated at temperatures from 220°C to 280°C (e.g. SUTL 2045/2046; Figure 5-25). Due to the wide distribution/scatter in equivalent doses no dependence on equivalent dose and preheat was observed.

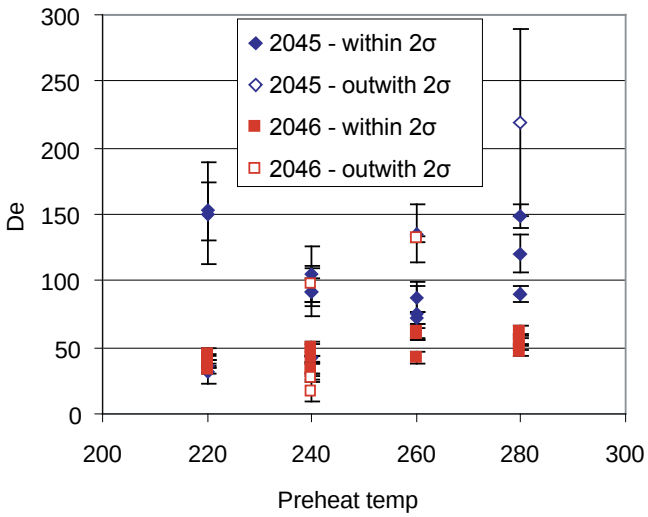

Figure 5-25: Preheat plateaus for quartz extracted from samples SUTL 2045/2046. Due to scatter, no dependence of equivalent dose and preheat was observed. Closed squares/diamonds denote data that are within 2σ of the mean. Open squares/diamonds denote data that are outwith 2σ of the mean

The equivalent dose distribution histograms for all three samples are shown in Figure 5-26. The samples collected at Kolossi yielded equivalent dose histograms with wide, asymmetric profiles, whereas the sample collected at Akrotiri yielded a tight, symmetric profile (Figure 5-26). Equivalent doses were obtained from 16 aliquots produced from quartz extracted from a colluvial deposit at the Kolossi football stadium (henceforth referred to as site (i)). Of the

16 aliqouts measured, 15 were within 2 standard deviations of the mean (Figure 5-26a). The equivalent dose distribution obtained for the sample collected at site (i) is a multi-peaked spectra spanning 152.4 ± 22.1 to 31.5 ± 9.7 Gy, but dominated by clusters at 90.1 ± 1.7, 73.6 ± 2.9 and 36.3 ± 5.2 Gy (Figure 5-26b). Equivalent doses were obtained from 20 aliquots produced from quartz extracted from an aeolinite deposit at the Kolossi goat farm (henceforth referred to as site (ii)). Of the 20 aliqouts measured, 16 were within 2 standard deviations of the mean (Figure 5-26a). The equivalent dose distribution obtained at site (ii) is largely bimodal and dominated by clusters at 41.5 ± 0.9 and 33.2 ± 0.3 Gy (Figure 5-26b). Equivalent doses were obtained from 5 aliquots produced from quartz extracted from an aeolinite deposit at Akrotiri (henceforth referred to as site (iii)). The equivalent dose distribution obtained at site (iii) is symmetric, with a dominant cluster at 25.0 ± 0.3 Gy (Figure 5-26b).

Age estimates for samples collected at site (ii) and (iii) were obtained by using the mean equivalent dose (following the procedure outlined in section 5.7.5.1). OSL ages of 76.58 ± 16.43 and 56.46 ± 8.17 ka were obtained for the samples collected at (ii) and (iii), respectively. The age estimate obtained for the sample collected at site (i) was obtained by using a value of 84.58 ± 8.70 Gy: a young population of equivalent doses (i.e. 36.3 ± 5.2 Gy) was disregarded as it is deemed to be contamination from the overlying unit; an old population of equivalent doses (i.e. that above 105.1 ± 20.6 Gy) was disregarded as it is deemed to be an inherited signal.

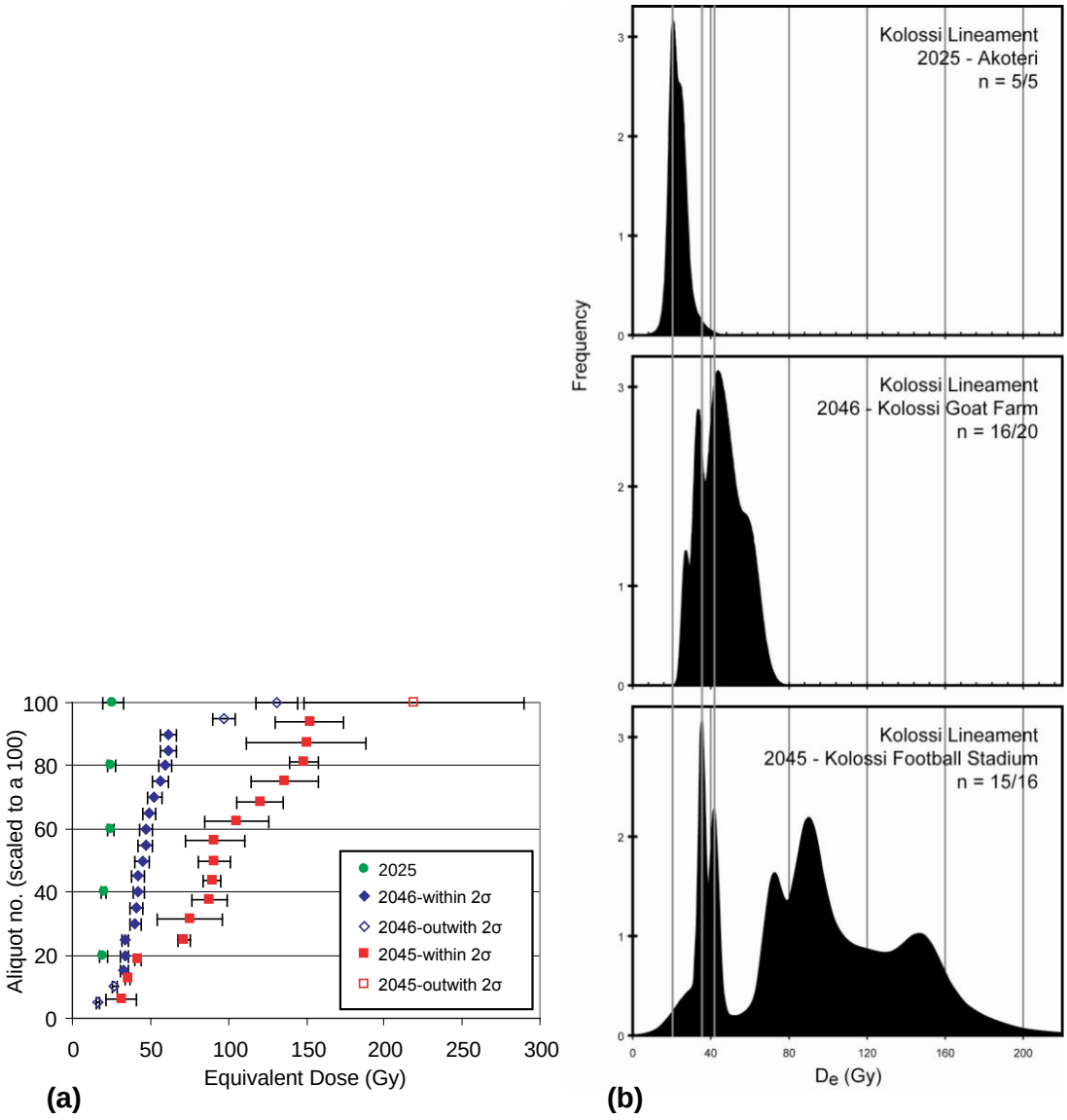

Figure 5-26: (a) equivalent dose distributions of quartz extracted from samples 2025 (Akotiri), 2045 (Kolossi football stadium) and 2046 (Kolossi goat farm). Closed squares/diamonds/circles denote data that are within 2σ of the mean. Open squares/diamonds/circles denote data that are outwith 2σ of the mean and (b) Weighted histograms of SAR equivalent doses

As a control, the median, mean, robust mean and logged and non-logged central age modelled estimates of Galbraith (1999) were calculated, to compare averaged equivalent dose estimates (Figure 5-27). In general, there was a good agreement between the different methods. However, at site (i) a discrepancy of c. 20 Gy was noted between the estimated mean equivalent dose, and the value used in the age calculation above. The calculations used in estimating a mean equivalent dose do not identify contamination, or inherited geological signals, and thus give anomalous values.

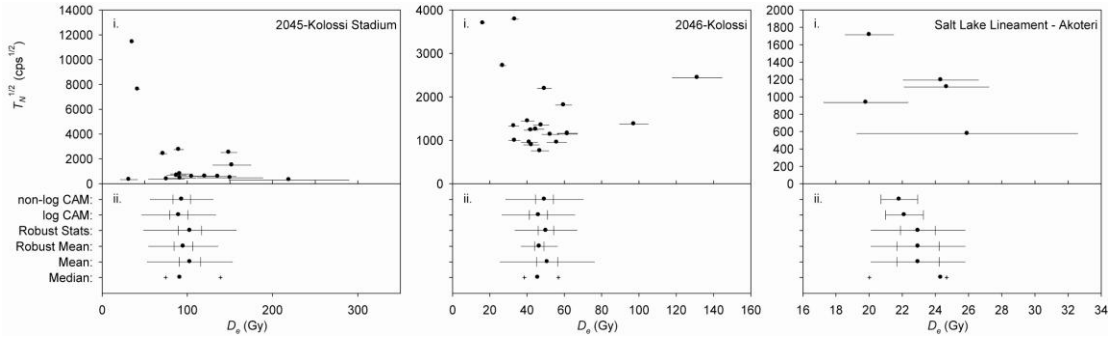

Figure 5-27: Equivalent dose distributions of quartz extracted from samples 2025 (Akrotiri), 2045 (Kolossi football stadium) and 2056 (Kolossi goat farm). The median, mean, robust mean and logged and non-logged central age model of Galbraith (1999) estimates of equivalent dose are shown.

The results of the OSL study are shown in Figure 5-28. The Kolossi fault juxtaposes Pakhna and Nicosia Formation strata against Fanglomerate gravels. Deformed Fanglomerate gravels at the base of the Kolossi fault are dated at 174.1 ± 20.9 ka. The Kolossi Fault is overlain by middle Pleistocene gravels dated at 76.6 ± 16.4 ka. There has been no displacement along the fault since the deposition of the Middle Pleistocene gravels. Thus, the Kolossi Fault was active at 176 ± 20.9 ka. Movement on the fault had ceased by 76.6 ± 16.4 ka.

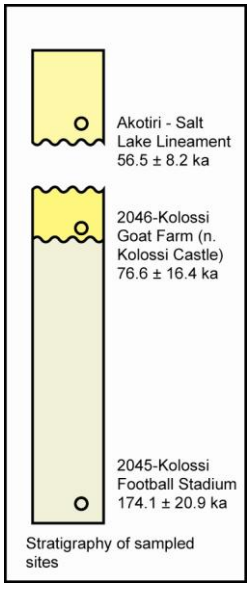

Figure 5-28: OSL ages obtained at Kolossi and Akotiri; constraining movement on the Kolossi Fault lineament

5.7.5.3 The Cape Kiti lineament

Table 5-9 summarises the SAR characteristics and results, together with age determinations based on unweighted and weighted combinations of data from the individual discs, obtained for a sample collected at Cape Kiti.

Sample (SUTL)	**2026**
Location:	**Cape Kiti**
Recycling ratio	
D_e at 220°C / Gy	27.04 ± 3.79
D_e at 240°C / Gy	19.50 ± 1.26
D_e at 260°C / Gy	21.28 ± 1.14
D_e at 280°C / Gy	26.87 ± 1.49
Combined D_e / Gy	23.67 ± 1.10
Total dose rate / $mGya^{-1}$	0.648 ± 0.035
Age / ka	36.52 ± 1.96
Age / years BP	36523 ± 1965
Weighted D_e / Gy	24.74 ± 8.49
Age / ka	**38.17 ± 13.18**
Age / years BP	38169 ± 13182

Table 5-9: Summary of SAR results from the site at Cape Kiti

A broad distribution in equivalent doses was obtained from the sample collected inland of Cape Kiti (Figure 5-29a). Equivalent doses were obtained from 16 aliquots produced from quartz extracted from an aeolinite deposit at Cape Kiti. Of the 16 aliqouts measured, 15 were within 2 standard deviations of the mean. The equivalent dose distribution obtained for the sample collected at Cape Kiti is a multi-peaked spectra spanning 11.3 ± 0.6 to 38.3 ± 2.5 Gy, but dominated by clusters at 29.6 ± 1.8 and 18.1 ± 0.7 Gy. The calculated estimates of the mean equivalent dose are similar (and within error; Figure 5-29b).

An OSL age of 38.17 ± 13.18 ka was determined for sands collected at the base of the aeolinite.

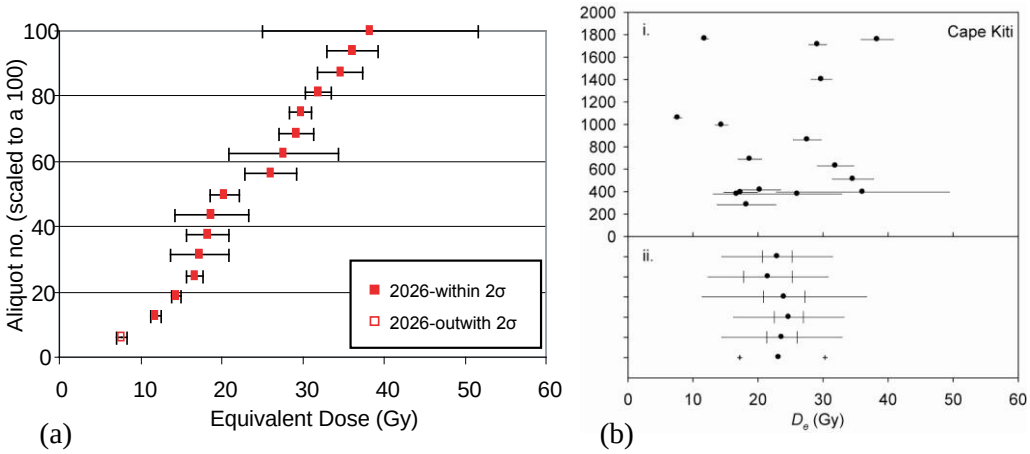

Figure 5-29: (a) Equivalent dose distributions of quartz extracted from the sample collected at Cape Kiti, SUTL 2026. The median, mean, robust mean and logged and non-logged central age model of Galbraith (1999) estimates of equivalent dose are shown in (b).

5.7.5.4 Amargeti

Table 5-10 summarises the SAR characteristics and results, together with age determinations based on unweighted and weighted combinations of data from the individual discs, obtained from samples collected near the village of Amargeti.

In total, three full dating and four profiling samples were dated by the SAR OSL protocol. Due to a limited amount of quartz in the sediment, only a limited number of aliquots could be prepared for each full dating sample. Equivalent doses for the full dating samples in the footwall of the fault are 89.20 ± 12.95 and 27.76 ± 2.63 Gy, respectively and in the hangingwall of the fault, 43.40 ± 2.14 Gy. The profiling samples were collected in the hangingwall of the fault; from the base to the top the averaged equivalent doses were 37.22 ± 8.41, 29.56 ± 0.82, 20.73 ± 0.75 and 8.24 ± 0.08 Gy. The results of the OSL study are shown in Figure 5-30.

Sample (SUTL)	**2019**	**2020**	**2021**
Location:	**Amargeti-1**	**Amargeti-2**	**Amargeti-3**
Recycling ratio			
D_e at 220°C / Gy	-	56.84 ± 4.86	74.02 ± 10.03
D_e at 240°C / Gy	43.74 ± 1.86	-	-
D_e at 260°C / Gy	37.85 ± 1.50	-	-
D_e at 280°C / Gy	-	-	-
Combined D_e / Gy	40.80 ± 2.95	-	-

Total dose rate / mGya^{-1}	0.940	±	0.053	2.047	±	0.084	0.830	±	0.043
Age / ka	**43.40**	**±**	**2.14**	**27.76**	**±**	**2.63**	**89.20**	**±**	**12.95**
Age / years BP	43404	±	2139	27764	±	2634	89203	±	12945
Weighted D_e / Gy	40.79	±	4.17	-			-		
Age / ka	43.41	±	3.96	-			-		
Age / years BP	43405	±	3964	-			-		

Table 5-10: Summary of SAR results from the site at Amargeti

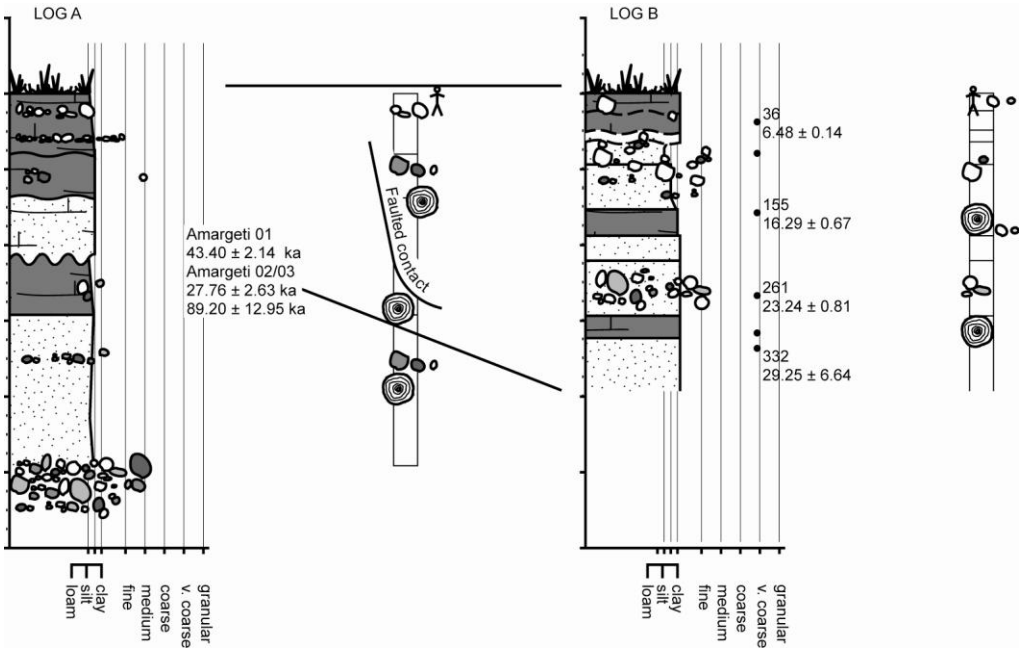

Figure 5-30: Sedimentary logs through the colluvium/palaeosol sequence at Amargeti. Horizons sampled for OSL profiling are indicated. The number beside the sampled horizon corresponds to its depth from the present land surface (in cm). The key to the sedimentary logs is given in Appendix A

5.7.6 Late Pleistocene – Recent depositional processes

5.7.6.1 Kalavasos

Table 5-11 summarises the SAR characteristics and results, together with age determinations based on unweighted and weighted combinations of data from the individual discs obtained from samples collected at, or near the village of Kalavasos.

Sample (SUTL)	2014	2017	2047
Location:	**Kalavasos- Márkou**	**Kalavasos-Vasilikós**	**Kalavasos- Vasilikós Drapia farm**
Recycling ratio			
D_e at 220°C / Gy	18.82 ± 2.51	22.13 ± 4.54	51.68 ± 1.59
D_e at 240°C / Gy	9.12 ± 1.00	-	-
D_e at 260°C / Gy	23.08 ± 1.49	-	-
D_e at 280°C / Gy	29.87 ± 1.55	-	-
Combined D_e / Gy	20.22 ± 0.86	-	-
Total dose rate / $mGya^{-1}$	0.584 ± 0.037	2.131 ± 0.083	0.660 ± 0.040
Age / ka	**34.62 ± 1.89**	**10.38 ± 2.17**	**78.25 ± 5.28**
Age / years BP	34616 ± 1889	10383 ± 2168	78249 ± 5282
Weighted D_e / Gy	20.22 ± 8.69	-	-
Age / ka	34.62 ± 15.04	-	-
Age / years BP	34616 ± 15035	-	-

Table 5-11: Summary of the SAR results from the sites at Kalavasos

In total, four full dating samples and twelve profiling samples were collected in the Vasilikós Valley, Kalavasos. A limited amount of quartz was extracted from the Vasilikós Valley samples: sample SUTL 2014 yielded enough quartz to make 4 aliquots, samples 2017 and 2047 yielded enough quartz to make 2 aliquots each, and sample SUTL 2048 didn't yield any quartz.

Consistent equivalent doses were obtained from sediment sampled at Kalavasos Márkou. The results of the OSL dating/profile study are shown in Figure 5-31a. The results are consistent with the stratigraphy established by Schrimer (1998). From the base of the section to the top the results are: 37.88 ± 4.74 ka, (31.97 ± 9.1 ka), 34.62 ± 1.89 ka*, 31.17 ± 4.50 ka, (27.44 ± 1.6 ka), 17.08 ± 2.85 ka, 17.31 ± 2.17 ka and 17.79 ± 8.35 ka. The dates in brackets indicate radiocarbon results obtained in the study of Schrimer (1998). The age denoted with an '*' indicates a fully dated sample. All other ages were derived from profiling samples.

Consistent equivalent doses were obtained from sediment sampled at Kalavasos Vasilikós. The results of the OSL dating/profile study are shown in Figure 5-31b. From the base of the

section to the top the results are: 8.25 ± 0.54 ka, 10.38 ± 2.17 ka*, 9.36 ± 4.03 ka, 8.00 ± 2.63 ka, 4.44 ± 1.64 ka, 2.21 ± 1.07 ka and 7.76 ± 2.85 ka.

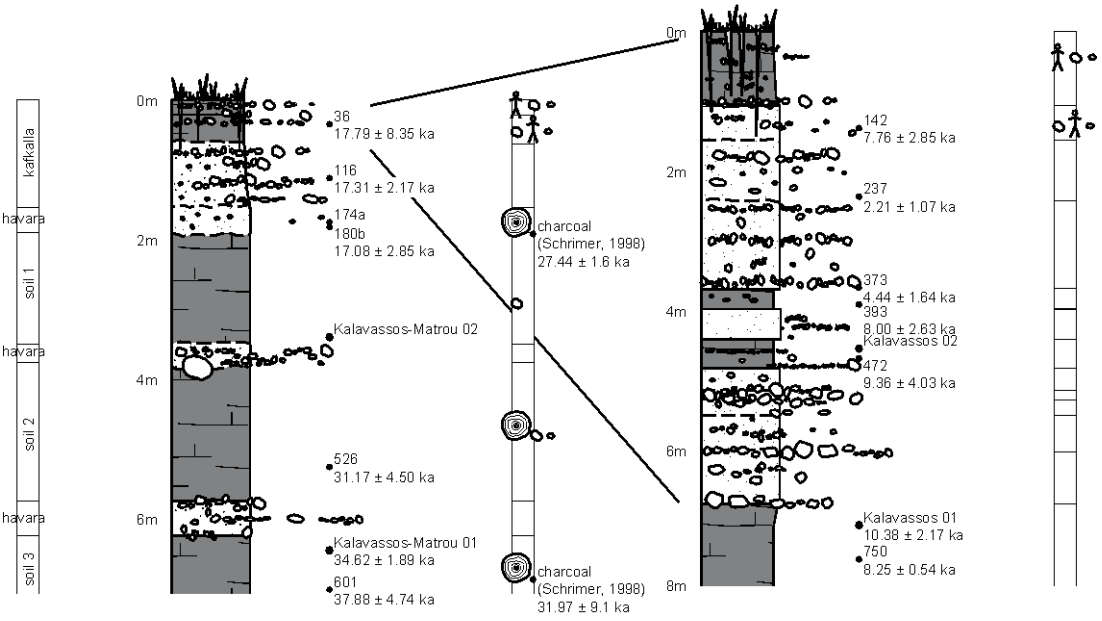

Figure 5-31: Sedimentary logs through the havara/palaeosol sequences: (a) at Kalavasos Márkou and (b) at Kalavasos Vasilikós. Horizons sampled for OSL profiling and for full OSL dating are indicated. The number beside the sampled horizon corresponds to its depth from the present land surface. The results of the OSL study are shown. The key to the sedimentary logs is given in Appendix A

The samples collected from Kalavasos Vasilikós-Drapia did not yield sufficient quartz to date. A single palaeosol horizon in the middle of the succession was dated at 78.25 ± 5.28 ka.

5.7.6.2 Souskiou

Table 5-12 summarises the SAR characteristics and results, together with age determinations based on unweighted and weighted combinations of data from the individual discs, for samples collected at Souskiou.

Sample (SUTL)	**1328**	**1330**
Location:	**Souskiou**	**Souskiou**
Recycling ratio		
D_e at 220°C / Gy	9.54 ± 1.24	4.05 ± 6.00
D_e at 240°C / Gy	25.97 ± 6.88	-
D_e at 260°C / Gy	17.10± 3.93	1.71 ± 1.52
D_e at 280°C / Gy	17.90 ± 4.90	3.10 ± 1.67

Combined D_e / Gy	17.62 ± 2.31	2.96 ± 2.14
Total dose rate / $mGya^{-1}$	1.466 ± 0.062	1.524 ± 0.061
Age / ka	**12.02 ± 1.60**	**1.94 ± 1.40**
Age / years BP	12021 ± 1599	1939 ± 1403
Weighted D_e / Gy	16.44 ± 9.26	3.02 ± 2.33
Age / ka	11.21 ± 6.33	1.98 ± 1.53
Age / years BP	11208 ± 6333	1978 ± 1528

Table 5-12: Summary of SAR results from the site at Souskiou

Two full-dating samples where dated in this study. A further two samples were dated by Spencer and Sanderson (2002). Consistent equivalent doses were obtained from 7 aliquots from quartz extracted from the lower palaeosol horizon at Souskiou. The equivalent dose distribution obtained for this sample is largely bimodal with clusters at 13.0 ± 1.7 and 6.45 ± 1.1 Gy. Consistent equivalent doses were obtained from 5 aliquots from quartz extracted from the higher palaeosol horizon sampled at Souskiou. The equivalent dose distribution obtained for this sample is symmetric, with a dominant cluster at 3.0 ± 2.3 Gy. The results of the OSL dating are shown in Figure 5-32. The results are consistent with the stratigraphy established by Spencer and Sanderson (2002). From the base of the section to the top the results are 12.02 ± 1.60 ka, (6.53 ± 0.31 ka, 3.80 ± 0.40ka) and 1.94 ± 1.40ka. The dates in brackets indicate the results obtained by Spencer and Sanderson (2002).

5.7.6.3 Pegeia

The results of the OSL profiling are shown in Figure 5-33. From the base of the section to the top these results are 47.2 ± 0.9 ka, 45.6 ± 1.3 ka, 48.5 ± 1.9 ka and 38.1 ± 0.7 ka.

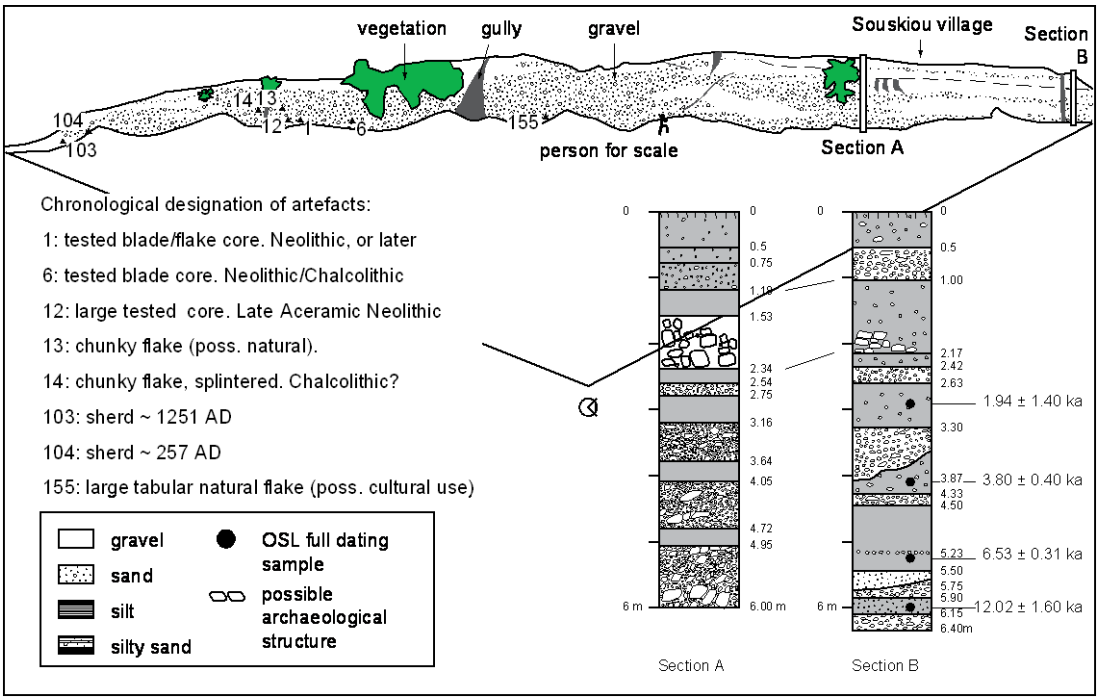

Figure 5-32: Sedimentary logs through the havara/palaeosol sequences at Souskiou (Kouklia). Horizons sampled for full OSL dating are indicated. The number beside the sampled horizon corresponds to its depth from the present land surface (K. Decker, personal communication). The OSL ages of 6.53 ± 0.31 and 3.80 ± 0.40 ka were obtained in an individual study by Spencer and Sanderson (2002). The results of the present OSL study are shown

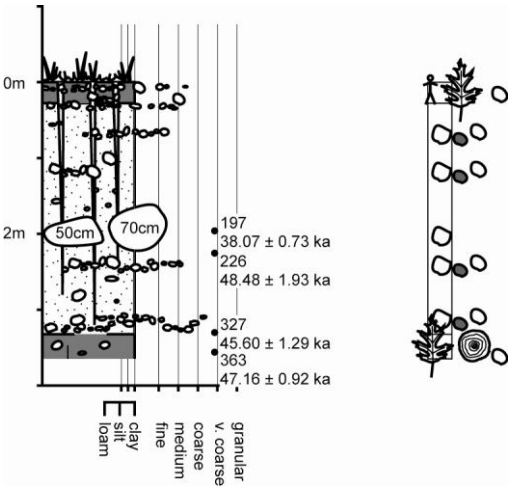

Figure 5-33: Sedimentary log through the colluvium/palaeosol sequence at Pegeia. Horizons sampled for OSL profiling are indicated. The number beside the sampled horizon corresponds to its depth from the present land surface. The key to the sedimentary logs is given in Appendix A

5.8 Discussion

5.8.1 Late Pleistocene – Holocene tectonic processes

The main objective of the luminescence study was to constrain the age of Pleistocene deformation. In chapter 3 the author proposed that the south coast of Cyprus was subjected to a period of compression/transpression in post-Miocene time. In west Cyprus, the Agia Marinouda Fold deforms Pleistocene strata; in central Cyprus, the Kolossi Fault cuts Pleistocene strata; and, in south central Cyprus, sinistral NNE-SSW-striking and dextral NNW-SSE-striking faults (Larnaka region) are believed to have been active in the Pleistocene/Recent.

The present study has established a preliminary chronology for the main Pleistocene compressional/transpressional events: (i) the Agia Marinouda Fold originated in the early middle Pleistocene at 76.8 ± 31.6 ka (~78.1 ka; chapter 4), and is still actively growing today; (ii) the Kolossi Fault Lineament originated in the early Pleistocene, and was active between 174.1 ± 20.9 ka and 76.6 ± 16.43 ka; and (iii) The Cape Kiti Fault lineament was active from the middle to late Pleistocene; Pleistocene movement on the Cape Kiti Fault is constrained to the period between 38.1 ± 13.2 ka and 12.1 ± 0.1 ka. It is believed that the Cape Kiti Fault may have originated earlier, possibly in the latest Pliocene (Harrison and Tsiolakis, 2006). Harrison and Tsiolakis (2006) state that a mimimum of 34m of stratigraphic throw occurred across the Cape Kiti fault in the Plio-Quaternary; the amount of horizontal displacement is indeterminable. The results of this study are intriguing as they indicate that transpressional/compressional lineaments were generated earlier in the east/southeast of the island than in the west.

Pleistocene extensional faulting is documented at Amargeti, Kalavasos and Pegeia. Extensional faults at Amargeti are believed to date to the late middle Pleistocene. The last episode of faulting at Amargeti occurred at ~ 43.4 ± 2.1 ka. In the Amargeti region, the interval between 29.3 ± 6.6 ka and 6.45 ± 0.1 ka is one of tectonic quiescence.

5.8.2 Late Pleistocene – Holocene depositional rates

Optically stimulated luminescence dating of havara/palaeosol sequences in the Vasilikós Valley, Kalavasos, was used as a tool to examine the controls on landscape evolution, in an

area of known tectonic instability. Three successions of interbedded havara and palaeosol were examined. To recap briefly, the site at Kalavasos Márkou was selected to assess whether it is possible to isolate a climatic signal in a sequence of havara/palaeosol; and sites at Kalavasos Vasilikós were selected to assess whether it is possible to isolate a tectonic signal in a sequence of havara/palaeosol. The site at Kalavasos Márkou is located on a stable slope-cut, approximately 30m above the valley bottom. There are no faults identified in the immediate area. In contrast, faults are observed cutting strata at the site at Kalavasos Vasilikós. It was hoped that through dating undeformed strata at Kalavasos Márkou and faulted strata at Kalavasos Vasilikós, that one could distinguish between climatic and tectonic signals. An additional aim was to constrain the age of faulting in the Vasilikós Valley.

Kalavasos Márkou

Radiocarbon ages derived from charcoal date the Kalavasos Márkou sequence as Middle to Upper Würmian (oxygen isotope stage 3; Schrimer, 1998); i.e. the palaeosol at the base of the sequence was dated at 31.97 ± 0.91 ka, and the havara horizon at the top of the sequence at 27.44 ± 1.60 ka (Figure 5-31a) (Schrimer, 1998). Based on this research, Schrimer (1998) correlated the havara/palaeosol units at Kalavasos Márkou with known stadial/interstadial periods from elsewhere in the eastern Mediterranean (Table 5-13): havara horizons were believed to correlate with the stadial phases of the Würmian glaciation and palaeosol horizons were believed to correlate with the interstadial phases of the Würmian glaciation. Schrimer (1998) reasoned that limited vegetation cover during stadial periods, coupled with frost action, would favour havara deposition and that extensive vegetation cover and stable climatic conditions during interstadial periods would favour formation of palaeosols. He admitted that alternatively, episodes of havara deposition and soil formation could instead equate with periods of heavy rainfall (i.e. pluvial conditions) and periods of aridity (i.e. interpluvial conditions), respectively. However, he argued that the havara sequences lack abundant organic material (e.g. humic streaks) as would be expected in the case of slope-wash processes in a vegetated area.

The chronological framework established for the havara/palaeosol sequence at Kalavasos Márkou during this study, is as follows: the lower, middle and upper palaeosols (the Tsiáko-Gondèssa soils of Schrimer (1998)) yield profiling/and full-age (*) date of 39.72 ± 6.07 ka, 36.29 ± 3.16 ka* and 32.68 ± 5.52 ka; the upper havara horizon yielded profiling age dates

of 17.91 ± 3.19 ka, 18.15 ± 2.57 ka and 18.65 ± 8.90 ka. Based on these data a new chronology is proposed: the lower palaeosol horizons equate to the Middle to Upper Würmian (i.e. oxygen stage 3), as proposed by Schrimer (1998); but the upper havara horizons equate to the Upper Würmian (i.e. oxygen isotope stage 2).

Oxygen Isotope Stages	Stage		Central European periglacial area	Cyprus (Kalavasos Márkou)
2	Upper Würmian		loess	havara
3	Middle Würmian	4	Sinzig soils 1-3: calcic cambisols	Tsiáko-Gondèssa soils 1-3: calcic regosols; havara
		3	Kripp stadial: loess	
		2	Remagen soils 1-5: calcic cambisols	
4		1	Stadial: loess	

Table 5-13: Middle Würmian of the Central European Glacial area and Cyprus (Schrimer, 1998)

In summary, a climatic signal is identified in the havara/palaeosol succession at Kalavasos Márkou.

Kalavasos Vasilikós

A chronological framework was established for the havara/palaeosol succession at Kalavasos Vasilikós: in which the lower palaeosol horizon is dated at 10.4 ± 2.2 ka*/8.25 ± 0.54 ka; the middle palaeosol horizon at 9.4 ± 4.0 ka; the upper palaeosol horizon at 8.00 ± 2.63 ka/4.4 ± 1.6 ka; and the upper havara horizon at 2.21 ± 1.07 ka. The OSL ages indicate that the succession was deposited in the present interstadial (i.e. oxygen isotope stage 1).

OSL dating of the havara/palaeosol succession at Drapia was not successful, as very little/to no quartz was contained with the havara/palaeosol horizons. A single horizon near the middle of the succession yielded an OSL age of 78.3 ± 5.3 ka. It had been envisaged that sedimentation rates at Kalavasos Vasilikós would be compared to those at Kalavasos Vasilikós-Drapia, allowing one to assess the impact that local faulting had on landscape evolution in the area. However, as the luminescence study at Kalavasos Vasilikós-Drapia was not successful this was not possible.

Extensional faulting in the Vasilikós Valley occurred in the late early to middle Pleistocene, between 78.3 ± 5.3 ka and 10.4 ± 2.2 ka. The havara/palaeosol succession at Kalavasos

Vasilikós-Drapia was rotated post-deposition by an inferred NW-SE-trending normal fault. A palaeosol horizon sampled near the middle of the Kalavasos Vasilikós-Drapia succession yielded an OSL age of 78.3 ± 5.3 ka, indicating that faulting must post-date deposition of this horizon. A palaeosol at the base of the Kalavasos Vasilikós succession yielded an OSL age of 10.4 ± 2.2 ka. This succession is not rotated to any degree, indicating that faulting had stopped prior to deposition of this unit.

Kalavasos/Pegeia/Souskiou

An additional objective was to assess depositional rates in areas of known tectonic disturbance. In order to achieve this aim, successions of interbedded havara and palaeosol were examined at (i) Kalavasos, (ii) Pegeia and (iii) Souskiou: to facilitate direct comparisons between depositional processes in areas of tectonic instability (sites (i) and (ii)) and stable areas (site (iii)).

Consistent equivalent doses were obtained from the sediment sampled at Pegeia. The results of the OSL profiling are as follows, from base to top, 47.2 ± 0.9 ka, 45.6 ± 1.3 ka, 48.5 ± 1.9 ka and 38.1 ± 0.7 ka. The havara/palaeosol succession profiled at Pegeia is interpreted as a wedge of fault colluvium. The most recent episode of faulting in the Pegeia region is gravitational in nature, and is influenced by pre-existing NW-SE- to WNW-ESE-striking faults. Sedimentation was almost instantaneous; all three dates from the lower third of the unit are within error of each other. Failure along one of the pre-existing NW-SE- to WNW-ESE-striking faults may have led to the sudden deposition of this unit. The palaeosol horizons at Pegeia may reflect periods of relative tectonic quiescence, or alternatively climatic variations (e.g. interstadial/stadial periods, or pluvial/interpluvial periods).

A chronological framework was established for the havara/palaeosol succession at Souskiou: in which the lower palaeosol horizon is dated at 12.0 ± 1.6 ka; the next at 6.53 ± 0.3 ka; the next at 3.8 ± 0.4 ka; and the upper palaeosol horizon at 1.9 ± 1.4 ka. The OSL ages indicate that the succession was deposited in the present interstadial (i.e. oxygen isotope stage 1). Sedimentation rates were calculated based on the depth of burial and age of each unit: an average sedimentation rate throughout the profile was calculated at 0.51 mm/yr; with individual rates of 1.47 mm/yr, 0.55 mm/yr, 0.50 mm/yr and 0.17 mm/yr. The sedimentation rates calculated at Souskiou are similar to those observed elsewhere, e.g. at Kalavasos, rates of 0.11mm/yr and 0.25 mm/yr were obtained. Leigh and Webb (2006) calculated average

sedimentation rates at Raven's Fork, Southern Blue Ridge Mountains, USA, on footslopes, toeslopes, between 0.3 and 11 mm/yr and alluvial/colluvial fans, between 2.0 and 2.7 mm/yr.

On the basis of these observations it is possible to distinguish between havara/palaeosol sequences in which the dominant control is climatic variation, or tectonic movements.

5.9 Conclusions

5.9.1 The Neolithic settlement of Mylouthkia-Kissonerga

Traces of some of the earliest successful human colonists on Cyprus can be dated to the late 10th millennium BP at Mylouthkia, in the southwest corner of the island. The OSL results contribute to an expanding catalogue of data on the Early Aceramic Neolithic occupation of Cyprus. This aids in understanding the processes of island colonisation, and the role of Cyprus in the Eastern Neolithic. The new evidence indicates that the Neolithic was introduced to Cyprus in the 10^{th} millennium BP, this is over a millennium earlier than is often assumed in studies of Mediterranean island colonisations (Peltenburg et al., 2003).

5.9.2 Late Pleistocene – Holocene tectonic processes

Early – late Pleistocene deformation events in south and south-central Cyprus are constrained by the luminescence study: transpressional lineaments originated in the late middle Pleistocene (i.e. Kolossi: 174.1 ± 20.9 – 76.6 ± 16.4 ka), and are still active today (Cape Kiti: 38.1 ± 13.2 ka – present); a compressional lineament (i.e. Agia Marinouda Fold) originated in the early middle Pleistocene at 76.8 ± 31.6 ka, and is still actively growing today. At surface level in localised areas extension continues: i.e. middle Pleistocene extension is observed at Amargeti (at c. 40 ± 2.1 ka), Pegeia (at c. 45 ka) and Kalavasos (post-78.3 ± 5.3 ka – pre-10.4 ± 2.2 ka).

5.9.3 Late Pleistocene – Holocene depositional processes and rates

If one has a detailed knowledge of the site/sample context and location, it is possible to determine the dominant control on havara/palaeosol cyclicity.

At Kalavasos Márkou and Vasilikós the deposition of havara and palaeosol interbeds were controlled by fluctuations in climate; havara horizons correlate with stadial phases of the Würmian glaciation and palaeosol horizons with interstadial phases. The Souskiou havara/palaeosol succession was also influenced by fluctuations in climate; havara horizons correlate with pluvial periods, palaeosols with interpluvail periods. In contrast at the sampled site at Pegeia, the thick (and rapidly deposited) successions of colluvium were probably controlled by faulting, i.e. a tectonic control.

Chapter 6: An integrated sedimentological and magnetostratigraphic study of the Pissouri Basin: constraints on the uplift of Cyprus.

6.1 Introduction

The Pissouri Basin (32º42'E, 34º40'N) is a discrete NNW-SSE-trending extensional basin, located in southwestern Cyprus. It is one of several Neogene extensional basins, e.g. Polemi, Pissouri and Maroni-Psematismenos (Figure 6-1), which formed during the Burdigalian to middle Miocene phase of palaeogeographic reorganisation related to the onset of subduction (Payne and Robertson, 1995; 2000) and/or transpression/continental collision to the south (Harrison et al., 2004a; Calon et al., 2005a,b).

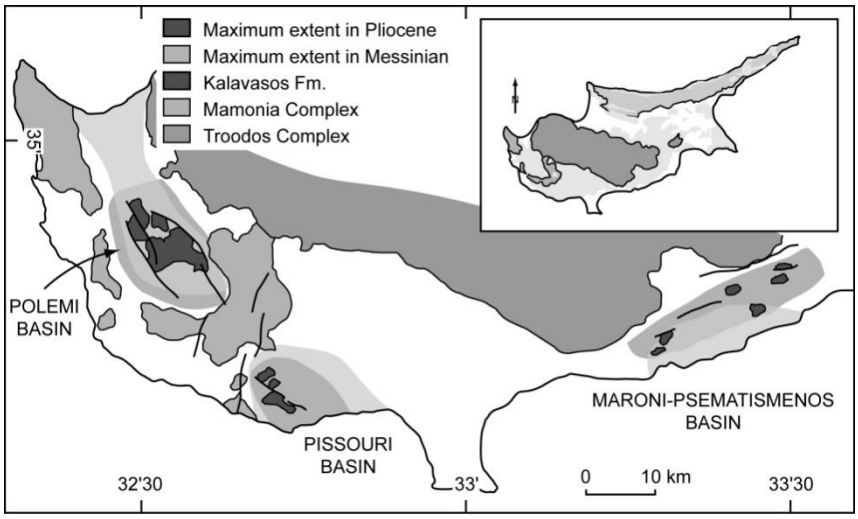

Figure 6-1: Messinian extensional basins located in south Cyprus. The maximum extent of the Messinian and Pliocene basins are shown, with the approximate locations of evaporate deposits exposed at present. Modified from Orszag-Sperber et al. (1989)

In this chapter an integrated sedimentological, structural and magnetostratigraphic study will be used to determine the Late Pliocene to Recent uplift history of the Troodos Massif. Plio-Quaternary marine to non-marine sediments in the Pissouri Basin provide an excellent record of subsidence and uplift. This study was additionally undertaken to review the Paleocene to Recent circum-Troodos sedimentary succession; the Pissouri Basin was identified as a favourable area to study as the entire circum-Troodos sedimentary succession is exposed there. Furthermore, several type-localities of the circum-Troodos sedimentary succession are located here.

In the concluding sections of this chapter a tectono-sedimentary model is proposed to explain the Miocene – Recent evolution of the basin. This has important implications for understanding the Neogene geological evolution of Cyprus and the Eastern Mediterranean region as a whole.

6.2 Basin Analysis

The Pissouri Basin encompasses an area of 23km east-west by 12km north-south, centred on Pissouri village. Its boundaries are marked by a transition from relatively uniform pelagic carbonate deposition (i.e. Lefkara sediments; Robertson, 1976; Kähler and Stow, 1998) to varied carbonate and clastic sedimentation (i.e. Pakhna sediments; Eaton and Robertson, 1993; Follows, 1992). Mio-Pleistocene units comprise the basin infill.

6.2.1 Lithostratigraphic units

Detailed mapping of the Pissouri Basin and the adjacent region has led to the recognition of several lithostratigraphic units, which are sub-divided into facies associations (Figure 6-2). A composite stratigraphic log is presented in Figure 6-3. Each lithostratigraphic package has a variable thickness, which reflects: (i) lateral and vertical variations in the depositional architecture, (ii) syn- and post- depositional faulting and (iii) erosion. The Aquitanian to Recent units overlie and are juxtaposed against the Mamonia Complex (Dhiarizos Group: see Chapter 2, section 2.2.2) in the west of the basin at Petra Tou Rominou.

Figure 6-2: Geological map of the Pissouri area, illustrating the distribution of lithostratigraphic units discussed in the text. Key to lithostratigraphic units shown on the composite log (Figure 6-3). Black lines denote roads. Thick black lines denote normal faults (downthrown side marked). Stars denote palaeomagnetic sampling sites (see section 6.3). Borehole data supplied by the Cyprus Geological Survey Department. Grid spacing is 1 kilometre.

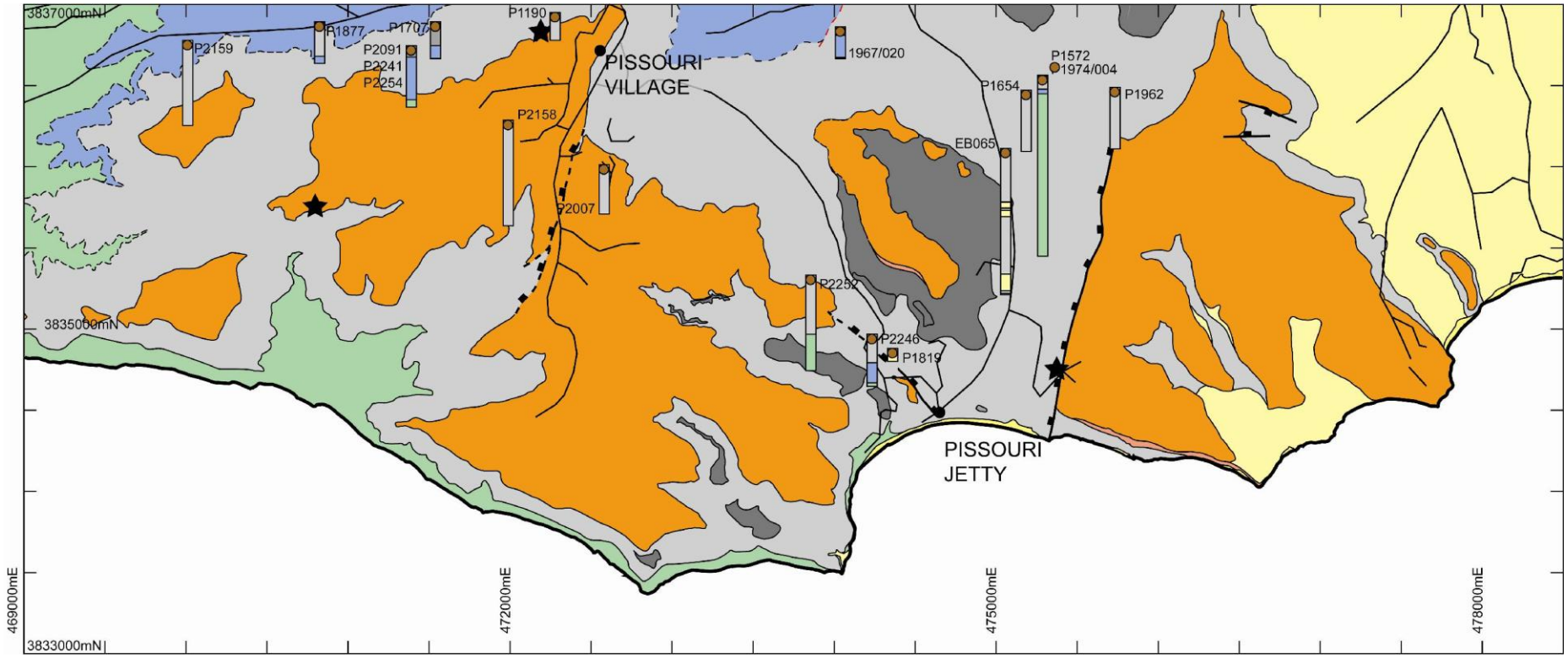

Figure 6-2: Geological map of the Pissouri area, illustrating the distribution of lithostratigraphic units discussed in the text. Key to lithostratigraphic units shown on the composite log (Figure 6-3). Black lines denote roads. Thick black lines denote normal faults (downthrown side marked). Stars denote palaeomagnetic sampling sites (see section 6.3). Borehole data supplied by the Cyprus Geological Survey Department. Grid spacing is 1 kilometre.

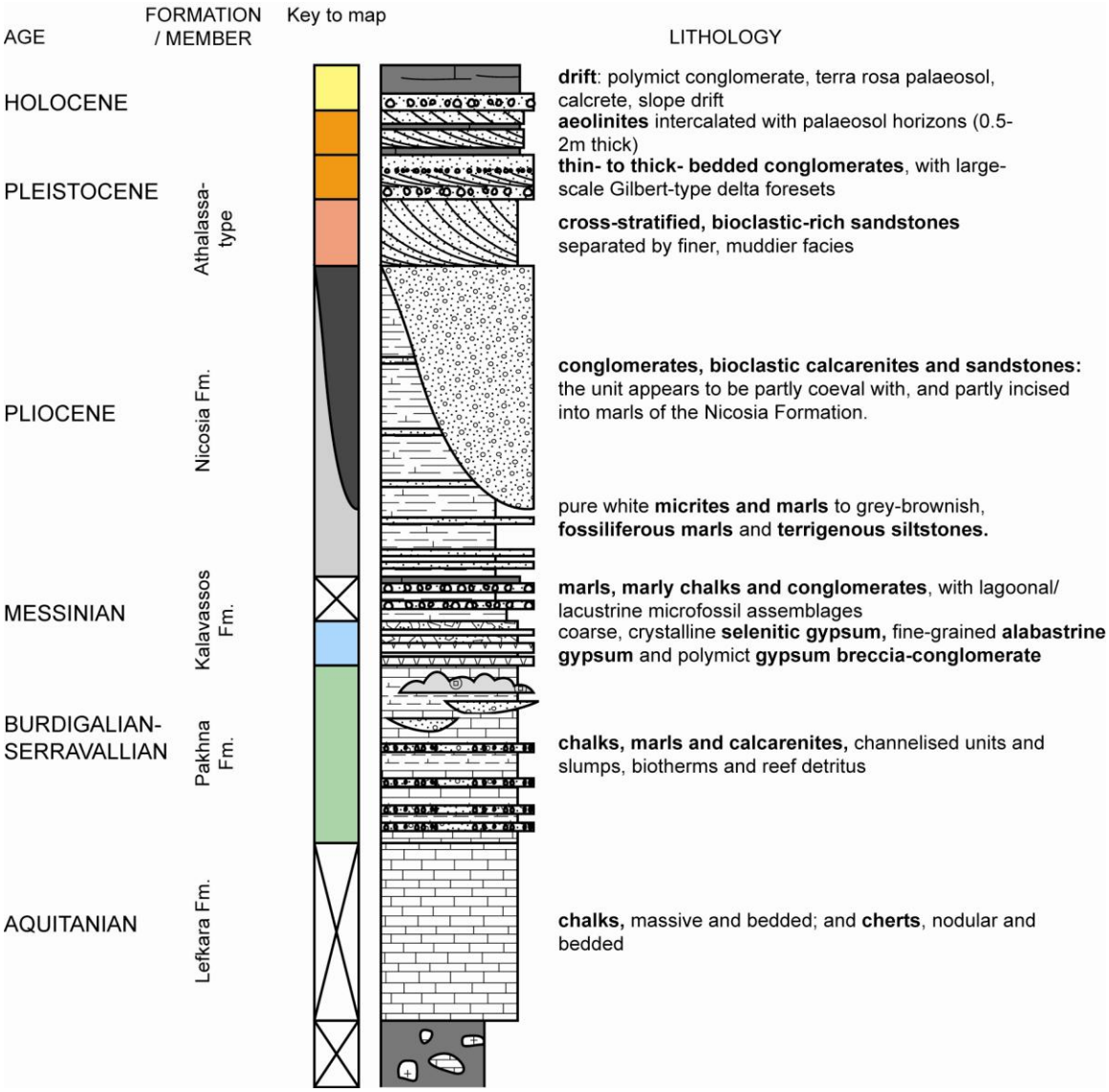

Figure 6-3: Lithostratigraphic units in the Pissouri Basin (modified from Stow et al. (1995))

The Mamonia Complex is overlain by the Lefkara Formation, an assemblage of white micritic limestones, interbedded with siliceous micrites and cherts. The transition between the Lefkara and Pakhna Formation is marked by a large influx of terrigenous material into the basin (see Figure 6-4). The Pakhna Formation is overlain by a marine to non-marine sedimentary succession, comprising evaporites, lagoonal and lacustrine deposits (Kalavasos Formation), deep-water marls (Nicosia Formation), Gilbert-type fan deltas and aeolinites/soils. Each of the lithostratigraphic packages will be described in terms of facies associations, and then interpreted in terms of their sedimentary environment and depositional processes.

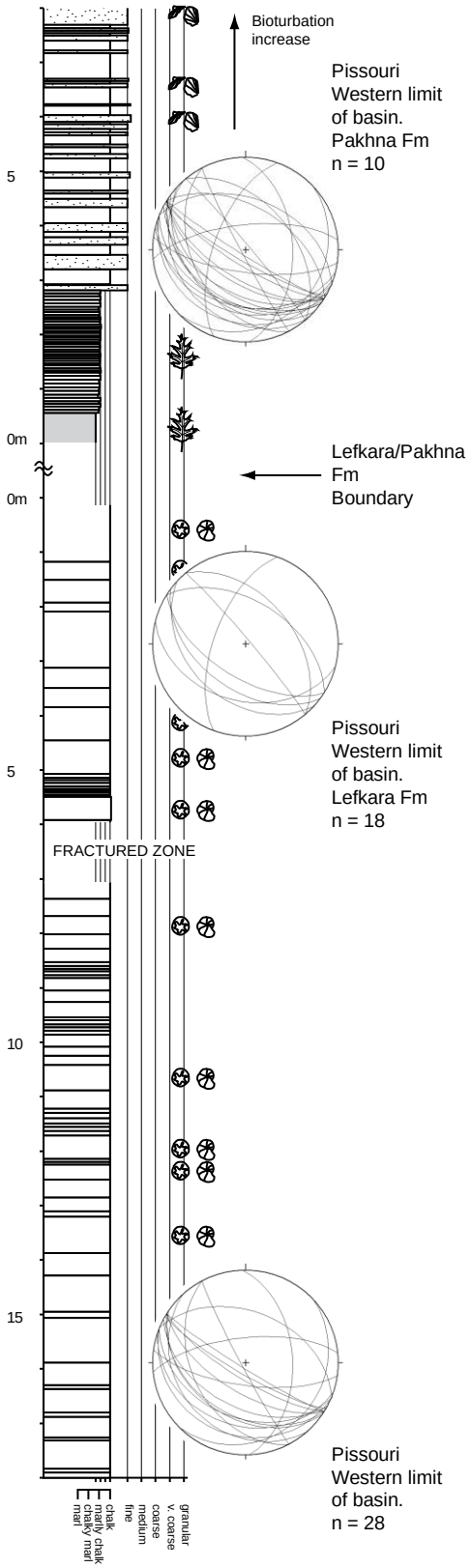

Figure 6-4: Sedimentary log through the contact between the Paleocene Lefkara and the Miocene Pakhna Formations. Fault data obtained along the section is shown in the stereographic plots; the fault data is presented as great circle trends on lower hemisphere plots. Key to sedimentary logs shown in Appendix A.

6.2.1.1 Facies association 1: shallow-water carbonates

Miocene chalks, marls and calcarenites of the Pakhna Formation were divided into four subordinate facies associations by Eaton and Robertson (1993), based on a study of the Lemesos area (Figure 1-4; Figure 6-5): PA1, basin-plain; PA2, basin-margin; PA3, gullied slope; and PA4, peripheral sands. A fifth facies association, PA5, is proposed here, a gradational unit with the overlying Messinian gypsiferous deposits (see facies association 2, section 6.2.1.2). Facies associations PA1, PA2, PA3 and PA5 are present in the Pissouri Basin, facies association PA4 is absent. PA1 and PA2 interfinger and are interbedded, with each other along the northern margin of the basin. PA1 and PA2 pass laterally to the east-northeast into PA3.

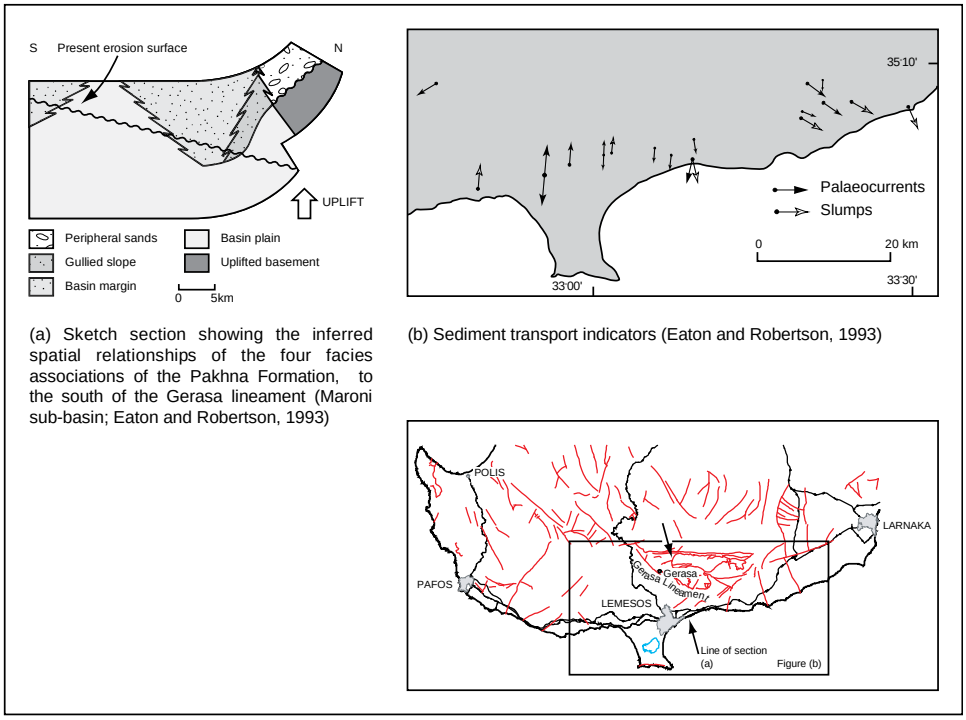

(a) Sketch section showing the inferred spatial relationships of the four facies associations of the Pakhna Formation, to the south of the Gerasa lineament (Maroni sub-basin; Eaton and Robertson, 1993)

(b) Sediment transport indicators (Eaton and Robertson, 1993)

Figure 6-5: (a) Sketch section showing the inferred spatial relationships of the four facies associations, to the south of the Gerasa lineament (Maroni-Psematismenos sub-basin; Eaton and Robertson, 1993). Note the shallowing-upward sequence and presence of margin facies, both to the north and south. Not to scale; (b) Sediment transport indicators (Eaton and Robertson, 1993)

PA1: Basin-plain

Description: The basin-plain association is comprised dominantly of planktonic foraminiferal, nannofossil chalk and marl, and less frequently bioturbated globigerinid mudstone, fine-grained terrigenous claystone and mudstone (Eaton and Robertson, 1993). Bioturbation is extensive, mainly of *Zoophycos*, *Chrondrites* and *Planolites* type.

Macrofossils are restricted to thin-shelled epipelagic bivalves, echinoids and rare fish teeth. Burrow fills contain a high proportion of globigerinid tests, commonly as grain-supported foraminiferal sands (Eaton and Robertson, 1993).

Interpretation: Eaton and Robertson (1993) envisage that facies association PA1 accumulated in an open marine, outer shelf to bathyal setting, with only minor fine-grained detrital input. *Zoophycos*, *Chrondrites* and *Planolites*-type bioturbation are indicative of deep-water deposition.

PA2: Basin-margin

Description: The basin-margin association is characterised by clastic packages of sporadic medium- to thin-bedded, graded fine-grained calcarenites, interbedded with bioturbated chalks and marls (Eaton and Robertson, 1993). Thin-bedded calcarenites occur as laterally extensive, 2-10 cm thick, parallel beds. Beds are graded, with sharp bases and intraclastic lags. The bed-tops are comprised of marl, and are commonly bioturbated. Medium-bedded (10-50cm thick) calcarenites are pebbly at the base and fine upward to coarse, medium or fine grain sizes. Eaton and Robertson (1993) identified flute casts, groove casts, parallel and low-angle cross-lamination and load and flame structures.

Interpretation: The calcarenitic facies of the basin-margin association is believed to be deposited from sheet-flow turbidity currents. Eaton and Robertson (1993) believe this to reflect basinal transport from line sources in areas where only limited uplift took place, i.e. erosional gullies did not develop. Background sedimentation is recorded in the chalk and marl facies.

PA3: Gullied-slope

Description: The gullied slope/channel-fill association consists of bioturbated foraminiferal chalks, silty marlstones and laminated calcarenites channelled into by polymict conglomerates, massive calcarenites, and minor thin marlstones (Eaton and Robertson, 1993; Figure 6-6; Figure 6-7; Figure 6-8). This unit laterally interfingers with the fine-grained facies of the basin-plain association. Two subfacies are recognised with the conglomerates based on bedding geometries, clast composition and clast abundance (Eaton and Robertson, 1993): subfacies (i) is comprised of predominantly clast-supported conglomerates, occurring within channelised bodies, or laterally extensive sheets. Clasts are, in general, well-rounded, < 15 mm in diameter, and composed of carbonate or Troodos lithologies; subfacies (ii) is

composed of predominantly matrix-supported conglomerates, confined to channel-fill sequences, cut into the background marls and chalks. Clasts are usually of the same composition as the local substrate. In general, channels within the Pissouri Basin are aligned N-S/NW-SE. Channel deposits, 2-5 m thick, are locally exposed in road sections along the Paphos-Lemesos highway. Channel widths are in the order of 1 – 5 m.

Figure 6-6: Calcarenitic facies in the Pakhna Formation, with mm-sized clasts of sub-angular to rounded Troodos-derived material, hammer for scale

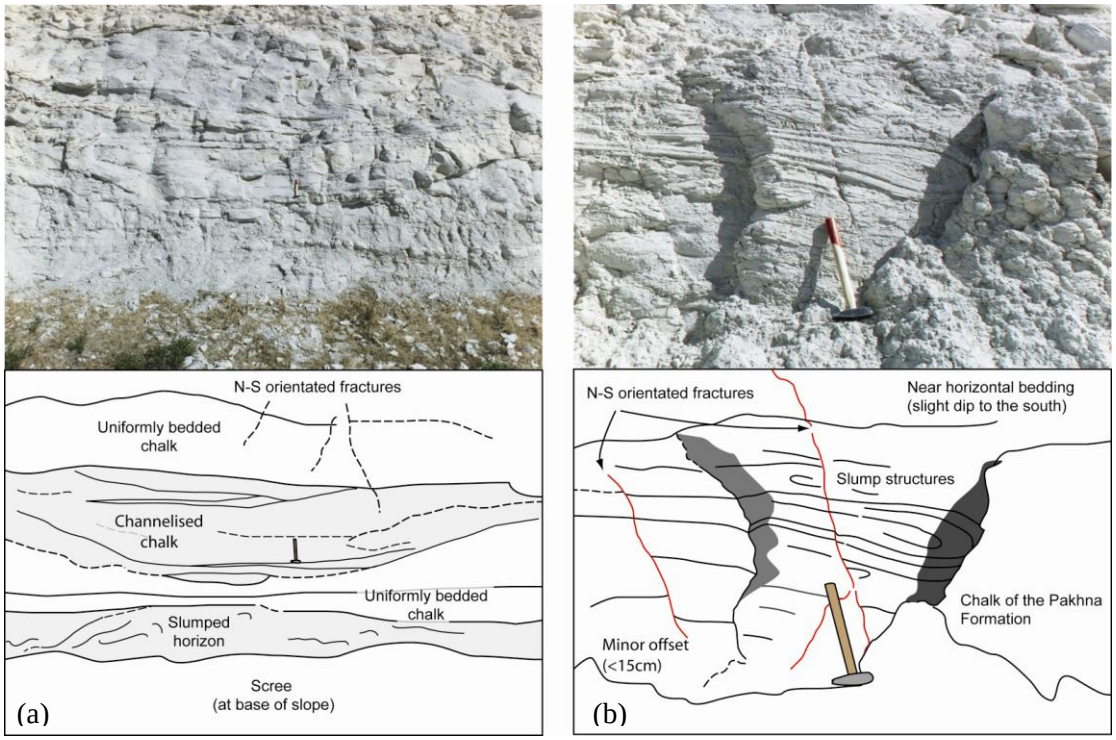

Figure 6-7: Syn-depositional (a) channelling and (b) slumping in the uppermost Pakhna Formation. Hammer for scale.

Figure 6-8: Channelised chalk of the Pakhna Formation with low-angle cross-lamination. Hammer for scale

The uppermost part of the Pakhna succession at Pissouri includes a 3.5 metre-thick slumped interval, characterised by large contorted fragments of laminated marls and carbonates. In the south of the basin this unit grades laterally into a chaotic accumulation of reef limestone blocks mixed with fragments of marls, diatomites and homogenous carbonates. This slump does not significantly deform the underlying deposits of chalk and marl. Syn-depositional slumps are comprised of overturned and recumbent folds above décollement surfaces. Asymmetrical fault-inception folds occur within multilayer deformed horizons, 1 - 4 m thick, sandwiched between un-deformed layers. Orientations of the slump folds were measured, and show a mean direction to the south. These deformation structures involved brittle deformation (faults, brecciation and décollement surfaces) and ductile deformation (recumbent and overturned folds).

Interpretation: The fine-grained facies of the gullied slope association accumulated on a sediment starved slope and are identified as heimipelagic (Eaton and Robertson, 1993). Sedimentation rates were relatively low; Eaton (1987) estimates a value of 0.001 cm/yr. An influx of terrigenous material (Figure 6-6) in the uppermost horizons of the Pakhna Formation indicates that the Troodos Massif was locally emergent (around the rim of the newly formed Pissouri Basin).

Syn-depositional channels and slumps in the Pissouri Basin are aligned (N-S/NW-SE) perpendicular to the inferred directions of Miocene extension (E-W/NE-SW) (see 6.2.2). A

channelised/slumped chalk body at Sotira Lemesou, in the east of the Pissouri Basin was dated using tetrapod assemblages: a Late Miocene (Serravallian to Tortonian) age of deposition was inferred due to the presence of *Vaginella acutissima* (Langhian to Serravallian) and *Diarria sangiorgii* (Tortonian to Messinian) (Cyprus Geological Survey Department, personal communication). During the Miocene the regional palaeo-slope trended generally southwards, towards the deeper sea, as evidenced by syn-depositional channelling (Figure 6-7a; Figure 6-8) and slumping (Figure 6-7b). The different slump morphologies and geometries may be explained by varying sediment behaviours, related to different pre-deformation conditions, e.g. (i) different degrees of lithification, (ii) different porosity and water contents, or (iii) different composition and/or variations in organic matter content (Spalluto et al., 2007).

PA5: restricted basin

Description: A sedimentary log of the uppermost 50 m of the Pakhna Formation is shown in Figure 6-9. This section is correlated against the magnetostratigraphy established by Krijgsman et al. (2002) in Figure 6-10. The transitional interval between carbonates and evaporates is known informally as the 'barre jaune' in the Pissouri Basin (Krijgsman et al., 2002). The section exhibits several different lithostratigraphic intervals. The pre-gypsiferous interval comprises graded, medium- to thin- bedded calcarenites, interbedded with chalks and marls, and pure, indurated, medium-bedded, white chalks. The gypsiferous interval additionally contains intercalations of centi- to deci- metre-thick horizons of reddish gypsiferous sands and dark organic-rich clay (the sapropels of Krijgsman et al. (2002)). Secondary growths of coarse gypsum crystals occur parallel to- and cross-cutting (along fractures) bedding/laminations within the Pakhna Formation. Krijgsman et al. (2002) identified abundant sponge spicules and varying amounts of diatoms, silicoflagellates and radiolaria. The top of the Pakhna Formation is marked by a band of white weathered chalk, containing abundant Discospirina foraminifers (Wade and Brown, 2005). Beneath this a prominent marker-horizon of cyclically bedded marine sediments comprised of diatomites, marls and carbonates, with thin (<1cm) lenses of gypsum (Krijgsman et al., 2002). The 'barre jaune' interval contains indurated and finely laminated limestones which show features characteristic of microbial deposits (stromatolites). High-resolution astrochronology has revealed that evaporitic deposition in the Pissouri Basin, southern Cyprus began at 5.96 ± 0.02Ma (Figure 6-10; Krijgsman et al., 2002).

Interpretation: An important palaeo-environmental change occurs at the top of the Pakhna Formation, between the lower part (i.e. the pre-gypsiferous interval) comprised of indurated marine marls, and chalk and the upper part (i.e. the gypsiferous interval) comprised of laminated sapropelitic and diatomaceous sediments. Palaeobathymetric analyses (Krijgsman et al., 2002; Kouwenhoven et al., 2006) indicate that shallowing of the Pissouri basin was minor or absent until the 'barre jaune'. Kouwenhoven et al. (2006) estimate a palaeodepth of ~300-500m. Kouwenhoven et al. (2006) identify a prominent change in palaeoenvironmental conditions at ~6.73 Ma in the Pissouri Basin: from open-marine, deep water taxa to more restricted, shallow water taxa. In addition, Kouwenhoven et al. (2006) identify a dominance of oligotypic and monospecific assemblages and frequent shifts in assemblage compositions after ~6.4 Ma, which indicate a severely stressed environment, probably related to increased salinity. Astronomical tuning of the succession indicates that the first gypsum bed was deposited at 5.96 ± 0.02 Ma, and overlies a 40 – 60 ka stromalite-bearing interval (Krijgsman et al., 2002). Thus, the restricted basin association reflects the final shallowing of the Pissouri Basin, prior to the onset of the Messinian salinity crisis.

Summary: The Pakhna Formation succession represents hemipelagic slope sedimentation within and around the shallowing Pissouri Basin, punctuated by influxes of turbidity currents, storm-reworked shell debris and mass wasting from reef talus slopes. An influx of terrigenous material (Figure 6-6) in the uppermost horizons of the Pakhna Formation indicates that the Troodos Massif was locally emergent around the rim of the newly formed Pissouri Basin.

Diatomaceous marls and microbial carbonates of the Pakhna Formation (Krijgsman et al., 2002; Wade and Brown, 2005) are overlain by the Kalavasos Formation, composed of a variety of gypsum facies (facies association 2: Robertson et al., 1995b) and/or lagoonal to lacustrine deposits and local palaeosols (facies association 3: the 'Lago Mare sequence of the Kalavasos Formation': Orszag-Sperber et al., 1989; Rouchy et al., 2001)

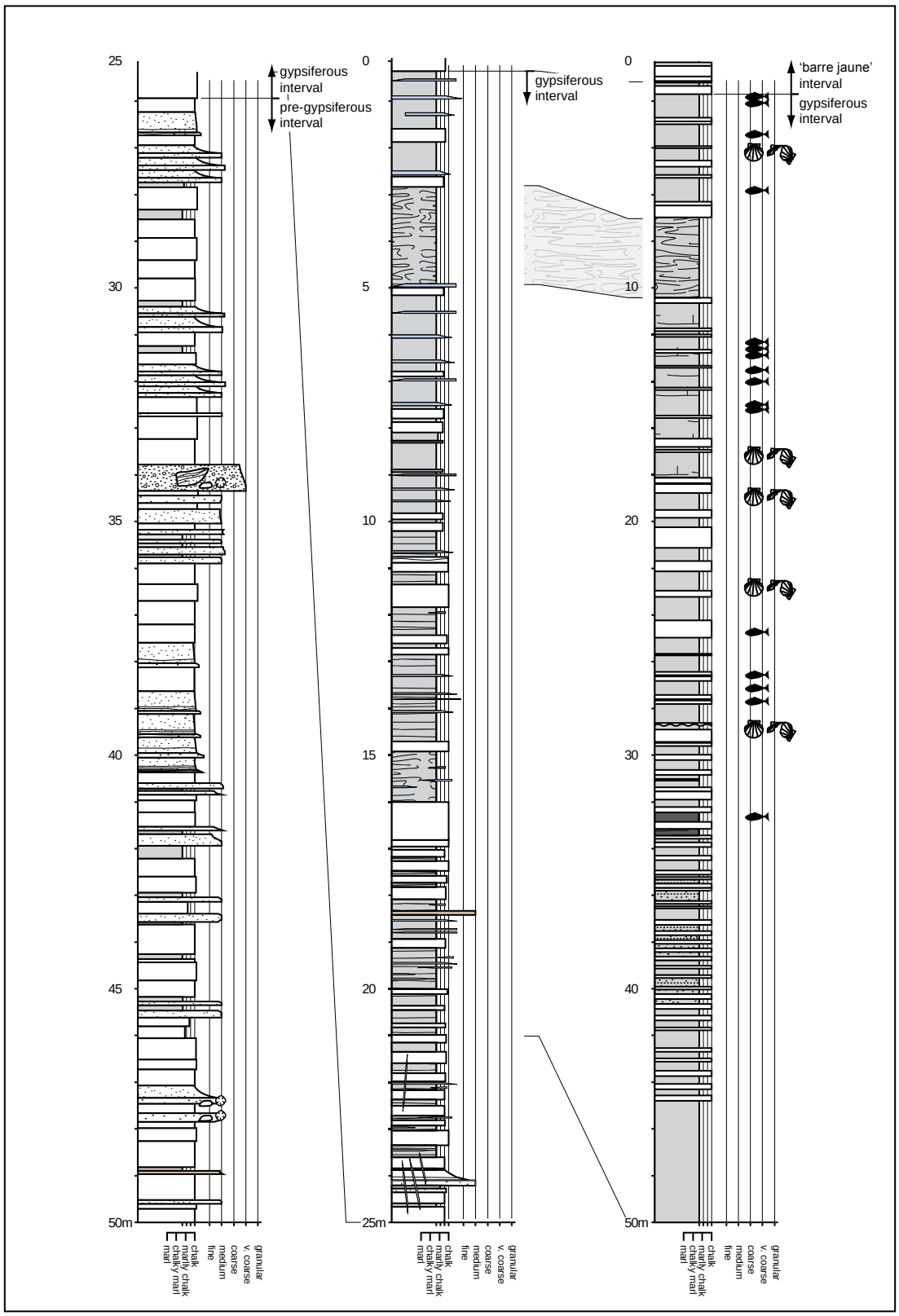

Figure 6-9: Sedimentary log through the uppermost 50 m of the Pakhna Formation; illustrating the three different stratigraphic intervals discussed in the text. The log is shown correlated with the log of Krijgsman et al. (2002). The key to the log is shown in Appendix A

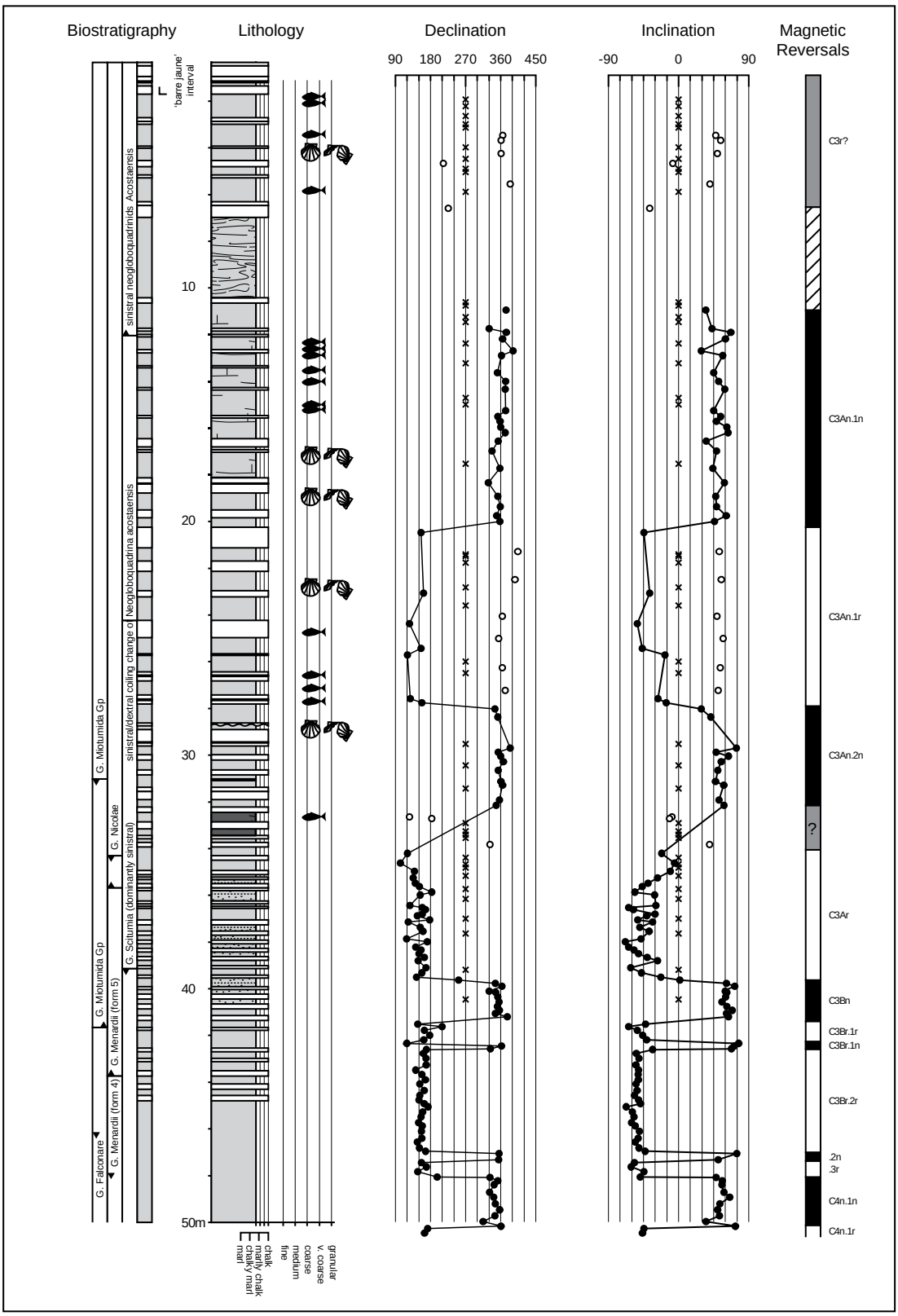

Figure 6-10: Magnetostratigraphy of the uppermost 50 m of the Pakhna Formation (Krijgsman, 2002). The key to the log is shown in Appendix A

The first column illustrates the biostratigraphy as established by Krijgsman et al. (2002) for the uppermost 25 m of the Pakhna Formation. The second column is a re-production of the sedimentary log as recorded by Krijgsman et al. (2002). The third column indicates the declination as determined

by Krijgsman et al. (2002) for each sampled horizon (a value around 000/360º indicates a normal polarity). The fourth column indicates the inclination as determined by Krijgsman et al. (2002) for each sampled horizon (a value of c. 45º indicates a normal polarity). The fifth column illustrates reversals in the magnetic polarity throughout the succession; black denotes normal polarity, white is reversed and grey indicates intervals of uncertain polarity.

6.2.1.2 Facies association 2: evaporites

A sedimentary log through the lower and middle parts of the evaporate succession at Pissouri is shown in Figure 6-11. A 3-6 m thick polygenic mega-breccia underlies the evaporitic succession. This is overlain by a lower unit of finely laminated gypsum, interbedded with redeposited selenitic gypsum. The lower unit is overlain by a distinctive gypsum mega-breccia. The overlying upper unit comprises intercalations of conglomerates (with well-rounded pebbles), banded stacked gypsum and swallow-tail gypsum.

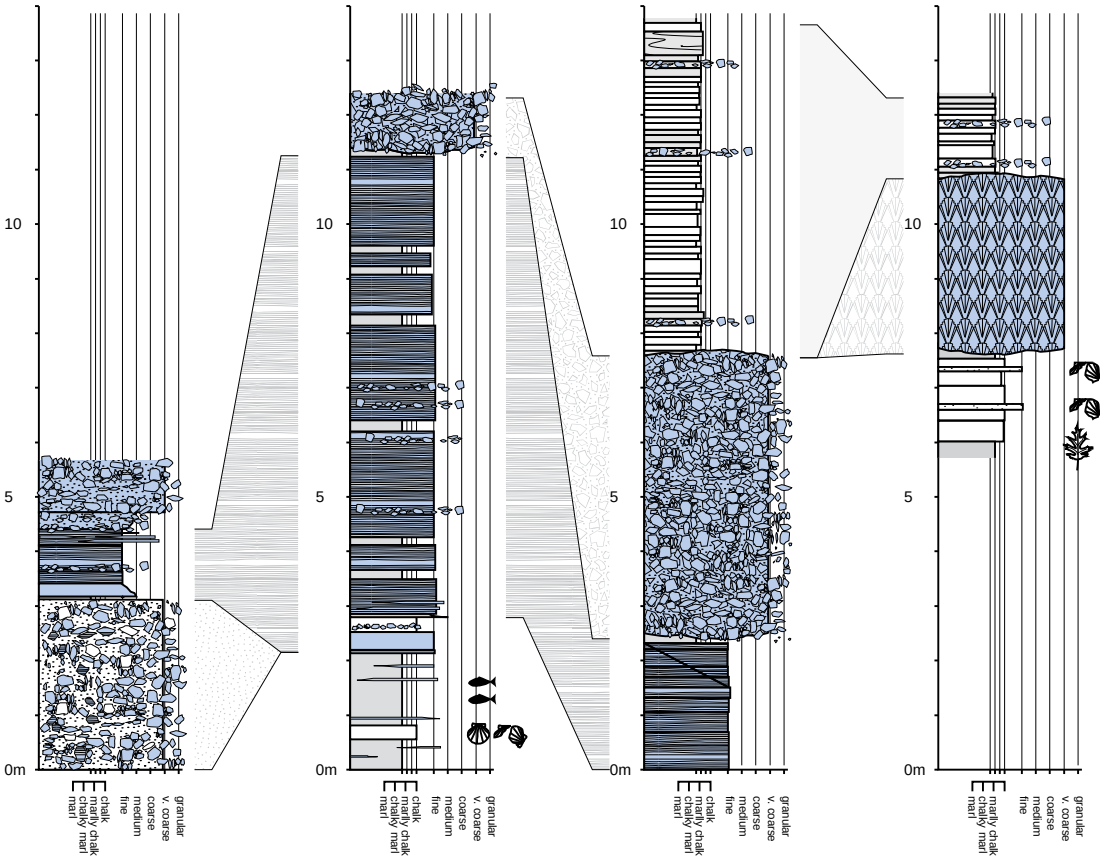

Figure 6-11: Correlated sedimentary logs of the Messinian evaporite succession in the Pissouri Basin. The key to the log is shown in Appendix A

EV1: Basin-plain

Description: The basin-plain association is characterised by parallel-laminated (marmara) gypsum and massive fine-grained (alabaster) gypsum, interbedded with thin beds of reworked, coarse crystalline selenite. Individual fine-grained gypsum partings are either massive, or more commonly, show subtle fine silt to clay-size normal grading. Marmara and alabaster are locally affected by small-scale slumping and soft-sediment normal faulting (on the millimetre- to centimetre scale).

Interpretation: Marmara and alabaster are believed to represent 'background' sedimentation in basinal areas; a product of chemical precipitation in hypersaline waters (Figure 6-12). After precipitation, this fine-grained gypsum was reworked by currents and/or gravity processes, and redeposited in the basin axis. The thin-bedded, graded massive gypsum partings are interpreted as low-density turbidites.

EV2: Basin-margin

Description: The basin-margin association is characterised by banded stacked selenite and swallow-tail selenite. Individual beds are not readily apparent, except where intercalated with alabastrine gypsum, or gypsiferous breccia-conglomerates. Banded-stacked gypsum consists of repeated layers of selenitic gypsum, intercalated with white bands, often composed of clastic gypsum, or carbonates. Individual layers are composed of up-right stubby selenite crystals. Swallow-tail gypsum consists of well-developed, near vertical columns of twinned gypsum (typically 10-100mm in length), forming a herringbone structure of paired selenite laths. The swallow-tails typically occur in aggregates of sub-parallel columns.

Interpretation: Banded-stacked selenite records repeated pulses of selenite growth, in well-aerated, very shallow settings (<3m), interrupted by emersion, erosion and/or reworking of detrital selenite (Robertson et al., 1995b). Selenite swallowtails record periods of undisturbed, subaqueous growth. Swallowtail selenite is, thus, inferred to have formed in slightly deeper water (< 10m) than the banded-stacked selenite, and probably in better protected, more continuously sub-aqueous parts of the lagoon (Robertson et al., 1995b).

EV3: Basin-slope

Desciption: The basin-slope association is comprised of polygenic, gypsum-breccias and normally-graded redeposited selenitic gypsum. A polygenic, gypsum-breccia underlies the

main evaporitic succession. The gypsum-breccia is a chaotic accumulation of cm- to m-scale blocks of calcarenite, selenitic gypsum and diatomites, bound within a calcarenitic matrix (Orszag-Sperber et al., 1989). Two sub-facies are recognised in the redeposited selenitic gypsum (Robertson et al., 2005b). Facies (a) consists of 1.5 m thick beds of angular to sub-rounded fragments of selenite, up to 5cm in size, with reworked marl, chalk and microbial limestones bound in a chalky, gypsiferous matrix. Beds exhibit sharp, scoured bases and gradational tops. Facies (b) consists of thickly bedded (<3 m), laterally discontinous, units of broken, mainly angular fragments of large, clear, or translucent selenite crystals up to 25cm long, bound in a chalky, gypsiferous matrix. This facies is seen to downcut into underlying units. Beds are either massive or show crude normal grading of clasts.

Interpretation: The thickly bedded, graded, detrital selenites are believed to have accumulated as high density turbidities. The more thickly bedded, chaotic assemblages of broken selenite crystals are interpreted as debris flows. The grain-size of the gravity redeposited units is believed to be largely controlled by available source material: low-density turbidites formed largely from re-suspension of fine-grained gypsum; gypsum turbidites were largely derived by break-up of banded-stacked gypsum, while debris-flow units formed by disintegration and downslope gravity transport of gypsum swallowtails (Robertson et al., 1995b). A 3-6 m thick gypsum-breccia underlies the main gypsum breccia at Alektora. This implies the presence of evaporites at the edge of the basin, and gravity reworking, before the onset of the main evaporitic formation.

Summary: The dominant control on the occurrence of evaporites in southern Cyprus (Robertson et al., 1995b) was the repeated desiccation of the Mediterranean during the Messinian Salinity Crisis (Hsü et al., 1973). Gypsum in the Pissouri Basin is interpreted as being entirely sub-aqueous, based on the presence of parallel, fine-grained marmara gypsum and coarse selenitic, banded-stacked and swallowtail, gypsum. The presence of slump units and gypiferous turbidites and debris flows indicates instabilities and re-sedimentation down steep basin margins. The polymict mega-breccia exposed at the base of the sequence, and the distinctive gypsum-breccia in the middle of the section indicates pronounced periods of instability in the Messinian basin.

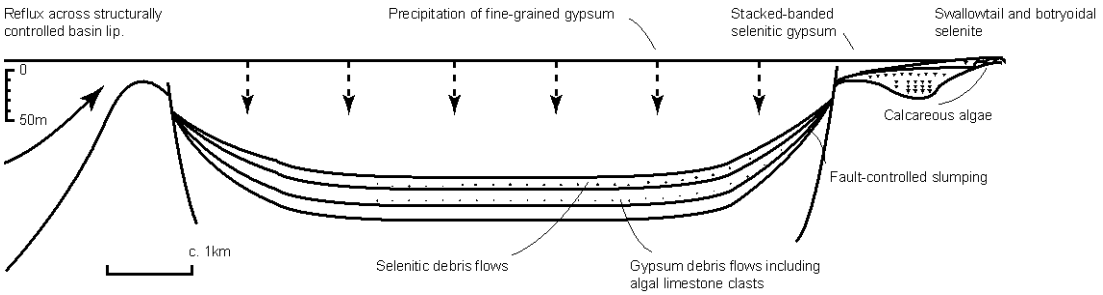

Figure 6-12: Simple facies model showing inferred processes of primary gypsum deposition in Cyprus. Modified from Robertson et al. (1995b)

6.2.1.3 Facies association 3: lagoonal – lacustrine marls and conglomerates

Three subordinate facies associations are recognised: LA1, restricted-basin; LA2, unstable slope; and LA3, emerged basin. Each of the facies associations is observed in the sedimentary logs presented in Figure 6-13. Units common to all three logs are:

i. A lower unit, ~ 2-5 m thick, of marl that contains an assemblage of *Ammonia beccarii tepida* and *Cyprideis pannonica* (Rouchy et al., 2001).
ii. A middle unit, ~ 9-13 m thick, of calcarenites intercalated with conglomerates and marls.
iii. An upper unit, ~ 8-9 m thick, of palaeosols intercalated with conglomerates and calcarenites.

LA1: Restricted-basin

Description: The restricted basin association of the Lago Mare succession is comprised of thin- to medium- bedded marls and silty marls, and medium- to thick- bedded calcarenites. The marls and silty marls contain an assemblage of *Ammonia beccarii tepida* and *Cyprideis pannonica* (Rouchy et al., 2001).

Interpretation: The microfossils identified by Rouchy et al. (2001) are diagnostic of a brackish water environment: the foraminfer *Ammonia beccarrii* is usually found in estuaries and similar settings where there are large variations in salinity; the ostracod assemblage dominated by *Cyprideis* can live at a depth of up to 50 metres and can tolerate high salinities.

LA2: Basin-slope

Description: Thickly-bedded (m-scale) conglomerates and medium- to thickly- bedded (dcm-scale) calcarenites are intercalated with thin horizons of marls. Together, these facies comprise the basin-slope association of the Lago Mare succession. The conglomerates are typically matrix-supported with a variety of sub-angular to rounded limestone clasts, of Lefkara and Pakhna Formation lithologies, (cm – dcm in diameter) set in a medium- to fine-grained calcarenitic matrix. The bases are sharp and commonly highly irregular, indicating loading and scouring, whereas the tops are either sharp or gradational to calcarenites. Some beds contain possible water escape structures. The calcarenites are composed of angular fragments of older carbonate deposits of Lefkara and Pakhna Formations lithologies, which include abundant reworked foraminifers. Orszag-Sperber and Rouchy (1979; in Rouchy et al., 2001) identified a scarce, dwarfed marine microfauna assemblage of *G. mediterranea* and *G. humerosa* in a single horizon of calcarenite. The calcarenite beds typically have sharp or erosive bases, are normally graded and have partial Bouma sequences.

Interpretation: The conglomerates and calcarenites were deposited from debris-flow and debris-flow turbitity currents, respectively; they indicate an input of terrigenous material into the restricted Lago Mare basin.

LA3: Emerged-basin

Description: Decimetre- to metre-thick, dark, marly horizons rich in centimetre-sized clasts of Lefkara and Pakhna Formation chalk are interbedded with conglomerates and calcarenites. Rouchy et al. (2001) identified fragmented bivalve and gastropod shells within one palaeosol horizon (8 m beneath the base of the Nicosia Formation), which could belong to *Dreissena*, *Didacna*, *Melanopsis* and *Melanoides*. Di Stefano et al. (1999) report a Lago-Mare type assemblage of *Ammonia beccarii tepida* and *Cyprideis pannonica* in the palaeosol horizons.

Interpretation: The macrofossils identified by Rouchy et al. (2001) are diagnostic of a freshwater environment: *Driessena* are indicative of clean, well oxygenated low-land rivers and lakes; *Didacna*, *Melanopsis* and *Melanoide* are indicative of freshwater lakes. The palaeosols indicate periods of subaerial exposure (associated with intense weathering of the Troodos Massif, and sedimentary cover). The brown colour of the soil suggests that prolonged subaerial exposure must have occurred.

Summary: The alternation of brackish- and fresh-water conditions, with prolonged periods of subaerial exposure, imply a varied climate, with contrasting wet and arid conditions. Syn-sedimentary instability is thought to be related to contemporaneous faulting at the margins of the basin. Erosion along the basin margin led to downslope re-sedimentation of carbonate conglomerates as debrites, and sand-grade material as turbidites.

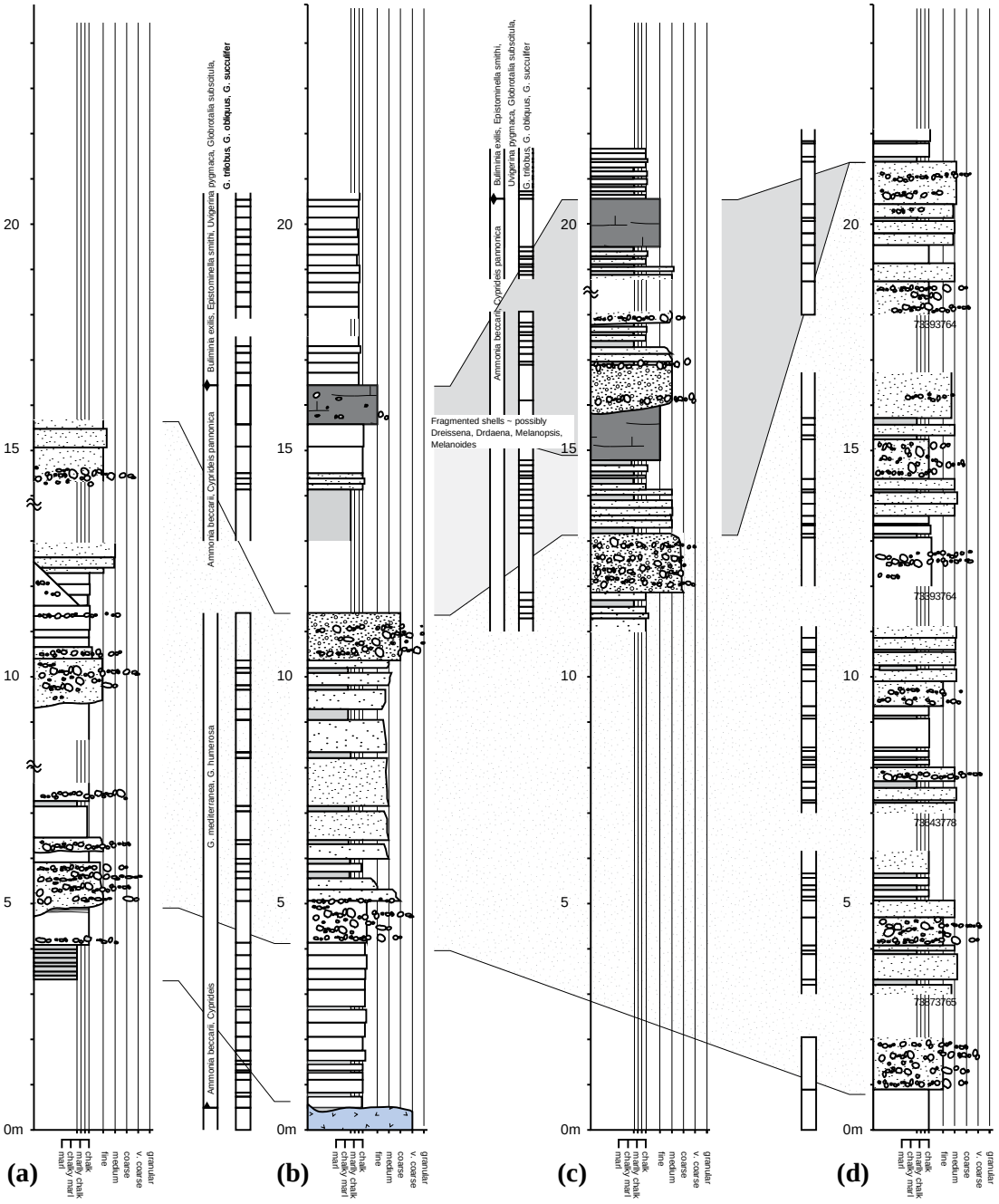

Figure 6-13: Sedimentary logs through the Messinian Lago Mare succession: at (a and b) the western entry of the lower Pissouri village, from several road-cuts on the left-hand side of the Limassol-Paphos road, (c) the motorway access road to Pissouri, and (d) the eastern entry of the lower Pissouri village, from several road-cuts on the left-hand side of the road. The key to the log is shown in Appendix A

6.2.1.4 Facies association 4: shallow-water marls and deltaic calcarenites

The Pliocene Nicosia Formation can be subdivided into several subordinate facies associations: NI1, basin-plain; N12, gullied-slope/channel-fill; and NI3, shallowing-basin. A sedimentological log of the uppermost 20 m of the Nicosia Formation is shown in Figure 6-14.

NI1: Basin-plain

Description: The basin-plain association of the Nicosia Formation is sub-divided into several units. The lower unit is comprised of regularly bedded marls (60-80cm thick) and pure white micrites (10-15cm thick). At the base of this unit (lower 5cm), marls are variably coloured, and contain a high density of planktonic foraminifers of an epipelagic (i.e. a depth of 0-200m) assemblage (*G. trilobus*, *G. obliquus* and *G. sacculifer*, Rouchy et al., 2001). This is associated with, at 14 cm, benthic microfauna dominated by *Buliminia exilis* and *Epistominella smithi* (Rouchy et al., 2001). The presence of the benthic foram, *Uvigerina pygmaea*, and the appearance of the nannoplankton, *G. subscitula*, in the lower layers suggest a bathymetry of less than 300 m (Rouchy et al., 2001). The middle unit is composed of regularly bedded marls (60-80 cm) and siltstone/sandstone beds. It is the first occurrence of very thin siltstone/fine sandstone beds that distinguishes the middle unit from the lower unit; the siltstone/sandstone beds increase in thickness from 5-10 cm up to a maximum of 70-80 cm up section (Figure 6-14a,b). These terrigenous beds typically show sharp planar to erosive bases and are normal graded. Partial Bouma sequences (T_{de}, T_{cde}, T_{bcde}) are recognised. The upper unit is characterised by medium- and thick-bedded (10-100 cm) marl interbedded with siltstones and sandstones in approximately equal proportions (Figure 6-14c). Faint laminations and low-angle laminations are preserved when the beds are not bioturbated. The uppermost layers of the Nicosia Formation are transgressed by Gilbert-type fan delta deposits (facies association GD).

Interpretation: The sediments indicate a return to more stable, deep-water basinal conditions, following the Messinian salinity crisis. The lower unit is interpreted as the product of low-energy pelagic sedimentation. The middle unit represents the influx of terrigenous turbidites derived from an uplifting Troodos Massif in the north, with the increase in thickness and proportion of turbidites reflecting increased uplift and/or tectonic adjustments at the basin margin (Stow et al., 1995). This trend continues into the upper unit, in which the less distinctly turbiditic sands towards the top indicate a general shallowing of the Pissouri Basin.

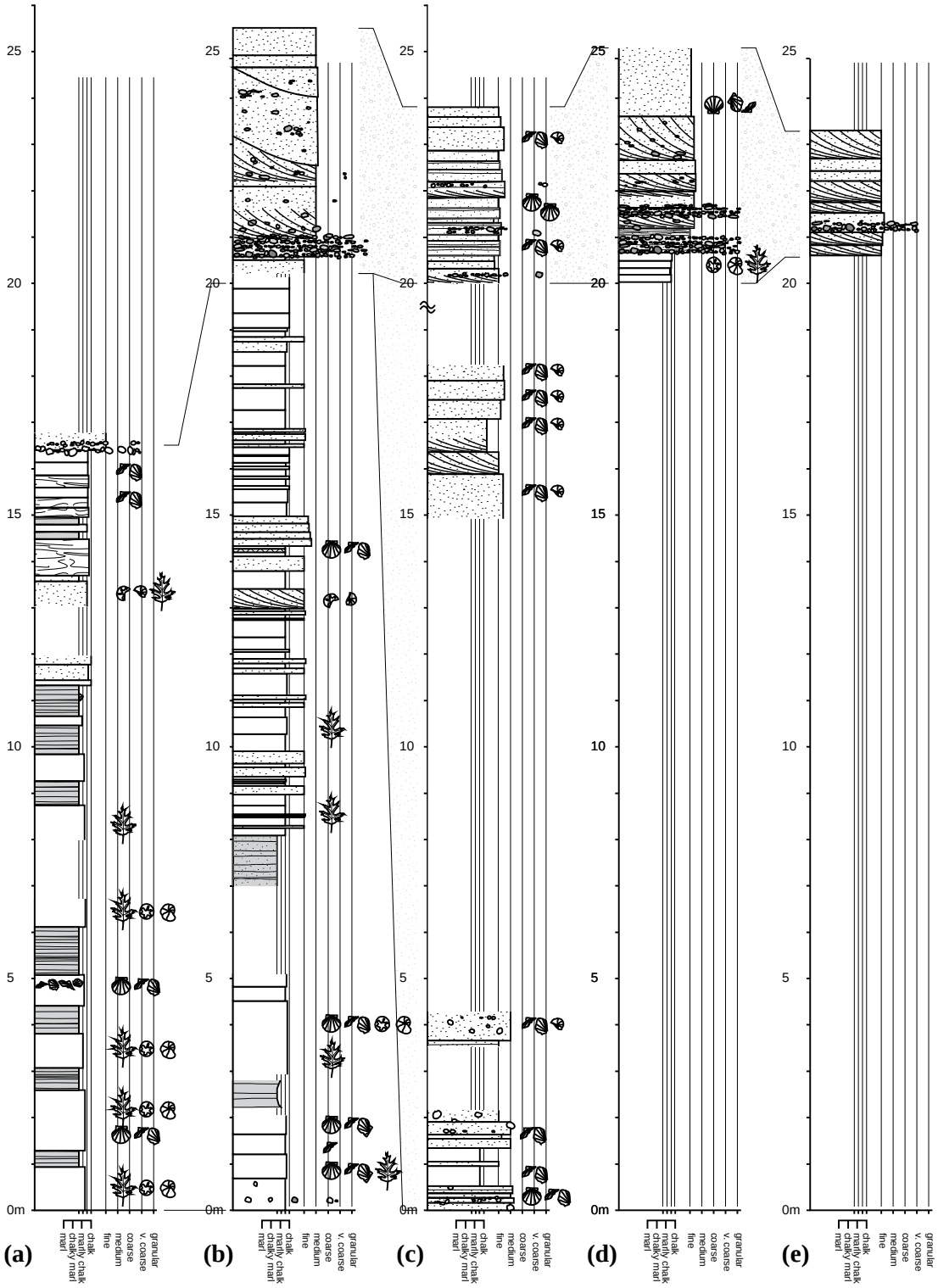

Figure 6-14: Correlated sedimenary logs through the Plio-Pleistocene sequence at Pissouri. Logs (a) and (b) correspond to the uppermost 20 metres of the Pliocene Nicosia Formation, observed at lower Pissouri village and at the western entry to upper Pissouri village, respectively. Log (c) is a stratigraphic section through a sequence of bioclastic sandstones observed at Pissouri Jetty village; a component member of the Nicosia Formation, see discussion in text. Nicosia Formation marls and bioclastic sandstones are transgressed by Gilbert-type fan deltas. Logs (d) and (e) are stratigraphic sections through calcarenites of the Gilbert-style fan deltas collected at Pissouri. The key to the log is shown in Appendix A

NI2: Gullied-slope/channel-infill

Description: A component member of the Nicosia Formation at Pissouri is a highly variable, and laterally discontinuous unit of conglomerates, bioclastic calcarenites and sandstones (Figure 6-14 and Figure 6-15). The gullied-slope/channel-infill association (NI2) appears to be partly coeval with, and partly incised into the basin-plain association (NI1) of the Nicosia Formation. Several facies are recognised within this unit: (i) *Conglomerates*: These are comprised of poorly to moderately sorted, sub-angular to mainly rounded, pebble-cobble conglomerates with occasionally interbeds of pebbly, coarse sandstones. The matrix is typically a muddy, fine- or medium-grained sandstone. The conglomerates occur interbedded with sandstones and siltstones. (ii) *Sandstones and siltstones*: These are comprised of thin (<10 cm), parallel beds of fine- to occasionally medium-grained, planar-stratified sandstones, with interbeds of siltstone. The beds are normally-graded, have 'loaded bases' and flamed tops; occasionally siltstone intraclasts are present. Bedding in both the conglomerates and sandstones is laterally lenticular over tens of metres. (iii) *Bioclastic calcarenites*: These contain thick (c.30-100cm) beds of poorly- to moderately-sorted, coarse-grained pebbly bioclastic sandstones or calcarenites, with crude parallel, sub-parallel and cross-stratification. There is a marked upward change in clast composition from dominantly bioclastic, including reef talus and thick-shelled bivalves, gastropods and scaphopods, to mainly terrigenous, including Troodos-derived igneous material (Stow et al., 1995). Coarse basal pebble lags are associated with shallow scour features. A SSW-directed component of flow is inferred from unidirectional cross-lamination. The bioclastic calcarenites are frequently intercalated with sandstones and siltstones comprised of massive, chalky sandstones and siltstones. Fine, powderly chalk, with little to no terrigenous material forms the matrix. (iv) *Mega-conglomerates*: These are comprised of thick (c.2-10 m) beds of massive, disorganised, matrix-supported, poorly sorted conglomerates, with block-sized clasts of reel limestone, chalk (Pakhna Formation) and marl (Nicosia Formation).

Interpretation: A submarine origin is proposed for facies NI2, due to its lateral equivalence within, and encasement in NI1. Sub-facies (i) to (iii) represent channel-fill. Sub-facies (i) to (iii) occur at a number of discrete levels, restricted to tongue-like bodies, with erosive bases cut down into the ubiquitous 'background' sediments of NI1. Sediment deposition is inferred to have been largely from turbidity currents and mass-flows. The conglomerates and bioclastic standstones are believed to be deposited from a variety of coarse-grained, high-density turbidity currents, by both rapid suspension settling and traction. The matrix-supported conglomerates are interpreted as relatively cohesive mass flows. The massive,

crudely layered, clast-supported conglomerates are interpreted as relatively non-cohesive mass flows. Both mass-flows and high-density currents were thus operative in the cutting and filling of individual submarine channels. Bioclastic detritus is believed to have been derived, from uplifted Pakhna reefal limestones around the rim of the sedimentary basins and from fringing shell-rich banks (Stow et al., 1995).

The sandstones and siltstones within facies (i) are interpreted as the product of rapid deposition from high-density turbidity currents, in this case carrying already sorted sand, perhaps largely shoreline-derived. Minor 'background' sedimentation took place from suspension (silt) and/or deposition from dilute turbidity currents.

Mega-conglomerates (facies iv) are interpreted as chaotic, non-cohesive debris-flow type deposits thar occur at the toes of tongue-like channelised bodies. As in sub-facies (i) to (iii), deposition is believed to be from a variety of coarse-grained, high-density turbidity currents. A triggering mechanism was required to generate these flows, for example, seismic shock. In the Pissouri Jetty section, large detached blocks of marl (Nicosia Formation) are observed in mega-conglomerates; these are believed to represent detached ramps of partly lithified sediment (Figure 6-15).

Figure 6-15 illustrates a possible mechanism to account for the genesis of the Nicosia Formation gullied-slope/channel-fill asscociation. Localised faulting along the northern margin of the Pissouri Basin resulted in a detachment in semi-lithified Pakhna Formation chalk (see inset in Figure 6-15). This detachment was perpendicular to the directions of Pliocene extension (i.e. WNW-ESE in the Pissouri Basin: see chapter 3) but parallel to the present-day coastline. The presence of syn-depositional channelling and slumping in Pliocene strata elsewhere in the Pissouri Basin implies a down-to-the-south palaeoslope. The detached (slumped) block was down-thrown to the south and southeast. Channelised turbidity currents and mass-flows associated with these episodes migrated down-slope, possibly carrying detached blocks of semi-lithified Nicosia marl (see inset in Figure 6-15).

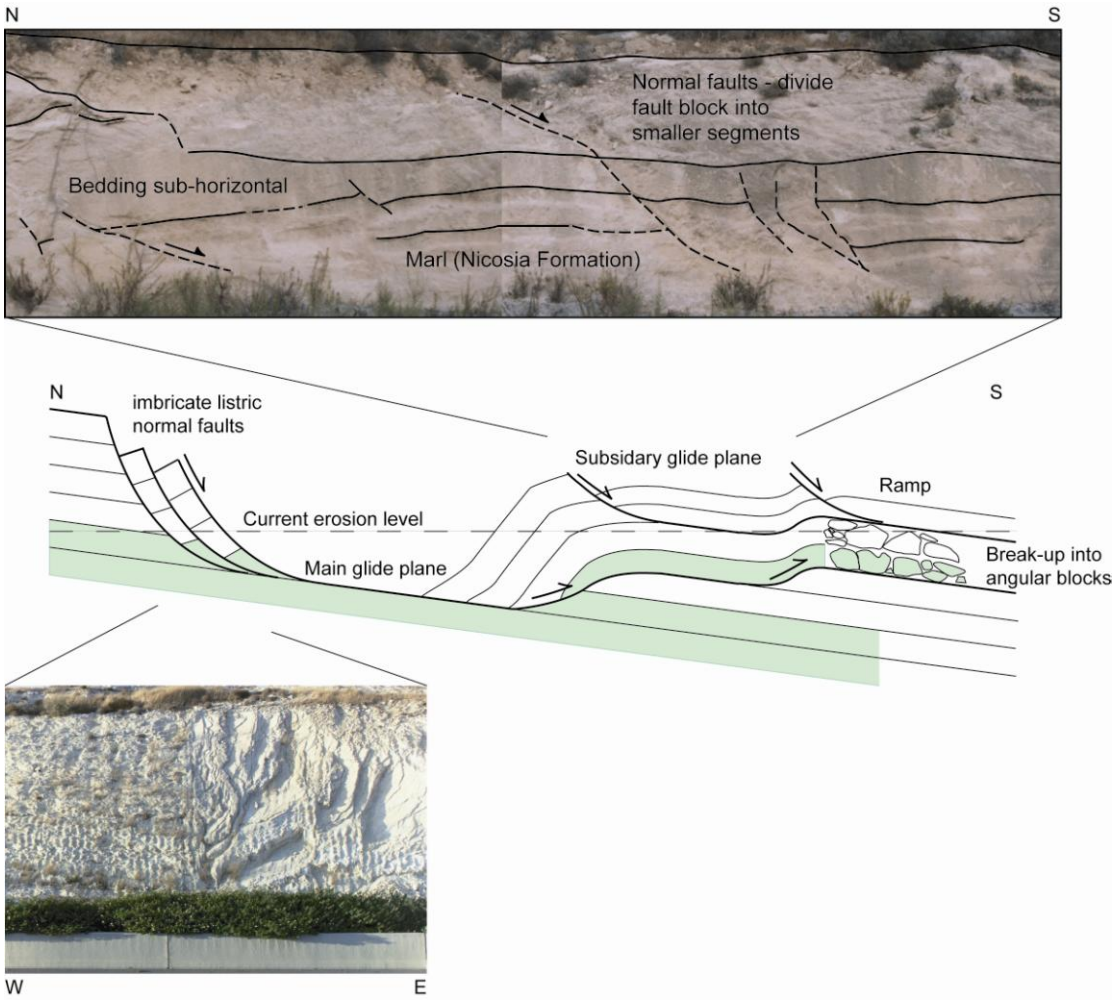

Figure 6-15: Possible mechanism to account for the genesis of the Pissouri Jetty Bioclastic sandstones.

The channels formed distally with respect to the coastal and subaerial parts of a series of small, very coarse-grained deltas. These were fed by alluvial fans located along the northern margin of the Pissouri Basin. These are no longer present, owing to erosion, leaving only the subaqueous toes of the fan deltas. Facies associations (i) to (iii) represent the more proximal units of the Pliocene channels, whereas facies association (iv) represents the more distal unit of the Pliocene channels. Marine influence is greatest to the southeast, as evidenced by rounding of pebbles, bivalve nests and more distinct lamination.

NI3: Shallow-marine, bioclastic sandbodies

Description: A third component member of the Nicosia Formation is a variable, laterally discontinuous unit of shallow-marine, cross-stratified, bioclastic sandstone. Sandstone beds are separated by finer, muddier facies (Figure 6-16). This unit is partly coeval with, as seen in the west, and partly incised into, as seen in the east, the NI1. Bioclastic detritus, including

reef talus and thick-shelled bivalves, gastropods and scaphopods is replaced up sequence by mainly terrigenous material, noteably Troodos-derived igneous material. Several sub-facies are recognised in the Pissouri region: (i) well-bedded, medium-grained, laminated to bioturbated, sandstones with irregular, discontinuous lenses of grits and muddier horizons (in the west); and (ii) medium- to coarse-grained, tabular and trough cross-laminated calcarenites (in the east).

Figure 6-16: Field photograph of cross-stratified, bioclastic rich sandstones of facies association NI3.

Interpretation: It is believed that carbonate sandbodies accumulated along the southern margin of the Troodos Massif in the Middle to Late Pliocene, this material was reworked offshore by storms. Tectonic activity and/or rapid eustatic sea-level change could have been responsible for triggering deposition of the bioclastic sediments.

A similar unit composed of bioclastic sandstones was identified by McCallum and Robertson (1995b) in the Mesaoria Basin. This unit was recognised by the Cyprus Geological Survey Department as a distinct unit, the Athalassa Member. A correlation is proposed between the two lithostratigraphic units.

Summary: Stable, deep-water basinal conditions, in which low-energy pelagic conditions prevailed, were established at the beginning of the Pliocene. In the middle part of the Nicosia Formation, an influx of terrigenous turbidites, derived from an uplifting Troodos source in the north, indicates increased uplift and/or tectonic adjustments at the margin of the basin. This trend continued into the upper parts of the Nicosia Formation, with an increase in the thickness and proportion of turbidites, reflecting the continuing shallowing of the basin, most likely due to tectonic uplift. Bioclastic calcarenitic bodies are incised into the Nicosia Formation. These bodies are believed to represent local channelised units of a fan-delta foreset system that prograded though the Pissouri Basin (Stow et al., 1995).

6.2.1.5 Facies association 5: Gilbert-type fan delta deposits

Nicosia Formation facies associations NI1, NI2 and NI3 are transgressed by a laterally persistent and distinctive upper unit; recognised as a separate facies association, GD, Gilbert-type fan delta deposits.

GD: Gilbert-type fan delta deposits

Description: This facies association is characterised by thin- to thick- bedded conglomerates, which form large-scale Gilbert-type delta foresets. Several sedimentary logs through this unit are shown in Figure 6-14d, Figure 6-14e and Figure 6-17. Stow et al. (1995) recognised several sub-facies within this lithostratigraphic unit: (i) Thick-bedded, fine- to medium-grained, laminated to bioturbated, sandstones; (ii) Fine- to medium-grained sandstones with irregular, discontinuous lenses of grits, pebbly sandstones and conglomerates; (iii) Generally thickly bedded, coarse-grained and pebbly sandstones, with parallel-lamination or trough cross-stratification; (iv) Very thick-bedded, medium- to coarse-grained, sandstones, showing large-scale Gilbert-type delta foresets in units up to 5m thick, commonly with intense bioturbation in the upper part of beds; and (v) Thin- to thick-bedded, poorly sorted, irregularly lenticular, conglomerates, with well-rounded clasts.

Topset strata of several of the Gilbert-type deltas are capped by laterally persistent molluscan shell beds containing diverse assemblages of bivalves, pectens and oysters (Stow et al., 1995).

Interpretation: Sub-facies (i) to (iv) tend to occur in sequence from the base to the top of the unit. Stow et al. (1995) interpreted these as a braided channel topset of a well-supplied fan delta that was feeding the bottomset and foreset facies of the Nicosia Formation associations NI1, NI2 and NI3. This significant sediment influx was principally controlled by intense uplift of the Troodos and its rapid erosion, possibly during the main pluvial periods of the Late Pliocene – early Pleistocene (Stow et al., 1995). Deposition occurred on the coastal plain above, or near sea level. Individual Gilbert delta geometries indicate that the Pissouri system was prograding in a south to south-east direction. The shell beds are interpreted as condensed intervals that record sedimentation during abandonment of the fan delta. The conglomerate sub-facies (v) occurs most commonly as a relatively wide spread basal unit and is thought to be indicative of local erosion and/or a depositional hiatus.

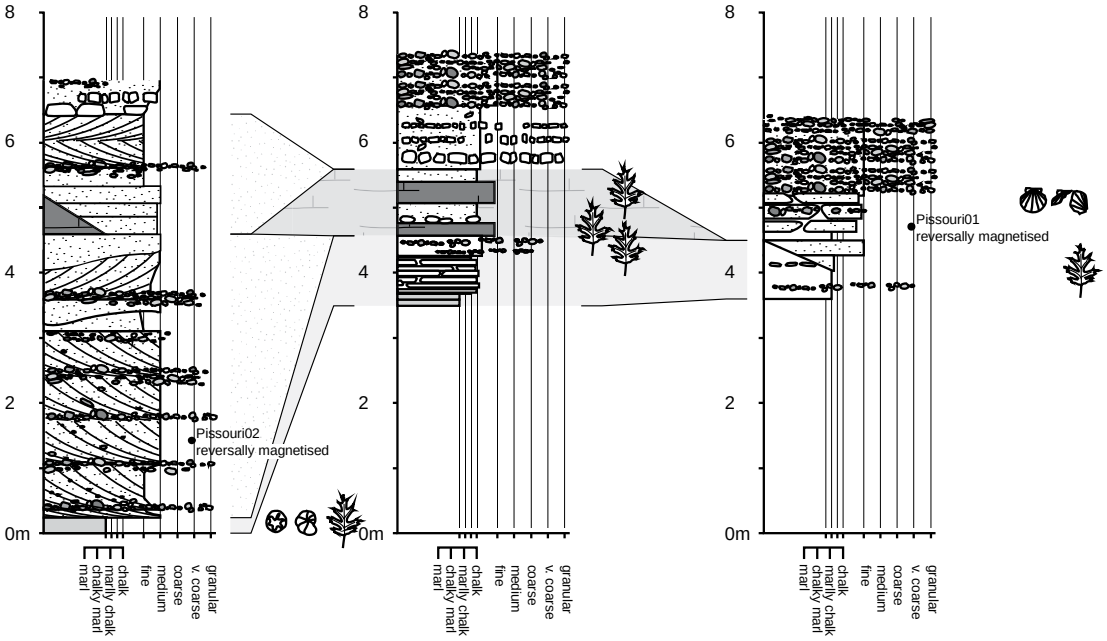

Figure 6-17: Correlated sedimentary logs through the Plio-Pleistocene Gilbert-type fan delta sequence at Pissouri. The key to the log is shown in Appendix A

6.2.1.6 Facies association 6: Recent alluvial fan/drift deposits

Description: Holocene sediments in the Pissouri fan-delta succession are variable in thickness and extent. They include a relatively thin (0.5-1.5m thick), very poorly sorted, moderately well-cemented, polymict conglomerate. The conglomerates are intercalcated with widespread, thick-bedded, red-coloured palaeosols.

Interpretation: The conglomerate is interpreted as an alluvial fan sheet deposit or fanglomerate.

6.2.2 Structural framework

Detailed mapping of the Pissouri Basin and the adjacent region led to the recognition of several fault populations.

6.2.2.1 Faults affecting Tortonian and older strata

Meso-structural information was collected from a number of faults affecting Miocene and Paleocene strata within the Pissouri Basin. Two fault populations are recognised: (i) N000-N020-striking (N-S), W- and E-dipping normal faults; and (ii) N300-N320-striking (NW-SE), SW- and NE-dipping, normal faults (Figure 6-4; Figure 6-18). Fault plane solutions, used as a first approximation of stresses (e.g. Marrett and Allmendinger, 1990) suggest that the stress regime responsible for generating the N-S-striking faults was characterised by broadly east-northeast/west-southwest extension, with a maximum principal stress (216/80°) orientated vertical, and intermediate and minimum principal stresses (350/07° and 051/70°, respectively) orientated sub-horizontal (see chapter 3). Facies analysis of Pakhna Formation carbonates indicates periods of tectonic instability during the Tortonian: (i) channel and slump orientations in the uppermost Pakhna (dated as Serravallian to Tortonian; Geological Survey Department, Cyprus, personal communication) are aligned ~ N-S, perpendicular to the direction of Late Miocene E-W extension. It is believed therefore that Late Miocene faults controlled the spatial distribution of channels; (ii) Koronia-type reefs colonised the faulted margins of the Pissouri Basin in the Tortonian (Follows et al., 1996); and (iii) influxes of Koronia-type reef detritus into the Pissouri Basin, as bioclastic calcarenites, probably reflect tectonic movements at the margins of the basin.

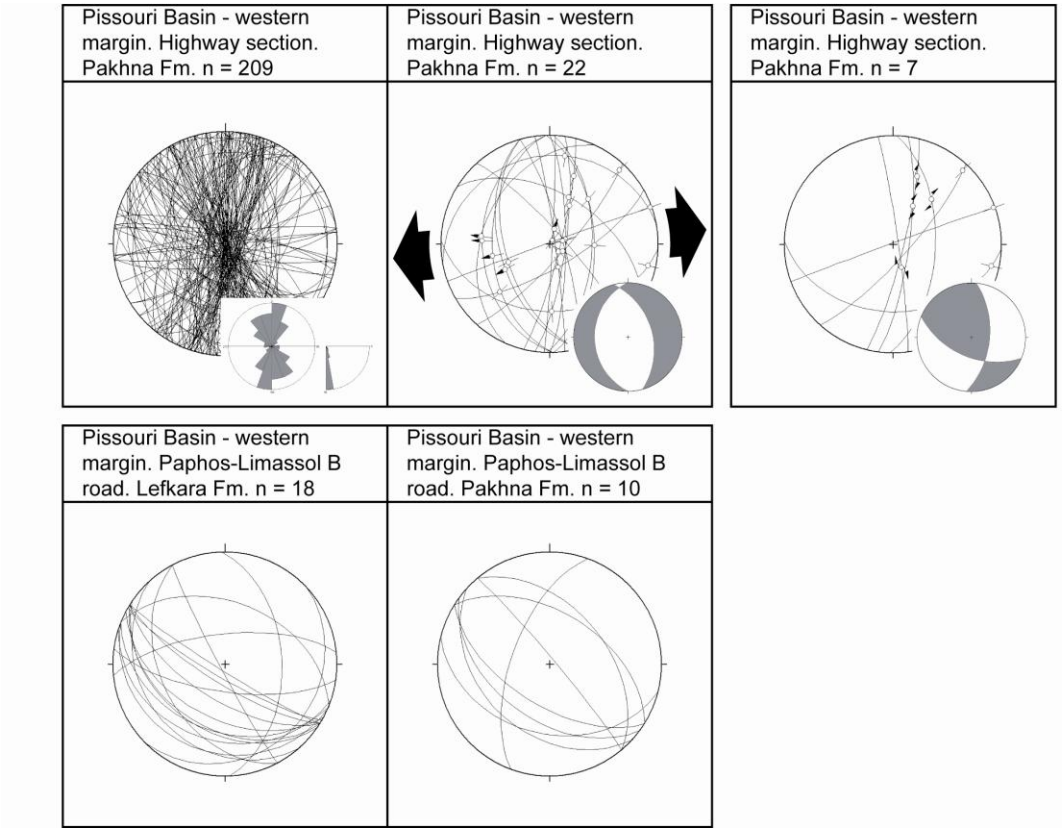

Figure 6-18: Structural data collected for faults affecting Miocene strata (Pakhna Formation) in the Pissouri Basin

6.2.2.2 Faults affecting Messinian strata

Hydro-geological boreholes (data supplied by the Cyprus Geological Survey) indicate that: (i) the spatial distribution and thickness of Messinian units and/or Pliocene marl varies throughout the basin; and (ii) Miocene and Pliocene units are juxtaposed (without the intervening Messinian units) (Figure 3-21). In the north of the basin, boreholes encounter a succession that pass down through Pliocene marls (Nicosia Formation, section 6.2.1.4), ~ 25-40 m thick, through gypsiferous deposits (Kalavasos Formation, section 6.2.1.2), ~ 5-100 m thick and into carbonates (Pakhna Formation, section 6.2.1.1). In the east of the basin, the boreholes reveal a similar succession, with marls, ~ 20 m thick, passing down through gypsiferous deposits, ~ 50 m thick, into carbonates. The gypsiferous units are inferred to pinch out laterally, and in the most eastern limit of the basin, Pliocene marls unconformably overlie Miocene carbonates. However, boreholes in the axis of the basin reveal a different stratigraphic succession: in general, Pliocene marls reach a maximum thickness of ~ 350 m, and pass down into Miocene carbonates, with no intervening Messinian evaporites; however, at a number of localities, Pliocene marls, ~ 70 m thick, pass down through gypsiferous

deposits, ~ 100 km thick, into Miocene carbonates). Two such successions, i.e. one containing evaporites (borehole P2246, Figure 3-21) and one without (borehole P2252, Figure 3-21) are noted 1km northwest of the resort of Pissouri Jetty. The two successions are separated by a horizontal distance of < 1km.

Meso-structural information was collected from faults affecting Messinian strata within the Pissouri Basin. Three populations of faults are recognised: (i) N340-N360-striking (NNW-SSE), ENE- and WSW-dipping normal faults; (ii) N000-N020-striking (NNE-SSW), WNW- and ESE-dipping normal faults; and (iii) N090-striking (E-W), S-dipping normal faults Figure 6-19). Faults of a ~N-S orientation trend parallel to faults identified in the underlying deposits. They are observed cutting the gypsum sequence in its entirety. In contrast, faults of a E-W orientation are not observed in strata younger than the Messinian. Facies analysis of Kalavasos Formation evaporates and Lago Mare deposits indicate several periods of tectonic instability during the Messinian: (i) Slumped and re-deposited gypsum probably indicates active faulting at, or near the margins of, the basin during evaporite deposition; (ii) Gypsum mega-breccias (i.e. the mega-rutite of Robertson et al., 1995b, and the polygenic breccia and gypsum mega-breccia of Orszag-Sperber et al., 1989) indicate periods of pronounced instability, with large slumps transporting material basin-ward from the margins of the basin. The polygenic breccia, noted by Orszag-Sperber et al. (1989) at the base of the evaporite succession, contains clasts of gypsum, diatomites and carbonates; which indicate that gypsum was precipiated, and reworked, prior to the main phase of evaporite deposition; (iii) The Lago Mare interval and the lowermost Pliocene deposits, which overlie the Messinian evaporites, are intensely disturbed, due to the cumulative affect of syn-sedimentary deformation, later dissolution and collapse.

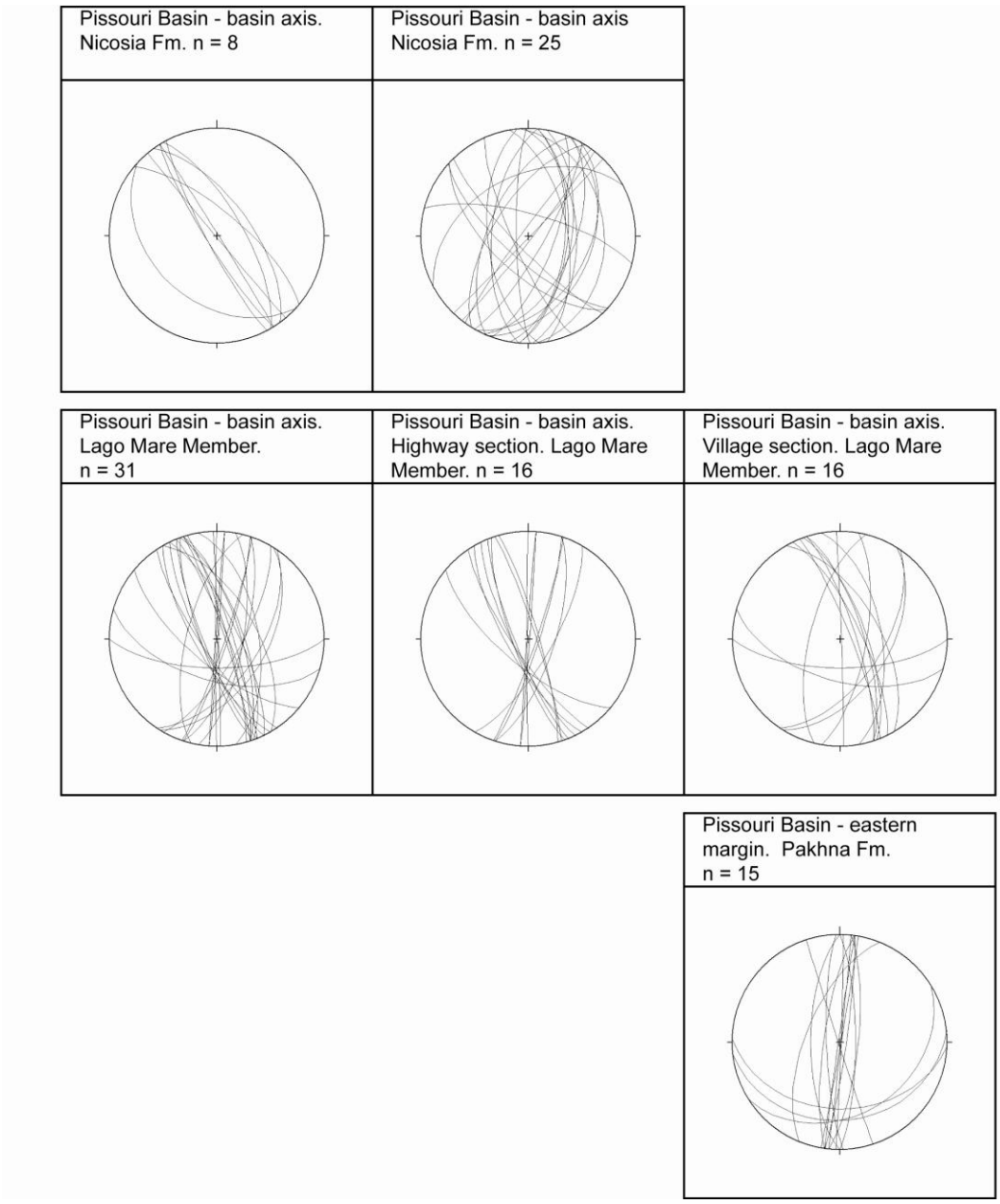

Figure 6-19: Structural data collected for faults affecting Messinian and Pliocene strata in the Pissouri Basin (see discussion in Chapter 3, section 3.3.3.3)

Dissolution of the gypsum deposits has created large (metre-wide) cavities, which where infilled by Lago Mare deposits (Figure 6-20). Deposits within the cavities typically display collapse structures, indicating that karstification was active during sedimentation. Large undulations, decimetre in amplitude in the Lago Mare strata, as observed along the Lemesos – Paphos motorway, are a product of this phenomenon. Metre-scale normal faults are found in association with the undulating strata. These normal faults have a range of orientations, ranging from ~N-S to ~E-W. It is proposed that the ~N-S faults formed in the Tortonian,

when they controlled the distribution of gypsum deposits. They continued to be active in the Messinian. The generation of ~E-W-striking faults occurred in the Late Messinian. These faults presumably formed due to the dissolution and collapse of the underlying gypsum.

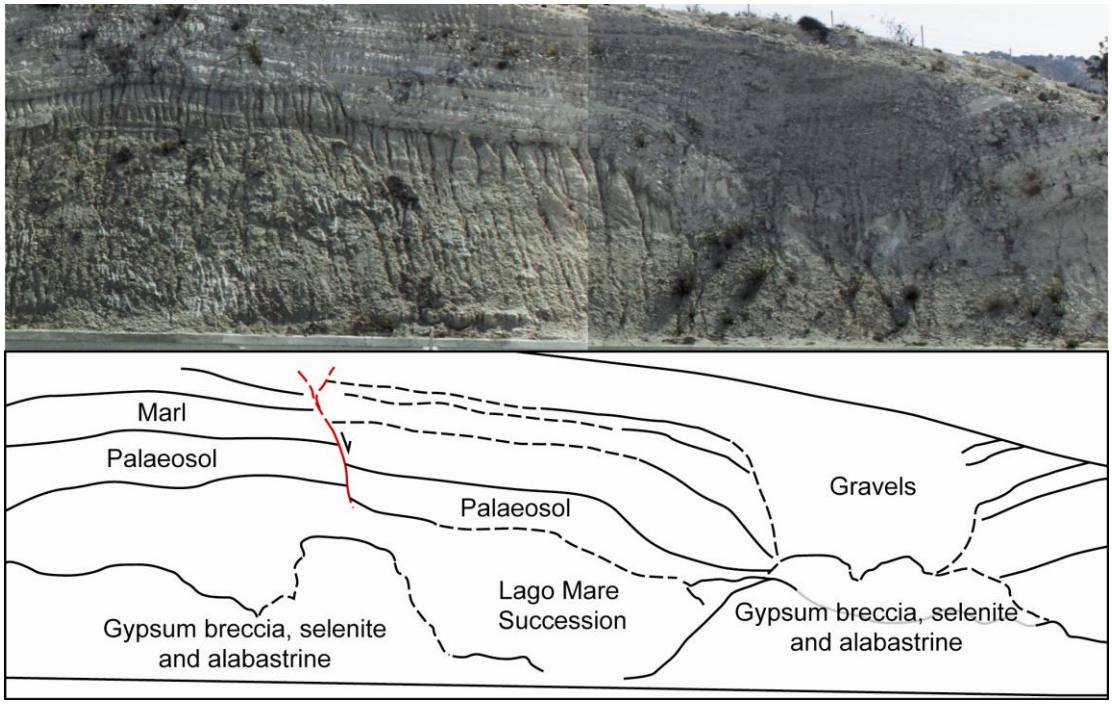

Figure 6-20: Dissolution of Kalavasos Formation evaporites. Note syn-sedimentary normal faulting.

Orszag-Sperber et al. (1989) identify three main phases of tectonic instability during the Messinian (Figure 6-21): (i) the first phase predates the main period of gypsum deposition; a polygenic breccia, containing reworked blocks of carbonates, diatomites and gypsum, underlies the succession, implying that gypsum must have previously been present on the margin of the basin; (ii) the second phase occurs during the main period of gypsum deposition, as recorded by a gypsum mega-breccia (the mega-rutite of Robertson et al., 1995b) part way through the evaporite succession; and (iii) the third phase occurs during the latest Messinian as recorded in the Lago Mare succession. Orzsag-Sperber et al. (1989) identified several palaeosol horizons separated by unconformities. They associate these depositional hiatuses with fault movements; each successive palaeosol horizon corresponding to subsidence on basin bounding normal faults.

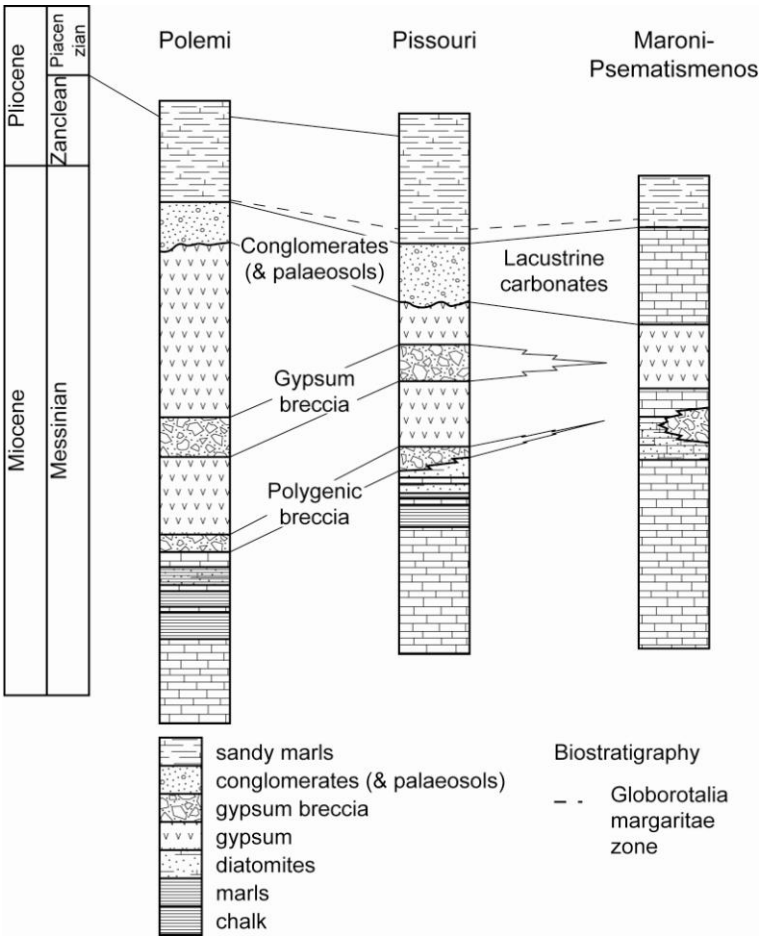

Figure 6-21: The structural study of Orszag-Sperber et al. (1989): schematic sections of the Polemi, Pissouri and Psematismenos basins, demonstrating the relationships between three Messinian tectonic events

Orszag-Sperber et al. (1989) believe that the gypsum breccias identified in the Messinian succession in each Neogene Basin occur at a similar stratigraphic level; this led them to state that tectonic events in each basin correlate. Whether or not, the gypsum breccias in the Pissouri, Polemi and Maroni-Psematismenos sub-basins are coeval, and, thus, possibly related to a more regional, rather than local event, cannot be determined without improved dating. Their third deformation event related to cyclic deposition of palaeosols within the basin is ambiguous. Further evidence is required to test this hypothesis. It is equally plausible, and thought more likely that climatic variations controlled the deposition of the Lago Mare palaeosols.

6.2.2.3 Faults affecting Late Pliocene to Recent sediments

Active structures identified in the Pissouri area include the Souskiou Fault (Soulas et al., 2005), the Alekhtora Fault (Soulas et al., 2005), the Pissouri Jetty-Patima Fault and the Pissouri village fault scarps. The Souskiou Fault is located south of the Neolithic settlement of Souskiou, ~3 km east-northeast of Kouklia village, i.e. near the western margin of the Pissouri Basin. It consists of an echelon network of N-S and NNW-SSE-striking faults, which follows the western boundary of the Oritis Forest, an uplifted plateau for a distance of 2 kilometres (Soulas et al., 2005). Soulas et al. (2005) have inferred a right-lateral sense of displacement to the fault. A single sub-vertical, strike-slip fault was identified in a Pleistocene marine terrace northwest of Kouklia and east of Souskiou. A 2m wide zone is cut by several strands of an E-W-trending en echelon fault, in an otherwise undeformed sequence of stratified, matrix-supported pebble conglomerates. Pebbles in the deformed area are imbricated parallel to the fault. This fault is interpreted as a conjugate fault to the main N-S- to NNW-SSE-trending Souskiou Fault. The Alekhtora Fault is located ~ 4 km north-northwest of Pissouri village. It consists of a set of NNE-SSW-trending faults, which total ~ 3 km in length (Soulas et al., 2005). Soulas et al. (2005) envisage that the Alekhtora Fault influenced/controlled deposition of the Pliocene Nicosia Formation. They identify a possible fault scrap, which may indicate movement in the Quaternary. Active fault scarps are present in and around Pissouri village. The largest of these is the NNE-SSW-trending Pissouri Jetty-Patima Fault, which forms a prominent escarpment above the resort of Pissouri Jetty. Smaller active scarps are observed on the slope east of Pissouri village.

Messinian Lago Mare chalks and marls, Pleistocene Fanglomerate Group gravels and Holocene Terra Rosa soils are cut by a number of additional NNW-SSE- and NNE-SSW- to NE-SW- striking faults in the northeast of the basin. The NNW-SSE and ~NE-SW faults are believed to have formed in the Late Pleistocene. Facies analysis of the Fanglomerate Group gravels indicates that they were deposited during an episode of extension: (i) channelised units/palaeosols are ‘banked’ against fault planes; (ii) pebbles/cobbles within channelised bodies of gravels are smeared along fault planes; and (iii) drag folds are associated with the fault planes. Messinian Lago Mare units are frequently reworked in close proximity to the fault planes. The Lago Mare, Fanglomerate Group and Terra Rosa soils overlie the Kalavasos Formation, a succession of gypsiferous deposits. The Kalavasos Formation is cut by Late Miocene (Tortonian) and Messinian faults. In general, faults affecting Late

Messinian and younger strata trend in a similar orientation to those observed cutting the Kalavasos Formation. It is believed that the orientation of the Late Miocene (Tortonian) and Messinian faults have largely controlled the distribution of post-Messinian faults. The slight scatter in the orientation of the post-Messinian faults is presumably related to recent dissolution and collapse. These faults are believed to be 'young', i.e. Late Pleistocene/early Holocene.

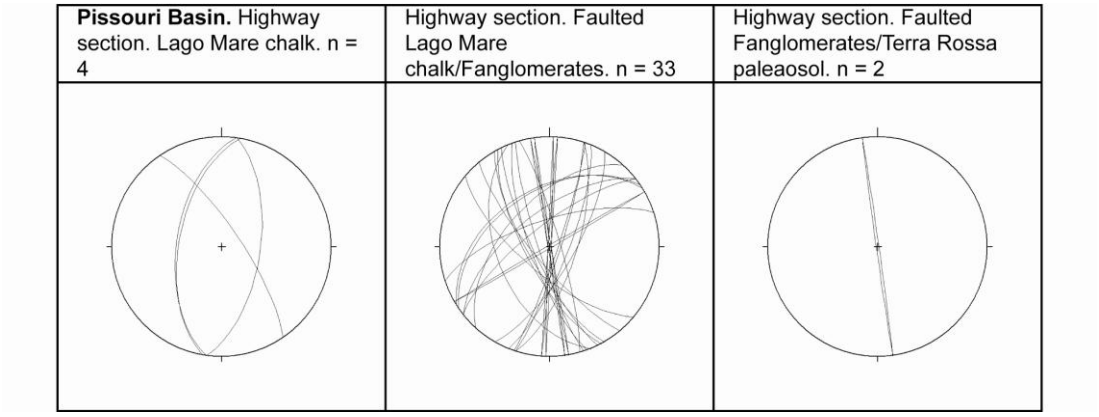

Figure 6-22: Structural data collected from faults affecting Messinian and Pleistocene strata in the Pissouri Basin

It is believed that the ~N-S faults observed cutting Pakhna Formation chalk at the western limit of the basin were reactivated. Many of the slickensided surfaces that occur in association with the N-S faults have two slickenlines preserved on them: steps associated with the development of the slickenlines indicate that one displacement was normal dip-slip, and that the other was dextral strike-slip. The reactivated structures at Kouklia occur in close proximity to the right lateral Souskiou fault, which is known to affect early/middle Pleistocene strata. For this reason, reactivation of the fault was deemed to have occurred in the early/middle Pleistocene. A regional compressional/tectonic event is recognised throughout the south of Cyprus in the Pleistocene (chapter 3). The Soukiou Fault was presumably generated at this time, along with the reactivation of the ~N-S faults.

6.2.2.4 Discussion: development of faults and fractures within the Pissouri Basin

Figure 6-23 summaries the data discussed above. On the basis of fault trend/kinematics and the age of the affected unit, four deformation events are recognised in the Pissouri Basin: *Late Miocene (Serravallian-Tortonian) east-west extension (D1a):* ~ N-S- and NW-SE-trending normal faults were generated during this event (Figure 6-23). N-S orientated faults are believed to have influenced the spatial distribution of Serravallian – Tortonian channels

(Pakhna Formation) and Tortonian reefs (Koronia Member). Borehole data has revealed that the deposition, and subsequent preservation of, Messinian evaporates (Kalavasos Formation) was controlled by Tortonian-Messinian faults; *Messinian extension (D1b):* ~ NNW-SSE- and NNE-SSW- and NE-SW-trending normal faults formed during this event. Latest Messinian extension, controlled by dissolution and collapse of the gypsum deposits, formed ~ NNW-SSE-, NNE-SSW- and NE-SW-trending normal faults (Figure 6-23); *Pleistocene compression/transpression (D3)*: Early – middle Pleistocene compression/transpression led to the reactivation of ~N-S-striking D1 structures. ~N-S-trending structures at the western margin of the basin are believed to have been reactivated in dextral transpression; *Late Pleistocene/Holocene extension (D4):* Late Pleistocene/Holocene dissolution and collapse of the Kalavasos Formation has led to extension in the overlying Lago Mare Member, Fanglomerate Group and Terra Rosa soils. The similar orientation of faults in the Kalavasos Formation and the overlying deposits has led the author to suggest that early Tortonian/Messinian structures (D1) partly controlled the spatial distribution of post-Messinian faults.

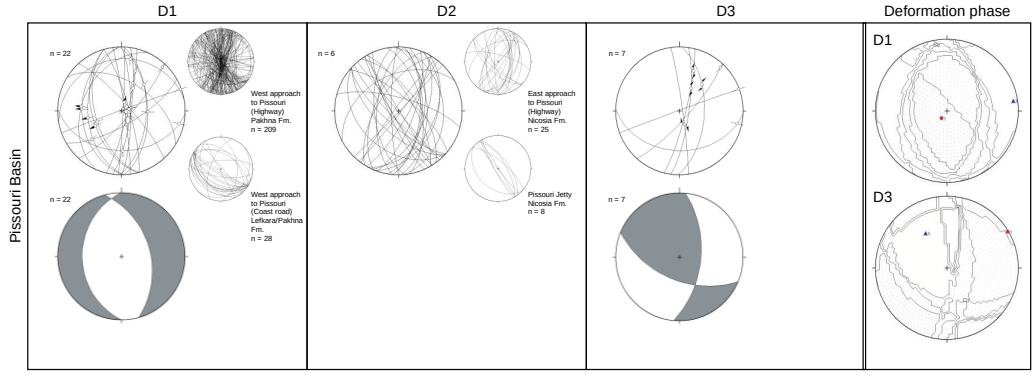

Figure 6-23: Deformation phases recognised in the Pissouri Basin: D1:- ~ N-S orientated faults formed during Tortonian E-W extension; D2:- ~ NE-SW orientated faults formed due to dissolution and collapse of gypsum; and, D3:- reactivation of D1/D2 structures in a dextral sense

6.3 Magnetostratigraphy

A magnetostratigraphy was generated for the Plio-Pleistocene fill of the Pissouri Basin to determine the timing of uplift in the basin (see chapter 4, section 0). The composite stratigraphic section shown in Figure 6-24 was compiled from data collected at Mandra tou Yerolemou (Pissouri), Pissouri village and Patima (Pissouri Jetty). This incorporates sedimentological data (e.g. logs) from the upper part of the Nicosia Formation (section

6.2.1.4), Gilbert-type fan delta deposits (section 6.2.1.5) and the upper sequence of interbedded aeolintes and palaeosols (section 6.2.1.6).

The upper part of the Nicosia Formation was deposited during either the Reunion (2.15 – 2.14 Ma) or Olduvai subchron (1.95 - 1.77 Ma) of the Matuyama chron. Gilbert-type fan deltas prograded into the Pissouri Basin in the Late Pliocene to Early Pleistocene, during the Matuyama chron, either prior to or after the Olduvai subchron, i.e. between 2.14 and 1.95 Ma or between 1.77 and 1.66 Ma, respectively. Terra Tosa-type palaeosols and aeolinites overlie the Gilbert-type fan deltas. The lower horizons were deposited in the Late Pliocene to Early Pleistocene, with deposition during the Matuyama chron, either prior to or after the Olduvai subchron, i.e. between 2.14 and 1.95 Ma or between 1.77 and 1.66 Ma, respectively. The upper horizons were deposited in the early Pleistocene to Recent during the Brunhes chron (< 0.78 Ma). Efthimios Tsiolakis, of the Cyprus Geological Survey Department, is in the process of generating a biostratigraphy for the upper part of the Nicosia Formation preserved at Pissouri. When complete, this will enable comparisions between the palaeomagetic and biostratigraphic data.

Pronounced uplift of the Troodos Massif is believed to be coincident with the progradation of the Gilbert-type fan-deltas into the Pissouri Basin (Stow et al., 1995). Hence, pronounced uplift of the Troodos Massif began in the Late Pliocene to early Pleistocene. This timing of uplift is comparable to results obtained from elsewhere around the Troodos Massif i.e. the Mesaoria Basin (see chapter 4). A magnetostratigraphy generated for the Mesaoria Basin indicates a pronounced uplift of the basin during the latest Pliocene (i.e. between 2.14 and 1.95 Ma), coincident with the progradation of the Kephales (Kakkaristra) fan-delta into the Mesaoria Basin.

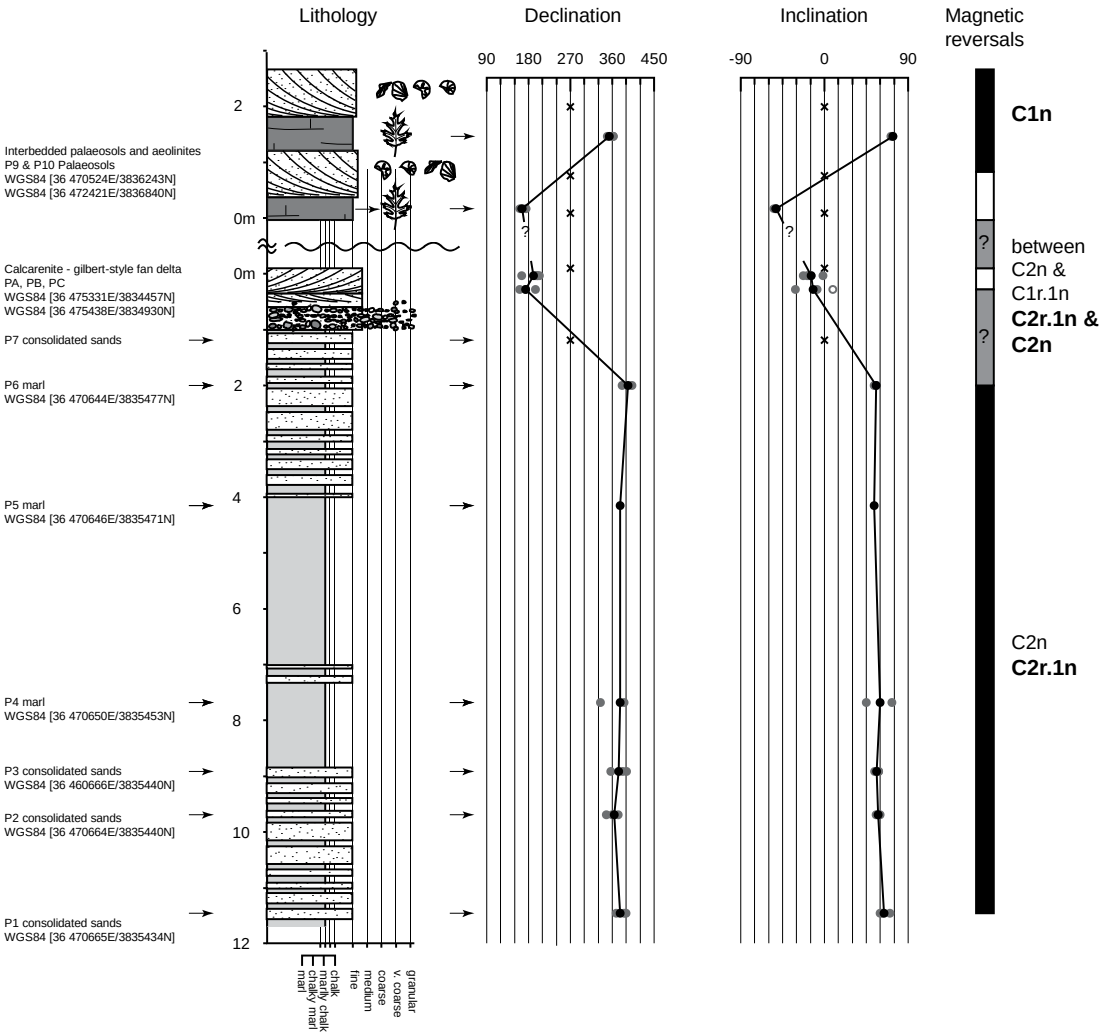

Figure 6-24: Composite stratigraphic section through the upper units of the Nicosia Formation, Stows et al.'s (1995) Gilbert-style fan deltas and overlying palaeosols and aeolinites. The key to the log is given in Appendix A. Sample horizons marked (Samples that didn't yield a palaeomagnetic signal are marked by a cross). The figure incorporates the results of the palaeomagnetic study (the presentation of the palaeomagnetic data is as in Figure 6-10). Possible correlations to the geomagnetic polarity timescale (Cande & Kent, 1995) are indicated; the favoured correlation is indicated in bold

6.4 Tectonic setting and evolution of the Pissouri Basin

The tectonostratigraphic evolution of the Pissouri Basin is summarised below:

6.4.1 Paleocene to Oligocene (Early Miocene?)

From Paleocene to Late Oligocene times, the Troodos-Mamonia terrain was subjected to a period of relative tectonic quiescence. This is represented by undisturbed pelagic carbonate

deposition of the Lefkara chalk formation. In the Pissouri area, pelagic sediments were deposited directly above pillow lavas and metalliferous chemogenic deposits.

6.4.2 Mid to Late Miocene (Burdigalian – Tortonian)

The Pissouri Basin formed during a period of tectonic instability, in response to a Burdigalian to middle Miocene phase of palaeogeographic/palaeoenvironmental reorganisation, associated with the beginning of uplift in Cyprus. On a regional scale, this uplift is attributed to the unstable position of Cyprus, broadly in a fore-arc setting at this time, within the complex zone of convergence between Africa and Anatolia (Robertson and Woodcock, 1986; Kemplar and Ben-Avraham, 1987). Early - Middle Miocene compression formed several WNW-ESE trending compressional lineaments, the Gerasa lineament, the Agia Mavri lineament, the Akrotiri lineament, and the Petounda lineament (see Chapter 3), in response to the migration of the convergent plate boundary from within the Kyrenia Range, in north Cyprus, to its present position (Kemplar and Ben-Avraham, 1987). Compressional lineaments compartmentalised the Miocene-Pliocene sedimentary succession in south Cyprus into several sub-basins: including the Pissouri, the Polemi, and the Maroni-Psematismenos Basins (Figure 6-1; Eaton and Robertson, 1993; Robertson et al., 1995b).

Tortonian E-W extension generated a well defined structural depression in the present Pissouri area, in which open to restricted marine sediments were deposited (see section 6.2.2). This is evidenced by marked facies differentiation at the top of the Pakhna Formation, in which small mounded biotherms surrounded by reef-talus interfinger with shallow-water algal laminites and deeper-water marls, micrites and bioclastic turbidites (Stow et al., 1995). Koronia Member reefs are thought to have colonised faulted blocks at the margin of the basin (Follows et al., 1996); faulting at the margin of the basin led to the redeposition of reefal detritus down-slope as bioclastic turbidites. Micro-structural studies of faults affecting Miocene strata within the Pissouri Basin suggest that these faults were orientated along N-S and NW-SE trends. Serravallian – Tortonian channels in the uppermost Pakhna Formation are aligned ~ N-S, which is approximately perpendicular to the direction of Late Miocene extension, suggesting that early faults controlled the spatial distribution of Pakhna channels.

6.4.3 Late Miocene (Messinian)

By the Late Miocene, the Pissouri Basin existed as a shallow, fault-bounded depression semi-isolated from the Mediterranean Sea. A prominent change in palaeoenvironmental

conditions occurred at ~ 6.73 Ma in the Pissouri Basin, as evidenced by a change from open-marine, deeper water taxa to more restricted, shallower water taxa (Kouwenhoven et al., 2006). This major change in palaeoenvironmental conditions (e.g. oxygen deprivation due to stagnation and hyper-salinity) can be explained on a regional scale by hydrographical changes in the Mediterranean basin, which were probably caused by tectonic movements in the Rif Corridor acting in concert with astronomical cyclicity (Jolivet et al., 2006). The deposition of the evaporites was not an abrupt event but the culmination of increasing restriction and salinity in response to the ongoing closure of the marine gateways under predominant tectonic control (Rouchy and Caruso, 2006). A study of palaeo-depth proxies in the Pissouri Basin (Rouchy et al., 2001; Kouwenhown et al., 2006) indicates a constant water depth of ~300 – 500 m, prior to deposition of the 'barre jaune', the interval preceding deposition of the evaporites (see section 6.2.1.1). At a local scale, another mechanism is necessary to explain the spatial distribution/facies variation in upper Pakhna Formation carbonate deposits and lower Kalavasos Formation gypsum deposits. Late Miocene extension (D1) is believed to have controlled the spatial distribution of evaporites in the basin (see section 6.2.2): with deposition of evaporites and lagoonal – lacustrine deposits of the Kalavasos Formation confined to the central part of the Pissouri Basin. Fault-controlled subsidence presumably isolated the Pissouri Basin from the Troodos Massif during the Messinian.

Coarsely crystalline gypsum formed in situ along the margins of the Pissouri Basin and within fringing shallow-water lagoons. Fine-grained gypsum was precipitated within the basin, and then occasionally reworked by weak traction currents and low-density turbidity currents. In addition, marginal and lagoonal selenites were reworked basin-wards by high-density turbidity currents and debris flows. Syn-sedimentary faulting is inferred from the presence of gypsum breccias, slump units and turbidites (D1).

During the latest Miocene, the Pissouri Basin continued to exist as a semi-enclosed, shallow-water basin, subject to repeated influxes of marine- and fresh- water, with no direct supply of sediment from the Troodos ophiolite. Small fan-deltas prograded from the fault-active basin margins into ephemeral lakes overlain by palaeosols. Erosion along the basin margin led to down-slope re-sedimentation of carbonate conglomerates as debrites and sand-grade material as turbidites. Dissolution and collapse of the underlying gypsum deposits led to syn-sedimentary faulting of Lago Mare chalks and marls (D2). Dissolution of the gypsum deposits created large (metre-wide) cavities, which where infilled by Lago Mare deposits.

Deposits within the cavities typically display collapse structures, indicating that karstification was active during sedimentation. Rouchy et al. (2001) state that Troodos ophiolite-derived material was introduced during deposition of the Lago Mare succession. Their evidence was the presence of conglomerates comprised of poorly to moderately sorted, sub-angular to mainly rounded, pebble to cobble sized clasts of Troodos ophiolite-derived material, interbedded with horizons of pebbly, coarse sandstones. The matrix is typically a fine, powdery chalk (Figure 6-25). However, detailed sedimentary logging, facies analysis and geomorphological studies indicate that these conglomerates are instead terrace deposits of early to middle Pleistocene age (when by general agreement uplift was occurring, Poole and Robertson, 1991). Conglomerates within the Lago Mare interval are comprised predominantly of sub-angular to mainly rounded clasts of chalk (and minor chert) with only very small amounts of Troodos-derived material.

Figure 6-25: Field photograph of the 'Messinian' conglomerates (Rouchy et al. 2001), that were re-assigned to the Pleistocene during this study

How consistent is the distribution of gypsiferous facies in the Pissouri Basin with the 'popular' picture for Messinian drawdown in the Mediterranean Basin? The Messinian succession of the Pissouri Basin may be described in terms of two units: a lower unit of thick evaporites, and an upper unit of lacustrine/lagoonal deposits. A similar stratigraphic framework is recognised throughout the whole Mediterranean (1st and 2nd evaporite stages – Rouchy and Caruso, 2006). The deposition of thick evaporites in each of the Neogene basins may be correlated with major evaporative drawdown and higher aridity throughout the entire Mediterranean; this event is believed to have occurred during the glacial period recorded in

ocean sediments between 6.3 and 5.6Ma (first evaporitic stage; Rouchy and Caruso, 2006). The deposition of the Lago Mare succession (second evaporitic stage; Rocuhy and Caruso, 2006) occurred during an interval of warming and global sea level rise (5.6-5.5Ma) in the Mediterranean. The Messinian Mediterranean Basin was a mosaic of sub-basins of different size and depth, with water exchanges between the basins dependent on eustatic sea-level changes and local uplift and subsidence.

6.4.4 Early to Middle Pliocene

Marine conditions were re-established at the beginning of the Pliocene, as evidenced by widespread and uniform deposition of pelagic marls and micrites. At this stage the Pissouri Basin appears to have deepened and increased in lateral extent, as the lowermost pelagic micrites and marls are seen to overstep the earlier basin margins, although they are deposited in apparent angular conformity with the underlying Pakhna Formation (Stow et al., 1995).

Localised uplift and faulting at the northern margin of the Pissouri Basin generated channelised turbidity currents and mass-flows (facies association NI2). Channelised units prograded as lenticular tongue-like bodies several kilometres across the basin to the south and southeast. Channel orientations and slumps in the Nicosia Formation remain similar to those observed in the Pakhna Formation, despite the presence of the intervening Messinian salinity crisis. This implies that the early Pliocene was subjected to similar extensional stresses as the Late Miocene.

Nicosia Formation marls and bioclastic sandstones were transgressed by Athalassa-type, shallow-marine, cross-stratified, bioclastic rich sandstones. Tectonic activity and possibly eustatic sea-level change may have been responsible for triggering deposition of the Athalassa-type sediments.

6.4.5 Late Pliocene

The Eratosthenes Seamount, a continental fragment rifted from, and pushed in front of the Africa plate as it advanced north collided with the Cyprus Arc in the Late Pliocene (~ 2 Ma; Robertson et al., 1995a, Robertson, 1998a); this led to the emergence, uplift and erosion of the Troodos Massif. Terrigenous material was introduced to the basin, as siltstone and sandstone turbidites, related to periods of uplift of the Troodos Massif and/or sea-level changes.

Pronounced uplift of the Troodos Massif began in the Late Pliocene (between 2.14 – 1.95 Ma; see section 6.3). Individual, stacked, Gilbert-type deltas prograded into the Pissouri Basin in the latest Pliocene/earliest Pleistocene (between either **2.14 – 1.95 Ma** or 1.77 – 1.66 Ma) from the northern margin of the basin towards the south/southeast a distance of c. 4 km. Stow et al. (1995) interpreted these as a braided channel topset of a well-supplied fan delta that was feeding the bottomset and foreset facies of the Nicosia Formation marls. This significant sediment influx was principally controlled by intense uplift of the Troodos and its rapid erosion, possibly during the main pluvial periods of the Late Pliocene – early Pleistocene. Deposition occurred on the coastal plain above or near sea level. Interpluvial periods were possibly represented by aeolinite and palaeosol development. Delta abandonment may have been caused by upstream avulsions and autocyclic lateral switching of fan-delta lobes during relatively uniform rates of subsidence. Alternatively it is possible that delta abandonment was caused by large episodic faulting events, which submerged each pre-existing fan-delta plain, substantially slowed detrital input by drowning of alluvial feeder channels, and created new accommodation space for each new Gilbert-type fan delta.

6.4.6 Late Pliocene – early Pleistocene

Continued uplift of the Troodos Massif, led to shallowing in the Pissouri Basin. By the early to middle Pleistocene, the regional stress regime had reverted from one of extension to transpression (sinistral?). Tortonian and Messinian NNW-SSE- and NNE-SSW-striking faults were reactivated in a strike-slip sense (D3). An E-W-striking fault is observed cutting Pleistocene marine terrace deposits at Kouklia. The fault is believed to be a conjugate to the right-lateral, NNW-SSE-trending Souskiou Fault. A synthesis indicating the evolution of regional stress with time is given in chapter 7.

Extension was still occurring at a surficial level, above the uplifting Pissouri region, as evidenced by a faulted sequence of Fanglomerate gravels and underlying Messinian Lago Mare deposits in the north of the basin.

6.4.7 Middle Pleistocene to Recent

Recent sediments (0.78 Ma – present) are of an alluvial-fluvial origin, and include aeolinites, palaeosols, alluvial fan sheets, and valley and slope unconsolidated drift deposits. They reflect continued uplift of the Troodos Massif and valley incision into the underlying units.

6.5 Conclusions

The discrete NNW-SSE-trending Pissouri Basin was initiated during Late Miocene E-W/NE-SW extension (D1), related to changes in regional stress patterns related to subduction, transpression and/or continental collision to the south. A possible cause of extension was relative 'roll-back' of the subducting/colliding plate to the south. The Pissouri Basin remained an extensional depocentre through the Messinian and into the Early Pliocene (D2). In the early to middle Pleistocene, the regional stress regime reverted from one of extension to one of transpression (D3).

The Pissouri Basin experienced a transition from deep-water pelagic sediments of the Maastrichtian - Upper Oligocene Lefkara Formation, to more varied shallower water, mixed carbonate and terrigenous sediments of the Upper Oligocene - Lower Miocene Pakhna Formation. By the latest Miocene (Messinian) the basin existed as a shallow, fault-bounded, silled depression semi-isolated from the Mediterranean Sea to the south. A range of pre-evaporitic, to evaporitic, facies accumulated, including minor amounts of microbial carbonate, overlain by fine- to coarse-grained and redeposited gypsum. Facies analysis indicates several periods of tectonic instability during the Messinian, associated with sediment redeposition and slumping. During the latest Miocene, small fan-deltas prograded from the fault-active basin margins into ephemeral lakes overlain by palaeosols ('Lago Mare' facies). Dissolution and collapse led to extensional faulting within Lago Mare deposits (D2). The sea flooded back at the end of the Messinian, followed by deposition of marginal fan-deltas, which pass basin-wards into shelf-depth marls (Nicosia Formation). These sediments are intercalated with terrigenous siltstone/sandstone turbidites, previously interpreted as the bottomsets and foresets of large marine fan-deltas. Large, intercalated lenses of bioclastic calcarenites and ophiolite-derived sandstones are interpreted as conduits for marginal shelf and terrigenous material. Soft-sediment deformation and slump structures (e.g. overturned and recumbent ductile folds) characterise the margins of these channels. The orientation of the channelling and slumping indicate a generally southward palaeo-slope towards the deep Mediterranean Sea. Higher within the Plio-Pleistocene succession, stacked micro-Gilbert-type fan-deltas (2.14 – 1.95 Ma, or 1.77 – 1.66 Ma) are interpreted as prograding fan-delta topsets; these are interbedded with Terra Rosa-type palaeosols. Middle to early Pleistocene transpression led to the reactivation of D1 structures.

To determine timing of uplift a magnetostratigraphy for the basin was generated by palaeomagnetically analysing each unit of the Plio-Pleistocene basin-fill. The results indicate that rapid uplift (in the Pissouri Basin) began in the latest Pliocene/earliest Pleistocene (between 2.14 and 1.95 Ma or between 1.77 and 1.66 Ma.), coincident with the large-scale progradation of the Gilbert-type fan-deltas. This timing of uplift is compatible with results from elsewhere around the Troodos Massif (Mesaoria Basin).

Chapter 7: Alternative tectonic models for the Early Tertiary to Recent development of Cyprus in its Eastern Mediterranean context: considered in light of new evidence

7.1 Introduction

The aim of this chapter is to summarise and discuss each of the alternative reconstructions proposed for the Early Tertiary to Recent tectonic evolution of Cyprus. Three alternative models will be considered in light of important information gained over the last three and a half years. I will highlight the components of each model, indicating where more recent data supports, or discounts a model. This discussion is intended to clear the way for future, improved tectonic reconstructions, in which the scrutiny of structural data, basin analysis studies, and geochronological investigations will continue to play an important role. In the concluding sections of this chapter a new model is proposed to explain the Early Tertiary to Recent tectonic evolution of Cyprus.

7.2 Alternative tectonic models

Three alternative models have been proposed to account for the tectonic evolution of Cyprus in its easternmost Mediterranean setting:

Model 1: Subduction/incipient collision

Northward subduction was initiated to the south of Cyprus in the Late Oligocene to Early Miocene (Eaton and Robertson, 1993), when the convergent plate boundary migrated southwards from within the Kyrenia Range of northern Cyprus to near its present position (Kemplar and Ben-Avraham, 1987). A possible explanation for the southward migration of this subduction zone is that as Early Mesozoic oceanic crust was consumed, younger, supra-subduction zone-type Late Cretaceous oceanic crust was juxtaposed against the then active margin to the north. This young, more buoyant crust was harder to consume, so the subduction zone relocated itself within Early Mesozoic oceanic crust further south. Robertson (1990) suggested that the 'Early Neogene subduction zone' could have effectively reactivated the 'Late Cretaceous subduction zone', above which the Troodos is believed to have formed by supra-subduction spreading. The transition between Paleocene-Oligocene

deep-water pelagic carbonates (Lefkara Formation) and Miocene shallower, mixed detrital and carbonate sediments (Pakhna Formation) may represent the onset of subduction (at c. 23 Ma; Eaton and Robertson, 1993). Eaton and Robertson (1993) infer that the existence of compressional lineaments in southern Cyprus (i.e. the Gerasa lineament) reflect a regional build up of stress immediately prior to the onset of northward subduction to the south of Cyprus.

From the Early Miocene onwards, Cyprus was located on the over-riding plate of a northward-dipping subduction zone. As older Neotethyan crust was consumed in the trench, the subducted plate may have undergone 'roll-back' (i.e. retreat of the subduction hinge, Royden, 1993), with southward migration of the trench and consequent extension in the overriding plate. This extension could have given rise to the dominantly extensional regime within the Middle to Late Miocene, i.e. in western (Polis Graben, Payne and Robertson, 1995; 2000), southwestern (Pissouri Basin, Elion, 1983), southern (Maroni-Psematismenos Basin, Robertson et al., 1995) and central Cyprus (Mesaoria Basin, Follows and Robertson, 1990). More widespread extension in the easternmost Mediterranean is reflected in the development of the Antalya, Cilicia and Adana basins between Turkey and Cyprus (Figure 1-1; Robertson and Woodcock, 1986). A pulse of accelerated subduction in the Late Miocene, possibly related to a change in convergence direction between Africa and Eurasia, is inferred to have sped up 'roll-back' at the trench (Payne and Robertson, 1995). This led to a phase of Late Miocene extensional faulting in the Polis Graben, and the Pissouri and Maroni-Psematismenos Basins. This occurred prior to the onset of westward tectonic escape of Anatolia along the North and South Anatolian Faults, which began in Early Pliocene time (c. 5 Ma: Şengör et al., 1985).

The Eratosthenes Seamount, a continental fragment rifted from North Africa, collided with the trench in the Middle to Late Pliocene (c. 2 Ma; Robertson et al., 1995; Robertson, 1998). Collision of the Eratosthenes Seamount with the active margin locally impeded subduction to the south of Cyprus, due to the difficulty of consuming thickened, continental crust. While subduction was locally impeded in the area of collision, neighbouring unrestricted areas of the trench could have continued to undergo subduction roll-back (Payne and Robertson, 1995). Northward underthrusting of the African plate beneath Cyprus, coupled with serpentinite diapirism, resulted in uplift of Cyprus, centred on the Troodos Massif (Poole and Robertson, 1991). Coarse clastic sediment (Fanglomerate Group) was shed radially from the rising Troodos Massif during Late Pliocene to Recent time. In late Pleistocene to Recent

times, the rate of uplift of the Troodos Massif appears to have diminished (Poole and Robertson, 1991). The present tectonic setting of Cyprus as envisaged in model 1 is shown in Figure 7-1.

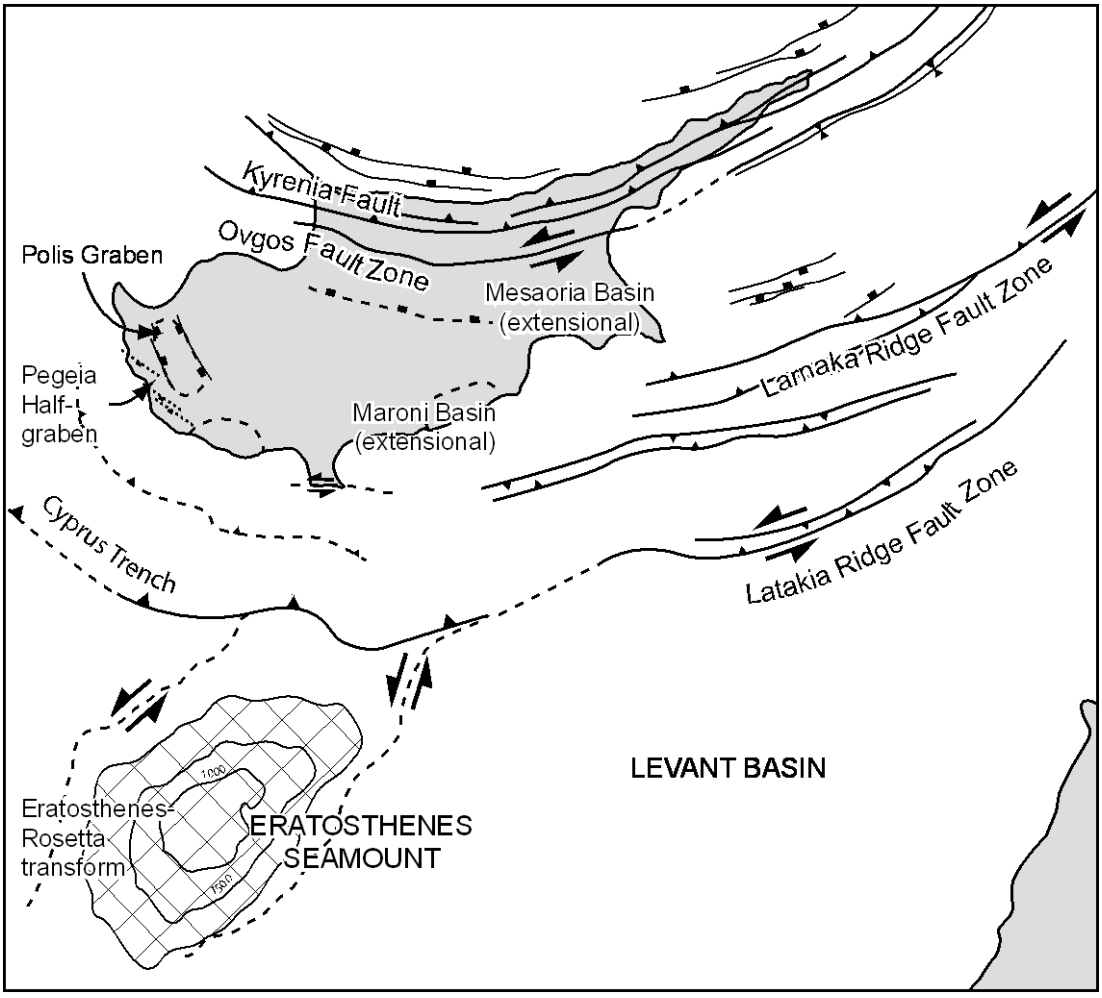

Figure 7-1: The present tectonic setting of Cyprus as envisaged in model 1

Criticisms: Several criticisms of the subduction model exist: (a) one is that there is an absence of volcanism in the vicinity of Cyprus at any time during the Middle to Late Cenozoic; another (b) is that focal mechanisms for shallow (<100km), major earthquakes (Mw > 5.0) indicate a mixture of faulting styles, but are dominantly strike-slip (Arvidsson et al., 1998; Dziewonski et al., 1998; Pinar and Kalafat, 1999; Makris et al., 2000; Pilidou et al., 2004; Papadimitriou and Karakostas, 2006); another (c) is that there is an apparent absence of a northerly dipping Wadati-Benioff zone beneath Cyprus; it is argued that recorded seismicity occurs in NNW-SSE linear trends (Makris et al., 2000), which are near vertical (see section 7.3); and yet another (d) is that known onshore Late Pliocene to Recent faults are strike-slip and transpressive.

Model 2: Advanced collision

Africa collided with Anatolia in the Late Eocene (c. 35 - 38 Ma); deep-rooted south-vergent thrusting at this time led to the prominent growth of the Troodos- Larnaka culmination, and concurrent imbrication in the Kyrenia Range (Calon et al., 2005a,b). The active front of the Tauride thrust system was situated along the southern margin of the Troodos microplate and its onland expression was the Gerasa fold/thrust belt (Calon et al., 2005a,b). Calon et al. (2005a,b) infer that the floor thrust of this system was directly linked with the then active subduction zone. Northward retreat of the active thrust front in the Oligocene–Miocene led to the development of a foredeep basin across the root of the Kyrenia fold/thrust belt. The facies changes from Paleocene-Oligocene deep-water pelagic carbonates (Lefkara Formation) to Miocene flysch deposits (Kythrea Group); and a rapid northward increase in the thickness of the latter unit, may be evidence of the development of this foredeep. Calon et al. (2005b) proposed that during the Eocene – Miocene interval, the depositional hinge line migrated northwards from a position near the crest of the Troodos-Larnaka culmination to the southern edge of the present-day Kyrenia Range.

Crustal contraction continued into the Miocene, with thrusting along the front of the Troodos-Larnaka culmination, i.e. the Gerasa fold/thrust belt (Calon et al. 2005b). In the late Miocene, thrusting became widespread in the forearc region with structural contraction focused on the Kyrenia fold/thrust belt. Pliocene thrusting in the forearc region is primarily focused on the Kyrenia fold/thrust belt with significant uplift occurring in the Middle to Late Pliocene, and continuing to the present (Calon et al. 2005b).

Calon et al. (2005b) propose that the Mesaoria Basin and its marine extensions evolved from the Eocene–Oligocene to Recent as a large piggy-back basin nestled between the active fronts of the Troodos-Larnaka culmination and the Kyrenia fold/thrust belt. Variations in the thickness and facies of the sedimentary successions deposited in this piggy-back basin during this time are directly related to shifts in the positions of the active fronts within the orogenic wedge.

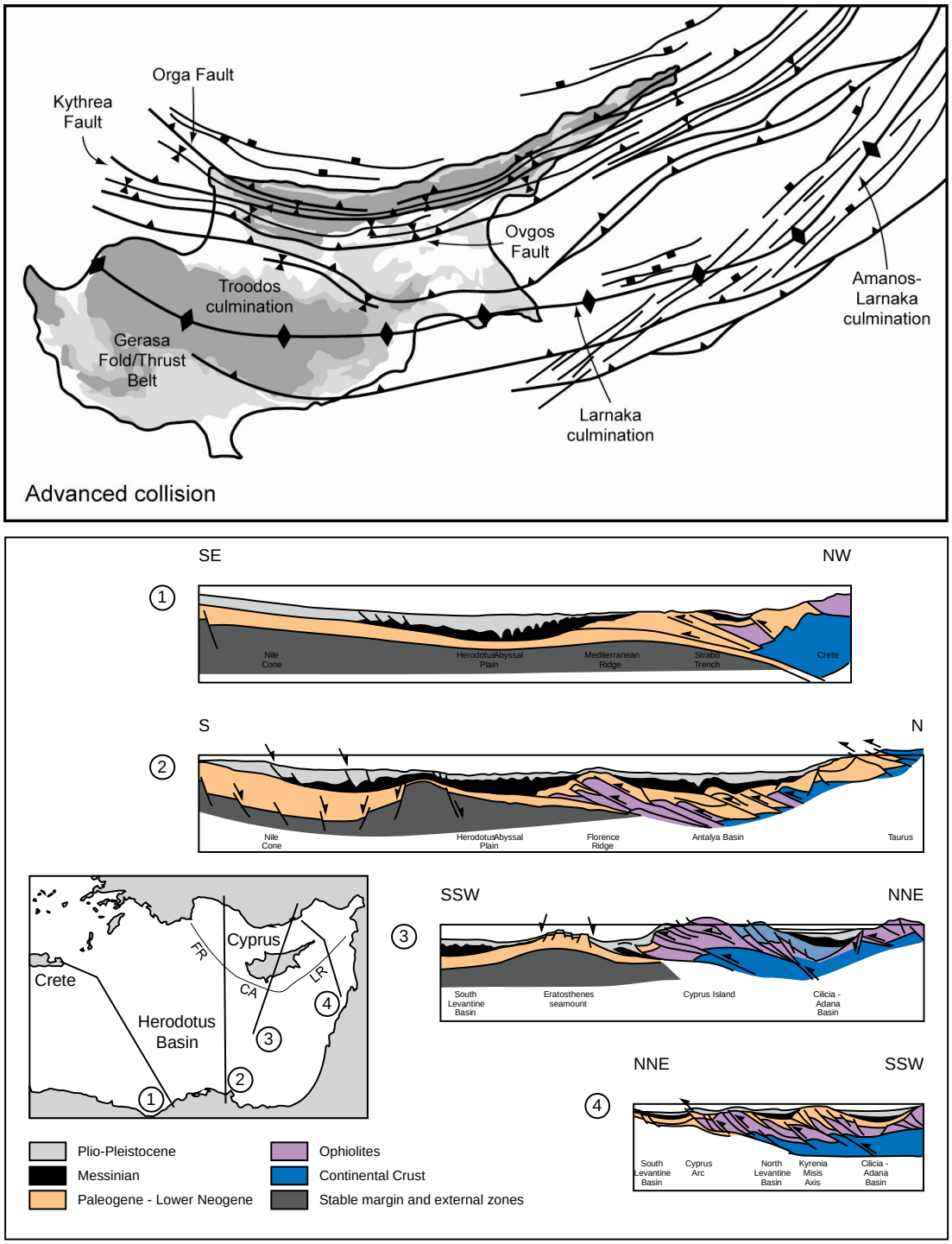

Figure 7-2: The present tectonic setting of Cyprus as envisaged in model 2: (a) tectonic map of Cyprus, western Latakia and eastern Antalya Basins (Calon et al., 2005b); (b) geological cross-sections through the Herodotus Basin, Cyprus and the Latakia/Larnaka ridges (Sage and Letouzey, 1990). Abrreviations as follows: CA = Cyprus Arc, FR = Florence Rise, LR = Larnaka Ridge

To summarise, Calon et al. (2005a,b) envisage a regional, south-verging, linked fold/thrust system, in which: (i) a footwall imbricate thrust fan system, extends into the Cyprus Basin, in front of the Tauride thrust front; (ii) the 'Troodos-Larnaka culmination' is a large

ophiolite-cored anticline, developed above a deep-rooted south-verging thrust; (iii) the leading edge of the fold/thrust system, the Mesaoria Fault is, at present, located in the middle of the Mesaoria Basin; (iv) the Kyrenia fold and thrust belt, is a trailing thick-skinned imbricate fan system, and occupies a middle position in this system; and (v) the Mesaoria Basin evolved in the Miocene to Pliocene as a piggy-back basin. Soulas (2003) envisages a local, south-vergent, linked fold/thrust system, the Paphos Thrust System, in west and south-west Cyprus. The present tectonic setting of Cyprus as envisaged in model 2 is shown in Figure 7-2.

Criticisms: Several criticisms of the advanced collision model exist: (a) one is recent seismic reflection data, multibeam bathymetric data, coupled with gravity and magnetic observations, (Ben-Avraham et al., 1995; 2002; Vidal et al., 2000a,b; Woodside et al., 2002; ten Veen et al., 2004; Ergün et al, 2005) indicate that the plate boundary is located south of Cyprus, between the island and the Eratosthenes Seamount; another (b) is that Neogene sedimentary basins formed in response to WNW-ESE/E-W directed extension, in south/southwest Cyprus, and NW-SE directed extension in south Cyprus (chapter 3); another (c) is that compressional related thrusting in southwest Cyprus (Soulas, 2003) may arguably relate to high-level extensional gravity tectonism.

Model 3: Transpression

At approximately 9 Ma (early Tortonian), a change in convergence direction between Africa and Eurasia (Dewey et al., 1989) resulted in compressional, or transpressional, tectonics in the Middle East and Eastern Mediterranean, including the northern part of Cyprus (Ducloz, 1972; Baroz, 1979; Robertson and Woodcock, 1986) and south-eastern Turkey (Kelling et al., 1987). Harrison et al. (2004a) suggests that a restraining bend initiated within this strike-slip setting in the early Tortonian (c. 9Ma). Correspondingly, sedimentation within the Kyrenia terrane changed from deep-water turbidite deposition of the Kythrea Group (Bellapais through to Davlos Formations) to shallower-water carbonate deposition (Lapatza Formation) (Harrison et al., 2004a). Harrison et al. (2004a) interpret this as indicative of uplift in the northern part of Cyprus.

From the Early Tortonian to the Early Pliocene (i.e. the interval between 9 and 5 Ma), Cyprus was dominated by transpressive strike-slip faulting. Contractional/transpressive deformation was underway by the Messinian: in the central part of Cyprus, Messinian evaporate deposits rest with an angular unconformity over strongly deformed turbidite

deposits (Kythrea Group); further north, Messinian evaporites were deposited in fault bounded basins (Robertson et al., 1995a), interpreted as pull-apart grabens (Harrison et al., 2004a).

Another change in regional tectonics occurred in the early Pliocene (c. 5 Ma), when the motion of the African plate changed to a more northerly direction (Dewey et al., 1973; Morris and Tarling, 1996; Harrison et al., 2004a). Strike-slip tectonics became prevalent throughout the Eastern Mediterranean–Middle East region at this time (c. 5 Ma: Şengör et al., 1985; Westaway, 1994). On Cyprus, the tectonic change at 5 Ma is marked in the stratigraphic record by a rapid re-establishment of marine conditions in the Early Pliocene (Lord et al., 2000). N–S compression began in the Early Pliocene and produced E-W trending contractional tectonism, including major thrusting in the Kyrenia Range. The Eratosthenes Seamount collided with the southern margin of Cyprus during the Middle to Late Pliocene (Robertson et al., 1995b; Robertson, 1998b); this led to accelerated uplift (Poole and Robertson, 2000) and a change in tectonism in the northern part of Cyprus (Harrison et al., 2004a). From that time to the present, tectonism in the northern part of Cyprus has been dominated by strike-slip faulting along east-west trends, conjugate strike-slip faulting along northwest-southeast and northeast-southwest trends, and subordinate thrusting along east-west trends (Harrison et al., 2004a). Quaternary deformation has been dominated by strike-slip faults along northwest-southeast and northeast-southwest trends.

To summarise, deformation since the Late Miocene has been due, predominantly, to left-lateral strike-slip tectonics (transpression) in a collisional setting. The major strike-slip faults were the Ovgos Fault in the north and the Cyprus 'Transform plate boundary' in the south (Figure 7-3); constraining strike-slip deformation to the area between the Eratosthenes Seamount to the south, and the Kyrenia Range to the north. The present tectonic setting of Cyprus as envisaged in model 3 is shown in Figure 7-3.

Criticisms: Several criticisms of the transpressional model exist: (a) focal mechanisms calculated for deep (76-85 km) and major (M > 5-6) earthquakes at the plate boundary are indicative of crustal shortening (Makris et al., 2000; Salamon et al., 2003; Pilidou et al., 2004); (b) Neogene sedimentary basins formed in response to WNW-ESE/E-W directed extension, in southwest Cyprus, and NW-SE directed extension in southeast Cyprus (chapter 3); and finally (c) detailed field mapping of the southern coast of Cyprus has revealed the

continuing presence of a down-to-the-south palaeoslope from the Paleocene to the Pliocene, towards the inferred position of the plate boundary (chapters 3 and 6).

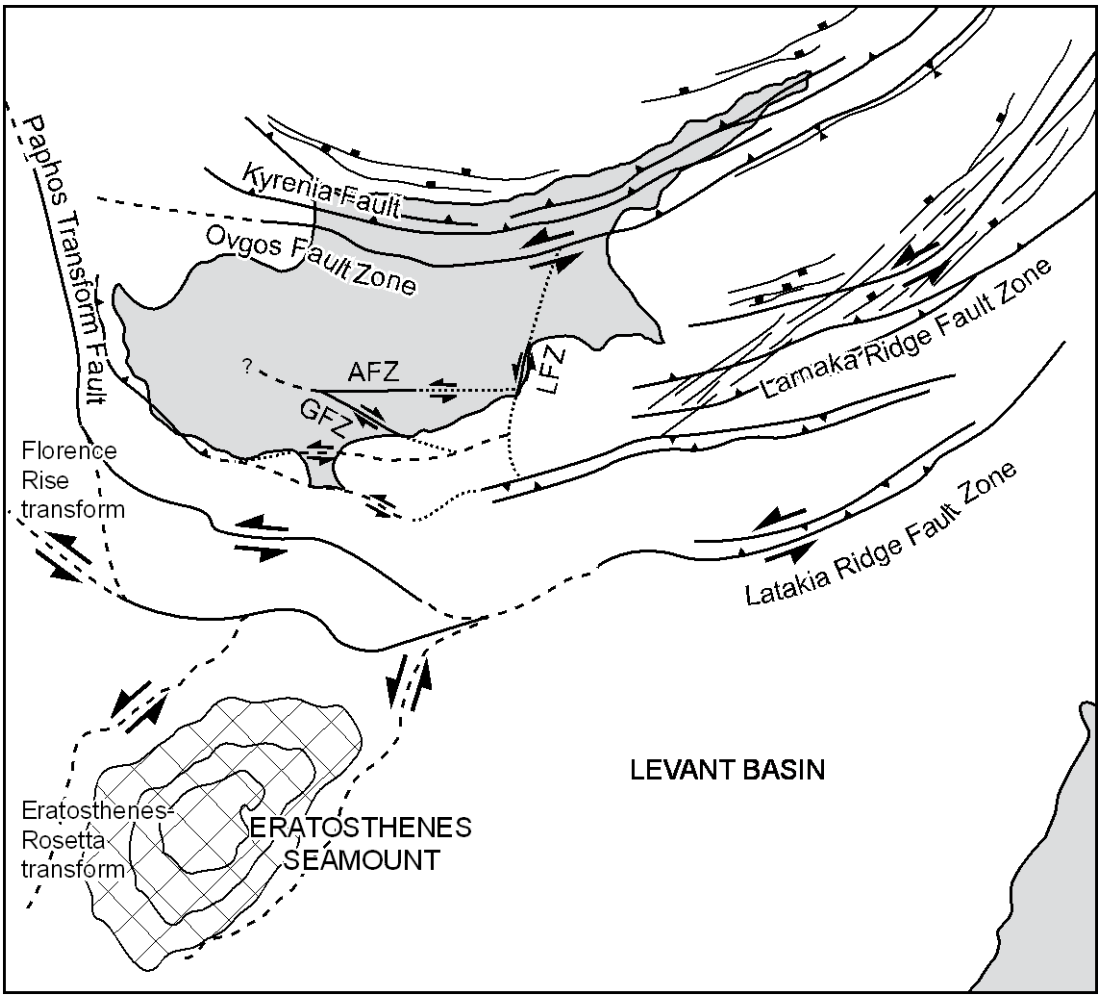

Figure 7-3: The present tectonic setting of Cyprus as envisaged in model 3

7.3 Current controversies

A number of contrasting issues exist between the main alternative tectonic models outlined above. Key points to be resolved include the following: (i) is the basement of the Levant Basin, continental or oceanic?; (ii) does the seismicity of the Cyprus region imply underthrusting (i.e. subduction) or transpression?; (iii) does a Wadati-Benioff zone exist beneath Cyprus which would imply that underthrusting of the Africa plate beneath Cyprus occurred?; and (iv) what is the plate motion of Cyprus relative to Africa and Anatolia?

Is the basement of the Levant Basin, continental or oceanic crust?

There is a disagreement in all three models as to whether the Levant Basin floor is composed of stretched continental crust, oceanic crust, or both. A series of geophysical studies, such as refraction–reflection profiles (Makris et al., 1983; Ben-Avraham et al., 2002; Netzeband et al., 2006), gravity (Rybakov et al., 1997; Seber et al. 2001), receiver function (Sandvol et al. 1998; Hofstetter and Bock, 2004; Mohsen et al., 2005), complex seismic and magnetic studies (Ginzburg and Ben-Avraham, 1992) have provided information about the crustal structure in the Eastern Mediterranean. The tomographic inversion of local ISC data indicates that the crust in the eastern Mediterranean is composed of two types: (i) oceanic/stretched continental (Levant Basin and Herodotus Abyssal Plain) and (ii) continental (Asia Minor, Zagros, Cyprus and the Eratosthenes seamount) (Koulakov and Sobolev, 2006). Geophysical gravity investigations (Makris et al., 1983; Rybakov et al., 2000; Seber et al. 2001), tomographic inversion of local ISC data (Koulakov and Sobolev, 2006) and the analysis of the dispersive characteristics of surface waves (Luccio and Pasyanos, 2007) suggest that Cyprus is underlain by ~ 30-35 km of continental crust, the Eratosthenes Seamount is underlain by ~ 22-28 km of continental crust and that the Levant basin is underlain by ~ 9-11 km of oceanic crust/stretched continental crust. Seismic-refraction measurements support this interpretation (Ben-Avraham et al., 2002).

Discussion. The nature of the crust beneath Cyprus, the Eratosthenes Seamount and the Levant Basin is an issue of contention in all three tectonic models. At present the composition of the crust in the Levantine Basin remains enigmatic (see list of publications above). The general consensus is that the Levant Basin and Herotodus Abyssal plain are underlain by oceanic crust/stretched continental crust that it ‘transitional’ in nature (Z. Garfunkel, personal communication).

Does seismicity in the Cyprus region imply underthrusting or transpression?

Figure 7-4 illustrates the distribution of earthquake epicentres from deep and shallow earthquakes in the immediate vicinity of Cyprus.

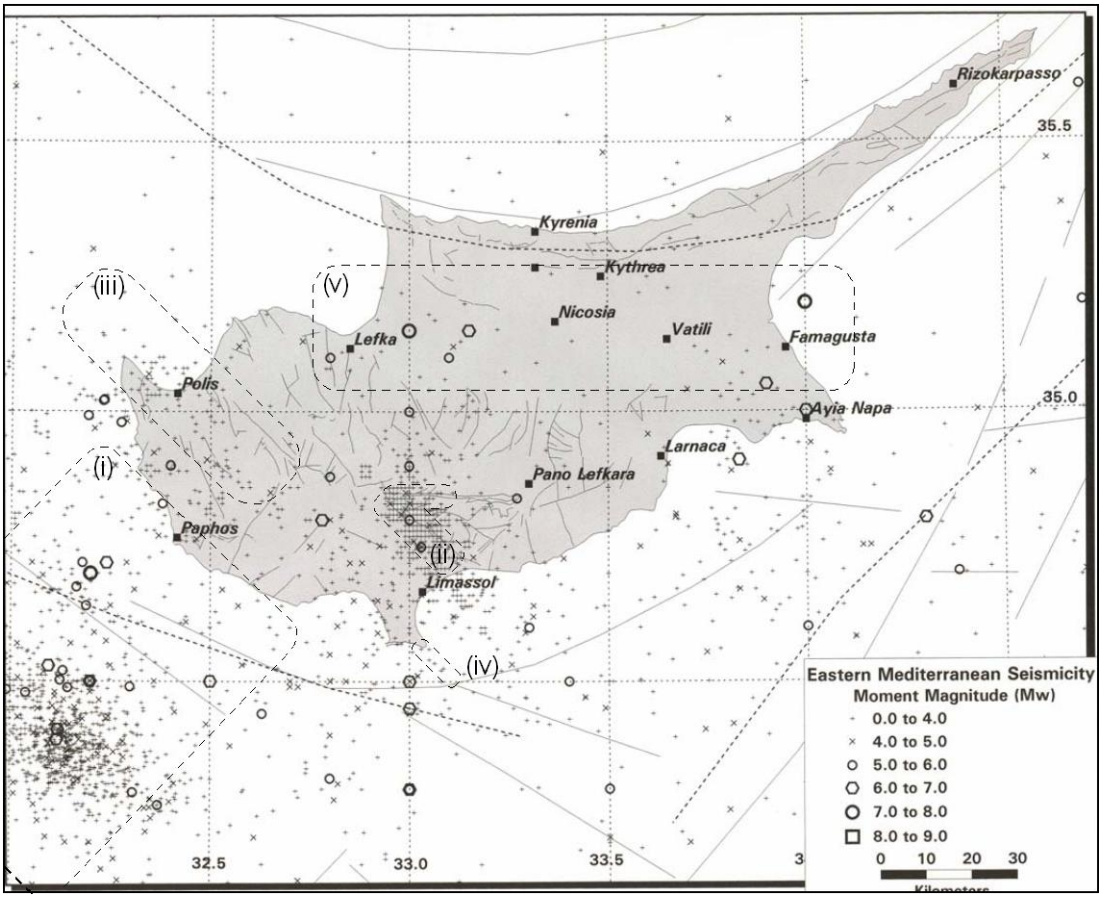

Figure 7-4: A map of all earthquakes in the historical record in the immediate vicinity of Cyprus (Algermissen and Rogers, 2004). The solid lines offshore depict faults inferred from bathymetric data and geophysical surveys (adapted from Neev et al, 1985); the dashed lines are inferred faults (U.S. Geological Survey, 2000). The faults on Cyprus are mapped and inferred faults of unspecified age (Geological Map of Cyprus, 1995).

Figure 7-4 illustrates that much of the seismicity in Cyprus is clustered: (i) a dense cluster of small to moderate earthquakes, striking NW-SE is located offshore SW Cyprus at the plate boundary between the Eratosthenes Seamount and the leading edge of Cyprus; (ii) dense clusters of small earthquakes occur along the Gerasa Fault Belt (striking NW-SE) and the Arakapas Fault Belt (striking E-W); (iii) a dense cluster of small earthquakes occurs in the Polis Graben, west Cyprus, and along strike offshore; (iv) a dense cluster of small earthquakes strikes north-northwest from the Akrotiri Gulf coast suggesting active crustal deformation in that region; several faults have been identified in that region (Soulas, 1999, 2001); and (v) several large earthquakes occur beneath the Mesaoria plain.

Papadimitriou and Karakostas (2006) compiled a list of earthquakes that have occurred in the Cyprus area, between 1896 and 1999; the focal mechanism solutions of which are shown in Figure 7-5. The Cyprus area is characterized by low-to-moderate seismic activity; the larger events are distributed unevenly along the arc, in three clusters (Wdowinski et al., 2006). The

clusters are located, from left to right, in (a) the northwestern corner of the plate boundary, (b) southwestern Cyprus, and (c) southeastern Cyprus. The northwestern cluster consists of 6 small events (M <5), indicating a variety of faulting styles (normal, reverse and transcurrent). The southwestern Cyprus cluster is characterized by strike-slip and thrust events reflecting a transpressional setting. The largest event in this cluster was the Mw = 6.8, 1996 Paphos earthquake, which has been modeled as a dextral failure on a NE-SW-plane at intermediate depth (76-85km; Arvidsson et al. 1998; Pilidou et al. 2004). The other solutions in this cluster correspond to smaller magnitude events (M < 6). The southeastern Cyprus cluster consists mainly of thrust events showing both N–S and NW–SE faulting direction of moderate size earthquakes (M < =6).

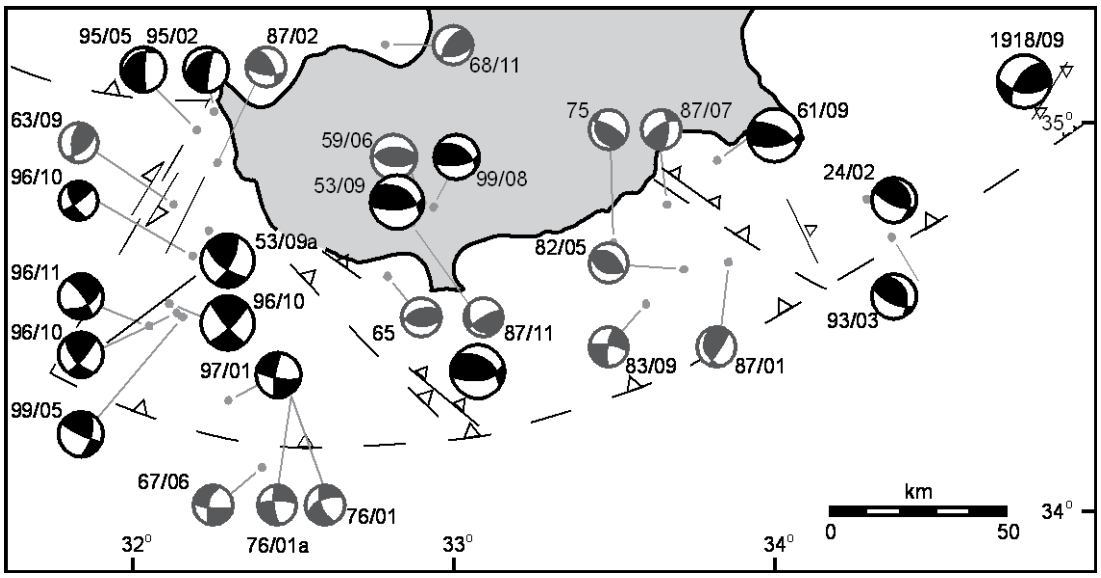

Figure 7-5: Focal mechanism solutions for earthquakes in the immediate vicinity of Cyprus (Papadimitriou and Karakostas, 2006). The numbers beside each focal mechanism solution give the occurrence year and month. The plate boundaries and offshore faults shown are as envisaged by Papadimitriou and Karakostas (2006)

The irregular seismicity along the western arc may be explained by two possible mechanisms: (i) Avridsson et al. (2004) suggest that strike-slip activity along an intermediate depth, NE-SW-trending tear fault (>30km) separates the 'arc' south and west of the island into two segments: subduction to the north of the tear fault and continental collision to the south; (ii) Papazachos and Papaioannou (1999) suggest that strike-slip activity occurs along a transform fault, which transfers the convergence in southwestern Cyprus to convergence in the Antalya Basin. According to their model, the western 'arc' is segmented and its northwestern segment is located about 100 km northeast of the western 'arc' assumed in this study. A similar model is proposed by Papadimitriou and Karakostas (2006). The transform

fault model of Papazachos and Papaioannou (1999) fails to explain the depth distribution of the seismic events along the western 'arc'. The recent study of Pilidou *et al.* (2004), which determines the epicentral depth of the 1996 events at a deeper level (76–85 km) would favour a tear fault model.

Discussion. Focal mechanisms calculated for deep and shallow earthquakes in the Cyprus area are indicative of a variety of faulting styles; thus, it is not possible to champion one model above another, based on earthquake data alone. It is important to note though, that the spatial distribution of earthquake epicentres suggests that the inferred plate boundary fault south of Cyprus (Figure 2-5; Figure 7-4), and structures mapped in west and southwest Cyprus (i.e. Polis Graben, Agia Marinouda Fold), south-central Cyprus (i.e. the Gerasa/Arakapas Fault Belts) and south Cyprus (i.e. the Larnaka Fault Zone) are active.

Does a Wadati-Benioff zone exist beneath Cyprus?

Figure 7-6 shows a map and cross-section of earthquakes located near Cyprus since 1997 with moment magnitude (Mw) $\geq$ 3.0 and depth $\geq$ 33 km (Algermissen and Rogers, 2004). A weakly defined northeast dipping hypocenter lineation suggests a Wadati-Benioff zone underlying Cyprus extending to at least 80 km depth. Algermissen and Rogers (2004) estimate the thickness of this zone to be 20km, which is somewhat larger than expected for oceanic crust (about 10 km). However, a similarly broad Wadati-Benioff zone is also observed in the Hellenic Arc (Rotstein and Ben-Avraham, 1985) and in the north-western part of the Cyprus Arc (Papazachos and Comninakis, 1978; Papazachos and Papaioannou, 1999). A similar slab trending in the same orientation is located 100 km northwest underlying the Antalya basin (Papazachos and Papaioannou, 1999).

In addition, a steep vertical zone of seismicity extending to a depth in excess of 60 km is located at the Cyprean Arc (Figure 7-6).

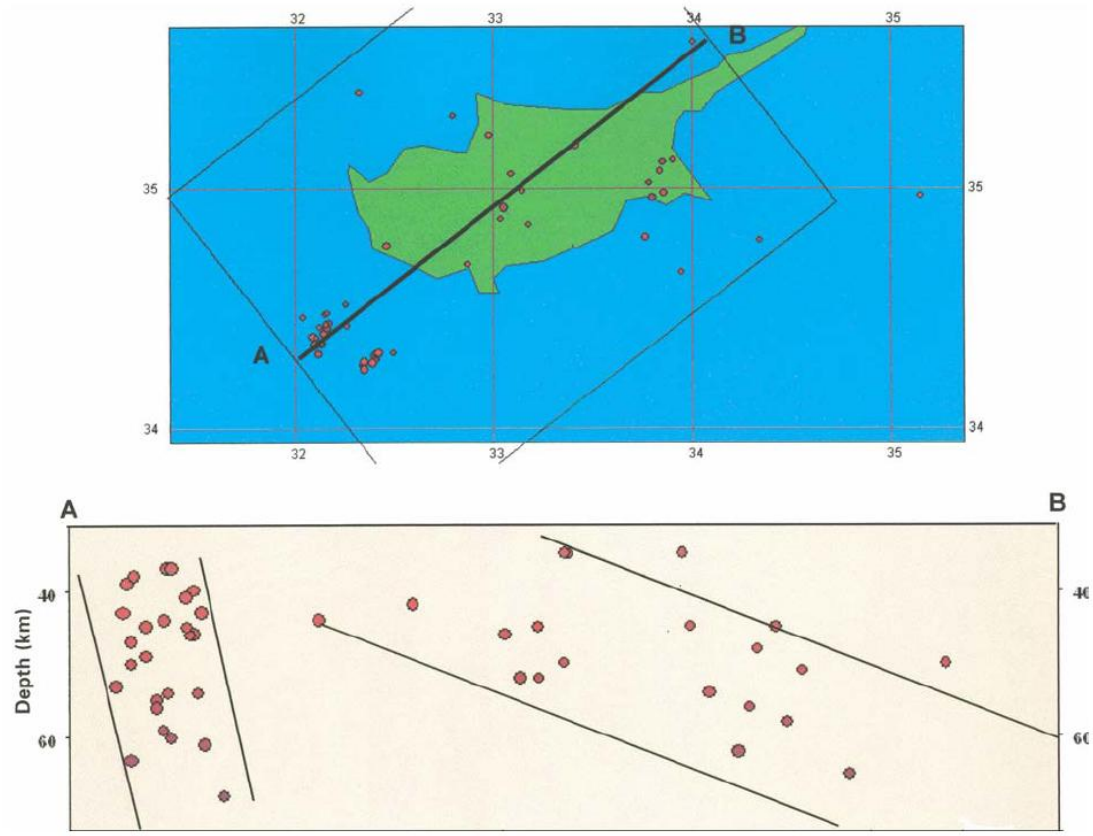

Figure 7-6: The map and cross-section shows the location and orientation of earthquakes located near Cyprus since 1997 with moment magnitude (Mw) ≥ 3.0 and depth ≥ 33 km. The box indicates the earthquakes included in the cross-section; earthquakes out with the line of section are projected onto the cross-section. The cross-sectional view is from the southeast looking northwest with 2×vertical exaggeration. Symbols are scaled by magnitude. The lines are interpretative positions of two possible Wadati-Benioff zones (Algermissen and Rogers, 2004)

Discussion: Subduction zones commonly have three principal seismic elements: (i) the mega-thrust (or subduction) zone, defined by large, shallow earthquakes, which accommodate reverse-slip as oceanic crust underthrusts continental crust (e.g. Alaska, St. Elias region (Doser and Lomos, 2000); Aleutian Arc, Attu Island (Lallemant, 1996); Appennines Arc (Doglioni et al., 2007)); (ii) the Wadati-Benioff zone, defined by intermediate- and deep-focus earthquakes, which accommodate normal and strike-slip faulting in the downgoing slab (e.g. Hellenic Arc (Doglioni et al., 2007); Central America Wadati-Benioff zone (Špičák et al., 2007)); and (iii) one or more transform faults, producing shallow earthquakes, which exist to accommodate horizontal slip between sections of the subducting oceanic crust (e.g. Aleutian Arc, Attu Island (Lallemant, 1996); SW Cyprus (Arvidsson et al., 1998; Pilidou et al., 2004; Wdowinski et al., 2006)).

As stated above, focal mechanisms derived for deep and shallow earthquakes in Cyprus are indicative of a range of faulting styles (i.e. reverse-slip, normal-slip and strike-slip focal mechanisms; Rotstein and Kafka, 1982; Arvidsson et al., 1998; Kalogeras et al., 1999; Papazachos and Papaioannou, 1999; Makris et al., 2000; Salamon et al., 2003; Pilidou et al., 2004). Recent seismicity indicates that the plate boundary between Africa and Anatolia may be divided into several segments (Wdowinski et al. 2006); (i) an eastern segment, characterised by strike-slip and normal fault events; (ii) a south-eastern segment, characterised by thrust events with both N-S and NNE-SSW fault directions; and (iii) a south-western segment, characterised by strike-slip and thrust events, reflecting a transpressional setting. The strike-slip focal mechanisms indicate dextral slip on a NE-SW plane; and (iv) a western segment, characterised by normal, reverse and transcurrent events. Therefore, it may be argued that most of the prerequisites for a subduction zone are met, i.e. low-angle thrust faulting in the 'forearc' (Figure 7-5; Papadimitriou and Karakostas (2006)), normal faulting due to down-bending of the slab south of the trench (Wdowinski et al. 2006) and, strike-slip faulting accommodating horizontal slip between sections of the subducting oceanic crust (Figure 7-5; Arvidsson et al., 1998; Pilidou et al., 2004). However, there is one exception; no large, shallow reverse-slip focal mechanism has been modelled, which would indicate that a megathrust zone exists. Many workers have suggested the presence of an active subduction zone in this region (e.g. Robertson, 1990; 2000; Eaton and Robertson, 1993; Payne and Robertson, 1995; 2000; Pilidou et al., 2004). An active Wadati-Benioff zone was identified beneath Cyprus by Algermissen and Rogers (2003; 2004). The absence of a megathrust zone does not necessitate the dismissal of a subduction zone model. It is entirely feasible that subduction is impeded while a previously subducted oceanic plate(s) beneath Cyprus continue(s) to break and generate earthquakes. The cluster of seismicity to the southwest of Cyprus may relate to an intermediate depth, NE-SW-trending tear fault (>30km) which separates the arc into two segments: subduction to the north of the tear fault and continental collision to the south. It would seem that as the Mediterranean seafloor 'subducts' beneath Cyprus it is subject to east-west shortening, due to the need to bend the slab beneath a curved plate boundary (Pilidou et al., 2004).

Cypriot and U.S. Geological Survey scientists believe that the vertical zone of seismicity located at the Cyprean Arc (Figure 7-6) is indicative of strike-slip faulting between the African and Anatolian plates. In their model, the cluster of focal mechanisms with a dextral solution (along a NE-SW plane) in the south-west and west of the plate boundary are thought to directly relate to the plate motion between Africa and Anatolia.

What is the plate motion of Cyprus, with respect to Africa and Anatolia?

New geodetic studies (Reilinger et al., 1997; Kahle and Mueller, 1998; Kahle et al., 1998; McClusky et al., 2000; Anzidei et al., 2001; Nocquet and Calais, 2004; Mahmoud et al., 2005) provide an accurate tectonic framework for understanding current plate movements and crustal deformation in the Eastern Mediterranean. In a fixed Africa/Sinai reference frame, at the western segment of the Cyprus Arc the Anatolian and African plates converge in a NE-SW to NNE-SSW direction (Figure 7-7).

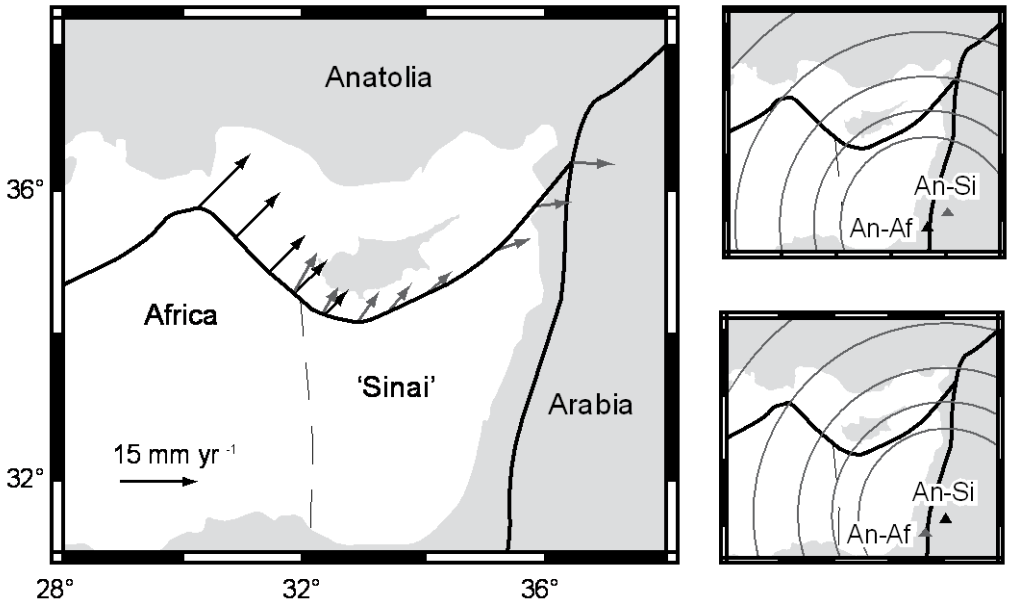

Figure 7-7: Predicted motion along the Cyprean Arc as calculated from Anatolian-Africa and Anatolia-Sinai poles (Wdowinski et al., 2006). The black arrows show the relative motion between Anatolia and Africa (Africa in fixed reference frame) and the grey arrows the relative motion between Anatolia and Sinai (Sinai in fixed reference frame)

The convergence rate is in the range of 9-14 mm yr^{-1} (Wdowinski et al., 2006). In the central segment of the Arc, Anatolia convergences with Sinai (Africa) at a slightly lower rate (7-8mm yr^{-1}) and in a more northernly direction than to the west (Wdowinski et al., 2006). This region, southwest of Cyprus, is seismically the most active region in the vicinity of the island and is characterized by compressional and NE–SW right-lateral strike-slip faulting (see above). In the eastern segment of the arc, the relative motion between Anatolia and Sinai is predominantly left-lateral with increasing extension towards the east. The calculated rates are in the range of 7–8 $mmyr^{-1}$ (Wdowinski et al., 2006). McClusky et al. (2003) derived higher rates (8– 10 mmyr−1) with a similar direction using Anatolia-African relative plate

motion (Eurasia in a fixed reference frame). Mahmoud et al. (2005) predict 8.9 ± 0.4 mm/yr of convergence along the western and central segments of the Cyprus Arc, and ~6.0 ± 0.4 mm/yr of left-lateral displacement along the eastern segment (Figure 2-4). A single GPS station is located on Cyprus (NICO): this station indicates that Cyprus is moving westwards with respect to Eurasia, in a similar direction and magnitude to the GPS sites in central Anatolia. Kahle et al. (1998) determined crustal deformation strain rates for the region comprising the Hellenic Arc, the Aegean Sea, western Anatolia and the Cyprus Arc. The Cyprus Arc is associated with slight to moderate arc-parallel compression (Figure 2-3a) within a weak transpressional setting (Figure 2-3b).

7.4 New evidence

New evidence from southern Cyprus, in the form of detailed geological maps at the 1:5,000 scale, reconnaissance maps at the 1:50,000 scale, a database of fault orientations and kinematics and a series of sedimentological logs has shed light on the tectono-stratigraphic framework of Cyprus. A review of the alternative models for the tectonic evolution of Cyprus would not be complete without a perusal of existing geological investigations, well log and geophysical data. Frequently, the hypotheses discussed below include data, or inferences based upon data, from published literature/reports; where this is the case, a distinction is drawn between my data and that of others.

7.4.1 Stratigraphic/sedimentological data

In the last chapter the sedimentary facies and basin architecture of the Pissouri Basin was reviewed. An attempt is now made to correlate between lithostratigraphic units in each of the Neogene basins of south and central Cyprus. A brief overview of each stratigraphic unit is provided, followed by a short description of the possible correlations between the Neogene basins. A related geochronological study combining palaeomagnetic and luminescence methods of dating is presented in section 7.4.3. The depositional age of each lithostratigraphic unit is appraised, so that one can better assess the uplift history of the Troodos Massif.

Lefkara Formation chalks and marls: In each region (Polis, Pissouri, Maroni-Psematismenos and Mesaoria) the transition from relatively uniform pelagic carbonate deposition (i.e. Lefkara Formation sediments) to varied carbonate and clastic sedimentation

(i.e. Pakhna Formation) marks the onset of basin deposition. This 'transition' is now widely accepted to have occurred in the Early Miocene (Aquitanian ~ 23 Ma); when a large influx of terrigenous material entered each basin.

Pakhna Formation chalks and calcarenites: The Lefkara Formation is overlain by the Pakhna Formation. The Pakhna Formation is characterised by foraminiferal chalk and marl channelled into (in the upper part of the succession) by conglomerates, massive calcarenites and minor, thin marlstones. In the marginal areas of each of the Neogene basins (Polemi, Pissouri, Maroni-Psematismenos and Mesaoria) Pakhna Formation chalk is locally intercalated with algal laminites and bioclastic calcarenites. Isolated carbonate mounds or reef knolls are present at the top of succession. Two reef limestone units are recognised in the Pakhna Formation: the Aquitanian – Burdigalian (c.23 – 16 Ma) Terra Member and the Tortonian (c. 12 – 7 Ma) Koronia Member (Follows and Robertson, 1990; Follows, 1992).

Correlations: Reefal facies of the Pakhna Formation are recognised in each of the Neogene basins (Eaton, 1987; Payne and Robertson, 1995). The model proposed for the formation of the Polis Graben, and development of the Polemi Basin, is based largely on the temporal and spatial distribution of reefs in W Cyprus (Payne and Robertson, 1995; 2000). In the region now known as the Polis Graben a broad basin is believed to have existed in the Aquitanian - the structurally higher basin margins were colonised by Terra Member reefs, while the basin was partly infilled with hemipelagic and redeposited carbonates of the Pakhna Formation. By the Tortonian, extensional faults had reconfigured the basin. Koronia Member reefs colonised localised highs (Follows, 1990), controlled by extensional faulting, on either side of a linear basin (that had narrowed since Terra Member time).

The channelled and slumped horizon in the upper part of the Pakhna succession at Pissouri is also recognised in the Maroni-Psematismenos Basin at Choirokoitia. Channelised calcarenites, polymict conglomerates and minor thin-bedded marlstones protrude as lenticular tongue-liked bodies for several kilometres into the Maroni-Psematismenos basin from the northwest/north-northwest. The age of the Choirokoitia channel network has, until recently, been a matter of debate. Submarine channels in the Maroni-Psematismenos Basin were first mapped by Bagnall (1960) during his work for the Geological Survey Department of Cyprus. Bagnall (1960) originally attributed the channels to the Pakhna Formation, due to their topographic position beneath the *Discospirina* band (a biostratigraphic marker for the upper Miocene within the Pakhna Formation, see section 2.2.4). Houghton et al. (1990)

investigated the channel fill further with the aid of biostratigraphical dating (calcareous nannoplankton and foraminifera), and stated that they were uppermost Pliocene in age and not Miocene. To account for their topographic position below the *Discospirina* Band, Houghton et al (1990) attributed them to be part of a canyon fill that was cut into the Paleocene-aged Lefkara Formation and Miocene-aged Pakhna Formation. Within the Maroni River valley, Schirmer (2000) identified, a succession of 10 individual channels cut into a sequence of basinal silty marlstones. Each channel ranges from 0.7-10 m in thickness and contains poorly sorted chalk, reworked coralline material and Troodos derived basic igneous clasts. Schirmer (2000) suggested that all facies associations within the Choirokoitia channel network (channel fill sands and conglomerates, basinal marlstones and marly chalk) are stratigraphically within the Pakhna Formation. Within the Choirokoitia-Psematismenos fan complex, Davies (2001) identified, six separate cycles comprised of coarse-grained conglomerates and breccias, representing periods of intense debrite activity. Each cycle is separated by relatively condensed beds of fine- to medium- grained calcarenites and marls, which Davies (2001) identified as low-density turbidites and the accumulation of background carbonate rain and fine-grained terrigenous material, during relative debrite quiescence. Davies (2001) suggested that the six cycles observed span an age of Lower Pliocene to mid-upper Pleistocene. Davies (2001) assumption was based on a biostratigraphic study of grey siltstones and fine-grained sandstone facies at Vasiliko, which were believed to represent the basinal equivalent of the Choirokoitia-Psematismenos fan complex. The Choirokoitia channel network has recently been dated using tetrapod assemblages (samples were collected from terrigenous muds which interfinger with the channels): a Middle to Late Miocene age of deposition was inferred due to the presence of *Stylda* (Late Oligocene to Recent), *Diacrolinia elidi* (Serravallian), *Diarria sangiorgii* (Tortonian to Messinian), *Clio pyramidata* (Late Miocene to Recent) and *Edithenella varaneca* (Langhian to Serravallian; Cyprus Geological Survey Department, personal communication).

The Pakhna Formation is thought to represent hemipelagic slope sedimentation, punctuated by influxes of turbidity currents, storm reworked shell detritus and mass-wasting of talus slopes (Eaton, 1987; Eaton and Robertson, 1993). The lower and middle parts of the succession reflect a shallowing of the Mediterranean Sea prior to the main phase of basin development in the late Miocene (Tortonian?). It is envisaged that tectonic adjustments in each basin led to instabilities on the slope and created localised channels and slumps. By the late Miocene (Tortonian), topographic highs surrounding the northern rim of each basin were

colonised by Koronia Member reefs. It is likely that the spatial distribution of Koronia Member reefs was controlled by early basin-bounding faults (Follows et al., 1996). Faulting is believed to have triggered erosion of the reefs, and led to the re-deposition of the material down-slope as calcarenites.

Kalavasos Formation evaporites/chalks, calcarenites and conglomerates: The Pakhna Formation is overlain by the Kalavasos Formation, composed of a variety of gypsum facies and/or lagoonal to lacustrine deposits (the 'Lago Mare sequence of the Kalavasos Formation': Orszag-Sperber et al., 1989; Rouchy et al., 2001). Gypsiferous deposits are recognised in all the Neogene basins, Lago Mare deposits are only recognised in the Pissouri Basin.

Correlations. Gypsiferous deposits are recognised in each of the Neogene basins (Orszag-Sperber et al., 1989; Payne and Robertson, 1995; Robertson et al., 1995b). Messinian successions described in the Polemi and Maroni-Psematismenos Basins by Orszag-Sperber et al. (1989) and Robertson et al. (1995b) share similar characteristics with the Pissouri succession described in chapter 6 (Figure 6-21): (i) in all three basins, a lower unit of gypsum, composed of a variety of fine-grained gypsum facies (e.g. laminar gypsum) is overlain by a disturbed horizon of slumped blocks and mega-breccias (e.g. detrital selenite and turbidites), in turn overlain by an upper unit of gypsum (e.g. gypsiferous marls, banded stacked and swallowtail selenite); and (ii) in the Polis and Pissouri Basins, the evaporitic sequence is underlain by a 3-6 m thick polygenic mega-breccia (described above). The slumped units and mega-breccias are attributed to catastrophic, tectonically induced events (i.e. slumping of the marginal gypsum towards the basin depocentre). Lacustrine and lagoonal deposits of the Lago Mare succession are only recognised in the Pissouri Basin; however, Payne and Robertson (1995) document evidence of Messinian emergence and local karst formation in the Polis Graben, which they believe correlate with the Lago Mare event.

The deposition of thick evaporites in each of the Neogene basins may be correlated with major evaporative drawdown and higher aridity throughout the entire Mediterranean; this event is believed to have occurred during the glacial period recorded in ocean sediments between 6.3 and 5.6Ma (first evaporitic stage; Rouchy and Caruso, 2006). The Messinian Salinity Crisis may have occurred slightly earlier and more intensively in the Easternmost Mediterranean than elsewhere, as the Cyprus 'Messinian' basins were dependent on water transit across the western Mediterranean. The deposition of the Lago Mare succession

(second evaporitic stage; Rocuhy and Caruso, 2006) correlates with an interval of warming and global sea level rise (5.6 - 5.5Ma); deposits of the Lago Mare are prevalent throughout the entire Mediterranean.

A Messinian extensional event is recognised in Kalavasos Formation and Lago Mare deposits in the Pissouri Basin. Further evidence of tectonism during the Messinian is noted in the Polis Graben (Payne and Robertson, 1995). In the northern part of the Polis Graben, Payne and Robertson (1995) documented evidence of emergence and local karst formation during the Messinian: on the flanks of the Polis Graben, fissured and potholed palaeo-karst surfaces, with up to 30 m of relief are developed on reef limestones of both the Upper Miocene Koronia Member (e.g. at Pelathousa village in the east; Figure 3-9) and the Lower Miocene Terra Member (e.g. at Drouseia village in the west; Figure 3-9; Payne and Robertson, 1995); in the axis of the graben, a less pronounced erosion surface may have developed on chalky talus or locally-derived conglomerates and breccias. Karst development is bracketed as Messinian in age, as it affects Tortonian limestones, and the karst fissures contain Lower Pliocene chalks (correlated with the *Sphaeroidinellopsis* Acme Zone; West, 1988 in Payne and Robertson, 1995).

New structural and sedimentological data collected at Evretou dam during the course of this study confirms Payne and Robertson's (1995) hypothesis. At the Evretou Dam spillway, Miocene and Pliocene units are juxtaposed along a ~ N-S-trending, W-dipping normal fault. A vertical displacement of 20-50 m is estimated. The Pakhna Formation is overlain by a 12 metre-thick succession of conglomerates and palaeosols (Figure 7-8). This succession is in turn overlain by Nicosia Formation marls.

The conglomerates and palaeosols are believed to be of Messinian age, due to an absence/lack of Troodos-derived clasts. Post-Messinian deposits in the Polemi Basin contain Troodos-derived clasts/material. Therefore, Messinian faulting controlled sediment supply, and preservation of material, within the Polemi Basin.

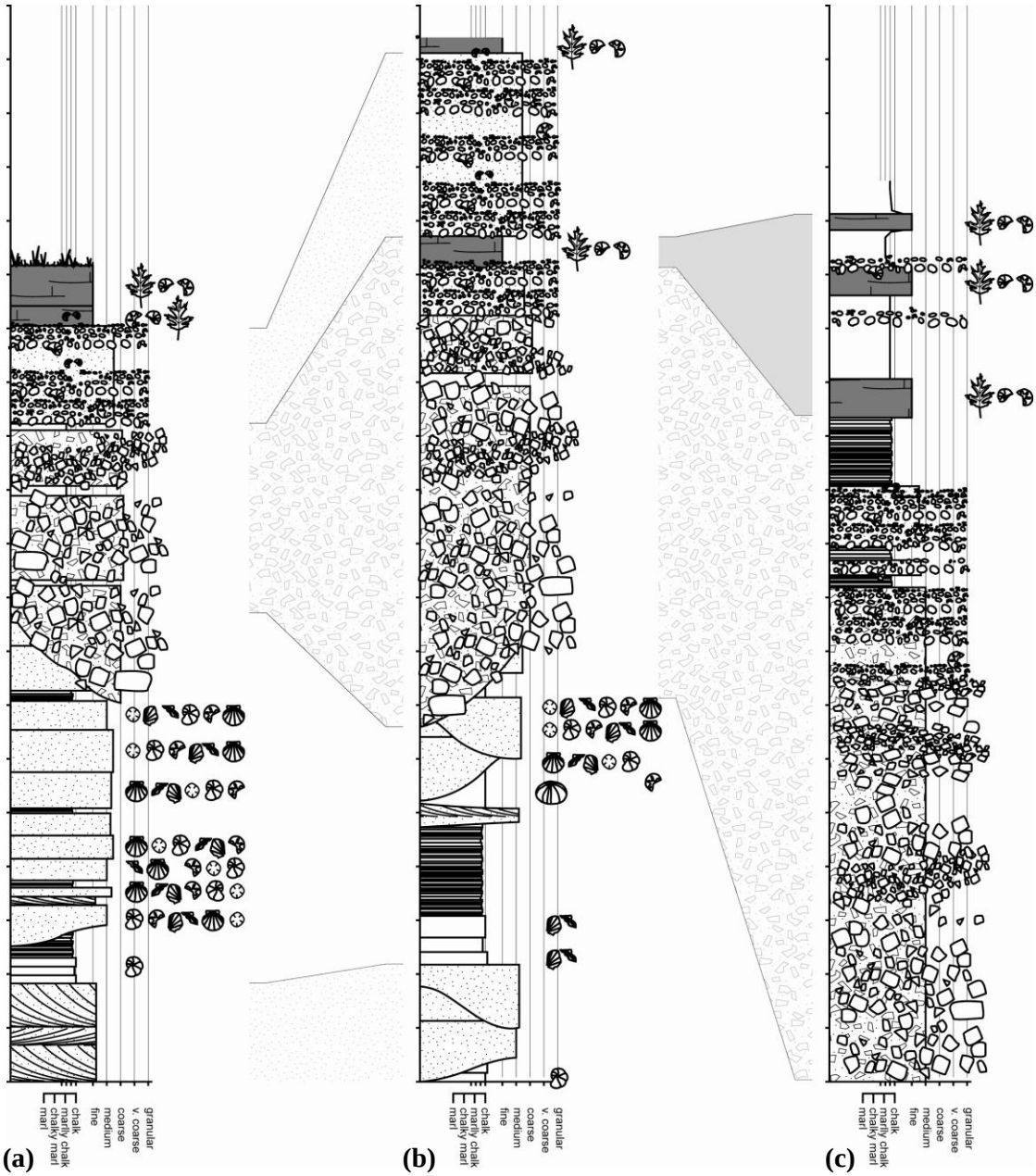

Figure 7-8: Sedimentary log of a Messinian sequence of conglomerates and palaeosols overlying Pakhna chalks, at Evretou Dam. Logs (a) and (b) were recorded at the Evretou Dam spillway. Log (c) was recorded on the northern boundary of the Evretou Dam reservoir. A key to sedimentary logs is shown in Appendix A.

Nicosia Formation chalk, marl and calcarenites: The Kalavasos Formation is overlain by the Nicosia Formation. Pliocene marine marls are recognised in all the Neogene basins. The component members of the Nicosia Formation are different to the north and south of the Troodos Massif.

Correlations. The Nicosia Formation is comprised predominantly of regularly bedded marls and pure white micrites, with thin sand- and silt-stones interbeds. This dominant facies is recognised in all of the Neogene Basins: furthermore, in each basin it can be sub-divided into three units – a lower unit of regularly bedded marls and micrites, a middle unit comprised of regularly bedded marls and siltstone/sandstone beds and, an upper unit characterised by medium- and thickly-bedded marl interbedded with siltstones and sandstones. The lower unit is interpreted as the product of low-energy pelagic sedimentation. The middle unit represents the influx of terrigenous turbidites derived from an uplifting Troodos Massif, with the increase in thickness and proportion of turbidites reflecting increased uplift and/or tectonic adjustments at the basin margin (Stow et al., 1995). The upper unit represents a pronounced shallowing of the individual basin, as indicated by distinctly less turbiditic sands entering the basin.

In the Polis Graben, the lower part of the Pliocene succession is typically fine-grained, and consists of pink chalks rich in planktonic foraminifera, which pass up into muddier chalks and marls (Payne and Robertson, 1995). On the flanks of the graben, the pink chalks fill fissures of Messinian age developed in the underlying Miocene limestones (Payne and Robertson, 1995). Above this basal unit, on the flanks of the graben, grey and white chalks are interbedded with fine-grained calcarenites, whilst muddier facies of chalk and marl are noted in the axis of the basin. The upper part of the succession is marked by the first occurrence of coarse-grained material in calcarenitic horizons (interbedded with muddy and sandy marls). Coarse-grained bioclastic calcarenites are coeval with this unit.

The component members of the Nicosia Formation are different to the north and south of the Troodos Massif. Two fan-delta systems are recognized in the Plio-Pleistocene deposits of the Mesaoria Basin (McCallum and Robertson, 1995a). The oldest of these is the Nicosia fan-delta (Nicosia Formation). Sub-facies internal to this unit are similar to those observed in the Pissouri Basin. The youngest of these is the Kephales fan-delta (Kephales Member, formerly the Kakkaristra Formation). The Kephales Member of the Nicosia Formation is a sequence of fan-delta deposits which include ‘Gilbert-type’ marine delta, bay and lagoonal deposits, and consists of a series of siltstones, cross-bedded conglomerates and fine-grained sands (with conglomeratic intercalations) (McCallum and Robertson, 1995a; Panayides et al., 2004). This unit is not recognized in the Polemi, Pissouri, Maroni-Psematismenos Basins. Shallow-marine bioclastic sandbodies migrated across the Mesaoria Basin in Upper Nicosia time. These sandbodies are comprised of fossiliferous medium- to coarse-grained, cross-

bedded sandstones, separated by sandy fossiliferous marls, are assigned to the Athalassa Member of the Nicosia Formation (formerly the Athalassa Formation). In both the Pissouri and Polemi Basins, cross-stratified, bioclastic-rich sandstones are observed in the upper part of the Nicosia Formation. It is believed that the bioclastic sandstone bodies in each of the Neogene basins are broadly correlative, indicating that distinct palaeoenvironmental/palaeogeographical conditions occurred throughout Cyprus in the Late Pliocene/early Pleistocene.

Apalos Formation gravels, Fanglomerate Group gravels and Terra Rosa soils: The Nicosia Formation is overlain alternatively by stacked micro-Gilbert-type fan deltas (Pissouri Basin), Fanglomerate Group gravels (Polemi and Maroni-Psematismenos Basins) and Apalos Formation gravels (Mesaoria Basin).

In the Pissouri Basin, stacked micro-Gilbert-type fan deltas prograded into the Pissouri region in Upper Nicosia time. Individual Gilbert deltas can be seen to prograde in a generally S to SE direction for a distance of 4 km. Stow et al. (1995) envisage that the basin was first flooded by a major influx of terrigenous sediment via a well-supplied fan delta, which rapidly prograded across the margin of the basin. In the Polemi and Maroni-Psematismenos Basins, the Nicosia Formation is unconformably overlain by the Pleistocene Fanglomerate Group, a series of coarse poorly sorted fluvial conglomerates (Ducloz, 1965; Poole, 1992; Poole and Robertson, 1998). Fanglomerate Group deposits contain well-rounded clasts, up to 40cm in diameter, of mainly Troodos-derived material, set in a sandy matrix (Poole and Robertson, 1998). In the Mesaoria Basin, the Nicosia Formation is overlain by a succession of continental fluvial deposits and palaeosols of the Apalos Formation; a stacked sequence of basal channel-gravel, channel-fill sand and gravel, overbank sand, silt, and clay, and finally a palaeosol horizon.

Correlations. No direction correlations can be made between the lithostratigraphic units which overlie the Nicosia Formation in each Neogene basin. However, all units imply a pronounced period of uplift of the Troodos Massif immediately post-dating Upper Nicosia time. Magnetostratigraphies were generated in the Mesaoria and Pissouri Basins to futher constrain this episode of uplift (see section 7.4.3).

7.4.2 Structural data

In chapter 3 the Cenozoic tectonic framework of the south coast of Cyprus was reviewed. This included an appraisal of fault kinematics in each of the Neogene basins and adjacent areas, so that the deformation history of each could be established. In addition, the author documented E-W-, NNE-SSW- and NNW-SSE-trending strike-slip faults in the Lemesos and Larnaka districts and a WNW-ESE-trending fold in the Paphos District. In this section, the aforementioned structures are considered in light of regional tectonics so that a model can be developed for the Cenozoic tectonic evolution of the island. The descriptions given below utilise a comprehensive set of new structural data, but also draw upon existing literature/publications. A distinction is drawn between my data and the work of others.

7.4.2.1 The Neogene basins

The Polis Graben: The northern and southern parts of the Polis Graben both have distinct palaeogeographies and deformation histories. The development and spatial distribution of Koronia Member (Tortonian) reefs along linear trends in the north Polis Graben was cited as evidence by Payne and Robertson (1995) that topography and sedimentary deposition was controlled by faulting (see section 7.4.1; ***Pakhna Formation chalks and calcarenites.*** *Correlations*). An analysis of the sedimentary facies and spatial distribution of the Koronia Member on the eastern margin of the graben by Follows (1990) led him to suggest that reef development migrated progressively up-slope (i.e. towards the north). There is no evidence of Tortonian reef growth in the southern part of the Polis Graben at this time (Follows, 1990). Based on these data, Payne and Robertson (1995) proposed that faulting and graben development initiated in the north of the Polis Graben in the Tortonian then migrated southwards. The existing fault-controlled topography of basins and highs resulted in localised evaporite precipitation (Robertson et al., 1995b).

North Polis Graben. The Messinian in the northern part of the graben was characterised by local emergence, as evidenced by karst formation and the deposition of locally-derived fluvial and sub-aerial deposits (see section 7.4.1; ***Kalavasos Formation evaporites/chalks, calcarenites and conglomerates***). Evaporites are neither exposed, nor known from boreholes (1:250,000 scale Geological Map of Cyprus, Cyprus Geological Survey (1995); Payne and Robertson, 1995). In axial parts of the basin, such as at Evretou dam, a Messinian-age topography of sub-aerially exposed active fault scraps and associated talus and

conglomerates is preserved. Payne and Robertson (1995) believe that the contrast between karst development on the flanks of the graben and fluvial-dominated erosion and deposition in the graben axis indicate that the basin was a topographically distinct faulted basin.

South Polis graben. The Messinian in the southern part of the basin was characterised by evaporite deposition, as indicated by the deposition of laminated gypsiferous marls and selenitic gypsum (see section 7.4.1; ***Kalavasos Formation evaporites/chalks, calcarenites and conglomerates***). Slumped and re-deposited gypsum horizons indicate active faulting on, or near the margins, of the basin during evaporite deposition. A slumped interval, ~ 20 m thick, was identified in the middle of the Messinian succession by Orszag-Sperber et al. (1989) and Robertson et al. (1995b). The transverse structures mapped at Evretou Dam and Pegeia could have been active in the Tortonian and early Messinian and acted as a barrier to southwards fault propagation. The transverse structure apparently formed a topographic high during the Messinian against which the evaporites of the Polemi sub-basin (Messinian basin) thinned abruptly (Payne and Robertson, 2000).

In the present study three deformation events were recognised in the Polis Graben: the first, a *Late Miocene extensional event (D1)*, led to the formation of NNW-SSE- to N-S-striking faults; the second, a *Pliocene extensional event (D2)*, led to the formation of WNW-ESE-striking faults; the third, *a Pleistocene/Holocene compressional/transpressional event (D3)*, led to reactivation of D1 and D2 strucutres. Figure 7-9 summerises the structural data that led to the recognition of the Late Miocene extensional event. Figure 7-10 summerises the structural data that led to the recognition of the Pleistocene compressional/transpressional event. Fault plane solutions, often used as a first approximation of stress (e.g. Marrett and Allmendinger, 1990), suggest that the stress regime responsible for generating the NNW-SSE- and NNE-SSW-striking faults was characterised by broadly east-northeast/west-southwest extension, with a maximum principal stress (σ_1) orientated vertical (049/86˚) and intermediate and minimum principal stresses (σ_2 and σ_3) orientated sub-horizontal (161/02˚ and 251/04˚, respectively).

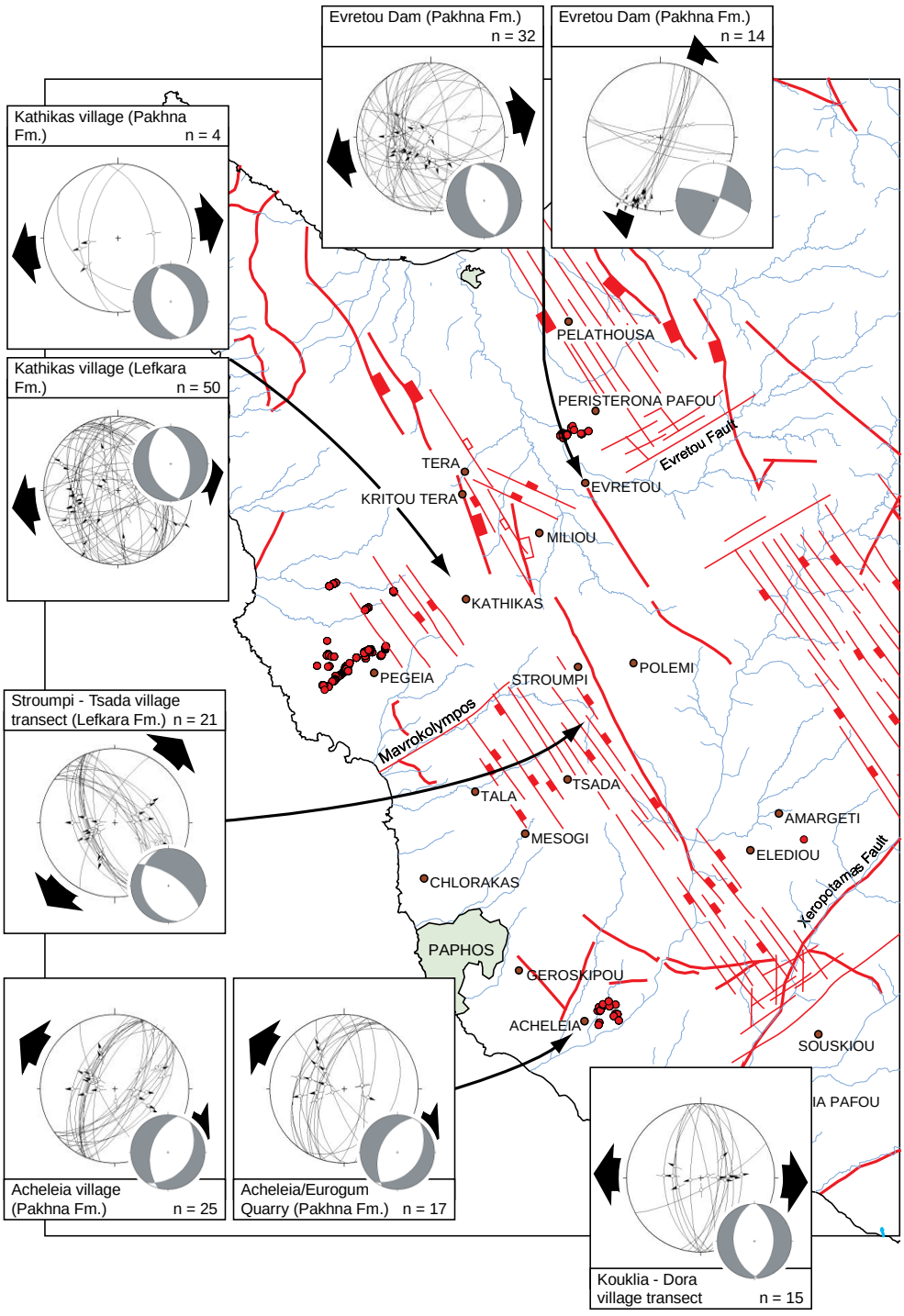

Figure 7-9: Late Miocene extension in the Polis Graben: structural data collected throughout the Graben alludes to a period of extension in the Polis region. This event is broadly constrained to the late Miocene (see discussion in text). The faults shown in this figure are as mapped by Payne and Robertson (1995); many as yet, have not been ground-truthed by the author

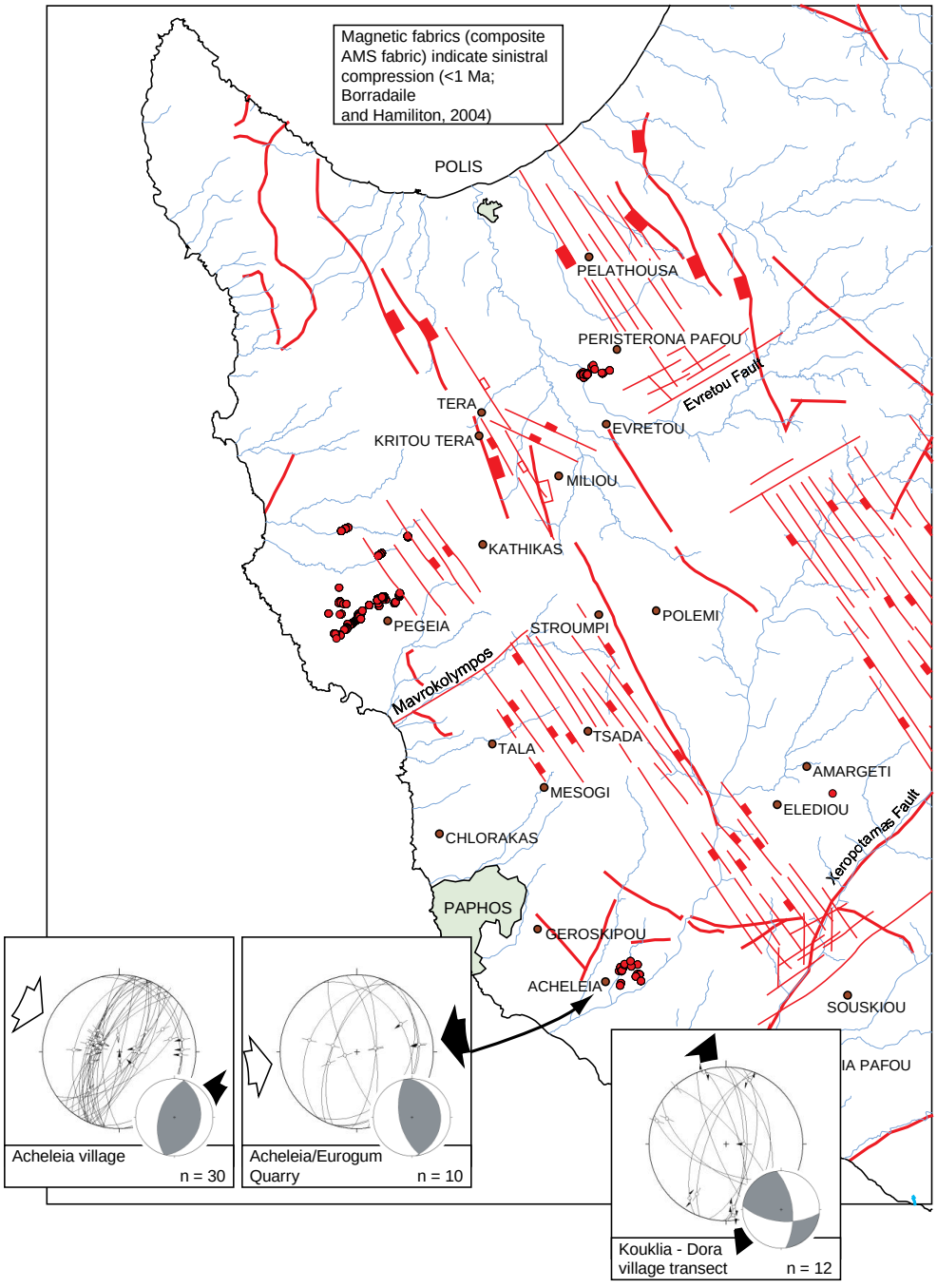

Figure 7-10: Post-Miocene compression: structural data collected throughout the Polis Graben alludes to a period of compression in the Polis region. This event is broadly constrained to the Pleistocene/Recent (see discussion in text). The faults shown in this figure are as mapped by Payne and Robertson (1995); many as yet, have not been ground-truthed by the author

Pegeia. Payne and Robertson (1995; 2000) proposed that the topography of the area to the south and west of the Polis Graben, the Pegeia region, (Figure 3-1) was controlled by a system of mainly southerly dipping, WNW-ESE normal faults, which bound a series of down-faulted blocks of latest Cretaceous to Pliocene chalks, i.e. a half-graben (Figure 3-10; cross-section b).

This interpretation was challenged based on reconnaissance mapping in the area (see chapter 3). The author has identified three populations of faults within the Pegeia-Mesogi region: NNW-SSE-striking normal faults; WNW-ESE-striking normal faults; and NNE-SSW-striking sinistral faults. Fault orientations and kinematics identified during the present study differ from those measured by Payne and Robertson (1995): the most significant is that WNW-ESE-striking, NNE-dipping faults are more prevalent than WNW-ESE-striking, SSW-dipping faults. In a half-graben configuration, it would be expected that the latter fault population would be more dominant (i.e. extensional collapse towards the sea). The presence of NW-SE- and WNW-ESE-striking normal faults in both the Polis Graben and Pegeia region imply that both areas were subject to the same tectonic processes.

Payne and Robertson proposed the following chronology for tectonic events in the west of Cyprus:

(i) Faulting in the northern part of the Polis Graben began in the Tortonian;
(ii) The main period of fault activity, with NNW-SSE-striking faults and an apparent ENE-WSW extension direction, occurred during the early to mid-Messinian. Faulting initiated in northern part of the Graben in the early to mid-Messinian and in the southern part of the Graben in the mid-Messinian;
(iii) Faulting continued with the same extensional orientation into the earliest Pliocene in the southern part of the Polis graben. Activity in the northern part of the Graben ceased in the mid- to late Miocene;
(iv) A period of relative tectonic quiescence occurred in the Early to mid-Pliocene;
(v) Latest Pliocene or Early Pleistocene inferred NNE-SSW extension direction led to the formation of WNW-ESE-striking faults. This phase of faulting was responsible for the development of the Pegia half-graben to the west of the Polis graben, in what previously had been a stable block.

The Pissouri Basin: The Pissouri Basin was established as a tectonically driven depocentre in the Burdigalian (Stow et al., 1995), in response to the beginning of uplift in Cyprus. A model for the tectonostratigraphic evolution of the Pissouri Basin is given in chapter 6; distinct palaeogeographies and deformation events are recognised in each stratigraphic interval. Koronia Member reefs colonised the northern margin of the Pissouri Basin. Reef facies are now preserved at only one locality, Happy Valley (Eaton and Robertson, 1993; Follows et al., 1996). Abundant reef-derived talus, along with ophiolite detritus (see section 7.4.1; ***Pakhna Formation chalks and calcarenites***) is preserved in channel deposits within the upper part of the Pakhna Formation succesion. It is envisaged that faulting at the margin of the basin led to the erosion and subsequent re-deposition of Koronia Member detritus down slope as turbidites (see chapter 6). A channelised/slumped chalk body at Sotira Lemesou, in the east of the Pissouri Basin was dated using tetrapod assemblages: a Late Miocene (Serravallian to Tortonian) age of deposition was inferred due to the presence of *Vaginella acutissima* (Langhian to Serravallian) and *Diarria sangiorgii* (Tortonian to Messinian) (Cyprus Geological Survey Department, personal communication).

Tortonian faulting controlled the spatial distribution of gypsiferous deposits. Outcrop and borehole data indicate that Messinian deposits are restricted to the northern margin of the Pissouri Basin (see section 7.4.1; ***Kalavasos Formation evaporites/chalks, calcarenites and conglomerates***). Locally, the gypsiferous succession is underlain by a 3-6 m thick polygenic mega-breccia, comprised of a chaotic accumulation of centimetre- to metre-scale blocks of calcarenite, selenitic gypsum and diatomites (Orszag-Sperber et al., 1989). Selenitic gypsum precipitated in shallow-water lagoons around the northern rim of the Pissouri Basin, was subsequently reworked and redeposited down-slope as mega-breccias. It is envisaged that faulting at the margin of the basin controlled this process. Slumped and redeposited gypsum in the basin are indicative of active faulting within, or on the margins of, the basin during evaporite deposition. A slumped and brecciated interval was identified in the middle of the evaporite succession (Orszag-Sperber et al., 1989; Robertson et al., 1995b). Dissolution of the underlying gypsum led to collapse and syn-sedimentary deformation of the latest Messinian Lago Mare interval and the lowermost Pliocene deposits. Locally, Pleistocene Fanglomerate deposits are affected.

In the present study four deformation events were recorded in the Pissouri Basin (Figure 6-23): *Late Miocene (Serravallian-Tortonian) east-west extension (D1a):* ~ N-S- and NW-SE-trending normal faults were generated during this event. N-S orientated faults are

believed to have influenced the spatial distribution of Serravallian – Tortonian channels (Pakhna Formation) and Tortonian reefs (Koronia Member). Borehole data has revealed that the deposition, and subsequent preservation of, Messinian evaporates (Kalavasos Formation) was controlled by Tortonian-Messinian faults. Fault plane solutions suggest that the stress regime responsible for generating the N-S- and NW-SE-striking faults was characterised by broadly east/west to east-northeast/west-southwest extension, with a σ_1 orientated vertical (216/90°), and σ_2 and σ_3 orientated sub-horizontal (350/07° and 051/07°, respectively); *Messinian extension (D1b):* ~ NNW-SSE- and NNE-SSW- and NE-SW-trending normal faults formed during this event. Latest Messinian extension, controlled by dissolution and collapse of the gypsum deposits, formed ~ NNW-SSE-, NNE-SSW- and NE-SW-trending normal faults; *Pleistocene compression/transpression (D3)*: Early – middle Pleistocene compression/transpression led to the reactivation of ~N-S-striking D1 structures. ~N-S-trending structures at the western margin of the basin are believed to have been reactivated in dextral transpression. Principal stress calculations suggest the stress regime responsible for the reactivation of the N-S- and NW-SE-striking faults was characterised by NNE-SSW transpression, consistent with an approximate northeast-orientated σ_1 (059/01°) and an approximate northwest-orientated σ_3 (328/43°); *Late Pleistocene/Holocene extension (D4):* Late Pleistocene/Holocene dissolution and collapse of the Kalavasos Formation has led to extension in the overlying Lago Mare Member, Fanglomerate Group and Terra Rosa soils. The similar orientation of faults in the Kalavasos Formation and the overlying deposits has led the author to suggest that early Tortonian/Messinian structures (D1/D2) partly controlled the spatial distribution of post-Messinian faults. It is believed that faults in the evaporitic succession acted as conduits for groundwater; hence dissolution cavities trend in a similar orientation to Messinian fault traces. Collapse structures are associated with the margins of these cavities.

The Maroni-Psematismenos Basin. The Maroni-Psematismenos Basin was established as a tectonically driven depocentre in the Early to Mid- Miocene, in response to the beginning of uplift in Cyprus. A number of distinct palaeogeographies and discrete deformation events are recognised in the Maroni-Psematismenos Basin. Koronia Member reefs are believed to have colonised the northern margin of the Maroni-Psematismenos Basin. A submarine channel network at Choirokoitia village records the first emergence and erosion of the Troodos Massif. Here, large channels contain poorly sorted chalk (Lefkara and Pakhna Formation) reworked coralline material (Koronia Member-type) and Troodos derived basic igneous clasts. The Choirokoitia channel network was recently dated using tetrapod assemblages; a

Middle to Late Miocene age (Serravallian to Tortonian) was inferred (Geological Survey Department of Cyprus, personal communication). A number of WSW-ENE-striking normal faults were identified in the Choirokoitia region by Bagnall (1960). Facies analysis indicates that these faults were responsible for positioning and maintaining the palaeo-slope gradient during debrite sedimentation in this area.

Tortonian faulting controlled the spatial distribution of gypsiferous deposits. In the Tochni-Maroni-Psematismenos area, extensional faults dissect the gypsiferous deposits into smaller segments. A conjugate system of fractures at Maroni, acted as conduits to super-saline, strontium-enriched groundwater (Figure 7-11). Celesite mounds developed at the intersections of the fractures (Figure 7-11; A.H.F. Robertson, personal communication). The celesite mounds are dated as Messinian in age (A.H.F. Robertson, personal communication); hence the fractures must be the same age.

Figure 7-11: Evidence of Messinian extension: (a) a conjugate system of fractures acted as conduits for super-saline, strontium-enriched waters; (b) selenite crystals within one such fracture; (c) celesite mounds develop at the intersection of the fractures; (d) detail of a celesite mound (B. Bailey for scale)

Localised slumped units and re-deposited units within the evaporate succession are indicative of localised faulting, within, or on the margins of, the basin during evaporite

deposition i.e. the middle to late Messinian. A slumped and brecciated interval was identified in the upper part of the evaporite succession (Orszag-Sperber et al., 1989; Robertson et al., 1995b).

A Pleistocene-Recent compressional/transpressional deformation phase has been recognised in SW Cyprus; it is believed that NE-SW-striking faults observed cutting Miocene and Messinian strata in the Maroni-Psematismenos Basin were reactivated during the same event. Many of the slickensided surfaces that occur in association with the NE-SW faults have two slickenlines preserved: steps associated with the development of the slickenlines indicate that one displacement was normal dip-slip, and that the other was reverse oblique-slip. In addition, a number of compressional and transpressional structures were identified in the Maroni-Psematismenos Basin. Top to the NW thrusting is observed in Messinian marls/gypsum, in a roadcut near to northern entrance to Psematismenos village (Figure 7-12). Soulas et al. (2005) identified an active structure, the NNW-SSE-trending Maroni River Fault, in the axis of the Maroni-Psematismenos Basin. Its presence was inferred based on a number of field observations (Soulas et al., 2005): (i) lateral facies variations and thicknesses were noted on either side of the Maroni River valley (i.e. basinal facies juxtaposed against reefal facies); (ii) different structural geometries are observed on either side of the river valley (i.e. orthogonal and oblique faults occur to the E; faults are largely absent to the W); and different rates of uplift are inferred on either side of the river valley (i.e. stronger Quaternary uplift has occurred in the east producing marine terraces at a higher elevation, and less poorly developed than in the west). Soulas et al. (2005) estimate a slip rate of 0.2mm/yr.

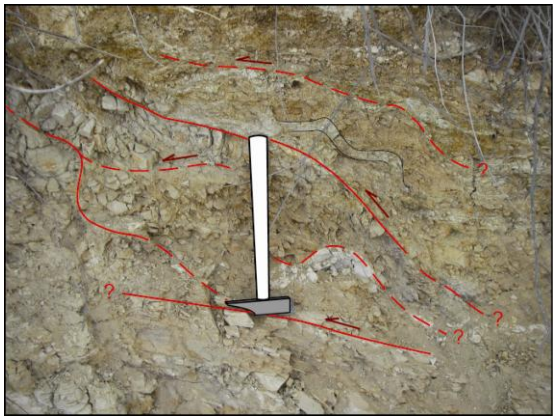

Figure 7-12: Evidence of post-Messinian compression: top to the NW thrusting in Messinian marls/gypsum (hammer for scale). Several of the more prominent fault planes are picked out in red. Photograph taken looking NNE

In the present study three deformation events were recorded in the Maroni-Psematismenos Basin: *Late Miocene (Serravallian-Tortonian) northwest-southeast east-west extension (D1a):* NE-SW-trending normal faults were generated during this event. Fault plane solutions suggest that the stress regime responsible for generating the NE-SW-striking set of faults observed cutting Miocene strata (pre-Messinian) in south Cyprus was characterised by broadly northwest/southeast extension, with σ_1 orientated vertical (332/82°), and σ_2 and σ_3 orientated sub-horizontal (074/01° and 164/06°, respectively); *Messinian extension (D1b):* ENE-WSW-trending normal faults formed during this event. A conjugate system of WNW-ESE- and N-S-stiking fractures controlled fluid pathways in the Messinian Maroni-Psematismenos Basin; *Pleistocene compression/transpression (D3)*: Early – middle Pleistocene compression/transpression led to the reactivation of ~NE-SW-striking D1 and D2 structures.

Figure 7-13 summerises the structural data that led to the recognition of the Late Miocene extensional event. Figure 7-14 summerises the structural data that led to the recognition of the Pleistocene compressional/transpressional event

Figure 7-13: Outline map of the Maroni region: structural data collected throughout the Maroni-Psematismenos Basin alludes to a period of extension in the Maroni region. This event is broadly constrained to the Late Miocene (see discussion in text). The faults shown in this figure are as mapped by the Geological Survey Department of Cyprus

Figure 7-14: Outline map of the Maroni region: structural data collected throughout the Maroni-Psematismenos Basin alludes to a period of compression in the Maroni region. This event is broadly constrained to the Pleistocene (see discussion in text). The faults shown in this figure are as mapped by the Geological Survey Department of Cyprus

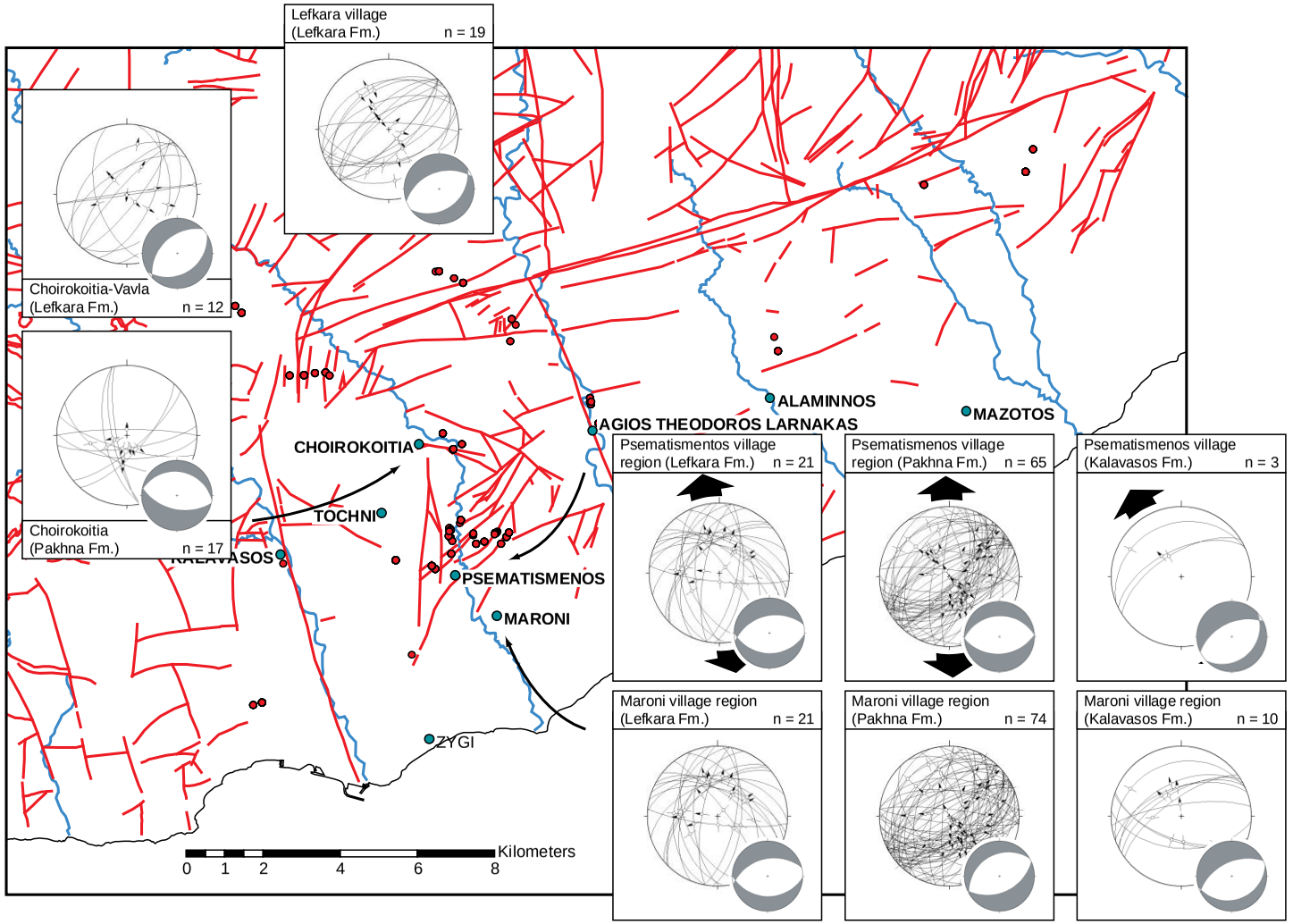

Figure 7-13: Outline map of the Maroni region: structural data collected throughout the Maroni-Psematismenos Basin alludes to a period of extension in the Maroni region. This event is broadly constrained to the Late Miocene (see discussion in text). The faults shown in this figure are as mapped by the Geological Survey Department of Cyprus

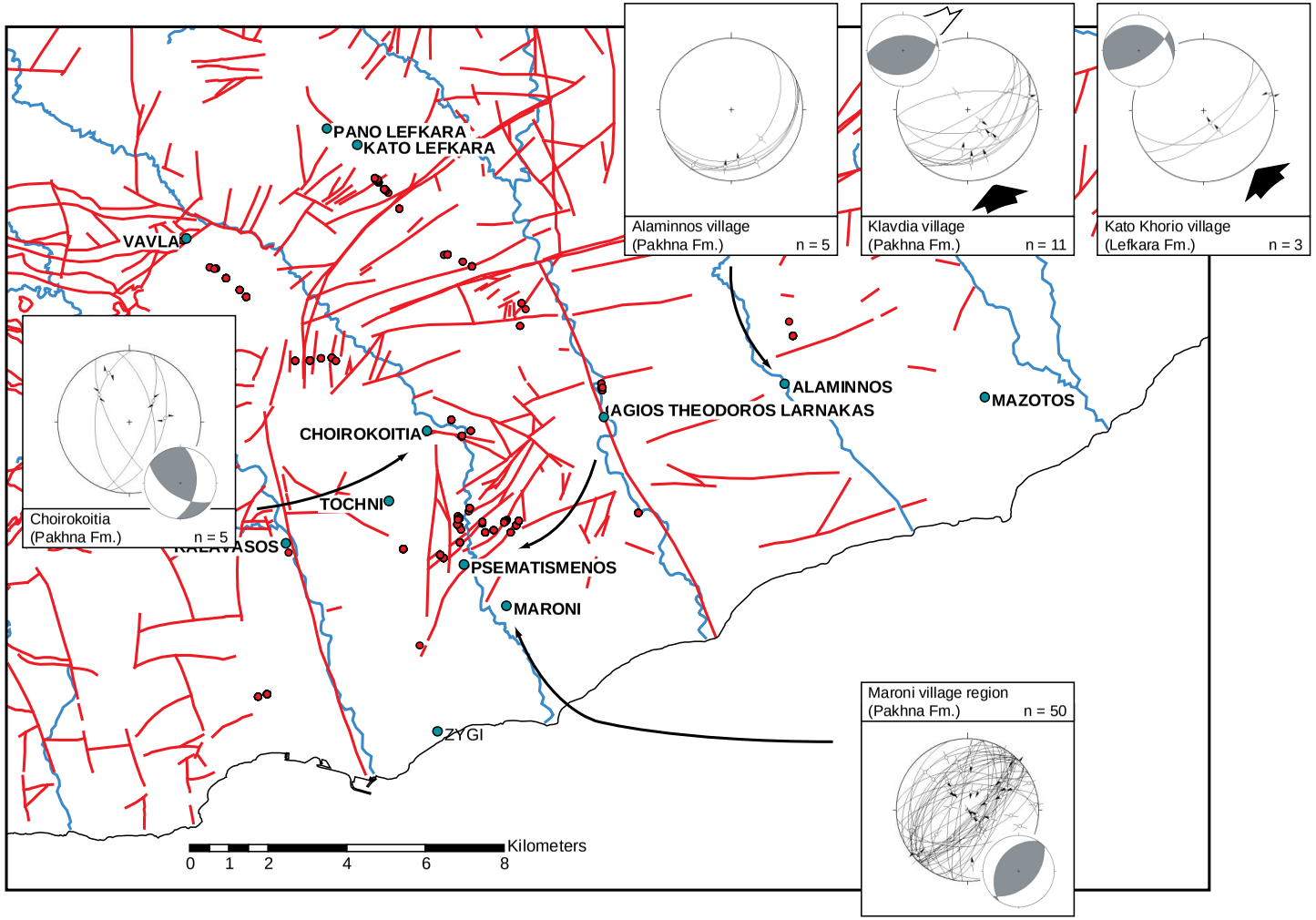

Figure 7-14: Outline map of the Maroni region: structural data collected throughout the Maroni-Psematismenos Basin alludes to a period of compression in the Maroni region. This event is broadly constrained to the Pleistocene (see discussion in text). The faults shown in this figure are as mapped by the Geological Survey Department of Cyprus

Mesaoria Basin: The Mesaoria Basin is a W-E-trending depocentre located in central Cyprus, between the ophiolitic Troodos Massif to the south and the Kyrenia range to the north. In early work, the Mesaoria Basin and its marine extensions were viewed as an arcuate Neogene depocentre situated within the central portion of a broad S-verging fold/thrust system (Weiler, 1969; Biju-Duval et al., 1978; Sage and Letouzey, 1990). More recently, McCallum and Robertson, (1990), Follows and Robertson (1990), Robertson et al. (1991) and Robertson (1998a) proposed that the basin formed as an asymmetric half-graben, during a phase of forearc extension that initiated in the Oligocene and lasted until the middle Pliocene (Figure 7-15a). Lately, Calon et al. (2005a,b) proposed that the basin and its marine continuation evolved from the Eocene–Oligocene to Recent as a large piggy-back basin nestled between the active fronts of the Troodos-Larnaka culmination and the Kyrenia fold/thrust belt (Figure 7-15b). Harrison et al. (2004a) propose that the basin developed as a foredeep in front of the left-lateral, steeply N-dipping Ovgos Fault (Figure 7-15c)

In the central axis of the Mesaoria Basin, the Ovgos fault, a steeply N-dipping reverse fault emplaces chalks of the Lapithos Group and marls of the Kythrea Group southward over the Myrtou Marl, Nicosia and lower Athalassa Formation/Members (Figure 7-3). The fault zone is unconformably overlain by the upper part of the Athalassa Member (Figure 7-3; Harrison et al., 2004a). To the south a similar thrust, the Mesaoria Fault, is buried beneath Pleistocene to Recent sediments (Harrison et al., 2004a). The frontal thrust of the Kyrenia Range, the Kythrea Fault, is an E–W trending, S-verging thrust, which emplaces slices of Lapithos and Trypa groups over the Kythrea Group (Robertson and Woodcock, 1986; Calon et al., 2005a,b).

An asymmetric half-graben? Robertson and Woodcock (1986) proposed that the Oligocene to Miocene represents a period of subsidence due to crustal extension in a forearc setting. Payne and Robertson (1995; 2000) suggested that this may be related to roll-back of a subduction zone to the south of Cyprus. In this model, the Mesaoria Basin evolved in the Late Miocene to Middle Pliocene as an asymmetric half graben, with maximum subsidence on S-dipping growth faults along its northern margin, and minimal subsidence on antithetic N-dipping faults along its southern margin (Figure 7-15a; McCallum and Robertson, 1990; Robertson et al., 1991; Robertson, 1998a). N-dipping extensional faults were developed during the late Miocene to early Pliocene along the southern margin of the Mesaoria Basin (Follows and Robertson, 1990; Robertson et al., 1991). McCallum and Robertson (1990) proposed that extension continued into the mid-Pliocene based on facies and borehole data

for the Nicosia Formation. Lateral and vertical thickness variations, in the Miocene units of the Kythrea Group, were taken as evidence by McCallum and Robertson (1990) to infer a phase of extension on S-dipping faults south of the Kyrenia Range (e.g. the Mesaoria, Ovgos and Kyrenia Faults).

Robertson and Woodcock (1986) proposed an episode of crustal contraction during late Pliocene to Pleistocene that resulted in uplift in the Kyrenia Range. S-dipping extensional faults were re-activated in a compressional sense and tilted to north, to form N-dipping high-angle reverse faults (Figure 7-15a). This was associated with concurrent imbrication in the Kyrenia Range. The event was coeval with uplift of the Troodos massif, recorded by the deposition of the Kephales fan-delta and Apalos continental gravels (McCallum and Robertson, 1990; Robertson, 1998a).

A foreland basin? In this model, the Mesaoria Basin and its marine extensions evolved from the Eocene–Oligocene to Recent as a large piggy-back basin within a crustal-scale linked thrust system between the active fronts of the Troodos-Larnaka culmination and the Kyrenia fold/thrust belt (Figure 7-15b; Calon et al., 2005a,b). Variations in the thickness and facies of the sedimentary successions deposited in this piggyback basin during this interval are directly related to shifts in the positions of the active fronts within this orogenic wedge.

A transpressional basin? In this model, the Mesaoria Basin evolved in the Late Miocene to Early Pliocene as a foredeep in front of the Ovgos Fault, within a linked crustal-scale, left-lateral strike-slip system (Figure 7-15c; Harrison et al., 2004a). In the late Miocene, pull-apart basins formed along the Ovgos Fault consistent with left-lateral strike-slip faulting (Harrison et al., 2004a). Messinian evaporites accumulated in the fault-bounded basins. Further south, on the northern margin of the Troodos Massif, concurrent extensional faulting was occurring. The extensional faults controlled the spatial distribution of Koronia Member reefs and Messinian gypsiferous deposits.

Figure 7-15: Models for the tectonic evolution of the Mesaoria Basin, and Kyrenia belt (modified from Calon et al., 2005b), proposed by (a) McCallum and Robertson (1990), Follows and Robertson (1990) and Robertson et al. (1991), (b) Calon et al. (2005a,b), and (c) Harrison et al. (2004a) (MF = Mesaoria Fault, OF = Ovgos Fault, KF = Kyrenia Fault)

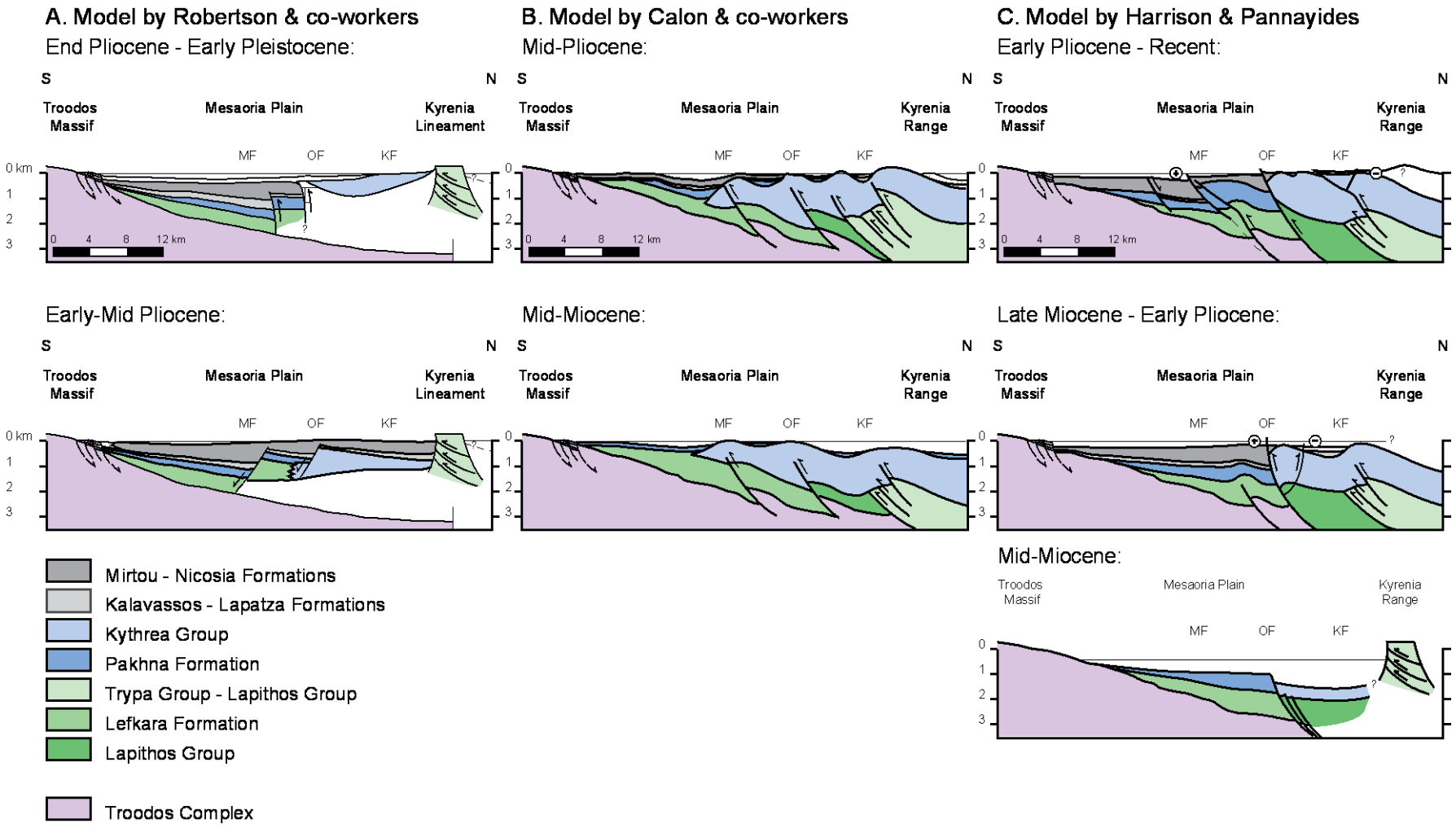
A. Model by Robertson & co-workers
End Pliocene - Early Pleistocene:
S
N
Troodos Massif
Mesaoria Plain
Kyrenia Lineament
MF
OF
KF
0 km
1
2
3
0
4
8
12 km
Early-Mid Pliocene:
B. Model by Calon & co-workers
Mid-Pliocene:
Kyrenia Range
Mid-Miocene:
C. Model by Harrison & Pannayides
Early Pliocene - Recent:
Late Miocene - Early Pliocene:
Mid-Miocene:
Mirtou - Nicosia Formations
Kalavassos - Lapatza Formations
Kythrea Group
Pakhna Formation
Trypa Group - Lapithos Group
Lefkara Formation
Lapithos Group
Troodos Complex

The above models need to be re-evaluated in light of new structural data collected during the present study. This data is directly relevant to the formation of the southern margin of the basin; however, due to the different tectonic regimes evident on either side of the Ovgos Fault (McCallum and Robertson, 1990; Follows and Robertson, 1990; Robertson et al., 1991; Harrison et al., 2004a) it is not possible to extrapolate this data to generate a synthesis on the tectonic evolution of the Mesaoria Basin as a whole. More structural data needs to be collected from along the northern margin of the Mesaoria Basin.

The new data sheds light on the tectonic evolution of the southern margin of the Mesaoria Basin:

(i) Faulting along the southern margin of the Mesaoria Basin began in the Middle to Late Miocene (pre-Tortonian);
(ii) This phase of faulting generated ~N-S-striking faults in an apparent east-west extension regime. Faulting initiated in the southeastern part of the Mesaoria Basin first, before propagating westwards (Figure 7-16);
(iii) In the Tortonian to Messinian north-south extension generated ~E-W-striking faults. Again, faulting initiated in the southeastern part of the Mesaoria Basin first, before propagating westwards. The location and development of Tortonian Koronia Member reefs was controlled by this phase of extension. This existing topography of basins and highs led to localised evaporite precipitation (Figure 7-16);
(iv) North-south extension continued into the Early Pliocene. E-W-trending faults continued to be active into the Messinian and Early Pliocene. The lower part of the Nicosia Formation is cut by E-W-trending faults (Figure 7-16). Intra-Messinian tectonic disturbance is recorded by tilted selenite botryoids and debris flows in the evaporite sequence;
(v) NE-SW-trending transverse structures were active in the Tortonian, and remain active today. E-W-striking depocentres were compartmentalised by the transverse structures.

Figure 7-16: Geological map of the Polikito-Agrokipia-Kato Moni region (southern margin of the Mesaoria basin). Structural data shown. Note that N-S-directed extension propagates from the east through to the west; N-S-directed extension affects Paleocene rocks at Politiko, Early to Middle Miocene rocks at Agrokipia, and Late Miocene (Messinian) rocks at Kato Moni

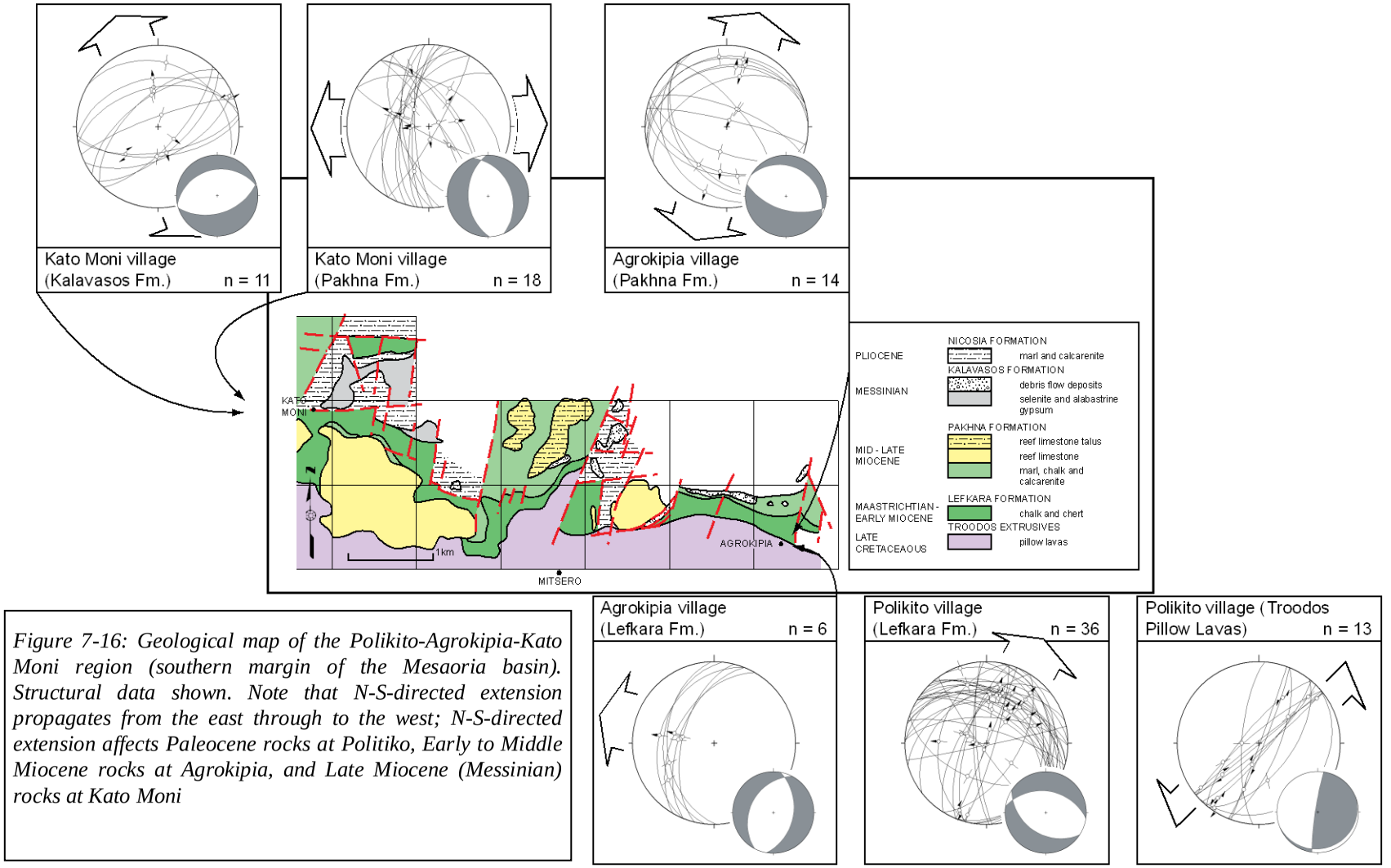

Figure 7-16: Geological map of the Polikito-Agrokipia-Kato Moni region (southern margin of the Mesaoria basin). Structural data shown. Note that N-S-directed extension propagates from the east through to the west; N-S-directed extension affects Paleocene rocks at Politiko, Early to Middle Miocene rocks at Agrokipia, and Late Miocene (Messinian) rocks at Kato Moni

Discussion. The Polemi and Pissouri Basins correspond to small tectonically controlled depressions elongated ~ NNW-SSE, and the Maroni-Psematismenos Basin to a depression elongated NE-SW. The general consensus, until relatively recently, was that these basins formed during a period of back-arc extension, related to the retreat of the Cyprus Arc to the south (Figure 7-1; Robertson, 2000; and references therein). In recent years a number of different explanations have been proposed. Harrison et al. (2004a) proposes that the Neogene basins formed as pull-apart structures, within a linked crustal-scale left-lateral strike-slip system. The major strike-slip faults were the Ovgos Fault in the north and the Cyprus 'Transform plate boundary' in the south; constraining strike-slip deformation to the area between the Eratosthenes Seamount to the south, and the Kyrenia Range to the north (Figure 7-2). Alternatively, Calon et al. (2005a,b) proposes that they formed as foreland basins within a S-verging fold/thrust system. Calon et al. (2005a,b) believe that the Gerasa Fold and Thrust Belt represents the active front of the Taurides thrust system. In this model, the Polemi and Pissouri basins would have formed as foreland basins in front of the active front of the Taurides thrust system, and the Maroni-Psematismenos Basin would have formed as a piggy-back basin between the active fronts of the Gerasa Fold and Thrust Belt and the Troodos-Larnaka culmination (Figure 7-3). Evidence for the middle model is E-W-trending sinistral faults in the north and south of Cyprus, and conjugate NNW-SSE-striking dextral faults and NNE-SSW-striking sinistral faults throughout Cyprus. Evidence for the latter model is inferred compression-related thrusting in SW Cyprus, the Paphos Thrust system (Soulas et al., 2005; discussed below).

It has been suggested that extensional faulting in the Polis Graben (SW Cyprus) is purely gravitational in nature, and not a representation of processes at depth (Soulas et al., 2005). Instead, Soulas et al. (2005) infer a southward propagating, NE-dipping thrust system in the Paphos-Polis area (see chapter 3; Agia Marinouda Fold). In this model, the extensional faulting observed in the Polis region is surficial – gravitational collapse above a developing collisional zone.

The arguments above highlight a contentious issue between all three tectonic models: is extension in the southern Neogene basins deep-rooted, and thus a representation of crustal-scale tectonic processes, or shallow-rooted, and thus not a true representation of such processes? This is an important issue – it has implications in each of the Neogene basins – does the structural data collected in the Polis Graben and the Pissouri, Maroni-Psematismenos and Mesaoria Basins reflect crustal-scale tectonic extensional processes, and

thus relate to the tectonic evolution of the island, or localised gravitational collapse away from uplifting zones, and thus relate to isolated events? In the following section, the term 'gravitational fault or gravitational faulting' is used to describe faults that are shallow-rooted. Shallow-rooted faults do not penetrate the basement. Examples of gravitational faults include recent landslides in the Pegeia and Pissouri areas and shallow-rooted gravitational sliding of Pliocene marl along bedding planes in the Pissouri Basin, which led to slumped horizons. The author has assigned an arbitrary value of 3km to represent the divide between deep- and shallow-rooted faulting; this is the depth at which the basement typically occurs in each of the Neogene basins.

In the following discussion, faults are considered gravitational (< 3km) if they meet several of the following criteria: that (i) the trace of the fault is parallel to relief; (ii) the fault plane is listric in nature; (iii) the dip of beds within a rotated fault block 'curve' in towards the fault plane; and (iv) (to accommodate displacements caused by landslides) compressional structures are (possibly) preserved down-slope. A further prerequisite is that there is a suitably weak rock for detachment to occur within, which underlies the faulted unit, i.e. in southwest Cyprus possible lithologies include: (i) bentonitic clays of the Kannaviou Formation; (ii) the clay matrix of the Kathikas Formation; and (iii) the siltstones, mudstones and clays of the Mamonia Complex (Figure 7-18). Spatial and temporal variations in fault data can also provide a clue as to whether faults are gravitational in nature (see below).

Figure 7-17: Models for the tectonic evolution of the Polis Graben proposed by (a) Payne and Robertson (1995; 2000) and Robertson (2000), and (b) Soulas (2003) and Soulas et al. (2005)

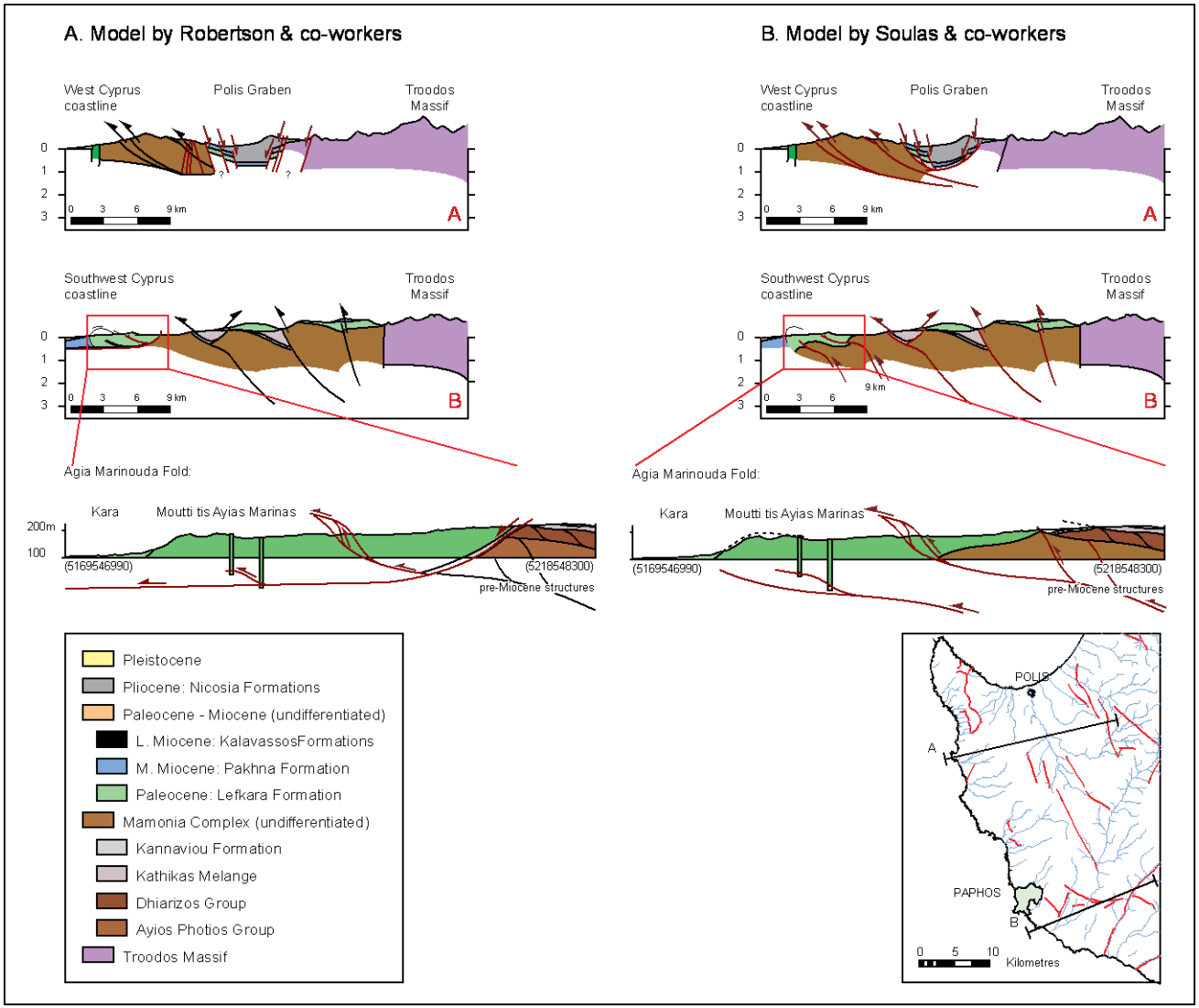

Figure 7-17: Models for the tectonic evolution of the Polis Graben proposed by (a) Payne and Robertson (1995; 2000) and Robertson (2000), and (b) Soulas (2003) and Soulas et al. (2005)

Let us considered the question proposed above in relation to the structures observed in the Polis region. In the Polis region, the interpretation of the origin of the faults as gravitational is in contradiction with: (i) the dip of the limestone beds in the region (blocks of limestone have been rotated as single units); (ii) the trace of the fault failure; and (iii) the absence of compressional structures down-slope. Faults observed in the Polis region, all show linear traces at outcrop, with no significant curvature. Furthermore, throughout the entire Polis region faults in Paleocene and Miocene strata strike preferentially at NW-SE and NE-SW; the NW-SE-striking faults are all normal in nature, whereas the NE-SW-striking faults are all sinistral in nature. If faulting was shallow-rooted and controlled by local events a range of orientations would be predicted. Discrete deformation events in the Polis Graben (D1 and D2) have been correlated with distinct periods of deposition; this led Payne and Robertson (1995) to believe that faulting initiated in the northern part of the Polis Graben in the Tortonian, but did not start in the southern part of Graben till the mid-Messinian. If faulting was localised, such a regimented chronological scheme would not be predicted.

Now let us consider the question again, in light of the new structural data collected throughout the south of Cyprus. In each of the basins several discrete populations of faults are identified: each population has been constrained an arbitrary age. Distinct deformation events are recognised in each basin (D1-D4): in general, these events occur simultaneously throughout south Cyprus. In addition, structural data collected in areas adjacent to the basins indicate that these deformation events are pervasive throughout Cyprus. Therefore, a regional tectonic control is proposed: related to Africa/Eurasia plate interactions.

There are exceptions to this: faulting in the Pegeia region is believed to be gravitational in nature. The presence of NW-SE- and NNE-SSW-striking faults, as observed in the Polis region, implies a prior regional tectonic control. However, the trace of the WNW-ESE-striking faults (which follows the topography), the dip of the limestone beds in the region (blocks of limestone have been rotated en mass) and the presence of compressional structures down-slope (e.g. Mesogi); suggest that these faults may be gravitational in nature. Detailed geological mapping of the region revealed that structures in Lefkara and Pakhna Formation chalk, detach in the underlying Kathikas Melange (Figure 7-18). The Pegeia region is not unique. Isolated ‘gravitational’ events are recognised in each of the basins e.g. in the Pissouri Basin dissolution and collapse of gypsiferous deposits has led to extension in the overlying deposits. The author proposes that regional tectonic processes have controlled the distribution and tectonic evolution of each of the Neogene basins, but that the affects of

gravitational collapse away from the uplifting Troodos Massif have been superimposed on this.

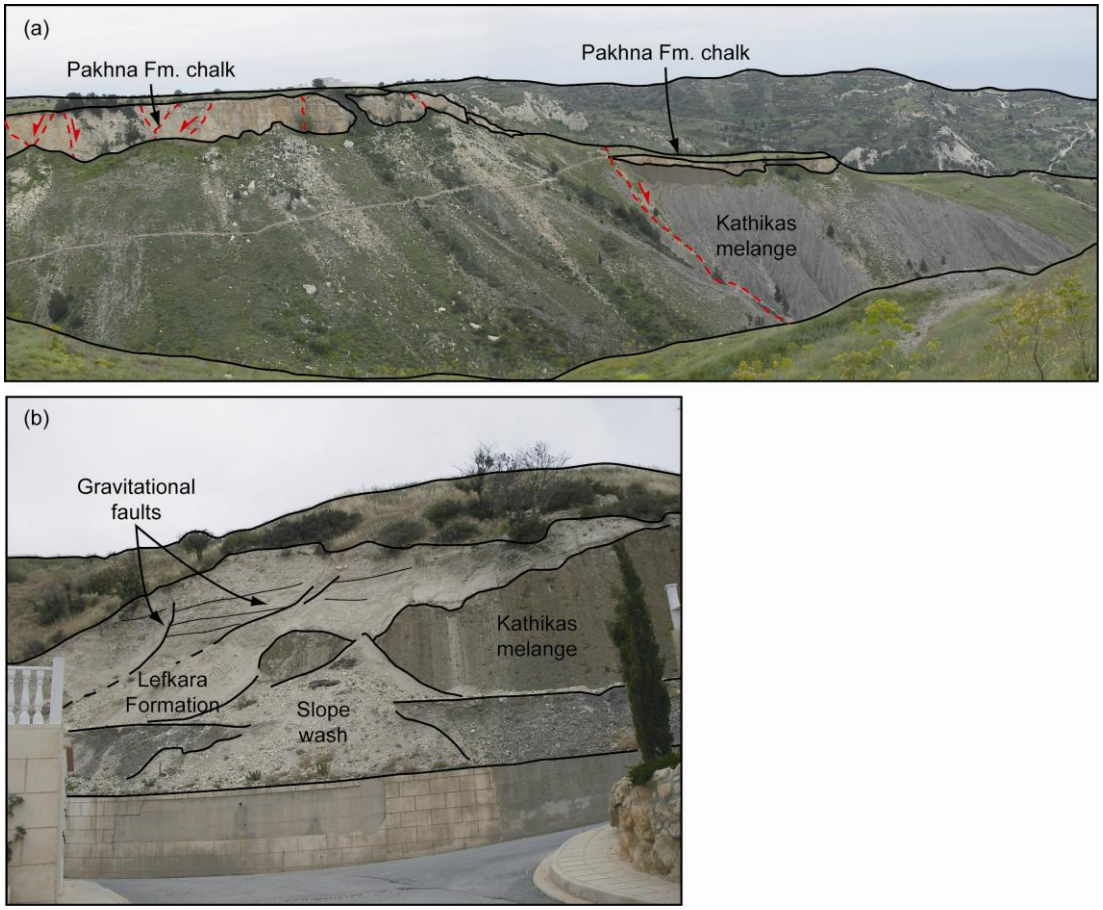

Figure 7-18: NW-SE-striking faults in Paleocene-Miocene strata overlying Kathikas Melange: (a) NW-SE faults cutting Pakhna Formation strata 1km NW of Pegeia, on the Pegeia-Kathikas road and (b) NW-SE faults cutting Lefkara Formation strata in Pegeia village

7.4.2.2 Strike-slip lineaments: E-W-striking sinistral faults and conjugate NNE-SSW-striking sinistral and NNW-SSE-striking dextral faults

E-W-striking sinistral faults and conjugate NNE-SSW-striking sinistral and NNW-SSE-striking dextral faults were documented by the author in the Lemesos and Larnaka District (see chapter 3). Faults a E-W orientation have been documented by Harrison et al. (2002, 2004a,b) in the north of Cyprus, and in the south of Cyprus by Soulas et al. (2005).

North Cyprus. Harrison et al. (2002, 2004a,b) and Panayides et al. (2004) document E-W-trending, left-lateral strike-slip Pleistocene movement on the Ovgos Fault. Additional work

was undertaken by the author and Gillian McCay to characterise the Ovgos Fault: dextral NNE-SSW- (N000-N020) and normal-dextral NW-SE- (N320-N340) faults were observed cutting Pliocene strata (Figure 7-19). Conjugate left-lateral NE/SW- trending and right-lateral NW-SE-trending strike-slip faults were recognised by Harrison et al. (2004a,b). Strike-slip faults were mapped in the Lefkosia (Nicosia) area during a seismic hazard and risk assessment project (DeCoster et al., 2004): five major NNE/SSW-trending left-lateral, strike-slip faults (Arkhangelos, Pedieos, Skali, Xeri, and Laxia faults) and one significant north-northwest-trending, right-lateral strike-slip fault (Sehir Bakan fault) were observed (Figure 3-48).

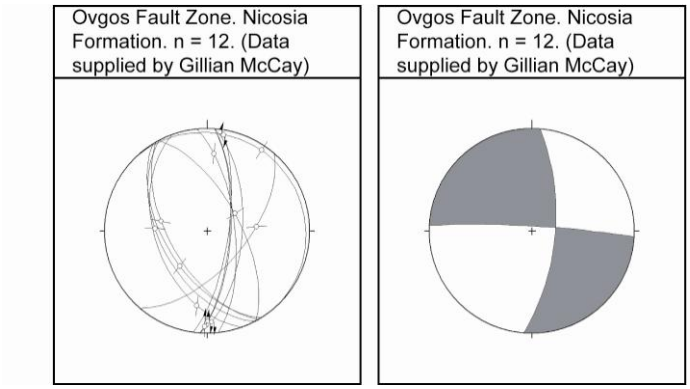

Figure 7-19: Structural data collected from faults affecting the Nicosia Formation (data collected by Gillian McCay)

Paphos International Airport. Soulas et al. (2005) identified an active, left-lateral en echelon system of strike-slip faults near to the Paphos International Airport. A chain of elongate hills, comprised of aeolinites, stretches east of the airport towards the churches of Agia Arkona and Agios Minas. Possible anticlinal stratification is evident in the aeolinitic mounds. The presence of marine pebbles at the top of these hills is interpreted as evidence of tectonic uplift in the area (Soulas et al., 2005).

Kolossi Fault Lineament. A description of the Kolossi Fault Lineament was given in chapter 3.

Arakapas/Gerasa Fault Belts. Significant Quaternary movement is believed to have occurred along the Arakapas and Gerasa Fault belts in the Limassol Forest area (Soulas, 2001; 2003; Soulas et al., 2005). New structural data collected in the Arakapas region (between the villages of Eptagoneia, Arakapas and Agios Mamas; Figure 3-59) and in the Gerasa region

(between the villages of Agios Mamas, Gerasa and Parekklisia; Figure 3-59) was presented in chapter 3.

Larnaka District. Several strike-slip faults are observed in the Larnaka district, including: (i) the sub-parallel, sub-vertical NNW-SSE- to NW-SE- -trending, right-lateral Maroni, Tremithos and Roundabout-airport Faults (Figure 3-69; Soulas et al., 2005); and (ii) the Cape Kiti fault, part of the Larnaka Fault Zone (LFZ), a braided network of NNE-SSW-trending, left-lateral, steeply dipping fault strands (Figure 3-73; R. Harrison and E. Tsiolakis, personal communications).

7.4.2.3 Compressional lineaments: The Agia Marinouda and Kouklia Folds

A description of the Agia Marinouda and Kouklia Folds are given in chapter 3. Optically stimulated luminescence dating was undertaken on deformed Pleistocene/Holocene strata, to characterise the growth of the Agia Marinouda Fold (see chapter 5): strata at the base of the succession (tilted at 50º) are dated at 68.7 ± 28.2 ka, strata in the middle of the succession (tilted at ~ 25º) at 33.03 ± 6.74 ka, and strata at the top of the succession at 6.68 ± 4.0 ka. The Kouklia fold locally deforms a Pleistocene marine terrace at the Happy Valley junction of the Paphos-Lemesos highway. Middle to upper Pleistocene marine terrace deposits are tilted to sub-vertical on the western flank of the fold and to 45° on its eastern flank (see chapter 3). Marine terrace deposits along strike to the west, i.e. at Paphos, and along strike to the east, i.e. Aphrodite's Hill Resort and Kolossi village yield palaeomagnetic ages of < 78.1 ka. Based on this evidence, the Agia Marinouda fold must have been generated in the Early to Middle Pleistocene.

Discussion. In SW Cyprus, the Troodos Complex is juxtaposed against the older Mamonia Complex along a series of serpentinite-filled fault zones that define the Mamonia Complex Suture Zone (MCSZ) (Bailey et al. 2000). A southerly suture passes through the villages of Loutra tis Aphroditis, Mavrokolymbos, Marathounta, Agia Varvara and Phasoula (Figure 7-20).

Soulas (2003) proposed that early Pleistocene to Recent compression resulted in a reactivation of the Late Cretaceous sutures. Furthermore he proposed that a forward-propagating thrust system, termed the Paphos Thrust System (PTS) developed at this time. In this model, the PTS represents the forward propagation of a Late Cretaceous suture zone

reactivated at depth. It is believed to be, in general a blind structure (Soulas, 1999; 2003), except in two key areas: (i) between Kouklia village and the Khaporuni River mouth; and (ii) between Agia Marinouda and the Paphianna hotel, to the NE of Geroskipou (Figure 7-21).

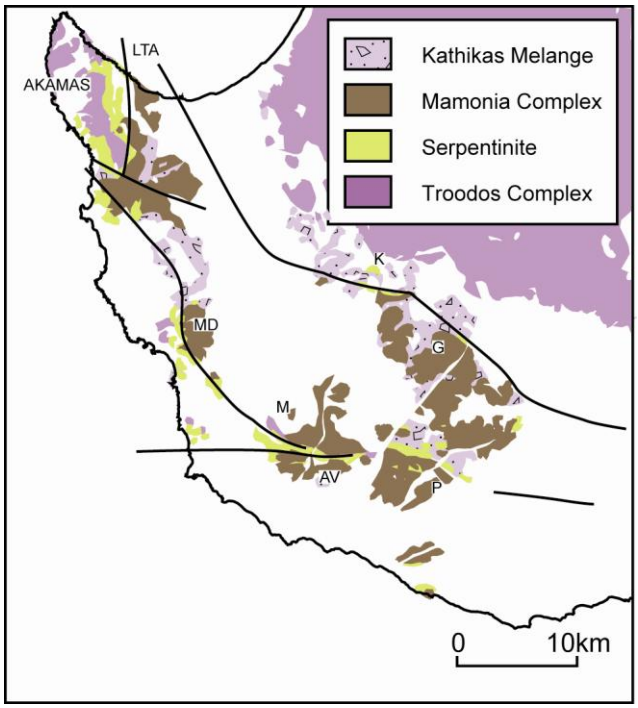

Figure 7-20: Geological map of SW Cyprus (modified from Bailey et al., 2000; geological data supplied by the Cyprus Geological Survey Department). The Mamonia Complex suture zone is defined by two main, serpentinite-filled fault zones, which are shown as black lines. Localities referred to in the text are Galataria (G), Kannaviou (K), Loutra tis Aproditis (LTA), Mavrokolymbos Dam (MD), Marathounta (M), Agia Varvara (AV) and Phasoula (P).

Two main active transverse structures divide the PTS into three segments: (i) the Eastern Cape Aspro Fault; (ii) the Agia Marinouda Fault; and (iii) the northern Akamas Fault (Figure 7-21). In this model, the Eastern Cape Aspro Fault is responsible for uplift in the Pissouri Basin, an area 23 km east-west by 12km north-south, between Kouklia village in the west, Evidhivou Bay in the east, and Archimandrita village to the north. In support of this model, Plio-Pleistocene Gilbert-type fan deltas (originally defined by Stow et al., 1995) occur at an elevation of 280m above mean sea level, Quaternary marine terraces at 300m and Fanglomerate deposits at 500m (Soulas, 2003). Soulas (2003) infers that the Agia Marinouda and Kouklia folds developed as arcuate, ~ NW-SE-trending anticlines above blind thrusts, part of the Agia Marinouda Fault network (Figure 7-21; Figure 7-22). The Akamas Fault, as mapped by Soulas (2003) is an isolated splay, trending ~ NW-SE NW of the PTS. It is located in the Akamas peninsula. Soulas (2003) believes that the fault shows evidence of Quaternary uplift of the Akamas ridge, increasing erosion and inducing the formation of

sheets of talus and piedmont fanglomerates. Soulas (2003) states that the Akamas fault is a piggyback fault of the PTS; shallower in nature than the main strand of the PTS.

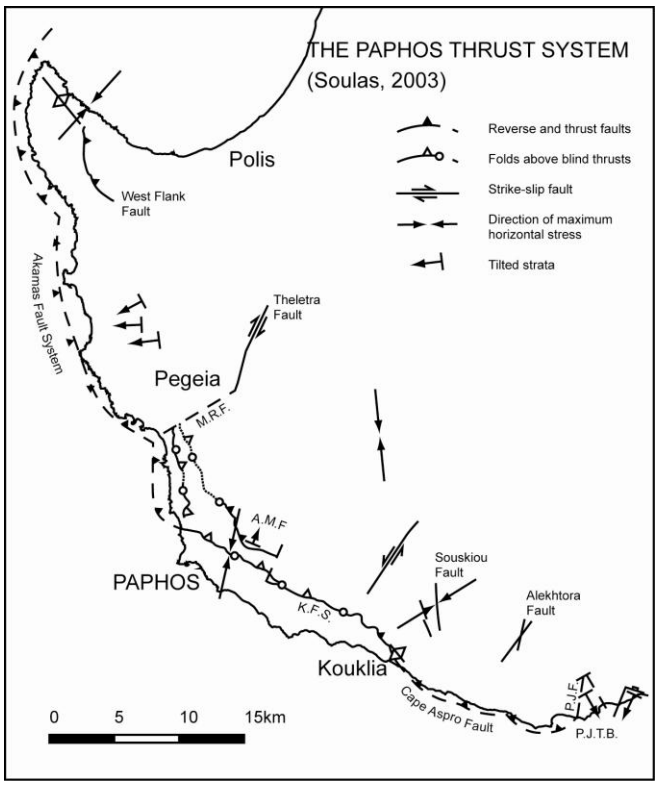

Figure 7-21: Outline map of the Paphos Thrust Zone, as envisaged by Soulas 2003. Abbreviations are as follows: A.M.F = Agia Marinouda Fold; K.F.S = Ktima Fault System; M.R.F = Mavrokolymbos River Fault; P.J.F = Pissouri Jetty Fault; P.J.T.B = Pissouri Jetty Tilted Fault Block

An alternative hypothesis was tested during the course of the study, as several contradictions in the compressional model were noted: (i) the Late Miocene to Early Pliocene tectonic regime was extensional (transtensional?); (ii) the area inland of the Kouklia and Agia Marinouda are both cut by an extensive array of normal faults; and (iii) repetitions in the stratigraphy are not known (determining stratigraphic markers within the Lefkara and Pakhna Formations is questionable). It was considered that the Kouklia and Agia Marinouda folds could have developed as buckle folds, above extensional detachments at depth (Figure 7-23). In this model, extension at depth was accommodated by gravitational sliding on Kannaviou Formation clay. However, several contradictions to this hypothesis became evident during subsequent fieldwork: (i) strike-slip lineaments mapped at Paphos International Airport, Kolossi, and Larnaka, indicate that the late Pliocene to Recent tectonic regime is transpressional in nature; (ii) WNW-ESE-trending, NNE-dipping faults, with a top to the SW sense of displacement and NNE-SSW-trending, ESE-dipping faults, with a top to

the WNW sense of displacement were mapped at Agia Marinouda and Acheleia, respectively; (iii) structural data collected in southwest Cyprus (and elsewhere in Cyprus, e.g. Pissouri, Maroni and Larnaka) indicate that structures generated in the Miocene to Early Pliocene were subsequently reactivated in a transpressional (compressional?) stress regime; and (iv) no detachment is seen inland of the Kouklia and Agia Marinouda folds, as would be expected in gravitational induced slumps.

The current hypothesis is as follows: early Pleistocene to Recent localised compression, in a regional transpressional stress regime, reactivated Late Cretaceous suture zones and the Agia Marinouda and Kouklia Folds formed above blind structures. A large, southward propagating thrust system is not envisaged; instead, compression is localised. Strike-slip lineaments at Paphos International Airport, Kolossi, and Larnaka, indicate that the late Pliocene to Recent tectonic regime is transpressional in nature. Structural data indicates that Miocene to Early Pliocene extensional structures have been subsequently reactivated in a transpressional (compressional?) stress regime (i.e. Acheleia). This hypothesis with be tested later in the chapter.

Figure 7-22: Geological cross-sections through the Agia Marinouda – Kouklia fold: as envisaged if the area is in compression (Soulas et al., 2005). The location of cross-sections 1 – 4 are shown on Figure 3-49

Figure 7-23: Geological cross-sections through the Agia Marinouda – Kouklia fold: as if envisaged if the area is in extension. The location of cross-sections 1 – 4 are shown on Figure 3-49

Figure 7-22: Geological cross-sections through the Agia Marinouda – Kouklia fold: as envisaged if the area is in compression (Soulas et al., 2005).

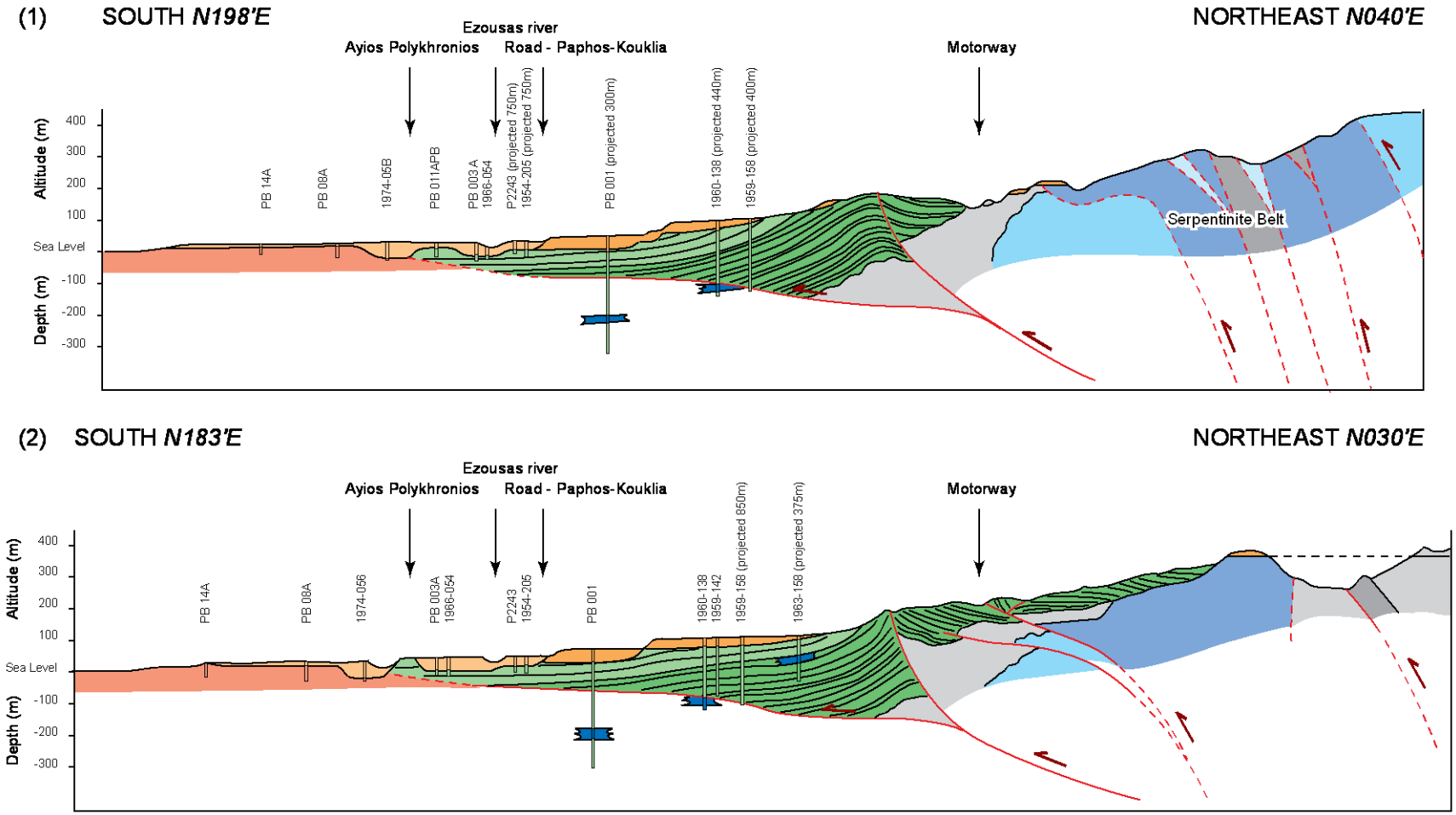

Figure 7-22 (contd)

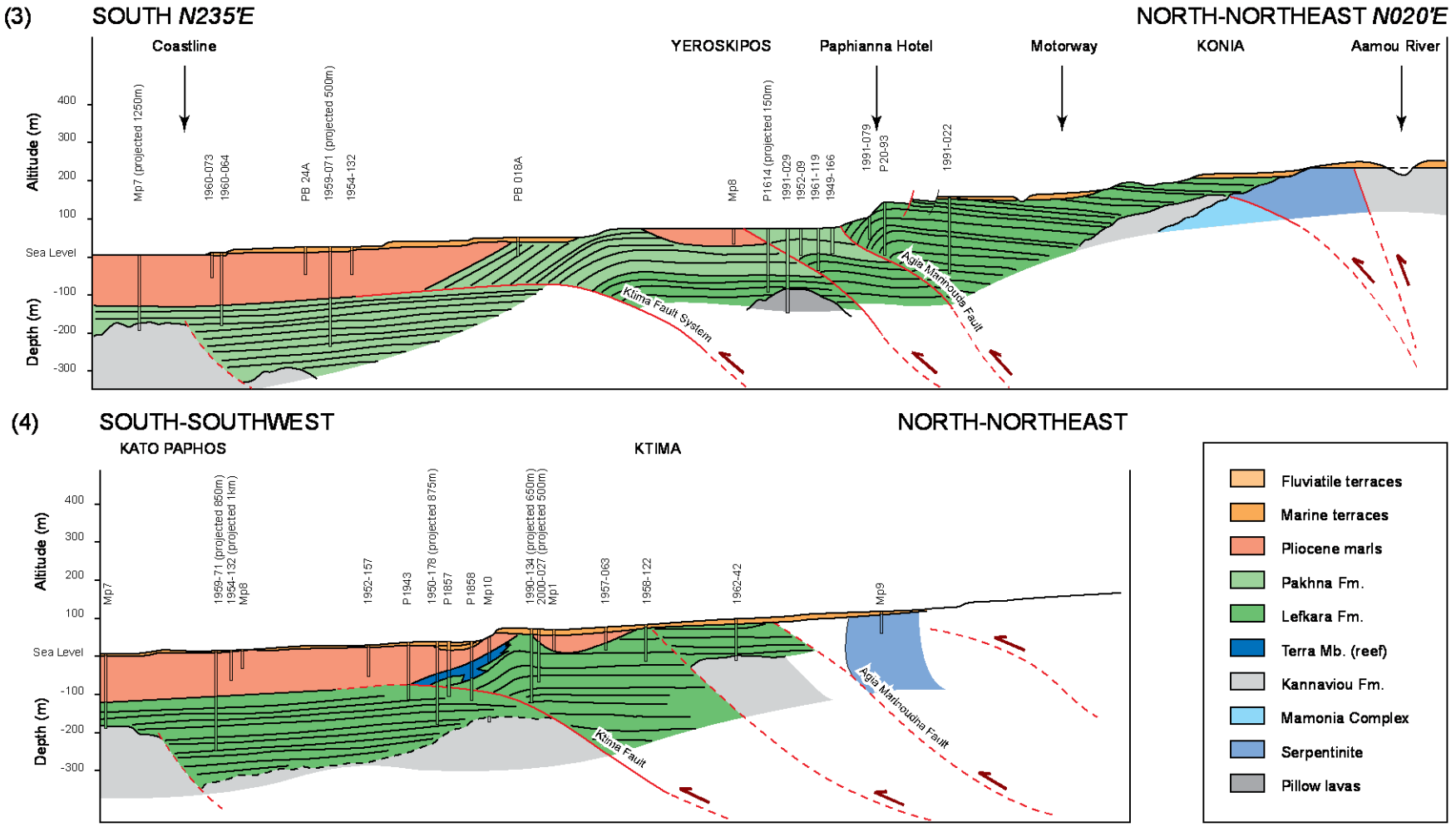

Figure 7-23: Geological cross-sections through the Agia Marinouda – Kouklia fold: as if envisaged if the area is in extension.

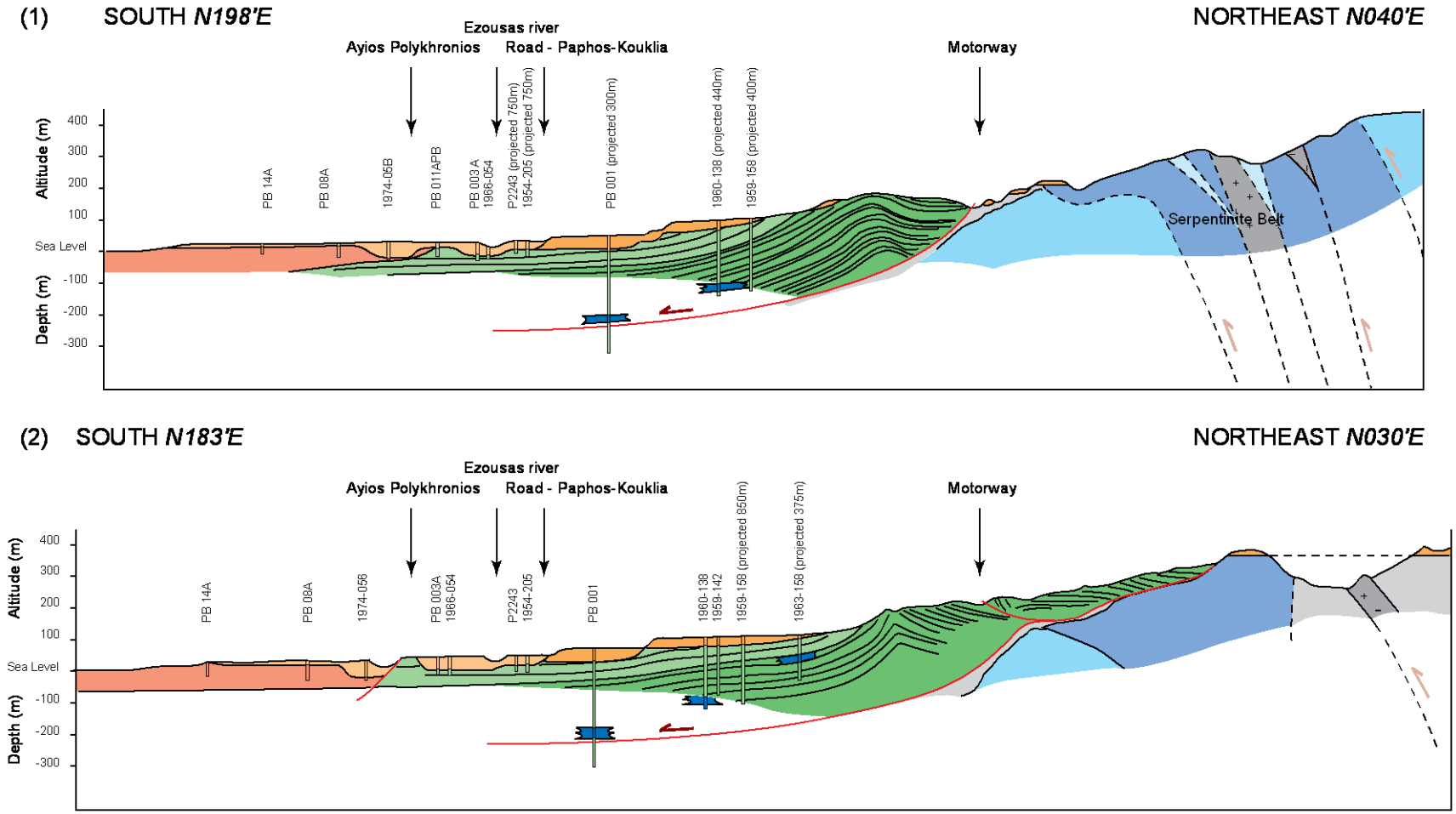

Figure 7-23 (contd)

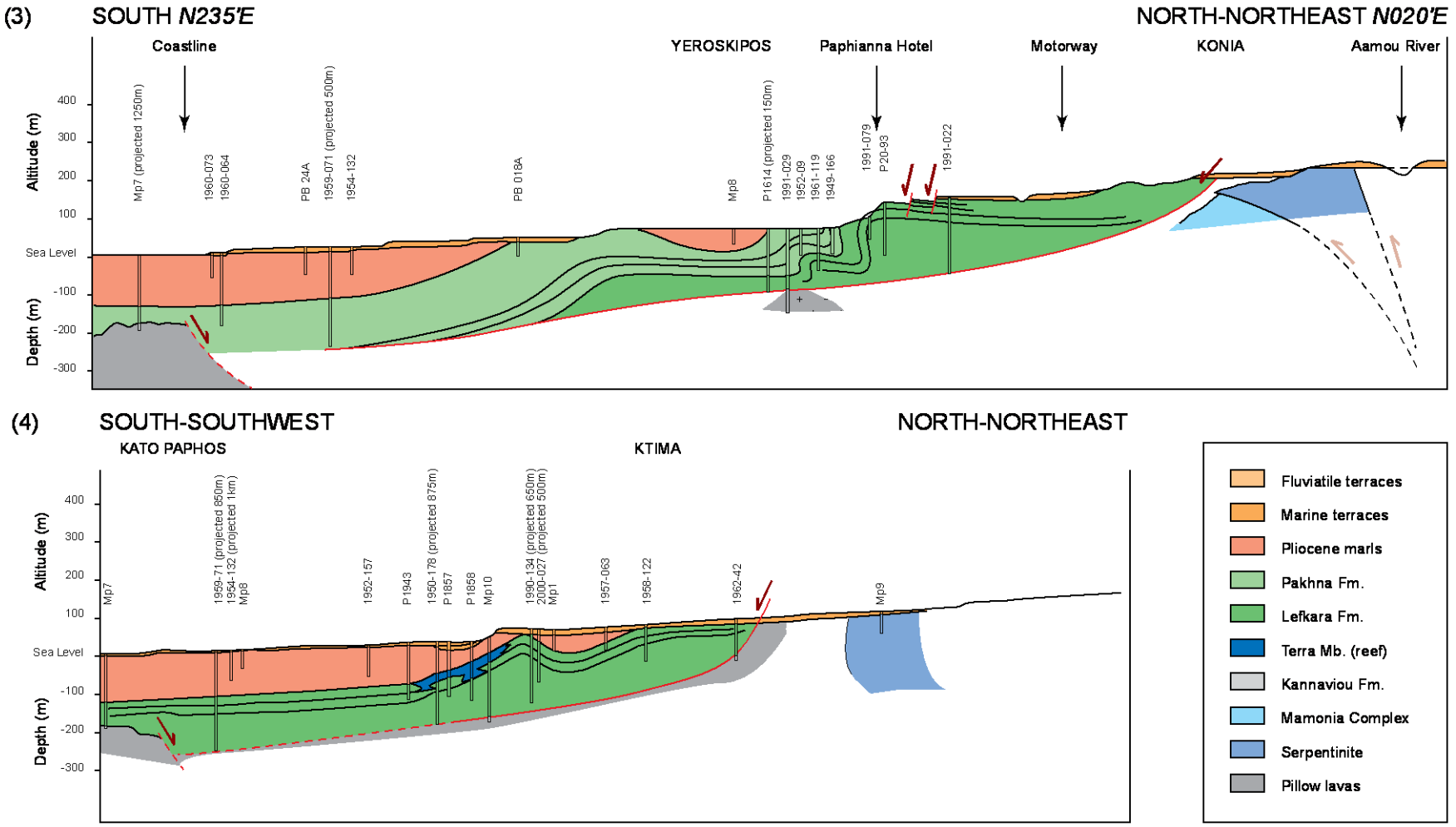

Offshore data

Marine geophysical surveys south and west of the Cyprus Arc have mapped geological structures indicating N-S convergence across the arc, i.e. Cyprus and the Eratosthenes Seamount (e.g. Robertson et al., 1998; Woodside et al. 2002). Recently, PGS Geophysical AS acquired 70,000 km^2 of seismic data, covering the Eratosthenes Seamount, Levant Basin and Cyprus Arc.

Figure 7-24 illustrates the distribution and orientation of faults in the eastern Mediterranean. In general two trends are recognised, a NE-SW trend, and a WNW-ESE trend. The Eratosthenes Seamount is bound in the north and south by WNW-ESE-striking faults and to the west and east by NE-SW-striking faults. The approximate locations of the cross-sections discussed below are shown.

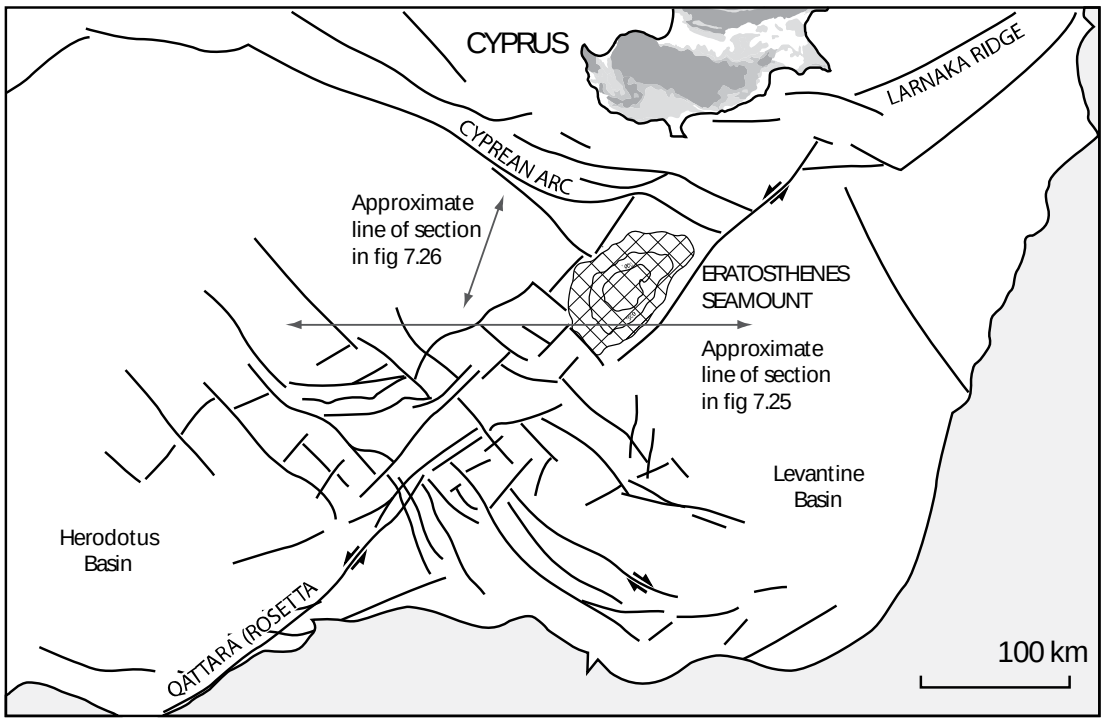

Figure 7-24: Offshore fault trends (Publicity flyer - 'Offshore Cyprus MC2D-CYP 2006', PGS Geophysical AS) (http://www.mcit.gov.cy/mcit/; Roberts and Peace, 2007)

Figure 7-25 is a regional E-W cross-section through the Levantine and Herodotus Basins, including the Eratosthenes Seamount. It illustrates the spatial and temporal distribution of faults in the region.

Figure 7-26 is a regional N-S cross-section through the Herodotus Basin. It illustrates two phases of deformation: a pre-Messinian phase of extension; and a post-Messinian phase of compression. Post-Messinian deformation has resulted in contractional faulting along WNW-ESE trends.

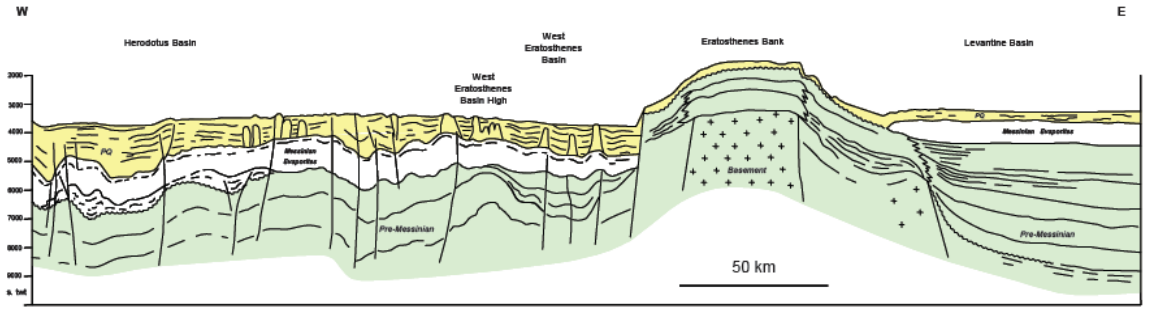

Figure 7-25: Regional cross-section through the Levantine Basin to the Herodotus Basin through the Eratosthenes Seamount (http://www.mcit.gov.cy/mcit/)

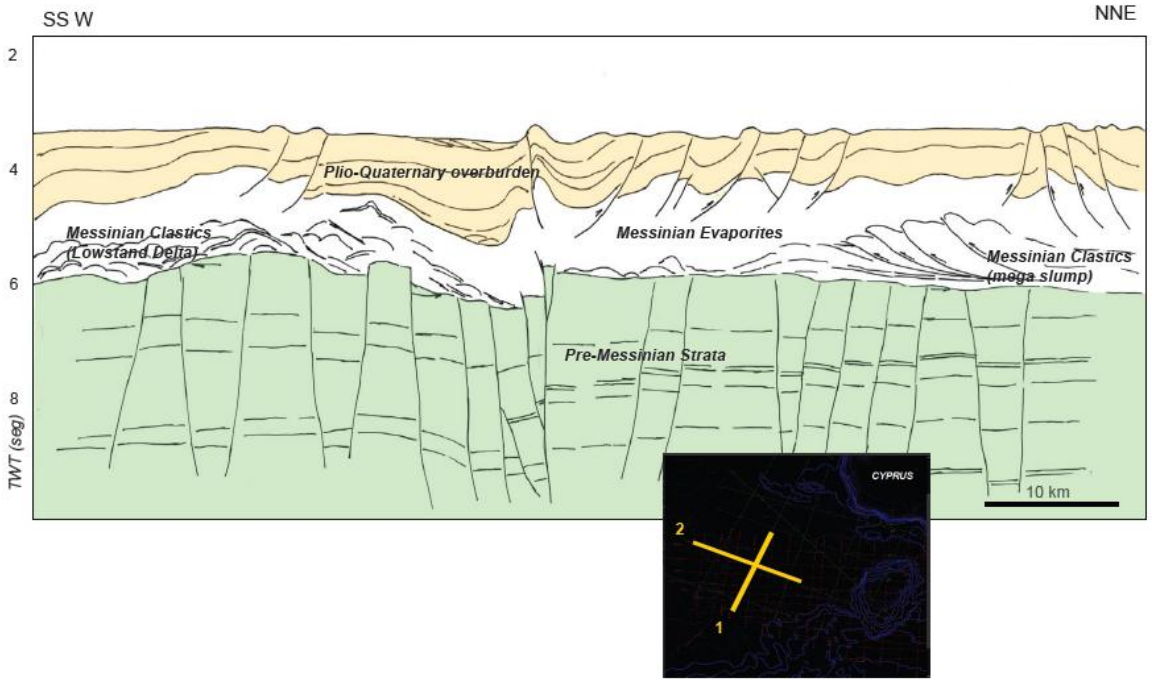

Figure 7-26: Regional N-S cross-section (http://www.mcit.gov.cy/mcit/)

7.4.3 Geochronological data

A geochronological framework for the Plio-Pleistocene sedimentary successions of central and south Cyprus is presented.

Palaeomagnetic data: Palaeomagnetic profiling of the Plio-Pleistocene circum-Troodos sedimentary cover was used as a tool to constrain the timing of uplift in Cyprus. Magnetostratigraphies were generated for the Plio-Pleistocene sedimentary fill of the Pissouri and Mesaoria Basins.

Pissouri. The Nicosia Formation forms the bulk of the Plio-Pleistocene fill of the Pissouri Basin, which reflects widespread and uniform blanket deposition of pelagic marls and micrites in a stable deep-water basin. In the middle and upper parts of the succession an influx of terrigenous turbidites, derived from an uplifting Troodos Massif to the north, indicates increased uplift and/or tectonic adjustments at the basin margin (see section 7.4.1). The upper part of the succession is marked by an increase in the thickness and abundance of terrigenous sands, which are distinctly less turbiditic and this trend reflects the gradual shallowing of the Pissouri Basin (see section 7.4.1). Palaeomagnetic data constrain the upper part of the Nicosia Formation to the Late Pliocene, with deposition of this unit occurring either during the Reunion (**2.15 – 2.14 Ma**) or Olduvai subchron (1.95 - 1.77 Ma) of the Matuyama Chron.

Rapid uplift of the Troodos Massif began in the latest Pliocene/earliest Pleistocene; coincident with the progradation of Gilbert-type fan-deltas into the Pissouri basin (see section 7.4.1). Palaeomagnetic age constraints date deposition of the Gilbert-type fan deltas at **2.14 – 1.95 Ma**, or 1.77 – 1.66 Ma, between the Reunion and Olduvai subchrons, or Olduvai and Gibsa subchrons of the Matuyama Chron, respectively. Deposition of the Gilbert-type fan-delta succession was followed by rhythmically bedded basal clastic lags, aeolinites and palaeosols (1.77 Ma to present). The age constraint in bold is the favoured interpretation.

Mesaoria. This timing of uplift is compatible with results from the Mesaoria Basin. Uplift of the Troodos Massif in the latest Pliocene is coincident with the progradation of the Kephales fan-delta system into, and the migration of Athalassa-type sandbodies, across the Mesaoria Basin. Palaeomagnetic age constraints date deposition of the Kephales fan-delta at 2.14 – 1.95 Ma, between the Reunion and Olduvai subchrons of the Matuyama Chron, and deposition of the Athalassa sandbodies at 2.14 – 1.24 Ma, between the Reunion and Cobb Mountain subchrons of the Matuyama Chron. Uplift of the Troodos Massif continued into the early Pleistocene, as recorded by rhythmically bedded fluvial gravels, silty overbank fines and palaeosols of the Apalos Formation (< 0.78 Ma).

Optically Stimulated Luminescence (OSL) data: Optically stimulated luminescence dating was used as a tool to constrain the age, and characterise the kinematic development of transpressional structures in southern Cyprus. The structural lineaments studied were the left-lateral E-W-trending Kolossi Fault, the left-lateral NNE-SSW-trending Cape Kiti Fault (part of the larger left-lateral Larnaka Fault Zone) and the Agia Marinouda-Kouklia Folds (see chapter 5).

(i) The earliest identified phase of strike-slip faulting in south Cyprus is at Larnaka. A left-lateral displacement is believed to have occured along the NNE-SSW-striking Cape Kiti Fault in the Late Pliocene (Harrison and Tsiolakis, 2006). Post-Pliocene movement along the fault was restricted to the Middle to Late Pleistocene between 38.1 ± 13.2 ka and 12.1 ± 0.1 ka. The latter date was obtained by R. Harrision (E. Tsiolakis, personal communication);

(ii) Faulting in south central Cyprus occurred in the early to middle Pleistocene. The Kolossi Fault juxtaposes Pakhna and Nicosia Formation strata against Fanglomerate gravels. Deformed Fanglomerate gravels at the base of the Kolossi Fault are dated at 174.1 ± 20.9 ka. The Kolossi Fault is overlain by middle Pleistocene gravels dated at 76.6 ± 16.4 ka. There has been no displacement along the fault since the deposition of the Middle Pleistocene gravels;

(iii) The Agia Marinouda – Kouklia fold originated in the early middle Pleistocene, with active growth to the present day. The Kouklia fold locally deforms a Pleistocene marine terrace at the Happy Valley junction of the Paphos-Lemesos highway. Palaeomagnetic age profiling of similar terraces exposed along strike dates this event to >78.1 ka. At Geroskipou, the Agia Marinouda Fold locally deforms middle Pleistocene strata at Geroskipou. Luminescence age dating of the lower horizons of colluviums date this event from 68.9 ± 28.2 ka

A number of conclusions are drawn from these results: (i) the south coast of Cyprus has been subjected to tangential shear along E-W faults and orthogonal transpressional components across NNE-SSW- and NNW-SSE-striking faults since at least the Late Pliocene/early Pleistocene (i.e. Cape Kiti/Kolossi Faults); (ii) the end of deformation on the Kolossi Fault coincides with the start of deformation on the Agia Marinouda Fold; hence, transpression may have propagated west through time; (iii) the Agia Marinouda Fold is still actively growing at present (Earthquake data imply the region is still seismically active (Algermissen and Rogers, 2004, see section 7.3); and (iv) the Cape Kiti Fault was an active structure until

fairly recently. Fault movements of Holocene age (< ~ 10 ka) are of particular significance, as they represent failure on faults that are probably still favourably orientated in the present stress field, and therefore, likely to fail in the future.

An additional aim of this study was to constrain the age of gravitational faulting in southwest and south-central Cyprus. Locallised extension, related to gravitational collapse away from the uplifting Troodos Massif, led to the generation of normal faults at a number of discrete localities – including sites at Amargeti, Pissouri and Kalavasos. Extensional faults at Amargeti are believed to date to the late middle Pleistocene. The last episode of faulting at Amargeti occurred at ~ 43.4 ± 2.1 k (the age of the youngest affected unit); the interval between 29.3 ± 6.6 ka and 6.45 ± 0.1 ka was one of tectonic quiescence. Extensional faulting in the Vasilikós Valley, Kalavasos occurred in the late early to late Pleistocene, between 78.3 ± 5.3 ka and 10.4 ± 2.2 ka (the age of the youngest and oldest affected units).

7.5 Discussion

The preceding sections of this chapter have detailed the sedimentology and structure of the Neogene basins and interpreted them in terms of local tectonic controls (i.e. extension vs. transtension). Four pervasive deformation events were recognised in west and south Cyprus:

Deformation phase D1a: Late Miocene (Serravillian –early Messinian) extension

The Neogene basins of south Cyprus (i.e. the Polis Graben, the Pissouri and Maroni-Psematismenos Basins) formed during a period of crustal extension in the Late Miocene (D1). This extensional event was pervasive through the entire south coast of Cyprus: (i) in west Cyprus, the faults responsible for the formation of the northern part of the Polis Graben were generated in the Tortonian, in response to broadly ENE-WSW extension (Figure 7-27); (ii) in southwest Cyprus, Late Miocene E-W to NE-SW extension generated N/S- to NW/SE-striking faults (Figure 7-28), which led to the formation of the Pissouri Basin; (iii) in south Cyprus, the faults responsible for the formation of the Maroni-Psematismenos Basin were formed in the Late Miocene in response to broadly NW-SE extension (Figure 7-29); and (iv) in regions adjacent to the Neogene basins D1 extension produced N-S- to NNE-SSW-striking faults in the Acheleia and Kouklia regions (Figure 7-30 and Figure 7-31, repectively); and NE-SW-striking faults in the Choirokoitia and Larnaka regions (Figure 7-32 and Figure 7-33, respectively).

Deformation phase D1b: Late Miocene (late Messinian) extension

Faulting continued with a similar extensional direction into the latest Messinian: (i) in west Cyprus, the main period of fault activity, with N/S- to NNW/SSE-striking faults is believed to have occurred during the early to mid-Messinian in the northern part of the Polis Graben, and during the mid-Messinian in the southern part of the Polis Graben; (ii) in southwest Cyprus, Tortonian through to Messinian faulting controlled the spatial distribution of evaporite deposits in the Pissouri Basin. Messinian deposits are confined to the northern and central parts of the Pissouri Basin; (iii) in south Cyprus, Messinian faulting controlled the distribution of facies within the Messinian Maroni-Psematismenos Basin. Facies analysis indicates several periods of tectonic instability during the Messinian, associated with sediment redeposition and slumping; (iv) in south-central Cyprus, the main period of fault activity, with E-W-striking faults is believed to have occurred along the southern margin of the Mesaoria Basin in the Tortonian to mid-Messinian; and (v) in the late Miocene, pull-apart basins formed along the Ovgos Fault (central-north Cyprus); Messinian evaporites accumulated in these fault-bounded basins.

Deformation phase D2: Early to Middle Pliocene extension

A later phase of localised extension in the Early to Middle Pliocene resulted in the formation of a second generation of faults (D2). D2 NNE-SSW to NE-SW extension generated WNW-ESE- to NW-SE-striking faults in the Polis region; most noteably in the Polis Graben, but also in the Pegeia region (Payne and Robertson, 1995). There is also evidence that D2 extension led to a re-orientation of the Maroni-Psematismenos Basin; and the generation of NW-SE-striking normal faults.

In all three Neogene basins, Pliocene and younger strata are affected by faulting and slumping associated with dissolution and collapse of the gypsum deposits. Tortonian and Messinian faults and fractures acted as conduits for groundwater migration; hence, dissolution cavities/collapse structures are frequently orientated in a similar direction to faults. Messinian fractures are aligned N340-N020 (~ N-S) and N280-N300 (WNW-ESE) (see section 7.4.2).

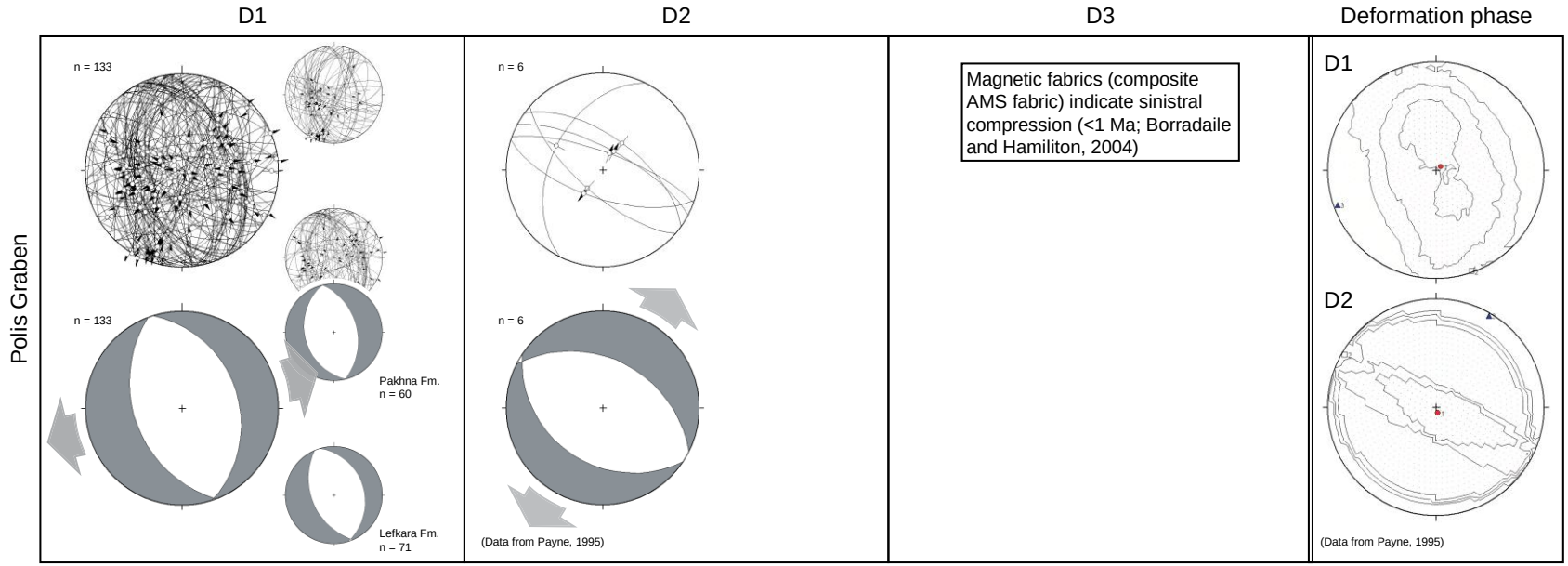

Figure 7-27: Deformation events recognised in the Polis Graben are: (i) Late Miocene ENE-WSW to E-W extension (D1); (ii) post-Miocene NNE-SSW extension (D2); and (iii) Pleistocene-Recent compression (D3)

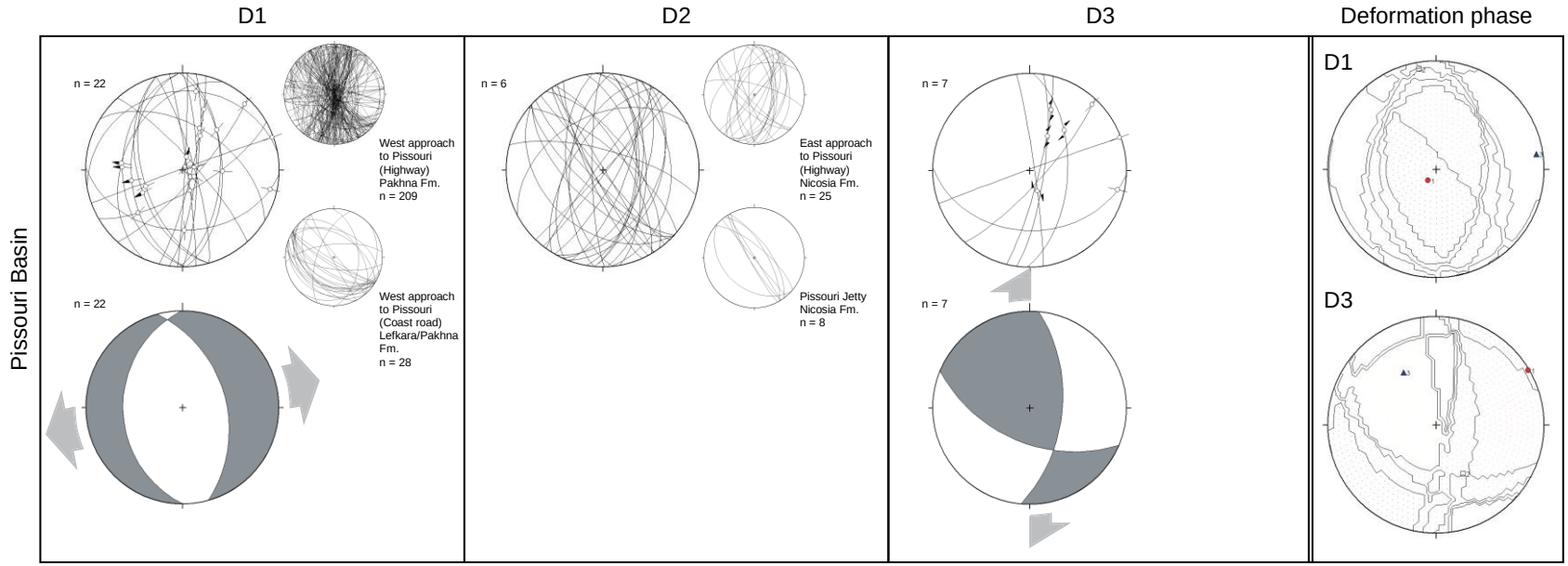

Figure 7-28: Deformation phases recognised in the Pissouri Basin are: (i) Late Miocene (Tortonian?) E-W extension (D1a); Messinian E-W extension (D1b); and (iii) Pleistocene-Recent transpression (right-lateral displacement on a N-S plane; D3)

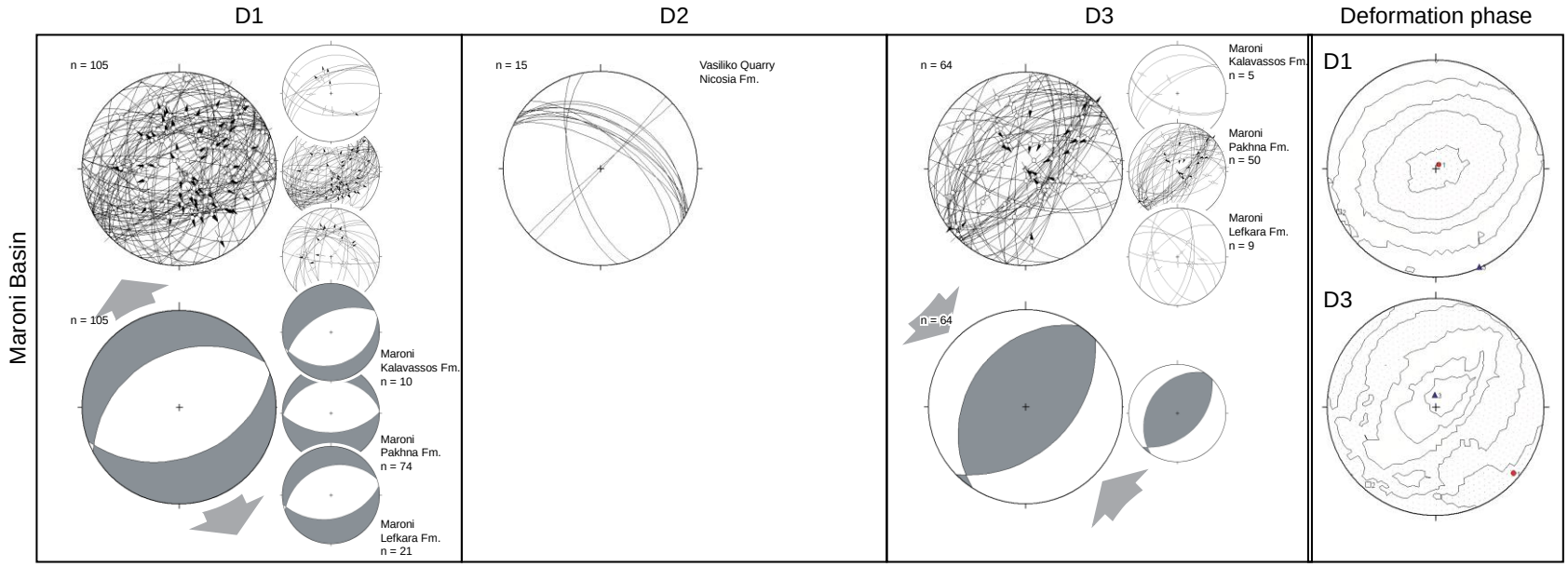

Figure 7-29: Deformation events recognised in the Maroni-Psematismenos Basin are: (i) Late Miocene NW-SE to N-S extension (D1a); Messinian NNW-SSE extension (D1b); and Pleistocene-Recent compression (D3)

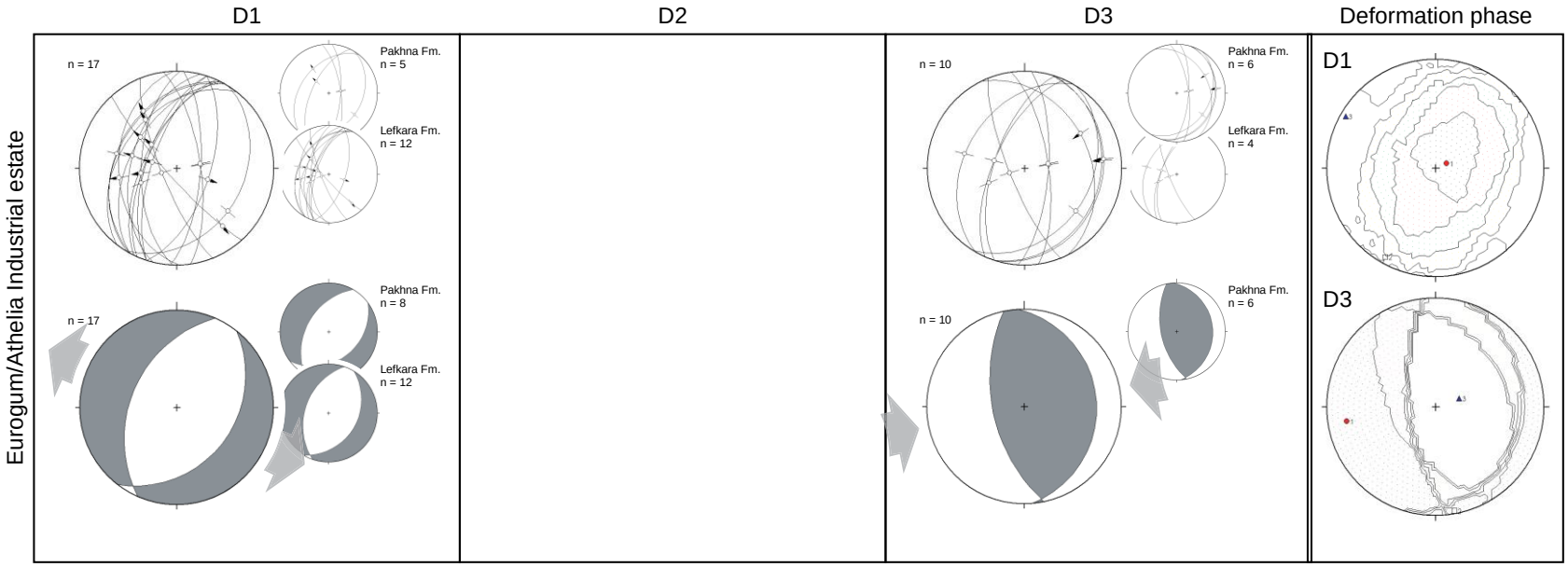

Figure 7-30: Deformation phases recognised at Acheleia (including the quarry at the Eurogum Factory) are: Late Miocene WNW-ESE extension (D1); and (ii) Pleistocene-Recent compression (D3)

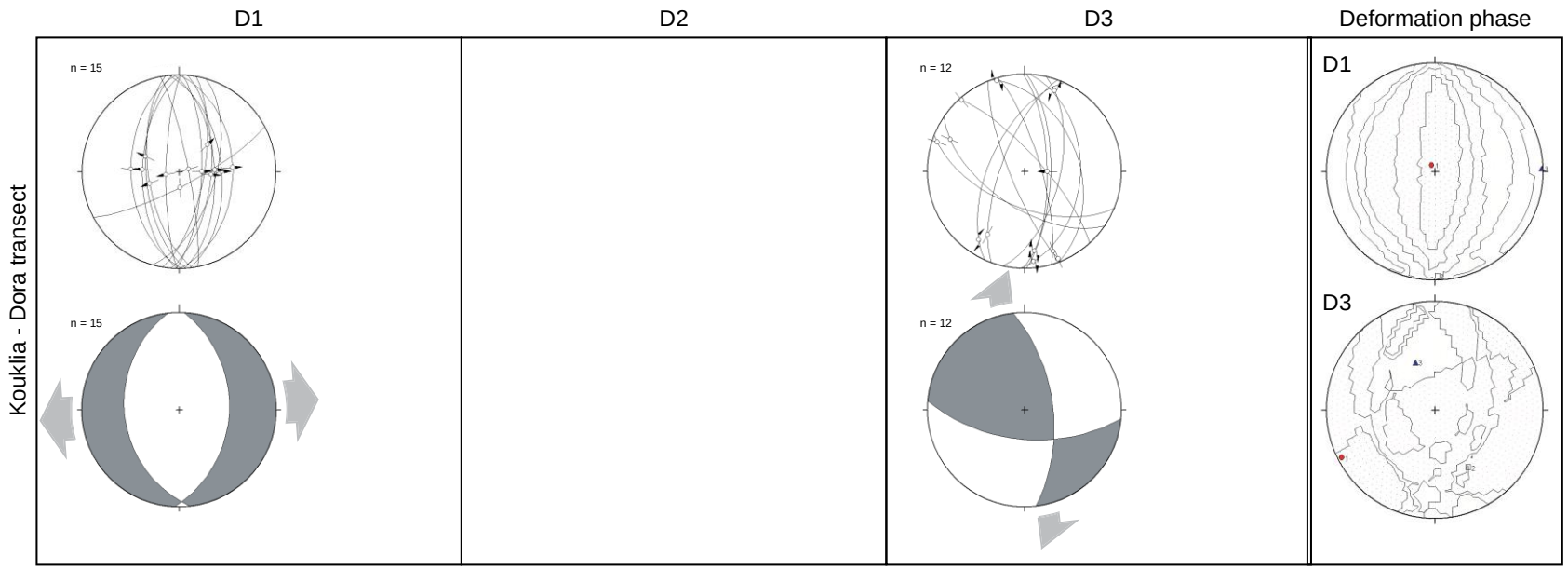

Figure 7-31: Deformation phases recognised at Kouklia are: (i) Late Miocene W-E extension (D1); and (ii) Pleistocene-Recent transpressional (right-lateral displacement on a NNW plane; D3)

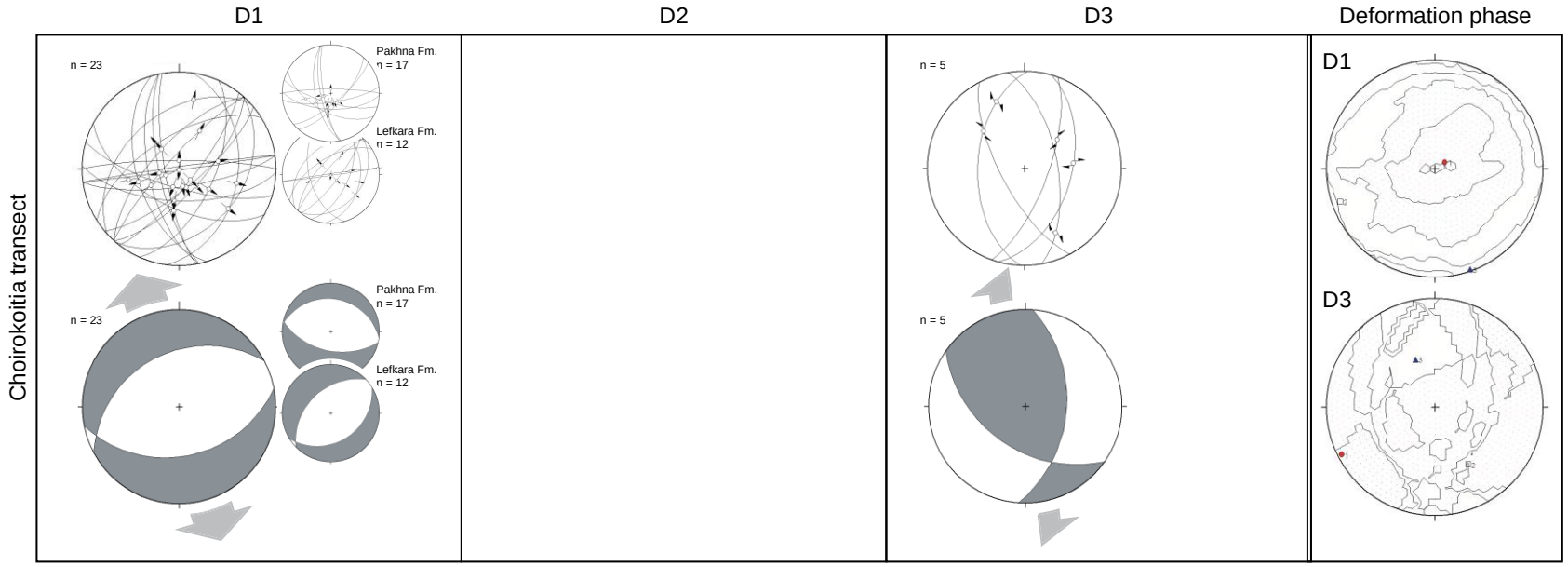

Figure 7-32: Deformation events recognised at Choirokoitia are: (i) Early Late Miocene N-S extension (D1); and (ii) Pleistocene-Recent transpression (right-lateral displacement on a N-S to NNW-SSE plane; D3)

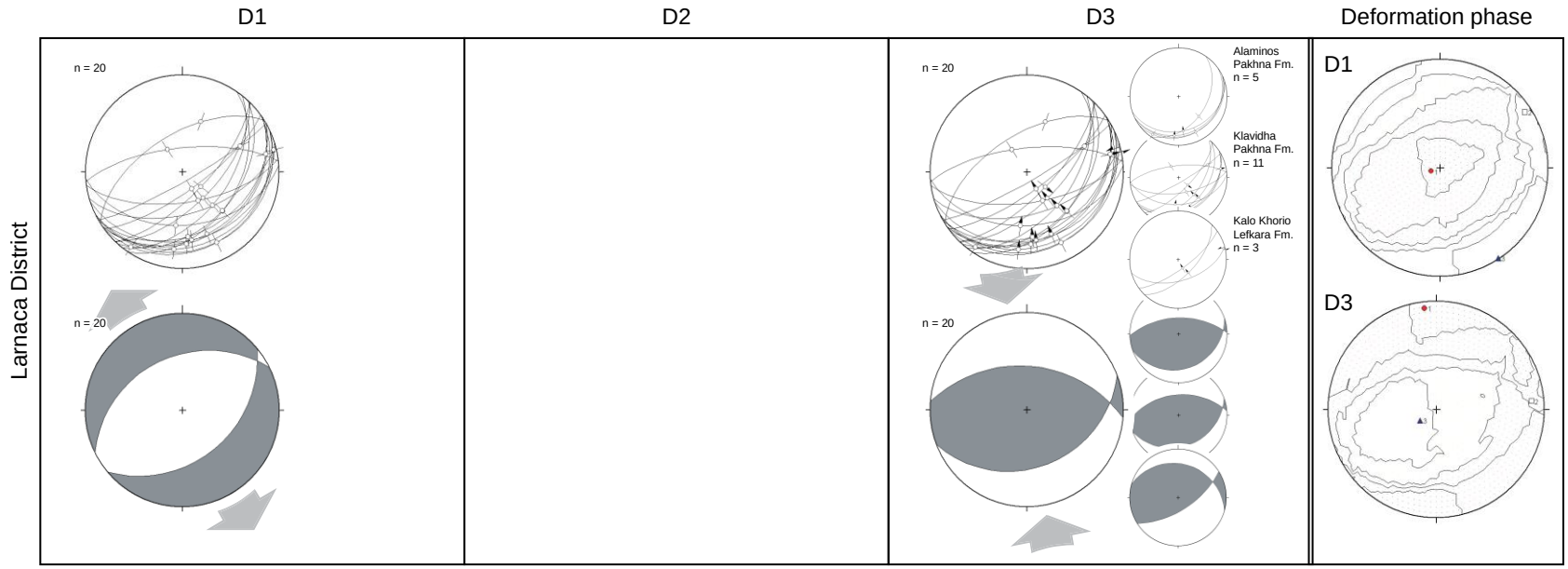

Figure 7-33: Deformation events recognised in the Larnaka District are: (i) early Late Miocene NW-SE extension (D1); and (ii) Pleistocene-Recent N-S contraction (D3)

Deformation phase D3: Early Pleistocene to Recent Compression/Transpression

A Pleistocene to Recent compressional/transpressional tectonic event is recognised in south Cyprus. E-W-trending sinistral faults and conjugate NNW-SSE-trending dextral and NNE-SSW-trending sinistral faults were generated during this phase of deformation. Luminescence dating has revealed that transpressional/compressional structures originated in the east of the island prior to propagating westwards: the Cape Kiti Fault was active in the Late Pliocene, the Kolossi Fault was active in the middle Pleistocene and, the Agia Marinouda fold was actively growing in the middle Pleistocene to Recent. Early Pleistocene to Recent compression/transpression additionally reactivated earlier D1 and D2 structures.

Kinematic analyses of fault slip data obtained from reactivated D1 and D2 structures throughout Cyprus have revealed a parititioning of stress. Prinicipal stress directions were computed for compressional/transpressional structures in several different geographic domains: east, west, central and north Cyprus. The results of this study are shown in Table 7-1.

				Principal stress directions					
Location		Age of affected strata	No.	σ_1		σ_2		σ_3	
				Azimuth	Dip	Azimuth	Dip	Azimuth	Dip
Acheleia	W	Miocene	30	284°	12°	015°	1°	111°	78°
Eurogum Quarry	W	Paleocene/Miocene	6	261°	19°	170°	3°	070°	71°
Kouklia	W	Miocene	12	044°	1°	135°	54°	314°	36°
Pissouri Basin	W	Miocene	7	059°	1°	151°	47°	328°	43°
Maroni	E	Miocene	64	156°	4°	248°	15°	51°	74°
Choirokoitia	E	Miocene	5	243°	4°	150°	39°	338°	51°
Larnaka	E	Paleocene	20	353°	7°	85°	13°	237°	75°
Larnaka†	E	Paleocene	-	NNE	hor.	-	-	ENE	hor.
Gerasa	C	Cretaceous/ Paleocene	292	032°	30°	301°	2°	207°	60°
Arakapas	C	Cretaceous	190	054°	19°	243°	70°	145°	3°
Ovgos	N	Miocene	12	227°	16°	081°	71°	320°	10°
Ovgos*	N	Miocene/Pliocene	-	NNE	hor.	-	-	ENE	hor.

*Table 7-1: Parameters of the deviatic stress tensors resolved from Cretaceous-Pliocene structures believed to have been reactivated in the Pleistocene to Recent. Abbreviations as follows: No. = number of structural measurements; W = west; E = east; C = central; N = north; * = result obtained by Harrison et al. (2004a); † = result obtained by Harrison and Tsiolakis (2006); hor = horizontal*

East Cyprus. Present deformation along the Kato Khorio, Klavdia and Alaminno fault lineaments is consistent with an approximate NNW-SSE-orientated horizontal maximum

prinicipal stress (σ_1) and an approximate NE-SW-orientated vertical least principal stress direction (σ_3). The intermediate prinicipal stress (σ_2) trends ENE-WSW. The results are consistent with an independent study by Harrison et al. (2004a); who propose that deformation in east Cyprus is consistent with an approximate horizontal σ_1 orientated NNE- and an approximate horizontal σ_3 orientated ENE. Harrison and Tsiolakis (2006) have inferred a Pliocene displacement along the Cape Kiti fault.

West Cyprus. A partition in present deformation is observed in west Cyprus, with the existence of two states of stress: in west Cyprus, the stress regime is compressional - σ_1 trends broadly E-W, σ_2 trends broadly N-S and σ_3 is vertical; in southwest Cyprus, the stress regime is transpressional - σ_1 trends broadly NE-SW, σ_3 trends broadly NW-SE and σ_2 becomes vertical.

Central Cyprus. Deformation along the Arakapas Fault Belt, central Cyprus, is consistent with an approximate NE-orientated horizontal σ_1 (054˚) and an approximate SE-orientated horizontal σ_3 (145˚). Deformation along the Gerasa Fault Belt, central Cyprus, is consistent with an approximate NE-orientated horizontal σ_1 (032˚) and a sub-vertical, SSW-orientated σ_3 (207˚).

North Cyprus. The deformation in the north of Cyprus is consistent with an approximate NNE-orientated horizontal maximum principal stress direction (σ_1) and an approximate ENE-orientated horizontal least principal stress direction (σ_3; Harrison et al., 2004a).

The results of this study have shown that transpressional/compressional stress was partitioned along the Cyprus plate boundary, and that this transpressional stress has propagated east-west with time, such that: the east coast of Cyprus was subject to transpression in the Late Pliocene, and the west coast of Cyprus was subject to transpression in the Middle Pleistocene to present. The Cape Kiti Fault was initiated during Late Pliocene transpression. The Agia Marinouda Fold was generated in the late middle Pleistocene, and continues to be an active structure in the present day.

Theoretical considerations: transtension. The incremental strain, and by implication stress, in a homogenous body of rock subject to strike-slip activity is shown in Figure 7-34a (Waldron, 2005). For infinitesimal simple shear, the shear body is a line of no extension. Extensional structures (e.g. normal faults) and shortening structures (e.g. thrust faults and

folds) are predicted to develop in orientations at 45º to the shear boundary, consistent with inferred directions of instantaneous shortening and extension.

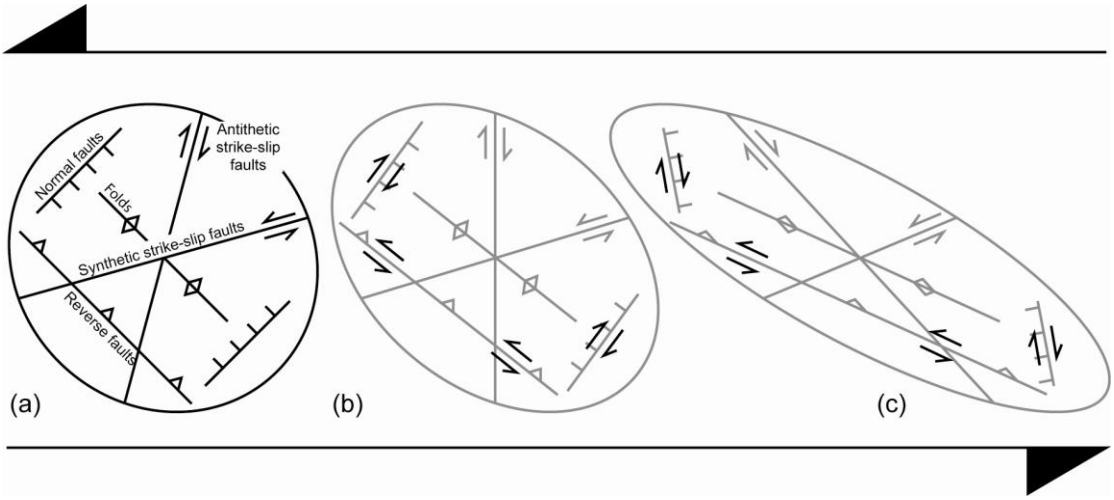

Figure 7-34: (a) Incremental strain associated with simple-shear deformation in a strike-slip zone; (b) modification of (a) by continued simple shear, showing that previous (grey) normal and thrust faults acquire oblique slip (black); (c) continued shear leads to inversion (black) of previous (grey) normal faults (modified from Waldron, 2005).

This model is complicated by rotation when finite strain is considered (Figure 7-34: Waldron, 2005). Any normal fault that initiated in the position shown in Figure 7-34a would be expected to rotate anticlockwise, and acquire a strike-slip component of motion. This would be synthetic to the sense of the main shear zone in the case of rotated thrust faults and antithetic for rotated normal faults (Figure 7-34b: Waldron, 2005). If the angle of shear exceeds 45º, a normal fault would rotate through an orientation perpendicular to the shear zone boundary, and experience incremental shortening (i.e. develop reverse-slip) (Figure 7-34c: Waldron, 2005). This would result in the inversion of the normal structures.

Discussion: In presenting this theory the author is not implying a rotation of the D1 and D2 structures. Indeed, palaeomagnetic analyses of Miocene to present rock samples imply no major (fault) rotations. The figure illustrates that NNW/SSE-striking faults in the Polis Graben and N/S-striking faults in the Pissouri Basin are aligned in a favourable position to be reactivated in transpression. The same can be said of ~ N/S-striking faults in the Kouklia-Dora region which cut Miocene strata, and Choirokoitia-Vavla region which cut Paleocene strata (Figure 7-35 (west)). In the Maroni-Psematismenos Basin and the Larnaka distinct, faults are aligned in an orientation that is more suited to compressional reactivation in a broadly NW-SE direction (Figure 7-35 (east)). If the present tectonic situation was to continue, as recent geodetic studies indicate, then rotation of the D1 and D2 structures is

envisaged in future. Prinicipal stress directions were computed for reactivated structures (D3) in east and west Cyprus: in east Cyprus deformation is consistent with an approximate NW-SE-orientated horizontal maximum prinicipal stress (σ_1) and an approximate E-W-orientated vertical least principal stress direction (σ_3). The intermediate prinicipal stress (σ_2) is horizontal and trends NE-SW; in west Cyprus deformation is consistent with a horizontal σ_1 orientated SSW-NNE, a sub-vertical σ_2 orientated E-W and a sub-horizontal σ_3 orientated NW-SE.

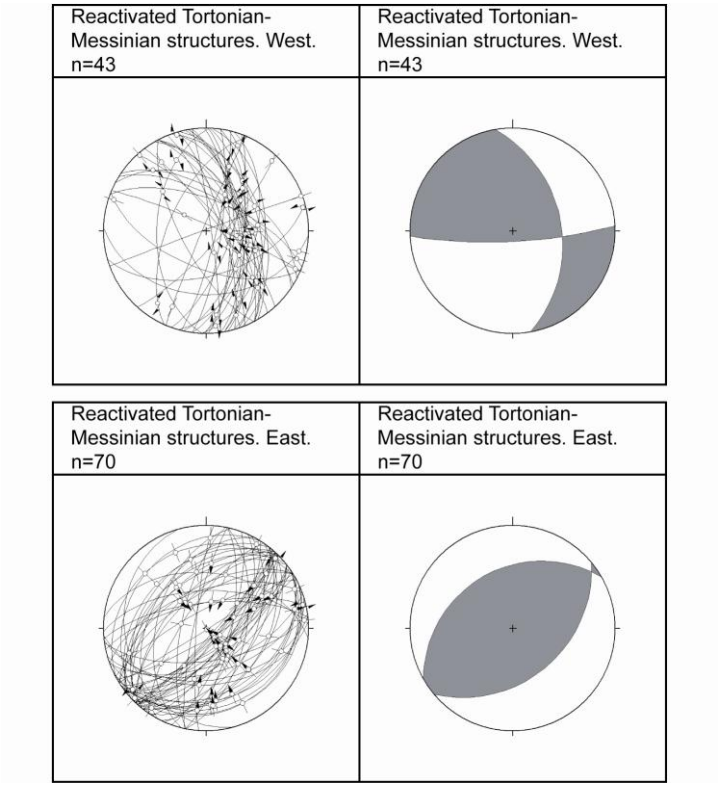

Figure 7-35: Fault data collected from Tortonian-Messinian ~N-S (top) and NE-SW to ENE-WSW (bottom) extensional structures, which have undergone subsequent reactivation.

D4: Late Pleistocene to Recent gravitational collapse

As stated above, the present stress regime is believed to be transpressional/compressional in nature. However, at a high structural level extension is still occurring. It is believed that in south and southwest Cyprus gravitational collapse is occurring away from an uplifting Troodos Massif. Luminescence dating indicates that extensional faulting is still occurring (or has occurred recently) at, or near to the villages of Amargeti, Pegeia, and Kalavasos. Geomorphological evidence in the form of exposed fault scarps, linear ridges and depressions, topographic breaks and offset streams and ridges, indicates that extensional

faulting played an important role in landscape evolution in the Pleistocene to Recent. New chronological constraints obtained during this study reveal a partitioning of stress during the Plio-Quaternary: in east Cyprus, extensional faulting was still occurring in the Polis Graben in the Middle to Late Pliocene (section 3.3.3.1); whereas in west Cyprus, the Cape Kiti fault formed during Middle to Late Pliocene transpression (section 3.3.4.5).

The term 'gravitational collapse' was introduced in section 7.4.2.1 (of this chapter) to refer to structures that are surficial in nature i.e. structures which do not penetrate the basement. It is important to distinguish between 'D1/D2' normal faults and 'gravitational' faults; as faults formed in the former event reflect crustal-scale processes, whereas faults formed in the latter are localised phenomena. An important outcome of the present structural study was the observation that many 'gravitational' or recent extensional faults trend in a similar direction to earlier structures. It is proposed that the trend of late Pleistocene to Recent faults is intrinsically linked to structures in the basement (i.e. Troodos Massif, Mamonia Complex, Paleocene to Miocene chalk). For example: in west Cyprus, WNW-ESE-striking faults in the Pegeia region trend in a similar direction to those in the Polis Graben; and in southwest Cyprus, active fault scarps/landslides in the Pissouri Basin follow structural trends identified in the basin sedimentary fill.

7.6 Tectonic comparisons

The tectonic setting of Cyprus is comparable to that of Crete in the Aegean region. The island of Crete is located on the over-riding plate of an arcuate subduction zone, the Hellenic trench (Le Pichon and Angelier, 1979). Today, Cyprus and Crete both lie above the same plate boundary (Figure 1-1); the western and central segments of the Hellenic and Cyprus 'Arcs' are perpendicular to the present-day relative motion of the African and Anatolian plates, forming the 'subduction sutures' or regions of incipient collision; however, the Pliny-Strabo trenches and the Latakia-Larnaka-Tartus ridge are sub-parallel to the slip vector, with a predominantly sinistral transform motion (Figure 1-1; Le Pichon et al., 1979). The over-riding plate of the Hellenic Arc has been subject to extension since the Middle Miocene (ten Veen and Postma, 1999; ten Veen and Kleinspehn, 2002; ten Veen et al., 2004); roll-back and extension behind the Hellenic trench are believed to have resulted in the Corinth rift system and the eastern Peloponnese gulfs. Extension in the Hellenic Arc is attributed to (i) the rapid retreat (roll-back) of the African slab (Le Pichon and Angelier, 1979) and (ii) the

westward extrusion of the Anatolian block along the North Anatolian Fault (Şengör, 1979). Reilinger et al. (1997) predict N-S extension at 14 ± 5 mm/yr across the Aegean extensional provenance. In contrast, the extension behind the Cyprus Arc is much less extensive. The over-riding plate of the Cyprus Arc has been subject to extension since the Middle to Late Miocene; roll-back and extension behind the Cyprus Arc are believed to have resulted in the Polis Graben and the formation of the Pissouri and Maroni-Psematismenos Basins.

A distinction between the Hellenic and Cyprus Arc extensional systems is that the Hellenic Arc has a 'volcanic arc', whereas no volcanic activity is known related to the present-day Cyprus Arc. Payne and Robertson (1995) attribute this to the different convergent rates over the two segments of the plate boundary. In the Hellenic Arc, present day convergence is calculated at 20-40 mm/yr (Wdowinski et al., 2006), whilst convergence in the Cyprus Arc is estimated at 7-9 mm/yr (Wdowinski et al., 2006; Mahmoud et al., 2005). The higher rate of convergence observed in the Hellenic Arc yields a significantly higher level of seismicity in the region, and generates earthquakes at a greater depth. Hence, the rate of roll-back and thus extension in the over-riding plate is today much greater in the Hellenic Arc than in the Cyprus Arc (Payne and Robertson, 1995). This is assumed to be have been true throughout the Neogene.

The Cyprus plate boundary displays geometric elements similar to other curved convergent plate boundaries, such as the Aleutian arc, the Sunda Arc, the Leeward Antilles arc, or Hikurangi subduction zone**.** However, its early history of increasing arc curvature and expanding overriding plate, and late history of incipient collision with Eratosthenes seamount make it distinct geodynamically.

7.7 A new model for the Cenozoic tectonostratigraphic evolution of Cyprus

In light of the new data presented above and published geophysical data, a new model for the Neogene tectonostratigraphic evolution of the southern part of Cyprus is proposed. In the following discussion, the rate of subduction is defined as the rate of convergence between an arbitrary point in the rigid interior of a downgoing plate and the outer part of a trench or foredeep basin located in front of the subduction zone; whereas, the rate of convergence is defined as the rate of motion between points within the rigid interiors of two converging plates (Royden, 1993). The subduction trench, or foredeep basin, will retreat when the rate of

subduction exceeds the rate of overall plate convergence; in such situations the ‘subduction zone’ is characterised by: (i) low topographic elevations; (ii) little erosion or denudation; (iii) regional extension within the overriding plate; (iv) little to no involvement of crystalline basement in shortening; (v) a protracted history of flysch deposition in front of the advancing orogenic belt and; (vi) by thin-skinned arcuate thrust belts that are concave towards the overriding plate (Royden, 1993).

A northward-dipping subduction zone is believed to have been initiated to the south of Cyprus during the Late Oligocene to Early Miocene (~ 23 Ma; Figure 7-36; Eaton and Robertson, 1993), when the convergent plate boundary migrated southwards from the vicinity of the Kyrenia lineament of northern Cyprus to near its present position (Kempler and Ben-Avraham, 1987). The convergent plate boundary migrated southwards following the docking of the Kyrenia Range thrust belt with the oceanic Troodos terrane during the Middle to Late Eocene (Robertson and Woodcock, 1986; Robertson, l990). The last remnant of oceanic crust to the south of the then active (Kyrenia) subduction zone was consumed during this time. The only substantial oceanic/stretched continental crust remaining in the gap between Africa and Eurasia then lay to the south and southwest of Cyprus. Subject to continued N-S convergence, the crust failed along pre-existing zones of crustal weakness. South of Cyprus a northward-dipping subduction zone was activated as a precursor to the present day active margin. The existence of compressional lineaments, trending NW-SE to WNW-ESE in onshore and offshore Cyprus (see chapter 3, McCallum and Robertson, 1993; Robertson, 1998b) may reflect a regional build up of stress immediately prior to the onset of northward subduction to the south of Cyprus (Eaton and Robertson, 1993; Ziegler et al., 1998). The compressional lineaments are restricted to southern Cyprus and areas directly offshore and are not recognized in other parts of Cyprus (i.e. north of the Troodos ophiolite). At this time the convergence of the African and Eurasian plates was approximately north-south.

As old Neotethyan oceanic crust was consumed at the trench the subducting plate underwent ‘roll-back’ (i.e. retreat of the subduction zone hinge; Figure 7-36; Royden, 1993), resulting in southward migration of the trench. D1 west-northwest/east-southeast extension of the Polis Graben and Pissouri Basin, and northwest-southeast extension of the Maroni-Psematismenos Basin is interpreted as a response to Late Miocene southward migration of the plate boundary.

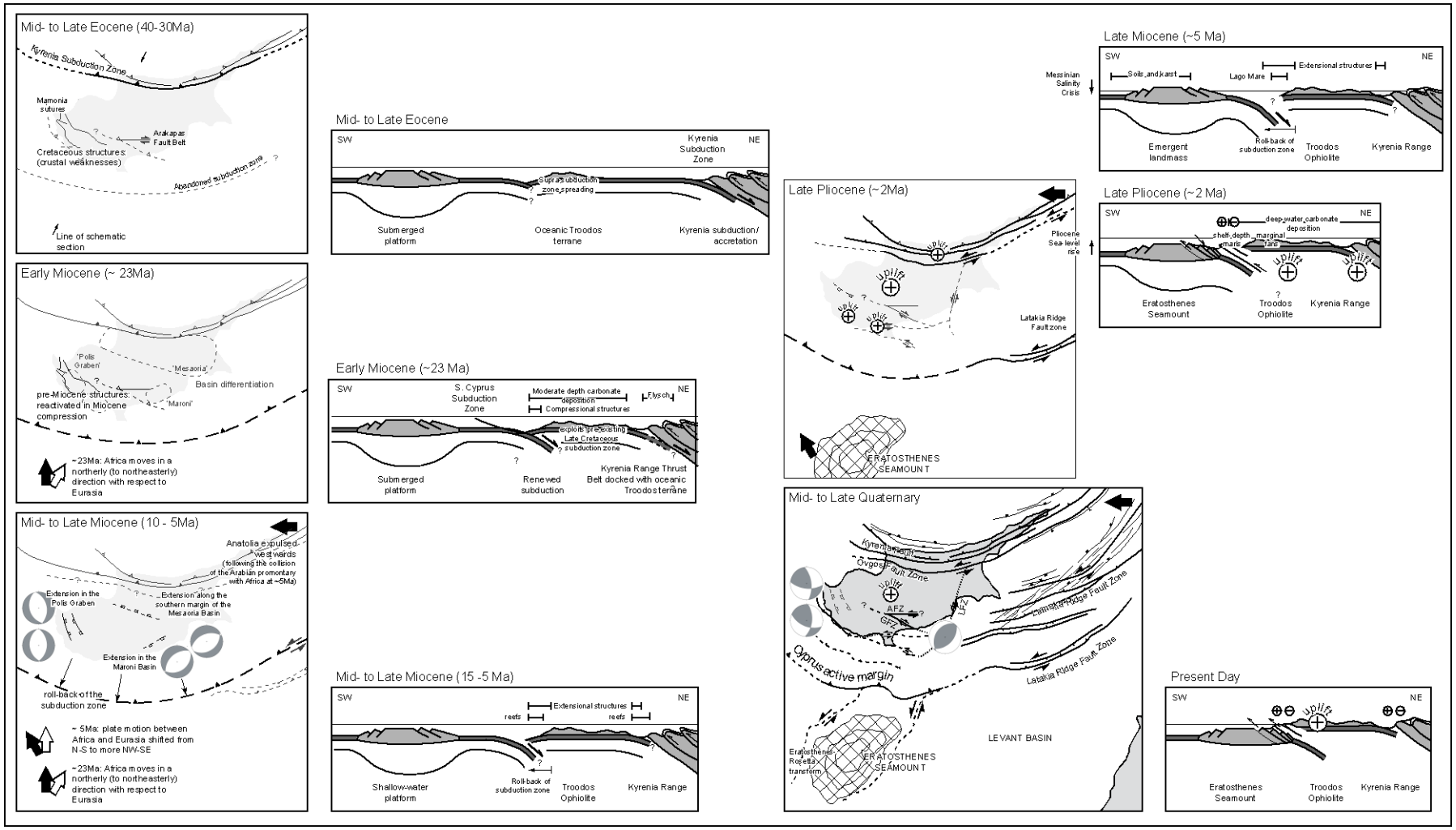

Figure 7-36: Plate reconstruction for the tectonic and sedimentary evolution of Cyprus (see discussion in text)

It is believed that the plate boundary lengthened as its curvature increased from a more east-west Early Miocene (~23 Ma) plate margin to its present position. The author attributes increased curvature of the arc to several individual or combined processes: (i) roll-back of the subduction interface related to the down-going African plate; (ii) Miocene supra-subduction zone extension in the Polis Graben (Payne and Robertson, 1995; 2000; this study), Pissouri (this study) and Maroni-Psematismenos Basins (this study); and latterly (> 5Ma), (iii) the westward expulsion of the Anatolian block along the North and East Anatolian Faults. Lallemand et al. (2005) have shown that back-arc stress correlates with slab-dip, i.e. supra-subduction zone extension (e.g. back-arc spreading) is observed for steep subduction dips (>50°), whereas supra-subduction zone shortening only occurs for deep dips less than 30°. In addition, slab dip correlates with the absolute motion of the overriding plate; slabs tend to dip more steeply for rapidly retreating subducting plates. Southward retreat of the Cyprus active margin led to a slight increase in the plate boundary curvature and corresponding supra-subduction zone extension.

The tectonics of the eastern Mediterranean Sea changed drastically in Mid- to Late Miocene time as the relative plate motion between Africa and Eurasia shifted from N–S (or NNE-SSW) to more NW–SE (Le Pichon and Angelier 1979; Jolivet and Faccenna, 2000; Harrison et al., 2004a; Jolivet et al., 2006). This kinematic change followed the collision of the Arabian and Eurasian plates in eastern Turkey and in the Caucasus, which initiated the westward extrusion of the Anatolian-Aegean Plate along the North Anatolian Fault Zone (in the Late Miocene-Early Pliocene (~5Ma); Şengör, 1979; Şengör et al., 1985) and the East Anatolian Fault (in the Early Pliocene age; Şengör et al., 1985). This resulted in compressional or transpressional tectonics in the Eastern Mediterranean, including the north of Cyprus, the Middle East and south-eastern Turkey (Ducloz, 1972; Robertson and Woodcock, 1986; Kelling et al., 1987; Harrison et al., 2004a). In the Mid- to Late Miocene the Cyprus–Hellenic subduction zone evolved into two distinct separate arcs.

In the Cyprus region this change produced: (i) an increase in the curvature of the plate boundary; (ii) an adjustment of the Africa-Anatolia convergence vectors; (iii) an outward shift in the absolute position of the plate boundary (associated with back-arc extension), and (iv) an arc-parallel lengthening of the western and eastern segments of the plate boundary. Zitter et al. (2003) note that the geometrical configuration of two highly arcuate subduction zones in the eastern Mediterranean Sea results in difficulties in accounting for plate convergence in the area between the two arcs. Ten Veen et al. (2004) suggest that

deformation is distributed throughout a very broad zone (~250km wide); from the Isparta Angle in the north (Zitter et al., 2003) to the Anaximander Mountains in the south (ten Veen et al., 2004).

The kinematic change in plate convergence vectors between Africa and Anatolia at ~5 Ma is reflected in the results of the present structural study in the Neogene basins and adjacent areas of Cyprus. An important reconfiguration of the stress field occurred during the tectonic hiatus between the late Messinian and the late Pliocene, a hiatus of a maximum of 2 million years. Minimal extensional faulting within the marls of the lower and middle Nicosia Formation (McCallum, 1989; McCallum et al., 1993) suggests that normal subduction, with little or no roll-back, resumed after the inferred Middle to Late Miocene rapid pulse (Payne and Robertson, 1995). By late Pliocene time (~ 2.5 – 1.8 Ma) the Polis Graben and Maroni-Psematismenos Basin were responding to D2 deformation. The Middle to Late Pliocene D2 extensional phase reoriented the Polis Graben and resulted in syn-depositional NE-SW extension.

During Middle to Late Pliocene times (post-3.16 Ma), the convergence rate between Africa and Anatolia decreased by approximately 25% in the eastern Mediterranean, with the relative plate motion direction becoming more oblique, i.e. west-northwesterly (Calais et al., 2003). The Eratosthenes Seamount collided with the Cyprus trench in the Late Pliocene (~ 2 Ma; Figure 7-36; Robertson et al., 1995a; Robertson, 1998b) and it appears that this has impeded subduction. The collision resulted in intense, focused uplift of southern Cyprus. For example**,** in the Pissouri region, Gilbert-type fan delta deposits occur at an elevation of 280m above mean sea level; Quaternary marine terraces at 300m and Fanglomerate deposits at 500m; and in Paphos region Quaternary marine terraces occur at an elevation of 500m (see chapter 4). To constrain the timing of regional uplift in south and central Cyprus, a magnetostratigraphy was generated for the Pissouri Basin and the Mesaoria Basin during this study. The results indicate that rapid uplift began in the latest Pliocene (c. 2.14 – 1.95 Ma), coincident with the large-scale progradation of Gilbert-type fan deltas into the Pissouri Basin, and large deltaic/fluvial deposition in the Mesaoria Basin.

A change in the regional tectonic regime from extension (transtension) to transpression (compression) occurred in the Late Pliocene/Early Pleistocene (~ 2 Ma) (see chapter 3). The Cyprus Arc is inferred to have migrated southwards throughout the Miocene and Pliocene, but remained fixed at its western (Anaximander Mountains) and eastern limits (Latakia,

Syria; Hardenberg and Robertson, 2007). This resulted in plate convergence along the easternmost and westernmost segments of the Cyprus Arc changing to transpression. The onset of the D3 kinematic phase at the end of the Pliocene/beginning of the Pleistocene (~2 Ma) suggests a threshold of obliquity was reached whereby the region north of the present plate boundary experienced oblique transpression. The author proposes a latest Pliocene/earliest Pleistocene threshold at which the plate boundary became sufficiently arcuate to force the plate boundary to begin to partition into oblique-slip and strike-slip (Figure 7-36). The Larnaka-Latakia ridges correspond to en echelon segmented bathymetric highs and lows, thought to demarcate sub-parallel sinistral strike-slip zones within the forearc (Ben-Avraham et al., 1995; Vidal et al., 2002a). Although sinistral wrench tectonics have been indicated offshore (Latakia-Larnaka Ridges), prior to recent studies (this study; Harrison et al., 2002; Harrison et al., 2004a,b; Harrison and Tsiolakis, 2006) no major strike-slip faults had been identified in the Cyprus region. Convergence between African and the Cyprus is nearly perpendicular in western/south-western Cyprus and highly oblique (>30˚) in eastern Cyprus (i.e. along the Larnaka-Latakia ridges). By 1.8 Ma, transtension due to east-west sinistral shear fully controlled the tectonic evolution of at least the southern part of Cyprus. The initial manifestation of this kinematic change was the generation of E-W-trending strike-slip faults (this study; Soulas, 2001; Harrison et al., 2004a; Soulas et al., 2005) and the development of conjugate left-lateral NNE-SSW-trending and right-lateral NNW-SSE-trending strike-slip faults (D3) (this study; Harrison et al., 2004a; Panayides et al., 2004,) e.g. the Kolossi Fault (Soulas, 2001), the Larnaka Fault Zone (Harrison and Tsiolakis, 2006), and the Roundabout-airport, Tremithos and Maroni River Faults (Soulas et al., 2005). Borradaile and Hamilton (2004) studied magnetic fabrics in the Polis Graben and identified a composite AMS fabric related to young (< 1 Ma) transpression (see chapter 4). In situ stress measurements and fracture logging in the Troodos Massif, central Cyprus (drill hole CY-4) have revealed a maximum principal stress orientated N070˚E, which is consistent with left-lateral strike-slip along the east-west plane; consistent with the westward expulsion of Cyprus along the southern boundary of the Anatolian plate. Subsequent deformation was manifested as the NW-SE-trending Agia Marinouda and Kouklia Folds (see chapter 3; Soulas, 1999). NNE-SSW-trending D1 structures in the Acheleia region were reactivated in WNW-ESE compression (this study, chapter 3).

To constrain the timing of deformation in the Pleistocene, optically stimulated luminescence dating was carried out on the Kolossi and Cape Kiti Faults, and the Agia Marinouda Fold (see chapter 5): the Kolossi Fault was active in the early to middle Pleistocene, i.e. between

174.1 ± 20.9 ka and 76.6 ± 16.43 ka; whilst the Agia Marinouda has been active since the early middle Pleistocene (~ 68.7 ± 28.2 ka) to the present day. Oblique convergence generated sinistral transpression in south and southeast Cyprus; this hypothesis is supported by shortening throughout the Latakia-Larnaka ridges. As the Mio- Pliocene plate boundary expanded outward from Anatolia, increasing its length and curvature, the deformed region stretched both parallel to the plate boundary and relative to a point in the central Anatolian realm. This combined stretching resolves into sinistral tangential shear along E-W faults and orthogonal transpressional components across NNE-SSW- and NNW-SSE- structures in Cyprus.

The present tectonic framework, in which compressional and transpressional stress is partitioned along the Cyprus active margin, is consistent with recent geodetic studies which indicate convergence to the south and southwest of Cyprus at 7-14mm yr^{-1} and left-lateral strike-slip convergence to the west at 6-10mm yr^{-1} (Figure 7-37; McClusky et al., 2003; Mahmoud et al., 2005; Wdowinski et al., 2006). In addition, a single GPS station located on Cyprus (NICO) indicates that Cyprus is moving westwards with respect to Eurasia, in a similar direction and magnitude to the GPS sites in central Anatolia (Wdowinski et al., 2006). This hypothesis is strengthened when one considers the recent seismicity that has occurred at the present plate boundary. The southern segment of the plate boundary is characterised by strike-slip and compressional events (Figure 7-5). Along the eastern part of the plate boundary, the relative motion between Anatolia and Africa (Sinai) is predominately left-lateral with increasing extension towards the east. It is characterised by strike-slip and normal events (Figure 2-6; Wdowinski et al., 2006).

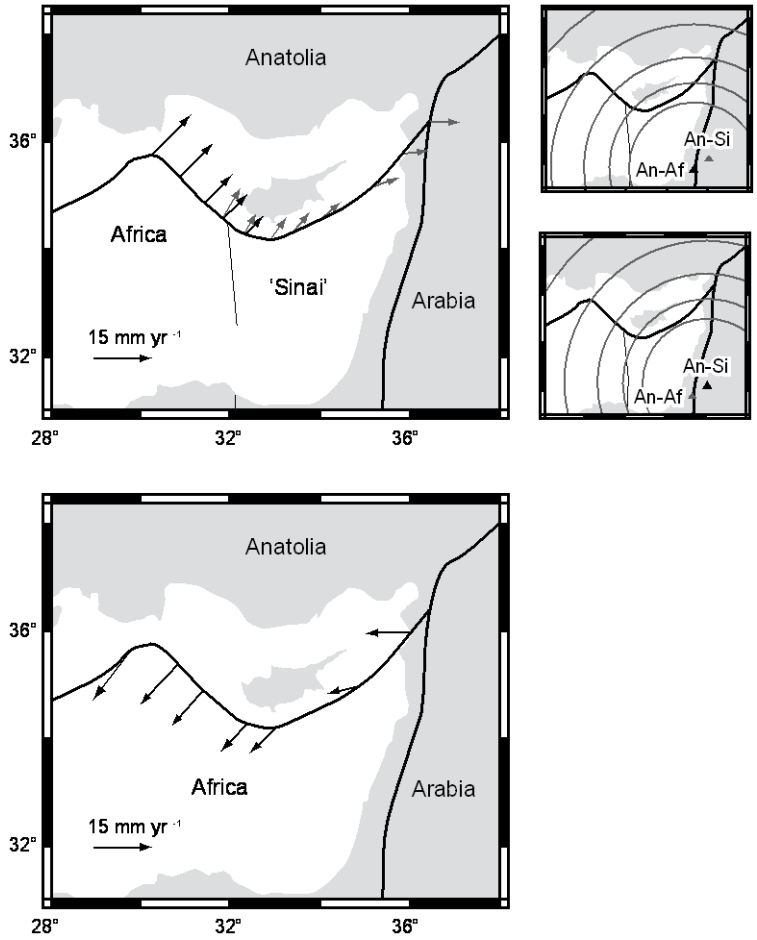

Figure 7-37: Predicted motion along the Cyprus Arc as calculated from (a) Anatolian-Africa and Anatolia-Sinai poles (Wdowinski et al., 2006). The black arrows show the relative motion between Anatolia and Africa (Africa in fixed reference frame) and the grey arrows the relative motion between Anatolia and Sinai (Sinai in fixed reference frame); and (b) Africa-Eurasia poles (McClusky et al., 2003). The black arrows show the relative motion between Africa and Anatolia (Anatolia in fixed reference frame)

Offshore Data: Data from offshore Cyprus including seismic reflection data and bathymetric trends on the continental slopes around Cyprus (Robertson, 1998b) and in the deep-marine Levantine Basin (Vidal et al., 2000a) are key to assess the broader significance of the structural relations observed onshore in Cyprus (Figure 7-24). The present-day boundary between the African and Anatolian plates is represented by a deformation front, commonly termed the Cyprus Arc, located south of Cyprus, between the island and the Eratosthenes Seamount (Ben-Avraham et al., 1995; Robertson et al., 1995a; Papazachos and Papaionnou, 1999; Vidal et al., 2000a,b; Woodside et al., 2002; Zitter et al., 2003). To the west of Cyprus, the Cyprus Arc extends along the Florence Rise (Woodside et al., 2002), and is probably connected to the Hellenic Arc in the Anaximander Mountains and/or Isparta Angle (ten Veen et al., 2004; Zitter et al., 2003). To the east of Cyprus, the plate boundary is suggested to

extend from south Cyprus through the Iskenderun Bay towards the junction of the East Anatolian Fault (Ben-Avraham et al., 1995; Vidal et al., 2000a,b; Al-Riyami et al., 2002; Hardenberg and Robertson, 2007). The tectonic character of the plate boundary changes along the Cyprus Arc from collision south of Cyprus, in the area between the Eratosthenes Seamount and the island, to transform deformation in the east (Figure 7-38).

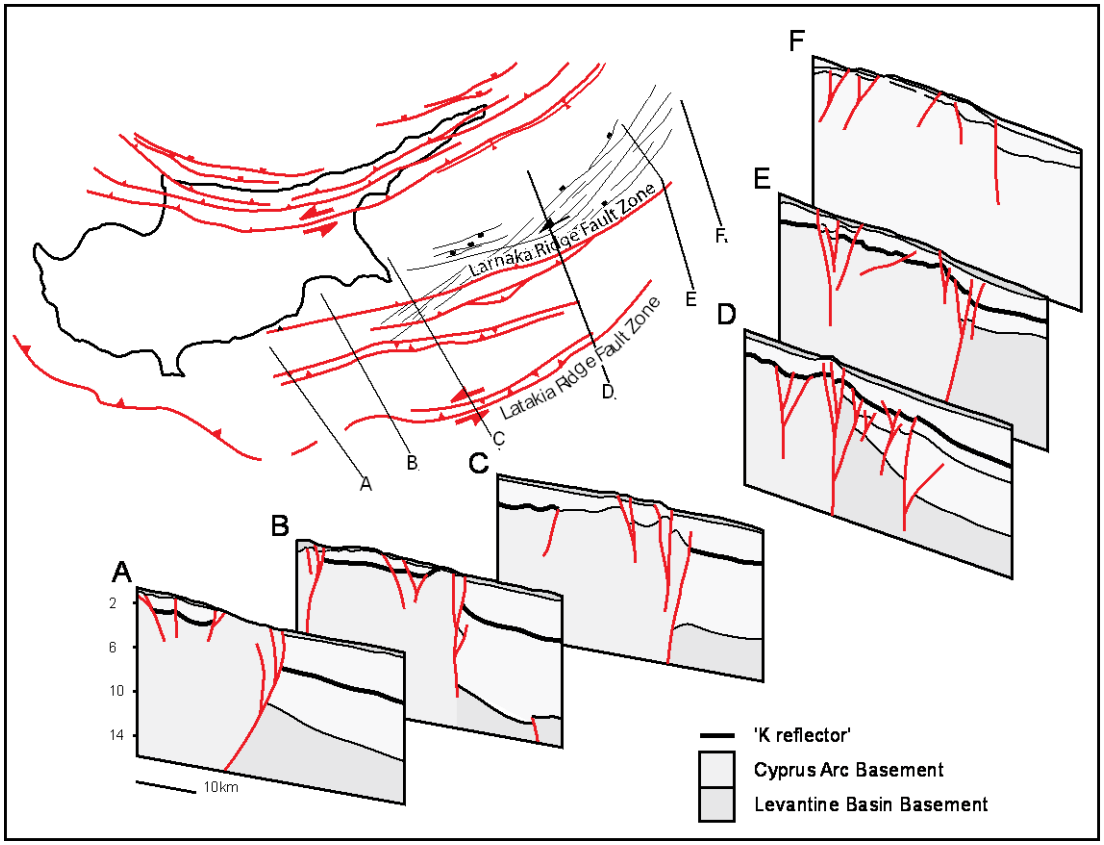

Figure 7-38: The structure of the African-Anatolia plate boundary as imagined by seismic reflection data; interpreted by Vidal et al. (2000a)

In the central part of the Cyprus Arc, defined as the part of the arc which is located between Cyprus and the Eratosthenes Seamount, a 2 km-deep asymmetrical basin and sediment-filled trench (Northern Trough; Robertson et al., l995; North Eratosthenes Basin; Vidal et al., 2000a) separates the island from the seamount. At the base of the northern slope of the seamount, an ENE-WSW-oriented asymmetrical fold with an axial surface dipping northwards, a seafloor relief of abount 40km, and a width of c. 2.5km was identified in the Pliocene-Quaternary unit above an inferred reverse fault (which affects pre-Messinian sedimentary rocks). This structure indicates that the direction of recent compression in this area was ~NNW-SSE, i.e. orothogonal to the ridge (Robertson et al., l995a; Galindo-Zaldivar et al., 2001; Robertson, 1998b).

High resolution seismic and deep-tow sonar data revealed that extensional deformation is occuring over most of the seamount, whereas compressional deformation was observed within the trench basin to the north and along its southern margin. Normal faults are located mainly in the seamount plateau area. The main fault set has a preferred E-W orientation and a northward dip. Faults are inferred to be active or have been active recently, because they reach the seafloor and are exposed as sediment-free scarps (as observed by deep-tow side-scan sonar and sub-bottom profiler; Robertson et al., l995a). Compressional structures were observed around the seamount. Folds and reverse faults facing southwards towards the seamount were observed in this basin. The Eratosthenes Seamount is bounded by two sets of strike-slip faults; one set strikes roughly NE-SW and forms the southeast margin of Eratosthenes, and the other strikes roughly NW-SE and forms the southwest margin. Considering the present N-S to NNW-SSE compressional stress field, determined by earthquake focal mechanisms, these faults probably have a transpressive sinistral slip along the NE-SW branch and a transpressive dextral slip along the NW-SE branch (Galindo-Zaldivar et al., 2001). Post-collisional deformation of this seamount includes the development of small-scale crestal flexural extensional faults and of thrust structures along its northern and southern flanks (Sage and Letouzey, 1990; Robertson et al., l995; Robertson, 1998b). The Eratosthenes seamount is currently in the process of tectonic collision with Cyprus and is beginning to disintegrate and collapse perhaps because it resists subduction (Robertson et al., l995a; Galindo-Zaldízar et al., 2001; Robertson, 1998b).

The deformation in the eastern part of the Cyprus Arc is partitioned along strike-slip fault systems distributed in sets of flower structures. The bathymetric expression of this strike-slip system is a series of three ridges, with associated linear depressions (Ben-Avraham et al., 1995; Vidal et al., 2002a,b). The sub-vertical fault zone and the structures observed within the Cyprus Arc to the east indicate that lateral movements govern the present tectonics in the area, and they also indicate a rapid change in the character of the plate boundary east of the collisional zone of the Eratosthenes Seamount. Ben-Avraham et al. (1995) suggest a Late Miocene sinistral-slip history for the aseimic Latakia-Larnaka ridges, as the ridges formed before the deposition of the Messinian evaporites.

Other fault trends similar to those observed onland occur offshore Cyprus (Figure 7-24). On the basis of bathymetric scarps and/or seismic profiles, NNE-SSW, and WNW-ESE faults of the D1 and D2 phases are pervasive throughout the continental slopes south of Cyprus and

the Levantine Basin (Roberts and Peace, 2007). The continuous faulting along the Cyprus Arc and across it, suggests a strong coupling between both sides of the Arc.

7.8 Conclusions

Three principal alternative plate tectonic models have been discussed for the Late Tertiary to Recent tectonic evolution of Cyprus. The results of numerous local interpretations have also been considered.

Model 1: Subduction/Incipient collision (Robertson, 1990; 2000). In this model, deformation since the Late Miocene was driven by supra-subduction extension above a southward migrating trench at the Cyprus active margin. A Late Miocene phase of extension was accommodated by a rapid pulse of subduction, and subsequent retreat of the subduction hinge. A Plio-Pleistocene phase of faulting was accommodated by differential extension in the overriding plate between an area where roll-back was occurring and an area where subduction was impeded.

Model 2: Advanced collision (Sage and Letouzey, 1990; Soulas, 2003; Calon et al., 2005a,b). In this model, deformation since the Late Eocene (~ 35 – 38 Ma) has been due, dominantly to broadly north-south crustal contraction. South-vergent thrusting is accommodated in the Troodos-Larnaka culmination, and the Kyrenia Range. The Mesaoria Basin evolved in the Eocene-Oligocene to Recent as a large piggy-back basin, nestled between the active fronts of the Troodos-Larnaka culmination and the Kyrenia fold/thrust belt.

Model 3: Transpression (Harrison et al., 2004a; Panayides et al., 2004). In this model, deformation since Late Miocene time (~ 9 Ma) has been due, dominantly to left-lateral transpression, in a collisional setting. The restraining blocks were the Kyrenia range to the north and the Eratosthenes Seamount to the south.

In light of the new data presented in this thesis and published geophysical data (see section 7.3), a new model for the Neogene tectonostratigraphic evolution of Cyprus is proposed. This model is distinct from previous models in that several spatially and temporally distinct tectonic events are recognised. The author recognises an abrupt transition from an extensional stress regime in the Mio-Pliocene to a transtensional/compressional stress regime

in the Pleistocene. It recognises for the first time strain partitioning along the Cyprus Arc; with transpressional structures originating in the east of Cyprus prior to propagating west. The high resolution at which structural data was collected has allowd one to identify new trends, such as the progration of E-W extension along the southern margin of the Mesaoria Basin in the Late Oligocene to Early Miocene.

Areas to the east of Cyprus (Syria, S Turkey) were in a collisional setting from Mid-Miocene time onwards. Cyprus remained in an oceanic embayment (Levant Sea) further west and subduction continued during Miocene time. Compressional processes may have been active at depth during this time. Southward extension (trench roll-back) was taking place at a high structural level in S Cyprus, as with many other convergent margin settings (e.g. SW Peloponnese; Aleutians; Sunda arc). The southward migration of the trench gave rise to a dominantly extensional regime within the Middle to Late Miocene and basin differentiation began at this time. Subsequently, the collision of the Eratosthenes Seamount with the Cyprus Arc obstructed subduction and initiated rapid uplift of the Troodos Massif. From the Late Pliocene onwards, the island of Cyprus has been subjected to E-W transpressional stress. The initial manifestation of this kinematic change was the generation of E-W-trending strike-slip faults and the development of conjugate left-lateral NNE-SSW-trending and right-lateral NNW-SSE-trending strike-slip faults. Subsequent deformation is documented in a compressional lineament in SW Cyprus. Transpression resulted in the reactivation of Late Miocene NNE-SSW- and NNW-SSE-striking structures. In addition, the over-riding plate in southwest Cyprus still appears to be undergoing gravity spreading outwards from the developing collision zone.

Chapter 8: Conclusions

The following points summarise the new data, interpretations and conclusions presented in the preceding chapters of this thesis.

Structural data/interpretations

1. On the basis of new structural data, including data obtained from penetrative structures (faults, folds and their kinematic development in time) and information from syn-sedimentary structures (syn-sedimentary folds, growth strata and growth faults), four deformation events are recognised in south Cyprus. In total 3,294 faults and 1,613 fractures were measured in south and central Cyprus. Of this total, 1,413 faults yielded slip data.

2. In west Cyprus (i.e. Polis Graben), a Late Miocene (Tortonian – Messinian) phase of extension generated NW-SE- to NNW-SSE-striking normal faults (D1). Faults of this orientation are observed cutting Palaeogene (at Kathikas village and between Stroumpi and Tsada villages) and Miocene strata (at Kathikas village and Evretou Dam). In southwest Cyprus (i.e. Pissouri Basin), the same event generated N-S- and NW-SE-striking normal faults, whilst in south Cyprus (i.e. Maroni-Psematismenos Basin) it generated NE-SW-striking normal faults.

Fault-plane solutions, often used as a first approximation of stress (e.g. Marrett and Allmendinger, 1990), were resolved for faults in each of the Neogene basins (Polis, Pissouri and Maroni-Psematismenos). The stress regime responsible for generating the NW-SE- to NNW-SSE-striking faults in the Polis and Pissouri Basins was characterised by broadly east-northeast/west-southwest extension, with a maximum principal stress (σ_1) orientated vertical, and intermediate and minimum principal stresses (σ_2 and σ_3, respectively) orientated sub-horizontal. In contrast, the stress regime responsible for the generating the NE-SW faults in the Maroni-Psematismenos Basin was characterised by broadly northwest/southeast extension, with σ_1 orientated vertical, and σ_2 and σ_3, orientated sub-horizontal, respectively.

3. A localised, Middle to Late Pliocene D2 phase of NE-SW extension (transtension?) generated NW-SE- to WNW-ESW-trending faults: (i) in west Cyprus, NW-SE- to WNW-ESE-striking faults cut Pliocene strata near the villages of Miliou, Skoulli, Pelathousa and Amargeti (see chapter 3); and (ii) in south Cyprus, WNW-ESE-striking faults cut Pliocene

strata in Vasiliko Quarry (see chapter 3). The fault trend is distinct from the earlier phase of faulting which formed the southern Neogene basins.

4. Early Pleistocene to Recent transpression (D3a) generated left-lateral strike-slip faults along E-W trends and associated conjugate left-lateral NNE-SSW-striking and right-lateral NNW-SSE-striking strike-slip faults. In south Cyprus, the Kolossi Fault lineament and the Paphos Airport Fault are examples of faults generated along E-W trends. The left-lateral, NNE-SSW-trending Cape Kiti Fault and the right-lateral, NNW-SSE- to NW-SE-striking Airport-roundabout, Tremithos and Maroni River Faults formed as conjugate faults within regional left-lateral E-W transpressional stress.

In southwest Cyprus, NNE-SSW- and NNW-SSE-striking structures formed during Late Miocene E-W to ENE-WSW extension (D1) were reactivated in the Pleistocene (D3a): (i) normal N-S-striking faults within the Pissouri Basin were reactivated in a dextral sense; and (ii) at Kouklia village, normal N-S- to NNW-SSE-striking faults were reactivated in a dextral sense. Meso-scale structures in south Cyprus, trending NE-SW, were also reactivated: (i) normal NE-SW-striking faults in the Maroni-Basin were reactivated during NW-SE compression; and (ii) normal ENE-WSW-striking faults in the Larnaka region were reactivated during NW-SE compression (minor left-lateral slip is noted on a ENE-WSW plane).

5. The NW-SE-trending Agia Marinouda and Kouklia folds were generated during middle Pleistocene to Recent compression (transpression?) (D3b). WNW-ESE-striking, NNE-dipping imbricate thrusts formed during the same event. Normal NNE-SSW-trending faults (D1) at Acheleia Dam were reactivated during E-W compression.

6. Extensional faults, trending WNW-ESE, and dipping to the NNE and SSW affect Pliocene and Pleistocene strata near Pegeia and Amargeti village. Faults at Pegeia and Amargeti were previously mapped as normal structures; however, they are re-interpreted here as gravitational in origin. The Kalavasos Vasilikós valley is bounded by NE-SW-trending, NE- and SW-dipping and WNW-ESE-trending, NNE- and SSW-dipping normal faults. These data indicate that at a surficial level, localised areas of Cyprus (e.g. Pegeia, Amargeti and Kalavasos) are undergoing gravity spreading away from the developing collisional zone (D4).

Sedimentological/stratigraphical data/interpretations

1. New sedimentological data in the form of geological maps, sedimentary logs, palaeocurrent data and sedimentary facies analysis have shed light on the tectono-sedimentary evolution of the Pissouri Basin.

The Pissouri Basin developed as a localised depocentre in the early Miocene, as recorded in the transition from deep-water pelagic sediments of the Maastrichtian - Upper Oligocene Lefkara Formation, to more varied shallower-water, mixed carbonate and terrigenous sediments of the Upper Oligocene - Upper Miocene Pakhna Formation. Sedimentary logs indicate a large influx of terrestrial material into the basin coincident with the deposition of the Pakhna Formation. Channel orientations in the uppermost (Serravallian – Tortonian) Pakhna Formation are aligned ~N-S, perpendicular to the direction of Late Miocene ~E-W extension (D1).

2. By the latest Miocene (Messinian) the Pissouri Basin existed as a shallow, fault-bounded, silled depression semi-isolated from the Mediterranean Sea to the south. A range of pre-evaporitic to evaporitic facies accumulated, including minor amounts of microbial carbonate, overlain by fine to coarse-grained and redeposited gypsum. Facies analysis indicates several periods of tectonic instability during the Messinian, associated with sediment redeposition and slumping.

3. During the latest Miocene, small fan-deltas prograded from the fault-active basin margins into ephemeral lakes overlain by palaeosols (‘Lago Mare’ facies). Previous workers have assigned ophiolite-derived pebble-conglomerates to the Lago Mare succession. Thus, pronounced uplift, emergence and erosion of the Troodos Massif had occurred by the Late Miocene. However, detailed sedimentary logging, facies analysis and geomorphological studies during this work, indicate that these conglomerates are instead terrace deposits of Early-Mid Pleistocene age (when, by general agreement, uplift was already occurring: see below).

4. The end of the Messinian salinity crisis was marked by deposition of marginal fan-deltas, which pass basinwards into shelf-depth marls (Nicosia Formation). Facies associations within the Nicosia Formation were identified, and their spatial and temporal distribution mapped, so that one could determine the Pliocene evolution of the basin. Fine-

grained basinal facies are intercalated with terrigenous siltstone/sandstone turbidites, interpreted as the bottomsets and foresets of large marine fan-deltas. Large, intercalated lenses of bioclastic calcarenites and ophiolite-derived sandstones are interpreted as conduits for marginal shelf and terrigenous material. Soft-sediment deformation and slump structures (e.g. overturned and recumbent ductile folds) characterise the margins of these channels.

5. The orientation of the channelling and slumping indicate a generally southward palaeo-slope towards the deep Mediterranean Sea. Also, the orientation of channels and slumps in the lower and middle Nicosia Formation remain similar to those observed in the Pakhna Formation, despite the presence of the intervening salinity crisis. This may imply that the extensional stress first noted in the Late Miocene, was still prevalent in the Pliocene, influencing sedimentation.

6. Higher within the Plio-Pleistocene succession, stacked micro-Gilbert-type fan-deltas are interpreted as prograding fan-delta topsets; these are interbedded with Terra Rosa-type palaeosols. The Gilbert-type fan deltas contain the first occurrence of abundant Troodos-derived clasts, indicating that by this time the Troodos Massif was emerged and being eroded.

Chronological data/interpretations

1. Palaeomagnetic analysis of Plio-Pleistocene units in the Pissouri and Mesaoria Basins was undertaken to constrain the regional Plio-Pleistocene stratigraphic framework and date uplift of the Troodos Massif. In total 119 samples were analysed. Of this total, 29 samples were from the Pissouri Basin and 90 samples were from the Mesaoria Basin.

In south Cyprus, rapid uplift of the Troodos Massif is marked by the progradation of Gilbert-type fan-deltas into the Pissouri basin (see above). The new palaeomagnetic age data constrain deposition of the Gilbert-type fan deltas to 2.14 – 1.95 Ma, or 1.77 – 1.66 Ma, between the Reunion and Olduvai subchrons, or the Olduvai and Gibsa subchrons of the Matuyama Chron, respectively. Therefore, pronounced uplift of the Troodos Massif is dated as the latest Pliocene/earliest Pleistocene.

2. This timing of uplift is compatible with new palaeomagnetic data obtained from the Mesaoria Basin. Uplift of the Troodos Massif in the latest Pliocene is coincident with: (i) the

progradation of the Kephales fan-delta system into the Mesaoria Basin; and (ii) shallow-marine Athalassa Member sandbodies migrating across the Mesaoria Basin. New palaeomagnetic ages constrain deposition of the Kephales fan-delta as 2.14 – 1.95, between the Reunion and Olduvai subchrons of the Matuyama Chron and deposition of the Athalassa sandbodies at 2.14 – 1.24 Ma, between the Reunion and Cobb Mountain subchrons of the Matuyama Chron.

3. Marine terrace deposits at Paphos, Kouklia, Lemesos and Larnaka were sampled (N = 20, n = 48) and dated palaeomagnetically. In the Paphos region, terraces were sampled at approximate elevations of 0m, 0-10m, 50, 100, 125, 200, 270 and 500m. All terraces yielded a normal polarity. The best estimate of their age is that they were deposited prior to 0.78 Ma. The upper terraces (i.e. at 270m and 500m) were previously estimated as Late Pliocene; the new palaeomagnetic data indicate that the terraces are substantially younger.

4. Optically stimulated luminescence (OSL) dating was used as a tool to constrain the age of Pleistocene deformation. OSL age constraints were established for: (i) faulted strata and overlying sediments along the Kolossi Fault; (ii) an uplifted aeolinitic terrace on the Cape Kiti Fault; (iii) growth strata preserved on the northern limb of the Agia Marinouda Fold; and (iv) extensional faulting near to Amargeti and Kalavasos. Full dating protocols were carried out on 12 samples, profiling work was undertaken on an additional 21 samples.

The OSL results indicate that transpressional lineaments (D3) in south Cyprus originated in the early Pleistocene (i.e. movement on the Kolossi Fault occurred between 174.1 ± 20.9 ka and 76.6 ± 16.43), and are still active today (i.e. Pleistocene movement on the Cape Kiti Fault is constrained between 38.1 ± 13.2 and 12.1 ± 0.1 ka).

OSL ages obtained from growth strata preserved on the northern limb of the Agia Marinouda fold, indicate that the structure has been active since prior to 76.8 ± 31.6 ka. This implies that the compressional lineaments (D3) in southwest Cyprus originated in the middle Pleistocene and are still actively growing today.

Extensional faulting observed at Amargeti was dated using the OSL technique. Samples were collected from the hangingwall and footwall of a WNW-ESE-striking normal fault. Faults at Amargeti were still actively extending in the late middle Pleistocene: (i) the last major episode of faulting predates 43.4 ± 2.1 ka; and (ii) the interval between 29.3 ± 6.6 ka

and 6.45 ± 0.1 ka was one of tectonic quiescence. Extensional faulting in the Vasilikós Valley, south Cyprus occurred in the late early Pleistocene – late Pleistocene, between 78.3 ± 5.3 ka and 10.4 ± 2.2 ka.

Regional tectonic setting

1. Three alternative models for the Late Cenozoic to Recent tectonostratigraphic evolution of Cyprus have been considered in light of the new evidence and published geophysical data, i.e. (i) subduction/incipient collision; (ii) advanced collision; and (iii) transpression. Problems have been identified in detail in all of the three models, as discussed in the thesis (Chapter 7).

2. A new working hypothesis for the tectonic setting and development of Cyprus, in its regional context, is proposed as follows:

Northward subduction initiated to the south of Cyprus in the Late Oligocene to Early Miocene (~23 Ma). During the Miocene the subduction zone retreated southwards, leading to extension in the over-riding plate. The southern Neogene basins (Polis/Polemi, Pissouri and Maroni-Psematismenos Basins) formed during this initial phase of extension (D1). In west and southwest Cyprus D1 extension was in a broadly E-W to NE-SW direction, and N-S- to NW-SE-striking faults formed as a result. In south Cyprus D1 extension was in a NW-SE extension, so that NE-SW-striking faults formed. The difference between the direction in west and south Cyprus is attributed to the curvature of the Cyprus Arc. A later phase of extension in the Early to Middle Pliocene resulted in the formation of a second generation of faults (D2). The Eratosthenes Seamount collided with the Cyprus active margin in the late Pliocene (~3 Ma). Both regional and local controls triggered transpression in the over-riding plate. Transpression resulted in left-lateral E-W-trending and conjugate left-lateral NNE-SSW- and right-lateral NNW-SSE-trending strike-slip faults (D3a). Earlier structures (D1/D2) were reactivated. Compression resulted in intense NE-SW contractional deformation oriented along NW-SE trend (D3b). At a surficial level, in localised areas (e.g. Pegeia, Amargeti and Kalavasos) Cyprus appears to be undergoing gravity spreading outwards from the developing collisional zone (D4).

3. In a regional context, the results of this work suggest that Cyprus is undergoing a transition from a long-lived subduction system to one of diachronous collision accompanied

by westward tectonic escape, accommodated by E-W-trending sinistral faults and conjugate dextral NNW-SSE- and sinistral NNE-SSW-striking faults.

Chapter 9: References

Aitken, M.J. 1983. Dose rate data in S.I. units. *PACT*, **9,** 69-76.

Aitken, M.J. 1999. Archaeological dating using physical phenomena. *Reports on Progress in Physics*, **62**, 1333-1376.

Aksu, A.E., Hall, J., Yaltırak, C. 2005. Editorial: Miocene to Recent tectonic evolution of the eastern Mediterranean: New pieces of the old Mediterranean puzzle. *Marine Geology*, **221**, 1-13.

Algermissen, T. and Rogers, A. 2003. Seismic hazard studies of Cyprus: A progress report. In: Petrides, G., Chrysostomou, Chr., Kyrou, K. and Hadjigeorgiou, Chr. (eds), Proceedings: Earthquake Risk Minimization; International conference. *Cyprus Geological Survey Department, Lefkosia.*

Algermissen, T. and Rogers, A. 2004. Chapter 5: A Cyprus earthquake hazard assessment: maps of probabilistic peak ground acceleration and uniform – Hazard Pseudo – absolute acceleration spectral response. In: DeCoster, M., Zomeni, z., Panayides, I., Petrides, G. and Berksoy, O. Seismic hazard and risk assessment of the Greater Nicosia Area. *Internal report, Cyprus Geological Survey Department.*

Allen, M. 2004. Late Cenozoic reorganisation of the Arabia-Eurasia collision and the comparison of short-term and long-term deformation rates. *Tectonics*, **23**.

Al-Riyami, K., Robertson, A.F.H.R., Dixon, J. and Xenophontos, C. 2002. Origin and emplacement of the Late Cretaceous Baer-Bassit ophiolite and its metamorphic sole in NW Syria. *Lithos*, **65**, 225-260.

Ambraseys, N.N. 1962. Data for the investigation of the seismic sea-waves in the Eastern Mediterranean. *Bulletin of the Seismological Society of America*, **52**, 895-913.

Ambraseys, N.N. and Adams, R.D. 1993. Seismicity of the Cyprus region. *Terra Nova*, **5**, 85-94.

Angelier, J. and Mechler, P. 1977. Sur une méthode graphique de recherche des contraintes principales également utilisable en tectonique et enséismologie: la methode des diédres droits. Bull. Soc. Géol. France , **19**, 1309-1318.

Anzidei, M., Baldi, P., Casula, G., Galvani, A., Mantovani, E., Pesci, A., Riguzzi, F. and Serpelloni, E. 2001. Insights into present-day crustal motion in the central Mediterranean area from GPS surveys. *Geophysical Journal International*, **146**, 98-110.

Armijo, R., Lyon-Caen, H. and Papanastassiou, D. 1992. E-W extension and Holocene normal fault scarps in the Hellenic Arc. *Geology*, **20**, 491-494.

Arvidsson, R., Ben-Avraham, Z., Ekstrom, G. and Wdowinski, S. 1998. Plate tectonic framework for the October 9, 1996, Cyprus earthquake. *Geophysical Research Letters*, **25**, 2241-2244.

Bagnall, P.S. 1960. The Geology and Mineral Resources of the Pano Lefkara-Larnaca Area. *Geological Survey Department Cyprus, Memoir*, **5**, 116.

Bailey, W.R., Holdsworth, R.E. and Swarbrick, R.E. 2000. Kinematic history of a reactivated oceanic suture: the Mamonia Complex Suture Zone, SW Cyprus. *Journal of the Geological Society of London*, **157**,1107-1126.

Baroz, F. 1979. Etude geologique dans le Pentadaktylos et la Mesaoria (Chypre Septentrionale). Tome 2: les structures, la synthése. (Geological investigation in Pentadaktylos and Mesaoria (North Cyprus). Volume 2: structures, the synthesis). *Unpublished PhD thesis.* Université de Nancy 1, U.E.R. Sciences de la Terre, Métallurgie, Chimie Minérale, Laboratoire de Pétrologie.

Bear, L.M. 1960. The geology and mineral resources of the Akaki-Lythrodondha area. *Geological Survey Department Cyprus, Memoir*, **3**, 122.

Bear, L.M. and Morel, S.W. 1960. Geological map of the Agros-Apsiou area, 1:31,680 scale. *Geological Survey Department of Cyprus.*

Bellamy, C.V. and Jukes-Brown, A.J. 1905. The Geology of Cyprus. *W. Brendan and Son Plymouth.*

Ben-Avraham, Z., Tibor, G., Limonov, A.F., Leybov, M.B., Ivanov, M.K., Tokarev, M.Yu. and Woodside, J.M. 1995. Structure and tectonics of the eastern Cyprian Arc. *Marine and Petroleum Geology*, **12**, 263-271.

Ben-Avraham, Z., Ginzburg, A., Makris, J and Eppelbaum, L. 2002. Crustal structure of the Levant Basin, eastern Mediterranean. *Tectonophysics*, **346**, 23-43.

Biju-Duval, B., Letouzey, J. and Montadert, L. 1978. Structure and evolution of the Mediterranean Basins. In: Hsü, K., Montadert, L., et al., (Eds.), Initial Reports of the Deep Sea Drilling Project XLII, Part I. *US Government Printing Office, Washington*, 951–984.

Blome, C.D. and Irwin, W.P. 1985. Equivalent radiolarian ages from ophiolitic terranes of Cyprus and Oman. *Geology*, **13**, 401-404.

Borradaile, G.J. and Hamilton, T. 2004. Magnetic fabrics may proxy as neotectonic stress trajectories, Polis rift, Cyprus. *Tectonics*, **23**.

Bøtter-Jensen, L. Bulur, E., Duller, G.A.T. and Murray, A.S. 2000. Advances in luminescence instrument systems. *Radiation Measurements*, **32**, 407-411.

BouDagher-Fadel, M.K. and Lord, A.R. 2006. Illusory stratigraphy decoded by Oligocene-Miocene autochthonous and allochthonous foraminifera in the Terra Member, Pakhna Formation (Cyprus). *Stratigraphy*, **3**, 217-226

Cande, S.C. and Kent, D.V. 1995. Revised calibration of the geomagnetic polarity timescale for the Late Cretaceous and Cenozoic. *Journal of Geophysical Research*, **100**, 6093-6095.

Calais, E., DeMets, C. and Nocquet, J.-M. 2003. Evidence for a post-3.16 Ma change in the Nubia-Eurasia-North America plate motions? *Earth and Planetary Science Letters*, **216**, 81-92.

Calon, T.J., Aksu, A.E. and Hall, J. 2005a. The Neogene evolution of the Outer Latakia Basin and its extension into the Eastern Mesaoria Basin (Cyprus), Eastern Mediterranean. *Marine Geology*, **221**, 61– 94.

Calon, T.J., Aksu, A.E. and Hall, J. 2005b. The Oligocene-Recent evolution of the Mesaoria Basin (Cyprus) and its western marine extension, Eastern Mediterranean. *Marine Geology*, **221**, 95– 120.

Clube, T.M.M. 1985. The palaeorotation of the Troodos microplate. *Unpublished PhD thesis, University of Edinburgh.*

Clube, T.M.M., Cleer, K.M. and Robertson, A.H.F. 1985. The palaeorotation of the Troodos microplate. *Nature*, **317**, 522-525.

Clube, T.M.M. and Robertson, A.H.F. 1986. The palaeorotation of the Troodos microplate, Cyprus, in the Late Mesozoic-Early Cenozoic plate tectonic framework of the Eastern Mediterranean. *Surveys in Geophysics*, **8**, 375-437.

Davis, Q.J. 2001. Climate and tectonic controls on deep water sedimentary cyclicity: evidence from the Miocene to Pleistocene of Cyprus. *Unpublished PhD thesis*, The Open University.

DeCoster M., Zomeni Z., Panayides I., Petrides G., Berksoy O. (eds) 2004. Seismic hazard and assessment of the Greater Nicosia Area. *Cyprus Geological Survey Department, Lefkosia.*

Deckers, K. 2002. Cypriot archaeological sites in the landscape: an alluvial geo-archaeological approach. *Unpublished PhD thesis, University of Edinburgh.*

Dercourt, J., Ricou, L.E. and Vrielynck, B. 1993. Atlas Tethys Palaeoenvironmental Maps. *Beicip-Franlab.*

Dercourt, J., Zonenshain, L.P., Ricou, L.E., Kazmin, V.G., Le Pichon, X., Knipper, A.L., Grandjacquet, C., Sbortshhikov, I.M., Geyssant, J., Lepvrier, C., Perchersky, D.H., Boulin, J., Sibuet, J.-C., Savostin, L.A., Sorokhtin, O., Westphal, M., Bazhrnov, M.L.,

Lauer, J.-P. and Biju-Duval, B. 1986. Geological evolution of the Tethys belt from the Atlantic to the Pamirs since the Lias. *Tectonophysics*, **123**, 241-315.

Doglioni, C., Carminati, E., Cuffaro, M. and Scrocca, D. 2007. Subduction kinematics and dynamic constraints. *Earth-science Reviews*, **83**, 125-175.

Dewey, J.F., Pittman, W.C., Ryan, W.B.F. and Bonnin, J. 1973. Plate tectonics and the evolution of the Alpine system. *Geological Society of America Bulletin*, **84,** 3137-3180.

Dewey, J.F., Helman, M.L., Turco, E., Hutton, D.H.W. and Knott, S.D. 1989. Kinematics of the western Mediterranean. In: Coward, M.P., Dietrich, D. and Park. R,G (eds), Alpine Tectonics, *Geological Society of London, Special Publication*, **45**, 265-283.

Di Luccio, F. and Pasyanos, M.E. 2007. Crustal and upper-mantle structure in the Eastern Mediterranean from the analysis of surface wave dispersion curves. *Geophysical Journal International*, **169**, 1139-1152.

Di Stefano, E., Cita, M.B., Spezzaferri, S., Sprovieri, R. 1999. The Messinian-Zanclean Pissouri section (Cyprus, Eastern Mediterranean). *Memorie della Societa Geologica Italiana* **54**, 133–144.

Doser, D.I. and Lomas, R. 2000. The transition from strike-slip to oblique subduction in southeastern Alaska from seismological studies. *Tectonophysics*, **316**, 45-65.

Ducloz, C. 1965. Revision of the Pliocene and Quaternary stratigraphy of the Central Mesaoria. *Geological Survey Department, Cyprus. Annual Report*, **1964**, 31-42.

Ducloz, C. 1972. The geology of the Bellapais-Kythrea area of the central Kyrenia Range. *Cyprus Geological Survey Bulletin*, **6**.

Duller, G.A.T. 2004. Luminescence dating of Quaternary sediments: recent advances. *Journal of Quaternary Science*, **19**, 183-192.

Duller, G.A.T., Bøtter-Jensen, L. and Murray, A.S. 2000. Optical dating of single sand-sized grains of quartz: sources of variability. *Radiation Measurements*, **32**, 453-457.

Dunlop, D. J. 1972. Magnetic mineralogy of unheated and heated red sediments by coercivity spectrum analysis. *Geophysical Journal International*, **27**, 37-35.

Dziewonski, A.M., Ekstrom, G. and Maternovskaya, N.N. 1998. Centroid-moment tensor solutions for October-December, 1996. *Physics of the Earth and Planetary Interiors*, **105**, 95-108

Eaton, S. 1987. The sedimentology of mid to late Miocene carbonates and evaporites in southern Cyprus. University of Edinburgh. *Unpublished PhD thesis.*

Eaton, S. and Robertson, A.H.F. 1993. The Miocene Pakhna Formation, southern Cyprus and its relationship to the Neogene tectonic evolution of the eastern Mediterranean. *Sedimentary Geology*, **86**. 273-296.

Elion, P. 1983. Etude structurale et sédimentologique du bassin Neogène de Pissouri (Chypre). *Unpublished PhD thesis*, University of Paris.

Enkin, R., Wuolle, K., Mccann, C., Carretero, M., Voroney, M., Baylis, T., Morton, K., Jaycock, D., Baker, J. and Beran, L. PMGSC. Palaeomagnetism Data Analysis. Version 4.2. *Geological Survey of Canada.* www.pgc.nrcan.gc.ca/tectonic/enkin.htm

Ergün, M., Okay, S., Sari, C., Oral, E.Z., Ash, M., Hall, J. and Miller, H. 2005. Gravity anomalies of the Cyprus Arc and their tectonic implications. *Marine Geology*, **221**, 349-358.

Flecker, R. and Ellam, R.M. 1999. Distinguishing climatic and tectonic signals in the sedimentary successions of marginal basins using Sr isotopes: an example from the Messinian salinity crisis, Eastern Mediterranean. *Journal of the Geological Society, London*, **156**, 847-854.

Flecker, R., de Villiers, S. and Ellam, R.M. 2002. Modeling the effect of evaporation on the salinity - 87Sr/86Sr relationship in modern and ancient marginal-marine systems: the Mediterranean Messinian Salinity Crisis. E*arth and Planetary Science Letters*, **203**, 221-233.

Follows, E.J. 1990. Sedimentary and tectonic setting of the Miocene reefs and related sediments in Cyprus. University of Edinburgh, *Unpublished PhD thesis*.

Follows, E.J. 1992. Patterns of reef sedimentation and diagenesis in the Miocene of Cyprus. *Sedimentary Geology*, **79**. 225-253.

Follows, E. and Robertson, A.H.F. 1990. Sedimentology and structural setting of Miocene reefal limestones in Cyprus. In: Malpas, J., Moore, E.M., Panagiotou, A. and Xenophontos, C. (eds), Ophiolites: Oceanic crustal analogues: Proceedings of the international Symposium. *Cyprus Geological Survey Department, Lefkosia.*

Follows, E., Robertson, A.H.F. and Scoffin, T.P. 1996. Tectonic controls on Miocene reefs and related carbonate facies in Cyprus. In: Franseen, E.K., Esteban, M., Ward, W.C. and Rouchy, J-M. (eds), Models for carbonate stratigraphy from Miocene reef complexes of Mediterranean regions. *SEPM Concepts in sedimentology and paleontology*, **5**, 295-325.

Fuchs, M. and Lang, A. 2001. OSL dating of coarse-grain fluvial quartz using single-aliquot protocols on sediments from NE Peloponnese, Greece. *Quaternary Science Reviews*, **20**, 783-787.

Galbraith, R.F. 1990. The radial plot: graphical assessment of spread in ages. *Nuclear Tracks and Radiation*, **17**, 207-14.

Galbraith, R.F., Roberts, R.G., Laslett, G.M., Yoshida, H. and Olley, J.M. 1999. Optical dating of single and multiple grains of quartz from Jinmium rock shelter, northern Australia: Part 1, experimental design and statistical models. *Archaeometry*, **41**, 339-364.

Galindo-Zaldívar, J., Nieto, L.M., Robertson, A.H.F. and Woodside, J.M. 2001. Recent tectonics of Eratosthenes Seamount: an example of seamount deformation during incipient continental collision. *Geo-Marine Letters*, **20,** 233-242.

Gapaisa, D., Cobbolda, P.R., Bourgeoisa, O., Roubya, D. and de Urreiztieta, M. 2000. Tectonic significance of fault-slip data. *Journal of Structural Geology*, **22**, 881-888.

Gass, I.G. and Masson-Smith, D. 1963. The geology and gravity anomalies of the Troodos Massif, Cyprus. *Philosophical Transactions of the Royal Society of London*, **A255**, 417-467.

Gass, I.G., MacLeod, C.J., Murton, B.J., Panayiotou, A., Simonian, K.O. and Xenophontos, C. 1994. The geology of the South Troodos Transform Fault Zone. *Geological Survey Department, Cyprus. Memoir*, **9**.

Geological Survey Department. 1995. Geological Map of Cyprus. 1:250,000. *Geological Survey Department of Cyprus, Lefkosia*.

Ginzburg, A. and Ben-Avraham, Z. 1992. Crustal structure and tectonic processes in the Levant and the eastern Mediterranean. *Israel Journal of Earth Sciences*, **40**, 125-133.

Glover, C. and Robertson, A.H.F. 1998. Neotectonic intersection of the Aegean and Cyprus tectonic areas: extensional and strike-slip faulting in the Isparta Angle, SW Turkey. *Tectonophysics*, **298**, 103-132.

Greitzer, Y. and Constantinou, Ch. 1968. The geology and hydrogeology of the Kouris River valley. *U.N. Special Fund Project, Survey Groundwater Mineral Resources, Cyprus*, **71**.

Guilaine, J., François, B., Vigne, J-D. and Carrère, I. 2000. New discovery of an early Cyprus preceramic Neolithic (late 9th, early 8th millenia cal. BC), related to the Early/Middle PPNB of the northern Levant: Découverte d'un Néolithique précéramique ancien chypriote (fin 9^{e}, début 8^{e} millénaires cal. BC), apparenté au PPNB ancien/moyen du Levant nord. *Comptes Rendus de l'Académie des Sciences - Series IIA - Earth and Planetary Science*, **330**, 75-82.

Hadjistavrinou, Y. and Constantinou, G. 1977. Hydrogeology of the Akrotiri Peninsula. *Bulletin of the Cyprus Geological Survey Department*, **7**.

Haimson, B.C., Lee, M.Y., Baumgartner and Rummel, F. 1990. Plate tectonics and structure inferences from in situ measurements and fracture logging in drillhole CY-4, Troodos ophiolite, Cyprus. In: (eds.) J. Malpas, J., Moores, E.M., Panayiotou, A. and Xenophoutos, C. *Ophiolites, Ocean Crustal Analogues* Published by the Geological Survey Department of Cyprus, 131–138.

Hardenberg, M.F. and Robertson, A.H.F. 2007. Sedimentology of the NW margin of the Arabian plate and the SW-NE-trending Nahr El-Kabir half-graben in northern Syria during the latest Cretaceous and Cenozoic. *Sedimentary Geology,* **201**, 231-266.

Harrison, J.W., Newell, W.L. and Necdet, M. 2002. Karstification along an active fault zone in Cyprus. US Geological Survey Karst Interest Group Proceedings. Shepherdstown, West Virginia, August 20-22, 2002. http://water.usgs.gov/ogw/karst/kig2002/rwh_karstification.html

Harrison, R.W., Newell, W.L., Batihanli, H., Panayides, I., McGeehin, J.P., Mahan, S.A., Ozhur, A., Tsiolakis, E. and Necdet, M. 2004a. Tectonic framework and Late Cenozoic tectonic history of the northern part of Cyprus: implications for earthquake hazards and regional tectonics. *Journal of Asian Earth Sciences*, **23,** 191-210.

Harrison, R., Newell, W., Tsiolakis, E., Necdet, M., Panayides, I., Batihanli, H., Zomeni, Z., Ozhur, A., Berksoy, O., Stone, B. and Lord, A. 2004b. Appendix A1: Bedrock Geological Map of Nicosia. In: DeCoster, M., Zomeni, Z., Panayides, I., Petrides, G. and Berksoy, O. Seismic hazard and risk assessment of the Greater Nicosia Area. *Internal report, Cyprus Geological Survey Department.*

Harrison, R. and Tsiolakis, E. 2006. Change from convergent to collisional transform boundary conditions between the African and Anatolian Plates, based on the geology of Cyprus. *Geological Society of America, Abstracts*, **38**, 277. Philadelphia Annual Meeting, 22-25 October, 2006.

Henson, F.R.S., Browne, R.V. and McGinty, J. 1949. A synopsis of the stratigraphy and geological history of Cyprus. *Quaternary journal of the Geological Society of London*, **105**, 1-41.

Hofstetter, A. and Bock, G. 2004. Shear-wave velocity structure of the Sinai subplate from receiver function analysis. *Geophysical Journal International*, **158**, 67-84.

Holdsworth, R.E., Butler, C.A. and Roberts, A.M. 1997. The recognition of reactivation during continental deformation. *Journal of the Geological Society, London*, **154,** 73-78.

Homke, S., Vergès, J., Garcés, M., Emami, H. and Karpuz, R. 2004. Magnetostratigraphy of Miocene–Pliocene Zagros foreland deposits in the front of the Push-e Kush Arc (Lurestan Province, Iran). *Earth and Planetary Science Letters*, **225,** 397– 410.

Houghton, S.D., Jenkins, D.G., Xenophontos, C. and Gass, I.G. 1990. Microfossil evidence for a latest Pliocene age for the Amathus and Khirokitia channel deposits, southern Cyprus and thereby unroofing of the Troodos Massif. In: Malpas, J., Moore, E.M., Panagiotou, A. and Xenophontos, C. (eds), Ophiolites: oceanic crustal analogues. Proceedings of the symposium 'Troodos 1987'. *Cyprus Geological Survey Department, Lefkosia*.

Hsü, K.J., Cita, M.B. and Ryan, W.B.F. 1973. The origin of the Mediterranean evaporates. In: Ryan, W.B.F., Hsü, K.J. and Cita, M.B. (eds), Initial reports of the DSDP 13, *DC, U.S. Government Printing Office, Washington*, 1203-1231.

Isacks, B. and Molnar, P. 1972. Distribution of stresses in the descending lithosphere from a global survey of focal-mechanism solution of mantle earthquakes. *Reviews of Geophysics and Space Physics*, **9**, 103-174.

Jackson, J.A. and McKenzie, D. 1984. Rates of active deformation in the Aegean Sea and surrounding areas. *Basin Research*, **1**, 121-128.

Jaffey, N., Robertson, A.F.H. and Pringle, M. 2004. Latest Miocene and Pleistocene ages of faulting, determined by $^{40}Ar/^{39}Ar$ single-crystal dating of airfall tuff and silicic extrusives of the Erciyes Basin, central Turkey: evidence for intraplate deformation related to the tectonic escape of Anatolia. *Terra Nova*, **16**, 45–53.

Jaffey, N. - Robertson, A.H.F. 2001. New sedimentological and structural data from the Ecemis Fault Zone, southern Turkey: implications for its timing and offset and the Cenozoic tectonic escape of Anatolia. *Journal of the Geological Society*, **158**, 367-

Jolivet, L., Augier, R., Robin, C., Suc, J-P., Rouchy, J.M. 2006. Lithospheric-scale geodynamic context of the Messinian salinity crisis. *Sedimentary Geology*, **188-189**, 9-33.

Jolivet, L. and Faccenna, C. 2000. Mediterranean extension and the Africa-Eurasia collision. *Tectonics*, **19**, 1095-1106.

Kahle, H.-G. and Mueller, S. 1998. Structure and dynamics of the Eurasian-African/Arabian plate boundary system: objectives, tasks and resources of the Wegner Group. *Journal of Geodynamics*, **25**, 303-325.

Kahle, H-G., Straub, C., Reilinger, R., McClusky, S., King, R., Hurst, K., Veis, G., Kastens, K. and Cross, P. 1998. The strain rate field in the eastern Mediterranean region, estimated by repeated GPS measurements. *Tectonophysics*, **294**, 237-252.

Kähler, G. and Stow, D.A.V. 1998. Turbidites and contourites of the Palaeogene Lefkara formation, southern Cyprus. *Sedimentary Geology*, **115**. 215-231.

Kalogeras, I., Stavrakakis, G., and Solomi, K. 1999. The October 9, 1996 Earthquake in Cyprus: Seismological, Macroseismic and Strong Motion Data. *Annali Di Geofisica*, **42**, 85-97.

Kelling, G., Gokcen, S.L., Floyd, P.A. and Gokcen, N. 1987. Neogene tectonics and plate convergence in the eastern Mediterranean: New data from southern Turkey. *Geology*, **15**, 425-429.

Kemplar, D. and Ben-Avraham, Z. 1987. The tectonic evolution of the Cyprean Arc. *Annales Tectonicae*, **1**, 58-71.

Kemplar, D. and Garfunkel, Z. 1994. Structures and kinematics in the northeastern Mediterranean: a study of an irregular plate boundary. *Tectonophysics*, **234**, 19-32.

Kinnaird, T.C., Sanderson, D.C.W., Burbidge, C. and Peltenburg, E. 2008. OSL dating of Neolithic Kissonerga-Mylouthkia, Cyprus. *Neolithics*, **2/07**, 51-56.

Koulakov, I. and Sobolev, S.V. 2006. Moho depth and three-dimensional P and S structure of the crust and uppermost mantle in the Eastern Mediterranean and Middle East derived from tomographic inversion of local ISC data. *Geophysical Journal International*, **164**, 218-235.

Kouwenhoven, T.J., Morigi, C., Negri, A., Giunta, S., Krijgsman, W. and Rouchy, J.-M. 2006. Palaeoenvironmental evolution of the eastern Mediterranean during the Messinian: Constraints from integrated microfossil data of the Pissouri Basin (Cyprus). *Marine Micropaleontology*, **60**, 17–44.

Krijgsman, W., Blanc-Valleron, M.M., Flecker, R., Hilgen, F.J., Kouwenhoven, T.J., Orszag-Sperber, F. and Rouchy, J.M. 2002. The onset of the Messinian salinity crisis in the Easternmost Mediterranean (Pissouri basin, Cyprus). Earth and Planetary Science Letters, **194,** 299-310.

Lagroix, F. and Borradaile, G.J. 2000. Tectonics of the circum-Troodos sedimentary cover of Cyprus, from rock magnetic and structural observations. *Journal of Structural Geology*, **22**, 453-469.

Lallemand, H.G.A. 1996. Displacement partitioning and arc-parallel extension in the Aleutian volcanic island arc. *Tectonophysics*, **256**, 279-293.

Lallemand, S., Heuret, A. and Boutelier, D. 2005. On the relationships between slab-dip, back-arc stress, upper plate absolute motion, and crustal nature in subduction zones. *Geochemistry, Geophysics, Geosystems*, **6**.

Lapierre, H. 1972. Les formations sédimentaires et éruptives des nappes de Mamonia et leurs relations avec le massif de Troodos (Chypre). *Unpulblished PhD thesis*, University of Nancy, France.

Lapierre, H., Bosch, D., Narros, A., Mascle, G.H., Tardy, M. and Demant, A. 2007. The Mamonia Complex (SW Cyprus) revisited: remnant of Late Triassic intra-oceanic volcanism along the Tethyan southwestern passive margin. *Geological magazine*, **144**, 1-19.

Leigh, D.S. and Webb, P.A. 2006. Holocene erosion, sedimentation, and stratigraphy at Raven Fork, Southern Blue Ridge Mountains, USA. *Geomorphology*, **78**, 161-177.

Lepper, K., Agersnap, Larsen, N. and McKeever, S.W.S. 2000. Equivalent dose distribution analysis of Holocene aeolian and fluvial quartz sands from Central Oklahoma. *Radiation Measurements*, **32**, 603-608.

Le Pichon, X. and Angelier, J. 1979. The Hellenic Arc and trench system: a key to the neotectonic evolution of the Eastern Mediterranean. *Tectonophysics*, **60**, 1-42.

Le Pichon, X., Angelier, J., Aubouin, J., Lyberis, N., Monti, S., Renard, V., Got, H., Hsu, K., Mart, Y., Mascle, J., Matthews, D., Mitropoulos, D., Tsoflias, P. and Chronis, G. 1979. From subduction to transform motion: a seabeam survey of the Hellenic Trench system. *Earth and Planetary Science*, **44**, 441-450.

Lord, A.R., Panayides, I., Urquhart, E. and Xenophontos, C. 2000. A biochronostratigraphical framework for the Late Cretaceous-Recent circum-Troodos sedimentary sequence, Cyprus. In: Panayides, I., Xenophontos, C. and Malpas, J. (eds), Proceedings of the Third International Conference on the Geology of the Eastern Mediterranean. *Cyprus Geological Survey Department, Lefkosia.*

Lourens, L.J., Antonarakou, A., Hilgen, F.J., Van Hoof, A.A.M., Vergnaud-Grazzini, C., and Zachariasse, W.J. 1996. Evaluation of the Plio-Pleistocene astronomical timescale. *Paleoceanography*, **11**, 391-413.

Lundgren, P., Giardini, D. and Russo, R.M. 1998. A geodynamic framework for eastern Mediterranean kinematics. *Geophysical Research Letters*, **25**, 4007-4010.

MacLeod, C.J. and Murton, B.J. 1993. Structure and tectonic evolution of the Southern Troodos Transform Fault Zone, Cyprus. In: Prichard, H.M., Alabaster, T., Harris, N.B.W. and Neary, C.R. (eds), Magnetic Processes and Plate Tectonics. *Special Publication of the Geological Society of London*, **76**, 141-176.

Mahmoud, S., Reilinger, R., McClusky, S., Vernant, P. and Tealeb, A. 2005. GPS evidence for northward motion of the Sinai Block: implications for E. Mediterranean tectonics. *Earth and Planetary Science Letters*, **238**, 217-224.

Malpas, J., Xenophontos, C. and Williams, D. 1992. The Agia Varvara Formation of S.W. Cyprus, a product of complex collisional tectonics. *Tectonophysics*, **212**, 193-211.

Malpas, J., Calon, T. and Squires, G. 1993. The development of a late Cretaceous microplate suture zone in S.W. Cyprus. In: Prichard, H.M., Alabaster, T., Harris, N.B.W. and Neary, C.R. (eds), Magmatic processes and plate tectonics. *Geological Society, London, Special publications*, **76**, 177-196.

Malpas, J. and Xenophontos, C. 1992. Geological map of the Akamas-Polis Area, 1:25,000 scale. *Geological Survey Department of Cyprus.*

Malpas, J. and Xenophontos, C. 1999. Geological map of the Agia Varvara-Pentalia Area, 1:25,000 scale. *Geological Survey Department of Cyprus.*

Mantis, M. 1970. Upper Cretaceous-Tertiary foraminiferal zones in Cyprus. Scientific Research Centre of Cyprus. *Epetiris*, **3**, 227-241.

Makris, J., Ben-Avraham, Z., Behle, A., Ginzburg, A., Giese, P. and Steinmetz, L. 1983. Seismic reflection profiles between Cyprus and Israel and their interpretation. *Geophysical Journal of the Royal Astronomical Society*, **75**, 575–591.

Makris, J., Stacker, J. and Kramvis, S. 2000. Microseismic studies and tectonic implications of Cyprus. In: Panayides, I., Xenophontos, C. and Malpas, J. (eds), Proceedings of the Third International Conference on the Geology of the Eastern Mediterranean. *Cyprus Geological Survey Department, Lefkosia.*

Marrett, R.A. and Allmendinger, R.W. 1990. Kinematic analysis of fault-slip data. *Journal of Structural Geology*, **12**, 973-986.

Martinod, J., Hatzfeld, D., Brun, J.P., Davy, P. and Gautier, P. 2000. Continental collision, gravity spreading, and kinematics of Aegea and Anatolia. *Tectonics*, **19**, 290-299.

Mejdahl, V. 1979. Thermoluminescence dating: beta dose attenuation in quartz grains. *Archaeometry*, **21,** 61-72.

McCallum, J.E. 1989. Sedimentation and tectonics of the Plio-Pleistocene of Cyprus. *Unpublished PhD Thesis, University of Edinburgh*.

McCallum, J.E. and Robertson, A.H.F. 1990. Pulsed uplift of the Troodos massif – evidence from the Plio-Pleistocene Mesaoria basin. IN: E.M. Moore *et al*. *(eds)*, Ophiolites Crustal Analogues. Proceedings of the International Symposium 'Troodos 1987', *Geological Survey Department, Cyprus*. 217-230.

McCallum, J.E. and Robertson, A.H.F. 1995a. Sedimentology of two fan delta systems in the Pliocene – Pleistocene of the Mesaoria Basin, Cyprus. *Sedimentary Geology*, **98**. 215-244.

McCallum, J.E. and Robertson, A.H.F. 1995b. Late Pliocene-early Pleistocene Athalassa Formation, north central Cyprus: carbonate sand bodies in a shallow seaway between two emerging landmasses. *Terra Nova*, **7,** 255-264.

McCallum, J.E., Scrutton, R.A., Robertson, A.H.F. and Ferrari, W. 1993. Seismostratigraphy and Neogene-Recent depositional history of the south central continental margin of Cyprus. *Marine and Petroleum Geology*, **10**, 426-438.

McClusky, S., Balassanian, S., Barka, A., Demir, C., Ergintav, S., Georgiev, I., Gurkan, O., Hamburger, M., Hurst, K., Kahle, H., Kastens, K., Kekelidze, G., King, R., Kotzev, V., Lenk, O., Mahmoud, S., Mishin, A., Nadariya, M., Ouzonis, A., Paradissis, D., Peter, Y., Prilepin, M., Reilinger, R., Sanli, I., Seeger, H., Tealeb, A., Toksöz, M.N. and Veis, G. 2000. Global positioning system constraints on plate kinematics and dynamics in the eastern Mediterranean and Caucasus. *Journal of Geophysical Research*, **105**, 5695–5720.

Nocquet, J.-M. and Calais, E. 2004. Geodetic measurements of crustal deformation in the Western Mediterranean and Europe. *Pure and applied geophysics*, **161**, 661-681.

Mohsen, A., Hofstetter, R., Bock, G., Kind, R., Weber, M., Wylegalla, K., Rümpker, G. 2005. A receiver function study across the Dead Sea Transform. *Geophysical Journal International*, **160**, 948-960.

Moores, E.M. and Vine, F.J. 1971. The Troodos Massif, Cyprus and other ophiolites as oceanic crust: evaluations and implications. *Philosophical Transactions of the Royal Society*, **A268**, 433-466.

Morel, S.W. 1960. Geological map of the Apsiou-Akrotiri Area, 1:31,680 scale. *Geological Survey Department of Cyprus.*

Morris, A. 1990. Palaeomagnetic studies of the Mesozoic-Tertiary tectonic evolution of Cyprus, Turkey and Greece. *Unpublished PhD thesis*, University of Edinburgh, Edinburgh.

Morris, A. 2003a. The Late Cretaceous palaeoatitude of the Neotethyan spreading axis in the eastern Mediterranean region. *Tectonophysics*, **377**, 157-178.

Morris, A. 2003b. A palaeomagnetic and rock magnetic glossary. *Tectonophysics*, **377**, 211 –228.

Morris, A., Anderson, M.W., Inwood, J. and Robertson, A.H.F. 2006. Palaeomagnetic insights into the evolution of Neotethyan oceanic crust in the eastern Mediterranean. In: Robertson, A.H.F. and Mountrakis, D. (eds), Tectonic development of the eastern Mediterranean region. *Geological Society, London, Special Publication*, **260**, 351-372.

Morris, A., Creer, K.M. and Robertson, A.H.F. 1990. Palaeomagnetic evidence for clockwise rotations related to dextral shear along the Southern Troodos Transform Fault (Cyprus). Earth and Planetary Science Letters, 99, 229-253.

Morris, A. and Tarling, D.H. 1996. Palaeomagnetism and tectonics of the Mediterranean region: An introduction. In: Morris, A. and Tarling, D.H. (eds), Palaeomagnetism and tectonics of the Mediterranean region. *Geological society of London, Special Publication*, **105**, 1-17.

Mukasa, S.B. and Ludden, J.N. 1987. Uranium-lead ages of plagiogranites from the Troodos ophiolite, Cyprus, and their tectonic significance. *Geology*, **15**, 825-828.

Murray, A. and Wintle, A.G. 2000. Luminescence dating of quartz using an improved single-aliquot regenerative-dose protocol. *Radiation Measurements*, **32**, 57-73.

Murton, B.J. and Gass, I.G. 1986. Western Limassol Forest Complex. *Geology*, **14**, 255-258.

Nocquet, J.-M. and Calais, E. 2004. Geodetic measurements of crustal deformation in the Western Mediterranean and Europe. *Pure and applied Geophysics*, **161**, 661-681.

Neev, D., Greenfield, L., and Hall, J.K. 1985. Slice Tectonics in the Eastern Mediterranean Basin. In: Stanley, D.J., and Wezel, F.C. (eds), Geological Evolution of the Mediterranean Basin, *Springer-Verlag, New York*. 249-269.

Netzeband, G.L., Gohl, K., Hübscher, C.P., Ben-Avraham, Z., Dehghani, G.A., Gajewski, D. and Liersch, P. 2006. The Levantine Basin - crustal structure and origin. *Tectonophysics*, **418**, 167–188.

OECD. 1994. JEF-PC – a personal computer programme for displaying nuclear data from the Joint Evaluated File Library. *OECD. Nuclear Energy, Paris.*

Olley, J.M., Caitcheon, G.G. and Murray, A.S. 1998. The distribution of apparent dose as determined by optically stimulated luminescence in small aliquots of fluvial quartz: implications for dating young sediments. *Quaternary Science Reviews*, **17**, 1033-1040.

Olley, J.M., Caitcheon, G.G. and Roberts, R.G. 1999. The origin of dose distributions in fluvial sediments, and the prospect of dating single grains from fluvial deposits using optically stimulated luminescence. *Radiation Measurements*, **30**, 207-217.

Orszag-Sperber, F., Rouchy, J.M. and Elion, P. 1989. The sedimentary expression of regional tectonic events during the Miocene-Pliocene transition in the southern Cyprus basins. *Geological magazine*, **126**, 291-299.

Orszag-Sperber, F. and Rouchy, J-M. 2000. The Messinian-Zanclean transition in the Pissouri area (Cyprus): a well documented section in the Eastern Mediterranean. In: (eds) Panayides, I., Xenophontos, C. and Malpas, J. Proceedings of the Third International Conference on the Geology of the Eastern Mediterranean. *Cyprus Geological Survey Department, Lefkosia.* 243-255.

Panayides, I., Necdet, M., Harrison, R., Newell, W., Batihanlı, H., Tsiolakis, E., Zomeni, Z., Berksoy, O., Özhűr, A., McGeenin, J. and Mahan, S. 2004. Chapter 2: Geology. In: DeCoster, M., Zomeni, Z., Panayides, I., Petrides, G. and Berksoy, O. Seismic hazard and risk assessment of the Greater Nicosia Area. *Internal report, Cyprus Geological Survey Department.*

Pantazis, Th.M. 1967a. Geological map of the Pharmakas-Kalavasos Area, 1:31,680 scale. *Geological Survey Department of Cyprus.*

Pantazis, Th.M. 1967b. The geology and mineralogy of the Pharmakas-Kalavasos area. *Geological Survey Department Cyprus, Memoir*, **8**, 190.

Papadimitriou, E.E. and Karakostas, V.G. 2006. Earthquake generation in Cyprus revealed by the evolving stress field. *Tectonophysics*, **423**, 61–72.

Papazachos, B.C. and Comninakis, P.E. 1978. Deep Structure and Tectonics of the Eastern Mediterranean. *Tectonophysics*, **46**, 285-296.

Papazachos, B.C. and Papaioannou, Ch.A. 1999. Lithospheric boundaries and plate motions in the Cyprus area. *Tectonophysics*, **308**. 193-204.

Payne, A.S. 1995. The structural and sedimentary evolution of the Polis graben system, West Cyprus. University of Edinburgh, *Unpublished PhD thesis*.

Payne, A.S. and Robertson, A.H.F. 1995. Neogene supra-subduction zone extension in the Polis graben system, west Cyprus. *Journal of the Geological Society, London*, **152**. 613-628.

Payne, A.S. and Robertson, A.H.F. 2000. Structural evolution and regional significance of the Polis graben system, western Cyprus. In: Panayides, I., Xenophontos, C. and Malpas, J. *(eds)*. Proceedings of the Third Internal Conference on the geology of the Eastern Mediterranean. *Cyprus Geological Survey Department, Lefkosia.*

Pearce, J.A., Lippard, S.J. and Roberts, S. 1984. Characteristics and tectonic significance of supra-subduction zone ophiolites. In: Kokelaar, B.P. and Howells, M.F. (eds), Marginal Basin Geology. *Special publication of the Geological Society, London*, **16**.

Peltenburg, E. (eds). 2003. The colonisation and settlement of Cyprus: investigations at Kissonerga-Mylouthkia, 1976-1996. *Lemba Archaeological Project, vol.* **1***; Studies in Mediterranean Archaeology*.

Peltenburg, E., Colledge, S., Croft, P., Jackson, A., McCartney, C. and Murray, M.A. 2000. Agro-pastoralist colonization of Cyprus in the 10th millennium BP: initial assessments. *Antiquity*, **74,** 844-853.

Pilidou, S., Priestley, K., Jackson, J. and Maggi, A. 2004. The 1996 Cyprus earthquake: a large, deep event in the Cyprean Arc. Geophysical Journal International, **158**, 85-97.

Pinar, A. and Kalafat, D. 1999. Source processes and seismotectonic implications of the 1995 and 1996 Cyprus, Eastern Mediterranean region, earthquakes. *Tectonophysics*, **301**, 217-230.

Poole, A.J. 1992. Sedimentology, neotectonics and geomorphology related to tectonic uplift and sea-level change: Quaternary of Cyprus. *Unpublished PhD thesis*, University of Edinburgh.

Poole, A.J. and Robertson, A.H.F. 1991. Quaternary uplift and sea-level change at an active plate boundary, Cyprus. *Journal of the Geological Society, London*, **148**. 909-921.

Poole, A.J. and Robertson, A.H.F. 1998. Pleistocene fanglomerates deposition related to uplift of the Troodos Ophiolite, Cyprus. In: Robertson, A.H.F., Emeis, K.-C., Richter, C. and Camerlenghi, A. (eds), *Proceedings ODP Scientific Results*, **160**, 544-568.

Poole, A.J. and Robertson, A.H.F. 2000. Quaternary marine terraces and aeolinites in coastal south and west Cyprus: implications for regional uplift and sea-level change. In: Panayides, I., Xenophontos, C. and Malpas, J. *(eds)*. Proceedings of the Third Internal Conference on the geology of the Eastern Mediterranean. *Cyprus Geological Survey Department, Lefkosia*.

Poole, A.J., Shimmield, G.B. and Robertson, A.H.F. 1990. Late Quaternary uplift of the Troodos ophiolite, Cyprus: Uranium-series dating of Pleistocene coral. *Geology*, **18,** 894-897.

Prescott, J.R. and Hutton, J.T. 1994. Cosmic ray contributions to does rates for luminescence and ESR dating: large depths and long-term variations. *Radiation Measurements*, **23,** 497-500.

Prescott, J.R. and Robertson, G. 1997. Sediment dating by luminescence: a review. *Radiation Measurements*, **27**, 893-922.

Ramsey, B. 2003. Oxcal v.3.9. *Research Lab for Archaeology, Oxford.* http://c14.arch.ox.ac.uk/.

Read, T.J. 1993. The sedimentology of the Oligocene to Miocene Transition in the Limassol - Larnaca Area, Southern Cyprus. *Unpublished PhD thesis*, University of London.

Reilinger, R.E., McClusky, S.C., Oral, M.B., King, R.W., Toksoz, M.N., Barka, A.A., Kinik, I., Lenk, O. and Sanli, I. 1997. Global Positioning System measurements of present-day crustal movements in the Arabia-Africa-Eurasia plate collision zone. *Journal of Geophysical Research*, **102**, 9983-9999.

Richter, C., Roberts, A.P., Stoner, J.S., Benning, L.D. and Chi, C.T. 1998. Magnetostratigraphy of Pliocene-Pleistocene sediments from the eastern Mediterranean Sea. In: Robertson, A.H.F., Emeis, K., Richter, C. and Camerlenghi, A. *(eds)* Proceedings of the Ocean Drilling Program, Scientific Results, **160**. 61-73.

Rizzetto, C., Marotta, A.M. and Sabadini, R. 2004. The role of trench retreat on the geometry and stress regime in the subduction complexes of the Mediterranean. *Geophysical Research Letters*, **31**.

Roberts, G. and Peace, D. 2007. Hydrocarbon plays and prospectivity of the Levantine Basin, offshore Lebanon and Syria from modern seismic data. *GeoArabia*, **12**, 99-124.

Robertson, A.H.F. 1976. Pelagic chalks and calciturbidites from the Lower Tertiary of the Troodos massif, Cyprus. *Journal of Sedimentary Petrology*, **46**, 1007-1016.

Robertson, A.H.F. 1977. Tertiary uplift of the Troodos massif, Cyprus. *Geological Society of America Bulletin*, **88**, 1763-1772.

Robertson, A.H.F. 1990. Tectonic evolution of Cyprus. In: Malpas, J., Moores, E.M., Panayiotou, A. and Xenophontos, C. *(eds.)* Ophiolites Oceanic Crustal Analogues. Proceedings of the Symposium, 'Troodos 1987', *Geological Survey Department of Cyprus, Nicosia*.

Robertson, A.H.F. 1998a. Mesozoic – Tertiary tectonic evolution of the Easternmost Mediterranean area: Integration of marine and land evidence. In: Robertson, A.H.F., Emeis, K., Richter, C. and Camerlenghi, A. *(eds)* Proceedings of the Ocean Drilling Program, Scientific Results, **160**. 723-782.

Robertson, A.H.F. 1998b. Tectonic significance of the Eratosthenes Seamount: a continental fragment in the process of collision with a subduction zone in the eastern Mediterranean (Ocean Drilling Program Leg 160). *Tectonophysics*, **298**, 63-82.

Robertson, A.H.F. 2000. Tectonic evolution of Cyprus in its Easternmost Mediterranean setting. In: Panayides, I., Xenophontos, C. and Malpas, J. (eds) Proceedings of the Third International Conference on the Geology of the Eastern Mediterranean.

Robertson, A.H.F. 2002. Overview of the genesis and emplacement of Mesozoic ophiolites in the Eastern Mediterranean Tethyan region. *Lithos*, **66**, 1-67.

Robertson, A.H.F. 2004. Development of concepts concerning the genesis and emplacement of Tethyan ophiolites in the Eastern Mediterranean and Oman regions. *Earth-Science Reviews*, **66**, 331-387.

Robertson, A.H.F. and Dixon, J.E. 1984. Introduction: aspects of the geological evolution of the Eastern Mediterranean. In: Dixon, J.E. and Robertson, A.H.F. (eds), The geological evolution of the eastern Mediterranean. *Geological Society, Special Publications*, **17**, 77-112.

Robertson, A.H.F., Dixon, J.E., Brown, S., Collins, A., Morris, A., Pickett, E., Sharp, I. and Ustaömer, T. 1996. Alternative tectonic models for the Late Paleozoic-Early Tertiary development of Tethys in the Eastern Mediterranean region. In: Morris, A. and Tarling, D.H. (eds), Palaeomagnetism and Tectonics of the Mediterranean Region. *Geological Society, Special Publication*, **105**, 239-263.

Robertson, A.H.F., Eaton, S., Follows, E.J. and McCallum, J.E. 1991. The role of local tectonics versus global sea-level change in the Neogene evolution of the Cyprus active margin. *Special publication of the international Association of Sedimentologists*, **12,** 331-369.

Robertson, A.H.F., Eaton, S., Follows, E.J. and Payne, A.S. 1995b. Depositional processes and basin analysis of Messinian evaporites in Cyprus. *Terra Nova*, **7**, 233-253

Robertson, A.H.F. and Grasso, M. 1995. Overview of the late Tertiary tectonic and palaeo-environmental development of the Mediterranean region. *Terra Nova*, **7**. 114-127.

Robertson, A.H.F. and Hudson, J.D. 1974. Pelagic sediments in the Cretaceous and Tertiary history of Cyprus. In: Hsü, K.J. and Jenkyns, H.C. (eds), Pelagic sediments: on land and under the sea. *Special Publication of International Association of Sedimentologists*, **1**, 403-436.

Robertson, A.H.F. and Hudson, J.E. 1974. Pelagic sediments in the Cretaceous and Tertiary history of the Troodos Massif, Cyprus. In: Hsü, K.J. and Jenkyns, H.C. (eds), Pelagic sediments on land and under the sea. *Special Publication of the International Association of Sedimentologists*, **1**, 403-436.

Robertson, A.H.F., Kidd, R.B., Ivanov, M.K., Limonov, A.F., Woodside, J.M., Galindo-Zaldivar, J., Nieto, L. and the Scientific Party of the 1993 'TTR-3' Cruise. 1995a. Eratosthenes Seamount: collisional processes in the easternmost Mediterranean in relation to the Plio-Quaternary uplift of southern Cyprus. *Terra Nova*, **7**, 254-264.

Robertson, A.H.F., Poisson, A. and Akinci, O. 2003. Developments in research concerning Mesozoic-Tertiary Tethys and neotectonics in the Isparta Angle, SW Turkey. *Geological Journal*, **38**, 195-234.

Robertson, A.H.F. and Woodcock, N. 1979. The Mamonia Complex, southwest Cyprus: the evolution and emplacement of a Mesozoic continental margin. *Geological Society of America Bulletin*, **90**, 651-665.

Robertson, A.H.F. and Woodcock, N. 1986. The role of the Kyrenia Range Lineament, Cyprus, in the geological evolution of the eastern Mediterranean. *Philosophical Transactions of the Royal Society of London*, **317**, 141-177.

Robertson, A.H.F. and Xenophontos, C. 1993. Development of concepts concerning the Troodos ophiolite and adjacent units in Cyprus. In: Prichard, H.M., Alabaster, T., Harris, N.B.W. and Neary, C.R. (eds), Magmatic Processes and Plate Tectonics. *Special Publication of the Geological Society of London*, **76**, 85-120.

Rotstein, Y. and Ben-Avraham, Z. 1985. Accretionary processes at subduction zones in the Eastern Mediterranean. *Tectonophysics*, **112**, 551-561.

Rotstein, Y. and Kafka, A.L. 1982. Seismotectonics of the southern Boundary of Anatolia, Eastern Mediterranean Region: Subduction, Collision, and Arc Jumping. *Journal of Geophysical Research*, **87**, 7694-7706.

Rouchy, J.M. and Caruso, A. 2006. Review: The Messinian salinity crisis in the Mediterranean basin: A reassessment of the data and an integrated scenario. *Sedimentary Geology*, **188–189**, 35–67.

Rouchy, J.M., Orszag-Sperber, F., Blanc-Valleron, M.-M., Pierre, C., Riviere, M., Combourieu-Nebout, N. and Panayides, I. 2001. Palaeoenvironmental changes at the Messinian – Pliocene boundary in the eastern Mediterranean (southern Cyprus basins) significance of the Messinian Lago-Mare. *Sedimentary Geology*, **145**. 93-117.

Royden, L.H. 1993. Evolution of retreating subduction boundaries formed during continental collision. *Tectonics*, **12**, 629-638.

Rybakov, M., Goldsmith, V. and Rotstein, Y. 1997. New compilation of the gravity and magnetic maps of the Levant. *Geophysical Research Letters*, **24**, 33-36.

Rybakov, M., Goldsmith, V., Fleischer, L. and Ben-Gai, Y. 2000. 3-D gravity and magnetic interpretation for the Haifa Bay area (Israel). *Journal of Applied Geophysics*, **44**, 353-367.

Sage, L. and Letouzey, J. 1990. Convergence of the African and Eurasian plates in the Eastern Mediterranean. In: Letouzey, J. (eds), Petroleum and Tectonics in Mobile Belts. *Editions Technip, Paris*, 49-68.

Salamon, A., Hofstetter, A., Garfunkel, Z. and Ron, H. 2003. Seismotectonics of the Sinai subplate-the eastern Mediterranean region, *Geophysical Journal International*, **155,** 149-173.

Sanderson, D.C.W. 1988. Thick Source Beta Counting (TSBC): a rapid method for measuring beta dose rates. *Nuclear Tracks (International Journal of Radiation Applications and Instrumentation. Part D. Nuclear Tracks and Radiation Measurements)*, **14,** 203-207.

Sanderson, D.C.W., Bishop, P., Houston, I., Boonsener, M. 2001. Luminescence characterisation of quartz-rich cover sands from NE Thailand. *Quaternary Science Reviews*, **20**, 893-900.

Sandvol, E., Seber, D., Calvert, A. and Barazangi, M. 1998. Grid search modelling of receiver functions: Implications for crustal structure in the Middle East and North Africa. *Journal of Geophysical Research*, **103**, 26899-26918.

Schrimer, W. 1998. Havara on Cyprus - a surficial calcareous deposit. *Eiszeitalter u. Gegenwart*, **48**, 110-117.

Schrimer, W. 2000. Neogene submarine relief and Troodos uplift in southeastern Cyprus. In: Panayides, I., Xenophontos, C. and Malpas, J. (eds), Proceedings of the Third

International Conference on the Geology of the Eastern Mediterranean. *Cyprus Geological Survey Department, Lefkosia.*

Seber, D., Sandvol, E., Sandvol, C., Brindisi, C. and Barazangi, M. 2001. Crustal model for the Middle East and North Africa region: implications for the isostatic compensation mechanism. *Geophysical Journal International*, **147**, 630-638.

Şengör, A.M.C. 1979. The North Anatolian transform fault: its offset and tectonic significance. *Journal of the Geological Society, London*, **136**, 269-282.

Şengör, A.M.C., Yilmaz, Y. and Süngürlu, O. 1984. Tectonics of the Mediterranean Cimmerides: nature and evolution of the western termination of Palaeo-Tethys. In: Dixon, J.E. and Robertson, A.H.F. (eds), The geological evolution of the eastern Mediterranean. *Geological Society, Special Publications*, **17**, 77-112.

Şengör, A.M.C., Gorur, N. and Saroglu, F. 1985. Strike-slip faulting and related basin formation in zones of tectonic escape: Turkey as a case example. In: Biddle, K.T. and Cristie-Blick, N. *(eds)* Strike-slip Deformation, Basin Formation and Sedimentation. *Society of Economical Paleontologists and Mineralogists, Special Publication,* **37**, 227-264.

Simonian, K.O. and Gass, I.G. 1978. Arakapas fault belt, Cyprus: a fossil transform fault. *Bulletin of the Geological Society of America*, **98**, 1220-1230.

Spalluto, L., Moretti, M., Festa, V., Tropeano, M. 2007. Seismically-induced slumps in Lower-Maastrichtian peritidal carbonates of the Apulian Platform (southern Italy). *Sedimentary Geology*, **196**, 81-98.

Špičák, A., Hanuš, V., Vaněk, J. and Běhounková, M. 2007. Internal tectonic structure of the Central American Wadati-Benioff zone based on analysis of aftershock sequences. *Journal of Geophysical Research*, **112**.

Sprovieri, R., Stefano, Di., Howell, M., Sakamoto, T., Di Stefano, A. and Marino, M. 1998. Integrated calcareous plankton biostratigraphy and cyclostratigraphy at site 964. In: Robertson, A.H.F., Emeis, K.-C., Richter, C. and Camerlenghi, A. (eds), *Proceedings of the Ocean Drilling Program, Scientific Results*, **160**.

Soulas, J. P. 1999. Active tectonic studies in Cyprus for seismic risk mitigation: the greater Limassol area. *Final report for Geological Survey Department, Cyprus*.

Soulas, J. P. 2001. Active tectonic studies in Cyprus for seismic risk mitigation: the greater Paphos area. *Final report for Geological Survey Department, Cyprus*.

Soulas, J.P. 2003. Active tectonics in southern Cyprus: Fundamentals of seismic risk analysis. In: Petrides, G., Chrysostomou, Chr., Kyrou, K. and Hadjigeorgiou, Chr. *(eds)*. Proceedings: Earthquake Risk Minimization; International conference. *Geological Survey Department, Cyprus*.

Soulas, J.P. 2005. Study of active tectonics in Cyprus for seismic risk mitigation. *Final report for Geological Survey Department, Cyprus*.

Spencer, J.Q. and Sanderson, D.C.W. 2002. Optically stimulated luminescence of fluvial sediments from Western Cyprus. In: Deckers, K. 2002. Cypriot archaeological sites in the landscape: an alluvial geo-archaeological approach. *Unpublished PhD thesis, University of Edinburgh.*

Spencer, J.Q., Sanderson, D.C.W., Deckers, K. and Sommerville, A.A. 2003. Assessing mixed dose distributions in young sediments identified using small aliquots and a simple two-step SAR procedure: the *F*-statistic as a diagnostic tool. *Radiation Measurements*, **37**, 425-431.

Stokes, S. 1999. Luminescence dating applications in geomorphological research. *Geomorphology*¸ **29**, 153-171.

Stokes, S., Bray, H.E. and Blum, M.D. 2001. Optical resetting in large drainage basins: tests of zeroing assumptions using single-aliquot procedures. *Quaternary Science Reviews*, **20**, 879-885.

Stow, D.A.V., Braakenburg, N.E. and Xenophontos, C. 1995. The Pissouri Basin fan-delta complex, southwestern Cyprus. *Sedimentary Geology*, **98,** 245-262.

Swarbrick, R.E. 1980. The Mamonia Complex of S.W. Cyprus: a Mesozoic continental margin and its relationship with the Troodos Complex. In: (eds) Panayiotou, A. Ophiolites: Proceedings of the International Ophiolite Symposium, Nicosia, 1979. 86-92.

Swarbrick, R.E. and Naylor, M.A. 1980. The Kathikas Mélange, Southwest Cyprus; late Cretaceous submarine debris flows. *Sedimentology*, **27**, 63-78.

Tarling, D. H. 1983. Palaeomagnetism: principles and applications in geology, geophysics and archaeology. *Chapman and Hall, London.*

Taymaz, T., Jackson, J. and Westaway, R. 1990. Earthquake mechanisms in the Hellenic Trench near Crete. *Geophysical Journal International*, **102**, 695-731.

ten Veen, J.H. 2004. Extension of Hellenic forearc shear zones in SW Turkey: the Pliocene-Quaternary deformation of the Esen Cay Basin. *Journal of Geodynamics*, **37**, 181-204.

ten Veen, J.H. and Postma, G. 1999. Neogene tectonics and basin fill patterns in the Hellenic outer-arc (Crete, Greece). *Basin Research*, **11**, 223-241.

ten Veen, J.H. and Kleinspehn, K.L. 2002. Geodynamics along an increasingly curved convergent plate margin: Late Miocene-Pleistocene Rhodes, Greece. *Tectonics*, **21**.

ten Veen, J.H., Woodside, J.M., Zitter, T.A.C. and Dumont, J.F., Mascle, J. and Volkonskaia, A. 2004. Neotectonic evolution of the Anaximander Mountains at the junction of the Hellenic and Cyprus Arcs. *Tectonophysics*, **391**, 35-65.

Vasiliev, L., Krijgsman, W., Stoica, M. and Langereis, C.G. 2005. Mio-Pliocene magnetostratigraphy in the southern Carpathian foredeep and Mediterranean–Paratethys correlations. *Terra Nova*, **17,** 376–384.

Vidal, N. Alvarez-Marron, J. and Klaeschen, D. 2000a. The structure of the Africa-Anatolia late boundary in the eastern Mediterranean. *Tectonics*, **19**. 723-739.

Vidal, N., Klaeschen, D., Kopf, A., Docherty, C., Von Huene, R. and Krasheninnikov, V.A. 2000b. Seismic images at the convergence zone from south of Cyprus to the Syrian coast, eastern Mediterranean. *Tectonophysics*, **329**. 157-170.

Vita-Fizi, C. 1993. Evaluating late Quaternary uplift in Greece and Cyprus. In: Prichard, H.M., Alabaster, T., Harris, N.B.W. and Neary, C.R. *(eds)*. Magmatic processes and plate tectonics. *Geological Society Special Publications*, **76**. 417-424.

Wade, B.S. and Brown, P.R. 2005. Calcareous nannofossils in extreme environments: The Messinian Salinity Crisis, Polemi Basin, Cyprus. Palaeogeography, Palaeoclimatology, Palaeoecology, **233,** 271-286.

Waldron, J.W.F. 2005. Extensional fault arrays in strike-slip and transtension. *Journal of Structural Geology*, **27**, 23–34.

Weber, J., Schrimer, W., Heller, F. and Bachtadse, V. 2006. Magnetostratigraphy of a Plio/Pleistocene section of fluviatile sediments on Cyprus. *Geophysical Research Abstracts*, **8**.

Weiler, Y. 1969. The Miocene Kythrea flysch basin in Cyprus. *Giornale di Geologia*, **35**, 213– 229.

Westaway, R. 1994. Present-day kinematics of the Middle East and eastern Mediterranean. *Journal of Geophysical Research*, **99**, 12071-12090.

Westaway, R. - Jaffey, N. - Robertson, A.H.F. 2002. Discussion of new sedimentological and structural data from the Ecemis Fault Zone, southern Turkey: implications for its timing and offset and the Cenozoic tectonic escape of Anatolia. *Journal of the Geological Society*, **159**, 111-

Wdowinski, S., Ben-Avraham, Z., Arvidsson, R. and Ekström, G. 2006. Seismotectonics of the Cyprian Arc. *Geophysical Journal International*, **164**, 176–181.

Woodside, J.M. 1977. Tectonic elements and crust of the eastern Mediterranean Sea. *Marine geophysical researches*, **3**, 317 - 354.

Woodside, J.M., Mascle., J., Zitter, T.A.C., Limonov, A.F., Ergun, M., Volkonskaia, A. and the shipboard scientists of the PRISMED II Expedition. 2002. The Florence Rise, the Western Bend of the Cyprus Arc. *Marine Geology*, **185**. 177-194.

Xenophontos, C., Malpas, J. and Williams, D. 1994. Geological map of the Acheleia-Kouklia area, 1:25,000 scale. *Geological Survey Department of Cyprus.*

Zeigler, P.A., van Wees, J-D. and Cloetingh, S. 1998. Mechanical controls on collision-related compressional intraplate deformation. *Tectonophysics*, **300**, 103-129.

Zhang, J.F., Zhou, L.P. and Yue, S.Y. 2003. Dating fluvial sediments by optically stimulated luminescence: selection of equivalent doses for age calculation. *Quaternary Science Reviews*, **22**, 1123-1129.

Zimmerman, D.W. 1971. Thermoluminescent dating using fine grains from pottery. *Archaeometry*, **13**, 29-52.

Zitter, T.A.C., Woodside, J.M. and Mascle, J. 2003. The Anaximander Mountains: a clue to the tectonics of southwest Anatolia. *Geological Journal*, **38**, 375-394.

Zomenis, S.L. 1972. Stratigraphy and hydrogeology of the Neogene rocks in the northern foothills of the Troodos Massif. *Bulletin of the Cyprus Geological Survey Department*, **5**, 22-90.

Appendix A: Key to sedimentary logs

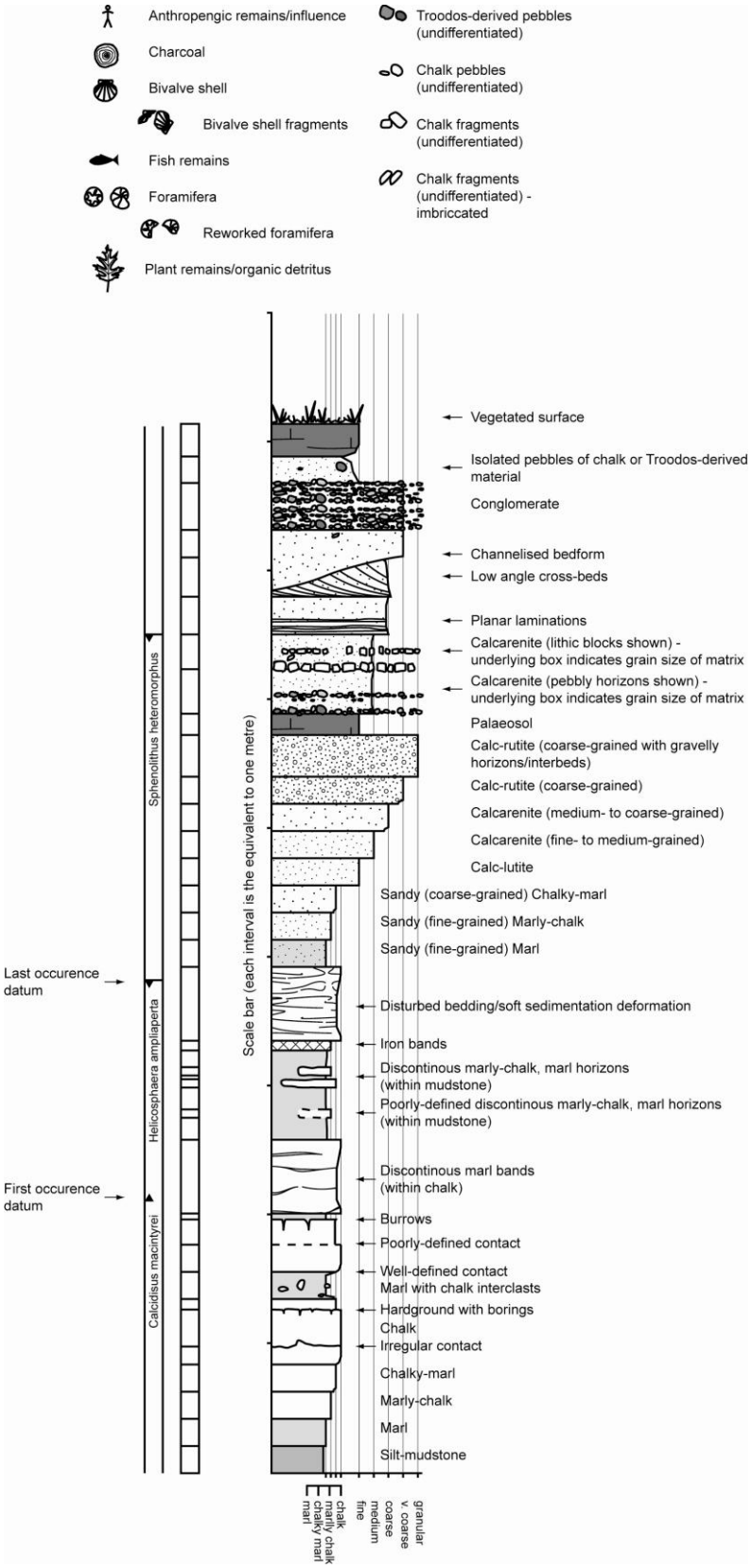

Key to sedimentary logs presented in this thesis